

UNCLASSIFIED

AD NUMBER

AD482152

LIMITATION CHANGES

TO:

Approved for public release; distribution is unlimited.

FROM:

Distribution authorized to U.S. Gov't. agencies and their contractors; Critical Technology; FEB 1966. Other requests shall be referred to Air Force Materials Laboratory, Wright-Patterson AFB, OH 45433. This document contains export-controlled technical data.

AUTHORITY

AFML ltr, 7 Dec 1972

THIS PAGE IS UNCLASSIFIED

ML-TDR-64-125
VOLUME III

487152

**IMPROVED GRAPHITE MATERIALS FOR
HIGH-TEMPERATURE AEROSPACE USE**
**VOLUME III. FURTHER RESEARCH AND
DEVELOPMENT FOR IMPROVED GRAPHITE MATERIALS**

UNION CARBIDE CORPORATION
Carbon Products Division

*Advanced Materials Laboratory, Lawrenceburg, Tennessee
and Research Laboratory, Parma, Ohio*

TECHNICAL REPORT ML-TDR-64-125, VOLUME III

FEBRUARY 1966

This document is subject to special export controls and each transmittal to foreign governments or foreign nationals may be made only with prior approval of the Metals and Ceramics Division (MAM), Air Force Materials Laboratory, Wright-Patterson AFB, Ohio.

**AIR FORCE MATERIALS LABORATORY
RESEARCH AND TECHNOLOGY DIVISION
AIR FORCE SYSTEMS COMMAND
WRIGHT-PATTERSON AIR FORCE BASE, OHIO**

NOTICES

When U. S. Government drawings, specifications, or other data are used for any purpose other than a definitely related Government procurement operation, the Government thereby incurs no responsibility nor any obligation whatsoever; and the fact that the Government may have formulated, furnished, or in any way supplied the said drawings, specifications, or other data, is not to be regarded by implication or otherwise as in any manner licensing the holder or any other person or corporation, or conveying any rights or permission to manufacture, use, or sell any patented invention that may in any way be related thereto.

Copies of this report should not be returned to the Research and Technology Division, Wright-Patterson Air Force Base, Ohio, unless return is required by security considerations, contractual obligations, or notice on a specific document.

**IMPROVED GRAPHITE MATERIALS FOR
HIGH-TEMPERATURE AEROSPACE USE**

**VOLUME III. FURTHER RESEARCH AND
DEVELOPMENT FOR IMPROVED GRAPHITE MATERIALS**

UNION CARBIDE CORPORATION
Carbon Products Division

This document is subject to special export controls and each transmittal to foreign governments or foreign nationals may be made only with prior approval of the Metals and Ceramics Division (MAM), Air Force Materials Laboratory, Wright-Patterson AFB, Ohio.

FOREWORD

This report was prepared by the Union Carbide Corporation, Carbon Products Division, under Contract No. AF 33(657)-11171. The contract was initiated under Project No. 7350, "Refractory Inorganic Nonmetallic Materials," Task No. 735002, "Refractory Nonmetallic Materials: Graphitic." The research and development program was accomplished at the Carbon Products Division, Advanced Materials Laboratory, Lawrenceburg, Tennessee, and the Carbon Products Research Laboratory, Parma, Ohio. The work was administered under the direction of the Air Force Materials Laboratory, Research and Technology Division; Major R. H. Wilson and C. A. Pratt, Jr., were the project engineers.

This report covers work conducted from 1 April 1964 to 31 May 1965 on "Research and Development for Improved Graphite Materials."

The program has been under the direction of Dr. P. G. Lafyatis. Work at the Carbon Products Research Laboratory was under the supervision of Mr. J. C. Bowman, with Dr. W. W. Lozier serving as Project Coordinator. Mr. J. A. Biehl of Marathon Oil Company coordinated the work at the pilot-scale coker at Robinson, Illinois. Scientists at the Research Laboratory were Messrs. M. Jones, I. C. Lewis, T. Edstrom, C. V. Mitchell, L. S. Singer, M. Haun, A. R. Cherry, C. E. Lowell, and Mrs. S. B. Wallon. Work at the Advanced Materials Laboratory was under the supervision of Dr. P. G. Lafyatis, with Mr. M. B. Carter serving as Project Coordinator. Experimentalists at the AML were Messrs. C. F. Stout (Group Leader), G. C. Tolley, E. R. McHenry, and J. H. Turner, with testing, processing and applications support by Dr. R. B. Dull and Messrs. C. W. Waters, W. E. Biles, J. D. Cannon, S. O. Johnson, R. C. Vaughan and D. C. Hiler.

The manuscript was released by the authors August 16, 1965, for publication as an RTD Technical Report.

This technical report has been reviewed and is approved.



W. G. RAMKE
Chief, Ceramics and Graphite Branch
Metals and Ceramics Division
Air Force Materials Laboratory

ABSTRACT

The pyrolysis mechanisms and thermal reactivity of aromatic and heterocyclic compounds are appreciably modified by substitution with nitrogen-, oxygen-, and halogen-containing groups. Aromatic nuclei with strongly activating side groups generally lead to a disordered graphitic structure. The hydrocarbons which yield well-ordered graphites consist largely of fused planar aromatic compounds. The complex mixtures of aromatic compounds that make up the normal raw materials for carbon and graphite form highly-ordered graphites. Pyrolysis studies have been performed for eleven model aromatic hydrocarbons and for two oxygenated aromatics. The planarity of the condensation products of the initial free radical intermediates determines the degree of ordering of the resulting graphite. Electron spin resonance (ESR) studies indicate that free radical intermediates may play an important role in the acid catalyzed rearrangements of methyl benzenes. Aromatic hydrocarbons and related heterocyclic compounds with two to four rings which produce no residue at atmospheric pressure have been thermally polymerized at super-atmospheric pressures. Graphite bodies have been fabricated using coke filler material prepared by pyrolysis of selected model aromatic compounds. The physical properties of the fabricated bodies are strongly influenced by the molecular structure of the starting compounds.

Examination of controlled commercial charge stocks was continued and an effort to correlate the nuclear magnetic resonance and electron spin resonance of these charge stocks with the final graphite properties was attempted. Bench-scale effort was centered around investigations into the preparation of isotropic high thermal expansion graphites and studies to improve binder qualities. Four pilot-scale coker runs to produce high thermal expansion isotropic cokes were made at the Marathon Oil Company in Robinson, Illinois. A commercial air-blown asphalt produced a lower thermal expansion and a higher strength material than that obtained from the air-blown vacuum residuum. A 2 per cent concentration of acetylene black in atmospheric residuum produced a coke with lower electrical resistance and higher strength than that of the 3 per cent concentration. Cokes from vacuum residuum and slurry oil charge stocks were formed into graphite. The test results show that original coke properties affect the final graphite properties. The high thermal expansion cokes were more difficult to process and resulted in graphite having a high compressive strength.

TABLE OF CONTENTS

	PAGE
1. INTRODUCTION	1
2. SUMMARY	3
3. PYROLYSIS MECHANISMS.....	6
3.1. Thermal Reactivity of Aromatic and Substituted Aromatic Hydrocarbons	6
3.1.1. Differential Thermal Analysis (DTA)	6
3.1.2. Thermally "Unreactive" Model Aromatic Compounds.....	7
3.1.3. Thermally "Reactive" Model Compounds.....	10
3.2. Chemical Structure and Graphitization - X-Ray Diffraction Studies of Graphites Derived from Model Compounds.....	39
3.2.1. Introduction	39
3.2.2. Experimental	39
3.3. Pyrolysis Mechanisms of Model Compounds	63
3.3.1. Introduction	63
3.3.2. Experimental Procedure.....	64
3.3.3. Experimental Results.....	67
3.3.4. Thermal Dehydrogenation of Aromatic Hydrocarbons	127
3.4. Electron Spin Resonance (ESR) and Optical Studies of the Electron Distribution in Aromatic Free Radicals.....	128
3.4.1. Introduction	128
3.4.2. Electron Spin Resonance of Radical Cations Produced by the Oxidation of Aromatic Hy- drocarbons with SbCl_5	129
3.4.3. Optical Spectra of Aromatic Radical Cations ..	154
3.4.4. The Electron Spin Resonance of the Radical Ion Formed by the Reaction of Hexamethyl- benzene with H_2SO_4	161
3.4.5. SESRS (Simulation of Electron Spin Resonance Spectra) Computer Program.....	176
3.5. ESR Studies of the Thermal Decomposition of Diaz Compounds.....	180

TABLE OF CONTENTS (CONT'D)

	PAGE
3.5.1. Introduction	180
3.5.2. 2-Diazo-1-acenaphthenone (LVI)	180
3.5.3. Diazophenanthrone (LVII)	
3.5.4. Thermally Decomposed Diazofluorene.	183
3.6. Synthesis of Organic Compounds for Pyrolysis Studies	183
3.6.1. 2-Diazo-2-(4-methoxyphenyl) acetophenone . .	183
3.6.2. 9,9'-Diphenyl-9,9'-Bifluorene.	185
3.6.3. (Chloromethyl)pentamethylbenzenc	186
3.6.4. Methylperinaphthene	186
3.6.5. Naphthacene Dimer	187
3.7. Polymerization of Aromatic Hydrocarbons and Heterocyclic Compounds Under Pressure.	188
3.7.1. Previous Investigations	188
3.7.2. Objectives of the Present Work	190
3.7.3. Equipment and Procedures	190
3.7.4. Effect of Hydrocarbon Structure on Polymer Properties	192
3.7.5. Kinetics of Thermal Polymerization	199
3.7.6. Stoichiometry of the Reaction	223
3.7.7. Possible Catalytic Effects.	231
3.7.8. Mechanisms of Thermal Polymerization Under Pressure	231
3.8. Preparation and Properties of Bulk Graphites from Model Aromatic Compounds	236
4. BENCH-SCALE INVESTIGATIONS.	239
4.1. Seeding Experiments.	239
4.1.1. Conducting Blacks as Seed Materials	240
4.1.2. Seeding of Gilsonite by Acetylene Black.	242
4.1.3. Lewis Acids	242
4.1.4. Investigation of Methods for Dispersing Acetylene Black in Coking Charge Stocks.	244
4.1.5. Effects of Diluents and High-Pressure Coking.	244
4.2. Air Blowing of Coker Charge Stocks	245
4.2.1. Laboratory Air-Blowing Experiments	245
4.2.2. Diluent Effects	247

TABLE OF CONTENTS (CONT'D)

	PAGE
4.2.3. Commercial Air-Blown Asphalts	253
4.2.4. Asphalt Characterization	259
4.2.5. Natural Asphalt.	259
4.2.6. Experiments to Develop Isotropic Cokes of Intermediate Thermal Expansion Levels	259
4.2.7. Preservation of High Thermal Expansion Properties Through Graphite Processing. . . .	269
4.2.8. Solvent Extraction Experiments	272
4.2.9. Characterization of Complex Raw Materials.	275
4.3. Pitch Binder Studies	295
4.3.1. Binders and the Sample Making Process	295
4.3.2. Solvent Extraction Experiments	301
4.3.3. Thermal and Catalytic Cracking Experiments.	303
4.4. Pilot-Scale Coker Experiments.	308
4.4.1. Isotropic High Thermal Expansion Coke	308
4.4.2. Pilot-Scale Coker Performance and Recommendations	315
4.5. Graphite Fabrication.	318
4.5.1. Low Thermal Expansion Cokes.	318
4.5.2. High Thermal Expansion Coke	335
5. REFERENCES	346

ILLUSTRATIONS

FIGURE	PAGE
1. DTA Thermograms of Thermally Unreactive Aromatic and Heterocyclic Model Compounds	9
2. DTA Thermograms of Thermally Reactive Aromatic Hydrocarbon Compounds	12
3. DTA Thermograms of Thermally Reactive Substituted Aromatic Hydrocarbons	18
4. DTA Thermograms of Thermally Reactive Substituted Aromatic Hydrocarbons	26
5. DTA Thermograms of Thermally Reactive Heterocyclic Compounds	33
6. Schematic Diagram of TGA-GE Apparatus	65
7. DTA, TGA-GE Thermograms for Acenaphthylene (Run 48)	68
8. Thermogravimetric-Gas Evolution and Weight Loss Rates for Acenaphthylene (Run 48).	69
9. Thermogravimetric-Gas Evolution and Weight Loss Rates for Acenaphthylene Expressed Relative to Amount of Residue in Reaction Cup (Run 48)	70
10. Ultraviolet Spectra of Chromatographic Fractions of Heat-Treated Acenaphthylene, Solvent: Benzene	73
11. Differential Thermal Analysis, Thermogravimetric and Gas Evolution Curves for the Pyrolysis of 7, 12-Dimethylbenz(a)anthracene (Run 56).	76
12. Weight Loss and Gas Evolution Rate Curves for the Pyrolysis of 7, 12-Dimethylbenz(a)anthracene (Run 56)	78
13. Weight Loss and Gas Evolution Rate Curves for the Pyrolysis of 7, 12-Dimethylbenz(a)anthracene Expressed Relative to Amount of Residue in Reaction Cup (Run 56)	79
14. Ultraviolet Spectra of Pyrolyzed 7, 12-Dimethyl(a)-anthracene	82
15. Infrared Spectra of Pyrolyzed 7, 12-Dimethylbenz(a)anthracene	83

ILLUSTRATIONS (CONT'D)

FIGURE		PAGE
16.	Postulated Carbonization Sequence for 7, 12-Dimethylbenz(a)anthracene.	87
17.	Thermogravimetric and Gas Evolution Curves for the Pyrolysis of Naphthacene (Run 55).	88
18.	Weight Loss and Gas Evolution Rates for Naphthacene (Run 55).	89
19.	Weight Loss and Gas Evolution Rates for Naphthacene (Run 55) Expressed Relative to Amount of Residue in Reaction Cup	89
20.	Infrared Spectra of Pyrolyzed Naphthacene	93
21.	Ultraviolet Spectra of Pyrolyzed Naphthacene	94
22.	Postulated Carbonization Sequence for Naphthacene	97
23.	Dehydrogenation Curve for Carbonized Fluoranthene	98
24.	Differential Thermal Analysis, Thermogravimetric and Gas Evolution Curves for the Pyrolysis of Periflanthene (Run 57).	100
25.	Weight Loss and Gas Evolution Rate Curves for the Pyrolysis of Periflanthene (Run 57).	101
26.	Weight Loss and Gas Evolution Rate Curves for the Pyrolysis of Periflanthene Expressed Relative to the Amount of Residue in Reaction Cup (Run 57)	101
27.	Infrared Spectra of Heat-Treated Periflanthene	104
28.	Differential Thermal Analysis, Thermogravimetric, and Gas Evolution Curves for the Pyrolysis of 9, 9'-Bifluorene (Run 51)	107
29.	ESR Spectrum of 9, 9'-Bifluorene at 260°C	109
30.	Variation of the ESR Intensity of 9, 9'-Bifluorene with Temperature.	110
31.	Differential Thermal Analysis, Thermogravimetric Analysis, and Gas Evolution Curves for the Pyrolysis of $\Delta^9,9'$ -Bifluorene (Runs 49 and 50).	112

ILLUSTRATIONS (CONT'D)

FIGURE		PAGE
32.	Thermogravimetric Gas Evolution and Weight Loss Rates for $\Delta^9,9'$ -Bifluorene (Run 49)	113
33.	Thermogravimetric Gas Evolution and Weight Loss Rates for $\Delta^9,9'$ -Bifluorene Expressed Relative to the Amount of Residue in Reaction Cup (Run 49)	113
34.	Variation of the ESR Line Intensity of $\Delta^9,9'$ -Bifluorene with Time at 384°C.	115
35.	Infrared Spectra of Heat-Treated $\Delta^9,9'$ -Bifluorene	116
36.	ESR Spectrum of 9,9'-Bianthryl at 550°C.	120
37.	Dehydrogenation Curve for Carbonized p-Terphenyl. . .	123
38.	Infrared Spectra of Heat-Treated 1,4-Naphthoquinone.	125
39.	Infrared Spectra of Heat-Treated 1,4-Naphthalenediol	126
40.	Vacuum Transfer Apparatus for the Preparation of Hydrocarbon - SbCl_5 Solutions at Low Temperatures . .	132
41.	ESR Spectra for the Radical Cations of (a) Tetraphenylethylene, (b) $\Delta^9,9'$ -Bifluorene, and (c) Naphthalene.	139
42.	Comparison of Experimental and Computed Stick Plots for the Radical Cation of Pyrene.	145
43.	Comparison of Experimental and Computed Stick Plots for the Radical Cation of Naphthalene	146
44.	Comparison of Experimental and Computed (SESRS) Curves for the Radical Cation of Naphthalene	147
45.	Comparison of Experimental and Computed (SESRS) Curves for the Radical Cation of Dibenzo(a, c)-Triphenylene.	148
46.	Comparison of Experimental and Computed Stick Plots for the Radical Cation of $\Delta^9,9'$ -Bifluorene.	149
47.	Comparison of Experimental and Computed Stick Plots for the Radical Cation of Tetraphenylethylene . . .	150

ILLUSTRATIONS (CONT'D)

FIGURE		PAGE
48.	Relation Between Experimental Coupling Constants, a_H , and Hückel Spin Densities, ρ , for Aromatic Hydrocarbon Negative Ions.	152
49.	Relation Between Experimental Coupling Constants, a_H , and Hückel Spin Densities, ρ , for Aromatic Hydrocarbon Positive Ions ^(es)	152
50.	Comparison Between Experimental Coupling Constants for Both Aromatic Negative and Positive Ions and Those Calculated from the Colpa-Bolton (CB) Theory ^(es)	153
51.	Comparison Between Experimental Coupling Constants for both Aromatic Negative and Positive Ions, and Those Calculated from the Giacometti-Nordio-Pavan (GNP) Theory ^(es)	155
52.	Optical Spectra of Naphthacene Radical Ion	156
53.	Optical Spectra of Aromatic Hydrocarbon Radical Ions	157
54.	Optical Spectra of Aromatic Hydrocarbon Radical Ions	157
55.	Ultraviolet Spectra of Pentamethylbenzene in H_2SO_4 . . .	161
56.	Ultraviolet Spectra of $\Delta^{1,1}$ -Biacenaphthene in H_2SO_4 . . .	162
57.	Optical Spectra of HMB in H_2SO_4	164
58.	ESR of HMB in H_2SO_4 ; Comparison Between Experimental Curve and Curve Synthesized by an SESRS Computation	164
59.	Experimental Line Spectrum for HMB in H_2SO_4 ; Line Positions and Intensities Taken from the Upper Spectrum in Figure 58.	165
60.	Line Intensities of the Central Group of Lines in Figure 59; Comparison with Those Computed from Three Different Sets of Coupling Constants (Dashed Curves)	166

ILLUSTRATIONS (CONT'D)

FIGURE	PAGE
61. Correlation Diagrams for the Intensities of the Central Group of Lines in the ESR Spectrum of HMB in H_2SO_4 ; Line No. Zero is the Central Line of the Spectrum; the Spacing $a/2$ Equals 1.68 Gauss . . .	167
62. Central Portion of the ESR Spectrum of HMB in H_2SO_4 at Three Different Temperatures	168
63. ESR of HMB in D_2SO_4 ; Comparison Between Experimental Curve and Curve Synthesized by an SESRS Computation	169
64. Line Intensities for the ESR of HMB in D_2SO_4 ; Comparison Between Experimental (Taken from the Upper Curve in Figure 63) and Computed Spectra	170
65. ESR of a 3×10^{-3} M Solution of HMB in Molten I_2 at 125°C	171
66. Correlation Diagrams for the ESR Spectrum of HMB in Molten I_2 ; Experimental Intensities Taken from the Curve in Figure 65; Line Number Zero is the Central Line of the Spectrum	172
67. Comparison of Experimental and Computed SESRS Spectra for Thermally Decomposed Diazobenzil.	179
68. ESR Spectrum of a 1:20 Solution of 2-Diazo-1-acenaphthenone (LVI) in Biphenyl at 196°C	181
69. Comparison of Experimental and Computed Line Spectra for (LVI)	181
70. Superposition of Spectra for the Two Radicals Formed During the Thermal Decomposition of (LVI); Measurement Made at 90°C	182
71. SESRS Comparisons of ESR Spectrum of Radical From Thermally Decomposed Diazofluorene	184
72. Exotherm in the Thermal Polymerization of Naphthalene (Experiment 128-17)	200
73. Transition to Solid Polymer in the Thermal Polymerization of p-Terphenyl (Experiment 160-84).	202
74. Transition to Solid Polymer in the Thermal Polymerization of Fluoranthene (Experiment 160-72).	203

ILLUSTRATIONS (CONT'D)

FIGURE		PAGE
75.	Arrhenius Plot for Transition to Solid Polymer - Naphthalene (θ in Hours)	206
76.	Arrhenius Plot for Transition to Solid Polymer - Fluoranthene (θ in Hours)	207
77.	Arrhenius Plot for Transition to Solid Polymer - p-Terphenyl (θ in Hours)	208
78.	Thermal Polymerization of Naphthalene - Reduced Density of 1.17 (Experiment 160-75)	217
79.	Thermal Polymerization of Naphthalene - Reduced Density of 2.00 (Experiment 159-57)	218
80.	Arrhenius Plot - Time to Minimum Pressure for First-Order Kinetics (Naphthalene)	220
81.	Arrhenius Plot - Time to Minimum Pressure for Second-Order Kinetics (Naphthalene)	221
82.	Time-Temperature-Pressure- ΔT Record for Polymerization of Fluoranthene (Experiment 255-145-15)	222
83.	Possible Mechanisms in the Thermal Polymerization of Naphthalene	233
84.	Cumulative Per Cent Linear Expansion Versus Temperature Relationships for Various High Thermal Expansion Materials	243
85.	Viscosity Versus Temperature Relationships for Dispersions of Acetylene Black in Residual Feedstocks	245
86.	Thermal Expansion (30-100°C) of Extruded Graphite Articles as a Function of Asphaltene Content of the Charge Stocks	250
87.	Viscosities of Diesel Oil Diluted Asphalt as Compared to Vacuum Residuum	254
88.	Viscosities of Light Catalytic Cycle Oil Diluted Asphalt as Compared to Vacuum Residuum	255
89.	Viscosities of Kerosene Diluted Asphalt as Compared to Vacuum Residuum	256

ILLUSTRATIONS (CONT'D)

FIGURE		PAGE
90.	Method of Separation and Densimetric Analysis	261
91.	Graphite Thermal Expansion as a Function of Mal- thene Molecular Weight and Number of Carbon Atoms per Molecule	264
92.	Billet Processing Variations Using Coke Produced in Pilot Coker (Cycles 68S and 69N) from Kerosene- Diluted Air-Blown Vacuum Residuum Produced by Trumbull Asphalt Company.	270
93.	Infrared Spectra of Vacuum Residuum P-4 and Air-Blown Products	286
94.	Infrared Spectra of Slurry Oil P-9, and Air-Blown Products	286
95.	NMR Spectra of Air-Blown Asphalts from Slurry Oil P-9.	288
96.	Saturation Measurements on Sample PS-111: (a) ESR Curves for Different Microwave Powers; (b) Normalized Intensity as a Function of Microwave Power	289
97.	ESR Signal for P-9; (The Parameters D and S_F and the Height of the Ruby Signal are used to Cal- culate Free Radical Concentration)	291
98.	ESR of Graphites Made from Air-Blown Asphalts: (a) PS-80, (b) PS-45.	292
99.	Relationship of Flexural Strength Versus Characteri- zation Factor ($BI \times C/H$ of Benzene Solubles $\times C/H$ of Benzene Insolubles).	301
100.	Extraction of 30 Medium and 30 Hard Pitch.	302
101.	Schematic of Pilot Scale Coker Operation for Pro- ducing a High Thermal Expansion Graphite-Source Material.	309
102.	Processing Raw Cokes	319
103.	Sampling Diagram of Graphite Blocks	320

ILLUSTRATIONS (CONT'D)

FIGURE		PAGE
104.	High-Temperature Thermal Expansion for With-Grain RT-0033 and RVA	327
105.	High-Temperature Thermal Expansion for Across-Grain RT-0033 and RVA	328
106.	High-Temperature Thermal Expansion for With-Grain RT-0034 and RVA	329
107.	High-Temperature Thermal Expansion for Across-Grain RT-0034 and RVA	330
108.	High-Temperature Thermal Expansion for With-Grain RT-0035 and CFZ	331
109.	High-Temperature Thermal Expansion for Across-Grain RT-0035 and CFZ	331
110.	High-Temperature Thermal Expansion for With-Grain RT-0036 and CFZ	332
111.	High-Temperature Thermal Expansion for Across-Grain RT-0036 and CFZ	332
112.	Pore Size Distribution of Grades RT-0033 and RVA . . .	333
113.	Pore Size Distribution of Grades RT-0034 and RVA . . .	333
114.	Pore Size Distribution of Grades RT-0035 and CFZ . . .	334
115.	Pore Size Distribution of Grades RT-0036 and CFZ . . .	334
116.	High-Temperature Thermal Expansion for With-Grain RT-0037 and RVA	340
117.	High-Temperature Thermal Expansion for Across-Grain RT-0037 and RVA	340
118.	High-Temperature Thermal Expansion for With-Grain RT-0040 and RVA	341
119.	High-Temperature Thermal Expansion for Across-Grain RT-0040 and RVA	341
120.	High-Temperature Thermal Expansion for With-Grain RT-0041 and RVA	342

ILLUSTRATIONS (CONCL'D)

FIGURE		PAGE
121.	High-Temperature Thermal Expansion for Across-Grain RT-0041 and RVA	342
122.	High-Temperature Thermal Expansion for With-Grain RT-0044 and RVA	343
123.	High-Temperature Thermal Expansion for Across-Grain RT-0044 and RVA	343
124.	Pore Size Distribution of Grades RT-0037 and RVA . . .	344
125.	Pore Size Distribution of Grades RT-0040 and RVA . . .	344
126.	Pore Size Distribution of Grades RT-0041 and RVA . . .	345
127.	Pore Size Distribution of Grades RT-0044 and RVA . . .	345

TABLES

TABLE		PAGE
1.	Thermally Unreactive Compounds	9
2.	Thermally Reactive Polynuclear Aromatics	13
3.	Thermal Properties of Oxygen Substituted Aromatic Hydrocarbons	15
4.	Thermal Properties of Chlorinated Polycyclic Hydrocarbons	19
5.	Thermally Reactive Amino Substituted Aromatic Compounds	21
6.	Thermally Reactive Substituted Polynuclear Aromatics .	25
7.	Thermally Reactive Nitro-Substituted Aromatic Hydrocarbons	27
8.	Thermally Reactive Substituted Aromatics	31
9.	Thermally Reactive Heterocyclic Oxygen Compounds . .	32
10.	Thermally Reactive Substituted Heterocyclic Nitrogen Compounds	34
11.	Thermal Properties of Heterocyclic Compounds Containing Both Oxygen and Nitrogen	36
12.	Thermal Properties of Heterocyclic Sulfur Compounds .	37
13.	002-Semilattice Spacings Obtained from Various Reflections for Some Graphitized Raw Materials	41
14.	002-Semilattice Spacings for Graphites Derived from Model Aromatic Hydrocarbons	42
15.	002-Semilattice Spacings for Graphites Derived from Alkyl and Aryl Substituted Aromatic Hydrocarbons	44
16.	002-Semilattice Spacings for Graphites Derived from Oxygenated Aromatics	46
17.	002-Semilattice Spacings for Graphites Derived from Nitrogen-Substituted Aromatics	49
18.	002-Semilattice Spacings for Graphites Derived from Halogen-Substituted Model Compounds	51

TABLES (CONT'D)

TABLES	PAGE
19. 002-Semilattice Spacings for Graphites Derived from Model Organic Compounds	52
20. 002-Semilattice Spacings for Graphites Derived from Heterocyclic Oxygen Compounds	52
21. 002-Semilattice Spacings for Graphites Derived from Heterocyclic Nitrogen Compounds	53
22. 002-Semilattice Spacings for Graphites Derived from Heterocyclic Sulfur Compounds	54
23. 002-Semilattice Spacings for Modified Aromatic Hydrocarbon Graphites	55
24. 002-Semilattice Spacings from Physical Mixtures of Cokes and Graphites Derived from Model Hydrocarbons Acenaphthylene and p-Terphenyl	56
25. Model Compounds Employed in Pyrolysis Mechanism Studies	63
26. Composition of the Fixed Gases Evolved During the Pyrolysis of Acenaphthylene in Helium, TGA-GE (Run 48)	71
27. Composition of Effluent Gas Collected at Various Temperatures During Pyrolysis of 7, 12-Dimethylbenz-(a)anthracene (TGA-GE Run 56).	80
28. Measured and Calculated Compositions of Total Fixed Gases Collected During Pyrolysis of 7, 12-Dimethylbenz(a)anthracene (TGA-GE Run 56)	81
29. Composition in Mole Per Cent of Effluent Gas Collected at Various Temperatures During Pyrolysis of Naphthacene (TGA-GE Run 55)	91
30. Measured and Calculated Compositions of Total Fixed Gases Collected During Pyrolysis of Naphthacene to 725°C (TGA-GE Run 55).	91
31. ESR Measurements of Naphthacene	92
32. Elementary Analysis for Pyrolyzed Fluoranthene.	98

TABLES (CONT'D)

TABLE	PAGE
33. Composition of Effluent Gas Collected at Various Temperatures During the Pyrolysis of Periflanthene (TGA-GE Run 57)	102
34. Measured and Calculated Compositions of Total Fixed Gases Collected During Pyrolysis of Periflanthene (TGA-GE Run No. 57)	103
35. Composition of the Fixed Gases Evolved During the Pyrolysis of 9, 9'-Bifluorene in Helium (TGA-GE Run 51).	107
36. Summary of ESR Experiments on 9, 9'-Bifluorene	108
37. Composition of the Fixed Gases Evolved During the Pyrolysis of $\Delta^{9,9'}$ -Bifluorene in Helium, TGA-GE Run 50	114
38. ESR Measurements for $\Delta^{9,9'}$ -Bifluorene	115
39. Elementary Analyses for Pyrolyzed p-Terphenyl	122
40. Hydrogen Content and Graphite Properties of Cokes Derived from Aromatic Hydrocarbons	127
41. Summary of ESR Observations on Aromatic Hydrocarbon Radical Cations Produced by SbCl_5 in CH_2Cl_2 Solvent--Resolved Spectra	133
42. Summary of ESR Observations of Aromatic Hydrocarbon Radical Cations Produced by SbCl_5 in CH_2Cl_2 Solvent--Unresolved Spectra	135
43. Coupling Constants for Aromatic Hydrocarbon Radical Ions	137
44. Optical Absorption of Aromatic Hydrocarbon Radical Ions	159
45. Data on Thermal Polymerization of Compounds Leading to Nongraphitizing Carbons	193
46. Characteristics of 3000°C Heat-Treated Polymers-Nongraphitizing Carbons	194
47. Data on Thermal Polymerization of Compounds Leading to Isotropic Graphites	196

TABLES (CONT'D)

TABLE	PAGE
48. Characteristics of 3000°C Heat-Treated Polymers - Isotropic Graphites.	196
49. Data on Thermal Polymerization of Compounds Leading to Anisotropic Graphite	197
50. Characteristics of 3000°C Heat-Treated Polymers - Anisotropic Graphites	198
51. Summary of Data on Temperature Dependence of Rate of Polymerization	209
52. Temperature Dependence of Time of Solid Polymer Formation.	210
53. Kinetic Order in Thermal Polymerization of Anthracene.	212
54. Critical Constants of Naphthalene	214
55. Reduced Parameters for the Initial Conditions of Naphthalene Polymerization.	215
56. Orthobaric Liquid and Vapor Densities of Naphthalene ⁽¹⁴⁷⁾	216
57. Coefficients and Statistics for Figures 80 and 81	222
58. Stoichiometry in Thermal Polymerization of Naphthalene	224
59. Composition of Gas in Vessel at Various Times, Experiment 160-84 (p-Terphenyl)	226
60. Composition of Pressure Distillate from Biphenyl Polymerization	227
61. Ultimate Analysis of Polymers.	228
62. Comparison of Stainless Steel and Glass Liners.	231
63. Analytical Data on Raw and Calcined Cokes from Acenaphthylene, Fluoranthene and p-Terphenyl.	236
64. Summary of Data on 0.75-Inch Diameter Extruded Rods Fabricated from Acenaphthylene, Fluoranthene, and p-Terphenyl Cokes	238

TABLES (CONT'D)

TABLE	PAGE
65. Summary of Data on 2.5-Inch Diameter Molded Plugs Fabricated from Acenaphthylene, Fluoranthene, and p-Terphenyl Cokes	238
66. Physical Characteristics of Cabot Vulcan XC-72R, Columbian Conducted SC and Shawinigan Acetylene Black	240
67. Physical Property Data for Graphitized Extruded and Molded Billets Produced from Atmospheric and Vacuum Residuum Cokes Seeded with Conductex SC and Vulcan XC-72R	241
68. Graphitized Extruded Billet Data for Vacuum Residuum Coking Charge Material Containing Ferric Chloride (Lewis Acid) and Ferrous Chloride (Not a Lewis Acid)	243
69. Physical Property Data for Graphitized Extruded and Molded Billets Processed From Seed Cokes, Effect of Diluent and Coking Pressure	246
70. Operating Conditions and Properties for the Paraffinic-Type Residuum Charge and Various Air-Blown Paraffinic-Type Residuum Samples	248
71. Operating Conditions and Properties for the Naphthenic Residuum Charge and Air-Blown Naphthenic-Type Residuum Samples	248
72. Graphite Properties for Extruded Billets Produced from Non Air-Blown and Air-Blown Paraffinic-Type Residuum	249
73. Graphite Properties for Extruded Billets Produced from Non Air-Blown and Air-Blown Naphthenic-Type Residuum	249
74. Graphite Properties for Molded Billets Produced from Non Air-Blown and Air-Blown Naphthenic-Type Residuum	251
75. Graphite Properties for Molded Billets Produced from Non Air-Blown and Air-Blown Paraffinic-Type Residuum	252
76. Evaluation of Air-Blown Vacuum Residuum	253

TABLES (CONT'D)

TABLE		PAGE
77.	Atmospheric Distillation Results (ASTM D-158) for Asphalt Diluents.	253
78.	Graphite Thermal Expansion Evaluation for Diluted Asphalt Coking Charges.	257
79.	Titles and Sources of Evaluated Commercial Air-Blown Materials.	257
80.	Properties of Commercial Air-Blown Material	258
81.	Physical Properties for Extruded Graphite Billets Produced from Commercial Air-Blown Materials.	260
82.	Coking Charge Characterization of Materials Used in the Densimetric Calculations	262
83.	Malthene Properties and Densimetric Calculations for Various Coker Charge Stocks and Asphalts	263
84.	Properties of Vacuum Residuum from Fourbear Crude Oil	264
85.	Thermal Expansion Values for Graphite Using a Topped Fourbear Crude Source.	265
86.	Physical Property Data for Graphitized $\frac{5}{8}$ -Inch Diameter Extruded Billets Processed from Cokes Produced from Gilsonite and Vacuum Residuum or Slurry Oil Mixtures.	266
87.	Physical Property Data for 3-Inch Diameter Graphitized Molded Billets Processed from Gilsonite and Vacuum Residuum or Slurry Oil Mixtures.	267
88.	Physical Property Data for Graphitized Extruded and Molded Billets Produced from Vacuum Residuum and Slurry Oil Cokes Produced in the Presence of High-Boiling Organic Compounds	268
89.	Graphitized 3-Inch Diameter by 3-Inch Length Molded Billet Properties for Billets Produced Using Fillers of Various Heat-Treatment Temperatures	271
90.	Volume Per Cent Sludge Removed from Vacuum Residuum with Various Solvents	273

TABLES (CONT'D)

TABLE	PAGE
91. Properties of Graphite Billets Made from Vacuum Residuum and its Heptane and Pentane Solubles and Insolubles	274
92. Properties of Vacuum Residuum and its Heptane and Pentane Solubles and Insolubles	275
93. Aromatic and Other Solvents Used with Vacuum Residuum	276
94. Graphite Property Data (Beaker Coked-Extruded Rods	277
95. Chemical Shifts, δ , of Protons in Graphite Raw Materials	278
96. Properties of Commercial Coker Charge Stocks	279
97. Hydrogen Composition of Graphite Raw Materials	281
98. Aromatic Carbon Content of Raw Materials	282
99. Hydrogen Composition of Slurry Oil P-9 and Chromatographed Fractions	282
100. Relationship of Aromatic Carbon Content to Coke Yield	283
101. Relationship of Thermal Expansion to Aromatic Carbon Content of Feed Stocks	284
102. Air-Blown Asphalts Examined	285
103. ESR Results for Air-Blown Refinery Oils	288
104. Comparison of Asphalt and Graphite Properties	294
105. Statistical Data for 3-Inch Diameter Molded Plugs	296
106. Analytical Properties of 30 Hard Pitch and an Experimental Petroleum Pitch	297
107. Binder Characteristics and Graphite Flexural Strength	299
108. Regression Equations Formed for Binder Properties Versus Flexural Strength	300

TABLES (CONT'D)

TABLE	PAGE
109. Properties of 30 Hard Pitch, 30 Hard Pitch Extract (α_1 , α_2 , and β Portions) and the Resultant Graphites	303
110. Properties of Marathon Oil Company Thermal Residuum and Pure Oil Company Thermal Tar	304
111. Thermal Cracking Conditions for Thermal Tar and Thermal Residuum (TT and TR)	304
112. Properties of Marathon Thermal Residuum Before and After High-Temperature Thermal Cracking.	305
113. Properties of Graphite Made From Thermally Cracked and Uncracked Thermal Residuum and From 30 Hard Pitch	305
114. Catalytic Cracking Conditions for Thermal Tar and Thermal Residuum (TT and TR)	306
115. Properties of Pure Oil Thermal Tar Before and After Catalytic Cracking Experiments	307
116. Properties of Graphite Made from Catalytically Cracked and Uncracked Thermal Tar and 30 Hard Pitch	307
117. High Thermal Expansion Isotropic Cokes, Operating Conditions and Yields	308
118. Extruded Billet Data for Cycles 68S and 69N Coke	310
119. Graphitized Molded Billet Data for Cycles 68S and 69N Coke	311
120. Extruded $\frac{5}{8}$ -Inch Diameter Billet Data for Cycles 78S and 79N.	312
121. Molded 3-Inch Diameter Billet Data for Cycles 78S and 78N	313
122. Processing and Physical Property Summary, Extruded and Molded Billets Processed from Acetylene Black-Seeded Atmospheric Residuum Coke Produced in Pilot Coker, Cycle 70S.	314

TABLES (CONT'D)

TABLE	PAGE
123. Processing and Physical Property Summary, Extruded and Molded Billets Processed from Acetylene Black-Seeded Atmospheric Residuum Coke Produced in Pilot Coker, Cycle 76N	346
124. Room-Temperature Properties of RT-0033 Through RT-0036, RVA and CFZ	321
125. Bulk Density, g/cc, Property Variation for RT-0035 . .	322
126. Bulk Density, g/cc, Property Variation for RT-0036 . .	322
127. Specific Resistance, 10^{-4} Ω -cm, Property Variation for RT-0035	323
128. Specific Resistance, 10^{-4} Ω -cm, Property Variation for RT-0036	323
129. Young's Modulus, 10^6 lbs./in. ² , Property Variation for RT-0035	324
130. Young's Modulus, 10^6 lbs./in. ² , Property Variation for RT-0036	324
131. Flexural Strength, lbs./in. ² , Property Variation for RT-0035	325
132. Flexural Strength, lbs./in. ² , Property Variation for RT-0036	325
133. Compressive Strength, lbs./in. ² , Property Variation for RT-0035	326
134. Compressive Strength, lbs./in. ² , Property Variation for RT-0036	326
135. Room-Temperature Thermal Expansion of RT-0035, RT-0036, and CFZ	327
136. Grade Designation for Graphites from Various Cokes . .	335
137. Physical Properties of Grades RT-0037, -0040, -0041, -0044	336
138. Bulk Density, g/cc Property Variations for RT-0037, -0040, -0041, and -0044	336

TABLES (CONCL'D)

TABLE		PAGE
139.	Specific Resistance, $10^{-4} \Omega\text{-cm}$, Property Variation for RT-0037, -0040, -0041, and -0044.	337
140.	Young's Modulus, 10^6 lbs./in.^2 , Property Variation for RT-0037, -0040, -0041, and -0044.	337
141.	Flexural Strength, lbs./in.^2 , Property Variation for RT-0037, -0040, -0041, and -0044.	338
142.	Compressive Strength, lbs./in.^2 , Property Variation for RT-0037, -0040, -0041, and -0044.	338
143.	Thermal Expansion ($30\text{-}100^\circ\text{C}$), $10^6/^\circ\text{C}$, Property Variation for RT-0037, -0040, -0041, and -0044.	339

1. INTRODUCTION

This volume covers the final year's work on "Research and Development for Improved Graphitic Materials," of a program to provide graphite materials for high-temperature aerospace use. This research and development effort is a continuation of selected portions of the program for studies leading to the understanding required for development of uniform reproducible carbon-based materials capable of being tailored to meet high-temperature materials requirements in advanced aerospace systems conducted under Contract AF 33(616)-6915. This work included scale-up, characterization, and evaluation of graphites to permit their successful use as engineering materials. Major emphasis was placed on acquiring a better understanding of the specific chemistry and pyrolysis reactions of raw materials; the limiting properties of single crystals; the relationship between the basic chemical and physical processes and processing techniques; and improved testing methods. The work conducted under Contract AF 33(616)-6915 is covered in the various volumes of WADD TR 61-72.

The objective of the present program is to obtain a more detailed understanding of the relation between the chemical characterization of the raw materials and the properties of the final graphite. This has been continued in a two-phase concurrent program. The first phase has been concerned primarily with the chemical mechanisms of pyrolysis, carbonization and graphitization of model compounds and the development of specific chemical and physical techniques to follow the reactions. The second phase has been directed to the examination of the commercially available charge stocks and their modification to produce graphites with a broad spectrum of physical properties. The final step has been to attempt to use the methods and information developed in phase one to correlate the results of phase two.

The approach in the first phase of the prior and current program has been to follow the carbonization of pure, model organic compounds and then mixtures by specialized physical and chemical techniques. Considerable progress has been made in the development of differential thermal analysis, nuclear magnetic resonance, electron spin resonance, polarographic, X-ray and spectral techniques for the detailed characterization and mechanism studies.

The applied research effort under the previous contract served as a basis for much of the present phase one effort and was concerned primarily with a survey of the carbonization behavior of various raw materials. These data formed the basis for choosing representative model compounds for the study of the relation between chemical structure and thermal reactivity.

The work relating thermal reactivity to chemical structure, emphasizing the effect of substituent groups on the thermal reactivity, has been continued.

Detailed studies have been made on the pyrolytic reaction mechanisms of several selected model compounds. Several of the intermediate radicals have been identified. The electron distribution and hence the reactivity of a number of aromatic radicals have been determined. Combining these various types of experimental information, we have clarified the mechanisms of carbonization and graphitization.

The parallel effort has been directed toward evaluating some of the commercially available raw materials, which are complex mixtures, as charge stocks to produce binder and filler materials for graphite. Bench-scale batch experimentation has demonstrated that the characteristics of coke can be varied over a wide range not only by varying the initial compositions of the material processed, but also by varying the time, temperature and pressure during the coking process.

Properties of the finished graphites are influenced by the characteristic of the raw materials, particularly the filler component. The major effort has been the investigation of reproducible raw materials with desirable combinations of thermal and physical properties.

During the period of this report, contact with Air Force Contractors and Subcontractors was maintained to expedite the awareness of improved materials developed under this program and to coordinate the evaluation of the materials from this program in the different locations.

2. SUMMARY

The pyrolysis mechanisms and thermal reactivity of aromatic and heterocyclic compounds are appreciably modified by substitution with nitrogen-, oxygen-, and halogen-containing groups. The activating effect of substituent groups is of particular interest in the development of new raw materials which will produce very high carbon yields on pyrolysis.

The degree of crystal order of graphites derived from model organic compounds exhibits a strong dependence on the starting chemical structure. The hydrocarbons which yield well-ordered graphites consist largely of fused planar aromatic compounds. Disordered graphites generally result from nonplanar molecules which are devoid of fused polycyclic systems. Aromatic nuclei with strongly activating side groups generally lead to a disordered graphitic structure. Heterocyclic compounds generally produced relatively disordered graphites. The complex mixtures of aromatic compounds that make up the normal raw materials for carbon and graphite form highly-ordered graphites. In general, the properties of the graphites obtained from model compounds show a dependence on two major factors: (1) the planarity and steric overcrowding in the original molecule and (2) the chemical reaction sequence and the nature of the thermally formed intermediates.

Pyrolysis studies have been performed for eleven model aromatic hydrocarbons and for two oxygenated aromatics. Differential thermal analysis (DTA), thermogravimetric analysis-gas evolution (TGA-GE), electron spin resonance (ESR), nuclear magnetic resonance (NMR), and chemical studies have been employed wherever applicable to the pyrolysis of acenaphthylene, 7, 12-dimethylbenz(a)anthracene, naphthacene, fluoranthene, perflanthene, 9, 9'-bifluorene, $\Delta^{9,9'}$ -bifluorene, 9, 9'-bianthryl, p-terphenyl, α -truxene, 9, 10-dibenzylanthracene, 1, 4-naphthoquinone, and 1, 4-naphthalenediol.

Reaction mechanisms have been proposed for each of the hydrocarbons. The carbonization reactions are consistent with an initial cleavage of a C-H or C-C bond at the most reactive site of the molecule. The planarity of the condensation products of the initial free radical intermediates determines the degree of ordering of the resulting graphite. The first dehydrogenation reactions are generally accompanied by intermolecular hydrogen transfers. At higher temperatures, direct dehydrogenation occurs at a rate influenced by the planarity of the aromatic intermediates.

Electron spin resonance (ESR) studies have been made of radical cations prepared by the oxidation of 24 aromatic hydrocarbons with SbCl_5 in CH_2Cl_2 solvent. The coupling constants for the ESR spectra of the radical cations of perylene, anthracene, 9, 10-dimethylanthracene, and naphthacene in SbCl_5 were essentially identical to those for the respective ions in H_2SO_4 . The ESR spectra for the radical cations of pyrene, naphthalene, dibenzo(a, c)triphenylene, $\Delta^{9,9'}$ -bifluorene, and tetraphenylethylene have also been reduced to coupling constants. The positive radical ion resulting from the oxidation of naphthalene is a symmetrical dimer with the unpaired electron divided equally between the two molecules. Quantitative

comparisons were made between experimental coupling constants and those computed from the Colpa-Bolton and Giacometti-Nordio-Pavan theories. Both theories were found to account for the differences in magnitude between the coupling constants for aromatic negative and positive ions.

Optical spectra were obtained for aromatic radical cations prepared by the oxidation of aromatic hydrocarbons with SbCl_5 in CH_2Cl_2 . Optical spectra of the radical ions of naphthalene, perylene, anthracene, pyrene, naphthalene, dibenzo(a, c)triphenylene, $\Delta^{6,6'}$ -bifluorene, and tetraphenylethylene are reported. For a number of the systems, competitive oxidations to dipositive ions were indicated at room temperature.

ESR studies indicate that free radical intermediates may play an important role in the acid catalyzed rearrangements of methyl benzenes.

Resolved ESR hyperfine structure has been observed during the thermal decomposition of 2-diazoacenaphthenone and diazophenanthrene. A computer program (SESRS) for simulating ESR spectra is described and several examples of the use of the program for verifying coupling constant assignments are presented.

The compounds, 2-diazo-2(-4-methoxyphenyl) acetophenone, 9, 9'-diphenyl-9, 9'-bifluorene, (chloromethyl)pentamethyl benzene, and methylperinaphthene were prepared for ESR investigations of thermal decomposition reactions.

Aromatic hydrocarbons and related heterocyclic compounds with two to four rings which produce no residue at atmospheric pressure have been thermally polymerized at super-atmospheric pressures. The structure of the initial compound has a dominant influence on the properties of the solid polymer. The compounds have been classified into those that lead to 1) nongraphitizing carbon, 2) isotropic graphite, and 3) anisotropic graphite. The transition from a liquid mixture to a polymer which is a solid at the temperature of the experiment occurs at a definite stage of the thermal reaction, and this transition is substantially exothermic. The reaction to the stage of solid polymer formation appears to follow second-order kinetics. A possible mechanism for the course of the thermal reaction is suggested.

Graphite bodies have been fabricated using coke filler material prepared by pyrolysis of selected model aromatic compounds. The physical properties of the fabricated bodies are strongly influenced by the molecular structure of the starting compounds.

In the parallel effort, examination of controlled commercial charge stocks was continued and an effort to correlate the NMR and ESR of these charge stocks with the final graphite properties was attempted.

Bench-scale effort was centered around investigations into the preparation of isotropic high thermal expansion graphites. Investigations

have included 1) the seeding of coker charge stocks and an asphaltic hydrocarbon with finely divided carbonaceous materials; 2) the air-blowing of various charge stocks prior to coking; 3) the coking of a naturally occurring asphalt; and 4) the effects of certain processing variations during graphite manufacture.

We have also attempted to produce isotropic cokes of intermediate thermal expansion levels by 1) causing the coking to occur in a liquid phase thus producing regular shaped coke particles; and 2) by coking selected mixtures of asphaltic hydrocarbon and other charge stocks.

Studies to improve binder qualities have included 1) removing by extraction those portions of coal tar pitches which do not contribute to binder strength; and 2) thermal and catalytic cracking of heavy petroleum stocks before distilling to a pitch. Statistical analyses have been performed in an attempt to correlate binder properties with flexural strength of 3-inch molded graphite plugs.

Four pilot-scale coker runs to produce high thermal expansion isotropic cokes were made at the Marathon Oil Company in Robinson, Illinois. Two runs were an atmospheric residuum charge stock seeded with acetylene black at two different concentrations. One run was made with air-blown vacuum residuum as the charge stock and the fourth run was made with a commercial air-blown asphalt.

The commercial air-blown asphalt produced a lower thermal expansion and a higher strength material than that obtained from the air-blown vacuum residuum. A 2 per cent concentration of acetylene black in atmospheric residuum produced a coke with lower electrical resistance and higher strength than that of the 3 per cent concentration.

Cokes from vacuum residuum and slurry oil charge stocks were formed into graphite. The test results show that original coke properties affect the final graphite properties. The high thermal expansion cokes were more difficult to process and resulted in graphite having a low flexural strength and a high compressive strength.

Under this contract six hundred pounds of coke having high and isotropic thermal expansion, prepared in Robinson coker runs 68S and 69N, were supplied to the USAEC for their evaluation. Several pounds of a similar coke prepared in the bench scale work was supplied to the Union Carbide Corporation, Carbon Products Division Research Laboratory for use in the Iridium Coating Program (Contract AF33(657)-11253).

3. PYROLYSIS MECHANISMS

3.1. Thermal Reactivity of Aromatic and Substituted Aromatic Hydrocarbons

3.1.1. Differential Thermal Analysis (DTA)

The thermal reactivity of a large number of model aromatic and heterocyclic compounds of interest as components of the complex raw materials used to manufacture carbon and graphite has been studied by the DTA technique.

DTA is a dynamic method for determining the thermal changes occurring in a sample as it is heated at a uniform rate. The DTA apparatus is so designed that the temperature of the reactive sample is continuously compared to the temperature of an inert reference substance having similar thermal properties while the two are heated together. When the sample undergoes a physical or chemical transition in which heat is either absorbed or evolved, its temperature will change from that of the reference. The plot of the temperature differential (ΔT) between the sample and the reference as a function of the reference temperature (T_r) is reported as the thermogram of the sample.

The DTA experiments reported here were carried out in a flowing argon atmosphere. Argon is introduced into the lower end of the combustion tube after passing through a heated copper wool purification tube to remove moisture and oxygen. A flow rate of 10 cc per minute is maintained. The argon is passed up the combustion tube through two diffuser rings and over the sample and reference cells and is exhausted from the top of the furnace into a KBr trap in which the condensable vapors from the sample are collected. The noncondensable gases pass through the trap and through a sulfuric acid bubbler which seals the system. A heating rate of 10°C per minute is maintained to 750°C when the sample has been converted essentially to carbon. The carbon residue is measured and reported herein.

The condensable reaction products collected in the KBr traps were all examined by infrared absorption spectroscopy using a Perkin-Elmer Model 21 or Model 221 double-beam spectrometer. The KBr pelleting technique was used most extensively because of the limited solubility of the materials studied.

A Kofler Hot Stage and accessories with an American Optical Spencer binocular microscope were used to help interpret the low temperature transitions indicated in the DTA experiments.

The compounds examined in this study were obtained from commercial chemical suppliers and in many cases were used as received. Purity and identification were verified by comparing spectra of each compound with published spectra. If contamination was suspected, the material was chromatographically purified and the purified compound reexamined in the DTA apparatus when possible.

The solvents used for chromatographic elution and for spectroscopic measurements were all Eastman Kodak Company, spectrograde solvents. The KBr powder used for collecting the DTA distillates and for IR sampling was IR quality powdered KBr purchased from the Harshaw Company. The anhydrous alumina used in chromatographic columns and as the DTA reference material was Fisher's Chromatographic grade anhydrous alumina, 80 to 200 mesh, Catalog No. A-540. The alumina used as a reference in DTA was specially treated by heating to 800°C and then stored in a sealed dispenser designed to avoid exposure of the bulk of the material to the atmosphere when transfer is made to the DTA cup.

The results of the continuing study to determine the relationship of the thermal reactivity of model compounds to their molecular structure are contained in this report. Compounds have been arbitrarily classified as thermally "unreactive" if they produce no carbonaceous residue at 750°C in the DTA experiment and thermally "reactive" if they undergo a condensation sequence and yield a measurable carbonaceous residue. The activating effect of substituent groups is of particular interest in the development of new materials which will produce very high carbon yields on pyrolysis.

3.1.2. Thermally "Unreactive" Model Aromatic Compounds

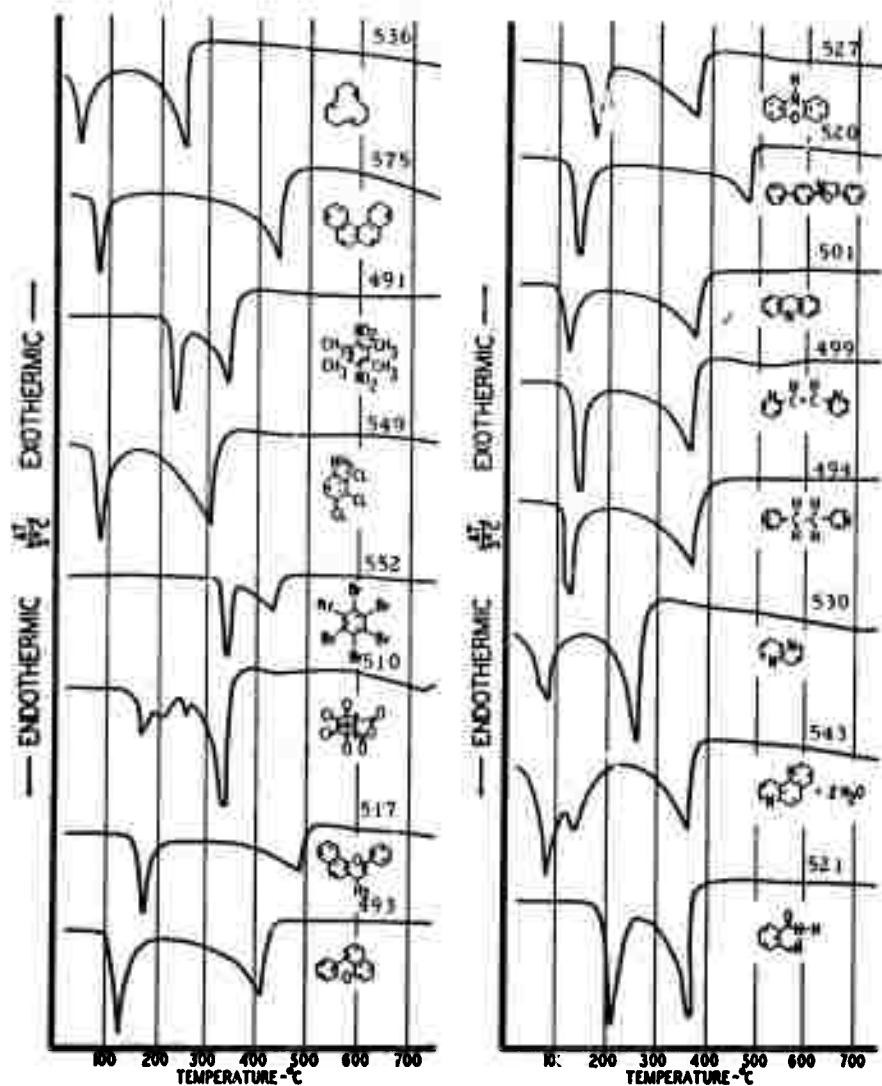
The DTA thermograms of 16 compounds which produced no significant residues on pyrolyzing at 10°C per minute to 750°C in an argon atmosphere are presented in Figure 1. The thermal properties of these compounds as determined by DTA are given in Table 1.

DTA offers a convenient if not precise method for measuring melting and boiling temperatures for organic compounds. In the case of extremely high boiling materials such as the polynuclear aromatics, it is extremely difficult to determine boiling points by any more conventional method, so volatility data are thus rather sparse in the literature.

The DTA method also provides a sensitive method for determining the presence of impurities if the melting point differs appreciably from that of the major constituent. The minor endotherms are due to impurities, usually isomers, in the commercial chemicals used in these studies. The melting point is measured from the DTA endotherm by extrapolating the forward slope of the endothermic peak up to the baseline and recording the intercept.

The boiling endotherms have no readily defined inflection points. The slope of the endotherm is a function of the vapor pressure of the sample with increasing temperature. The normal gradual slope to the endothermic minimum indicates a slowly increasing vaporization rate. The reported boiling points are the endothermic minima where the vaporization rate is at a maximum.

The thermograms are all typical of unreactive compounds, exhibiting normally sharp and deep melting and boiling endotherms with the



N-7055

Figure 1. DTA Thermograms of Thermally Unreactive Aromatic and Heterocyclic Model Compounds

Table 1. Thermally Unreactive Compounds

Compound (SM)	Structure	DTA No.	MP-°C Lit.	MP-°C DTA	BP-°C DTA	Rx.T-°C DTA	%C Residue	Remark-IR Exam. of Cond.
1,1,1,1,5,9-Cyclodecatriene		536	34	32	250	-	0.0	SM only in Condensate
1,4-Benzophenanthrene		575	68	70	440	-	0.0	SM only in Condensate
Dinitrofluorene		491	207.8	217	340	-	0.0	SM only in Condensate
2,3,4-Trichloroaniline		549	71.5	75	305	-	0.0	SM only in Condensate
Hexabromobenzene		552	306	330	435	-	0.0	SM only in Condensate
Chlorendic anhydride		510	230-4	150	338	210-285	0.0	SM plus new OH bands in Condensate.
2-Naphthoflavone		517	154-6	152	491	-	0.3	SM plus mixture of new products in Condensate
per(1,9)-Benzonanthrene		493	108	103	410	-	0.0	SM only in Condensate
Phenoxazine		527	156	150	370	-	0.0	SM only in Condensate
2-(4-Biphenyl)-5-phenylloxazole		520	112-3	120	475	-	0.0	SM only in Condensate
Iminodiphenyl		501	110	106	374	-	0.0	SM only in Condensate
1,2-Bis-(2-Pyridyl)-ethylene		499	49.5-50.5	120	362	-	0.4	SM only in Condensate
1,2-Bis-(4-Pyridyl)-ethane		494	110-111	110	372	-	0.2	SM only in Condensate
1,5-Naphthyridine		530	75	65	240	-	0.0	SM only in Cond. - Triple mp. indicate impure sample
m-Phenanthroline dihydrate		543	65.5	60	360	-	0.0	SM only in Cond. - Dehydration between 120-140°C
Phthalazone		521	183	195	365	-	0.0	SM only in Condensate

exception of chlorendic anhydride (510) (which exhibits two small additional endotherms), 1,5-naphthyridine (530) (which shows a multiple melting endotherm indicating possible impurities), and m-phenanthroline dihydrate (543) (which shows decomposition of the hydrate just over 100°C). In most cases, the condensates collected in the KBr traps consisted of only the starting compound, indicating no reactivity prior to complete distillation of the sample. However, chlorendic anhydride produced a condensate composed of starting material plus some products containing a hydroxyl group

probably due to opening of the anhydride ring; 2-naphthoflavone (517) also produced new condensable products of an unidentified nature. This latter compound, along with 1,2-bis-(2-pyridyl)-ethylene (499) and 1,2-bis-(4-pyridyl)-ethane (494), produced very small residues between 0.2 per cent and 0.4 per cent. They are arbitrarily included in the unreactive category because of the very low residue yields even though they might have undergone some chemical changes on pyrolysis.

Although 3,4-benzophenanthrene (575) was not expected to be thermally reactive under the conditions of the DTA experiment, it is an interesting aromatic compound because its configuration leads to non-planarity and strain due to the close approach of the 4' and 5 positions. The related compound, benzo (g, h, i) fluoranthene,



was examined previously and found to be slightly reactive, giving a carbon yield of 2.1 per cent. Benzo (g, h, i) fluoranthene, which has an ionization potential of 7.40 e.v., was predicted to be more reactive than 3,4-benzophenanthrene with an ionization potential of 7.77 e.v. On DTA examination, 3,4-benzophenanthrene proved to be unreactive: it exhibited only a melting and boiling endotherm, gave no carbon yield, and had only starting material in the condensate.

Dinitrodurene (491) is the first nitro-substituted aromatic examined in this study that did not react thermally to produce a carbon residue. Apparently, the vaporization temperature for dinitrodurene is below any reaction temperature.

In general, the heterocyclic compounds have been found to be relatively unreactive toward thermal treatment. Several additional examples are given in Table 1.

3.1.3. Thermally "Reactive" Model Compounds

Differential thermal analyses were performed on a variety of substituted aromatic and heterocyclic compounds. Substituents were chosen for their potential activating effect on the thermal reactivity of the aromatic or heterocyclic ring systems.

3.1.3.1. Thermally "Reactive" Substituted Aromatic Hydrocarbons

A total of 48 substituted aromatic compounds have been classified as thermally reactive in the DTA experiments. These will be discussed in the following sections where the compounds have been grouped by type of substituent.

3.1.3.1.1. Aromatic Hydrocarbons with Aryl and Alkyl Substituents

The DTA thermograms of 5 aromatic compounds substituted with aryl or alkyl groups are shown in Figure 2. Physical property and thermal reactivity data obtained from the DTA experiments are summarized in Table 2.

a. Ovalene (555)

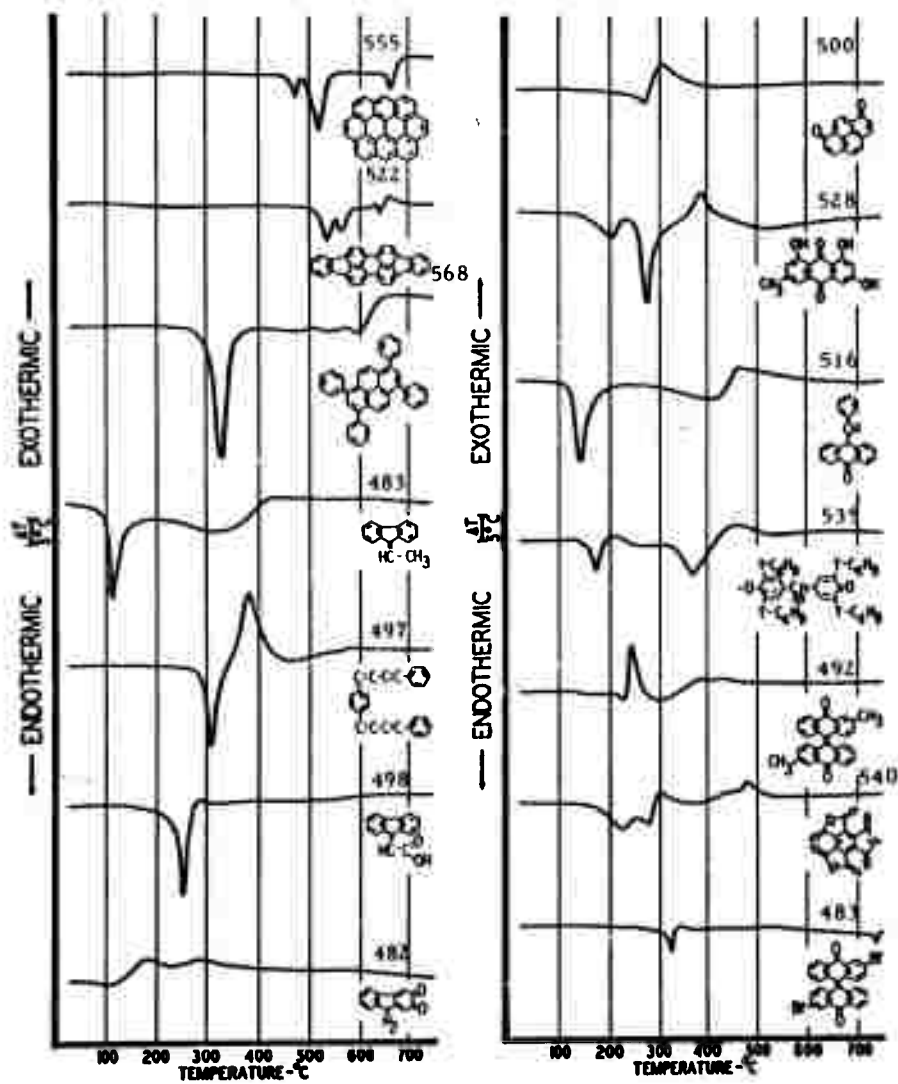
This very large polynuclear aromatic hydrocarbon produced a high yield of carbon of 64.9 per cent on pyrolysis to 750°C. The DTA thermogram shows three quite symmetrical endotherms. The first small endotherm may indicate contamination or may result from a phase transition. The extremely simple infrared absorption spectrum of this symmetrical molecule does not indicate any significant contamination. The second endotherm is in all probability the melting endotherm indicating a melting point of approximately 515°C as compared to 430°C for coronene. The final endotherm at 662°C may be the boiling endotherm but it is unusually sharp. It is followed by a sharp change in the baseline which often accompanies a decrease in the amount of sample in the DTA sample cup. The IR analysis of the condensate showed only starting material present. One would expect essentially no degradation of this compound, only dehydrogenation accompanied by molecular growth.

b. Diindeno(1,2,3-cd:1',2',3'-lm)perylene (Periflanthene)(522)

This compound is a dimer of fluoranthene. It is being studied in some detail as part of the investigation of the thermal reaction sequences involved in the conversion of fluoranthene to graphite. The large molecular size of this compound makes it stable to very high temperatures. The DTA thermogram indicates a melting point of about 520°C. This is followed by a series of endothermic and exothermic reactions at about 560°, 625°, and 660°C which result in a high carbon yield of 54.7 per cent at 750°C. Surprisingly, no new condensable products were found in the condensate collected during the pyrolysis. Apparently little or no degradation to benzene, perylene, fluoranthene, or indeno-perylene occurs.

c. 1,3,6,8-Tetraphenylpyrene (568)






The usual effect of the phenyl substituent on a polynuclear compound is to increase its physical thermal stability permitting the material to withstand higher environmental temperatures before vaporization becomes appreciable. In this case, the four phenyl groups increase the molecular size and, consequently, the boiling point of the compound to well over the temperature where thermal dehydrogenation occurs in most hydrocarbon systems. A carbon yield of 13.8 per cent was obtained from this tetraphenylpyrene. The DTA thermogram indicates two slight exothermic reactions between 500° and 600°C followed by a peculiarly small vaporization endotherm and possible shift of baseline. The condensate collected during the DTA pyrolysis contained only the starting compound. No new reaction products were found.



N-7056

Figure 2. DTA Thermograms of Thermally Reactive Aromatic Hydrocarbon Compounds

Table 2. Thermally Reactive Polynuclear Aromatics

Compound (SM)	Structure	DTA No.	MP-°C Lit.	MP-°C DTA	BP-°C DTA	Rx. T.-°C DTA	%C Residue	Remarks
Ovalene		555	> 325	460	?	622	64.9	SM only in Condensate
Diindeno(1,2,3-cd:1',2'3'-lm) perylene (perfluanthene)		522	> 360	520	?	560, + 626, + 657	54.7	SM only in Condensate
1,3,6,8-Tetraphenylpyrene		568	298	300	?	+ 510 + 570 + 590	13.8	SM only in Condensate
9-Ethylidenefluorene		483	104	100	Broad endotherm > 300°	?	5.0	Sample contained C=O groups as did condensate. Condensate was entirely new complex product.
1,4-Bis-(4-phenylbutadienyl)benzene		497	290-1	295	---	385 +	19.7	Condensate contained all new product, broad pitch- like spectrum.

d. 9-Ethylidenefluorene (483)

This compound, like dibenzofulvene, is expected to be very reactive to free radical polymerizations and so should be thermally reactive. The DTA thermogram shows the normal melting endotherm at 100°C followed by a broad attenuated vaporization endotherm that extends out to 400°C. No exothermic reactivity is discernible although the shape of the vaporization endotherm, with no abrupt end point, is indicative of the gradual degradation of a polymer. A carbon yield of 5 per cent was obtained. The condensate was an entirely new material consisting of a complex mixture of degradation products.

e. 1,4-Bis-(4-phenylbutadienyl) benzene (497)

This compound melts at 295°C and then exothermally polymerizes to produce a complex cross-linked polymer which gives a carbon yield of 19.7 per cent at 750°C. The volatile condensate obtained from the thermal degradation of the polymer was a complex pitch-like material.

3.1.3.1.2. Aromatic Hydrocarbons with Oxygen-containing Substituents

The DTA thermograms of nine polynuclear aromatic hydrocarbons substituted with oxygen or carboxylic acid groups are given in Figure 2. These compounds were all quite reactive thermally and produced high carbon yields. The physical properties and reaction conditions are tabulated in Table 3.

a. Biphenyleneacrylic Acid (498)

The DTA thermogram of this compound is uninformative. Following the melting endotherm at 235°C, the curve lies along the baseline all the way to 750°C. A carbon yield of 16.4 per cent indicates thermal reactivity which must occur slowly over a broad temperature range accompanied by gradual vaporization of the material. The IR spectrum of the condensate substantiates this general view. The condensate contains both starting compound and some new products.

b. 2,3-Fluorenoquinone (482-518)

This ortho-quinone of fluorene reacts exothermally below 200°C accompanied, apparently, by some vaporization. A large carbon yield of 73.6 per cent was obtained at 750°C. Examination of the condensate by IR analysis does not clarify the nature of the thermal reactions.

c. 1,8-Pyrenequinone (500)

The infrared absorption spectrum of this compound exhibits a C=O stretching frequency doublet at 5.70 and 5.85 microns which indicates that either the material we have examined is not 1,8-pyrenequinone, or the 1,8-pyrenequinone is not a true quinone. The higher frequency

Table 3. Thermal Properties of Oxygen Substituted Aromatic Hydrocarbons

Compound (SM)	Structure	DTA No.	Mp °C Lit.	Mp °C DTA	BP °C DTA	Rx. T °C DTA	% C Residue	Remarks - IR Spectra of condensates
Biphenylene acrylic acid		498	228	234	---	290 +	16.4	Condensate S. M. plus new compounds. Spectrum broadened.
2, 3-Fluorenoquinone		482 518	>300	---	---	180+ 280+	73.6	Mostly S. M. in condensate, small changes in spectrum.
1, 8-Pyrenequinone		500	270	255	---	305 +	58.4	Condensate was mostly new material.
1, 3, 8-Trihydroxy-6-methylanthraquinone (Emodin)		528	253	255	---	+390	52.8	Double melting endotherm possible impurity. Condensate mostly SM but some differences in IR bands.
9-Benzylidene anthrone		>16	127	123	420? broad	460 +	14.4	Condensate was S. M. plus small amount of new product.
Galvinoxyl		535	159	162	370	+450	12.2	Condensate trap contained all new products. Strong -OH band and strong aliphatic C-H bands.
2, 2'-Dimethylbianthrone		492	230-2	210	---	244 +	54.3	Condensate was mostly new material.
Mellitic Trianhydride		540	320-d	~ 250 - 300	?	+300, +480	25.2	IR indicates acid impurities were converted to anhydrides, which were condensed in KBr trap.
2, 2'-Dibromobianthrone		486	--	315	730? Br	500+ 730-	66.5	Almost nothing in KBr trap.

+ exothermic
- endothermic

absorption bands are more typical of aromatic ketones. The doublet indicates possible coupling between the carbonyl groups or a mixture of carbonyl-containing compounds.

The DTA thermogram exhibits an exothermic reaction peak immediately following the melting endotherm. A carbon yield of 58.4 per cent was obtained at 750 °C.

The IR spectrum of the condensate was quite different from that of the starting material but it still had the C=O stretching bands at 5.70 microns and 5.85 microns.

d. 1,3,8-Trihydroxy-6-Methyl-anthraquinone (Emodin) (528)

The parent compound, anthraquinone, has been found to be thermally unreactive under the conditions of pyrolysis in our DTA apparatus. However, multiple substitution, as in this case, greatly increased the reactivity and resulted in a large carbon yield. The DTA thermogram has a double melting endotherm, indicating an impurity; and the IR spectrum of the compound showed an impurity which contained a carboxyl group. An exothermic reaction followed melting, and some new reaction products appeared in the condensate. A carbon yield of 52.8 per cent was obtained at 750°C.

e. 9-Benzylidene Anthrone (516)

This compound produced a DTA thermogram typical of the moderately thermally reactive materials that have been examined. The normal melting endotherm is followed by a broad, weak vaporization endotherm that terminates in a moderate, but extensive, exothermic region. A carbon yield of 14.4 per cent was obtained.

The condensate contains a major portion of the starting material plus reaction products which are quite similar. The major effect on the IR spectrum is a broadening and smearing out of the absorption bands of the starting material rather than the addition of new strong bands.

f. Galvinoxyl (535)

This compound reportedly exists as a semiquinone ion. It is moderately thermally reactive, as evidenced by a carbon yield of 12.2 per cent upon pyrolysis in the DTA apparatus. The DTA thermogram has a small shoulder on the melting endotherm, suggesting the presence of impurities or an isomeric mixture. The large boiling endotherm is preceded by a shallow, broad endothermic region, indicating continuous vaporization above 225°C. Infrared analysis of the condensable products indicate all new products were formed. The spectra exhibited the broad bands of a complex mixture. Its principal features were the strong -OH bands, strong aliphatic C-H bands, and the skeletal out-of-plane bending absorptions of substituted aromatics. The strongest of these bands represents mono- or di-substitution. Thus, pyrolysis involves the rupture of the -CH- bridge as well as the t-butyl substituents in large part, and the reduction of the quinone as well as molecular growth to produce a carbon residue. The reaction sequence appears to be complex, as one would expect.

g. 2,2'-Dimethylbianthrone (492)

This compound, like bianthrone, undergoes a strong exothermic reaction with little evidence of melting. The dimethylbianthrone produced

a small endotherm at 210° to 225°C which indicates that the melting was interrupted by the large exothermic reaction peaking at 243°C. This was followed by possibly slow volatilization and additional exothermic reactivity around 380°C and 425°C. A final carbon yield of 54.3 per cent was obtained at 750°C.

The condensate was a complex mixture of new compounds still containing the anthrone or quinone structure.

h. Mellitic trianhydride (540)

This completely substituted benzene derivative is of potential interest as a reactive additive to aromatic systems. The sample examined hydrolyzed very readily; IR examination indicated that it consisted of a mixture of the anhydride and the carboxylic acids. On pyrolysis in the DTA apparatus, the acids were dehydrated at approximately 185°C followed by melting between 250°C and 300°C. Above 300°C, slow vaporization occurred. An exothermic reaction (or reactions) begins above 400°C and reaches a maximum at 480°C. The only material found in the condensate collected in the exit KBr trap was mellitic trianhydride plus a small amount of water. A carbon residue of 25.2 per cent was obtained on heating to 750°C. The volatile reaction products were apparently all non-condensable.

i. 2,2'-Dibromobianthrone (483)

This brominated derivative of bianthrone produced a carbon yield of 66.5 per cent in the DTA experiment. Bianthrone, which has a higher percentage of carbon in its molecule, gave a 74.3 per cent residue in the DTA experiment. The dibromobianthrone melted around 315°C and then appeared to have reacted with a very weak exotherm at 335°C and a broad, very weak exotherm between 425° and 575°C. The DTA curve also shows a small sharp endotherm at 730°C.

An extremely small amount of condensable material was found in the KBr trap. From the very weak IR spectrum obtained, it appeared to be mostly starting material. The TGA thermogram of the starting material will be examined to explain the 730° endotherm and the scarcity of condensate.

3.4.3.1.3. Chlorinated Polycyclic Compounds

The DTA thermograms for five polychlorinated polycyclic compounds are given in Figure 3. The physical properties and thermal reactivity data as obtained from the DTA curves are summarized in Table 4.

a. 1,2,3,4,9,9-Hexachloro-1,4,4a,8a-tetrahydro-1,4-methanonaphthalene-5,8-dione (507)

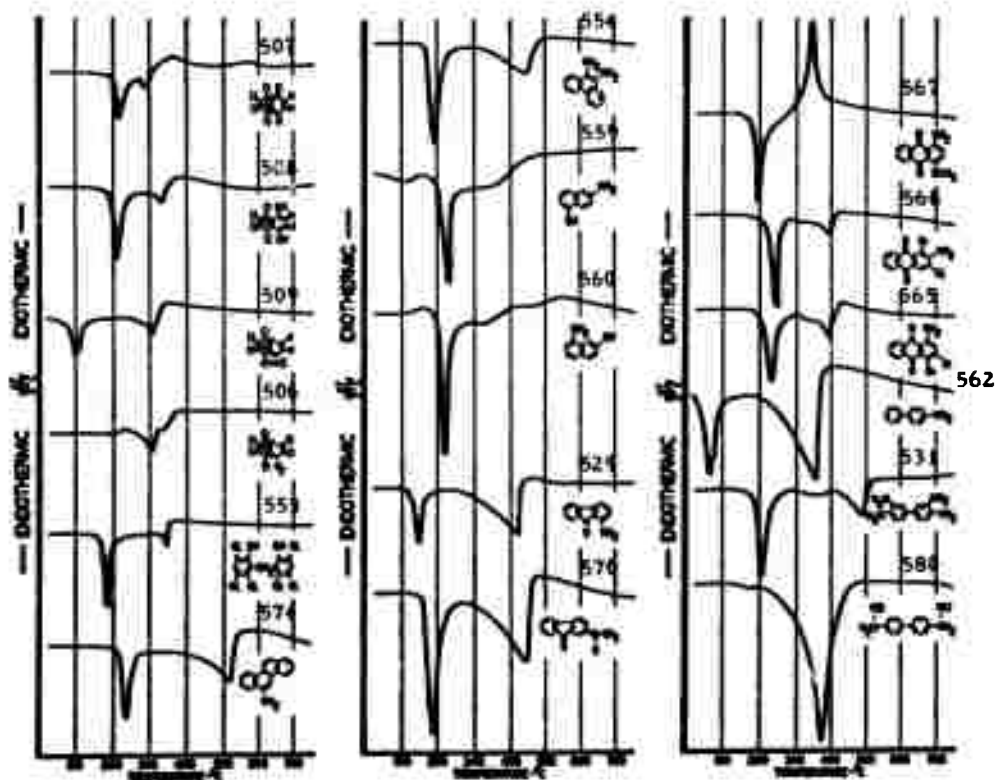




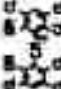


Figure 3. DTA Thermograms of Thermally Reactive Substituted Aromatic Hydrocarbons

N-7057

Table 4. Thermal Properties of Chlorinated Polycyclic Hydrocarbons

Compound (SM)	Structure	DTA No.	MP-°C Lit.	MP-°C DTA	BP-°C DTA	Ex. T-°C DTA	%C Residue	Remarks - IR Spectrum
1,2,3,4,9,9-Hexachloro-1,4,4a-tetrahydro-1,4-methanonaphthalene-5,8-dione		507	188	200	280.7	355 +	22.3	Conversion of C=O to -OH in condensate. Completely new volatile products similar to S. M. in DTA 508.
1,2,3,4,9,9-Hexachloro-1,4-dihydro-1,4-methanonaphthalene-5,8-diol		508	-	186	327	- 375 +	16.8	S. M. only in Condensate
1,4,9,6,7,8,8-Hexachloro-3a,4,7,7a-tetrahydro-4,7-methanonaphthalene		509	91-3	80	303	- 340 +	9.7	S. M. only in Condensate
2,3,4,5,6,7,8-Octachloro-3a,4,7,7a-tetrahydro-4,7-methanonaphthalene		506	-	-	303	232 + 330	6.0	S. M. only in Condensate
Hexachlorophene (2,2'-Dihydroxy-3,3',5,5',6,6'-hexachlorodiphenylmethane)		553	165	166	342	+ 330	22.2	New products in condensate, primarily chlorinated phenols.

- b. 1, 2, 3, 4, 9, 9-Hexachloro-1, 4-dihydro-1, 4-methanonaphthalene-5, 8-diol (508)
- c. 1, 4, 5, 6, 7, 8, 8-Heptachloro-3a-tetrahydro-4, 7-methanoindene (509)
- d. 2, 3, 4, 5, 6, 7, 8, 8-Octachloro-3a, 4, 7, 7a-tetrahydro-4, 7-methanoindene (506)

These four compounds, listed in Table 4, are all based on the chlorendic moiety with an attached 5- or 6-membered ring structure containing different substituents. The compounds are listed in order of decreasing carbon yield in the DTA experiments. All of these compounds were thermally reactive and produced appreciable carbon yields. The related compound, chlorendic anhydride, was also examined and found to produce no carbon residue. It is discussed under the unreactive compounds although it did undergo a series of reactions as evidenced by both the complex DTA thermogram and the changes in the condensate.

Compound (a) melted near 200°C, began to distill between 250°C and 285°C, and then underwent an exothermic reaction between 285°C and 355°C. Infrared analysis of the condensate showed that the dione (a) was converted to the diol (compound b) and also produced a carbon yield of 22.3 per cent. Compound (b) showed only a melting and boiling endotherm in the DTA thermogram but produced a carbon yield of 16.8 per cent. No new condensable products were found. Compound (c) also exhibited melting and boiling endotherms and produced no new condensable products. It gave a carbon yield of 9.7 per cent. Compound (d) showed slight exothermic reactivity, produced a 6.0 per cent carbon yield, but yielded no new condensable products. The reaction products of these highly chlorinated bridged compounds appear to be primarily carbon and noncondensable gases.

e. Hexachlorophene (553)

Hexachlorophene is a highly chlorinated phenol-formaldehyde dimer. It is quite reactive on pyrolysis and gave a 22.2 per cent carbon yield in the DTA apparatus. The DTA thermogram shows the melting endotherm at 160°C and a small exotherm at 330°C which interrupts the vaporization endotherm. Infrared analysis of the condensable volatile products indicate new products quite similar to the starting compound but completely lacking the methylene bridge, i.e., chlorinated phenols.

3.1.3.1.4. Nitrogen Substituents

The nitrogen-containing substituents included in this study are (1) amino, (2) amido, and (3) nitro-groups. All of these nitrogen groups have an activating effect on the thermal reactivity of aromatics. The effect varies with the position of substitution, with the aromatic structure, and, of course, is sensitive to the presence of other substituent groups.

3.1.3.1.4.1. Amino-compounds

The amino group has demonstrated a pronounced effect on the thermal reactivity of aromatic compounds although, in general, the nitro-group has a greater effect. The amino group is readily oxidized and also has a strong effect on the aromatic ring by contributing an electron pair to the π -electron system through resonance interaction.

The DTA thermograms of 12 amino compounds are shown in Figure 3, and the physical and thermal properties and behavior are summarized in Table 5.

Table 5. Thermally Reactive Amino Substituted Aromatic Compounds

Compound (SM)	Structure	DTA No.	MP-°C Lit.	MP-°C DTA	BP-°C DTA	Rx. T-°C DTA	%C Residue	Remarks
6-Amino Chrysene		574	-	220	510	-	0.8	SM only in Condensate
9,10-Diaminophenanthrene		554	165	165	435	-	3.0	SM in Condensate plus small amount of new products.
2-Amino-5-naphthol		559	200	~ 50, 190	-	Broad + 360- + 475	49.1	Double melting endotherm. Contains SM but with many IR bands missing. OH band broad and less intense. Only one new band at 12.35 μ .
8-Amino-2-naphthol		560	206	198	325	+ 400 + 520	42.1	SM only in Condensate
1-Amino-9-fluorenone		529	120	120, 127	415	-	0.7	SM only in Condensate
2-Methylamino-9-fluorenone		570	152	159	430	-	1.9	SM only in Condensate
1-Amino-4-methoxy-anthraquinone		567	180	180	-	+ 338	43.3	New compounds in condensate C=O bands at 6.0 μ gone. NH bands present; ether bands present.
2-Amino-1-bromo-3-chloro-anthraquinone		566	229	224	390	+ 280 + 425	33.0	SM only in Condensate
1-Amino-3,4-dibromo-anthraquinone		565	224	210	393	+ 300 + 428	22.5	Mostly SM in condensate plus two new IR bands -- cannot identify new products.
4-Aminobiphenyl		562	61	43	355	-	1.1	SM only in Condensate
3,3'-Diaminobenzidine		531	180	180	485?	-	23.5	SM only in Condensate
Benzidine Dihydrochloride		580	-	-	375	-	8.7	Condensate was pure benzidine

* SM-Starting Material.
+ - Exothermic Reaction.

a. 6-Aminochrysene (6-Chrysenamine) (574)

The introduction of the amino group in the 6-position increased the thermal reactivity of chrysene only slightly to yield a carbon residue of 0.8 per cent. The DTA thermogram shows only the melting and boiling endotherms at 220°C and 510°C, respectively. Analysis of the condensate indicated that no new pyrolysis products were formed. Only starting material was found in the condensate.

b. 9, 10-Diaminophenanthrene (554)

The DTA thermogram of 9, 10-Diaminophenanthrene shows only the melting endotherm at 165°C and a gradual vaporization endotherm starting at approximately 275°C and reaching a minimum at 440°C. A carbon residue of 3.0 per cent was obtained indicating about the same activating effect of the diamino-substitution on phenanthrene as on naphthalene. The condensate contained mostly starting compound with a small amount of new unidentified products.

c. 2-Amino-5-naphthol (559)

d. 8-Amino-2-naphthol (560)

Although a number of diaminonaphthalenes and naphthalenediols have been examined and found to be moderately thermally reactive, these are the first amino-naphthols studied to date. The amino-naphthols are much more reactive than either the diamines or the diols as judged by carbon yield.

DTA thermogram 559 of 2-amino-5-naphthol has a shallow endotherm beginning near 50°C that indicates a contaminant in the sample. The melting endotherm at 190°C agrees with the reported values. The melting endotherm is followed by a gradually rising curve which finally levels at approximately 500°C and is essentially flat as heating continued to 750°C. A carbon residue of 49.1 per cent was obtained. The condensate produced an IR spectrum very similar to that of the starting material but with many bands missing. The OH and NH bands were much broadened and of lower intensity, and one new band at 12.35 microns was observed.

The thermogram (560) of 8-amino-2-naphthol is somewhat similar but with no indication of an impurity and with somewhat sharper inflections in the rising portion of the curve following the melting endotherm. A carbon residue of 42.1 per cent was obtained. The condensate in this case contained only the starting material. The IR spectra were identical.

e. 1-Amino-9-fluorenone (529)

f. 2-Methylamino-9-fluorenone (570)

Fluorenone was found earlier to be unreactive in the DTA examination and the substitution with an amino- or a methylamino-group enhances the reactivity only slightly. The DTA thermograms of 1-amino-9-fluorenone and 2-methylamino-9-fluorenone given in Figure 3 show only the typical melting and boiling endotherms of unreactive or slightly reactive compounds. Similarly, analysis of the condensates collected during pyrolysis shows only the starting compounds present.

- g. 1-Amino-4-methoxy-anthraquinone (567)
- h. 2-Amino-1-bromo-3-chloro-anthraquinone (566)
- i. 1-Amino-3,4-dibromo-anthraquinone (565)

Although anthraquinone has been found to be thermally unreactive under the conditions which we have used to define this term, it has proved to be readily activated by a variety of substituent groups including methyl, ethyl, benzo, hydroxyl, and halogens. In general, multiple substitution results in increased thermal reactivity and higher carbon yields. The substituted anthraquinones listed above all proved to be thermally reactive and produced carbon yields ranging from 22.5 per cent to 43.3 per cent. The DTA thermogram of 1-amino-4-methoxy-anthraquinone (567) shows strong exothermic reactions which result in ultimate high carbon yields. The DTA thermograms of 2-amino-1-bromo-3-chloro-anthraquinone (566) and 1-amino-3,4-dibromo anthraquinone (565) are very similar in shape with only slight shifts in temperature among the several endothermic peaks. They both show sharp melting endotherms and broad gradual boiling endotherms and both have a peculiar slight exothermic peak immediately following the melting endotherm. With the exception of 2-amino-1-bromo-3-chloro-anthraquinone, new condensable products were found in the condensates.

- j. 4-Aminobiphenyl (562)
- k. 3,3'-Diaminobenzidine (534)

l. Benzidine Dihydrochloride (580)

The polyphenyl moiety has previously been shown to be extremely resistant to thermal reactivity. All unsubstituted polyphenyls from biphenyl through quinquephenyl examined to date have vaporized out of our system leaving no residue. Similarly, substitution with an acetyl-, benzyl- or phenyloxazole-group simply increased the melting and boiling points of biphenyl without inducing thermal reactivity. Substitution with one or more amino-groups, however, is seen to produce a thermally reactive polyphenyl. The 4-Aminobiphenyl is only slightly reactive, producing a scant 1.1 per cent carbon residue at 750°C. The thermogram shows only strong melting and boiling endotherms. The 3,3'-Diaminobenzidine is very reactive producing a carbon yield of 23.5 per cent; however, the DTA thermogram does not give much information on the reaction temperatures. Only the melting endotherm and an attenuated boiling endotherm with a

very shallow, broad endothermic region spanning almost the entire temperature range between melting and boiling are exhibited.

The DTA thermogram of benzidine dihydrochloride (580) shows a small endotherm starting near 140°C and reaching a maximum at 175°C, followed by a very large and broad endotherm peaking at 375°C. A carbon residue of 8.7 per cent was obtained at 750°C. Only the starting compounds were found in the condensates collected during the pyrolysis of 4-aminobiphenyl (562) and 3,3'-Diaminobenzidine (531). In the case of benzidine dihydrochloride (580), the condensate was benzidine. The large endotherm is apparently caused by a combination dehydrochlorination and distillation. The volatile reaction products are all noncondensable.

3.1.3.1.4.2. Amido-compounds

The DTA thermograms of 1-acetamidopyrene (541) and 9,10-Bis-(Formamido)-anthracene (533) are shown in Figure 4, and the physical and thermal properties as determined in the DTA experiment are summarized in Table 6.



a. 1-Acetamidopyrene (541)

The introduction of a highly functional substituent such as the acetamido-group to pyrene produced a thermally reactive material which gave a carbon yield of 15.9 per cent in the DTA experiment. The DTA thermogram does little to elucidate the reaction details, however. Only the melting and vaporization endotherms are found. The condensable volatiles also reveal nothing about the reaction since only the starting material was found. Degradation products of the substituent group appear to be noncondensable vapors.

b. 9,10-Bis-(Formamido)-anthracene (533)

The DTA thermogram of 9,10-bis-(formamido)-anthracene shows a series of broad shallow endotherms beginning at 200°C and finally terminating in a sharp, strong endotherm which reaches its minimum at 415°C. The reported melting point is 439°C, a value which is difficult to accept for a molecule of this size despite the possibility of strong intermolecular attraction. The shape of the 415°C endotherm is that of a boiling point. Since the carbon yield was only 4.7 per cent, considerable vaporization must have taken place. Examination of the condensate shows no starting material. The condensable volatiles were all new reaction products making up a complex mixture. Although no products could be identified from the IR spectrum of the condensate, several characteristic new bands appeared. The amide bands were considerably broadened and shifted, indicating less hydrogen bonding than in the starting compound, and a strong diazo band appeared. In addition, many new bands appeared in the longer wavelength region from 10 to 15 microns, indicating changes in positions of substitution.

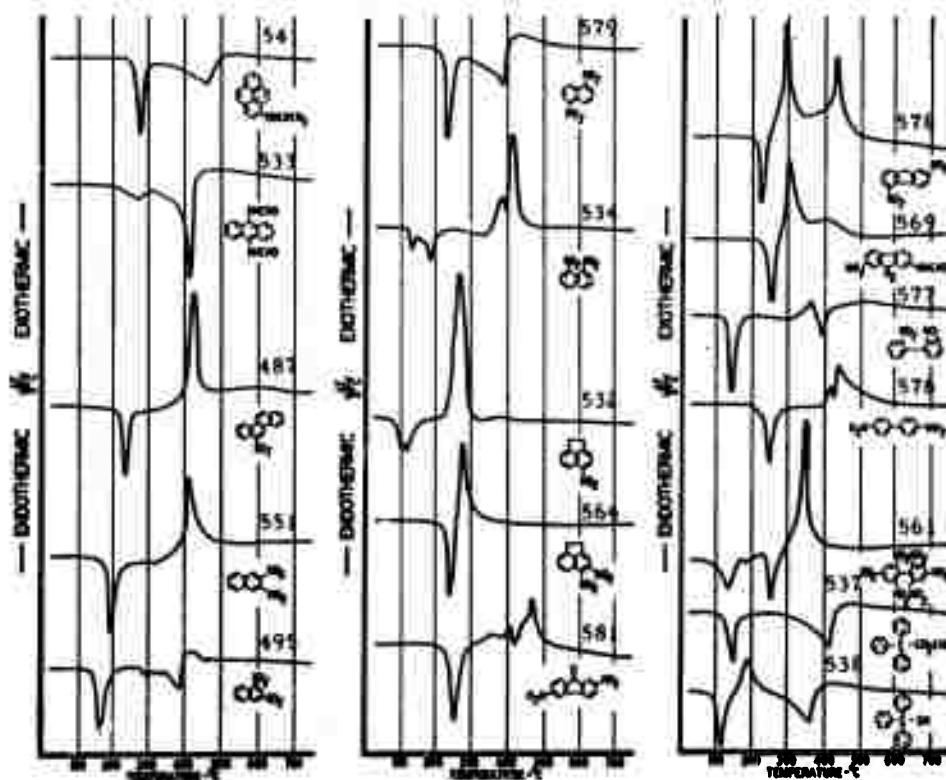
Table 6. Thermally Reactive Substituted Polynuclear Aromatics

Compound (SM)	Structure	DTA		MP-°C		BP-°C		Ex.T-°C		%C Residue	Remarks
		No.	Lit.	DTA	DTA	DTA	DTA	DTA	DTA		
1-Acetamidopyrene		541	245	255	465	-	-	-	-	15.9	SM only in condensate.
9,10-bis-(Formamido)-anthracene		533	439	-200	4157	-	-	-	-	4.7	Broad m.p. endotherm. Condensate contained no SM. Complex mixture of new products.

3.1.3.1.4.3. Nitro-compounds

Nitro-groups greatly increase thermal reactivity of aromatic hydrocarbons. Possible reaction routes include complex-formation, thermal elimination of the substituent, activation of other ring carbons by the substituent, and an oxidizing action of the nitro-compound.

The DTA thermograms of 13 nitro-substituted aromatic hydrocarbons are included in Figure 4. Physical and thermal property data obtained from the DTA experiments are summarized in Table 7.



N-7056

Figure 4. DTA Thermograms of Thermally Reactive Substituted Aromatic Hydrocarbons

Table 7. Thermally Reactive Nitro-Substituted Aromatic Hydrocarbons

Compound (SM)	Structure	DTA No.	MP-°C Lit.	MP-°C DTA	BP-°C DTA	Ra. T-°C DTA	%C Residue	Remarks
6-Nitrochrysene		487	209	220	-	425 +	34.3	Condensate was only SM
2, 3-Dinitronaphthalene		551	170.5	175	-	+410	10.5	SM only in Condensate
1, 3-Dinitronaphthalene		495	144-5	143	-310	300-350 + 400-425 +	5.3	Condensate contained SM only
1, 5-Dinitronaphthalene		579	216	216	382	-	3.4	Condensate contained SM and new products
1, 8-Dinitronaphthalene		534	172	122, 170	-	+380, +406	11.9	Double melting endotherm. Condensate contains mostly SM + 3 small new carbonyl bands between 5.7 and 6.0 μ.
5-Nitroacenaphthene		532	102	80, 98	-	+268	44.8	Double melting endotherm. SM only in Condensate
5-Amino-4-nitroacenaphthene		564	216	220	-	+272	56.1	Condensate mostly SM but two bands at 12.80 and 13.07 μ are missing. Three new bands.
2, 6-Dinitro-9-Fluorenone		581	-	237	415	+360 +405 +447	18.1	Condensate contains SM only
2, 5-Dinitrofluorene		578	207	205	-	+287 +426	36.5 ^a	Condensate all new products Strong C=O band
2-Formamido-7-nitrofluorene		569	223	225	-	+300, +400	48.8	Condensate contained no SM Complex mixture of new products.
2, 2'-Dinitrobiphenyl		577	125	126	390	+350 +360	4.8	SM only in Condensate
4, 4'-Dinitrobiphenyl		576	235	205, 233	420	+413 +433	9.2	Some impurity - SM only in Condensate
2, 2', 4, 4', 6, 6'-Hexanitrobiphenyl		561	242	100 170 240	7 255	+230 +350	6.2	SM only in Condensate

+ Exothermic reaction.

a. 6-Nitrochrysene (487)

The activating effect of the nitro-group is graphically illustrated in the DTA thermogram of 6-nitrochrysene. After melting at 220°C, the molten nitrochrysene undergoes a strong exothermic reaction which starts around 300°C and peaks at 425°C. The resultant reaction products yield a 34.3 per cent carbon residue at 750°C. The strong exothermic reaction apparently vaporizes a considerable amount of unreacted nitrochrysene, as only the starting material was found in the condensate fraction.

In comparison to the 34 per cent carbon yield from 6-nitrochrysene, unsubstituted chrysene gave no carbon residue, 6, 12-dibromochrysene gave a 15 per cent yield, and 2-aminochrysene produced 12 per cent carbon in DTA experiments.

b. 2, 3-Dinitronaphthalene (551)

c. 1, 3-Dinitronaphthalene (495)

d. 1, 5-Dinitronaphthalene (579)

e. 1, 8-Dinitronaphthalene (534)

The activating effects of substituent groups on the naphthalene nucleus has been examined quite extensively in this study. The effects of both the substituent and the position of substitution have been found to be important. Of the 10 possible dinitronaphthalene isomers, 5 have been examined in the DTA apparatus. All have been shown to be thermally reactive.

2, 3-Dinitronaphthalene (551) gave a very simple DTA thermogram consisting of a sharp melting endotherm and a strong, sharp exotherm peaking at 410°C. A carbon residue of 10.5 per cent was obtained.

The thermogram of 1, 3-dinitronaphthalene (495) shows a series of exothermic and endothermic reactions between 280°C and 450°C. Similar behavior was observed with 1, 4-dinitronaphthalene.⁽¹⁾ A carbon residue of 5.3 per cent was obtained from 1, 3-dinitronaphthalene as compared to 10.1 per cent from the 1, 4-isomer. In both cases, the condensates collected in the exit KBr traps consisted only of starting material.

The thermogram of 1, 5-dinitronaphthalene is the only one of the dinitronaphthalene isomers not showing an exothermic peak. This compound showed only a sharp melting endotherm at 216°C followed by a broad distillation endotherm which reached a maximum ΔT at 382°C. A carbon residue of 3.4 per cent was obtained. Unlike the other dinitro isomers, this one gave some new condensable products in the condensate.

The 1, 8-dinitronaphthalene appears to be a mixture as it gave two melting endotherms, the second one agreeing with the reported melting

point of this compound. Two strong exothermic reactions are indicated in the DTA thermogram. A carbon residue of 11.9 per cent was obtained. The condensate consisted almost entirely of starting material. The IR spectrum of the condensate had three small new carbonyl bands, indicating some oxidation products. Since in almost every case only the starting compounds are found in the condensed fractions after pyrolysis, additional studies such as thermo-gravimetric analysis and gas evolution analysis and fractionation and analysis of the residual, condensable, and noncondensable products of these nitro-substituted aromatics will be necessary to understand the nature of the reactions occurring.

f. 5-Nitroacenaphthene (532)

g. 5-Amino-4-nitroacenaphthene (564)

Acenaphthene which has a relatively low melting point and a high vapor pressure boils out of an unrestricted thermal reactor long before it can be carbonized. The substitution of a ring hydrogen with a nitro- or an amino-group greatly enhances the thermal reactivity.

The DTA thermogram of 5-nitroacenaphthene indicates that after melting near 100°C it undergoes a violent exothermic reaction starting near 225°C which results in a carbon yield at 750°C of 44.8 per cent. As expected with a nitro compound, the condensate was found to contain only the starting compound. The 5-Amino-4-nitroacenaphthene produced a very sharp, clean DTA thermogram. Immediately after melting near 220°C, the molten material underwent an exothermic reaction that peaked at 272°C and then leveled off all the way out to 750°C. A carbon residue of 56.1 per cent was obtained. The condensate was mostly starting material but with several small changes in the IR spectrum, indicating that some new products were trapped in the KBr condenser.

h. 2,6-Dinitro-9-Fluorenone (581)

The thermogram of this compound, which gave an 18.1 per cent carbon yield at 750°C, exhibits a complex series of exothermic and endothermic reactions between 350° and 470°C. The condensate collected in the KBr trap contained only starting material. In this case, as in most in which nitrocompounds are pyrolyzed, the reaction products appear to be carbon and noncondensable gases.

i. 2,5-Dinitrofluorene (578)

The DTA thermogram of this compound indicates that a very powerful exothermic reaction occurs immediately after melting is completed and is followed by a second, somewhat less violent, exothermic reaction. The first reaction peaked at 287° and the second at 426°C. Although a residue of 36.5 per cent was measured, it should be considerably greater, since the sample had foamed and overflowed the DTA container. Previous DTA examination of 2,7-Dinitrofluorene⁽¹⁾ showed no exothermic reactivity;

however, there was indication of high reactivity in that a carbon yield of 25.8 per cent was obtained. In the case of both dinitrofluorene isomers, the condensable volatile products were completely new materials. The infrared absorption spectra of the condensates had strong carbonyl bands indicating an oxidative effect of the nitro-groups. Some 9-fluorenone appears as one of the products in both instances along with other unidentified compounds.

j. 2-Formamido-7-nitrofluorene (569)

The DTA thermogram obtained from this compound shows that a very strong exothermic reaction begins soon after melting has occurred. This reaction is followed by a second less intense but broader exotherm. These reactions produce a 750°C residue of 68.8 per cent. Since the starting material contains only 66.1 per cent carbon, the 750°C coke must still retain a considerable quantity of oxygen and nitrogen as well as the usual small amount of hydrogen. Previously, 2-nitrofluorene was found to react similarly to give a 67.4 per cent yield in the DTA experiments, which was 91 per cent of the theoretical carbon yield. The formamido-group increases the reactivity somewhat in this case. The condensate collected during the DTA pyrolysis of 2-formamido-7-nitrofluorene consisted of a mixture of entirely new products. None of the starting compound vaporized without reacting. The IR spectrum of the condensate looks much like that of a pitch with broad bands, making any compound identification difficult.

k. 2, 2'-Dinitrobiphenyl (577)

l. 4, 4'-Dinitrobiphenyl (576)

The polyphenyl structure has been shown to be extremely resistant to thermal reaction. Substitution with the nitro-group usually increases the thermal reactivity of aromatic nuclei, and the two dinitrobiphenyls listed here proved to be thermally reactive.

The substitution of the biphenyl nucleus in the 4, 4' positions by nitro-groups produced a more reactive material than 2, 2' substitution. The DTA thermogram of 4, 4'-Dinitrobiphenyl showed a melting endotherm followed by a strong exotherm starting at 400°C. The doublet effect in this exotherm is probably caused by a rapid endothermic volatilization superimposed on the exotherm at 420°C. A carbon residue of 9.2 per cent was obtained, and only starting material was found in the condensate. Apparently, the volatile reaction products were all noncondensable gases. The 2, 2'-Dinitrobiphenyl thermogram is somewhat similar to that of the 4, 4'-isomer; however, the reaction exotherm occurs about 80°C lower in temperature. A carbon yield of 4.8 per cent was obtained and only starting compound was found in the condensate.

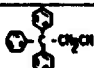

m. 2, 2', 4, 4', 6, 6'-Hexanitrobiphenyl (561)

The DTA thermogram for 2, 2', 4, 4', 6, 6'-Hexanitrobiphenyl is difficult to interpret. The melting point reported in the literature agrees with the third endothermic peak exhibited at 240°C. The two endotherms preceding indicate either considerable contamination or other physical or chemical transitions. Immediately following the 240°C endotherm, a very strong exothermic reaction begins which reaches a maximum at 350°C. This reaction generates sufficient heat to flash distill much of the starting material out of the reaction cup. This result is evidenced by the low yield of residue of 6.2 per cent and the composition of the condensate which contained only the starting material. Apparently, all volatile reaction products are noncondensable gases.

3.1.3.1.4.4. Miscellaneous Substituted Hydrocarbons

The DTA thermograms of two substituted triphenylmethyl compounds are shown in Figure 4. The physical and thermal properties of these compounds are summarized in Table 8.

Table 8. Thermally Reactive Substituted Aromatics

Compound (SM)	Structure	DTA No.	Mp.°C Lit.	Mp.°C DTA	Sp.°C Rx. T.°C DTA	% C Residue	Remarks
3, 3, 3-Triphenylpropionitrile		537	139	125	410	-	2.2 SM only in Condensate.
Triphenylmethylmercaptan		538	107	105	362	+192	1.6 SM plus new material of unidentified nature.

a. 3, 3, 3-Triphenylpropionitrile (537)

The DTA thermogram of this compound shows only the melting and boiling endotherms with no indications of thermal reactivity, although a small carbon yield of 2.2 per cent was obtained. The condensate was found to contain only the starting compound.

b. Triphenylmethylmercaptan (538)

The DTA thermogram of this compound shows a strong exothermic reaction occurring shortly after melting. The reaction products, however, are too volatile to produce a significant carbon residue, which in this experiment resulted in only a 1.6 per cent yield. The spectroscopic analysis of the condensable volatile products indicated that new compounds were formed, but we were unable to identify or characterize them because the condensate was predominantly the starting compound.

3.1.3.2. Thermally "Reactive" Heterocyclic Compounds

An additional 15 heterocyclic compounds have been examined by DTA during this report period and found to be thermally "reactive". The majority of these materials are substituted polycyclic compounds, and their reactivity is attributed in general to the activating effect of substituent groups or to multiple heteroatom substitutions in the ring systems. The compounds have been grouped by type of heteroatom substitution for discussion.

3.1.3.2.1. Heterocyclic Oxygen Compounds


a. 9-Xanthylideneanthrone (515)

Only one thermally reactive heterocyclic oxygen compound was examined by DTA at this time. The DTA thermogram is shown in Figure 5 and the physical and thermal properties determined by DTA are tabulated in Table 9.

This rather high molecular weight compound does not melt until 290°C. Upon melting it reacts rapidly and exothermally to produce an ultimate yield of 67.2 per cent carbon residue at 750°C.

The infrared spectrum of the condensate exhibits a strong -OH stretching band, not hydrogen-bonded, as well as a different C=O band shifted to lower frequency as in a true quinone. Other general features of the spectrum are quite different from the starting material indicating extensive alteration in the structure of the condensable volatile products.

Table 9. Thermally Reactive Heterocyclic Oxygen Compounds

Compound (SM)	Structure	DTA No.	Mp:°C Lit.	Mp:°C DTA	Bp:°C Rk. T. °C DTA	% C Residue	Remarks
9-Xanthylideneanthrone		515	301-2	292	--- 316+	67.2	Condensate new compounds. Strong OH band.

3.1.3.2.2. Heterocyclic Nitrogen Compounds

The nitrogen heterocyclic compounds, particularly those containing more than one nitrogen atom in a single ring, have been somewhat more thermally labile than the other heterocyclic compounds.

The DTA thermograms for eight heterocyclic nitrogen compounds are given in Figure 5. The physical and thermal properties are summarized in Table 10.

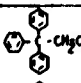
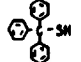
m. 2, 2', 4, 4', 6, 6'-Hexanitrobiphenyl (561)

The DTA thermogram for 2, 2', 4, 4', 6, 6'-Hexanitrobiphenyl is difficult to interpret. The melting point reported in the literature agrees with the third endothermic peak exhibited at 240°C. The two endotherms preceding indicate either considerable contamination or other physical or chemical transitions. Immediately following the 240°C endotherm, a very strong exothermic reaction begins which reaches a maximum at 350°C. This reaction generates sufficient heat to flash distill much of the starting material out of the reaction cup. This result is evidenced by the low yield of residue of 6.2 per cent and the composition of the condensate which contained only the starting material. Apparently, all volatile reaction products are noncondensable gases.

3.1.3.1.4.4. Miscellaneous Substituted Hydrocarbons

The DTA thermograms of two substituted triphenylmethyl compounds are shown in Figure 4. The physical and thermal properties of these compounds are summarized in Table 8.

Table 8. Thermally Reactive Substituted Aromatics

Compound (SM)	Structure	DTA No.	Mp.°C Lit.	Mp.°C DTA	Bp.°C Rx. DTA	T.°C DTA	% C Residue	Remarks
3, 3, 3-Triphenylpropionitrile		537	139	125	410	-	2.2	SM only in Condensate.
Triphenylmethylmercaptan		538	107	105	362	+192	1.6	SM plus new material of unidentified nature.

a. 3, 3, 3-Triphenylpropionitrile (537)

The DTA thermogram of this compound shows only the melting and boiling endotherms with no indications of thermal reactivity, although a small carbon yield of 2.2 per cent was obtained. The condensate was found to contain only the starting compound.

b. Triphenylmethylmercaptan (538)

The DTA thermogram of this compound shows a strong exothermic reaction occurring shortly after melting. The reaction products, however, are too volatile to produce a significant carbon residue, which in this experiment resulted in only a 1.6 per cent yield. The spectroscopic analysis of the condensable volatile products indicated that new compounds were formed, but we were unable to identify or characterize them because the condensate was predominantly the starting compound.

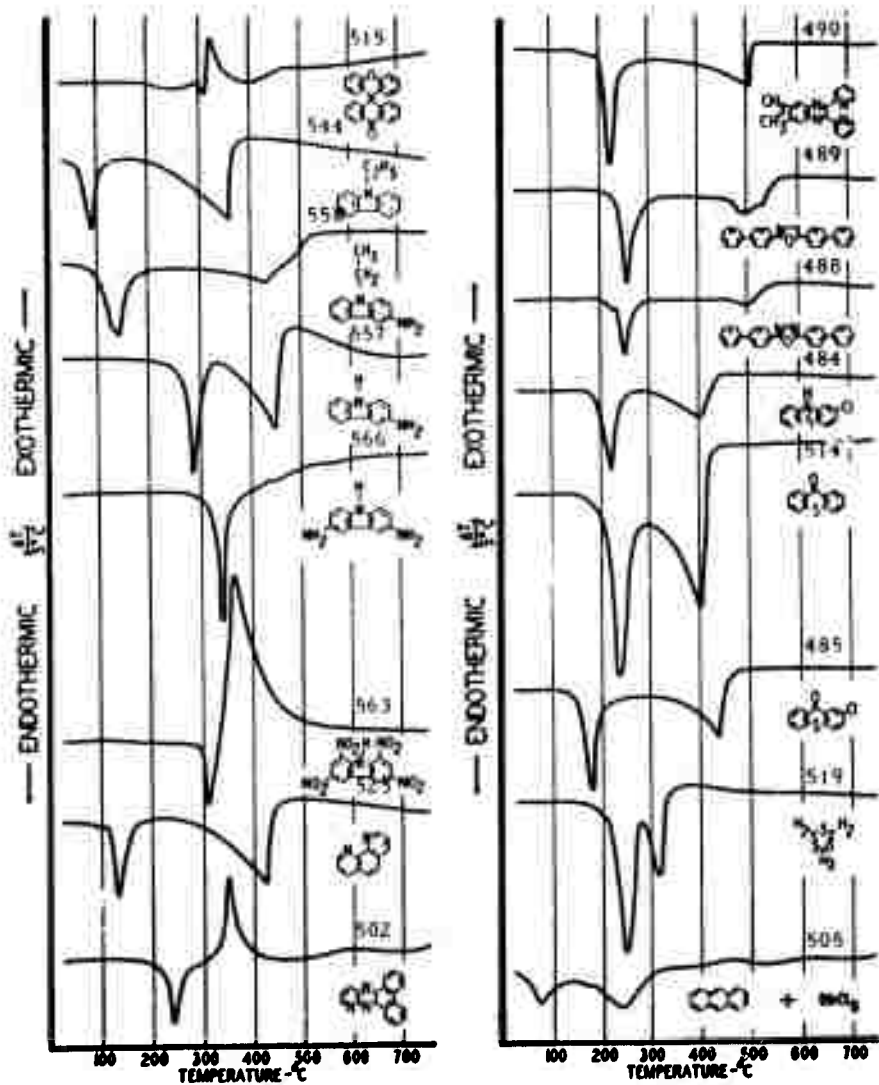

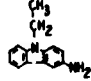
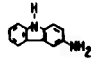
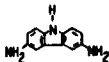
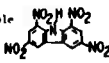

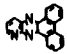



Figure 5. DTA Thermograms of Thermally Reactive Heterocyclic Compounds

N-7059

Table 10. Thermally Reactive Substituted Heterocyclic Nitrogen Compounds

Compound	Structure	DTA No.	MP. °C Lit.	MP. °C DTA	BP. °C DTA	Rr. T. °C DTA	% C Residue	Remarks*
N-Ethylcarbazole		544	68	65	357	-	1.8	SM only in Condensate.
3-Amino-9-Ethylcarbazole		558	-	101, 110	420 br	-	28.0	SM only in Condensate.
3-Aminocarbazole		557	254	255	440	-	3.0	SM only in Condensate.
3,6-Diaminocarbazole		556	>290	310	-	+425 br +520 br +580 br	48.2	Mostly SM in Condensate but all IR bands are broadened and several new bands occur. Spectrum is pitchlike in appearance.
1,3,6,8-Tetranitrocarbazole		563	294	295	-	+360	17.0**	**Overflowed -% Residue higher. SM only in Condensate.
1,10-Phenanthroline		523	91.5	110	425	-	1.3	SM only in Condensate.
10-Azaadibenzo(a,c)phenazine		502	215-17	218	---	+350	88.1	Condensate was a mixture of new tar-like products.
6,7-Dimethyl-2,3-di(2-pyridyl)-quinoxaline		490	--	195	495	---	3.4	Condensate contained S. M. only

*SM - Starting Material.
+ - Exothermic reaction.

a. N-Ethylcarbazole (544)

The DTA thermogram of N-ethylcarbazole is typical of an unreactive material although in this case a carbon residue of 1.8 per cent was obtained. Only the melting and boiling endotherms are evident in the thermogram. The condensable fraction contained only the starting material.

b. 3-Amino-9-Ethylcarbazole (558)

The thermal reactivity of N-ethylcarbazole (544) is greatly increased by the additional substitution with an amino-group. The compound, 3-amino-9-ethylcarbazole, produced a carbon yield of 28.0 per cent in the DTA apparatus. The DTA thermogram indicates possible contamination of the sample by exhibiting a double minimum on the melting endotherm. The boiling endotherm is shallow and broad, typical of reactive materials when no strong exothermic activity is evident. Following the minimum in the vaporization endotherm at 420°C, the curve rises slowly with several small inflections, indicating continued thermal activity in the residue remaining after the major volatilization was complete. Since the condensate consisted entirely of starting material, no information on the nature of volatile reaction products was obtained.

c. 3-Aminocarbazole (557)

Although carbazole was thermally unreactive, 3-aminocarbazole produced a carbon yield of 3.0 per cent in the DTA examination. The DTA thermogram (557) shows only the sharp melting and boiling endotherms with no indication of thermal reaction temperature or type. The condensate contained only the starting material.

d. 3,6-Diaminocarbazole (556)

Substitution with two amino groups increased thermal reactivity immensely. The 3,6-diaminocarbazole produced a 48.2 per cent carbon residue. The DTA thermogram shows a strong, sharp melting endotherm near 300°C followed by a series of broad, very weak exotherms on a gradually rising curve. The high residue yield indicates that exothermic and endothermic changes were probably occurring simultaneously and continuously over most of this upper temperature region. The IR spectrum of the condensate looks similar to that of the starting compound, but all bands are broadened and several new bands occurred. The spectrum reveals pitchlike absorption bands.

e. 1,3,6,8-Tetranitrocarbazole (563)

The DTA thermogram of this compound indicates that a very strong exothermic reaction occurred as soon as the material melted. The reaction was so violent that much of the sample was lost, and only a 17 per cent residue was measured after the run was completed. However, if compensation were made for these losses, the carbon yield would be much higher. As in the case of most nitro-substituted compounds which react violently exothermally, the condensate contained only the starting compound which appears to flash vaporize as a result of the rapid temperature rise brought about by the reaction.

f. 1,10-Phenanthroline (523)

In general, those unsubstituted heterocyclic compounds having only one heteroatom in any given 6-membered ring have exhibited a high

resistance to thermal reaction in our DTA examination. The 1,10-phenanthroline is one of the few that has produced a carbon residue. The DTA thermogram has a small endotherm preceding the major melting endotherm, probably caused by vaporization of excess water of crystallization. Above 250°C, vaporization increases gradually to the boiling point at 425°C. A carbon residue of 1.3 per cent was obtained. The condensate contained only the starting material. Apparently, no condensable reaction products were formed.

g. 10-Azadibenzo(a,c)phenazine (502)

This compound gave one of the largest carbon yields ever obtained by carbonizing a pure compound in the DTA experiment. The thermogram shows two sharp peaks. The first is a melting endotherm at 218°C, and the second a strong exotherm peaking at 350°C. A carbon yield of 88.1 per cent was obtained. The condensate was a tarlike material which gave an IR absorption spectrum having a few broad bands similar to pitch or asphalt residues.


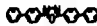
h. 6,7-Dimethyl-2,3-di(2-pyridyl)-quinoxaline (490)

The DTA thermogram of this highly substituted heterocyclic compound is typical for a moderately reactive material. There is no exotherm evident. The vaporization endotherm is broad and not too deep. A carbon yield of 3.4 per cent was obtained at 750°C. The volatile fraction consisted entirely of the starting compound.

3.1.3.2.3. Heterocyclic Compounds Containing both Nitrogen and Oxygen Atoms in One Ring

The DTA thermograms for thermally reactive oxazole and oxadiazole compounds are also shown in Figure 5. The physical and thermal properties of these compounds as determined in the DTA experiments are summarized in Table 11.

Table 11. Thermal Properties of Heterocyclic Compounds Containing Both Oxygen and Nitrogen

Compound (SM)	Structure	DTA No.	MP, °C Lit.	MP, °C DTA	BP, °C DTA	AgT, °C DTA	% C. Residue	Remarks
2,5-Di-(4-biphenyl)- oxazole		489	232-3	230.	490. several endotherms	-----	14.6	Condensate contained S.M. plus new products Some C=O bands at 5.90 to 6.0 microns.
2,5-Di-(4-biphenyl)- 1,3,4-oxadiazole		488	229-30	228.	490	-----	15.1	S.M. contained some impurity-double m.p. Condensate contained S.M. plus new products

+ Euthermic
- Endothermic

a. 2,5-Di-(4-biphenyl)-oxazole (489)

This compound is structurally similar to the next-listed compound (see Table 11) except that the heterocyclic ring contains one nitrogen atom instead of two. The effect of replacing one nitrogen with -CH- is almost negligible. The thermogram (DTA No. 489 in Figure 5) is very similar to DTA No. 488, showing a melting point of 230°C and a weak, but somewhat more complex, vaporization and reaction endotherm between 480°C and 525°C. The condensate contains some oxidized products as well as starting material. A carbon yield of 14.6 per cent was obtained.

b. 2,5-Di-(4-biphenyl)-1,3,4-oxadiazole (488)

The DTA thermogram for this compound shows a double melting endotherm, indicating the presence of an impurity. The melting point of the major constituent is 228°C. Following melting, no reaction occurs until the temperature reaches 460°C, at which point a weak vaporization endotherm begins. A carbon yield of 15.1 per cent was obtained. The condensate contained some reaction products in addition to starting material.

3.1.3.2.4. Heterocyclic Sulfur Compounds

Four heterocyclic sulfur compounds were examined in the DTA apparatus. The DTA thermograms are given in Figure 5, and the related physical properties and carbon residues obtained in the DTA experiments are summarized in Table 12.

Table 12. Thermal Properties of Heterocyclic Sulfur Compounds

Compound (SM)	Structure	DTA No.	MP-°C Lit.	MP-°C DTA	BP-°C DTA	% Residue	Remarks
2-Chlorophenothiazine		484	196-8	185	466-	10.5	Condensate contained mostly SM but all bands were broadened.
Thioxanthone		514	207	195	400-	1.3	Condensate contained SM only
2-Chlorothioxanthone		485	142	155	440	1.0	Condensate contained mostly SM plus small amount of new products.
Trithiane		519	215-6	205	315-	1.9	Condensate contained new products plus some SM.

+ Exothermic
- Endothermic

The majority of the heterocyclic sulfur compounds examined in this survey to date have been unreactive under the experimental conditions used. These four compounds are all reactive, but also have various additional structural features such as oxygen or halogen substituents, or multiple heteroatoms in a single ring.

a. 2-Chlorophenothiazine (484)

This compound was the most reactive of the group examined. The DTA thermogram shows a typical sharp, symmetrical melting endotherm and a somewhat attenuated vaporization endotherm also typical of a moderately reactive material. A carbon yield of 10.5 per cent was obtained. The condensate consisted primarily of starting material contaminated with a small amount of reaction products which broadened the absorption bands in the IR spectrum.

b. Thioxanthone (514)

The thermogram obtained from this compound gives no indication of thermal reactivity, showing only two large, sharp endotherms due to melting and boiling. The condensate collected in the KBr trap consisted only of the starting material. A small carbon residue of 1.3 per cent was obtained as a result of thermal treatment in argon.

c. 2-Chlorothioxanthone (485)

The thermogram of the 2-chloro-derivative of thioxanthone is similar to that of the parent heterocycle, showing only the melting and boiling endotherms. The condensate contained a small amount of unidentified new products in addition to starting material. A carbon residue of 1.0 per cent was obtained. The chlorine substituent apparently has little activating effect in this compound.

d. Trithiane (519)

Trithiane is a cyclic trimer of methylene sulfide which is of more interest as a carbonization initiator than as a primary source of carbon. Its thermal behavior is illustrated in the DTA thermogram which shows a slight forward shoulder on the melting endotherm and a second endotherm that indicates a boiling point of about 345°C. The condensate indicates considerable thermal decomposition occurred along with the vaporization. A carbon residue of 1.9 per cent was obtained.

3.1.3.3. Thermally "Reactive" Anthracene-SbCl₅ Complex

The interactions of aromatic hydrocarbons with a strong electron acceptor, SbCl₅, form thermally reactive complexes. Anthracene and SbCl₅ interact at room temperature to form a black, solid polymeric complex that reacts further with moisture in the atmosphere to introduce hydroxyl groups in the complex.

This anthracene-SbCl₅-H₂O complex was heated in the DTA apparatus at 10°C per minute in dry argon. The complex melts above 50°C and reacts endothermally above 200°C to produce a mixture of chloro-anthraquinones and a carbonizable residue. A carbon yield of 9.6 per cent was obtained in the DTA experiment. This result is low compared with the 72 per cent yield obtained in the standard UCC long-coking value test of heating at 60°C per hour to 1000°C in a nonoxidizing atmosphere, but it does indicate the strong activating effect of the Lewis acid. The DTA thermogram is shown in Figure 5.

3.2. Chemical Structure and Graphitization - X-Ray Diffraction Studies of Graphites Derived from Model Compounds

3.2.1. Introduction

An important aspect of this program is to relate graphite properties to chemical structure of the original raw material. A general survey of graphites derived from model compounds has therefore been undertaken. The model compounds examined are those which have been investigated in our DTA program for relating chemical structure to thermal reactivity.

It is generally accepted that the properties of graphites are related to the degree of ordering of the crystal structure. The most direct method for characterizing order-disorder phenomena is the X-ray diffraction technique. Previous reports have described some attempts to measure X-ray parameters of synthetic graphites.⁽²⁾ The average semilattice spacing as measured by the (00 ℓ) bands was found to be a roughly suitable method for classifying graphites. The direct measurement of the 002 peak position by diffractometer methods seemed to have a gross dependence on the experimental X-ray procedure employed. Such experimental variables as sample packing and sample size caused considerable variation in the width and position of the 002 line. The direct measurement of the 002 line by camera methods improved this situation but still resulted in poor reproducibility.

It had been suggested⁽³⁾ that the most reliable method for measuring the 002 reflection consists of measuring the higher order 004, 006, and 008 lines of graphite. By employing the appropriate factors, the line position of the 002 reflection can be determined accurately. These measurements have been made on the graphites prepared from model compounds which produced sufficient carbon yields. The results are discussed in terms of the chemical structure of the model compounds.

3.2.2. Experimental

3.2.2.1. Preparation of Synthetic Graphites

The DTA residues from 160 model compounds have been heated to 3000°C in a conventional graphitizing furnace. A number of organic

compounds which are of interest do not produce a carbonaceous residue in the DTA experiments. These compounds have been carbonized to 450°C in a closed pressure system, and the synthetic carbons obtained were then graphitized in a conventional manner.

3.2.2.2. X-Ray Measurements

The graphite samples were all ground through 100 mesh. They were mounted on a 5-mil thick tantalum fiber which had first been dipped in Apiezon grease. The function of the grease was to permit the graphite particles to adhere to the tantalum fiber. The use of tantalum permitted the accurate measurement of the 002, 004, 006, and 008 reflections in the synthetic graphites. The interference effects that had previously been found for tungsten were thus obviated. Tantalum additionally provides distinct lines in the back-reflection for film shrinkage corrections.

The X-ray patterns were measured on films with the use of a Norelco diffractometer and a Debye-Scherrer powder camera, 114.6 mm diameter. Copper radiation and a nickel filter were employed, and the films were exposed for a period of 20 hours. Each film was measured and corrected for shrinkage a total of four times. After each measurement, the film was removed from the film measuring device and then re-inserted. An average of the four measurements was then obtained for all values. A second correction for the thickness of the tantalum fiber mount was necessary to eliminate a systematic error between results calculated from the 008, 006, 004, and 002 reflections.

For the well-ordered graphites, the 008 rather than the 006 line gave the most accurate measure of the semilattice spacing. In the compounds where the 008 line could not be detected, the 006 line was measured and then corrected by 0.004 Å which is the average deviation between the 008 and 006 values. This correction reflects the error due to the thickness of the tantalum fiber mount. Materials which showed no 006 lines had extremely high semilattice spacings and the position of the 004 lines were then employed directly. The semilattice spacings expressed in Angstrom units for the 002 lines are reported along with the particular reflection employed in the measurement. It should be emphasized that for the purposes of this study it is the relative, rather than the absolute, x-ray values which are important.

3.2.2.3. Results

The 002 and 004 lines were observed in all the synthetic graphites. The 006 lines could be observed in nearly all of the materials while the 008 lines were discernible in approximately one-half of the films. The 008 reflections even when evident, however, were faint and difficult to measure. All the line positions were converted to comparable values in Angstroms by the use of the appropriate factors. In general, good agreement is found among the 004, 006, and 008 values. The 002-line positions appeared to be the most divergent in that the experimental error decreased in the higher order reflections. In several instances, there

was poor agreement between the 004 and 006 values. When the 008 line could not be measured, position of the 006 reflection was chosen as the most reliable measure of the 002 line position.

The graphites have been grouped according to structural type of the original compounds in order to facilitate evaluation of the results. The compounds have been listed in the tables in the order of increasing 002 values; thus, those compounds producing the best-ordered graphites are listed first.

3.2.2.3.1. Graphitized Raw Materials; Natural Graphites, Pitches and Cokes

The X-ray values for the semilattice spacings of graphites prepared from several of the raw materials conventionally used for the production of manufactured graphite products are listed in Table 13. All of the line positions were converted to comparable values of semilattice spacing in Angstroms by the use of the appropriate factors. These results are useful for comparison with the data from model compounds.

Table 13. 002-Semilattice Spacings Obtained from Various Reflections for Some Graphitized Raw Materials

Material	002 Å	2(004) Å	3(006) Å	4(008) Å
(1) Canadian Natural Graphite	3.353	3.347	3.350	3.354
(2) 30 Medium Pitch	3.358	3.351	3.350	-
(3) AX Coke	3.366	3.345	3.351	3.357
(4) 15 Vacuum Pitch	3.343	3.337	3.353	-
(5) Acenaphthylene Pitch	3.363	3.352	3.354	3.356
(6) DK Coke	3.363	3.352	3.355	3.358


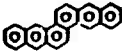
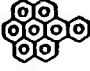


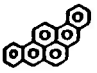

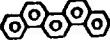
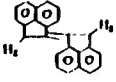




3.2.2.3.2. Aromatic Hydrocarbons

The 002 semilattice spacings listed in Angstroms along with the reflections from which they were derived, for graphites derived from 27 aromatic hydrocarbons are presented in Table 14. The DTA coking values are also included in Table 14.

3.2.2.3.3. Aromatic Hydrocarbons with Alkyl and Aryl Substituents

The 002 semilattice spacings for graphites derived from 17 Alkyl and Aryl-substituted aromatic hydrocarbons are given in Table 15; the DTA coking values are also given.

Table 14. 002-Semilattice Spacings for Graphites Derived from Model Aromatic Hydrocarbons

Aromatic Hydrocarbon	Structure	002, Å (Reflection)	DTA C.V., %
9,9'-Bianthryl		3.354 (008)	0.0
Dibenso(b,k)chrysene		3.354 (008)	22.0
Benzo(a)coronene		3.354 (008)	31.0
Acenaphthylene		3.356 (008)	23.5
Benzo(e)pyrene		3.356 (008)	0.0
Dibenso(a,l)pyrene		3.356 (008)	9.8
Dibenzo(a,l)pentacene		3.356 (008)	53.0
Picene		3.357 (008)	0.0
Biacenaphthylidene		3.357 (008)	40.9
Naphthacene		3.358 (008)	13.9
Decacyclene		3.358 (008)	66.3
Dibenso(h,rst)pentaphene		3.358 (008)	14.0
Ovalene		3.358 (008)	64.9

Continued . . .

Table 14. Continued



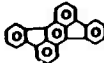






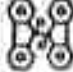
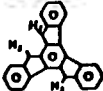
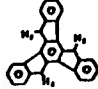

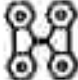
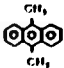
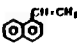

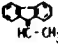
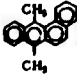
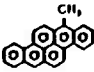
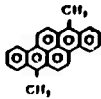
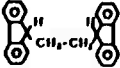

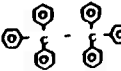



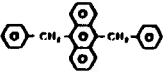
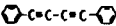
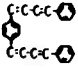
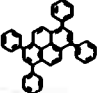
Pentacene		3.363 (006)	42.8
Periflanthene		3.363 (006)	54.7
Rubicene		3.363 (006)	9.0
Pyranthrene		3.363 (008)	60.1
14 H-Acenaph(1,2-)]indeno- (1,2-1)]fluoranthene		3.365 (006)	46.8
Quaterylene		3.368 (006)	91.8
Coronene		3.370 (006)	1.5
Fluoranthene		3.371 (006)	0.0
Dibenzo(a,c)triphenylene		3.373 (006)	0.0
9,9'-Bifluorene		3.374 (006)	5.8
14,15-Dihydro-9H-dilindeno (1,2-a;1',2'-c)]fluorene		3.380 (006)	13.5
10,15-Dihydro-5H-dilindeno-(1,2-a;- 2',1'-c)]fluorene		3.385 (006)	27.8
p-Terphenyl		3.437 (004)	0.0
Δ ^{9,10} -Bifluorene		3.474 (004)	28.0

Table 15. 002-Semilattice Spacings for Graphites Derived from Alkyl and Aryl Substituted Aromatic Hydrocarbons

Aromatic Hydrocarbon	Structure	002, Å (Reflection)	DTA C. V., %
9, 10-Dimethylantracene		3.354 (008)	0.4
1-Vinylnaphthalene		3.354 (008)	4.2
5, 6, 11, 12-Tetraphenylnaphthalene		3.356 (008)	44.0
9-Ethylidenefluorene		3.357 (008)	5.0
7, 12-Dimethylbenzo(a)anthracene		3.358 (008)	4.7
7-Methylbenzo(a,h)pyrene		3.358 (008)	22.7
7, 14-Dimethyldibenzo(a,h)pyrene		3.358 (008)*	33.6
Di-9-fluorenylethane		3.358 (008)	5.1
9, 10-Di-1-naphthylantracene		3.359 (008)	14.0
Hexaphenylethane		3.360 (006)	8.0
4-Vinylbiphenyl		3.362 (006)	8.1
2-Vinylnaphthalene		3.363 (006)	9.9
Di-p-xylylene		3.406 (004)	12.6
9, 10-Dibenzylantracene		3.412 (004)	8.9
Diphenyldiacetylene		3.421 (004)	38.0
1, 4-Bis (4-phenylbutadienyl)benzene		> 3.40 (002)	19.7
1, 3, 6, 8-Tetraphenylpyrene		> 3.40 (002)	13.8

3.2.2.3.4. Aromatic Hydrocarbon with Oxygen Substituents

X-ray data for graphites derived from 44 oxygenated aromatics are compiled in Table 16; the DTA coking values are also given. Compounds with a variety of oxygen-containing functional groups are included. These compounds are of special interest since they are believed to represent the kinds of structures formed during any oxidation of the usual graphite raw materials.

3.2.2.3.5. Aromatic Hydrocarbons with Nitrogen Substituents

Listed in Table 17 are the X-ray parameters for graphites prepared from 35 nitrogen-substituted aromatics, and the DTA coking values are also given. Nitrogen substitution has an extreme activating effect on the thermal reactivity of aromatics. None of the unsubstituted aromatic structures in Table 17 would be thermally reactive in the DTA experiment.

3.2.2.3.6. Aromatic Hydrocarbons with Halogen Substituents

The 002-semilattice spacings for 14 graphites prepared from halogen-substituted aromatic hydrocarbons are given in Table 18; the DTA coking value is also given. Halogen substitution generally increases the thermal reactivity of the aromatic moiety which results in enhanced carbon yields. The graphite semi-lattice spacings of the halogenated compounds are generally high.

3.2.3.7. Aromatic Compounds with Sulfur Substituents

The X-ray diffraction pattern of only one sulfur-substituted aromatic compound, p-xylylenedithiol has been measured. The results, shown in Table 19, include the organic structure, the 002-semilattice dimension, the reflection used, and the DTA coking value. An excellent graphitic structure was obtained from this material.

3.2.2.3.8. Heterocyclic Compounds



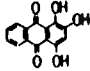
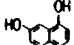
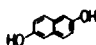
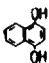
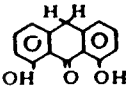
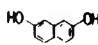
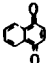
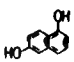
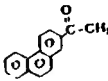
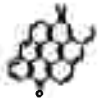

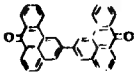
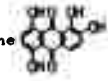
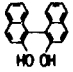
3.2.2.3.8.1. Oxygen Heterocyclics

The 002-semilattice spacings for graphites derived from four heterocyclic oxygen compounds, along with the DTA coking value, are listed in Table 20. In general, the graphites are relatively poor, with large 002 spacings, and exhibit very weak or no higher order reflections of the 002 bands.

3.2.2.3.8.2. Nitrogen Heterocyclics

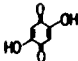
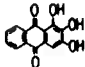
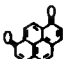
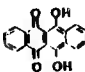
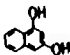
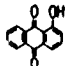
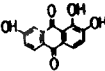
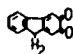

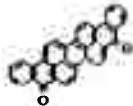
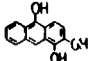
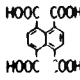
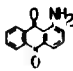
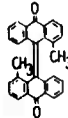
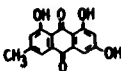
The thermal reactivity of the heterocyclic nitrogen compounds is increased by substitution and by the presence of more than one heteroatom in a ring as in the phenazines. The X-ray diffraction parameters for 15 graphites derived from heterocyclic nitrogen compounds, along with their DTA coking value are listed in Table 21. The L_c spacings

Table 16. 002-Semilattice Spacings for Graphites Derived from Oxygenated Aromatics

Compound	Structure	002, Å (Reflection)	DTA C.V., %
Anthanthrone		3.354 (008)	70.0
Perinaphthenone		3.356 (008)	25.6
Purpurin		3.358 (008)	30.5
1,7-Naphthalenediol		3.358 (008)	1.5
2,6-Naphthalenediol		3.359 (008)	4.3
1,4-Naphthalenediol		3.360 (008)	52.6
1,8-Dihydroxyanthranol		3.360 (006)	13.1
2,7-Naphthalenediol		3.363 (008)	6.7
1,4-Naphthoquinone		3.370 (006)	40.4
1,6-Naphthalenediol		3.372	21.9
3-Acetylphenanthrene		3.372 (006)	3.4
Isioviolanthrone		3.373 (006)	85.6
Mellitic trianhydride		3.376 (006)	25.5
13,13'-Dibenzanthronyl		3.378 (006)	77.2
1,2,5,8-Tetrahydroxyanthraquinone		3.381 (004)	12.0
1,1'-Bi-2-naphthol		3.382 (004)	9.6

Continued

Table 16. Continued

2,5-Dihydroxybenzoquinone		3.383 (004)	29.8
1,2,3-Trihydroxyanthraquinone		3.385 (004)	41.1
1,8-Pyrenequinone		3.386 (006)	58.4
6,11-Dihydroxynaphthacenequinone		3.387 (004)	20.6
1,3-Naphthalenediol		3.390 (006)	47.8
1-Hydroxyanthraquinone		3.390 (004)	3.8
1,2,7-Trihydroxyanthraquinone		3.392 (004)	46.9
2,3-Fluorenoquinone		3.392 (004)	73.6
Pyranthrone		3.393 (004)	79.8
Violanthrone		3.394 (004)	84.3
3,4-Dihydroxyanthranol		3.397 (006)	61.8
Naphthalene-1,4,5,8 tetracarboxylic acid		3.398 (002)	19.8
1-Aminoanthraquinone		3.402 (004)	12.9
4,4'-Dimethylbianthrone		3.406 (004)	48.8
Emodin		3.408 (004)	52.8

Continued

Table 16. Continued

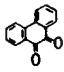
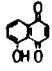
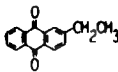
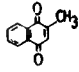

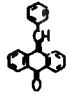
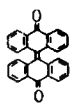
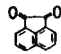
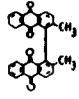
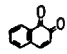
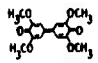
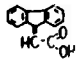
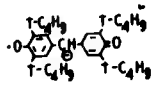

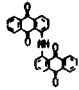
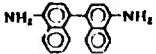
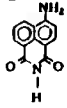
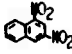
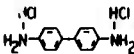
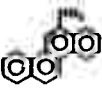
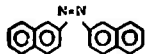

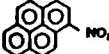
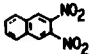
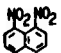
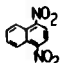
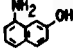
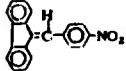
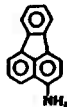
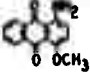
Phenanthrenequinone		3.411 (004)	40.3
5-Hydroxy-1,4-naphthoquinone		3.412 (004)	64.7
2-Ethylanthraquinone		3.412 (004)	6.9
2-Methyl-1,4-naphthoquinone		3.412 (004)	-
9-Phenyl-9-fluoreneol		3.414 (002)	43.4
9-Benzylideneanthrone		3.422 (002)	14.4
$\Delta^{10,10'}$ -Blanthrone		3.422 (004)	74.3
Acenaphthenequinone		3.426 (004)	14.6
2,2'-Dimethyl-1,1'-dianthraquinone		3.458 (002)	53.5
1,2-Naphthoquinone		> 3.40 (002)	27.5
Coerulignone		> 3.40 (002)	25.8
Δ^9 -Fluoreneacetic acid (Biphenylene acrylic acid)		> 3.40 (002)	16.4
Galvinoxyl		> 3.40 (002)	12.2

Table 17. 002-Semilattice Spacings for Graphites Derived from Nitrogen-Substituted Aromatics

Compound	Structure	002, Å (Reflection)	DTA C. V., %
1-Acetamidopyrene		3.358 (008)	15.9
1,1'-Iminodianthraquinone		3.359 (006)	70.8
Naphthidine		3.359 (006)	3.0
4-Amino-1,8-naphthalimide		3.359 (008)	15.2
1,3-Dinitronaphthalene		3.360 (006)	5.3
Benzidine dihydrochloride		3.361 (006)	8.7
2-Aminochrysene		3.362 (006)	11.9
2,2'-Azonaphthalene		3.362 (006)	12.1
1,8-Diaminonaphthalene		3.364 (008)	4.4
1-Nitropyrene		3.365 (006)	39.5
2,3-Dinitronaphthalene		3.372 (004)	10.5
1,8-Dinitronaphthalene		3.376 (004)	11.9
1,4-Dinitronaphthalene		3.382 (004)	10.1
8-Amino-2-naphthol		3.383 (006)	42.1
p-Nitrobenzylidene-fluorene		3.389 (004)	45.9
3-Amino-fluoranthene		3.398 (004)	36.2
1-Amino-4-methoxy-9,10-anthraquinone		3.399 (004)	43.3

Continued

Table 17. Continued

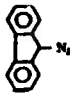

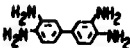
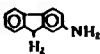

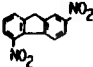

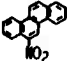
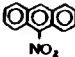
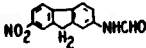
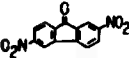
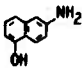
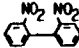
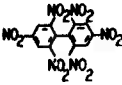
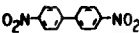
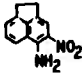
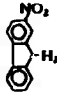
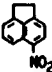
9-Diazofluorene		3.400 (004)	35.7
2-Amino-9-fluorenone		3.406 (004)	63.0
3,3'-Diaminobenzidine		3.407 (006)	23.5
2-Aminofluorene		3.437 (004)	12.9
9-Fluorenoneazine		3.408 (008)	42.7
2,5-Dinitrofluorene		3.409 (002)	36.5
2,7-Diaminonaphthalene		3.413 (004)	10.3
6-Nitrochrysene		3.416 (002)	34.3
9-Nitroanthracene		3.427 (004)	24.1
2-Formamido-7-nitrofluorene		3.435 (002)	68.6
2,6-Dinitro-9-fluorenone		> 3.40 (002)	18.1
2-Amino-5-naphthol		> 3.40 (002)	49.1
2,2'-Dinitrobiphenyl		> 3.40 (002)	4.8
2,2',4,4',6,6'-Hexanitrobiphenyl		> 3.40 (002)	6.2
4,4'-Dinitrobiphenyl		> 3.40 (002)	9.2
5-Amino-4-nitroacenaphthene		> 3.40 (002)	56.1
2-Nitrofluorene		> 3.40 (002)	67.4
5-Nitracenaphthene		> 3.40 (002)	44.8

Table 18. 002-Semilattice Spacings for Graphites Derived from Halogen-Substituted Model Compounds

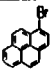
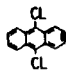
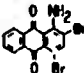
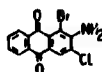
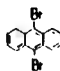
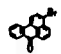
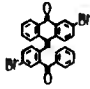


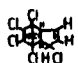
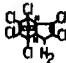
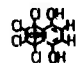
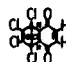
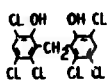
Compound	Structure	002, Å (Reflection)	DTA C.V., %
1-Bromopyrene		3.361 (006)	9.2
9,10-Dichloroanthracene		3.386 (004)	0.0
1-Amino-2,4-Dibromoanthraquinone		3.399 (004)	22.5
2-Amino-1-Bromo-3-Chloroanthraquinone		3.401 (004)	33.0
9,10-Dibromoanthracene		3.415 (004)	20.0
3-Bromobenzanthrone		3.466 (002)	14.9
2,2'-Dibromobianthrone		> 3.40	66.5
9-Chloro-9-phenylfluorene		> 3.40 (002)	51.7
Dichloroquinone chloroimide		> 3.40 (002)	39.4
Heptachlor		> 3.40 (002)	9.7
Octachlor		> 3.40 (002)	6.0
1,2,3,4,9,9-Hexachloro-1,4-dihydro-1,4-methanonaphthalene-5,8-diol		> 3.40 (002)	16.8
1,2,3,4,9,9-Hexachloro-1,4,4a,8a-tetrahydro-1,4-methanonaphthalene-5,8-dione		> 3.40 (002)	22.3
Hexachlorophene		> 3.40 (002)	22.2

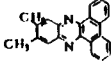

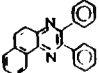
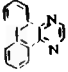
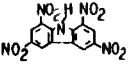
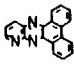
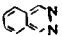
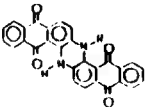
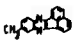
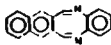
Table 19. 002-Semilattice Spacings for Graphites Derived from Model Organic Compounds

Compound	Structure	002, Å(Reflection)	DTA C. V., %
(1) p-Xylylenedithiol	<chem>HS-CH2-c1ccc(cc1)CH2-SH</chem>	3.356 (006)	15.5

Table 20. 002-Semilattice Spacings for Graphites Derived from Heterocyclic Oxygen Compounds

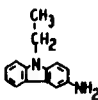

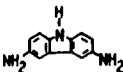


Compound	Structure	002-Å(Reflection)	DTA CV-%
2-Hydroxydibenzofuran	<chem>Oc1ccc2c(c1)oc3ccccc3o2</chem>	3.382 (004)	7.6
9-Xanthylideneanthrone	<chem>O=C1C(=O)c2cc3c(cc21)c4ccccc4c5ccccc35</chem>	3.406 (004)	57.2
9,9'-Bixanthylene	<chem>c1ccc2c(c1)c3ccccc3c2C4=CC=CC=C4C5=CC=CC=C5</chem>	3.422 (002)	35.0
Dicoumarin	<chem>O=C1C(=O)c2cc3c(cc21)c4ccccc4c5ccccc35C6=CC=CC=C6C7=CC=CC=C7</chem>	3.429 (004)	27.3

Table 24. 002-Semilattice Spacings for Graphites Derived from Heterocyclic Nitrogen Compounds

Compound	Structure	002-Å(Reflection)	DTA CV-%
11, 12-Dimethyldibenzo (a, c) phenazine		3. 362 (008)	9. 7
11-Methyl-dibenzo (a, c) phenazine		3. 362 (008)	7. 7
2, 3-Diphenyl 5,6-benzoquinoxaline		3. 362 (006)	7. 9
5, 6, 7, 8-Dibenzoquinoxaline		3. 363 (008)	10. 5
1, 3, 6, 8-Tetranitrocarbazole		3. 365 (006)	17. 0
Dibenzo (f, h) pyrido (3, 4-b) quinoxaline		3. 366 (006)	88. 1
Phthalazine		3. 392 (004)	2. 3
Indanthrone		3. 399 (004)	53. 9
9-Methylacenaphthoquinoxaline		3. 400 (004)	3. 2
2, 3-Benzo-1,4-diazo (2', 3', 6, 7-naphtho) - cyclooctatetraene		3. 407 (004)	32. 6

Continued

Table 21. Continued



3-Amino-9-ethylcarbazole		3.412 (004)	28.0
6-Nitroindazole		3.422 (002)	23.6
3,6-Diaminocarbazole		3.430 (004)	48.2
2,5-Di-(4-biphenyl)-oxazole		>3.40 (002)	14.6
2,5-Di-(4-biphenyl)-1,3,4-oxadiazole		>3.40 (002)	15.1

vary from those of an intermediately-ordered graphite to those of a highly-disordered graphite, depending on the initial heterocyclic structure.

3.2.2.3.8.3. Sulfur Heterocyclics

The graphites derived from only two heterocyclic sulfur compounds were examined by X-ray diffraction. The results are summarized in Table 22. The first compound listed, diacenaphtho(1,2-b:1',2'-d)-thiophene, produced a relatively well-ordered graphite with a 002 spacing of 3.358 Å. The second compound, 2-chlorophenothiazine (which is chloro-substituted and contains a heterocyclic ring with both sulfur and nitrogen atoms), gave a relatively disordered graphite with a semilattice dimension of 3.370 Å.

Table 22. 002-Semilattice Spacings for Graphites Derived from Heterocyclic Sulfur Compounds

Compound	Structure	002-Å (Reflection)	DTA CV-%
Diacenaphtho(1,2-b:1',2'-d)-thiophene		3.358 (008)	68.2
2-Chlorophenothiazine		3.370 (004)	10.5

3.2.2.3.9. Modification of Graphites from Aromatic Hydrocarbons by Reactive Additives and Rapid Heating Rates

Previous work has shown how reactive additives can modify the thermal reactivity of aromatic compounds. Such additives can affect the character of the derived graphite, as well. Several examples are given in Table 23. The addition of p-benzoquinone to naphthacene results in a poorly-ordered graphite. A similar effect is demonstrated for benzoquinone-fluorene and for anthracene-chloranil. Also shown in Table 23 are the effects of the powerful complexing agent SbCl_5 on two hydrocarbons which yield highly-ordered graphites when carbonized alone. High 002 spacings (the order of 3.42 Å) are observed for the mixtures. The final example in Table 23 illustrates how the heating rate can affect the graphite properties for 9,9'-bifluorene. The "rapid graphitization" sample was heated to 3000°C in 30 minutes directly from the 475° polymer stage. The "normal graphitization" sample was heated at 60°C/hour to 1000°C before graphitizing to 3000°C at the rapid rate. The rate of heating through the coke forming stage is seen to exert a marked effect on the 002 spacing of the graphite.

Table 23. 002-Semilattice Spacings for Modified Aromatic Hydrocarbon Graphites

System	002-Å (Reflection)	CV-%
Naphthacene-p-Benzoquinone (1:1)	3.398 (004)	36.1
Fluorene-p-Benzoquinone (1:1)	3.399 (004)	17.1
Anthracene-Chloranil (1:1)	>3.40 (002)	10.9
Acenaphthylene - SbCl_5 (1:1)	3.417 (004)	--
Anthracene - SbCl_5 (1:1)	3.420 (004)	9.6
9,9'-Bifluorene (Normal Graphitization)	3.374 (006)	5.8
9,9'-Bifluorene (Rapid Graphitization)	3.413 (004)	5.8

3.2.2.3.10 Physical Mixtures of Cokes and Graphites from Model Hydrocarbons Acenaphthylene and p-Terphenyl

X-ray measurements were performed on a graded series of mixtures of graphites derived from acenaphthylene and p-terphenyl. Acenaphthylene has been shown to produce an excellent highly-ordered graphite, whereas p-terphenyl graphite is very poorly-ordered. The purpose of these experiments was to determine the effects of possible contamination of the graphites derived from the model compounds with the highly-ordered graphite from the capsules in which the samples were graphitized. Occasionally, results had been obtained where the 002 reflection was rather diffuse and gave very approximate spacings near 3.40 Angstroms; but the

higher order 004, 006, and 008 reflections were also present and yielded values near 3.356 Angstroms, indicating a highly-ordered graphite. The data in Table 24, showing the 002 spacing parameters computed from the various order reflections, satisfactorily explains this type of diffraction pattern. The 1:4 mixture of acenaphthylene coke to p-terphenyl coke exhibits a similar X-ray pattern. The other mixtures show that if the concentration of good graphite is too high (1:1 mixture) the poor graphite is not definitely detected (but a possible increase in average spacing may be introduced); conversely, if the concentration of good graphite is too low (1:10 mixture), only the pattern of the poor graphite is obtained.

Table 24. 002-Semilattice Spacings from Physical Mixtures of Cokes and Graphites Derived from Model Hydrocarbons Acenaphthylene and p-Terphenyl

Mixture Components	Ratio	002-Spacing A	(Reflections)
Acenaphthylene Graphite	Only	3.356	(008)
		3.355	(006)
		3.349	(004)
		3.348	(002)
p-Terphenyl Graphite	Only	3.437	(004)
		3.419	(002)
Acenaphthylene Coke - p-Terphenyl Coke	1:1	3.362	(008)
		3.359	(006)
		3.358	(004)
		3.353	(002)
Acenaphthylene Coke - p-Terphenyl Coke	1:4	3.357	(006)
		3.354	(004)
		3.416	(002)
Acenaphthylene Coke - p-Terphenyl Coke	1:10	3.424	(004)
		3.437	(002)

3.2.2.4. Discussion of Results

The data presented in the previous Tables indicate that the nature of the final graphite is highly dependent on the chemical structure of the starting materials. The connection is not obvious in all cases; however, it appears that two major factors are involved:

1. The planarity and steric overcrowding in the original molecule;
2. The chemical reaction sequence and the nature of the thermally-formed intermediates.

Other factors, of course, also affect graphite structure (heating rate, pressure, atmosphere, and contamination), but they operate primarily through their effect on the chemical reaction sequence. These present results, therefore, do show the importance of detailed mechanism studies on model aromatic systems. Such studies can reveal the general types of thermal reactions, which can be related to the starting structure as well as to the ultimate structure of the graphite.

3.2.2.4.1. Natural Graphites and High-Grade Cokes

The raw materials normally used for the manufacture of synthetic carbon and graphite, coal tar pitches, and petroleum cokes form highly-ordered graphites, as illustrated in Table 13. The 002 spacings derived from the 008 reflections vary from 3.354 Å for Canadian Natural Graphite to 3.358 Å for DK coke. It is evident that the variation in graphite structure introduced by the raw materials alone covers a narrow range on the 002 lattice spacing scale as used in this study. These results are useful for comparison with the data from model compounds.

3.2.2.4.2. Aromatic Hydrocarbons

Nearly all of the compounds in Table 14 are known constituents of the usual raw materials for carbon and graphite, i.e., coal tar pitch and petroleum residues. The majority of these aromatic compounds yield highly-ordered graphites with low 002 spacings. Approximately one-half fall in the same range of well-ordered graphites as represented by the raw materials in Table 13.

Especially interesting are the compounds showing large 002 spacings. Most of the compounds with lattice spacings greater than 3.363 Å are either nonplanar or sterically overcrowded. The thermal reactions of these structures would very likely yield nonplanar reactive intermediates. The 002 spacing obtained for such planar aromatic systems as quaterylene and coronene are surprisingly large. Such symmetrical structures may not yield the mobile reactive species presumed necessary for rearrangement to planar graphitic structures. The large spacings for graphites derived from fluoranthene and fluorene derivatives are also likely a result of the nonplanarity of thermally formed reaction intermediates.

3.2.2.4.3. Aromatic Hydrocarbons with Alkyl and Aryl Substituents

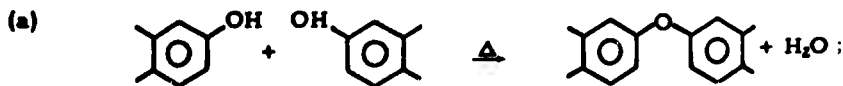
Of the 17 alkyl and aryl-substituted aromatic hydrocarbons listed in Table 15, approximately one-half produced graphites comparable to the

complex raw materials used in manufacturing synthetic graphite. For the compounds with low 002 values, reactivity seems to be of major importance. Alkyl substitution and side chains increase thermal reactivity and enhance the degree of graphitization. Such compounds readily form aromatic radicals on thermal treatment. The side chain groups offer a mobil means of rearrangement to planar conjugated systems through radical intermediates. This type of sequence has been proposed for the hydrocarbon acenaphthylene. The position of substitution influences graphite properties as well. This is illustrated by the difference between 1-vinylnaphthalene (3.354 Å) and 2-vinylnaphthalene (3.363 Å). The non-planar, nonfused aromatics exhibit high 002 values, grouped at the end of Table 15. The value for 9,10-dibenzylanthracene is surprisingly high; however, values near 3.40 Å have been obtained for several different samples of this material.

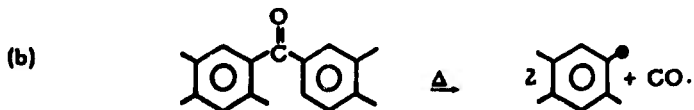
3.2.2.4.4. Aromatic Hydrocarbons with Oxygen Substituents

The oxygen-substituted aromatics are of interest in that they represent the types of structures presumed to be formed during the oxidation of aromatic raw materials for graphite. Although a total of 44 oxygen-substituted aromatics were examined, only five produced graphites with low 002 values (below 3.360 Å). These results substantiate the conclusions concerning the effects of oxidation on raw materials; oxidation results in a higher reactivity and a more disordered graphite structure.

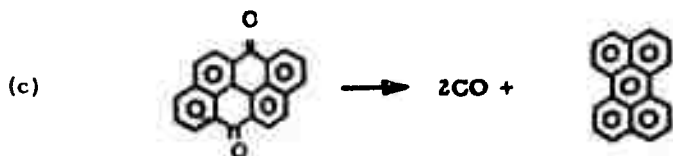
DTA studies have shown that oxygen substitution generally increases the coking value of aromatic hydrocarbons. The oxygen substituents usually encountered in the raw materials for graphite can either serve as reaction sites for thermal polymerization:



or they may serve as activated sites for carbon-carbon bond cleavage and radical formation:

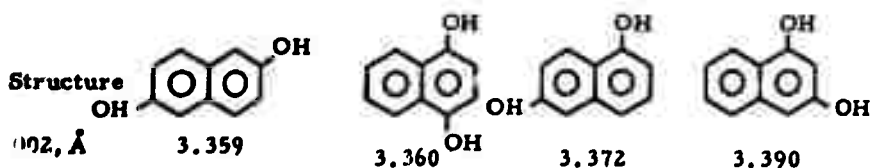


The nature of the graphite formed from oxygenated aromatics is variable, depending both on the nature of the substituent and the position of substitution. Highly-disordered graphites are obtained from the several nonplanar quinone materials listed at the end of Table 16. Anthanthrone, however, yields a well-ordered material, presumably as a result of the formation of planar intermediates which could be formed by the elimination of CO:



The effects of oxygen substituents are complex, however. The oxygen substituent can provide a direct site for thermal polymerization or can facilitate direct thermal cleavage of carbon-carbon bonds. Perinaphthenone and purpurin also produce highly-ordered graphites (sharp 008 lines). This result is expected for perinaphthenone, which could readily eliminate CO and produce vinylnaphthalene radical moieties. These radicals have been postulated as intermediates in the pyrolysis of acenaphthylene and would give rise to planar aromatics of the zethrene type. The formation of a well-ordered graphite from the hydroxyanthraquinone, purpurin, is unexpected. Only one other substituted anthraquinone, 1,1'-Iminodianthraquinone, produced a graphite having a well-ordered structure. The most striking feature of the results for the quinones (in addition to the very high coking yields) is the high graphite semilattice spacing.

The effect of the position of substitution on the nature of the final graphite can be seen in the following comparison for the naphthalenediols.



The symmetrical derivatives give rise to the best ordered graphites. It is evident that reaction mechanism studies are required to explain the effect of oxygen substitution on the nature of the final graphite. Oxygen substitution can cause a wide variation in graphite structure.

3.2.2.4.5. Aromatic Hydrocarbons with Nitrogen Substituents

Substitution with nitrogen-containing groups has a strong activating effect on the thermal reactivity of aromatics. None of the parent hydrocarbons of the compounds listed in Table 17 was thermally reactive enough to yield carbon residues in DTA. A variety of nitrogen groups are represented in our data, including -NH_2 , -NHCOCH_3 , -NH- , -N=N- , and NO_2 groups.

The amino group exerts an activating effect on the thermal reactivity of the aromatic compounds. The character of the final graphite, however, depends on the nature of substitution. Three aminonaphthalene derivatives, with the NH_2 group in the α -position, form well-ordered graphites. The compound 2,7-diaminonaphthalene, which contains $\beta\text{-NH}_2$ groups, produces a poorly-ordered material. The compound 2-amino-fluorene exhibits a behavior which is typical of fluorene derivatives. An explanation of these effects for aromatic amines must await further mechanism studies; however, the NH_2 substituent, unlike the C=O group, apparently does not generally induce a thermal rupture of the aromatic ring system.

The oxidative nitro group also exerts a strong activating effect on thermal reactivity; however, it generally produces a disordered graphite (high 002 values). This conclusion is well illustrated by 9-nitroanthracene, 6-nitrochrysene, and other examples in Table 17. In almost all cases, the nitro-substituted compounds produced more disordered graphites than did the corresponding amino-, hydroxy-, or alkyl-substituted compound. The NO_2 group in the majority of cases appears to cause rupture of the aromatic ring during pyrolysis, producing very reactive non-planar radical intermediates. Further mechanistic studies on nitrogen-substituted aromatics are necessary to understand these results.

3.2.2.4.6. Halogen-Substituted Aromatic Hydrocarbons

Halogen substitution appears to induce the cleavage of carbon-carbon bonds and a disruption of the planar aromatic system. This effect can be seen in the large 002 values for the halogenated anthracenes in Table 18. All of the organic halogen compounds examined showed poor graphite ordering (high 002 values). The majority of the compounds, unlike anthracene, are nonplanar and would be expected to yield rather poor graphite.

3.2.2.4.7. Aromatic Hydrocarbons with Sulfur Substituents

The p-xylylenedithiol was the only sulfur-substituted aromatic compound examined in this study (Table 19). This compound unexpectedly produced an excellent graphite, indicating the probability of simultaneous elimination and condensation reactions to produce a condensed ring system, perhaps of the anthracene type. The graphite spacing of 3.356 Å is comparable to that obtained from acenaphthylene, dibenzo(a,l)pentacene, and naphthacene. In contrast, the dimer, Di-p-xylylene, produced a graphite with an 002 spacing of 3.406 Å, a highly-disordered graphite structure.

3.2.2.4.8. Heterocyclic Compounds

A total of 22 heterocyclic compounds, including oxygen, nitrogen, and sulfur heterocyclics, were examined. Of this group, only one (the diacenaphthothiophene listed in Table 22) produced a highly-ordered graphite, comparable to those obtained from the complex raw materials used to produce synthetic graphite. In addition, several phenazine and quinoxaline compounds which contain two heteronitrogen atoms in 1,4-positions and a tetranitrocarbazole also produced fairly well-ordered graphites with 002 spacings between 3.362 Å and 3.366 Å. All other heterocyclics examined gave highly-disordered graphites. It is postulated that ring-opening reactions occur during pyrolysis, producing nonplanar radical intermediates.

3.2.2.4.9. Reactive Additives

In addition to modifying the thermal reactivity of aromatic hydrocarbons, additives such as benzoquinone, chloranil, and Lewis acids also alter the characteristics of the resultant graphite. In every case shown in Table 23, the effect of the additive was to increase the disorder of the graphite structure to produce a very hard, glassy-type graphites. The p-benzoquinone and chloranil are known to react with polynuclear aromatics through the formation of non-planar adducts. The inorganic SbCl_5 , unlike the organic quinones, cannot contribute materially to the graphite. It is likely that complex formation by the SbCl_5 prevents the continuous planar growth process observed for the uncomplexed hydrocarbons, anthracene, and naphthacene.

3.2.2.5. Conclusions

The results of this X-ray diffraction study have shown that the degree of crystal order of graphites derived from model organic compounds exhibits a strong dependence on the starting chemical structure. The following general conclusions can be made relating chemical structure and thermal reaction mechanisms to graphite properties.

- a. The complex mixtures of aromatic compounds that make up the normal raw materials for manufacturing carbon and graphite products, that is, coal tar pitches and petroleum cokes, form highly-ordered graphites.
- b. The graphites derived from unsubstituted aromatic hydrocarbons show a dependence on the starting molecular structure. The connection is not always obvious, however, and it appears that two major factors are involved:
 - 1) The planarity and steric overcrowding in the original molecule and
 - 2) The chemical reaction sequence and the nature of the thermally formed intermediates.

The hydrocarbons which yield well-ordered graphites (low 002 values) consist largely of fused planar aromatic entities. There is considerable graphite variation among even these types of structures and several exceptions, such as quaterylene and coronene, produce poorly-ordered graphites. In general, the hydrocarbons which yield highly-disordered graphites are largely nonplanar molecules which are devoid of fused polycyclic systems.

It is apparent that no relationship exists between thermal reactivity (carbon yield on pyrolysis) per se and graphite character.

c. Substitution of the aromatic nucleus with strongly activating side groups generally leads to a more disordered graphitic structure. Single or multiple substitution by halogens, nitro, amino, and azo groups results in almost all cases in a degradation of graphite ordering.

d. Oxygen substitution is seen in most instances to result in a more disordered graphite than that obtained from the unsubstituted hydrocarbon. This effect is variable, however, and depends on the site of substitution and the oxygen functionality. The results appear to depend specifically on the thermal reaction mechanism of the oxygenated structure.

These results substantiate empirical observations concerning the effects of oxidation on raw materials, namely, a higher thermal reactivity and a more disordered graphite structure.

e. Alkyl and Aryl substitution of the aromatic moiety enhances thermal reactivity and, in general, results in a highly-ordered graphite. These substituents readily form aromatic radicals and offer a mobile means of rearrangement to planar conjugated systems through radical intermediates.

f. The thermal reactivity of aromatic hydrocarbons can also be modified by reactive additives such as quinones and Lewis acids. These additives affect the character of the derived graphite as well by altering the reaction mechanisms through the formation of nonplanar intermediates. The results in all cases examined were to produce highly-disordered graphites.

g. Heterocyclic compounds generally produced relatively poor graphites with high 002 semilattice spacings compared with the complex raw materials. However, the degree of disorder was highly dependent on the nature of the heterocyclic ring system.

h. These present results illustrate the importance of detailed mechanism studies on model organic systems. Such studies will delineate the general types of thermal reactions which can be related to the starting molecular structure as well as to the ultimate structure of the graphite.

3.3. Pyrolysis Mechanisms of Model Compounds

3.3.1. Introduction

Sections 3.1. and 3.2. have described the general relationships between chemical structure, thermal reactivity, and graphitization behavior for an extensive series of model compounds. Both the thermal reactivity and the graphitization sequence are known to be intricately related to the reaction mechanisms during the initial stages of pyrolysis. A major effort of this program has been the investigation of the pyrolysis mechanisms for a selected group of model compounds. Compounds were chosen which show extremes in carbonization and graphitization behavior and which possess unique structural features.

The detailed pyrolysis studies involved the application of a variety of physical and chemical studies including: thermogravimetric analysis, chromatography, infrared and optical spectroscopy, and electron spin and nuclear magnetic resonance. These techniques have been employed wherever applicable to the pyrolysis mechanism studies of the 13 selected compounds. The compounds are listed in Table 25 along with their thermal reactivities (determined by DTA) and the semilattice spacings of the resultant graphites (measured by X-ray).

Table 25. Model Compounds Employed in Pyrolysis Mechanism Studies

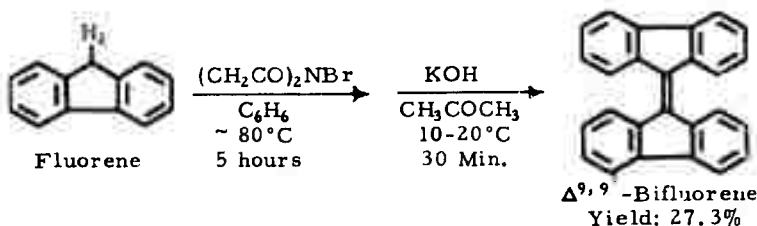
Compound	Coking Value DTA (750°C)	"002" - Spacing, Å°
Acenaphthylene	23.5	3.356
7,12-Dimethylbenz(a)anthracene	4.7	3.358
Naphthacene (tetracene)	13.9	3.358
Fluoranthene	0.0	3.371
Periflanthene	54.7	3.363
9,9'-Bifluorene	5.8	3.374
Δ ^{9,9'} -Bifluorene	28.0	3.474
p-Terphenyl	0.0	3.437
9,9'-Bianthryl	0.0	3.354
10,15-Dihydro-5H-diindeno- (1,2-a;-2'-1'-c)fluorene (α-truxene)	27.8	3.385
9,10-Dibenzylanthracene	8.9	3.412
1,4-Naphthalenediol	52.6	3.360
1,4-Naphthoquinone	40.4	3.370

The experimental techniques are described in Section 3.3.2.; the results are summarized for each compound in Section 3.3.3.; and, finally, our general conclusions on the mechanisms of carbonization are presented in Section 3.3.5.

3.3.2. Experimental Procedure

3.3.2.1. Model Compounds

The compounds listed in Table 25, with the exception of $\Delta^{9,9'}$ -bifluorene, were obtained from commercial sources. All the materials were purified by solvent recrystallization prior to use. The compound $\Delta^{9,9'}$ -bifluorene was synthesized by the method outlined below.



3.3.2.2. Thermal Analysis Measurements

3.3.2.2.1. Differential Thermal Analysis (DTA)

DTA measurements were made on the compounds before the more detailed pyrolysis studies. The apparatus, experimental conditions, and general techniques have been described previously⁽¹⁾.

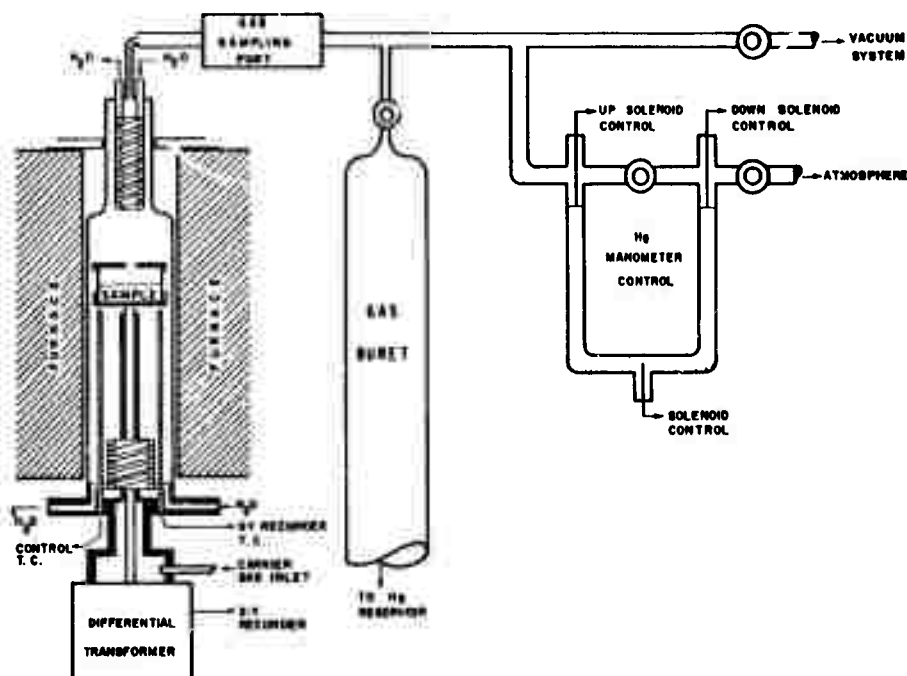
3.3.2.2.2. Thermogravimetric-Gas Evolution Analysis (TGA-GE)

Thermogravimetric analysis (TGA) is a commonly used technique which involves the continuous measurement of the weight of a sample while it is heated at a uniform rate. The simultaneous measurement of the weight change and the evolution of noncondensable gases from a hydrocarbon system during pyrolysis provides additional information important to an understanding of the carbonization mechanisms.

We have developed an apparatus in which materials can be pyrolyzed under precisely controlled conditions of atmosphere, pressure, and temperature. The sample weight and the volume of fixed gases evolved are monitored and recorded continuously. The condensable volatile products are collected and prevented from undergoing secondary reactions. From such experiments, the rate and extent of distillation of unreactive components, as well as considerable information about the thermally reactive species, can be deduced. Periodic removal and analysis of the

products during the course of the pyrolysis permits some inferences as to reaction mechanisms.

The TGA-GE apparatus⁽⁴⁾ has undergone continual evolutionary modification as a result of difficulties encountered with different materials. A schematic drawing of the modified TGA-GE apparatus is shown in Figure 6.



N-5818

Figure 6. Schematic Diagram of TGA-GE Apparatus

The tarry condensable products always produced in the pyrolysis of hydrocarbons have presented the major problems with the apparatus. These materials had to be removed from the pyrolysis zone and controlled so that they could not undergo secondary reactions or affect the operation of the balance.

The change from an argon to a helium atmosphere drastically changed the buoyancy of the hydrocarbon vapors. They descended to the lower end of the pyrolysis chamber instead of rising to the condenser

above the sample container. The most satisfactory pyrolysis chamber design for use with hydrocarbon systems is shown in Figure 6. The covered sample container with a small hole in the cover was used to maintain a relatively high vapor concentration over the reacting sample, thus favoring a thermal reaction process over simple distillation.

A method was developed for removing gas samples periodically using gas-tight syringes and storing them until they could be analyzed by gas chromatography. The disposable plastic syringes, available through medical supply houses, have been found to be superior to the Hamilton-type syringes.

Diffusion of helium and hydrogen through the plastic bodies was found to be negligible in the times involved in these experiments. A vestibule-type gas-sampling port which could be alternately evacuated and flooded with helium completely eliminated contamination of the gas samples with air. A gas sampling port was put in the pyrolysis chamber exit line so that gas samples could be taken with a minimum of mixing with the accumulated gases. A second gas sampling port (not shown in Figure 6) was also installed at the top of the gas buret to sample the accumulated gases.

The performance characteristics of the TGA-GE apparatus are as follows:

The sensitivity of the balance is 0.1 per cent.

The gas evolution detection system measures the change in height of the mercury column in the gas collection buret. A change in height of 0.25 mm can be detected. With the 20 mm diameter gas buret used in these experiments, a sensitivity of about 0.08 cc is achieved. A total volume change of 250 cc can be accommodated. The volume of the pyrolysis chamber and the inert gas flow rates had to be kept small. Measurements were made to determine the degree of reproducibility of the volume expansion of the gas in the furnace section of the system and the uniformity of the inert gas flow rates. The volume expansion and gas flow rates must be used to correct the measured evolution in order to determine the true gas evolution curves of the sample. We found that the volume expansion correction was reproducible at all temperatures to within 0.7 cc for any given inert atmosphere. Measurements on helium flow rates between 0.20 cc per minute and 2.0 cc per minute were made for periods of eight hours. In all cases, flow rates were found to fluctuate about ± 0.035 cc per minute on a 15- to 30-minute cycle. Consequently, fluctuations in gas evolution rates, as shown in the fine structure of the derivative gas evolution curves, are interpreted to have originated with the sample.

3.3.2.3. Electron Spin Resonance (ESR) Measurements

ESR investigations of the pyrolysis of a number of the compounds listed in Table 25 were performed by the general method described previously.^(5,6) The pyrolyses were performed in an improved high-temperature cavity which had been redesigned to accommodate larger samples

than previously possible. This cavity enabled measurement of samples in situ at temperatures as high as 550°C. Seven of the compounds in Table 25 were examined by this method. The hydrocarbons were generally measured as solutions in m-quinquephenyl. Several variations of temperature and concentration were employed for each system in an attempt to improve the resolution of the ESR spectra.

3.3.2.4. Chemical Studies of Pyrolysis

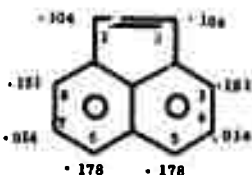
Independent chemical studies of the pyrolysis reactions for the compounds in Table 25 were conducted. The following procedure was employed:

The compounds were initially purified by solvent recrystallization. The pyrolysis assembly consisted of a Vycor tube inserted in a tube furnace and directly connected to a sulfuric acid trap. A 1-gram sample was placed in a ceramic boat and heated at approximately 15°C per minute in a continually flowing argon atmosphere. The compounds were heated to temperatures at which thermal reactions were indicated in the DTA thermograms. The condensates and residues were collected and examined by infrared and ultraviolet spectroscopy. A single residue was then selected and subjected to detailed study. The residue was chromatographically separated on an alumina column. The chromatographic column was protected from light and maintained in a nitrogen atmosphere. Infrared, ultraviolet and nuclear magnetic spectra, and melting point determination were made on individual chromatographic fractions.

3.3.3. Experimental Results

The experimental results from the pyrolysis mechanism studies for each compound are discussed individually. Quantitative estimates of the reactivity have been provided for most of the compounds.

3.3.3.1. Acenaphthylene



The mechanisms of the pyrolysis of acenaphthylene have been described previously.^(4,6,7) This report discusses additional attempts at isolation and identification of thermal reaction products of acenaphthylene.

3.3.3.1.1. TGA-GE Analysis of Acenaphthylene

Two thermogravimetric-gas evolution analysis experiments (Runs 47 and 48) were performed on acenaphthylene. This compound has been studied in considerable detail because its thermal behavior results in excellent carbon yields and because the carbon structure, being well-ordered, produces a good graphite upon heating to 3000°C.

The DTA and TGA-GE curves obtained for acenaphthylene are shown in Figure 7. The experimental conditions and results for Run 48 are given in Figure 7. In Run 47, argon was used to maintain an inert atmosphere and the flow rate averaged 1.96 ± 0.15 cc/minute over the approximate 8-hour period required to complete the run. This 8-hour period included 2 hours to measure the gas flow rate at constant temperatures before heating was started, 4 hours to heat and cool the sample, and 2 hours to recheck the gas flow rate at room temperature. In Run 48, the argon was replaced with helium gas and an average flow rate of 0.86 ± 0.10 cc/minute was used. The change to helium was made in order to increase the sensitivity of the gas chromatographic analysis of the fixed gas products and in order to permit the detection of oxygen in the gases.

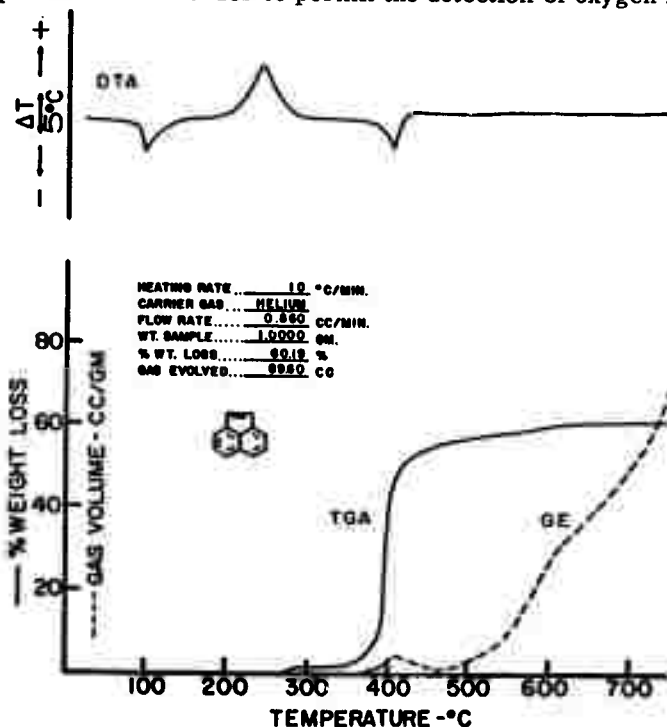


Figure 7. DTA, TGA-GE Thermograms for Acenaphthylene (Run 48)

N-7122

The results for Runs 47 and 48 are in close agreement, indicating no significant effect resulting from the differences in inert atmosphere or from differences in the flow rates. The derivative curves for Run 48 of the weight loss rate and gas evolution rate for acenaphthylene as a function of temperature are shown in Figures 8 and 9. In Figure 9, the weight loss and gas evolution curves have been corrected for the residue remaining in the reaction cup at the indicated temperature.

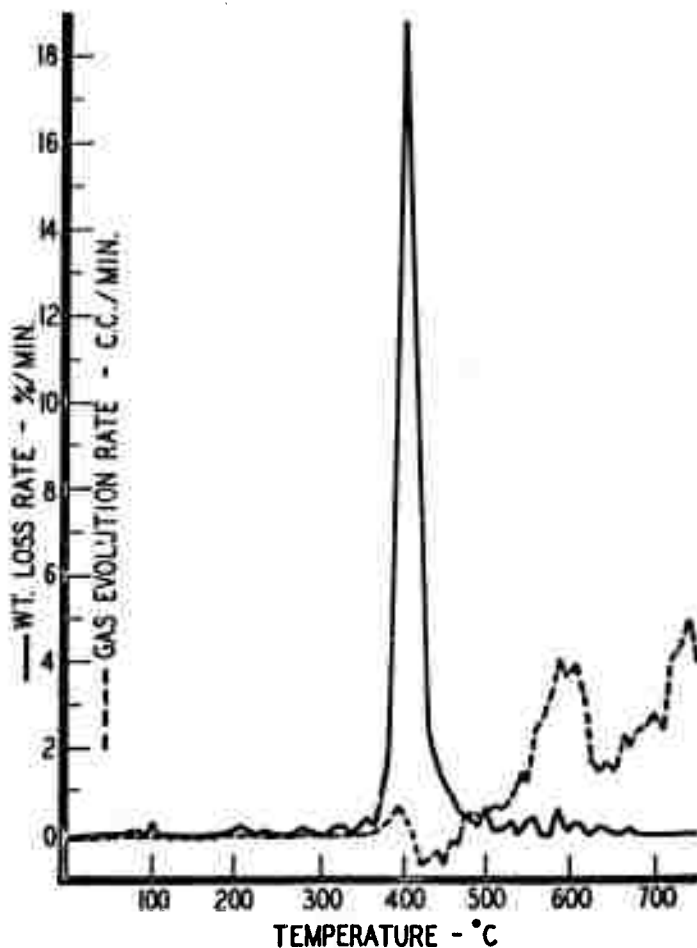
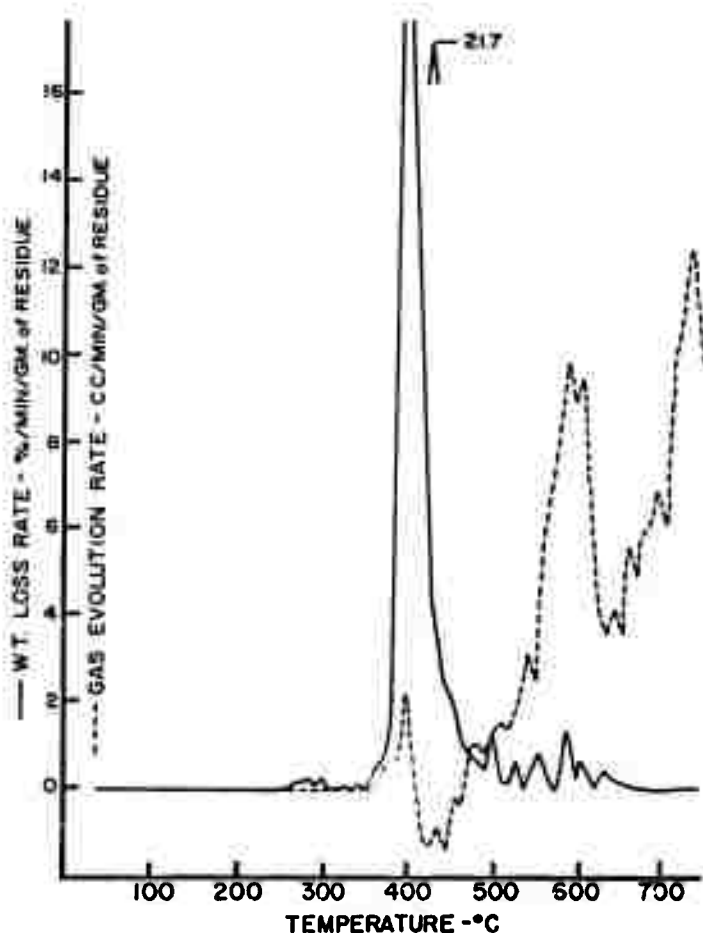


Figure 8. Thermogravimetric-Gas Evolution and Weight Loss Rates for Acenaphthylene (Run 48)

N-7118



N-7119

Figure 9. Thermogravimetric-Gas Evolution and Weight Loss Rates for Acenaphthylene Expressed Relative to Amount of Residue in Reaction Cup (Run 48)

Acenaphthylene melts at approximately 95°C, and a very slight weight loss was registered at this temperature. The vaporization of acenaphthylene between 100° and 200°C that was reported in an earlier experiment⁽²⁾ using a shallow open sample cup was largely suppressed

in these experiments. The plateau in the weight loss curve between 200° and 365°C, which occurs because of the thermal stability of the poly-acenaphthylenes, was at 1 per cent weight loss as compared with about 15 per cent in the open cup experiments. At 360°C, the polymer begins to react thermally, producing a large amount of volatile material. Infrared analysis of the condensate showed it to be 80 to 90 per cent acenaphthene, with small amounts of acenaphthylene, ethyl naphthalene, and some unidentified mixtures which are probably methyl naphthalenes and naphthalene. The weight losses above 500°C were small and were due to the loss of fixed gases rather than higher molecular weight hydrocarbons. The gas evolution curves indicate that low molecular weight gases begin to appear around 475° after the major weight loss has been completed. The gas evolution shows a maximum rate near 600°C and a second maximum at about 735°C.

The results of analyses of the fixed gases taken at progressively higher temperatures during the course of these runs are given in Table 26. Samples taken at temperatures below 500°C contained no evolved gas and are not listed in the table.

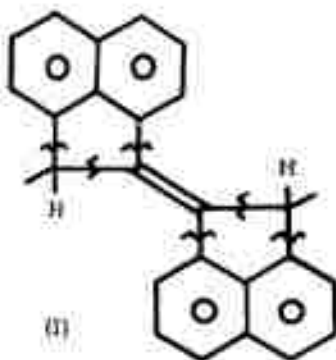
Table 26. Composition of the Fixed Gases Evolved During the Pyrolysis of Acenaphthylene in Helium, TGA-GE (Run 48)

Temp. When Sample Taken → Gas	Mol % of Gas in Fraction			
	510°C	613°C	735°C	750°C *
Hydrogen (H ₂)	87	67	70 **	81
Methane (CH ₄)	5	28	25	16
Ethane (C ₂ H ₆)	4	2	2	2
Ethylene (C ₂ H ₄)	0	1	1	~ 0.1
Carbon Monoxide (CO)	4	1	2	1
Carbon Dioxide (CO ₂)	0	0.4	0	trace

* Average of three duplicate analyses.
 ** Hydrogen peak reversed - not accurate.

3.3.3.1.2. Chemical Studies of Pyrolysis Intermediates

Extensive chemical studies of the carbonization of acenaphthylene have been reported previously. ^(2,4,5) The initial reactions of carbonization were shown to involve thermal carbon-carbon bond cleavage within the 5-membered ring systems of polymeric acenaphthylene units (I).



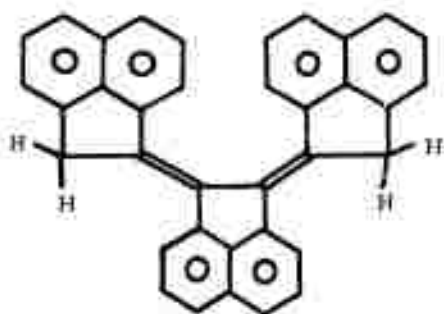
These reactions can lead to the formation of a variety of alkyl substituted naphthalene free radicals depending on the mode of bond cleavage. These mobile radicals can readily rearrange during the carbonization process to form planar conjugated aromatic hydrocarbons, such as zethrene (III). The condensation of such structures produces the planar aromatic units required for ordered graphite.

We have attempted to isolate some additional condensation products from the pyrolysis of acenaphthylene by chromatographic techniques. A sample of acenaphthylene was heated to 450°C, and the black residue was subjected to chromatographic separation. In addition to the reaction products such as acenaphthene, biacenaphthylidene, and decacyclene which could be readily identified and were reported earlier, the following materials were obtained.

1. Fraction 9 - A Red Hydrocarbon Product

The infrared spectrum of this material was quite similar to that of biacenaphthylidene. The ultraviolet-visible absorption spectrum of Fraction 9 is shown in Figure 10a. This spectrum shows a pattern of absorption bands identical to biacenaphthylidene; however, the absorption bands for Fraction 9 are all at a wavelength about 20 mμ longer than those of the latter compound. From the physical and spectral data, this red fraction appears to be identical to the hydrocarbon fluorocyclene which was first isolated by Dziewonski and Leyko.⁽⁷⁾ These investigators did not assign a structure to fluorocyclene, although they envisioned it as a tetramer of acenaphthylene. The structure of Fraction 9 is thought to be a conjugated triacenaphthylidene (II).

A cyclic product, decacyclene (IV), is known to form from the pyrolysis of acenaphthylene. The compound (II) may be considered a linear analog of decacyclene. The increased conjugation for (II) relative to biacenaphthylidene (I) could cause the shift in the UV absorption spectrum.



(II)

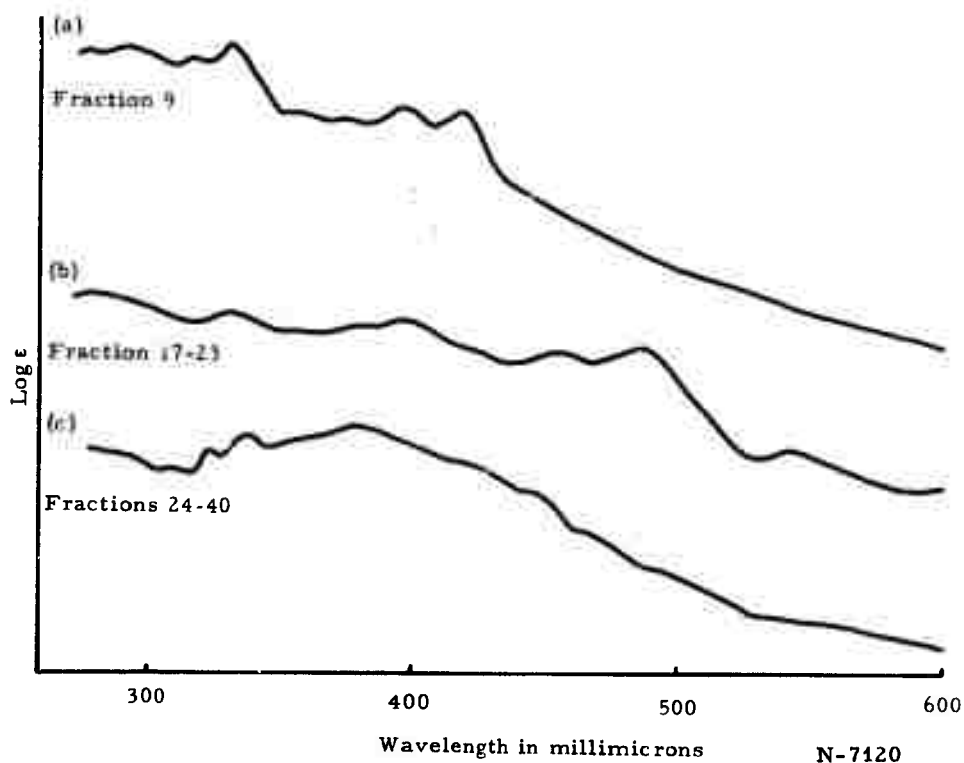
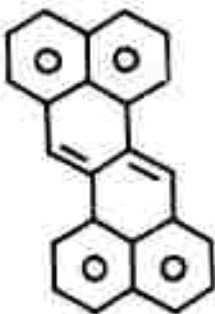


Figure 10. Ultraviolet Spectra of Chromatographic Fractions of Heat-Treated Acenaphthylene, Solvent: Benzene

2. Fraction 11 - Red Hydrocarbon

This material is believed to be the hydrocarbon zethrene (III). In the presence of light and air, it underwent rapid oxidation and self-hydrogen-transfer to form a green hydrogenated derivative.



(III)

3. Fractions 17 to 23 - Red Hydrocarbon

This compound was one of the major products obtained from the pyrolysis of acenaphthylene at 450°C. At first we thought that this substance was zethrene. The UV-visible spectrum, which is shown in Figure 10b, resembles that of zethrene but is definitely different.^(a) The infrared spectrum for Fractions 17 to 23 shows a strong aliphatic C-H absorption and a complicated aromatic substitution pattern.

This material was insoluble in concentrated H₂SO₄ but gave a purple solution with SbCl₅ which showed a paramagnetic resonance. No reference to a compound which resembled this substance could be found in the chemical literature. The visible absorption spectrum with bands at 544, 486, and 454 mμ is indicative of a highly conjugated aromatic system and resembles that of highly condensed pyrene and perylene derivatives.

This red hydrocarbon could be a hydrogenated derivative of an aromatic condensation product formed from three or four acenaphthylene units. Due to the mobility of the acenaphthylene side chain, numerous structural possibilities exist for such products. Further structural studies are needed to chemically characterize this hydrocarbon.

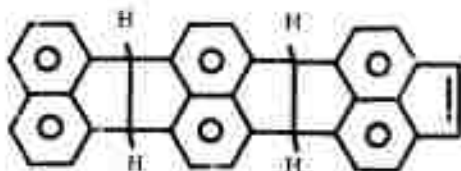
4. Fractions 24 to 40 - Brown Hydrocarbon

The last major product, Fractions 24 to 40, was a brown hydrocarbon which came off the column along with the decacylene (IV).



(IV)

The optical spectrum for Fractions 24 to 40 is shown in Figure 10c and exhibits a poorly resolved absorption region extending into the visible. This type of unresolved absorption is typical of nonconjugated acenaphthene or acenaphthylene units. The infrared spectrum of the brown fraction shows evidence of both acenaphthylene and acenaphthene ring units. The condensation product (V) postulated by Dziewonski⁽⁹⁾ is a likely structure for this material.



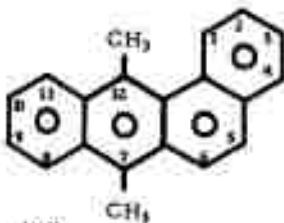
(V)

Structure (V), which has been named leukacene, could readily form through condensations at the reactive 1, 2 and 5, 6 positions of acenaphthylene molecules.

3.3.3.1.3. Thermal Reactions of Acenaphthylene

The TGA-GE and chemical data obtained for acenaphthylene are consistent with the thermal reaction sequence previously proposed.⁽⁴⁾ The important first reactions involve rearrangements of alkyl substituted naphthalene radicals to planar aromatic units. A number of different aromatic species of the shape and size of zethrene form between 400° and 500°C. Above 500°C, the aromatic growth occurs by direct dehydrogenation between these planar units. The formation of methane above 600°C is a result of the cleavage of the remaining aliphatic side chain groups.

3.3.3.2. 7, 12-Dimethylbenz(a)anthracene

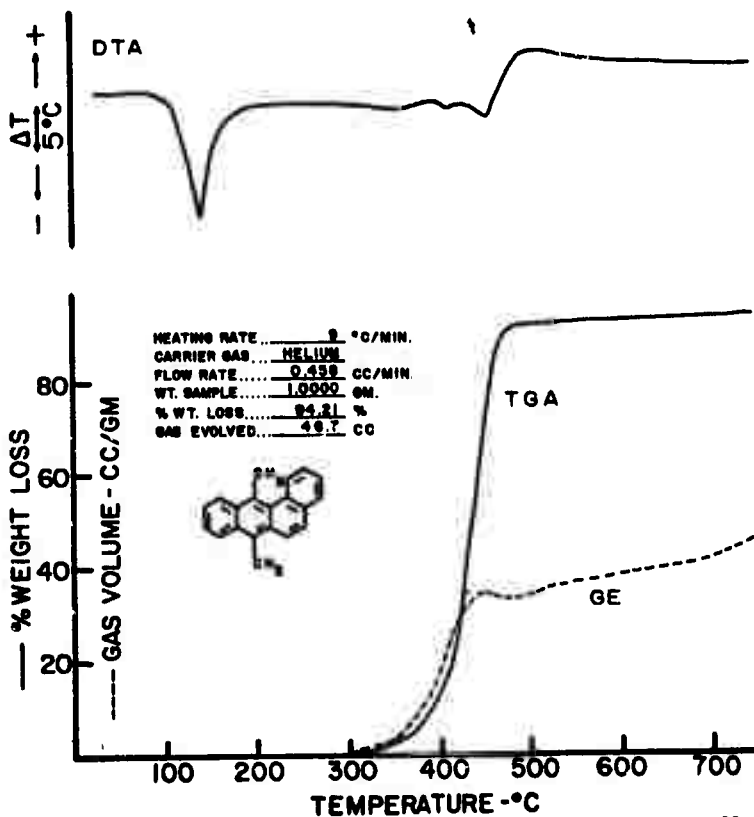


(VI)

The compound 7, 12-dimethylbenz(a)anthracene (VI) like acenaphthylene, can be converted to a highly-ordered graphitic carbon. The former compound was selected for study in order to determine the manner in which methyl substituents increase the thermal reactivity of aromatic hydrocarbons.

3.3.3.2.1. Differential Thermal Analysis (DTA)

The DTA thermogram for (VI) (shown in the upper portion of Figure 11) exhibits a complex thermal sequence between 300' and 500°C.⁽¹⁾ The strong endotherm associated with the rapid evolution of volatile products is almost entirely compensated for by the exothermic chemical reactivity in this temperature region.



N-6946

Figure 11. Differential Thermal Analysis, Thermogravimetric and Gas Evolution Curves for the Pyrolysis of 7, 12-Dimethylbenz(a)anthracene (Run 56)

Interrupted DTA experiments between 315°C and 425°C were performed in order to examine the condensates and residues. Both the condensate and the residue obtained at 300°C were primarily the starting compound, although there was some evidence that thermal reactions were progressing. The condensate obtained at 425°C was almost identical to that obtained at the end of the 750°C DTA and TGA experiments, a complex mixture of methyl- and di-methyl benzantracenes. The 425°C residue is a black, viscous tar which gave a very complex infrared spectrum. The spectrum showed very strong methyl C-H bands which were more intense than those given by the starting dimethyl compound. A strong band around 11.4 microns resulted from isolated ring hydrogens. Other bands indicated the presence of pyrenes and 3,4-benzopyrenes.

3.3.3.2.2. TGA-GE of 7, 12-Dimethylbenz(a)anthracene, (Run 56)

The TGA-GE thermograms of 7, 12-dimethylbenz(a)anthracene (VI) are shown in Figure 11. The derivative TGA-GE curves are given in Figures 12 and 13. In Figure 13, the derivative curves have been corrected for the weight of residue remaining in the reaction chamber at the indicated temperature. The experimental conditions are tabulated in Figure 11.

7, 12-Dimethylbenz(a)anthracene melts at 122°C and begins to distill slowly near 250°C. Distillation is nearly complete at 460°C. The evolution of fixed gases begins near 300°C and continues at a slow rate to approximately 340°C. Between 340° and 450°C, gas evolution is rapid; above 450°C, the rate again drops off. The decrease in total gas evolved that occurs between 450°C and 460°C is caused by the condensation of some of the volatiles after their formation has ceased. Above 460°C, the weight loss and gas evolution are caused by the dehydrogenation and demethylation of the residual polymer as it carbonizes.

The composition of the gases evolved during the pyrolysis was determined at 50°C intervals by gas chromatographic analysis. The results are summarized in Table 27. Below 350°C, no effluent gas, other than a small amount of residual oxygen, was detected. At 350°C, methane appeared; at 400°C, small amounts of ethane, ethylene, and propane were also found; and at 450°C, hydrogen was detected. At higher temperatures, the concentration of hydrogen increased and that of methane decreased. Methane was the major gaseous product, accounting for 84.5 mol per cent of all the gas evolved. In Table 28, the composition of the total gas collected is summarized in terms of volume, weight, and moles of each gas. The last column gives the ratio of the moles of gas evolved per mole of (VI) in the original sample.

Infrared and ultraviolet absorption analysis of the condensable products collected during the pyrolysis indicate these products are mostly methyl and dimethylbenzantracenes. NMR data also indicated the presence of dihydrobenz(a)anthracene.

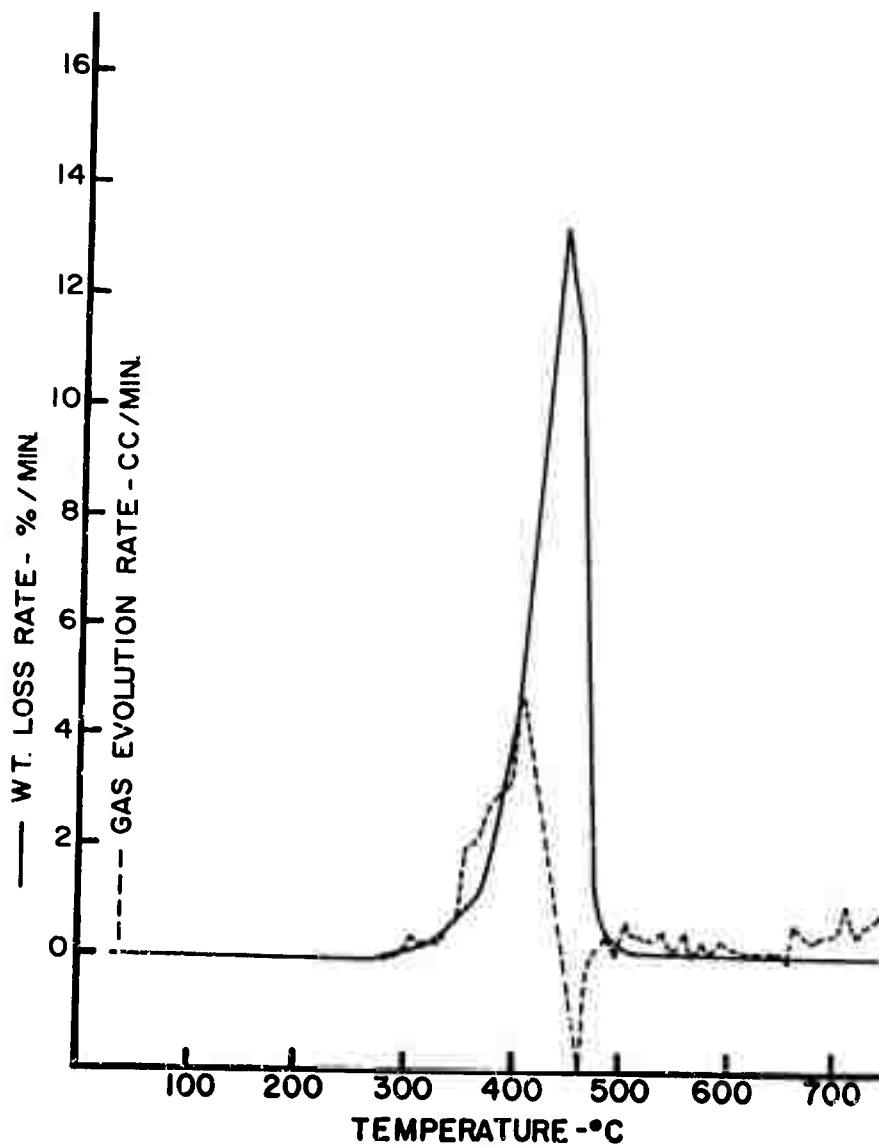
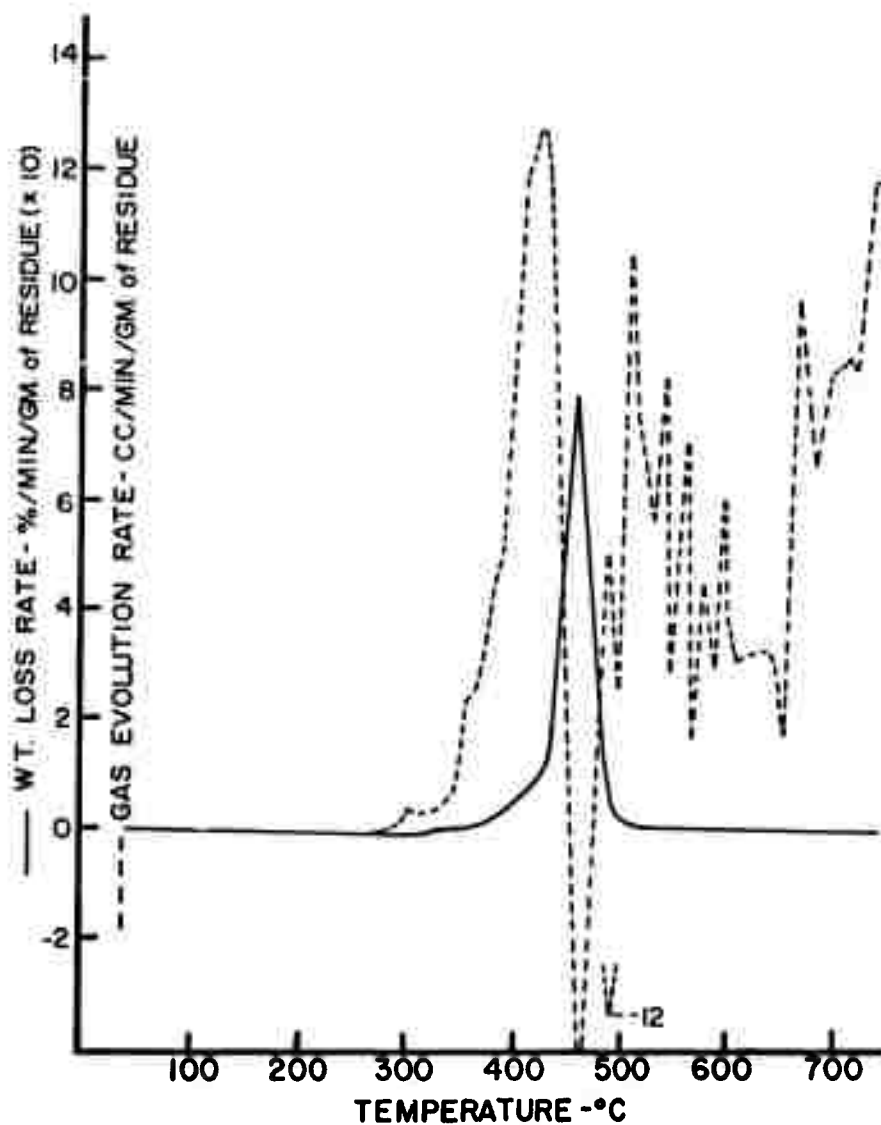


Figure 12. Weight Loss and Gas Evolution Rate Curves for the Pyrolysis of 7, 12-Dimethylbenz(a)anthracene (Run 56) N-6947



N-6948

Figure 13. Weight Loss and Gas Evolution Rate Curves for the Pyrolysis of 7, 12-Dimethylbenz(a)anthracene Expressed Relative to Amount of Residue in Reaction Cup (Run 56)

Table 27. Composition of Effluent Gas Collected at Various Temperatures During Pyrolysis of 7, 12-Dimethylbenz(a)anthracene (TGA-GE Run 56)

Gas	Temp. When Sample Taken		350°C Mol. %	400°C Mol. %	447°C Mol. %	553°C Mol. %	600°C Mol. %	648°C Mol. %	705°C Mol. %	750°C Mol. %	Gas Buret* Mol. %
	Mol. %										
O ₂	100		2.8	1.4	0.6	1.0	1.1	1.7	1.4	1.7	3.9
H ₂	-		-	-	sl.trace	9.5	14.1	18.7	25.4	41.1	9.0
CH ₄	-		97.2	94.5	95.4	85.2	80.8	76.3	70.8	55.0	84.5
C ₂ H ₆	-		-	2.3	3.0	3.4	3.3	2.7	1.7	1.0	2.0
C ₃ H ₈	-		-	1.7	0.9	0.7	0.7	0.6	0.7	1.0	0.6
C ₃ H ₆	-		-	trace	0.2	0.1	0.1	0.1	trace	sl.trace	trace
CO	-		-	-	-	-	-	-	-	0.1	-
CO ₂	-		-	-	-	-	-	-	-	-	-
Total	100		100	100	100	100	100	100	100	100	100

* Total accumulated gases evolved during entire pyrolysis. See Table 28 for more detailed analysis of these gases.

Table 28. Measured and Calculated Compositions of Total Fixed Gases Collected During Pyrolysis of 7, 12-Dimethylbenz(a)anthracene (TGA-GE Run 56)

Gas	Gas Sample #16 Taken From Gas Buret. Mol. %	Volume of Each Gas Evolved cc	Moles of Each Gas Evolved Moles	Total Weight of Each Gas Evolved Grams	Moles of Each Gas per Mole of Starting Material 1.0 gm = .00391 Moles
O ₂	3.9	1.82	.0000814	.0026	.021
H ₂	9.0	4.20	.000188	.0004	.048
CH ₄	84.5	39.40	.00176	.0282	.450
C ₂ H ₆	2.0	0.93	.0000415	.0013	.011
C ₄ H ₆	0.6	0.28	.0000125	.0004	.003
C ₃ H ₈	Trace	0.07 (by diff.)	.00000313	.0001	.001
CO	None	0.00	.00	.0000	.00
CO ₂	None	0.00	.00	.0000	.00
Total	100.0	46.70	.0020865	.0330	0.533

3.3.3.2.3. ESR Measurements

The pyrolysis of dimethylbenz(a)anthracene (VI) was studied by ESR. ESR experiments were performed for pure (VI) and for 10 per cent solutions of (VI) in m-quinquephenyl. With pure (VI), an ESR signal was first observed at 450°C. This signal was totally unresolved when measured at 200°C and consisted of a single line 10 gauss wide. A 10 per cent solution of (VI) did not exhibit any ESR until 500°C. The only spectrum obtained for this solution when measured at lower temperatures was that of a single broad line.

The dimethylbenz(a)anthracene ESR signal indicates that the observed broad line can be attributed to unresolved proton hyperfine structure of radicals in solution. The large number of inequivalent protons in the starting compound could lead to a considerable overlapping of the hyperfine components and a lack of resolution in the spectrum of the free radical. This result is consistent with the observation of a poorly-resolved spectrum for the radical cation of (VI) as discussed in Section 3.4.2.

3.3.3.2.4. Chemical Studies of Pyrolysis

Figures 14 and 15 show a series of infrared and ultraviolet spectral curves for residues of (VI) pyrolyzed between 400° and 500°C. Changes in band intensities at 6.9, 11.4, and 13.4 microns are evident in the infrared spectrum of the 400°C residue. A major change is observed in the 450°C spectrum. The 13.4 micron band intensity (four adjacent hydrogens)

has broadened and increased relative to the 12.4 micron band. The bands between 14 and 15 microns are largely gone. A major band at 11.4 microns (single hydrogen) has developed. The material has also become less aliphatic. At 500°C, the bands at 11.4 and 13.4 microns have become the dominant ones. Additional structural changes and greater aromatization are indicated by the remainder of the spectrum.

The ultraviolet spectra for the identical series show pronounced changes in the UV-visible region with progressing temperature. The major absorptions of the benz(a)anthracene ring system at 320 to 380 millimicrons diminish, and new bands at 370, 388, 410, 440, and 540 millimicrons develop.

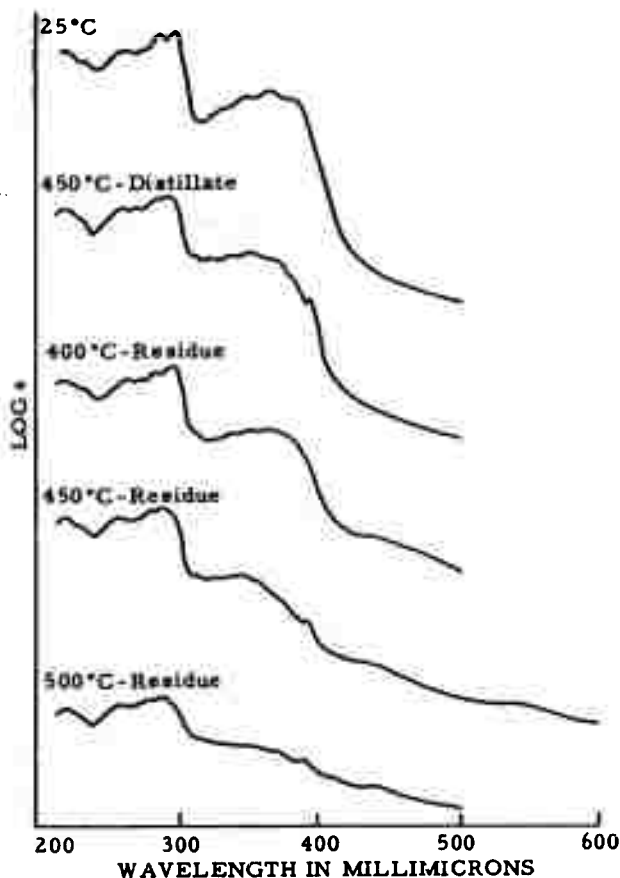


Figure 14. Ultraviolet Spectra of Pyrolyzed
7, 12-Dimethyl(a)anthracene

N-5852

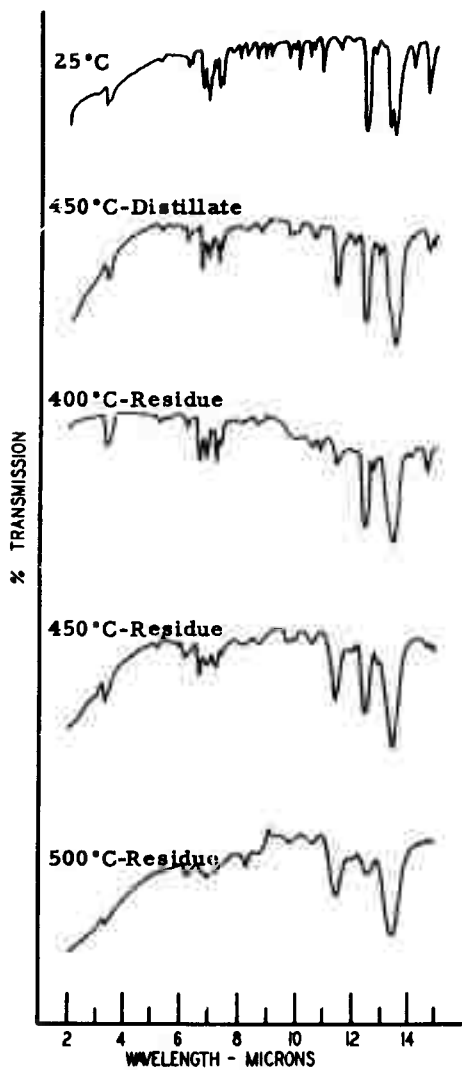
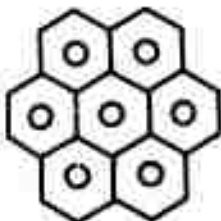


Figure 15. Infrared Spectra of Pyrolyzed 7, 12-Dimethylbenz(a)anthracene

N-5851

A one-gram sample of (VI) was heated to 450°C in the pyrolysis apparatus. The resultant black residue was chromatographically separated. The distillates of the 450°C pyrolysis were collected and their IR and UV absorption spectra are recorded in Figures 14 and 15.

NMR measurements were made on the distillate and residue obtained at 450°C. The NMR spectra showed a marked decrease in the 12-methyl group intensity, the formation of naphthenic ring hydrogens at 4.1 ppm., and the development of an extremely downfield aromatic proton peak at 8.8 ppm. The latter is similar to the chemical shift observed for the protons in coronene (VII) in which the large ring size results in an extensive ring-current effect.

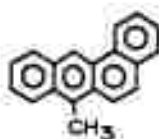


(VII)

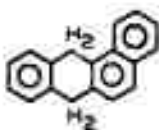
About 40 fractions were obtained from the chromatographic separation on an alumina column of the 450°C pyrolysis residue. In spite of precautionary measures taken to exclude oxygen during the chromatographic process, several of the last fractions were found to be aromatic quinones. Absorption spectra of these substances indicated that they were highly condensed and they are believed to have been formed by alumina catalyzed oxidation of reactive radical intermediates.

A close similarity was found between the infrared spectra of these oxidized products and those from naphthacene. Both showed a single dominant aromatic substitution band at 13.5 microns and major bands at 9.4, 8.9, 7.8, 6.9, 6.2, and 5.85 microns.

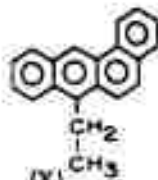
One of the major products separated in the early chromatographic fractions was identified as 7-methylbenz(a)anthracene (VIII). Two other low molecular weight products were characterized as dihydrobenz(a)anthracene (IX) and 7-ethylbenz(a)anthracene (X), based on IR and NMR spectra. A small quantity of a wax-like aliphatic hydrocarbon material was also isolated. The predominant condensation product separated from the 450°C residue was a red-brown methylated aromatic hydrocarbon. Its UV absorption spectrum contained bands at 532, 490, and 460 millimicrons. This product is also believed responsible for the NMR aromatic proton peak observed at 8.8 ppm for dimethylbenzanthracene pyrolysis residue.



(VIII)

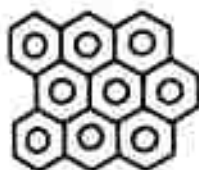


(IX)



(X)

The closest analogs that could be found in the published literature were dibenzo(bc, ef)coronene (XI) (with absorption bands at 536, 496, and 463 millimicrons) and 1,2,7,8-dibenzoperylene (XII) (with bands at 558, 516, and 478 millimicrons).⁽¹⁰⁾



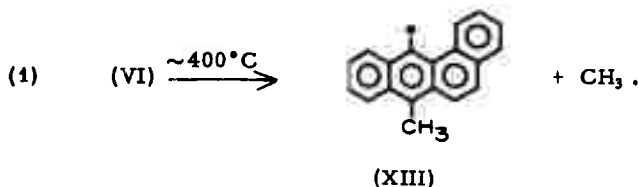
(XI)



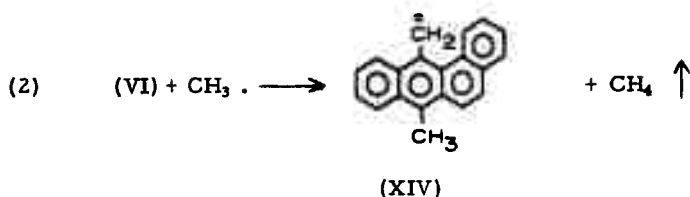
(XII)

3.3.3.2.5. Thermal Reactions of 7,12-Dimethylbenz(a)anthracene

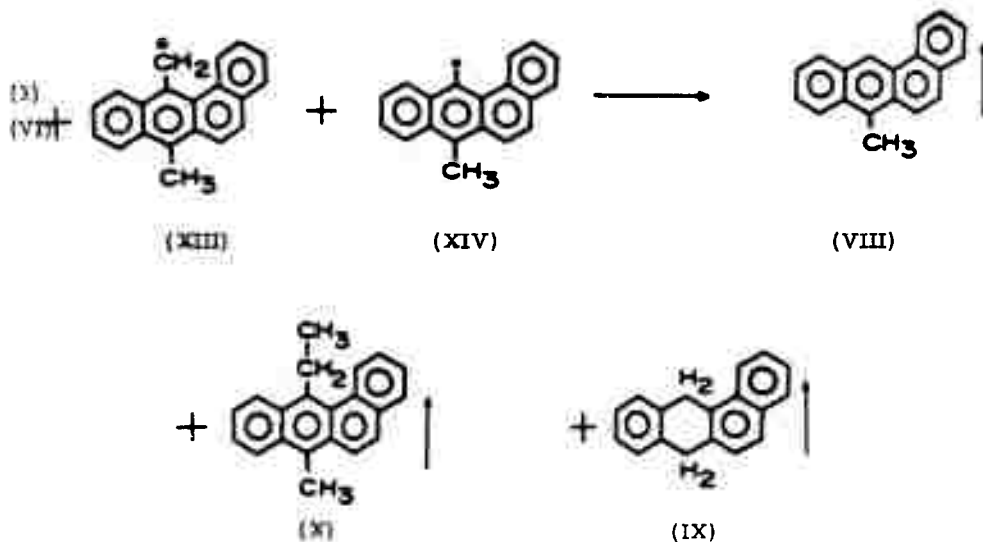
On the basis of the combined pyrolysis studies, a reaction sequence can be proposed for the carbonization of (VI). The initial step involves the cleavage of the methyl group at the 12-position to yield a methyl radical and a 7-methylbenz(a)anthryl radical (XIII).



The 7 and 12-positions are the most reactive in the benz(a)anthracene molecule. Molecular models show that the 12-methyl group is highly strained through interference with the hydrogen at the 1-position. Thus, the easy thermal cleavage of the 12-methyl group is expected. The reactive methyl radicals can readily abstract hydrogens from the starting material (VI) to form methane and 7-methyl-12-benz(a)anthryl-methyl radical (XIV) as the most likely products.



The free radicals (XIII) and (XIV) are thought to contribute to the ESR spectrum observed for (VI) at about 450°C. Due to the unsymmetrical nature of these radicals, the observation of hyperfine structure would not be expected in the ESR experiment. Both (XIII) and (XIV) can undergo hydrogen and methyl abstraction to form the various volatile hydrocarbon products, (VIII), (IX), and (X).



Hydrogen abstraction can also involve the protons on the aromatic ring. Subsequent methyl rearrangement would lead to the isomeric monomethylbenz(a)anthracenes.

The aromatic radicals (XIII) and (XIV) can condense into dimers of varying structural configuration, such as (XV), (XVI), and (XVII). These products are expected to show optical and NMR spectra similar to those found for the major condensation products of (VI).

Further reactions (Figure 16) would induce additional polymerization and aromatization through dehydrogenation and demethylation reactions. Because of the general symmetry of the dimeric products, these condensations are expected to produce large planar aromatic molecules, such as (XVIII).

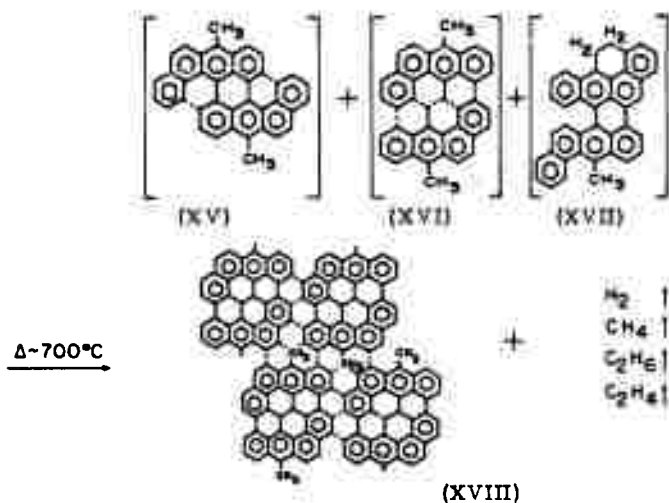
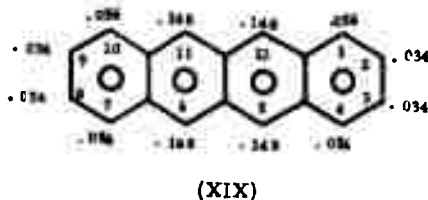


Figure 16. Postulated Carbonization Sequence for N-7121
7, 12 - Dimethylbenz(a)anthracene

3.3.3.3. Naphthacene



Naphthacene can be converted to a high yield of a well-ordered graphite. The unpaired spin densities for a naphthacene free radical are shown with the accompanying structural formula. The 5, 6, 11, and 12-positions possess the highest spin density and are expected to be the most reactive positions.

3.3.3.3.1. Differential Thermal Analysis (DTA) of Naphthacene

The DTA thermogram of naphthacene shows an endotherm starting at the melting temperature of 343°C followed by an exothermic reaction sequence between 450°C and 525°C. The DTA thermogram of naphthacene is shown in Figure 17 together with the TGA and GE thermograms.

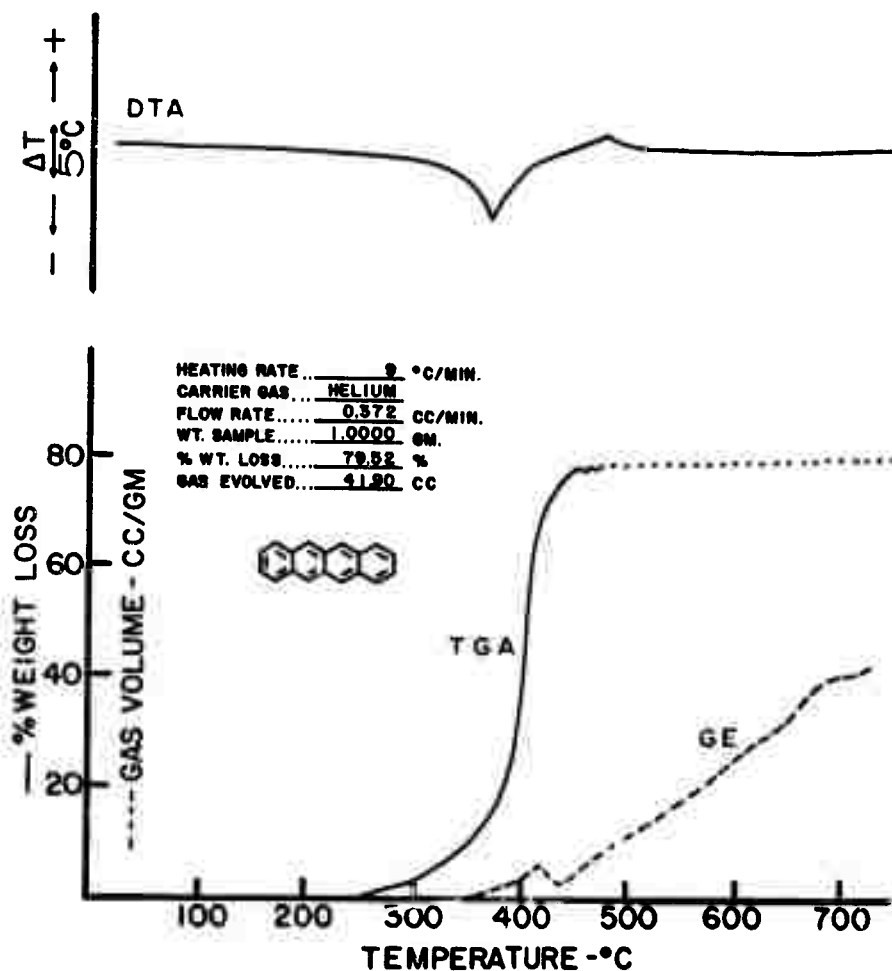


Figure 17. Thermogravimetric and Gas Evolution Curves for the Pyrolysis of Naphthacene (Run 55)

3.3.3.3.2. Thermogravimetric and Gas Evolution Analysis of Naphthacene (Run 55)

Naphthacene was an extremely difficult material to study in the TGA-GE apparatus. Its high volatility near the melting point and the very long, hairlike crystals which formed a bridge between the balance staff and the pyrolysis tube and the condenser coils forced us to make numerous modifications of the apparatus before a successful experiment was completed. Even in this run, the balance seized at 480°C; but, since 99 per cent of the total weight loss was recorded at this point, it was felt that a simple linear extrapolation of the data to the end of the run at 725°C was valid and that little or no information was lost.

The thermogravimetric and gas evolution curves are plotted in Figure 17. The derivative curves of the weight loss and gas evolution are given in Figures 18 and 19. In Figure 19, the derivative curves were recalculated relative to the amount of residue remaining in the reaction cup at the indicated temperature. The experimental conditions are tabulated in Figure 17.

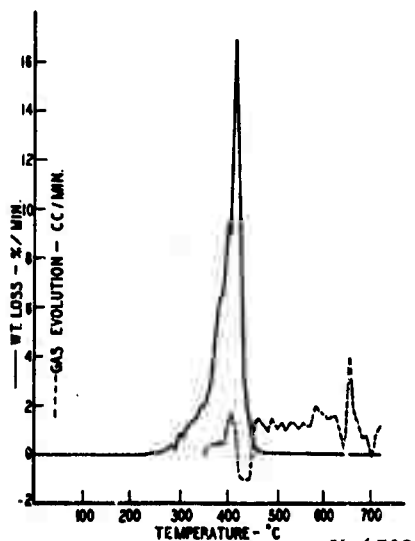


Figure 18. Weight Loss and Gas Evolution Rates for Naphthacene (Run 55)

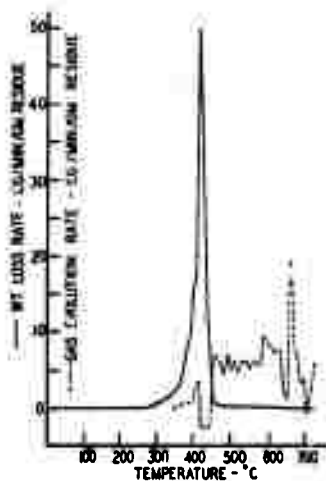


Figure 19. Weight Loss and Gas Evolution Rates for Naphthacene (Run 55) Expressed Relative to Amount of Residue in Reaction Cup

Naphthacene began to sublime approximately 100°C below its melting point of 343°C. After melting, the weight loss (Figure 19) rose very sharply for several minutes; at 420°C, it began to slow; and, above 460°C, very little additional weight loss occurred. Since the TGA balance seized at 480°C, an extrapolated dotted line is shown at the higher temperatures. The residue and cup were cooled to room temperature and weighed on an analytical balance to determine the final weight. The gas evolution curve indicates that fixed gases began to form near 430°C and were evolved at a fairly uniform rate until heating stopped at 725°C. The initial rise in the gas evolution curve between 350° and 430°C was caused by the rapid vaporization of condensable products.

Infrared absorption analysis of the condensable products obtained during this period of very rapid weight loss indicates that these products are principally 5, 12-dihydronaphthacene. A small amount (roughly 10 per cent) of naphthacene was also separated from the condensate. The absence of any evolved fixed gas until after the major weight loss has occurred indicates that the initial intermolecular transfer of hydrogen forms the volatile dihydronaphthacene. Above 430°C, the residual polymer begins to carbonize with the release of gaseous products. The curves in Figures 18 and 19 show that the gas evolution rates between 430° and 630°C are fairly constant. The sudden increase in rate at 650°C may have been caused by a drop of condensate falling from the upper condenser into the hot zone of the furnace.

The results of analyses of the fixed gases taken at progressively higher temperatures are given in Table 29. The gas samples (No. 7 through No. 14) were taken during the heating phase of the experiment from the gas stream flowing between the pyrolysis chamber and the gas collection buret. The final sample (No. 15), taken from the gas collection buret at the completion of the run, represents the average composition of the total gas evolved.

The data in Table 29 show that hydrogen is the major gaseous product formed during the conversion of the naphthacene polymer to carbon. The relative proportion of hydrogen in the effluent gas increases as the temperature increases, and the final composition of the accumulated gas contained 83.5 mole per cent of hydrogen. Methane is the next most abundant gaseous product. A relatively high proportion of methane occurs in the lower temperature samples, but the ratio decreases as the temperature increases. Ethane, ethylene, and propane are also present in higher proportions in the lower temperature samples than in the high temperature ones. Carbon monoxide increases in concentration as the temperature increases, approaching 2 mole per cent in the sample taken at 724°C just before the furnace shut off. The oxygen must have been adsorbed on the sample, since there was no detectable oxygen in the helium atmosphere at the start of the run.

In Table 30, the composition of the accumulated gaseous products has been converted into total molar quantities. In the last column of Table 30, the gaseous composition data have been recalculated to represent

Table 29. Composition in Mole Per Cent of Effluent Gas Collected at Various Temperatures During Pyrolysis of Naphthalene (TGA-GE Run 55)

Sample No. Temperature ° Gas	7 484°C	8 540°C	9 576°C	10 613°C	11 650°C	12 687°C	13 724°C	14 ^{ee} 690°C	15 ^{eee}
H ₂	72.8	69.2	75.4	81.5	81.9	83.3	84.2	85.6	83.5
CH ₄	17.3	19.3	18.1	14.4	14.1	13.4	12.5	11.7	12.2
CO	trace	0.4	0.9	1.1	1.6	1.7	1.8	1.5	1.0
C ₂ H ₆	4.4	7.2	4.1	2.3	1.8	1.3	1.1	0.9	2.2
C ₃ H ₈	1.1	1.0	0.4	0.2	0.2	0.3	0.3	0.3	0.4
C ₄ H ₁₀	4.4	2.9	1.1	0.5	0.4	0.1	0.1	trace	0.7
Total	100.0	100.0	100.0	100.0	100.0	100.0	100.0	100.0	100.0

^e Temperature when sample was taken.
^{ee} Sample taken while cooling.
^{eee} Sample taken from Gas Collector.

Table 30. Measured and Calculated Compositions of Total Fixed Gases Collected During Pyrolysis of Naphthalene to 725°C (TGA-GE Run 55)

Gas	Sample 15 Taken From Gas Collection Buret, Mol. %	Volume of Each Gas Evolved cc	Moles of Each Gas Evolved Moles	Total Weight of Each Gas Evolved Grams	Moles of Gas Per Mole of Naphthalene Monomer in Residue at 480°C
H ₂	83.5	35.23	.00157	.0031	1.71
CH ₄	12.2	5.15	.00023	.0037	0.25
CO	1.0	0.42	.000019	.0005	0.02
C ₂ H ₆	2.2	0.93	.000043	.0013	0.05
C ₃ H ₈	0.4	0.17	.000008	.0002	0.009
C ₄ H ₁₀	0.7	0.30	.000013	.0006	0.014
Total	100.0	42.20	.001882	.0094	(2.05)

the ratio of moles-of-gas to moles-of-naphthacene units in the polymer. The total calculated weight of gaseous products agrees closely with the TGA weight loss curve between 460° and 725°C. The weight loss above 460°C is caused by dehydrogenation and ring scission producing low molecular weight methyl, ethyl, or propyl fragments. The material balance indicates that no more than about 0.01 mole of products with molecular weights above C₃ per mole of naphthacene forms between 460° and 725°C.

3.3.3.3. ESR Studies

ESR investigations were made of the pyrolysis of naphthacene, (XIX) and for solutions of (XIX) in m-quinquephenyl. The conditions and results of these measurements are shown in Table 31.

Table 31. ESR Measurements of Naphthacene

Conc. in m-quinquephenyl	Decomp. Temp., °C*	Measurement Temp., °C	Resolved or Unresolved	Linewidth (Gauss)
100%	350	192	(U)	~5.5
10%	350	230	(U)	~5.0
3%	350	230-550	(U)	~5.5

* Lowest temperature at which an ESR signal was observed.

Naphthacene and solutions of naphthacene in m-quinquephenyl all showed intense ESR signals at 350°C. These spectra were measured at temperatures between 230° to 550°C and showed no trace of resolution. The overall width of the naphthacene spectrum was of the order of 5 gauss. This narrow spectrum, in contrast to the 40 gauss width observed for the naphthacene radical ion in solution (Section 3.4.2.), indicates that the ESR signal may be due to solid insoluble free radical intermediates. The insolubility of naphthacene in m-quinquephenyl would also explain the lack of any effect of dilution on the measured decomposition temperature.

3.3.3.4. Chemical Studies of Pyrolysis

Naphthacene was heated to temperatures of 400°, 450°, and 500°C. Infrared and ultraviolet spectra for distillates and residues of these reactions are shown in Figures 20 and 21, respectively. The presence of two new bands at 528 and 578 millimicrons in the UV show that some slight reactions have begun at 400°C. Significant changes in the spectra from the temperature increase to 450°C indicate that major reactions have begun. The UV spectrum of the 500°C product exhibits the complete lack of detail which is characteristic of complex highly aromatic materials. The infrared spectrum of the 500°C product shows a fairly simple aromatic substitution pattern. The band at 13.6 microns is the basic band (found in naphthacene) for four adjacent ring hydrogens. The band associated with

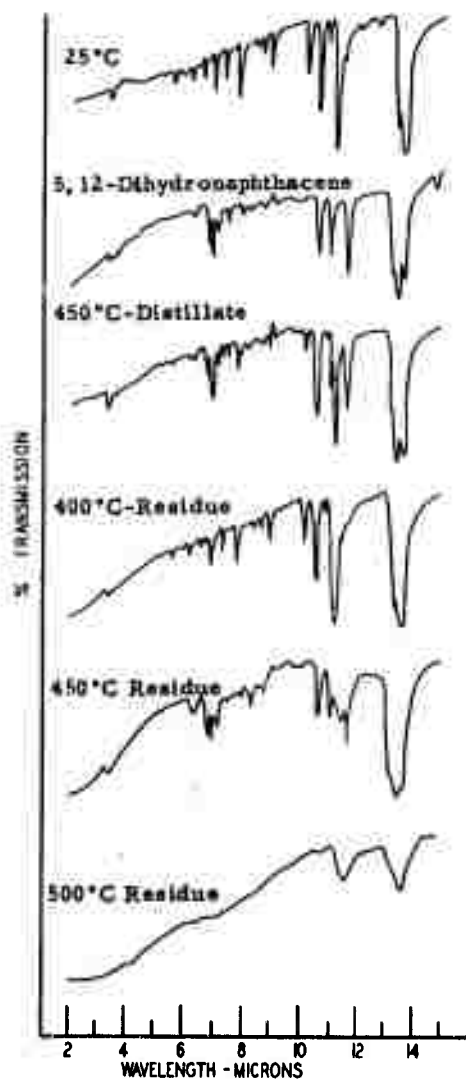


Figure 20. Infrared Spectra of Pyrolyzed Naphthalene

N-5849

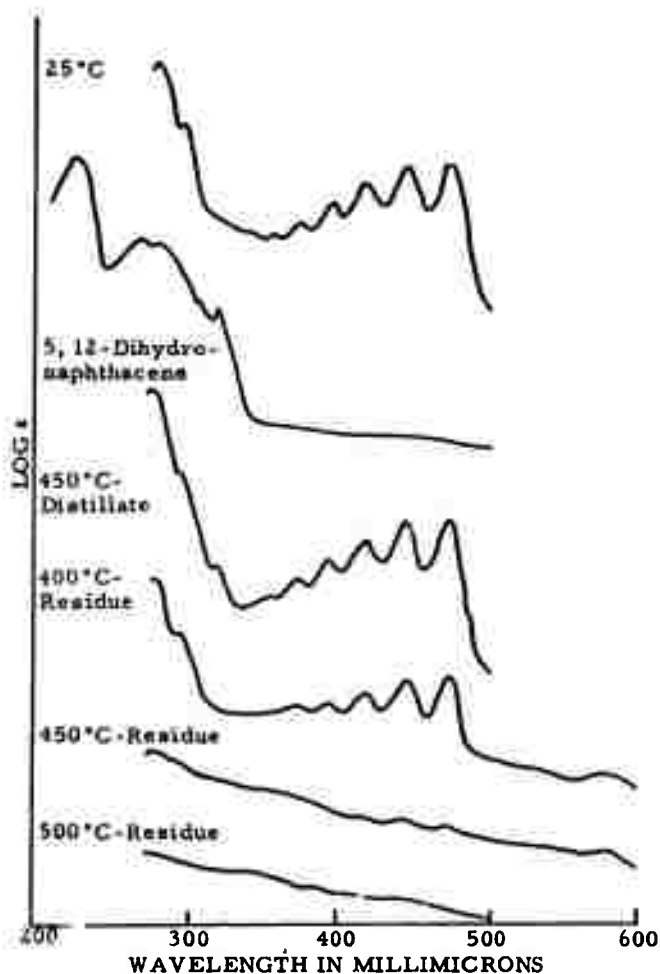


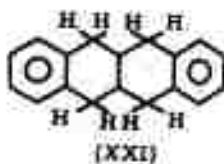
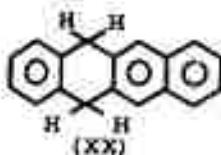
Figure 21. Ultraviolet Spectra of Pyrolyzed Naphthalene N-5850

the isolated hydrogen atoms at the 5, 6, 11, and 12 positions of naphthalene has been shifted from 11.1 to 11.5 microns and has broadened considerably.

The most significant chemical changes occur at 450°C, as shown by the spectral data of the residues. Spectral examination of the

distillate formed at this temperature showed the presence of considerable 5, 12-dihydronaphthacene.

The 450°C residue was subjected to an extensive chromatographic separation. A large amount of (XX) as well as some unreacted naphthacene and a more aliphatic material were separated in the early chromatographic extracts. The aliphatic product has been characterized through spectrometric examination as probably being 5, 6, 11, 12-tetrahydronaphthacene, (XXI).



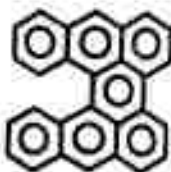
The pyrolysis of naphthacene largely involves reaction at the 5, 6, 11, and 12-positions and initiates with carbon-hydrogen cleavage at these sites. This result is consistent with the reactivity data presented for the naphthacene molecule.

The major condensation products which we isolated were a red and a brown hydrocarbon with closely related spectra. The first material had a characteristic UV spectra with major visible absorption bands at 528 and 567 millimicrons and a minor band at 407 millimicrons. The second material showed absorption bands at 505, 535, and 578 millimicrons in addition to distinct bands at 336 and 354 millimicrons. Infrared spectroscopy indicated that the basic naphthacene substitution pattern had not been extensively altered in these products, although the two main aromatic substitution bands were shifted to 11.45 and 13.75 microns. Both of these products were highly reactive and, on standing, underwent oxidation to quinone-type material.

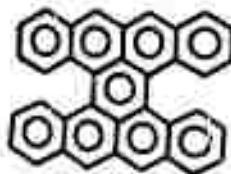
A search of the literature revealed no reported compounds which could be identified with these substances. The spectra appeared to be most closely related to those of the dibenzperylene (XXIIa) and (XXIIb).⁽¹⁰⁾



(XXII)

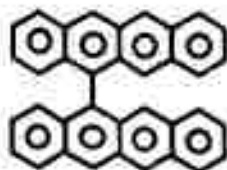


(XXII)



(XXIII)

The reaction products are thought to be tetrabenzoperylene derivatives such as (XXII) formed by direct fusions at the 5, 6, 11, 12 positions. This type of planar derivative would be expected to proceed to an ordered graphite system. Tetrabenzoperylene (XXIII) is unknown, although its quinone has been prepared.⁽¹¹⁾ The formation of XXXIII should involve a binaphthacene intermediate (XXIV). Our attempts to synthesize (XXIV) are described in Section 3.6.



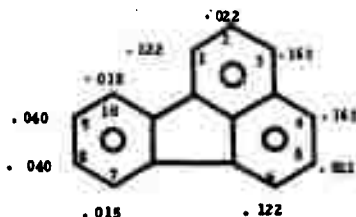
(XXIV)

3.3.3.3.5. Reaction Mechanisms

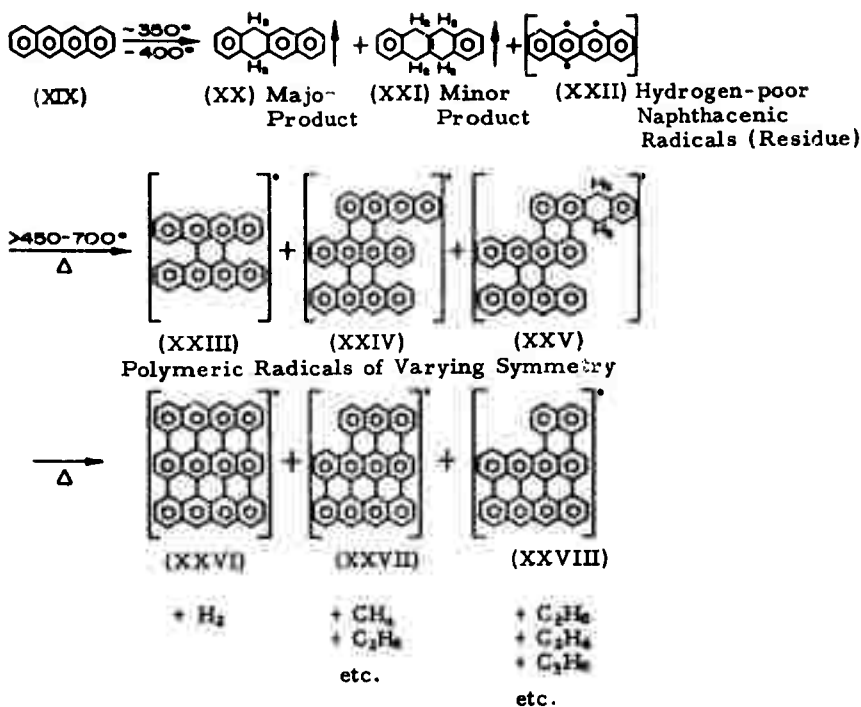
A postulated reaction sequence for the pyrolysis of naphthacene is given in Figure 22. The initial thermal reactions involve the cleavage of C-H bonds at the reactive 5, 6, 11, or 12 positions to form naphthacenyl radicals (XXII), and dihydronaphthacene (XX), by intermolecular hydrogen transfer. The failure to observe any hydrogen evolution during this process indicates that the reactions are bimolecular. The reactive free radicals can polymerize to dimeric and trimeric structures of varying symmetry, such as (XXIII), (XXIV), and (XXV). Structure (XXIII) is favored by both symmetry and reactivity considerations. Further thermal treatment induces dehydrogenations and polymerizations which could produce symmetrical trimeric aromatic structures such as (XXVI) from (XXIII). For other less symmetrical structures, protruding rings may open, leading to the formation of methane and ethane and to larger aromatic nuclei, such as (XXVII) and (XXVIII). These structures could exist either as hydrocarbons or as free radicals.

Elementary analysis of the residue at 725°C gave 2.27 per cent hydrogen. This low hydrogen content requires structures at least the size of (XXVI) in this residue.

3.3.3.4. Fluoranthene



(XXIX)



N-6706

Figure 22. Postulated Carbonization Sequence for Naphthacene

Fluoranthene (XXIX) is a relatively unreactive hydrocarbon and must be carbonized under pressure. At 3000°C, the fluoranthene carbon appears intermediate to a well-ordered and disordered graphite. The unpaired spin densities, computed for a fluoranthene radical ion, are shown. These data predict the 3,4-positions to be the most reactive in (XXIX).

3.3.3.4.1. Thermal Dehydrogenation of Fluoranthene

Initial studies of the carbonization of fluoranthene have been reported previously.⁽⁴⁾ A series of fluoranthene samples have been carbonized to temperatures up to 1000°C. Elementary analysis data were obtained for these products and are listed in Table 32.

Plotted in Figure 23 is the percentage hydrogen-versus-heat treatment temperature for fluoranthene. Above 600°C, a smooth dehydrogenation sequence is observed.

Table 32. Elementary Analysis for Pyrolyzed Fluoranthene

Pyrolysis Temp., °C	Weight % C	Weight % H	Atomic C/H
25	95.02	4.98	1.60
450	95.21	4.91	1.58
475	94.95	5.02	1.59
500	94.61	4.84	1.64
525	95.88	4.12	1.94
550	95.99	3.21	2.51
600	95.95	2.96	2.94
700	95.26	1.67	4.78
800	97.50	1.05	7.81
900	98.27	0.83	9.98
1000	99.70	0.50	16.60

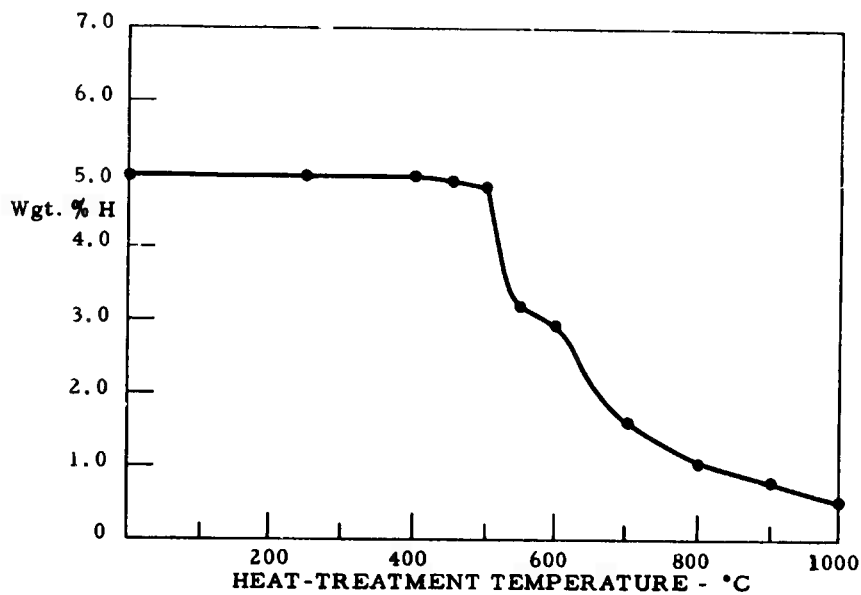
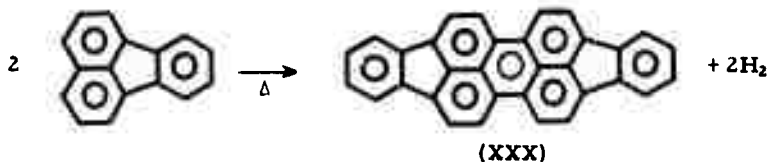


Figure 23. Dehydrogenation Curve for Carbonized Fluoranthene

N-5772

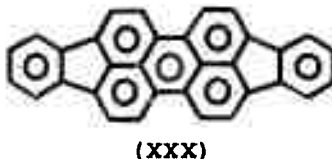
3.3.3.4.2. Chemical Studies of Pyrolysis

A portion of the residue obtained at 525°C from fluoranthene was chromatographically extracted. This residue had been obtained by heat treating fluoranthene under pressure. The only pure condensation product that could be extracted in quantity was the dehydrogenated dimer periflanthene, (XXX). A black, completely insoluble, carbonaceous residue remained on the column after the extraction was completed. There was very little indication of any aliphatic material in the 525°C pyrolysis product, indicating that the formation of periflanthene involves the direct loss of hydrogen. As predicted, this dehydrogenation sequence appears to involve primarily the reactive 3,4-positions.



The fluoranthene molecule itself is apparently a poor hydrogen acceptor. Further studies of the fluoranthene pyrolysis have been continued with periflanthene itself.

3.3.3.5. Periflanthene

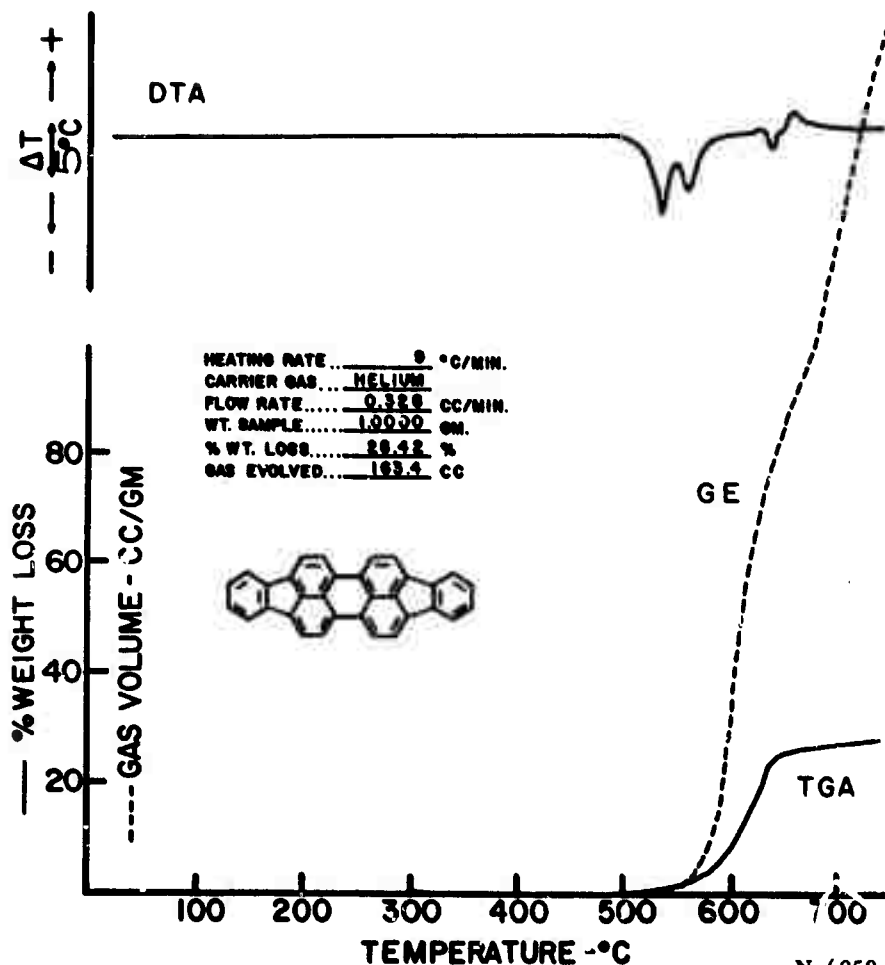


Periflanthene (XXX) is the first thermal reaction product of the pyrolysis of fluoranthene. This compound is quite stable and undergoes no reaction until about 550°C, where carbonization begins. An approximate 55 per cent yield of carbon can be obtained from this compound.

To obtain an experimental quantity of periflanthene, a portion of the 525°C fluoranthene residue was repeatedly chromatographed. This extracted product, along with some commercial material, was employed in the subsequent reaction studies.

3.3.3.5.1. Differential Thermal Analysis (DTA) of Periflanthene

The DTA thermogram for periflanthene shown in Figure 24 indicates melting at a temperature of approximately 520°C followed by a series of endothermic and exothermic reactions at higher temperatures.



N-6950

Figure 24. Differential Thermal Analysis, Thermogravimetric and Gas Evolution Curves for the Pyrolysis of Periflanthene (Run 57)

3.3.3.5.2. Thermogravimetric and Gas Evolution Analysis (TGA-GE) of Periflanthene

The TGA and GE curves for (XXX) are plotted in Figure 24. The derivative curves for the weight loss and gas evolution are given in Figures 25 and 26. In Figure 26, the derivative curves were corrected for the amount of reactants remaining at the indicated temperature. The experimental conditions are tabulated in Figure 24.

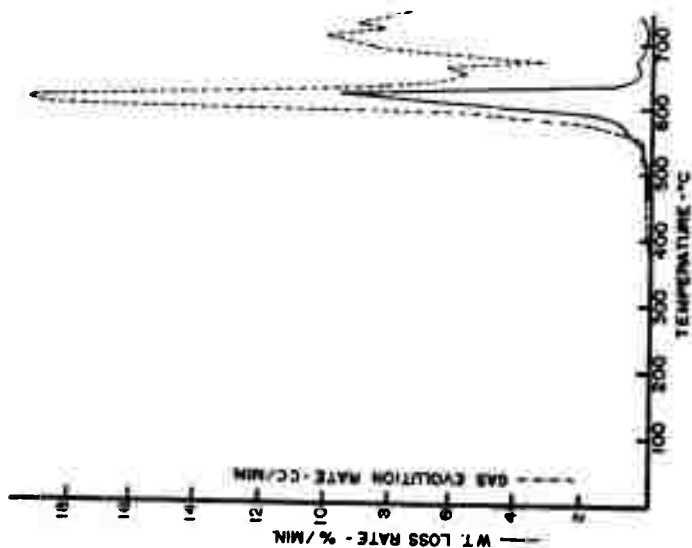


Figure 25. Weight Loss and Gas Evolution Rate Curves for the Pyrolysis of Perilanthene (Run 57)

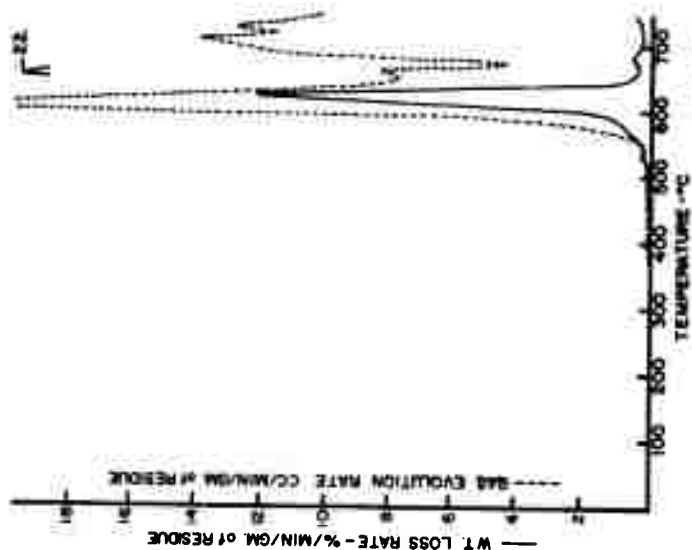


Figure 26. Weight Loss and Gas Evolution Rate Curves for the Pyrolysis of Perilanthene Expressed Relative to the Amount of Residue in Reaction Cup (Run 57)

Periflanthene begins to sublime slowly at approximately 475°C. After melting at 520°C, the weight loss rate increases slowly to about 575°C, then, very rapidly to a maximum at about 620°C. The rate drops very rapidly to a very low level above a temperature of 650°C. A carbon residue of 71.6 per cent was obtained in the TGA experiment. The gas evolution curve indicates that fixed gases begin evolving at approximately 500°C, although none was detected by gas chromatographic analysis in either the 500°C sample or the 550°C sample. The gas evolution rate increases rapidly above 550°C, reaching a maximum at about 615°C and then dropping off at higher temperatures to between one-fourth to one-half of the maximum rate. The compositions of the effluent gas samples at various intervals are given in Table 33. Hydrogen is the major gaseous product released during the entire heating period and the proportion of hydrogen in the effluent gas drops only slightly with increasing temperature. The second major gaseous product is methane. The proportion of methane was almost constant as the temperature increased. Minor amounts of ethane, ethylene, and propane were found in the 600°C sample, and their relative amounts decreased rapidly as the reaction temperature increased; only traces were found in the 750°C sample. Fairly large amounts of carbon monoxide were identified in all of the gas samples taken above 600°C.

Table 33. Composition of Effluent Gas Collected at Various Temperatures during the Pyrolysis of Periflanthene (TGA-GE Run 57)

(Mol %)						
Sample No.	7	8	10	11	12	Cumulative Gases
Temperature	550 °C	597°C	702°C	750°C	Cooling	Collected in Gas Buret during Entire Run
O ₂	-	-	0.6	0.7	0.9	0.3
H ₂	-	84.8	83.0	81.5	80.0	82.3
CH ₄	-	10.0	10.4	10.0	10.0	11.3
C ₂ H ₆	-	3.7	0.7	0.1	trace	1.3
C ₂ H ₄	-	0.9	0.1	trace	sl. trace	0.4
C ₃ H ₈	-	0.2	trace	-	-	trace
CO	-	0.2	5.2	7.7	9.1	4.4
CO ₂	-	-	-	-	-	-
Total	-	100.0	100.0	100.0	100.0	100.0

Although the atmosphere in the system was analyzed before heating began, and no oxygen was detected, a small amount of residual oxygen was detected in the high-temperature gas samples. The helium used in these experiments is passed through a molecular sieve column and has been checked many times and found to be oxygen free. The oxygen must originate with the sample, either as adsorbed gas or as a contaminant.

In Table 34, the composition of the total gases collected in the gas buret during the entire heating cycle are presented in several forms to aid us in understanding the physical and chemical changes occurring during the pyrolysis. Of the total weight loss, 14 per cent was due to gaseous products. The remaining 86 per cent was condensable and proved to be almost pure perflanthene. On this basis, it is reasonable to assume that ~25 per cent of the original perflanthene distilled off and that the remaining 75 per cent reacted thermally to produce the carbon residue and gaseous products. A material balance can be made which indicates that approximately 1 atom of carbon and 16.5 atoms of hydrogen are removed as gaseous products from every two molecules of reacting perflanthene. This result gives a carbon residue at 750°C containing approximately 2.0 weight per cent hydrogen, in good agreement with measured values on residues from fluoranthene, naphthacene, acenaphthylene, and terphenyl.

Table 34. Measured and Calculated Compositions of Total Fixed Gases Collected during Pyrolysis of Perflanthene (TGA-GE Run No. 57)

Gas	Average Composition of Gas from Buret at End of Run (Mol %)	Total Volume of Each Gas Evolved (cc)	Total Weight of Each Gas Evolved (gms)	Moles of Each Gas Evolved	Moles of Gas per Mole of Starting Compound. 1.00gm = 0.0025 mole	Moles of Gas per Mole of Perflanthene in Residue at 625°C. 0.775 gm = 0.00194 mole
O ₂	0.3	0.5	0.0067	0.0000223	0.01	0.01
H ₂	82.3	134.5	0.0120	0.00600	2.40	3.09
CH ₄	11.3	18.5	0.0132	0.000826	0.33	0.43
C ₂ H ₆	1.3	2.1	0.0028	0.0000938	0.04	0.05
C ₂ H ₄	0.4	0.6	0.0008	0.0000268	0.01	0.01
C ₃ H ₈	trace	trace	-	-	-	-
CO	4.4	7.2	0.0090	0.000322	0.13	0.17
CO ₂	0.0	0.0	-	-	-	-
Total	100.0	163.4	0.0385	0.00729	2.92	3.76

3.3.3.5.3. ESR Studies

A sample of perflanthene (XXX) was pyrolyzed in the ESk cavity. A signal was first observed at 450°C; a temperature well below the melting point of the compound. This signal, approximately 5.0 gauss wide, was totally unresolved.

A 10 per cent solution of perflanthene in m-quinquephenyl first showed an ESR signal at 542°C. This sample, when cooled and measured at 234°C, showed signs of resolution. A complex spectrum with lines 0.20 gauss wide was obtained at this temperature. Further work on this system should permit an analysis of the spectrum and a structural assignment of the free radical.

3.3.3.5.4. Chemical Studies of Pyrolysis

The pyrolysis reactions of perflanthene were quite difficult to control. This material is highly stable and undergoes only slight decomposition below 500°C. Initially, a sample of the perflanthene was heated to 565°C in an inert atmosphere. At this temperature, the perflanthene reacted instantly to form an infusible, porous carbon residue. In subsequent efforts, it was found that, at 545°C, the pyrolysis of perflanthene proceeds much more gradually. After a 30-minute hold at this temperature, a black but fusible residue is obtained. An infrared spectrum of this material is shown in Figure 27. Although the major bands of perflanthene are present, reaction is indicated by the appearance of a new band at 11.55 microns (isolated hydrogen) and a shift of the aromatic substitution band from 11.95 to 12.20 microns.

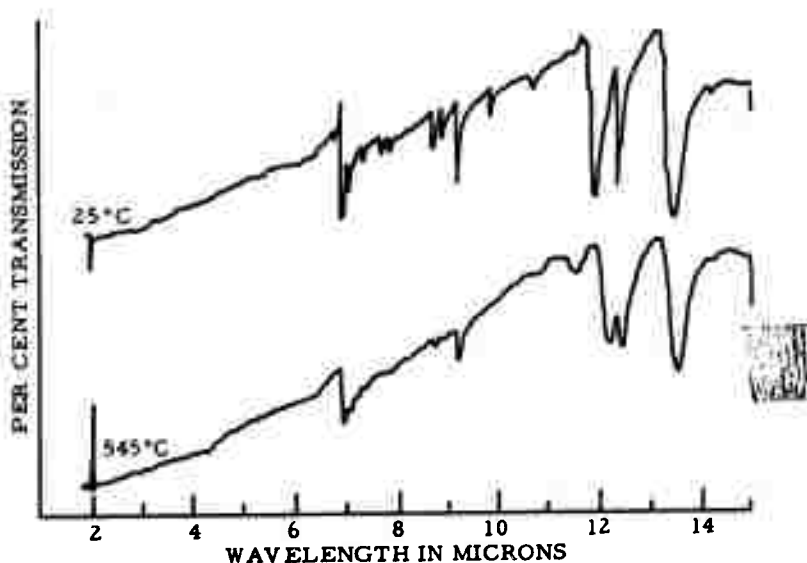


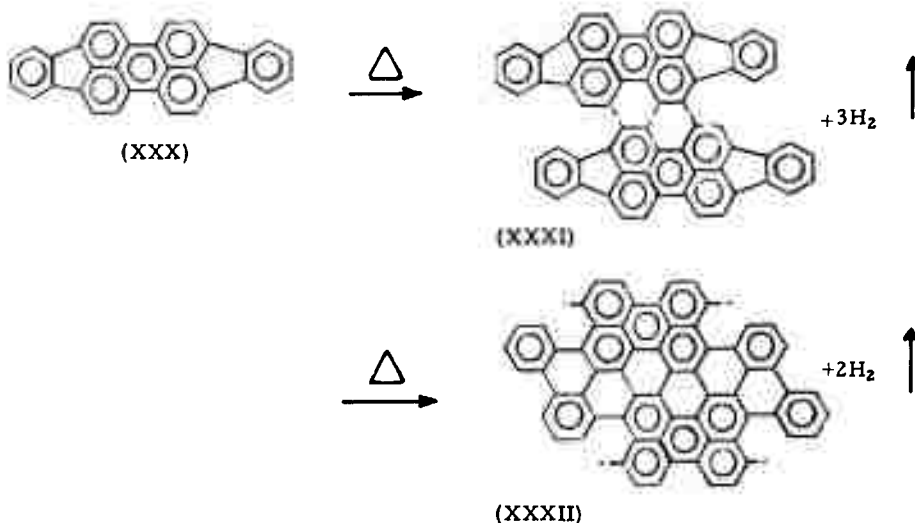
Figure 27. Infrared Spectra of Heat-Treated Perflanthene

N-6676

Chromatographic extraction of the 545°C material was attempted. After extraction with numerous solvents, the major portion was not dissolved and remained on the column as a black, pitch-like residue. The infrared spectrum of this material was similar to that of the original residue. The small portion which was eluted proved to be an oxidized aliphatic material. This material is thought to result from ring cleavage reactions involving the bridging phenyl group.

3.3.3.5.5. Thermal Reactions of Periflanthene

A thermal reaction sequence can be postulated which principally involves dehydrogenation and polymerization of the periflanthene moieties. Ring rupture and carbon bond cleavage are minor side reactions which produce the light hydrocarbon gases. The following thermal reaction sequence is readily suggested by the symmetry and reactivity of periflanthene

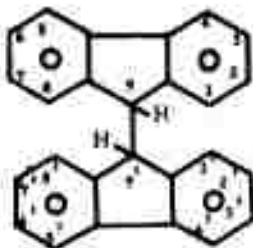


Condensations at the reactive 6, 7, and 14, 15 positions would lead to structures such as (XXXI). Such a structure would explain the infrared spectrum in Figure 27. The large molecule would also be insoluble and infusible. Structures such as (XXXI) could readily form free radicals by ring opening of the phenyl bridge. These large aromatic radicals could have several configurations but would all be nonplanar. As the temperature increases, some of the protruding rings will open and cleave off as methane, ethane, etc. In instances where growth occurs without further rearrangement, imperfections in the planar structure will result from the missing carbon atoms.

3.3.3.6. 9,9'-Bifluorene

The pyrolysis reactions of 9,9'-bifluorene (XXXIII) have been discussed previously.^(2,4) The initial thermal reactions involve the formation of $\Delta^{8,9'}$ -bifluorene (XXXV) and fluorene (XXXVI). TGA-GE analyses have been obtained for (XXXIII) and are presented along with additional ESR studies for this hydrocarbon.

3.3.3.6. 9,9'-Bifluorene (Cont'd)



(XXXIII)

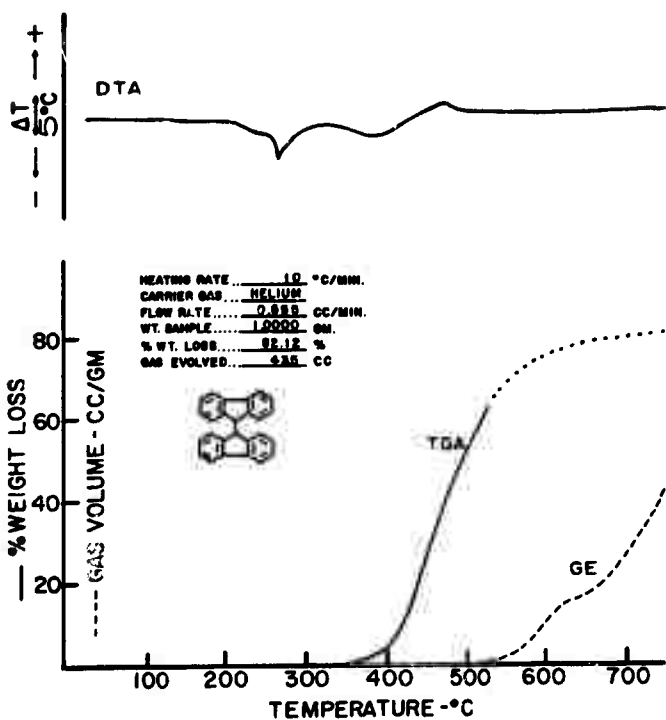
3.3.3.6.1. Differential Thermal Analysis of 9,9'-Bifluorene

The DTA thermogram of 9,9'-bifluorene which is given in Figure 28 shows a melting endotherm at 250°C, followed by a broad vaporization endotherm between 340°C and 400°C. Above 400°C, an exothermic reaction occurs, peaking near 460°C. At higher temperatures, no DTA activity is evident. A 5.8 per cent carbon yield was obtained in the DTA experiment. The compounds identified in the condensable volatile products included fluorene, $\Delta^{9,9'}$ -bifluorene, and dibenzo(a,c)triphenylene.

3.3.3.6.2. Thermogravimetric - Gas Evolution Analysis (TGA-GE) of 9,9'-Bifluorene

The thermogravimetric curve in Figure 28 shows that 9,9'-bifluorene begins to volatilize around 325°C. Above 400°C, the weight loss rate is very rapid. This material foamed so badly during the experiment that the TGA curve had to be terminated at 550°C and no derivative curves could be obtained. The gas evolution curve in Figure 28 is essentially the attenuated gas evolution curve for $\Delta^{9,9'}$ -bifluorene. Based on the carbon residue and the total gas evolution, the conversion of 9,9'-bifluorene to $\Delta^{9,9'}$ -bifluorene appears to be about 35 to 40 per cent. The condensate collected on the water-cooled condenser coil was predominantly fluorene, with appreciable amounts of 9,9'-bifluorene, $\Delta^{9,9'}$ -bifluorene, and dibenzo(a,c)triphenylene.

The results of gas chromatographic analysis of gas samples taken during this run are tabulated in Table 35. As in the case of acenaphthylene, naphthalene, and perflanthene, the major gaseous product is hydrogen, which accounts for approximately 87 per cent of the total gas evolved.



N-7123

Figure 28. Differential Thermal Analysis, Thermogravimetric, and Gas Evolution Curves for the Pyrolysis of 9,9'-Bifluorene (Run 51)

Table 35. Composition of the Fixed Gases Evolved During the Pyrolysis of 9,9'-Bifluorene in Helium (TGA-GE Run 51)

Temp. When Sample Taken → Gas	Mol. % of Gas in Fraction					
	500°C	558°C	605°C	652°C	698°C	750°C *
Hydrogen (H ₂)	Sl. trace	trace	81	79	83	87
Methane (CH ₄)	-	-	13	16	13	12
Ethane (C ₂ H ₆)	-	-	3	3	2	1
Ethylene (C ₂ H ₄)	-	-	1	1	1	trace
Carbon Monoxide (CO)	-	-	2	1	1	trace
Carbon Dioxide (CO ₂)	-	-	sl. tr.	sl. tr.	sl. tr.	sl. tr.

* Average of three analyses of final gas products.

3.3.3.6.3. ESR Studies

The compound 9,9'-bifluorene (XXXIII), when heated between 270°C and 400°C in a m-quinquephenyl solvent yields an ESR spectrum consisting of six poorly resolved lines.⁽⁵⁾ The pyrolysis of 9,9'-bifluorene has now been reinvestigated in order to determine the effects of temperature and hydrocarbon concentration on the ESR. The various ESR experiments which were performed, along with their results, are summarized in Table 36.

Table 36. Summary of ESR Experiments on 9,9'-Bifluorene

Concentration in m-Quinquephenyl	Decomp. Temp. °C*	Meas. Temp. °C	Resolved (R) or Unresolved (U)	Linewidth Gauss
10%	262	262-398	(R)	~2.5
		450-570	(U)	~9.0
10%	274	127	(R)	~0.25
Pure	250	260	(R)	~0.25

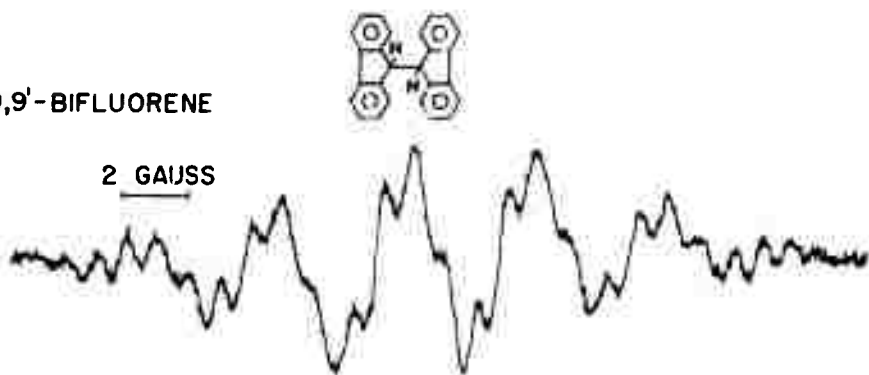
* Lowest temperature at which an ESR signal was observed.

The resolution and linewidths of the 9,9'-bifluorene spectrum varied with both the temperature of measurement and the sample concentration. A 10 per cent solution of 9,9'-bifluorene in m-quinquephenyl first showed an ESR signal at 262°C. This signal was completely unresolved when measured above 450°C. Between 260°C and 400°C, the 6-line spectrum with linewidth of 2.5 gauss was observed. At about 127°C, the resolution was appreciably improved, and lines on the order of 0.25 gauss wide were present.

A neat sample of 9,9'-bifluorene first gave a resonance at 250°C. At 260°C, this signal was resolved with lines on the order of 0.25 gauss wide. A portion of this spectrum is reproduced in Figure 29. Apparently, at 260°C, the unreacted bifluorenyl serves as a solvent for the free-radical intermediates, thus obviating the need for any additional solvent. Further study showed that the ESR resolution was limited at high temperatures by the effect of the current in the heating element of the heater cavity. This current produced a slightly inhomogeneous magnetic field on the order of a few hundred milligauss at the sample. This problem is being corrected.

ESR studies of pyrolysis provide a means of obtaining kinetic data for some of the reactions involved in the carbonization of aromatic hydrocarbons. We can measure spin concentrations as a function of time or temperature for any of the stable free radical intermediates.

9,9'-BIFLUORENE



N-7003

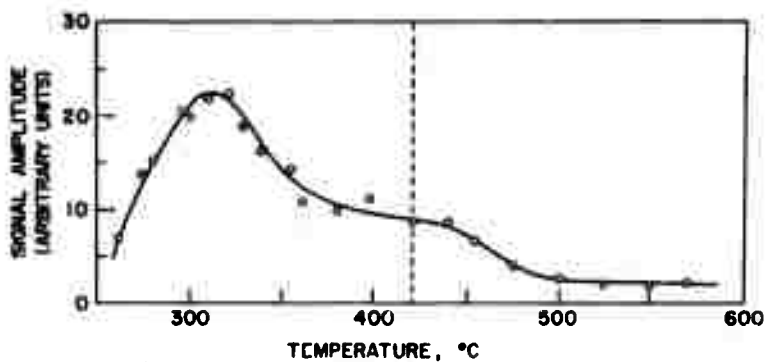
Figure 29. ESR Spectrum of 9,9'-Bifluorene at 260°C

Some preliminary experiments of this nature have been performed on the 9,9'-bifluorene system.

Figure 30 shows the effect of temperature on the line intensity of one of the resolved components of the 6-line 9,9'-bifluorene spectrum. This spectrum was measured for a 10 per cent solution of 9,9'-bifluorene in *m*-quinquephenyl. No signal is observed until a temperature of 250°C is reached. A steady-state concentration of radicals is reached rapidly at every temperature above 250°C. This steady-state concentration reaches a maximum at about 315°C, decreases abruptly between 315°C and 350°C, and decreases more slowly between 350°C and 575°C.* Although no radicals are formed below 250°C, radicals formed at higher temperatures can be quenched to a metastable state below 130°C. These radicals disappear rapidly when attempts are made to measure their ESR between 130°C and 250°C. Above 250°C, new radicals form and the steady-state situation again ensues. The clarification of the reactions involved in these effects awaits further experimental study.

ESR measurements were also made on some pyrolysis residue from 9,9'-bifluorene which had been graphitized to 3000°C. No signal was observed for either the pure material or for a dispersion of the graphite in SiO₂.

* The vertical dashed line in Figure 30 indicates the temperature (approximately 420°C) at which the hyperfine lines begin to broaden. Above this temperature, the signal amplitude is not a quantitative measure of the spin concentration.

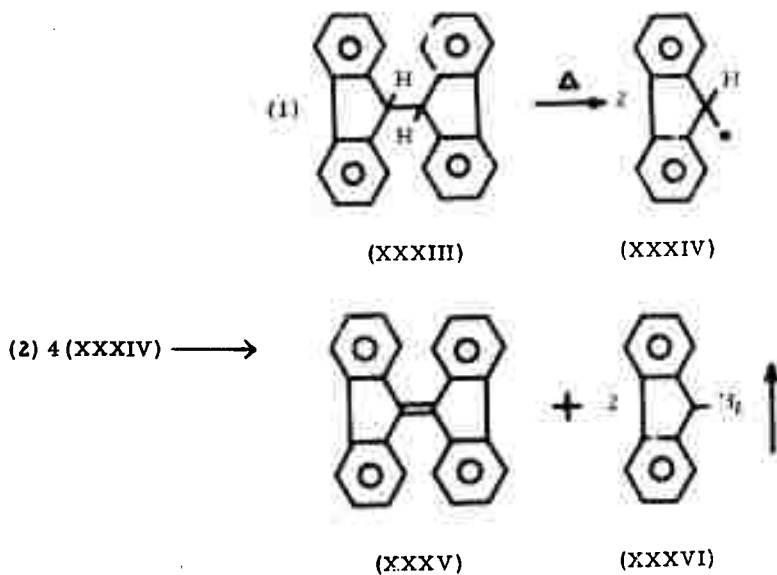


N-6690

Figure 30. Variation of the ESR Intensity of 9,9'-Bifluorene with Temperature

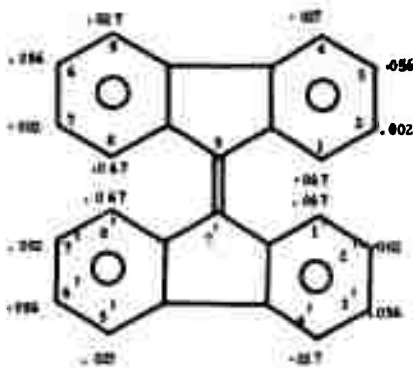
3.3.3.6.4. Thermal Reactions of 9,9'-Bifluorene

The studies included in this report are consistent with the following reaction sequence for 9,9'-bifluorene (XXXIII).



We believe that the ESR spectrum in Figure 29 results from the neutral fluorene radical (XXXIV). The carbonization reactions of 9,9'-bifluorene proceed by way of the unsaturated dimer (XXXV).

3.3.3.7. $\Delta^9,9'$ -Bifluorene



(XXXV)

The compound $\Delta^9,9'$ -bifluorene (XXXV) is the initial thermal reaction product of 9,9'-bifluorene. The computed spin densities for a $\Delta^9,9'$ -bifluorene radical cation are shown with the structure. The 9,9'-positions are the most active positions, but the 1,1', and 8,8'-positions are the most reactive of the hydrogen containing sites.

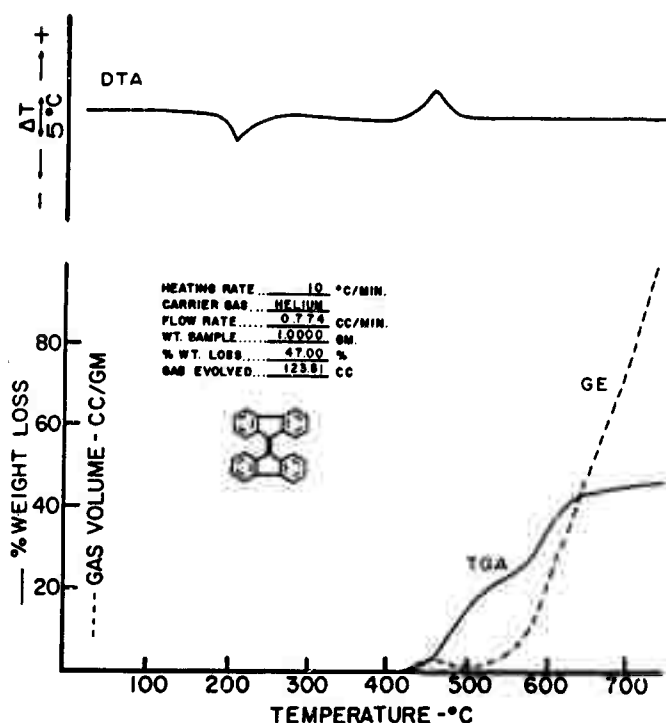
The carbon produced from (XXXV) forms a highly-disordered "graphite." The pyrolysis of (XXXV) has now been studied in detail in order to clarify the thermal reaction sequences.

3.3.3.7.1. Differential Thermal Analysis

The DTA thermogram given in Figure 31 shows a melting endotherm at 188°C. The liquid (XXXV) is quite stable up to 400°C, where an exothermic reaction ensues. A carbon yield of 31.5 per cent was obtained. The condensable volatile products consisted primarily of fluorene and a major aromatic product that could not be identified.

3.3.3.7.2. Thermogravimetric-Gas Evolution Analysis (TGA-GE)

Two TGA-GE analyses, Runs 49 and 50, have been completed on $\Delta^9,9'$ -bifluorene (XXXV). The experimental conditions for both runs were nearly identical. During Run 49, the gas chromatograph became inoperable and no gas analyses were obtained. The purpose of the second experiment was to obtain gas analyses of the fixed gases.

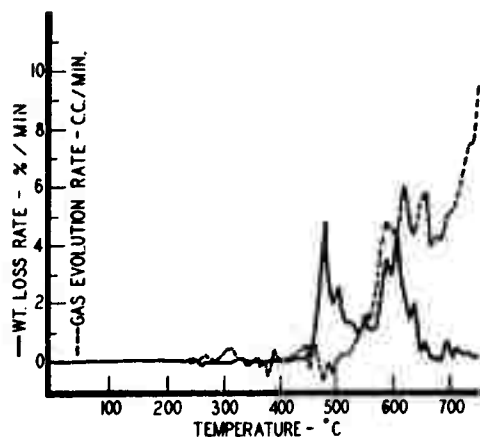


N-7125

Figure 31. Differential Thermal Analysis, Thermogravimetric Analysis, and Gas Evolution Curves for the Pyrolysis of $\Delta^{8,9}$ -Bifluorene (Runs 49 and 50)

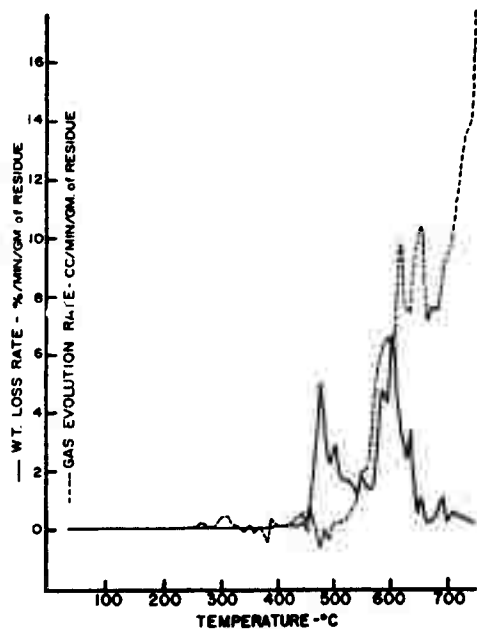
The TGA and GE curves for the pyrolysis of (XXXV) in a helium atmosphere are shown in Figure 31. Good agreement was obtained between Runs 49 and 50, particularly in the gas evolution data, despite the fact that this material foamed badly. The total weight losses of the two runs were in agreement. The knee in the TGA curve corresponds to the exothermic peak exhibited in the DTA thermogram at about 475°C. The evolution of low molecular weight gaseous products began just above 500°C, at a temperature corresponding to the second increase in weight loss rate. These effects are better illustrated in the derivative curves shown in Figures 32 and 33. The two major weight-loss-rate peaks have several superimposed minor peaks. The significance of these secondary peaks has not been determined; they may be the result of foaming or they may indicate specific reactions. The same comment is applicable to the gas evolution rate curve, which exhibits several consecutive maxima.

The results of chromatographic analysis of the fixed gases evolved at progressively higher temperatures during Run 50 are given



N-7127

Figure 32. Thermogravimetric Gas Evolution and Weight Loss Rates for $\Delta^9, 9^1$ -Bifluorene (Run 49)



N-7128

Figure 33. Thermogravimetric Gas Evolution and Weight Loss Rates for $\Delta^9, 9^1$ -Bifluorene Expressed Relative to the Amount of Residue in Reaction Cup (Run 49)

in Table 37. The evolved gas, predominantly hydrogen, also contains about 10 to 20 per cent methane and only a few per cent of ethane, ethylene, and carbon monoxide. We do not know how the oxygen gets into our system unless it is strongly adsorbed on the sample. The helium carrier gas is passed through a molecular sieve 13X trap before it is introduced into the TGA apparatus. The entire apparatus, except the molecular sieve trap, is evacuated to below 20 microns before each run to test for leaks as well as to purge the sample and assure an inert atmosphere. Despite these precautions, CO and in some cases CO₂ continue to be present in the off-gases. Samples taken at temperatures below 550°C did not contain any evolved gas. The condensable volatile products were collected on the water-cooled condenser, chromatographed on alumina, and separated into four relatively pure fractions. The first three were identified by infrared absorption as fluorene, $\Delta^9,9'$ -bifluorene, and dibenzo(ac)triphenylene. The highest molecular weight fraction (i.e., last to elute from the column) has a very simple IR spectrum, with only two sharp major bands at 13.10 and 13.68 microns, indicating three or four adjacent hydrogen atoms on aromatic rings as the principal structural feature; however, its structure has not been identified.

Table 37. Composition of the Fixed Gases Evolved During the Pyrolysis of $\Delta^9,9'$ -Bifluorene in Helium, TGA-GE Run 50

Temp. When Sample Taken → Gas	Mol % of Gas in Fraction					
	500°C	558°C	605°C	652°C	698°C	750°C*
Hydrogen (H ₂)	Sl. trace	trace	81	79	83	87
Methane (CH ₄)	--	--	13	16	13	12
Ethane (C ₂ H ₆)	--	--	3	3	2	1
Ethylene (C ₂ H ₄)	--	--	1	1	1	trace
Carbon Monoxide (CO)	--	--	2	1	1	trace
Carbon Dioxide (CO ₂)	--	--	sl. tr.	sl. tr.	sl. tr.	sl. tr.

*Average of three analyses of final gas products.

3.3.3.7.3. ESR Studies

Some preliminary ESR investigations for the pyrolysis of (XXXV) have been reported.^(2,4) The effects of temperature and hydrocarbon concentration on the ESR spectrum have been determined. Table 38 lists the various ESR experiments which have been performed for (XXXV).

No ESR is observed for (XXXV) until a temperature of 300°C is reached. This temperature is about 40°C higher than that required to observe an ESR in 9,9'-bifluorene (XXXIII). The resolution of the ESR signal of (XXXV), like that of 9,9'-bifluorene, is sensitive to changes in temperature and concentration.

Table 38. ESR Measurements for $\Delta^9,9'$ -Bifluorene

Concentration in m-Quinquephenyl	Decomp. Temp. °C*	Meas. Temp. °C	Resolved (R) or Unresolved (U)	Linewidth Gauss
Pure	300	340	(R)	~0.30
10%	384	160, 247	(R)	~3.0
10%	384	384	(R)	~2.5
10%	384	147, 160	(U)	~9.0

* Lowest temperature at which an ESR signal was observed.

The spectrum has not been sufficiently resolved to permit an analysis.

Kinetic data have also been obtained from the ESR experiments. Figure 34 is a graph of the line intensity for one of the resolved components of the six-line $\Delta^9,9'$ -bifluorene spectrum as a function of time at 384°C. It is evident that the radical formation is not a simple unimolecular process. After 60 minutes, the lines begin to broaden, and the line intensity is no longer a criterion of concentration. The optimum resolution of the $\Delta^9,9'$ -bifluorene signal occurs at about 350°C. Quenching the 350°C sample to lower temperatures does not affect the free radical concentration, but does impair the resolution.

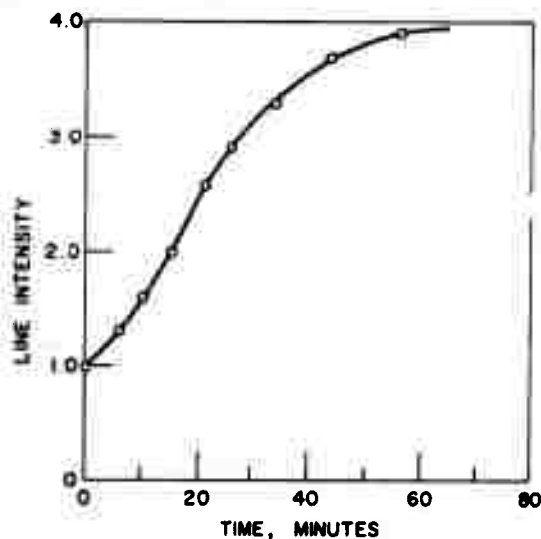


Figure 34. Variation of the ESR Line Intensity of $\Delta^9,9'$ -Bifluorene with Time at 384°C

3.3.3.7.4. Chemical Studies of Pyrolysis

Chemical studies have been performed on the pyrolysis of $\Delta^8,9'$ -bifluorene. Figure 35 shows infrared spectra of samples which have been heat-treated to temperatures between 390°C and 500°C. The thermal transformations are gradual, involving rearrangements as evidenced by the changes in the aromatic substitution region (10 to 14 microns) and in the 7 micron region. The spectrum of the distillate obtained in these pyrolyses has been identified as pure fluorene (XXXVI). The formation of fluorene requires a disproportionation of the molecules and an abstraction of hydrogen from the aromatic rings.

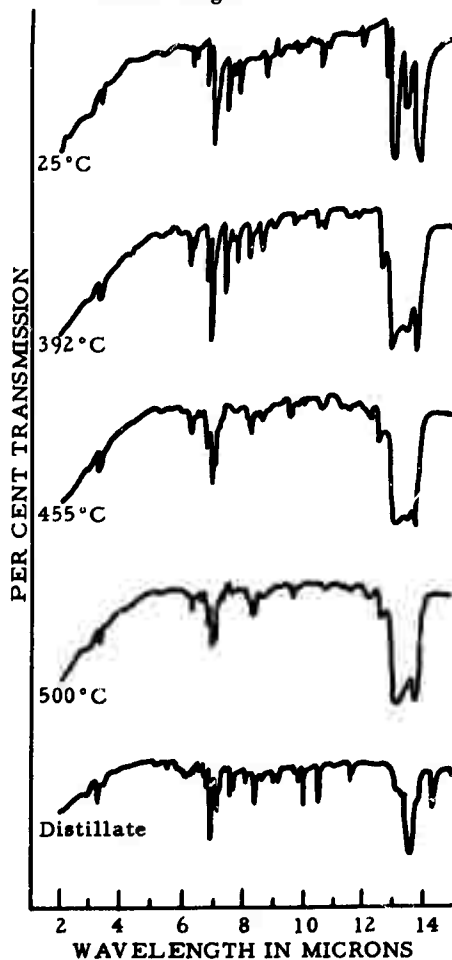


Figure 35. Infrared Spectra of Heat-Treated $\Delta^8,9'$ -Bifluorene

N-6678

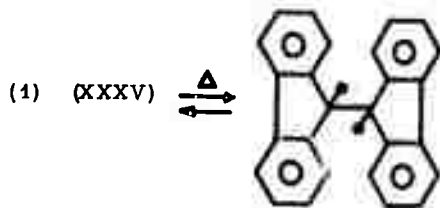
A considerable amount of dibenzo(ac)triphenylene was isolated from the 500°C residue by chromatographic extraction. A large quantity of a red hydrocarbon product was also separated from the residue. On the basis of UV and IR analysis, this product was shown to contain rubicene (XXXVII) in addition to some high molecular weight material.



(XXXVII)

3.3.3.7.5. Thermal Reactions of $\Delta^9,9'$ -Bifluorene

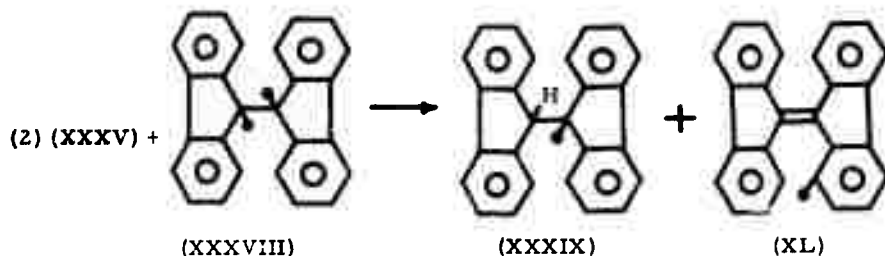
The ESR spectrum observed during the pyrolysis of $\Delta^9,9'$ -bifluorene (XXXV) is thought to be attributable to the biradical (XXXVIII).



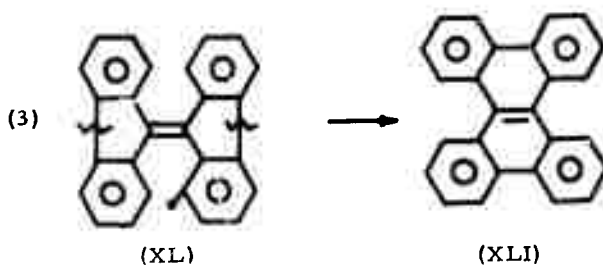
(XXXVIII)

The formation of (XXXVIII) through a thermal activation process would relieve the strain in the initial (XXXV) molecule.

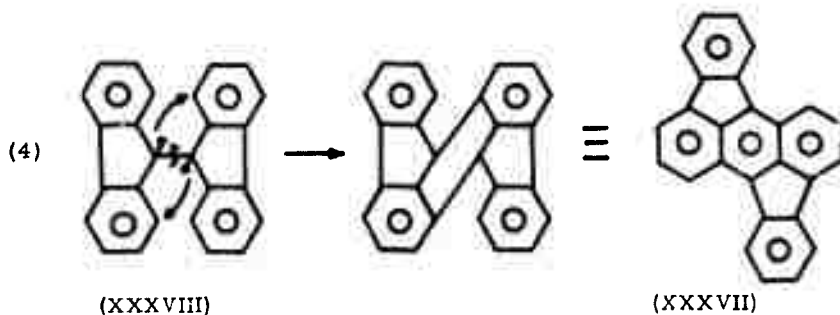
The radical (XXXVIII) can abstract hydrogen atoms from other $\Delta^9,9'$ -bifluorene molecules. These hydrogen abstractions are expected to occur at the reactive 1, 3-positions to produce radicals such as (XXXIX) and (XL).



The rearrangement of radicals like (XL) would result in the formation of the nonplanar dibenzo(a, c)triphenylene (XLI).

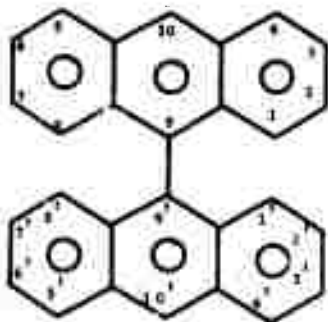


Radicals of structure (XXXIX) would produce fluorene by further hydrogen abstraction, while compound (XXXVIII) could react directly to form rubicene (XXXVII).



Additional nonplanar aromatic structures can be formed by recombination of various kinds of similar free radical intermediates. Thus, the carbonization of (XXXV) is expected to involve a nonplanar condensation process.

3.3.3.8. 9,9'-Bianthryl



(XLII)

The compound 9,9'-bianthryl (XLII) yields an extremely well-ordered graphite. Preliminary ESR and chemical pyrolysis studies are reported for this compound.

3.3.3.8.1. ESR Studies

A 10 per cent solution of (XLII) in *m*-quinquephenyl first exhibited on ESR signal at 550°C. This signal which consists of a complex pattern of lines with linewidths on the order of 0.25 gauss is shown in Figure 36. The spectrum is believed to be that of a neutral anthryl radical (XLIII) formed by thermal disassociation of (XLI). Further work will be required, however, to confirm this conclusion.

3.3.3.8.2. Chemical Studies

Since the compound 9,9'-bianthryl begins to pyrolyze at a fairly high temperature, its reactions are difficult to control. At 520°C, an infusible black product is formed which shows two major aromatic C-H absorptions at 11.3 to 11.7 μ and 13.2 to 13.6 μ in the infrared. The starting material (XLII) has major bands at 11.3, 12.8, and 13.7 μ .

At about 500°C, a fusible black product was obtained, a portion of which could be chromatographically extracted. A number of hydrogenated aromatic fractions were obtained in addition to some red aromatic products which had infrared absorption bands at 11.5, 12.3, and 13.1 μ and visible absorption between 420 and 550 $m\mu$. These spectral data are indicative of benzoperylene derivatives.

9,9'-BIANTHRYL

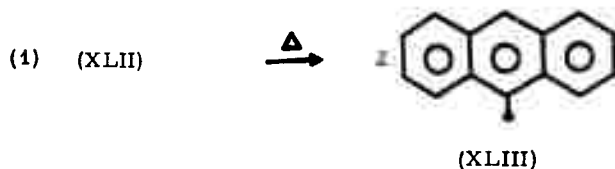


N-6999

Figure 36. ESR Spectrum of 9,9'-Bianthryl at 550°C

3.3.3.8.3. Thermal Reactions of 9,9'-Bianthryl

The initial thermal reactions of (XLII) are thought to involve a dissociation to anthryl radicals (XLIII).

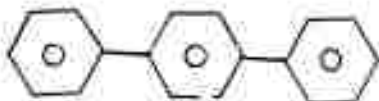


These planar free radicals can recombine to form the symmetrical, planar derivatives of perylene such as (XLIV) and (XLV).



The formation of 1,2,7,8-dibenzoperylene (XLIV) is favored from reactivity. Further carbonization reactions could proceed by condensation of these derivatives. Hydrogen abstraction by the radicals (XLIII) leads to the formation of the hydrogenated derivatives of (XLII), such as anthracene and dihydrodianthranyl, which have also been isolated in the reaction product.

3.3.3.9. p-Terphenyl



(XLVI)

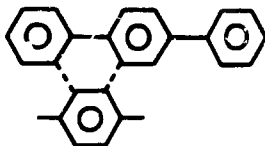
The compound p-terphenyl is an extremely stable aromatic hydrocarbon, precluding any TGA or ESR study. By thermal treatment under pressure, it can be converted to a highly-disordered carbon.

Previous results for the pyrolysis of p-terphenyl⁽⁴⁾ showed that carbon-carbon bond cleavage between phenyl rings was an important first reaction. Subsequently, the thermally formed phenyl and biphenyl radicals underwent hydrogen abstraction or condensation to infusible product.

3.3.3.9.1. Chemical Studies of Pyrolysis

Chromatographic extraction of the black residue prepared from p-terphenyl at 550°C⁽⁴⁾ was attempted. Although a variety of solvents were employed, only a slight amount was eluted from the column.

At 550°C, the major change in the p-terphenyl product appeared to be the formation of species with major infrared bands at 13.60, 12.70, and 12.15 microns. The first band is characteristic of aromatics containing four adjacent hydrogens of the triphenylene and 1,2,5,6-dibenzanthracene type. Such substituted structures could be formed through condensation reactions of the following type:



This type of fusion process would involve the reactive ortho positions. A variety of polyphenyl products ranging from benzene to quinquephenyl appear to be side products of the ring cleavage reaction.

The complete insolubility of the residue prevented further study of the condensation product by chemical methods. The carbon residues from p-terphenyl were studied by small angle X-ray methods. It was found that in the first stages of carbonization no unique reaction intermediates are formed. Instead, a mixture of nonplanar aromatic structures with little ordered layer stacking is observed. The layer growth accelerates between 600° and 800°C, but even at 3000°C the structure does not approach a graphite.

3.3.3.9.2. Thermal Dehydrogenation of p-Terphenyl

Elementary analysis data have been obtained for the series of thermal reaction products produced from p-terphenyl.⁽⁴⁾ These data are listed in Table 39.

Table 39. Elementary Analyses for Pyrolyzed p-Terphenyl

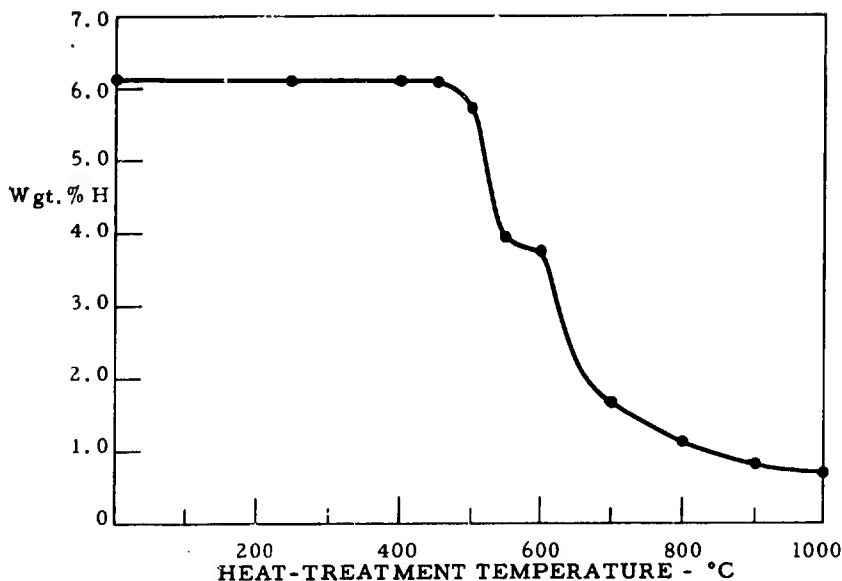
Pyrolysis Temp. °C	Wgt. % C	Wgt. % H	Atomic C/H
25	93.88	6.12	1.29
525 - 4 hrs	94.43	5.74	1.38
525 - 10 hrs	94.72	5.50	1.44
525 - 20 hrs	95.26	4.85	1.65
535	95.32	4.52	1.77
550	96.37	3.90	2.07
600	96.23	3.76	2.15
700	97.02	1.69	4.81
800	97.99	1.13	7.29
900	98.38	0.83	9.99
1000	99.27	0.70	12.0

The percentage hydrogen as a function of temperature is plotted in Figure 37 for p-terphenyl. As in the case of fluoranthene, major loss of hydrogen occurs in a smooth manner above 600°C.

3.3.3.10. 10, 15-Dihydro-5H-diindeno-(1, 2-a; 1', 2'-c)fluorene (α -Truxene)



(XLVII)



N-5773

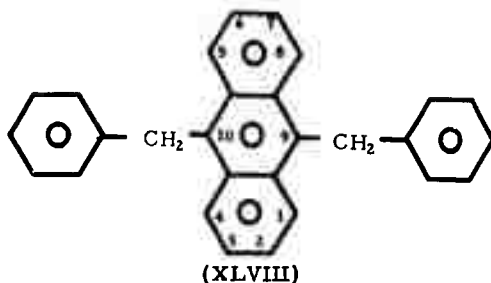
Figure 37. Dehydrogenation Curve for Carbonized p-Terphenyl

Pyrolysis studies were initiated on the hydrocarbon α -truxene (XLVII). This compound is thermally reactive and gives a 28 per cent carbon yield in the DTA experiment. The graphite derived from (XLVII) shows relatively low order.

A sample of (XLVII) has been pyrolyzed at 470°C, and the residue was chromatographically separated. Preliminary analyses of the products indicated an extensive amount of thermal hydrogen transfer within the molecule. Thermal cleavage of the strained 5-membered ring systems was also indicated by infrared analysis of the products. Such reactions would give rise to nonplanar aromatic radicals and are consistent with the ultimate structure of the graphite obtained from α -truxene. At 470°C, insufficient reaction product was separated to permit detailed analysis. Further studies on this system were discontinued.

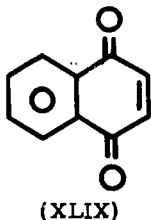
3.3.3.14. 9,10-Dibenzylanthracene

The compound 9,10-dibenzylanthracene (XLVIII) yields a relatively disordered graphite when heated to 3000°C. Some preliminary ESR pyrolysis experiments have been performed for this compound. Pure (XLVIII) first showed an ESR signal at 400°C. This signal was unresolved and consisted of a single 10 gauss wide line. When the hydrocarbon was



diluted in *m*-quinquephenyl, a resolved spectrum could be observed at 450°C. The individual linewidths in this spectrum were 0.25 gauss at 235°C. This spectrum has not yet been analyzed but can probably be attributed to the free radical formed by the dissociation of a single benzyl hydrogen atom.

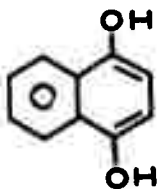
3.3.3.12. 1,4-Naphthoquinone



Quinones are presumed to be important intermediates in the oxidation of aromatic raw materials for graphite. The introduction of the carbonyl group on the aromatic ring has been shown to modify the thermal reaction sequence and to lead to a more disordered graphite. Some initial studies were therefore made on the pyrolysis of a representative quinone, 1,4-naphthoquinone.

3.3.3.12.1. Chemical Studies

The compound 1,4-naphthoquinone begins to pyrolyze at about 290°C. Figure 38 shows infrared spectra for the residue and distillate obtained from 1,4-naphthoquinone at 295°C. The distillate appears to be largely the reduction product, 1,4-naphthalenediol (L).



(L)
124

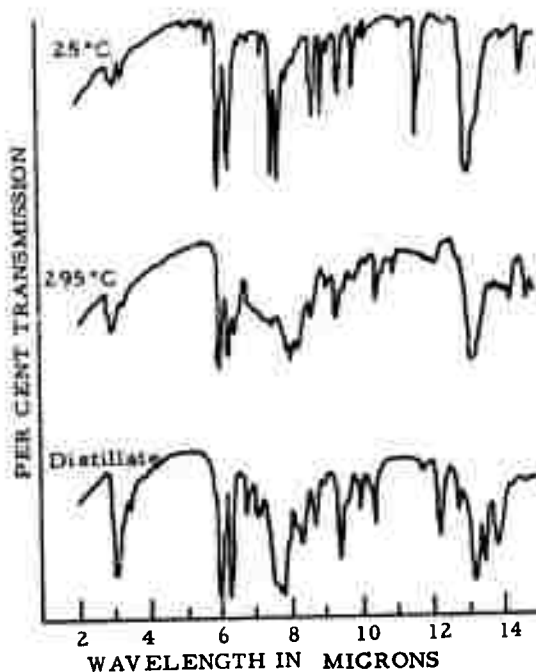
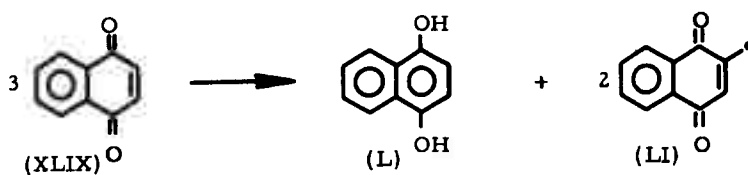


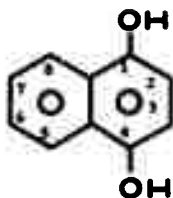
Figure 38. Infrared Spectra of Heat-Treated 1,4-Naphthoquinone N-6402

The dehydrogenation which leads to the formation of (L) is believed to involve the 2,3-positions, a conclusion which is based on the absence of the 11.60 micron IR band in the spectrum of the residue.



Further reaction could involve recombination of radicals such as (LI), followed by a rupture of the $\text{C}-\overset{\text{O}}{\text{C}}$ bond.

3.3.3. 13. 1,4-Naphthalenediol



(L)

Some preliminary thermal reaction studies were performed on 1,4-naphthalenediol. This reactive compound begins to pyrolyze at 245°C. The infrared spectrum of the pyrolysis product obtained at 245°C is presented in Figure 39.

At 245°C, the compound undergoes partial dehydrogenation to form quinone products as shown by the IR carbonyl band at 5.95 μ . Considerable change occurs in the aromatic substitution region at 13-13.5 μ as well as in the 7-7.5 μ region. More detailed studies of these reactions have not yet been attempted.

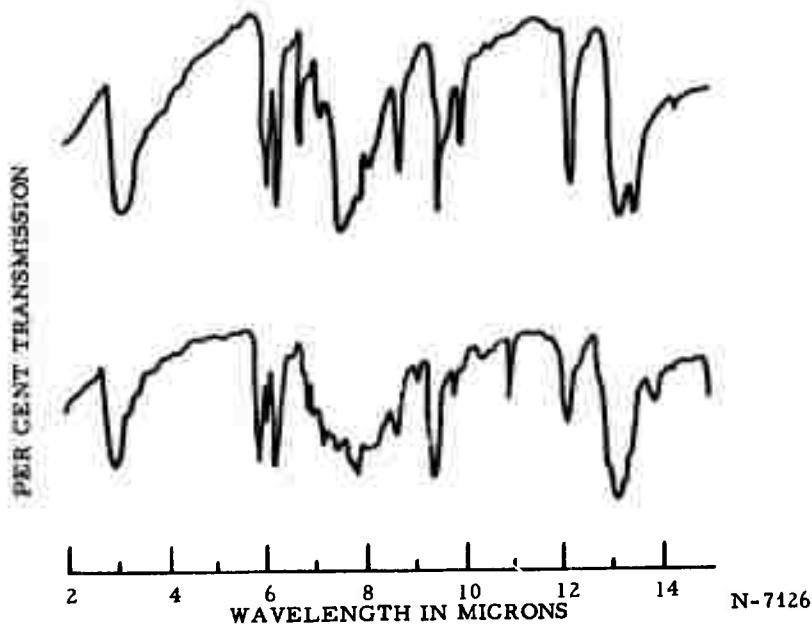


Figure 39. Infrared Spectra of Heat-Treated 1,4-Naphthalenediol

3.3.4. Thermal Dehydrogenation of Aromatic Hydrocarbons

Elementary analysis data have been obtained for the pyrolysis residues from 25°C to 1000°C for the four aromatic hydrocarbons; acenaphthylene, fluoranthene, 9,9'-bifluorene, and p-terphenyl. Table 40 compares the hydrogen content for the four aromatic hydrocarbons at 1000°C. Included are the semilattice spacings for graphites prepared from the same materials. These data show that the rate of thermal dehydrogenation can be related to the structure of the final graphite. The "well-graphitizing materials" graphitize at a faster rate. It would be expected that reactions which proceed through planar aromatic intermediates would result in products of greater stability than those involving non-planar entities and should occur more readily.

Table 40. Hydrogen Content and Graphite Properties of Cokes Derived from Aromatic Hydrocarbons

Aromatic Hydrocarbon	Weight Per cent H at 1000°C	002, Å
(1) Acenaphthylene	0.23	3.356
(2) Fluoranthene	0.50	3.371
(3) 9,9'-Bifluorene	0.53	3.374
(4) p-Terphenyl	0.70	3.437

3.3.5. General Conclusions Concerning the Mechanisms of Carbonization of Aromatic Hydrocarbons

On the basis of the studies which have been completed, the following general conclusions can be made concerning the mechanisms of carbonization of aromatic hydrocarbons:

- The mechanisms of carbonization are complex and do not involve single reactions occurring in discrete steps; however, a good representation of the general carbonization sequence for an aromatic hydrocarbon can be based on a knowledge of only a few of the many reactions occurring during pyrolysis.
- The initial carbonization reactions involve the thermal cleavage of a C-H or a C-C bond to form an aromatic free radical. This cleavage generally occurs at the most reactive site, the position of highest electron density, in the molecule.
- For condensed aromatic hydrocarbons containing no side chains, this initial reaction usually involves the thermal dissociation of a C-H bond. The formation of the aromatic free radicals is generally accomplished by a transfer of hydrogen from the most reactive site of one molecule to an acceptor site of a neighboring molecule.

The production of 5, 12-dihydronaphthacene during the initial free radical formation from naphthacene is a typical example of such a reaction. Direct dehydrogenation can occur in molecules which are poor electron acceptors.

d. In aromatic hydrocarbons containing side chain groups, the initial reaction proceeds with C-C bond cleavage in the side chain. If these groups are attached to planar condensed aromatic ring systems, such as in acenaphthylene, rearrangement of the mobile side chains leads to planar polycyclic structures. If the side chain is not joined to a condensed aromatic system, as in $\Delta^8,9$ -bifluorene, then cleavage of these side chains leads to the formation of nonplanar free radical intermediates.

e. Methyl substituents on aromatic rings are thermally cleaved to methyl radical. The ease of cleavage of these groups accounts for their activating effect on aromatic hydrocarbon pyrolysis.

f. The structure and properties of the final graphite can be related directly to the structure and reactivity of the initial free radical intermediates. Aromatic radicals which can readily condense or rearrange to form planar structures yield well-ordered graphite. Reactive nonplanar radicals polymerize to form nonplanar aromatic molecules producing a disordered graphite.

g. The initial free radical formations and condensations occur for most aromatic hydrocarbons below 500°C. The extent of molecular rearrangements to planar intermediates depends on the relative rates of the competing rearrangement and condensation reactions. If molecular growth occurs too rapidly and stable nonplanar polymers are produced, the molecular disorder is frozen in and results in a disordered graphite.

h. The condensations of the free radicals proceed at the most reactive positions or points of highest spin density.

i. At higher temperatures, between 500° and 750°C, the thermal polymerization proceeds by fusion of aromatic ring systems by a direct dehydrogenation process. Aromatic polymers containing approximately 100 carbon atoms are formed. Aliphatic side chains which have formed as a result of hydrogen transfers also cleave to form CH_4 , C_2H_6 , C_3H_8 , etc.

3.4. Electron Spin Resonance (ESR) and Optical Studies of the Electron Distribution in Aromatic Free Radicals

3.4.1. Introduction

The pyrolysis mechanism studies reported in Section 3.3. have shown the importance of free radical intermediates in the carbonization of aromatic hydrocarbons. The initial reactions were shown to involve a

thermal bond cleavage at the most reactive site in the molecule. The subsequent reactions of carbonization were related to the structure and reactivity of the first radical intermediate.

Section 3.4. presents the results of studies of the electron distribution in the free radicals of aromatic hydrocarbons. The ESR technique has been used to measure the proton hyperfine coupling constants for aromatic radical cations prepared by the oxidation of hydrocarbons with SbCl_5 . These data can be used to predict the course of thermal reactions of aromatic hydrocarbons. Optical studies have helped to clarify the chemistry of the aromatic hydrocarbon- SbCl_5 interactions. ESR studies are also presented for a completely methylated free radical prepared by the oxidation of hexamethylbenzene.

3.4.2. Electron Spin Resonance of Radical Cations Produced by the Oxidation of Aromatic Hydrocarbons with SbCl_5

3.4.2.1. Introduction

This section describes the electron spin resonance (ESR) of positive radical ions produced by the oxidation of aromatic hydrocarbons with SbCl_5 in CH_2Cl_2 solvent. This oxidation procedure is a general method for the preparation of aromatic hydrocarbon cations in solution. Furthermore, SbCl_5 and CH_2Cl_2 provide the proper combination of oxidant and solvent required for the observation of resolved ESR hyperfine structure. The proton hyperfine coupling constants determined in this study have enabled us to make a comprehensive comparison of Hückel (HMO) spin densities with experiment and to examine the generality of the McConnell relationship, $a_{\text{H}} = Q\rho$.⁽¹²⁾

ESR has been particularly successful in measuring electron distributions in aromatic radical anions and cations. The comparison of coupling constants for corresponding anions and cations provides an important additional test of HMO theory, which predicts identical spin densities for positive and negative ions of alternant hydrocarbons. However, the few cations of alternant hydrocarbons which have been examined⁽¹³⁾ were found to have coupling constants slightly higher than those for respective anions. Aromatic radical anions can generally be prepared by the reduction of the parent hydrocarbon with an alkali metal in an inert solvent. With this method, resolved ESR spectra have been obtained for the radical anions of benzene, toluene, naphthalene, anthracene, pyrene, perylene, tetracene,⁽¹³⁻¹⁷⁾ and a variety of other aromatic hydrocarbons.

Since aromatic radical cations are more difficult to prepare, they have been less extensively investigated. The most satisfactory method of preparation of aromatic radical cations for ESR studies has utilized 98 per cent H_2SO_4 as an oxidizing medium for the parent hydrocarbons.^(18,19) This oxidation process, however, requires a prior dissolution and concomitant protonation of the aromatic hydrocarbon. The unsubstituted aromatic hydrocarbons; anthracene, perylene, naphthacene biphenylene, and coronene have been oxidized in this manner.

Other oxidizing agents which have been employed in ESR studies of aromatic radical cations include: $\text{BF}_3\text{-CF}_3\text{COOH}$,⁽²⁰⁾ SbCl_5 ,⁽²¹⁾ SbCl_5 ,^(22, 23, 24) AlCl_3 ,⁽²⁵⁾ I_2 ,⁽²⁶⁾ V_2O_5 ,⁽²⁷⁾ $\text{SiO}_2\text{-Al}_2\text{O}_3$,⁽²⁸⁾ VOCl_3 ,⁽²⁹⁾ $\text{K}_3\text{Fe(CN)}_6\text{-HClO}_4$,⁽³⁰⁾ and $\text{SO}_2\text{-BF}_3$.⁽³¹⁾ None of these oxidants have yet been found superior to H_2SO_4 for studies of ESR hyperfine structure of radical cations. A more suitable system requires both an oxidizing agent of high electron affinity and a solvent of sufficient polarity. We have found that these criteria can be met by the oxidant SbCl_5 in conjunction with a CH_2Cl_2 solvent. This combination has permitted the preparation of a variety of previously unreported aromatic radical cations.

SbCl_5 has been employed by various investigators as an oxidant for aromatic hydrocarbons. Hilpert and Wolf⁽³²⁾ initially reported the formation of colored solutions for mixtures of aromatic hydrocarbons and SbCl_5 . The solid complexes of SbCl_5 and aromatics were studied by Brass.⁽³³⁾ Weissman, DeBoer, and Conradi⁽³⁴⁾ first observed a paramagnetic resonance spectrum for several of these aromatic hydrocarbon- SbCl_5 solid compounds. A number of investigators^(23, 34, 35) have measured the optical spectra of aromatic radical cations formed by the oxidation of hydrocarbons with SbCl_5 in solution. No observations of resolved ESR hyperfine structure have been reported for these systems. In all cases, either a single sharp line characteristic of a solid, or a broad unresolved line was observed.^(13, 35) Kinoshita⁽³⁷⁾ reported a partially resolved spectrum for the heterocyclic thianthrene with SbCl_5 in nitrobenzene.

Leftin and Hobson⁽³⁸⁾ recently found that the paramagnetic solid compounds formed from the addition of SbCl_5 to diphenylethylene could be dissolved in CH_2Cl_2 ; however, they reported only a broad unresolved ESR spectrum for this solution. We have found that if the oxidation of aromatic hydrocarbons with SbCl_5 is carried out in CH_2Cl_2 under carefully controlled conditions of atmosphere, concentration, and temperature, resolved hyperfine structure can be observed for numerous aromatic radical cations.

This section presents the results of ESR studies of radical cations prepared from 24 aromatic hydrocarbons. The experimental procedure for preparing and measuring the radicals is described in Section 3.4.2.2. Since the observations were critically dependent upon the experimental conditions of concentration and temperature, the ESR experiments are described in detail in Section 3.4.2.3. Section 3.4.2.4. contains a brief discussion of the reactions of SbCl_5 with aromatic hydrocarbons. The assignment and tabulation of coupling constants are given in Section 3.4.2.5. Employing coupling constant data for cations and anions from both this study and the literature, correlations with theoretical spin densities are presented in Section 3.4.2.6.

3.4.2.2. Experimental Procedure

ESR spectra were obtained for 24 aromatic hydrocarbons treated with SbCl_5 in CH_2Cl_2 solution. Three compounds, perylene, naphthacene,

and 9, 10-dimethylanthracene, exhibited well-resolved ESR spectra when solutions of the hydrocarbons in CH_2Cl_2 were treated with SbCl_5 in air at room temperature and then measured in the absence of oxygen. Since the majority of the hydrocarbons examined did not exhibit resolved spectra when treated in this manner, a low-temperature method of sample preparation in vacuum was devised.

The vacuum transfer apparatus is shown in Figure 40. A typical preparation procedure involved the following steps. The hydrocarbon- CH_2Cl_2 solution and SbCl_5 were deoxygenated separately by freezing, pumping, and thawing. A known quantity of SbCl_5 vapor was introduced into the 10 cm^3 bulb by controlling the temperature of the SbCl_5 reservoir.⁽³⁵⁾ The SbCl_5 in the bulb was transferred to the ESR sample tube by cooling the hydrocarbon solution (10^{-3} - 10^{-5} molar) to 77°K. The final concentration of SbCl_5 in the CH_2Cl_2 solution could be calculated by assuming that all the transferred SbCl_5 dissolved in the CH_2Cl_2 (about 0.06 ml. volume). For example, from SbCl_5 vapor pressure data⁽³⁵⁾ extrapolated by use of the Clapeyron equation, the vapor pressure of SbCl_5 at 25°C is 1.26 mm of Hg. Thus, a 10 cm^3 volume of SbCl_5 at this pressure dissolved in 0.06 ml. of CH_2Cl_2 yields a 1×10^{-5} M solution.

The sample tubes were sealed-off with a torch. The samples were melted and shaken in a Dewar containing solid CO_2 , and then inserted into the microwave cavity which had been precooled to -90°C. Since CH_2Cl_2 is extremely lossy at low temperatures, it was necessary to use sample tubes with an ID not greater than about 2 mm. Even so, the uneven distribution of H_1 (rf magnetic field) throughout the sample caused the ESR lines to be asymmetric as a result of the slight admixture of χ' . The line shapes became particularly distorted when the resonance was partially saturated. In order to minimize saturation and line distortion effects, superheterodyne detection was employed at microwave powers less than 0.1 mw.

3.4.2.3. Summary of ESR Observations

The aromatic hydrocarbons were reacted with SbCl_5 in CH_2Cl_2 solvent at -78°C in the absence of air. The ESR spectra were measured at temperatures near -90°C and, in some cases, at several higher temperatures. Table 41 summarizes the results for the compounds which exhibited resolved spectra. The ESR spectra of the 16 compounds in Table 41 all contained evidence of proton hyperfine structure. In most cases, the spectra were essentially completely resolved with the individual linewidths varying between 0.04 and 0.50 gauss. The spectra of the last three compounds in Table 41 were only partially resolved. In addition to the number and widths of the ESR spectral lines, the colors of the individual hydrocarbon- SbCl_5 solutions are listed in Table 41. In a number of instances, the colors were temperature dependent.

Similar data for the compounds which exhibited totally unresolved spectra are included in Table 42. The spectra for these hydrocarbons consisted of either a single sharp line with a linewidth on the order of several

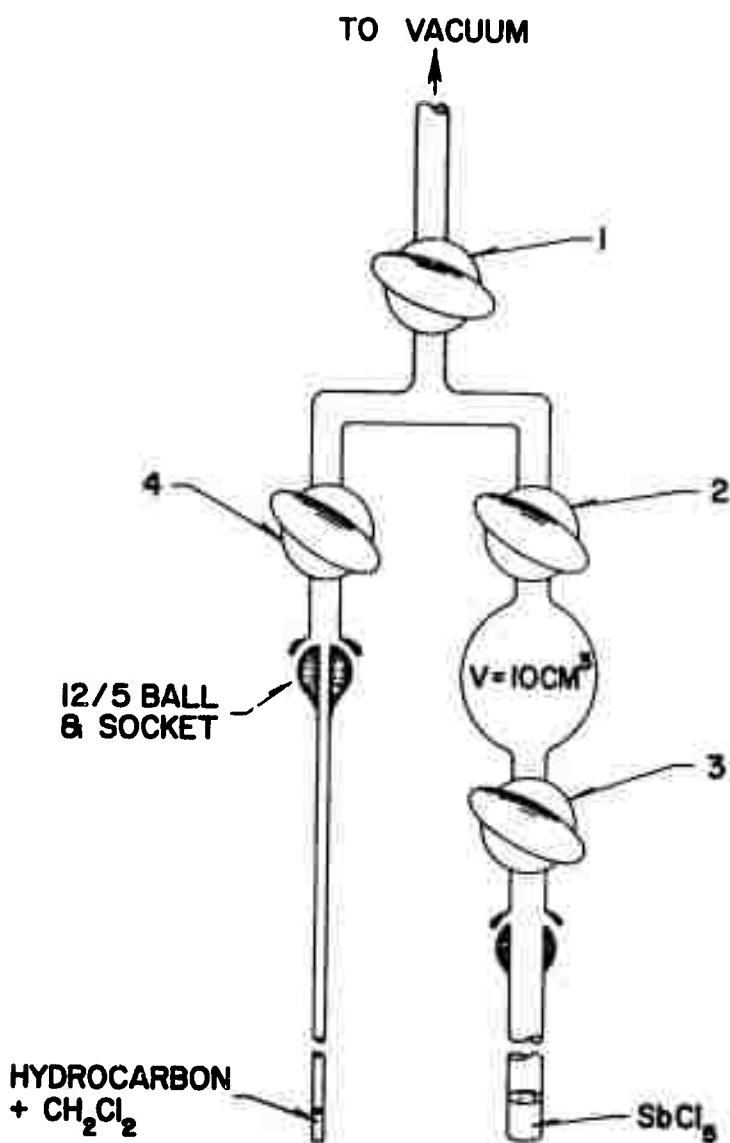










Figure 40. Vacuum Transfer Apparatus for the Preparation of
Hydrocarbon - SbCl₅ Solutions at Low Temperatures









N-6315

Table 41. Summary of ESR Observations on Aromatic Hydrocarbon Radical Cations Produced by SbCl_5 in CH_2Cl_2 Solvent--Resolved Spectra

Compound	Structure	Hydrocarbon Concentration (Molar)	SbCl_5 Concentration (Molar)	Measuring Temperature ($^{\circ}\text{C}$)	No. Lines	Line-width (Gauss)	Remarks: color, (a) etc.
Naphthalene		1×10^{-4}	1×10^{-2} One drop in air	25 25	~ 50	0.40	Blue
Perylene		5×10^{-5}	1×10^{-2} One drop in air	25 25	~ 75	0.25	Blue
9,10-Dimethyl-anthracene		1×10^{-4}	One drop in air	25	~ 60	0.50	Blue
Naphthalene		1×10^{-3}	2×10^{-3}	-91	81	0.12	Purple
Anthracene		5×10^{-4}	1×10^{-2}	-85	~ 50	0.20	Green
Pyrene		1×10^{-4}	6×10^{-3}	-38	75	0.15	Green
Tetraphenylethylene		5×10^{-4}	1×10^{-2}	-91	~ 100	0.05	Purple, fades at 25°C
Δ 9,9'-Bifluorene		5×10^{-4}	1×10^{-2}	-91	~ 100	0.04	Purple, fades at 25°C

Continued...

Table 41. Continued

Compound	Structure	Hydrocarbon Concentration (Molar)	SnCl ₄ Concentration (Molar)	Measuring Temperature (°C)	No. Lines	Line- width (Gauss)	Remarks; color, (a) etc.
Dibenzo (a, c)- triphenylene		10^{-3}	6×10^{-3}	-91	~ 70	0.15	Blue
Triphenylene		5×10^{-4}	1×10^{-2}	-91	~ 30	0.20	Green
Chrysene		5×10^{-4}	1×10^{-2}	-50	~ 50	0.20	Red-orange
3,4,5,6-Dibenz o- phenanthrene		1×10^{-4}	1×10^{-2}	-21	~ 75	0.15	
1,2,5,6-Dibenz- anthracene		5×10^{-4}	1×10^{-2}	-38	~ 30	0.15	Cherry red
Fluorene		1×10^{-4}	1×10^{-2}	-91	3	3	Blue-green
Fluoranthene		1×10^{-3}	6×10^{-3}	-38	Several	2	Red-orange at -90° C, blue at -38° C
7,12-Dimethylbenz- (a)-anthracene		1×10^{-3}	1×10^{-2}	-91	3 or 4	1	Blue

(a) The color observations were made at the ESR measuring temperature except where otherwise indicated.

Table 42. Summary of ESR Observations of Aromatic Hydrocarbon Radical Cations Produced by SbCl_5 in CH_2Cl_2 Solvent--Unresolved Spectra

Compound	Structure	Hydrocarbon Concentration (molar)	SbCl_5 Concentration (molar)	Measuring Temp. ($^{\circ}\text{C}$)	Lines with Gauss)	Remarks (color, etc.)
Coronene		2×10^{-4} 5×10^{-4}	1×10^{-2}	-91, -92, 0	11	Green
Benzenyl ^a		2×10^{-4} 1×10^{-3} 5×10^{-3}	1×10^{-2}	-91, -38	8-9	-91: Green -92: Blue
Acenaphthene		1×10^{-3}	1×10^{-2}	-91, -46	9-8	
Trans-Stilbene		1×10^{-3}	1×10^{-2}	-91	Broad, weak	-80: C Red 25: C Green
Phenanthrene		1×10^{-3}	1×10^{-2}	-91, -38	10	
Diphenyldiacetylene		1×10^{-3}	1×10^{-2}	-91, -38	10	Blue - Black
p-Xylene ^a		1×10^{-1}	1×10^{-2}	-91	Broad, weak	-80: C Orange (after 24 hrs. at 25: C) 25: C Purple
Benzene		1×10^{-1}	2×10^{-2}	-91 -91	No Signal 10	Colorless Light Green (after 2 hrs. at 25: C)
Acenaphthylene		1×10^{-3} 1×10^{-3}	1 drop in air 1×10^{-2}	25 -91 -38	12 No Signal	Green Green

(a) The color observations were made at the ESR measuring temperature except where otherwise indicated.

gauss or a single broad line with a width of about 10 gauss. Since the nuclear hyperfine structure in practically all aromatic free radicals extends over about 30 gauss, a simple broadening of the hyperfine components usually results in a Gaussian-shaped line with a peak-to-peak linewidth of about 10 gauss. On the other hand, a solid free radical or paramagnetic charge-transfer complex generally exhibits an exchange-narrowed single line only a few gauss wide, with either an asymmetric shape or a symmetrical line shape tending toward Lorentzian.

The hydrocarbon and SbCl_5 concentrations and the ESR measuring temperatures are given in Tables 41 and 42. These conditions were not the only ones tried. The stability of the radical ions and resolution of the spectra were critically dependent on both the hydrocarbon and SbCl_5 concentration as well as on the measuring temperature. Although attempts were made to optimize the experimental conditions, it is possible that the resolution could have been improved for several of the systems listed if additional combinations of concentrations and temperature had been tried. The ESR observations and their dependence on the experimental variations are discussed for each compound in order of appearance in the Tables.

3.4.2.3.1. Resolved Spectra




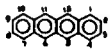







a. Naphthacene, Perylene, and 9,10-Dimethylantracene

These three hydrocarbons exhibited well-resolved, hyperfine structure when the SbCl_5 was added either in vacuum or air. A sharp signal characteristic of a solid free radical was observed, however, if the amounts of hydrocarbon or SbCl_5 present were excessive. Solutions less concentrated than 10^{-4} M in hydrocarbon were found to be adequately dilute for resolution of the hyperfine structure. In each instance, the hyperfine patterns proved to be virtually identical to those observed for the corresponding compounds in H_2SO_4 . The proton hyperfine coupling constants obtained from the analyses of these spectra are given in Table 43.

b. Naphthalene

A considerable effort was required to obtain a well-resolved ESR spectrum for naphthalene positive ion. A broad signal with no trace of resolved hyperfine structure was seen in samples measured at room temperature. Resolved structure was observed in a solution 10^{-3} M in naphthalene and 10^{-2} M in SbCl_5 , prepared and measured at -90°C . However, the signal became smaller with time and disappeared in about 20 minutes. One possible reason for the disappearance was a reaction of the radicals with excess SbCl_5 . To test this idea, several additional samples were prepared using smaller amounts of SbCl_5 . With the solution 6×10^{-3} M in SbCl_5 , although the initial decrease in signal was just as rapid, a small stable signal remained indefinitely. For a 2×10^{-3} M concentration of SbCl_5 , the signal grew for about 15 minutes and then remained stable indefinitely at -91°C . Figure 41 (c) shows the spectrum for this sample. The signal disappeared rapidly at -72°C , with no apparent broadening.

Table 43. Coupling Constants for Aromatic Hydrocarbon Radical Ions





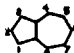



Compound	Structure	Position	ρ (HMO)	a_{1r} Negative Ion (Gauss)	a_{1r} Positive Ion, H_2SO_4 (Gauss)	a_{1r} $SbCl_5$ (Gauss)	
(1) Perylene		3 1 2	.108 ⁴² .083 .013	3.53 ¹⁵ 3.09 0.46	4.11 ¹⁵ 3.09 0.46	4.04 3.04 0.44	
(2) Anthracene		1 2 9	.097 ⁴² .048 .193	2.74 ¹⁵ 1.57 5.56	3.11 ¹⁵ 1.40 6.65	3.08 1.38 6.49	
(3) 9,10-dimethylanthracene		1 2 CH ₃	.078 ⁴³ .039 a	2.90 ⁴³ 1.52 3.88	2.54 ⁴³ 1.19 8.00	2.46 1.23 7.50	
(4) Benzo[a]anthracene		1 2 5	.056 ⁴² .034 .147	1.49 ¹⁵ 1.17 4.25	1.74 ¹⁵ 1.03 5.17	1.68 1.02 5.01	
(5) Pyrene		1 2 4	.136 ⁴² 0 .087	4.75 ¹⁷ 1.09 2.08	-	5.38 1.18 2.12	
(6) Naphthalene		1 2	.181 ⁴² .069	4.95 ⁴⁴ 1.87	-	2.77 (5.54) ^b 1.03 (2.06)	
(7) Triphenylmethyl radical		1 2 3 4	.027 .056 .002 .067	-	-	0.60 ^c 1.99 < 0.03 2.28	
(8) Tetraphenylmethyl radical		1 2 3 4 9	Anion .034 .017 .042 .009 .145	Cation .067 .002 .056 .027 .134	Undetermined ⁴⁵	-	2.14 ^c 0.15 1.98 0.46
(9) Tetraphenylethylene		2 3 4	.048 .019 .056	Undetermined ⁴⁶	-	2.06 ^c 0.52 2.93	
(10) Biphenylene		1 2	.027 ⁴⁷ .087	0.21 ⁴⁷ 2.86	0.21 ⁴⁷ 3.69	-	
(11) Coronene		1	.057 ⁴²	Undetermined ⁴⁰	1.53 ⁴⁸	-	

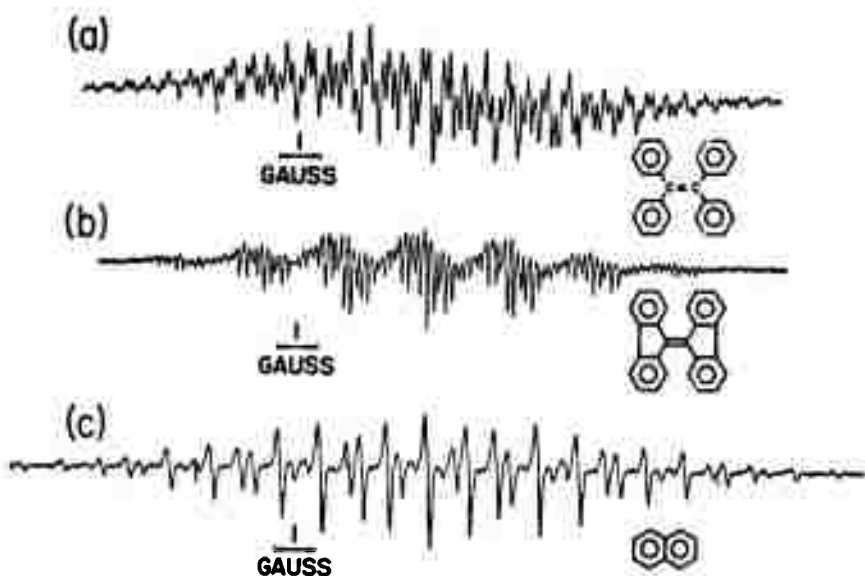
a) Values are for positive ion obtained from ref. 43, CH₃ splittings are by hyperconjugation.b) Values in parentheses are the experimental values multiplied by 2, on the assumption of a naphthalene dimer in SbCl₅.

c) The specific assignments of coupling constants to the molecular positions shown were made on the basis of a comparison between experimental and HMO spin densities.

Continued...

Table 43. Continued

Compound	Structure	Position	ρ (HMO)	a_{H^+} Negative Ion (Gauss)	a_{H^+} Positive Ion, H_2SO_4 (Gauss)	a_{H^+} SbCl ₅ (Gauss)
(12) Benzene		1	.167	3.75 ¹⁴	-	-
(13) Cyclooctatetraene		1	.125	3.21 ⁴⁹	-	-
(14) Biphenyl		2 3 4	.090 .020 .158	50 2.73 0.43 5.46	-	-
(15) Phenanthrene		1 2 3 4 9	.116 .002 .099 .054 .172	44 3.71 0.43 2.88 0.63 4.43	-	-
(16) Azulene		1 2 4 5 6	<u>Anion</u> .004 .100 .221 .010 .264 <u>Cation</u> .295 .000 .026 .113 .000	51, 52 ^ 27 3.95 6.22 1.34 8.83	-	-
(17) p-Terphenyl		1 2 3 4	.060 .008 .088 .049	53 2.07 0.56 3.30 0.95	-	-
(18) Acenaphthylene		1 2 3 4	<u>Anion</u> .104 .151 .014 .178 <u>Cation</u> .264 .044 .027 .060	54 3.06 4.51 0.46 5.60	-	-
(19) Pentacene		1 2 3 4	.035 .025 .106 .141	44 0.88 0.88 3.08 4.27	-	-



N-6689

Figure 41. ESR Spectra for the Radical Cations of (a) Tetraphenylethylene, (b) $\Delta^{9,9}$ -Bifluorene, and (c) Naphthalene

c. Anthracene

A 5×10^{-4} M solution of anthracene exhibited a large, fairly well-resolved signal at -85°C . At room temperature, the signal broadened irreversibly to a 15 line spectrum with linewidths ~ 0.6 gauss. The resonance disappeared completely in about 30 minutes. The broadening could be due to rapid electron exchange with the diamagnetic dipositive ion. Dipositive ion formation has been observed in other hydrocarbon ion systems.⁽³⁴⁾

d. Pyrene

The positive ion of pyrene has not yet been reported. This radical ion can be prepared in $\text{SbCl}_5\text{-CH}_2\text{Cl}_2$ at room temperature in air. However, only an incompletely resolved spectrum consisting of 15 lines 0.6 gauss wide is observed. If the concentrations of pyrene and SbCl_5 are too large, a solid precipitates and an intense signal about 0.3 gauss wide is observed. If the preparation is carried out in vacuum at low temperatures with small quantities of SbCl_5 and pyrene, no signal is observed at -90°C . Presumably, the hydrocarbon is not sufficiently soluble in CH_2Cl_2 .

at low temperatures. Upon warming a 5×10^{-4} M sample of pyrene-SbCl₅ to -38°C , some hydrocarbon dissolved and both the sharp peak due to the solid and a well-resolved hyperfine structure are observed. If the pyrene concentration is decreased to 1×10^{-4} M, only the well-resolved hyperfine spectrum is obtained. This spectrum, which consists of about 50 lines 0.15 gauss wide, broadens and loses its resolution irreversibly above -16°C . The irreversible broadening may, again, be due to electron exchange with the pyrene dipositive ion.

e. Tetraphenylethylene

At -91°C , a 10^{-3} M solution and a 5×10^{-4} M solution of hydrocarbon containing identical amounts of SbCl₅ gave about the same radical concentration and the same resolution of hyperfine structure. Under these conditions, a spectrum of about 100 lines with an average linewidth of 0.05 gauss was obtained. Figure 41(a) shows the ESR curve for a 10^{-3} M solution run at -91°C . A 4×10^{-5} M solution gave a smaller signal with no improvement in resolution. When a 2×10^{-4} M solution is warmed from -91°C to -56°C , a large increase in radical concentration occurs, but the individual lines broaden to about 0.3 gauss. These changes in radical concentration and linewidths are not reversible when the sample is recooled to -91°C . The radical concentration for the 5×10^{-4} M solution does not increase on warming. This behavior is similar to that observed for pyrene and again indicates the critical dependence of radical concentration on hydrocarbon solubility in CH₂Cl₂. The increase in linewidth for the more concentrated solution may be due either to rapid electron exchange or to dipolar broadening resulting from the high radical concentration. There is a broad background signal in Figure 41(a) which cannot be explained by line overlap alone. This signal must arise from a second radical species which exhibits a poorly resolved spectrum.

f. $\Delta^9, 9'$ -Bifluorene

Figure 41(b) shows the spectrum of 5×10^{-4} M hydrocarbon solution run at -91°C . This spectrum consists of about 100 lines with individual linewidths of 0.04 gauss. It was later found that the 0.1 mw value of microwave power used for this measurement partially saturated the resonance. Note that the individual hyperfine lines are not symmetrical. The asymmetry is presumably due to a slight admixture of χ^1 resulting from the very lossy CH₂Cl₂ solvent. There was no change in the signal when the sample was measured at -38°C .

g. Dibenzo(a, c)Triphenylene

A 10^{-3} M solution of this hydrocarbon gave an extremely intense signal at -91°C after treatment with SbCl₅. Approximately 70 lines with a linewidth of 0.5 gauss were recorded. The analysis of this spectrum is discussed in the following section. No paramagnetic solid formation was observed for this compound.

h. Triphenylene

The ESR spectrum of the triphenylene positive ion is of considerable interest because of the two-fold degeneracy of the energy levels of the ground state.^(40,41) At -91°C , a 5×10^{-4} M solution of triphenylene- SbCl_5 exhibited an incompletely resolved ESR spectrum with 30 lines approximately 0.2 gauss wide. The fairly narrow linewidth suggests that time-dependent Jahn-Teller distortions which lead to line broadening are probably absent.⁽⁴⁰⁾ More concentrated solutions of triphenylene exhibit a single sharp line of a paramagnetic solid in addition to the hyperfine structure.

i. Chrysene

Chrysene reacts with SbCl_5 at -78°C to form a paramagnetic solid which at -91°C exhibits a single ESR line 0.5 gauss wide. As the sample is warmed, the solid dissolves and hyperfine structure appears. At -56°C , a 5×10^{-4} M solution of chrysene exhibited more than 50 lines each about 0.2 gauss wide. HMO theory predicts a total of 729 lines for the chrysene radical cation. The incomplete resolution, to be expected for a spectrum consisting of so many lines, did not permit a detailed analysis.

j. 3,4,5,6-Dibenzophenanthrene

This hydrocarbon was quite insoluble in CH_2Cl_2 at low temperatures and only a weak signal was observed at -91°C . When dilute solutions of 3,4,5,6-dibenzophenanthrene- SbCl_5 were warmed to room temperature, the ESR signal intensity increased, consisting of a single sharp line of a paramagnetic solid superimposed on the hyperfine pattern of the soluble ion. In this instance, the radical ion as well as the hydrocarbon has a low solubility in CH_2Cl_2 . At -21°C it was possible to record the hyperfine structure in the absence of the solid signal for a 10^{-4} M solution of hydrocarbon. A complex pattern of approximately 75 lines was obtained under these conditions. The poor signal-to-noise ratio, however, made the analysis of the spectrum difficult.

k. 1,2,5,6-Dibenzanthracene

A 5×10^{-4} solution exhibited no signal at -91°C , but when the solution was warmed to -40°C , a partially resolved signal consisting of ~ 30 lines 0.2 gauss wide was observed. Above -30°C , the signal decreased rather rapidly with time. The complexity of the molecule and the incomplete resolution precluded a detailed analysis of the hyperfine spectrum.

l. Fluorene

At -91°C , a 10^{-4} M solution of fluorene- SbCl_5 gave a weak ESR signal consisting of three broad lines with a separation of about 4 gauss. No paramagnetic solid formation was observed in this case, but attempts to improve the resolution by varying temperatures and concentrations were unsuccessful.

m. Fluoranthene

At -91°C , the signal for a 10^{-3} M solution consisted of a 1-gauss wide, intense signal of a solid superimposed on several weak hyperfine peaks of about the same width. When the sample was warmed, the paramagnetic solid dissolved without producing any improvement in the hyperfine pattern. A more dilute solution showed no improvement in resolution.

n. 7, 12-Dimethylbenz(a)anthracene

This hydrocarbon gave a poorly resolved spectrum consisting of several broad lines. The observed poor resolution may be due in part to the large number of hyperfine lines which would be expected for such an unsymmetrical molecule. No improvement in resolution was observed for a more dilute solution.

3.4.2.3.2. Unresolved Spectra

By considering in detail the results for the hydrocarbons which gave resolved spectra, one may rationalize the lack of resolution or total absence of a signal for the hydrocarbons in Table 42.

A 10^{-4} M solution of coronene- SbCl_5 exhibited an intense signal approximately one gauss wide. Such a signal is characteristic of solid paramagnetic free radicals. Similar signals were also seen for samples of tetracene, perylene, chrysene, and others in which the hydrocarbon concentration was too high and in which solid precipitates were also observed. However, the solubility of the paramagnetic solid in those compounds was presumably sufficient to permit also the observation of the resolved signal from the radicals in solution (10^{-4} to 10^{-6} M). Apparently, CH_2Cl_2 is not a sufficiently good solvent for the coronene radical cation.

ESR signals were seen for biphenyl and azulene only at high concentrations of hydrocarbon (10^{-1} to 10^{-2} M). These hydrocarbons possess high ionization potentials and are apparently relatively unreactive to SbCl_5 . At these high concentrations, either totally unresolved broad lines or single sharp "solid" signals were observed for both compounds. Attempts to resolve the broad lines were unsuccessful. It may be that the required high concentrations of reactants introduced line broadening from electron exchange phenomena.

The compounds trans-stilbene, phenanthrene, and diphenyldiacetylene all exhibited broad, fairly weak signals. The broad signal is characteristic of a radical in solution with unresolved hyperfine structure. The broadening could again be due to electron exchange phenomena.

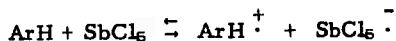
ESR was observed for p-xylene and benzene only after concentrated solutions of hydrocarbon and SbCl_5 stood at room temperature for

several hours. These solutions gave a weak, broad resonance when measured at low temperatures. Although the signals might be those of the simple xylene and benzene radical cations, it is more likely that they arise from products of chemical side reactions.

Solutions of acenaphthylene in CH_2Cl_2 turned deep green when treated with a large excess of SbCl_5 at room temperature. These samples exhibited broad, fairly strong ESR signals. Dilute solutions prepared in vacuum at low temperatures were also green but did not exhibit any signals. It is interesting that the green solution which forms when acenaphthylene is added to H_2SO_4 also shows no ESR. We have investigated the NMR of these solutions and found no proton resonance. The absence of NMR signal strongly indicates the presence of paramagnetic species. These phenomena may be associated with electron exchange or polymerization reactions involving several kinds of ionic species.

3.4.2.4. Reactions of SbCl_5 with Aromatic Hydrocarbons

These studies have shown that SbCl_5 is one of the most effective electron acceptor reagents found to date for aromatic hydrocarbons. With SbCl_5 , electron transfers can be achieved for hydrocarbons, such as naphthalene, with ionization potentials as high as 8 e.v. The initial reaction is believed to involve a reversible one-electron transfer from the aromatic hydrocarbon to SbCl_5 :



Although ESR signals were observed for concentrated solutions of SbCl_5 with benzene and its derivatives, it is felt that these signals resulted from complex reaction products rather than from the simple cations.

With the use of CH_2Cl_2 as solvent, stable solutions of many of the hydrocarbon unipositive ions can be produced by SbCl_5 at low temperatures. However, both the concentration of radicals in solution and the resolution of the ESR hyperfine structure depend critically on the concentrations of hydrocarbon and SbCl_5 . For many of the aromatics of high ionization potential, high concentrations of hydrocarbon and SbCl_5 are required to obtain sufficient quantities of free radical for ESR observation. With the aromatic hydrocarbons of large size, the concentration of reagents must be kept low to prevent paramagnetic solid formation at low temperatures. For the reactive aromatics, concentrations of hydrocarbons as low as 10^{-6} M are suitable for ESR study. At high temperatures or with SbCl_5 concentrations which are too high, further irreversible oxidation reactions leading to dipositive ions are thought to occur. Electron exchange reactions between uni- and dipositive ions can cause a loss of resolution in the ESR hyperfine structure.

With more effective control of these various factors, it may be possible to improve the ESR resolution and signal-to-noise ratio sufficiently to permit the determination of hyperfine coupling constants for all the hydrocarbons listed in Tables 41 and 42.

3.4.2.5. Coupling Constants and Spin Densities in Aromatic Hydrocarbon Radical Ions

The main result of this investigation was the determination of proton hyperfine coupling constants for a number of previously unreported aromatic hydrocarbon cations. Our data further confirm the validity of simple HMO theory for aromatic hydrocarbons and are consistent with previous observations that the coupling constants for positive ions are larger than those of corresponding negative ions. From the literature, we have compiled ESR coupling constants and HMO spin densities for unsubstituted aromatic hydrocarbons, and have presented these data along with the data obtained in the present investigation in Table 43.

The HMO spin densities, ρ , are listed in column 4 of Table 43. References are given for the spin densities obtained from the literature. For the alternant hydrocarbons, ρ values are identical for both the cations and anions. For the few nonalternant hydrocarbons in Table 43, the ρ values for both the positive and negative ions are included. Column 5 lists the experimental coupling constants a_H which have been reported for aromatic anions. Columns 6 and 7 list the proton coupling constants for the radical cations prepared with H_2SO_4 and $SbCl_5$. Literature references for the anion data and the H_2SO_4 data are indicated. The $SbCl_5$ data in the last column have all been determined in this study.

Our coupling constants were determined by comparing experimental line spectra (stick plots) with stick plots constructed from various coupling constant assignments. Of course for incompletely resolved spectra, line overlap can give rise to considerable error in the experimental line intensities. For those cases which were ambiguous, comparisons were made with spectra synthesized by an SESRS (Simulation of Electron Spin Resonance Spectra) computer program.⁽⁵⁵⁾ This program is described in detail in Section 3.4.5. The $SbCl_5$ data for each compound are discussed below.

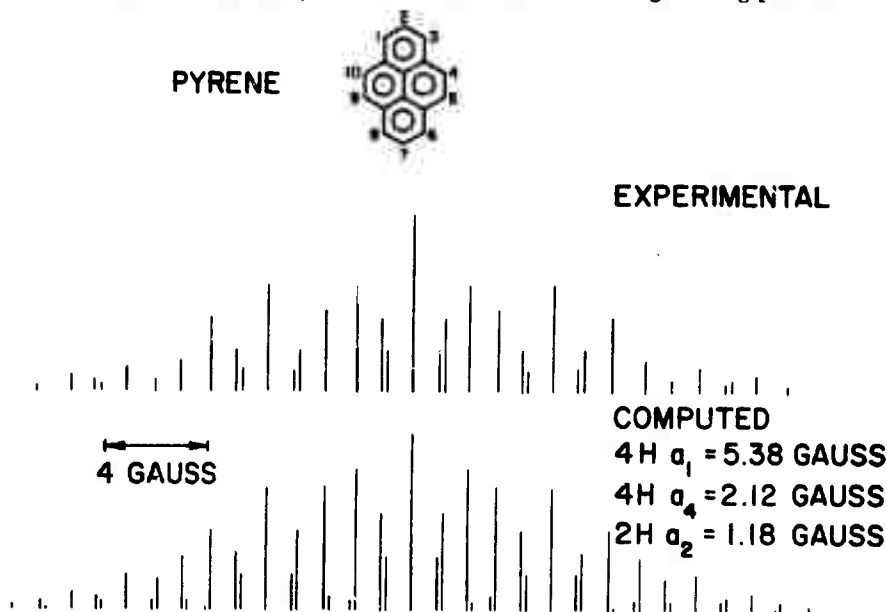
a. Perylene, Anthracene, 9,10-Dimethylantracene, and Naphthacene

The positive ions of perylene, anthracene, 9,10-dimethylantracene, and naphthacene have all been prepared previously in H_2SO_4 .^(15,43) Our coupling constants for the radical ions produced by $SbCl_5$ are remarkably close to those prepared by the H_2SO_4 method. This result leaves no doubt that the oxidation of these hydrocarbons with $SbCl_5$ leads to the formation of unipositive radical cations. It should be noted, however, that our $SbCl_5$ results are all lower than the H_2SO_4 results by 1 or 2 per cent. This difference may be due to a solvent effect.

b. Pyrene

The pyrene positive ion has not been reported previously. The coupling constants for the pyrene radical cation are given in Table 43.

A comparison of the experimental stick plot with that computed from these coupling constants is shown in Figure 42. It is of interest to compare the coupling constants with those obtained for the negative ion⁽¹⁷⁾ and with HMO theory.⁽⁴²⁾ The coupling constants for the positive ion are higher than those of the negative ion, especially at the reactive 1-position. A similar trend for other aromatic hydrocarbons has been discussed by various investigators.^(44, 56, 57) The pyrene radical ion is of additional interest because HMO theory predicts zero spin density at the 2- and 7-positions. This prediction is not borne out by either the negative or positive ion. In both species, a negative spin density corresponding to about 1.1 gauss is induced at these sites by the spin densities at the neighboring positions.



N-6698

Figure 42. Comparison of Experimental and Computed Stick Plots for the Radical Cation of Pyrene

c. Naphthalene

The results obtained for naphthalene were very unusual. The ESR experiments show that the positive ion of naphthalene exists as a dimer. The negative ion, which has been prepared by Tuttle, et al.,⁽⁵⁸⁾ and subsequently by Carrington, et al.,⁽¹⁵⁾ is a simple monomer. The coupling constants for the negative ion are in agreement with HMO theory, which predicts two sets of four equivalent protons with spin densities of 0.181 and 0.069.

Figure 43 shows a comparison of the experimental and two different computed stick plots for the ESR of naphthalene-SbCl₅. It is apparent that the expected 4-4 proton model (Figure 43c) does not agree at all with experiment. However, it is evident that an assignment resulting from two sets of eight equivalent protons (Figure 43b) is in excellent agreement with experiment. Furthermore, the coupling constants, 2.77 and 1.03 gauss, are much smaller (in fact, about a factor of two smaller) than those for the naphthalene negative ion. Final confirmation of the 8-8 assignment is provided by a comparison of the experimental and SESRS⁽⁶⁵⁾ curve shown in Figure 44.

The 8-8 assignment leads to the conclusion that the positive ion produced by the oxidation of naphthalene by SbCl₅ exists as a dimer with one unpaired electron equally distributed between the two naphthalene molecules. The sharp lines and measured g-value of 2.0023 suggest that the SbCl₅ does not interact strongly with the pi-system. As far as we are aware, this experiment is the first ESR observation of a radical cation for a dimer of an aromatic hydrocarbon.

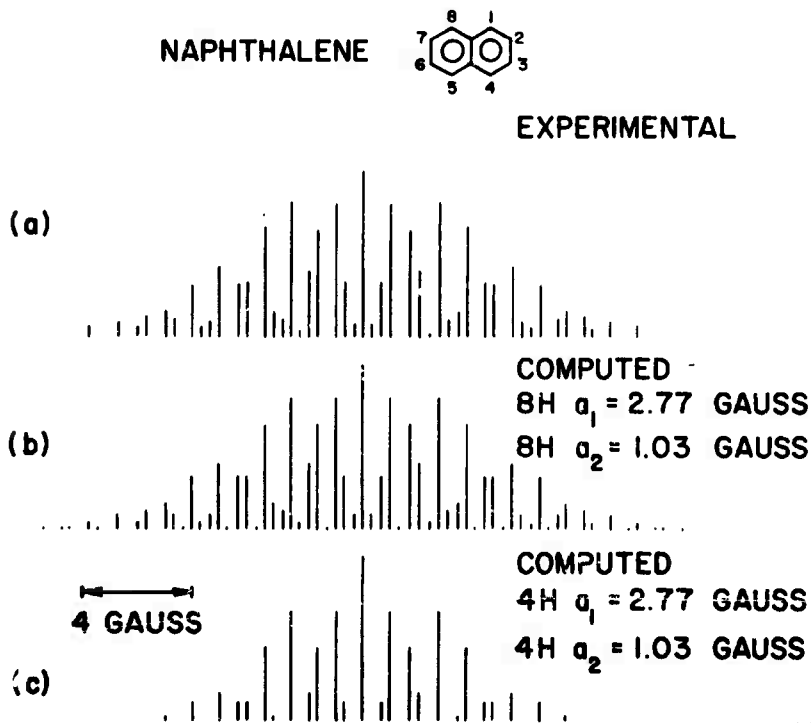
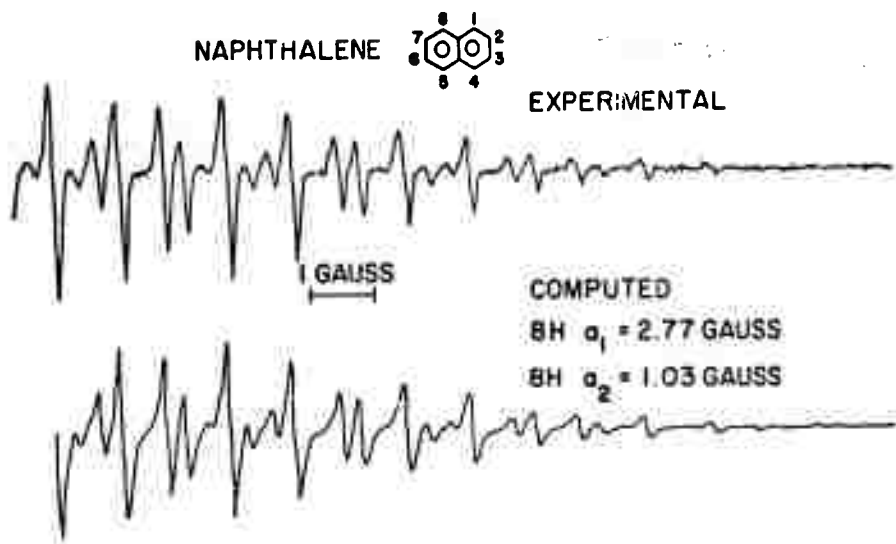


Figure 43. Comparison of Experimental and Computed Stick Plots for the Radical Cation of Naphthalene



N-7000

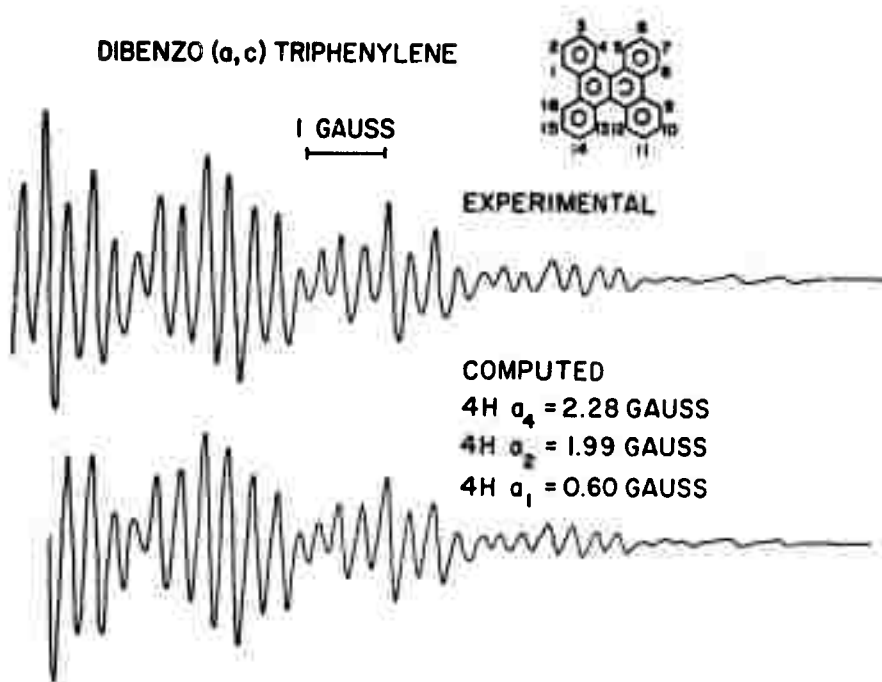
Figure 44. Comparison of Experimental and Computed (SESRS) Curves for the Radical Cation of Naphthalene

Dimers of neutral aromatic hydrocarbons, including naphthalene, have been shown to exist in excited states (eximers).⁽⁶⁰⁾ Our ESR results for naphthalene suggest that the radical cation of a dimer of an aromatic hydrocarbon can exist in the ground state. Dimeric complexes of aromatic hydrocarbons and $SbCl_5$ are also known. Tetracene⁽⁶¹⁾ and perylene⁽⁶¹⁾ both form solid complexes in which there is a 2:1 ratio of hydrocarbon to $SbCl_5$. Also, Handa⁽⁶²⁾ has recently obtained spectral evidence for the association of polycyclic aromatics in concentrated H_2SO_4 .

d. Dibenzo(a, c)Triphenylene

The ESR signal of the cation of dibenzo(a, c)triphenylene was one of the most intense observed. The spectrum was reduced to the coupling constants given in Table 43. A comparison of the experimental spectrum with an SESRS curve synthesized from these coupling constants is shown in Figure 45.

The symmetrical dibenzo(a, c)triphenylene molecule contains four groups of four equivalent protons. However, as seen from the coupling constant assignment, one of the groups has essentially zero spin density associated with it. Neither experimental data on the negative ion nor HMO calculations have been reported. We have calculated the HMO



N-7002

Figure 45. Comparison of Experimental and Computed (SESRS) Curves for the Radical Cation of Dibenzo(a, c)Triphenylene

spin densities for dibenzo(a, c)triphenylene and the agreement with experiment is excellent (see Table 43). The good agreement with Hückel theory which assumes planar aromatic systems, is unexpected in view of the non-planarity of the dibenzo(a, c)triphenylene molecule.⁽⁶³⁾

e. $\Delta^{\theta, \theta'}$ -Bifluorene

The nonalternant hydrocarbon $\Delta^{\theta, \theta'}$ -bifluorene is a structural isomer of dibenzo(a, c)triphenylene and, like the latter compound, is non-planar.⁽⁶⁴⁾ The HMO spin densities for the $\Delta^{\theta, \theta'}$ -bifluorene positive ion are identical to those for dibenzo(a, c)triphenylene ion. However, since $\Delta^{\theta, \theta'}$ -bifluorene is nonalternant, the spin densities of the positive and negative ions differ (see Table 43).

The $\Delta^{\theta, \theta'}$ -bifluorene exhibited the complex hyperfine structure shown in Figure 41 (b). Both the overall width of the spectrum and the individual lines were quite narrow. Small spin densities at the ring protons

are to be expected, since the central 9,9'-carbon atoms are shown in HMO theory to be regions of high spin density. The coupling constants for the $\Delta^{9,9'}$ -bifluorene cation are given in Table 43. Figure 46 shows a comparison of the experimental and computed stick plots. To compensate for line overlap, the computed spectrum was obtained by adding the calculated intensities of all lines within a linewidth of each experimental line position.

Employing a $Q \approx 30$, there is good agreement between the experimental coupling constants and those derived from simple Hückel theory. This agreement is rather remarkable for a nonalternant hydrocarbon which is known to be nonplanar.⁽⁶⁴⁾ It should be noted that the coupling constants for the $\Delta^{9,9'}$ -bifluorene cation are approximately the same as those for the cation of its structural isomer, dibenzo(a,c)triphenylene.

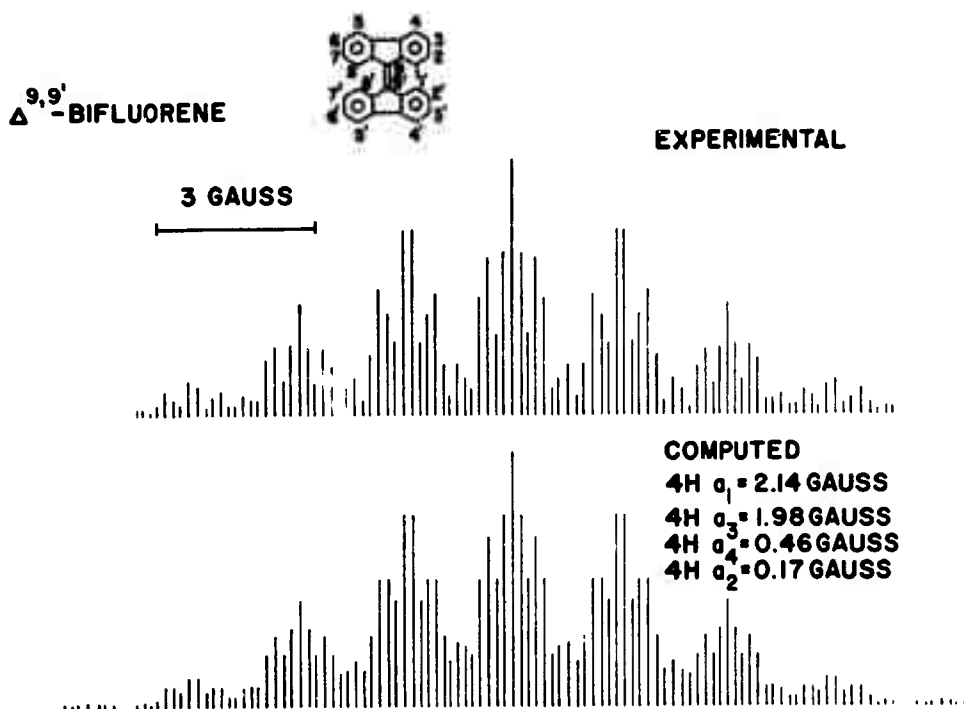
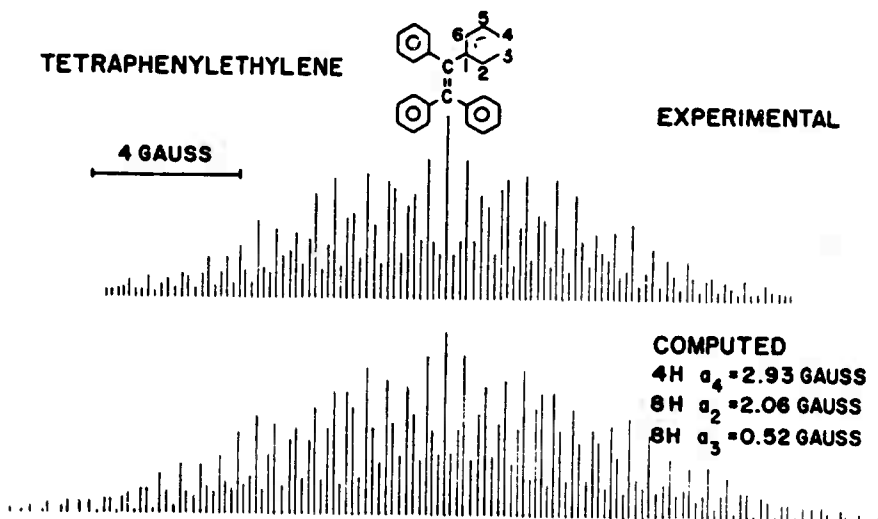


Figure 46. Comparison of Experimental and Computed Stick Plots for the Radical Cation of $\Delta^{9,9'}$ -Bifluorene

f. Tetraphenylethylene

The ESR spectrum for the tetraphenylethylene cation should contain a maximum of $9 \times 9 \times 5 = 405$ lines. The observed spectrum in Figure 41(a) contains 12 lines of about 0.05 gauss linewidth. The approximately equal spacing and partial line overlap make the assignment of coupling constants rather difficult. However, a good agreement between experimental and computed spectra is obtained for the assignment, 4H (2.93 gauss), 8H (2.06 gauss), and 8H (0.52 gauss). A comparison of experimental and computed stick plots is shown in Figure 47. The previously mentioned procedure of collecting and adding line intensities was again used for obtaining the computed spectrum in Figure 47. The approximate superposition of many of the 405 predicted lines leads to the much smaller number shown.



N-7030

Figure 47. Comparison of Experimental and Computed Stick Plots for the Radical Cation of Tetraphenylethylene

The coupling constants for the tetraphenylethylene cation are considerably larger than those predicted from HMO theory ($Q \approx 30$). This discrepancy cannot be explained by the nonplanarity of tetraphenylethylene alone, ⁽⁶⁵⁾ since one would expect deviations from planarity to decrease, rather than increase the unpaired electron density in the phenyl rings. ⁽⁶⁶⁾

3.4.2.6. Correlation of Spin Densities with Proton Hyperfine Coupling Constants

We have employed the experimental data in Table 43 to test quantitatively several of the theories which relate coupling constants to theoretical spin densities in aromatic radical anions and cations.

The McConnell relationship ^(1a)

$$a_H = Q\rho \quad (1)$$

states that the proton coupling constant, a_H , in aromatic free radicals is related to the unpaired spin density, ρ , at the attached carbon atom by a single constant, Q . However, the ESR data for the alternant hydrocarbons perylene, anthracene, naphthacene, pyrene, naphthalene, and biphenylene in Table 42 show that the measured coupling constants of aromatic hydrocarbon cations are generally larger than those for the corresponding anions. Since it has been shown⁽⁶⁷⁾ that the spin densities for positive and negative ions of alternant hydrocarbons should, to a high degree of approximation, be identical, the McConnell relationship must be modified accordingly.

In Figures 48 and 49, the proton coupling constants for the aromatic hydrocarbon anions and cations listed in Table 43 have been plotted separately against spin densities determined from simple HMO theory. These plots show good linear relationships for data which include both alternant and nonalternant radical ions.⁽⁶⁸⁾

Least squares fits to the data in Figures 48 and 49 yield expressions (2) and (3) for the anions and cations, respectively.

$$a_H^- = 28.6 \rho \text{ (Standard Error} = \pm 0.43 \text{ gauss)} \quad (2)$$

$$a_H^+ = 35.7 \rho \text{ (Standard Error} = \pm 0.38 \text{ gauss)} \quad (3)$$

The two different Q values show that the proton hyperfine coupling constants for hydrocarbon cations are, on the average, about 25 per cent greater than for the respective anions.

There have been several recent quantitative attempts to account for this apparent difference in Q . Colpa and Bolton⁽⁴⁴⁾ proposed a modification of the McConnell relationship which takes into account both the effects of spin density and excess charge density on the C-H bond. For the case of Hückel spin densities, they obtained the expression

$$a_H^\pm(CB) = -(Q\rho \pm K\rho^2). \quad (4)$$

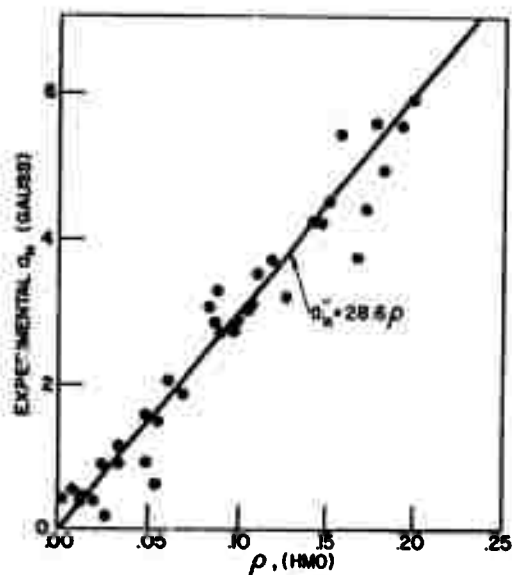


Figure 48. Relation Between Experimental Coupling Constants, a_H , and Hückel Spin Densities, ρ , for Aromatic Hydrocarbon Negative Ions N-7006

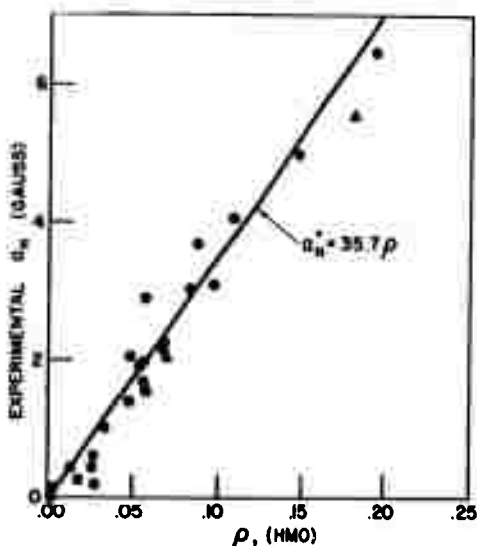


Figure 49. Relation Between Experimental Coupling Constants, a_H , and Hückel Spin Densities, ρ , for Aromatic Hydrocarbon Positive Ions^(es) N-7007

This relationship which employs a single value of Q , accounts for the difference between positive and negative ions by the excess charge density term $\pm K\rho^2$.

We have tested the Colpa-Bolton (CB) relationship (4), using the average of our Q values (32.2) for positive and negative ions. The value of K in equation (4) was determined to be 16 by a least squares analysis of the combined positive and negative ion data in Table 43.⁽⁸⁸⁾ Colpa and Bolton in their analysis employed $Q = 34.2$ and $K = 17$. In Figure 50, the experimental coupling constants a_H are plotted against the corresponding

coupling constants $a_{H(CB)}^\pm$ calculated from the equation

$$a_{H(CB)}^\pm = 32.2 \rho \pm 16 \rho^2. \quad (5)$$

The fit of the data in Figure 50 (Standard Error = ± 0.40 gauss) is as good as that obtained for the individual Q plots in Figures 48 and 49.

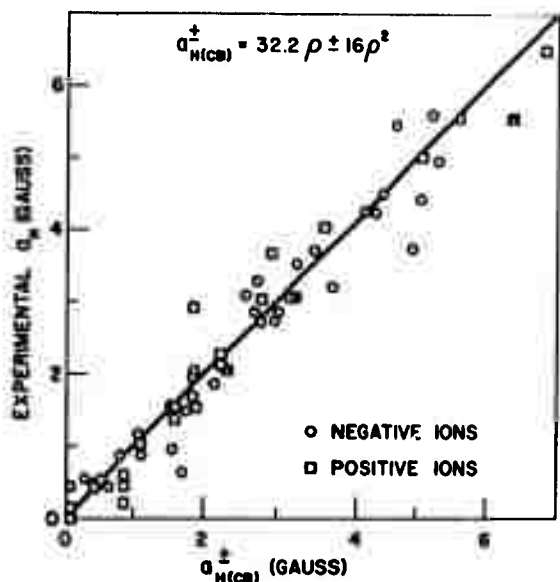


Figure 50. Comparison Between Experimental Coupling Constants for Both Aromatic Negative and Positive Ions and Those Calculated from the Colpa-Bolton (CB) Theory⁽⁸⁸⁾

N-7031

Recently Giacometti, Nordio, and Pavan⁽⁵⁶⁾ (GNP) have modified the McConnell relationship without introducing an explicit charge effect. Starting with Hückel theory, they derived expression (6) by a first order perturbation calculation which considered terms arising from hydrogen-next-nearest-neighbor-carbon p-orbitals. The result of their calculation was expressed in the form

$$a_{H_i}^{\pm}(\text{GNP}) = Q_1 \rho_1 \pm Q_2 \left| \sum_j c_i c_j \right| \quad (6)$$

and is analogous to the (CB) relationship (4), except that the second term involves the products of Hückel coefficients of neighboring carbon atoms.

We have also tested equation (6) using the combined data in Table 43, ⁽⁵⁸⁾ and the results are shown in Figure 51. The coupling constants $a_{H_i}^{\pm}(\text{GNP})$ were calculated from the equation

$$a_{H_i}^{\pm}(\text{GNP}) = 32.2 \rho_1 \pm 7.0 \left| \sum_j c_i c_j \right|, \quad (3)$$

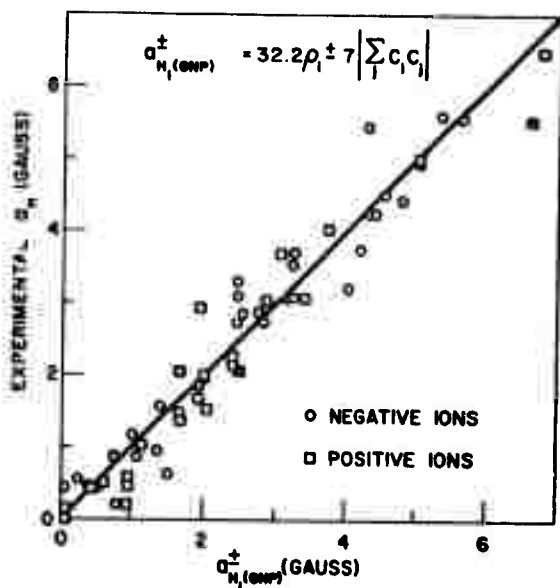
in which a value of $Q_2 = 7.0$ was determined by a least squares analysis. For Q_1 , we have again employed our average value of 32.2. The standard error for the fit of the data in Figure 51 is ± 0.38 gauss, which is only slightly better than the (CB) fit in Figure 50.

It appears that both the (CB) and (GNP) modifications of the McConnell relationship account for the differences in magnitude between the coupling constants for aromatic negative and positive ions. It is also evident that none of the relations provides precise quantitative agreement between experiment and theory. However, in view of the simplicity of HMO theory, the agreement between HMO spin densities and coupling constants for the wide variety of alternant, nonalternant, planar, and non-planar aromatic hydrocarbons included in Table 43 is impressive. Any better agreement with experiment will probably require more accurate calculations of spin densities such as those recently reported by Sayetta and Memory.⁽⁵⁷⁾

3.4.3. Optical Spectra of Aromatic Radical Cations

3.4.3.1. Aromatic Hydrocarbons - Antimony Pentachloride

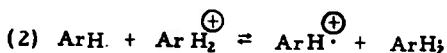
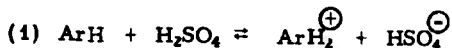
Optical spectra have been obtained for radical cations prepared by the interaction of aromatic hydrocarbons with SbCl_5 in CH_2Cl_2 solution. At room temperature, many of the systems examined proved to be unstable, and the spectra changed with time. The stability was generally found to be highest for solutions containing 10^{-3} M SbCl_5 and 10^{-4} M hydrocarbon.



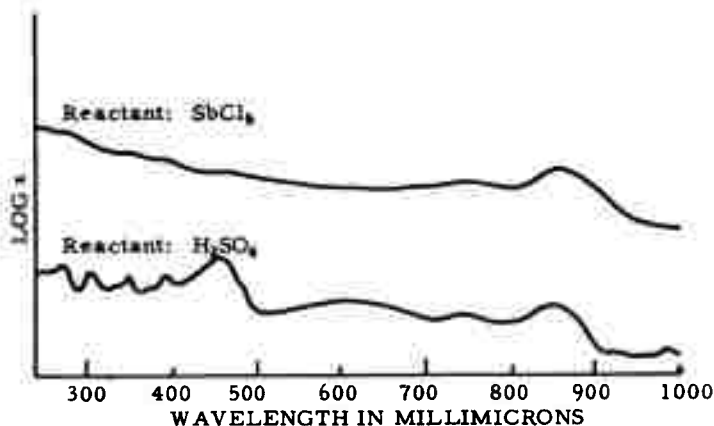
N-7032

Figure 51. Comparison Between Experimental Coupling Constants for both Aromatic Negative and Positive Ions, and Those Calculated from the Giacometti-Nordio-Pavan (GNP) Theory^(6a)

Figure 52 shows a spectrum of 10:1 SbCl_5 -naphthacene mixture in CH_2Cl_2 . This spectrum is compared with one obtained for a solution of naphthacene in the oxidizing medium H_2SO_4 . In H_2SO_4 , the following sequence of reactions has been shown to take place between polynuclear aromatic hydrocarbons and H_2SO_4 .^(6b)



The spectra of the diamagnetic cation (ArH_2^{\oplus}) and the radical cation (ArH^{\oplus}) are both generally observed when sulfuric acid is used as

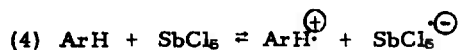


N-6250

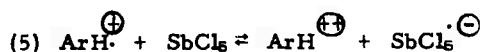
Figure 52. Optical Spectra of Naphthacene Radical Ion

the oxidizing agent for aromatic hydrocarbons. The major bands at 457 and 607 $m\mu$ for naphthacene in H_2SO_4 are attributed to the diamagnetic cation (ArH_2^+). The bands at 741 and 850 $m\mu$ have been assigned to the radical cation ($ArH^{\cdot+}$) of naphthacene.

Protonation is not a necessary prerequisite for radical-ion formation. Therefore, when the spectrum of naphthacene is recorded in the presence of the strong Lewis acid, $SbCl_5$, only the bands of the radical cation ($ArH^{\cdot+}$) are observed. The overall reaction is believed to involve a direct transfer of an electron from the aromatic hydrocarbon to $SbCl_5$.



Further oxidation is possible, leading to the formation of the diamagnetic dipositive ion (ArH^{2+}).



Optical spectra have been obtained for 1:10 mixtures of the aromatic hydrocarbons perylene, anthracene, 9, 10-dimethylantracene, pyrene, naphthalene, dibenzo(a, c)triphenylene, $\Delta^9, 9'$ -bifluorene, and tetra-

phenylethylene with SbCl_6 in CH_2Cl_2 . The spectra which were obtained for these deeply-colored solutions are shown in Figures 53 and 54.

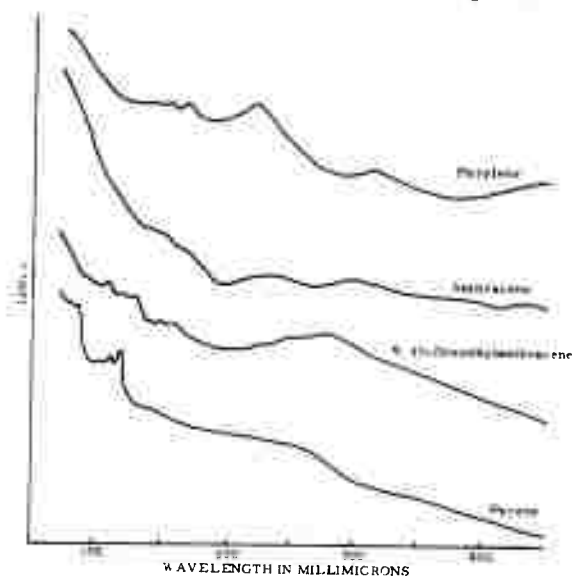


Figure 53. Optical Spectra of Aromatic Hydrocarbon Radical Ions N-7027

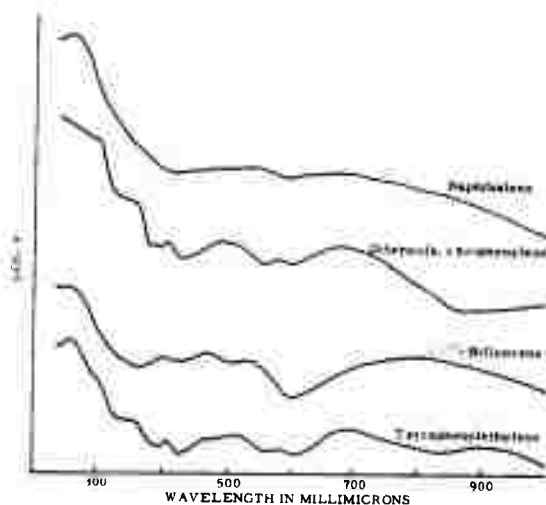


Figure 54. Optical Spectra of Aromatic Hydrocarbon Radical Ions N-7028

The wavelengths of the major absorption bands of each spectrum have been compiled in Table 44 together with the wavelengths of the corresponding radical cations and anions which have been prepared by other chemical methods. For alternant aromatic hydrocarbons, the negative and positive ions are expected to have similar spectra. Finally, columns 5 and 6 of Table 44 list the wavelengths of the absorption bands for the few dipositive and dinegative ions which have been reported. A brief discussion of the SbCl_5 spectra of each compound listed in Table 44 follows.

a. Naphthacene

The spectrum of naphthacene- SbCl_5 agrees fairly well with that reported for the radical cation prepared with sulfuric acid.⁽⁷⁰⁾ The bands in the SbCl_5 spectrum appear to be shifted to longer wavelengths and to be better resolved than the H_2SO_4 spectrum, however. After about 3 hours, the naphthacene- SbCl_5 spectrum changes, showing the development of a strong band at 650 m μ . The naphthacene dipositive ion also shows a strong absorption at 650 m μ . Thus, it appears that, with time, further oxidation of naphthacene by SbCl_5 leads to dipositive ion formation by reaction (5).

b. Perylene

Shown in Figure 53 is the ultraviolet-visible spectrum of perylene in $\text{SbCl}_5\text{-CH}_2\text{Cl}_2$ solution. It can be seen from Table 44 that the major absorption bands at 541 and 727 m μ agree very well with those reported by Aalbersberg, et al.,⁽⁷²⁾ for the radical cation prepared in $\text{CF}_3\text{COOH-BF}_3$, H_2O solution.

c. Anthracene

The spectrum of anthracene (Figure 53) shows strong absorption at 698 m μ which is presumed to correspond to that at 728 m μ for the radical cation prepared by Aalbersberg, et al.,⁽⁷²⁾ in $\text{CF}_3\text{COOH-BF}_3$, H_2O solution. The anthracene- SbCl_5 spectrum also shows strong absorption at 569 m μ which could possibly be that of the dipositive cation. The spectrum of the dipositive cation of anthracene has not been reported, but the dinegative ion has a strong band at 620 m μ .⁽⁷⁸⁾

d. Pyrene

The spectrum of pyrene (Figure 53) is poorly resolved, perhaps due to the presence of several ionic species in solution. The broad band in the 500 to 700 m μ region includes the absorption reported for the unipositive radical cation⁽⁷⁴⁾ and could also contain bands of the dipositive ion.

e. Naphthalene

The spectrum of naphthalene is shown in Figure 54. The absorption wavelengths in Table 44 do not agree with the data published by Paul, Lipkin, and Weissman for the negative ion.⁽⁷⁶⁾ However, the band with maximum at 680 m μ is broad and unresolved and extends over the absorption

Table 44. Optical Absorption of Aromatic Hydrocarbon Radical Ions

Compound	Experimental ^(a)				
	(SbCl ₅) λ, mμ	⊖ λ, mμ	⊖ λ, mμ	⊕ λ, mμ	⊕ λ, mμ
Naphthalene	281	271 ⁽⁷⁰⁾	358 ⁽⁷¹⁾	271 ⁽⁷⁰⁾	352 ⁽⁷⁰⁾
	358	348	400	333	398
	400	390	648 w	381	629
	466 w	762	706	551	709
	708 w	842	800	800	
	778				
	880				
Perylene	381 w	552 ⁽⁷²⁾	375 ⁽⁷³⁾		446 ⁽⁷³⁾
	409	728	676		558
	437		730		649
	541		769		704
	727				
Anthracene	382	314 ⁽⁷⁰⁾	403 ⁽⁷⁰⁾		621 ⁽⁷⁰⁾
	402	327 w	546		
	437	333 w	595		
	569	348	637		
	698	640 w	654		
		728	694		
9, 10-Dimethyl- anthracene			724		
	318				
	339				
	358				
	377				
	398				
	423				
	550				
	592				
	652				
Pyrene	273 w	508 ⁽⁷⁴⁾	364 ⁽⁷⁵⁾		
	367	750	383		
	320		450		
	337		490		
	385		736		
	500-700 (broad)				
Naphthalene	440		364 ⁽⁷⁰⁾		
	480		429		
	532		444 w		
	634 w		728		
	680		800		
Dibenzo(a, c)- triphenylene	301				
	355				
	384				
	406				
	483				
	579				
Δ ⁹ -Bifluorene	689				
	394				
	468				
	532				
Tetraphenyl- ethylene	810				
	335 w				
	342 w				
	352				
	359				
	384 w				
	406				
	509				
	595				
	574				
	912				
w = weak					

region reported for the negative ion. Here, again, the poor resolution may be due to the presence of more than one ionic species.

f. 9, 10-Dimethylantracene, Dibenzo(a, c)triphenylene,
 $\Delta^{9,10}$ -Bifluorene, Tetraphenylethylene

The compounds 9, 10-dimethylantracene, dibenzo(a, c)triphenylene, $\Delta^{9,10}$ -bifluorene, and tetraphenylethylene gave well-resolved and characteristic spectra with SbCl_5 . The spectrum of dimethylantracene exhibits the same radical ion bands which have been observed in H_2SO_4 .⁽⁴⁾ Dibenzo(a, c)triphenylene, $\Delta^{9,10}$ -bifluorene, and tetraphenylethylene are all insoluble in H_2SO_4 and no radical cation spectra have been previously reported for these compounds. The spectra in Figure 54 are believed to be those for the respective radical cations. The ESR of these solutions have already been discussed.

g. Miscellaneous Aromatics

Spectra were obtained for biphenyl, benzene, and fluorene with SbCl_5 in CH_2Cl_2 . They all gave colored solutions, the spectra of which were almost completely unresolved or changed with time. These results indicate the presence of more than one ionic species in each case.

3.4.3.2. Aromatic Hydrocarbons-Sulfuric Acid

Optical spectra are reported for two aromatic hydrocarbons, pentamethylbenzene and $\Delta^{1,1'}$ -biacenaphthene, in sulfuric acid.

a. Pentamethylbenzene

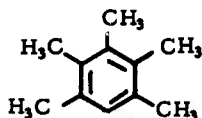


Figure 55 shows the spectra obtained for pentamethylbenzene in H_2SO_4 as a function of time. The behavior of this compound resembles that of hexamethylbenzene.⁽⁴⁾ A strong band forms at 385 millimicrons immediately; with time, a peak develops at 514 millimicrons.

It is likely that pentamethylbenzene in sulfuric acid rearranges to form hexamethylbenzene.

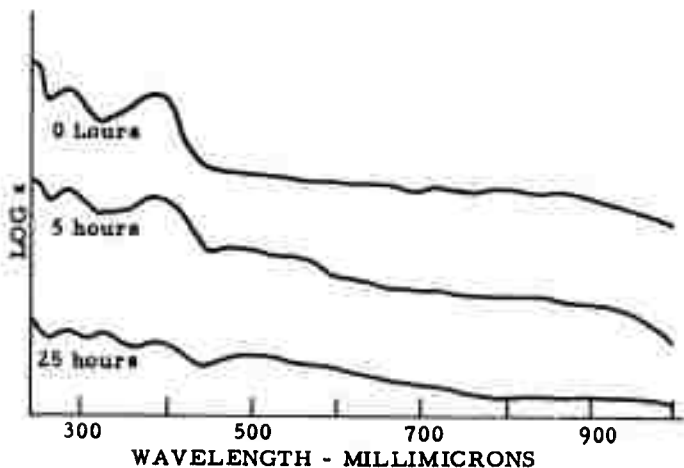
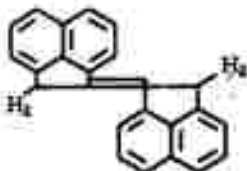


Figure 55. Ultraviolet Spectra of Pentamethylbenzene in H_2SO_4 N-5856

b. $\Delta^1,1'$ -Biacenaphthene



Biacenaphthene is an intermediate in the pyrolysis of acenaphthylene. It would be of interest to prepare a radical from this material by oxidation in sulfuric acid. $\Delta^1,1'$ -biacenaphthene does react in sulfuric acid initially forming a blue solution which later turns green. The spectra are shown in Figure 56 and are somewhat similar to that obtained for acenaphthylene itself. A major band develops at 630 millimicrons and some changes in the spectra occur in the 420-millimicron region.

3.4.4. The Electron Spin Resonance of the Radical Ion Formed by the Reaction of Hexamethylbenzene with H_2SO_4

3.4.4.1. Introduction

Polynuclear aromatic hydrocarbons are known to undergo one-electron oxidations in the presence of concentrated H_2SO_4 . ESR spectra

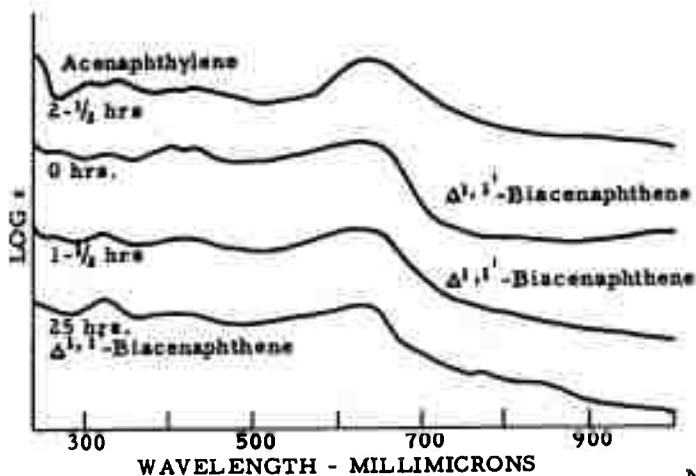


Figure 56. Ultraviolet Spectra of $\Delta^{1,1'}$ -Biacenaphthene in H_2SO_4 N-4939

have been reported for the stable unipositive radical ions of a number of polycyclic hydrocarbons in H_2SO_4 solution.^(16,19) The smaller aromatic hydrocarbons, such as naphthalene and benzene, are not oxidized by H_2SO_4 . We have found, however, that the methylated benzene derivative, hexamethylbenzene (HMB), does react with concentrated H_2SO_4 to form a deeply-colored solution which exhibits an intense ESR signal. Section 3.4.4. describes the results of ESR studies for this system and discusses the structure of the stable radical cation formed from HMB in strong oxidizing media.

ESR investigations of positive radical ions derived from methylated anthracenes have provided important support for the concept of hyperconjugation.⁽⁴³⁾ The ESR coupling constants for the negative radical ions prepared by the reduction of toluene and ortho-, meta-, and para-xylene,^(14,76,77) have been helpful in studying both hyperconjugation and the orbital degeneracies in the ground state of benzene.

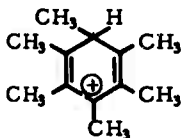
The direct oxidation of methylated benzenes to radical ions has been difficult to achieve. Although an ESR spectrum was observed for p-xylene in concentrated H_2SO_4 containing $\text{K}_2\text{S}_2\text{O}_8$, this spectrum was shown to be that of a dimethyl-p-semiquinone cation.^(78,79) Hulme and Symons⁽⁸⁰⁾ and, more recently, Carter and Vincow⁽⁸¹⁾ have reported the ESR of the hexamethylbenzene cation prepared by the oxidation of HMB. Hulme and Symons observed a 13-line ESR spectrum when a solution of HMB in H_2SO_4 was photolyzed. Carter and Vincow observed a similar spectrum for HMB in fuming H_2SO_4 .

We have found that, although HMB does not react immediately with 98 per cent H_2SO_4 , it does undergo a slow rearrangement to form a stable radical cation which is not the simple (HMB) cation. This reaction is related to the rearrangements found for other methylbenzenes in strong oxidizing environments. ^(62, 63)

In the Section 3.4.4.2., the optical spectra of HMB in 98 per cent H_2SO_4 are described. In Section 3.4.4.3., the ESR results for HMB in H_2SO_4 and HMB in D_2SO_4 are discussed. Section 3.4.4.3. also presents ESR data for HMB in two other oxidizing media, SbCl_5 and I_2 . In Section 3.4.4.4., NMR results for the ions formed from HMB with strong acids are described. Finally, in Section 3.4.4.5., a structure of the radical from HMB is proposed and the evidence in support of this structure is given.

3.4.4.2. Optical Spectra of Hexamethylbenzene in H_2SO_4

The ultraviolet-visible absorption spectra obtained over a period of time for HMB in concentrated H_2SO_4 are shown in Figure 57. HMB initially dissolves in H_2SO_4 to form a yellow solution. The spectrum of this solution (0 hours), which is shown in Figure 57, contains major absorption bands at 393 and 280 $\text{m}\mu$. These bands can be attributed to the protonated HMB cation (LII).



(LII)

This spectrum has been reported for solutions of HMB in CCl_3COOH and in $\text{CF}_3\text{COOH-H}_2\text{SO}_4$ mixtures. ⁽⁶⁴⁾

After 1 hour, the solution of HMB in H_2SO_4 turns red and the second absorption spectrum in Figure 57 is observed. This spectrum contains a broad band at 518 $\text{m}\mu$ and a second band at 330 $\text{m}\mu$. After 3 hours, the 518 and 330 $\text{m}\mu$ absorptions increase and the peaks due to the carbonium ion (LII) diminish. After 24 hours, the spectrum changes completely as a result of complex oxidation reactions.

3.4.4.3. ESR Results

3.4.4.3.1. Hexamethylbenzene in H_2SO_4

No ESR signal was observed in the yellow solution of HMB in H_2SO_4 . The red solution exhibited an intense ESR signal, which was stable for several days. The upper curve in Figure 58 shows one-half

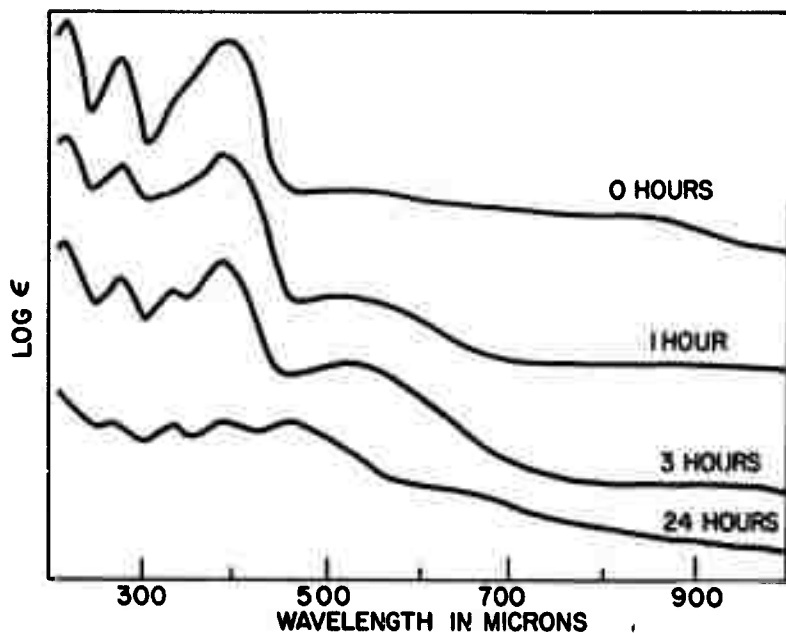


Figure 57. Optical Spectra of HMB in H_2SO_4 N-7005
 HEXAMETHYLBENZENE - H_2SO_4

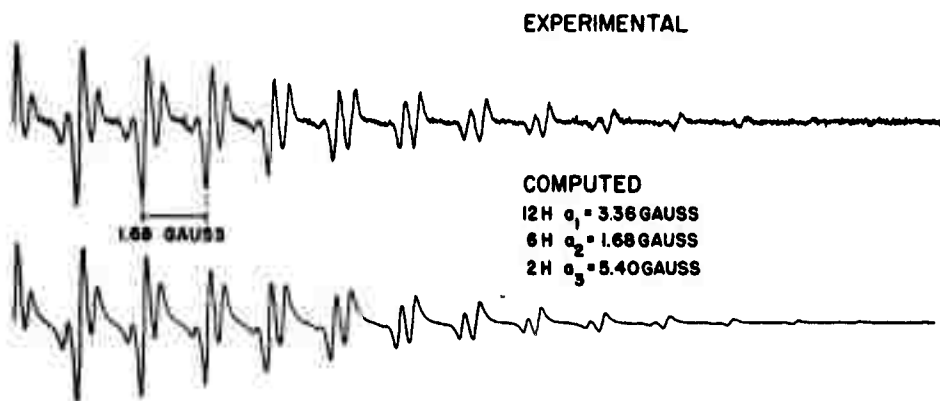


Figure 58. ESR of HMB in H_2SO_4 ; Comparison Between Experimental Curve and Curve Synthesized by an SESRS Computation N-7054

of the ESR spectrum. This complex pattern was not expected, since the 6 equivalent methyl groups of a HMB radical cation would be expected to give 19 equally-spaced lines having a binomial intensity distribution. ⁽⁷⁹⁾ Figure 59 shows the entire experimental line spectrum. There are 3 groups of lines separated by 5.40 gauss with an intensity ratio of 1:2.8:1. The individual lines within each group are spaced 1.68 gauss apart. The separation of the spectrum into three main groups of lines suggests a 5.40 gauss splitting by 2 equivalent protons. The deviation from the expected 1:2:1 intensity ratios will be discussed in detail in a later section.

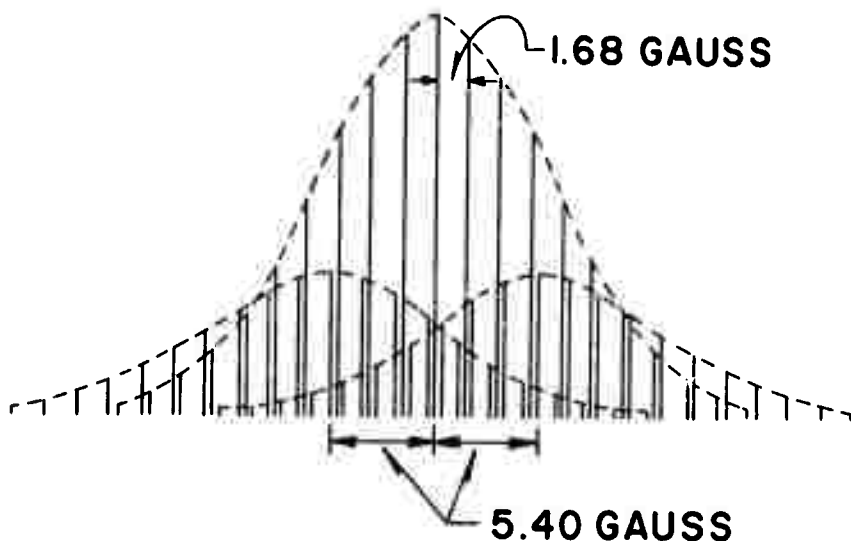


Figure 59. Experimental Line Spectrum for HMB in H_2SO_4 ; Line Positions and Intensities Taken from the Upper Spectrum in Figure 58 N-4605

To complete the analysis of this spectrum, it is necessary to consider only the central group, since the relative intensities of corresponding lines in each group are identical. The intensities of lines within the central group fall off extremely gradually. This result is illustrated in Figure 60, which compares the experimental intensity distribution with three possible assignments of coupling constants. The lines and bars in Figure 60 represent the experimental intensities. The lower two dashed curves show the intensity distributions for 18 and 36 equivalent protons with coupling constants of 1.68 gauss. It is apparent that the decrease in intensities for both assignments is much more rapid than for the experimental lines.

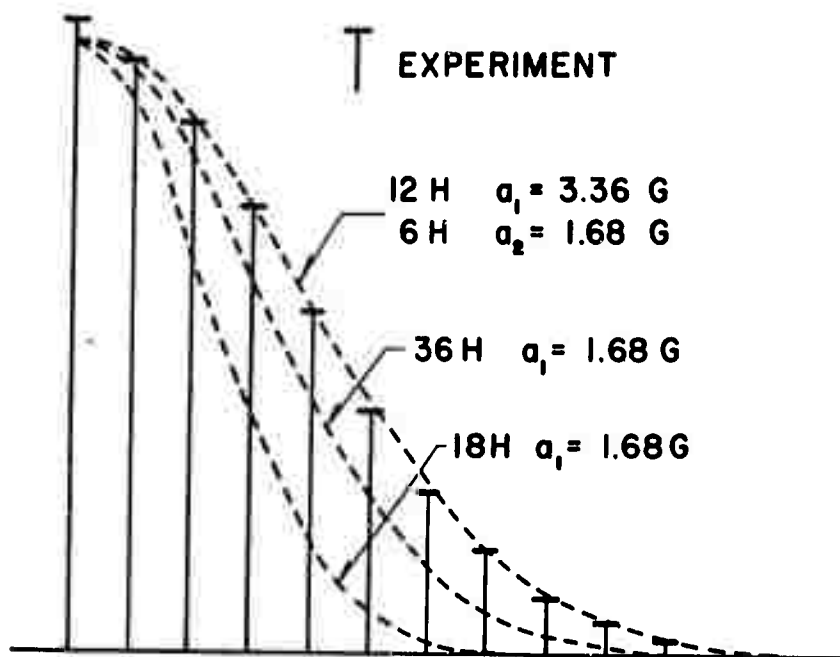


Figure 60. Line Intensities of the Central Group of Lines in Figure 59; Comparison with Those Computed from Three Different Sets of Coupling Constants (Dashed Curves) N-4606

The upper dashed curve is the intensity distribution for a radical containing 12 protons with $a_1 = 3.36$ gauss and 6 protons with $a_2 = a_1/2 = 1.68$ gauss. It can be seen that this assignment is in excellent agreement with experiment. Although this 12-6 assignment predicts 31 lines, our experimental signal-to-noise ratio permitted the observation of only 21 lines.

A considerable effort was made to show that the 12-6 assignment was unique. Figure 61 shows correlation diagrams for a number of alternative assignments for the lines within the central group; these diagrams show the per cent deviation between corresponding lines of the experimental and the various computed spectra. It can be seen that the correlation diagram for the 12-6 assignment is the only one in which the deviations are small and random.

As previously mentioned, the relative intensities of the 3 major groups of lines in Figure 59 are appreciably different from the 1:2:1 ratio to be expected from a splitting by two equivalent protons. It was noted,

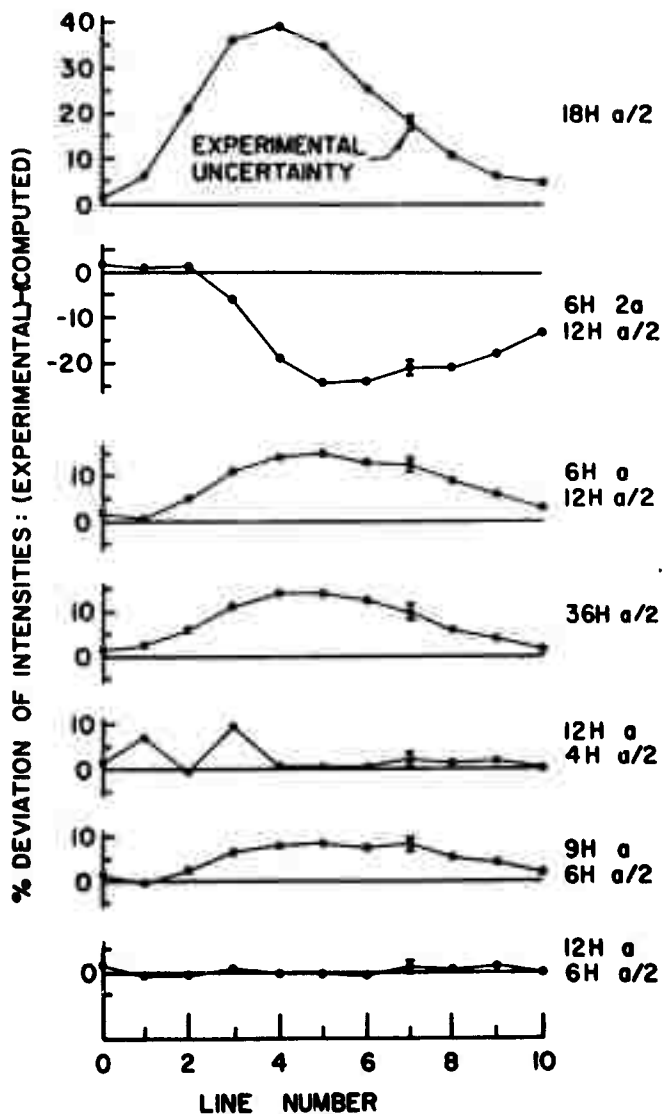
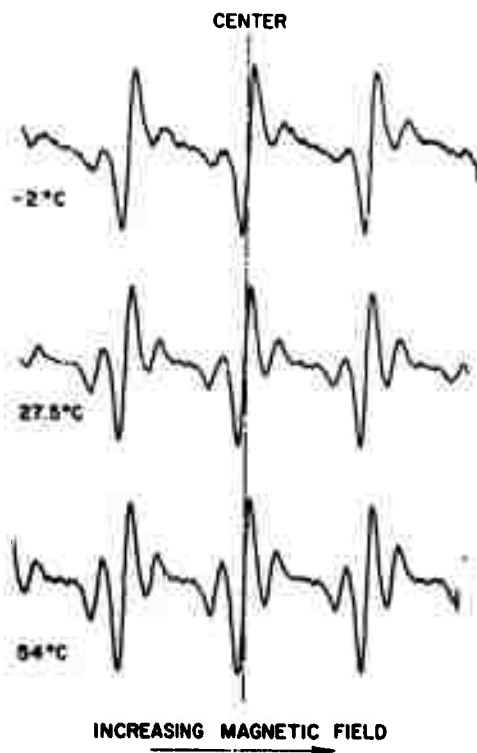


Figure 61. Correlation Diagrams for the Intensities of the Central Group of Lines in the ESR Spectrum of HMB in H_2SO_4 ; Line No. Zero is the Central Line of the Spectrum; the Spacing $a/2$ Equals 1.68 Gauss

N-7076

however, that the ESR lines belonging to the outer groups were slightly wider than those in the central group. A 10 to 20 per cent greater width of the outer lines would account for the observed deviation from an exact 1:2:1 ratio of intensities.

The observed linewidth variations suggest that there may be restricted rotation involving the two protons which give rise to the large splitting.⁽⁶⁵⁾ One might expect such linewidth variations to depend upon both temperature and viscosity. Figure 62 shows the central portion of the HMB spectrum at three different temperatures. Note that the width of the intense lines, which belong to the central group, do not vary with temperature. The satellite lines which belong to the outer groups narrow considerably with increasing temperature. At 54°C, the intensity ratios for the three main groups of lines are within 15 per cent of the expected 1:2:1 distribution. It was also found that the addition of trifluoroacetic acid to a solution of the radical in H_2SO_4 lowered the room-temperature viscosity sufficiently to decrease the widths of the satellite lines.



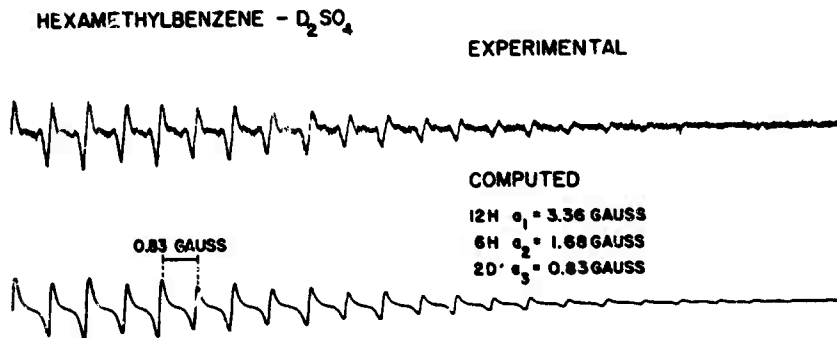
N-5042

Figure 62. Central Portion of the ESR Spectrum of HMB in H_2SO_4 at Three Different Temperatures.

From the preceding discussion, it was concluded that the radical formed from HMB in H_2SO_4 had the following coupling constants: 2H , $a_1 = 5.40$; 12H , $a_2 = 3.36$; and 6H , $a_3 = 1.68$ gauss. A final confirmation of this assignment is shown in Figure 58 in which a spectrum simulated from these coupling constants is compared with the experimental curve obtained at 25°C . The synthesized SESRS curve⁽⁵⁸⁾ contains two different linewidths: 0.157 gauss for the central group and 0.174 gauss for the two outer groups.

3.4.4.3.2. Hexamethylbenzene in D_2SO_4

The 12-6-2 assignment of coupling constants shows that the observed radical contains two more protons than the original hexamethylbenzene molecule. In order to determine whether the additional two protons involved the H_2SO_4 solvent, an ESR spectrum was obtained for HMB in D_2SO_4 . The upper curve in Figure 63 shows one-half of the experimental spectrum. There is no sign of the 3 groups of lines shown in Figure 59. Instead, 37 equally-spaced lines with a separation of about 0.84 gauss were observed.



N-7053
 Figure 63. ESR of HMB in D_2SO_4 ; Comparison Between Experimental Curve and Curve Synthesized by an SESRS Computation

This spectrum of HMB in D_2SO_4 is consistent with the previous 12-6-2 assignment only if the two protons which give rise to the large 5.4 gauss splitting are replaced by deuterons. Since the ratio of the deuterium coupling constant a_D to the proton coupling constant a_H is given by

$$\frac{a_D}{a_H} = \frac{\mu_D^{\text{I}}}{\mu_H^{\text{I}}} = \frac{0.8574(1/2)}{2.7927(1)} = 0.1535,$$

the $a_H = 5.4$ gauss becomes $a_D = 0.83$ gauss. This predicted splitting agrees within experimental error with the measured 0.84 gauss spacing. The particularly simple spectrum in Figure 63 results from the fact that the 0.84 gauss deuteron splitting is precisely one-half of the smallest proton splitting of 1.68 gauss.

In Figure 64, the experimental line intensities are compared with a line spectrum computed from a 12H, 6H, 2D assignment. The alternation

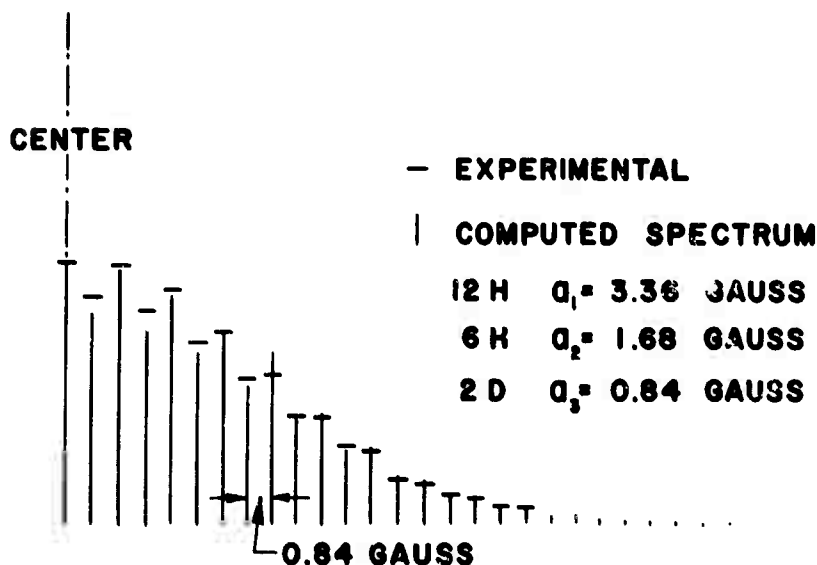


Figure 64. Line Intensities for the ESR of HMB in D_2SO_4 ; Comparison Between Experimental (Taken from the Upper Curve in Figure 63) and Computed Spectra

N-4608

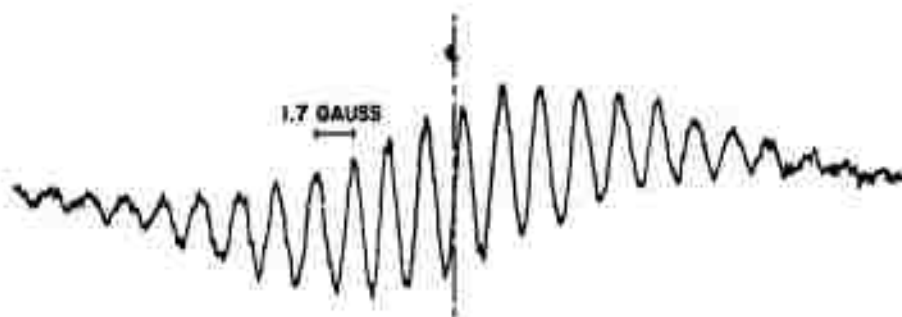
in line intensity is a result of the 1:2:3:2:1 distribution of intensities for two equivalent deuterons of spin 1. Final confirmation of the assignment is given in Figure 63 which shows an SESRS comparison of the computed and experimental spectra.

3.4.4.3.3. Hexamethylbenzene with Iodine and with $SbCl_5$

The most likely explanation of the D_2SO_4 results is that the two additional protons (deuterons) in the HMB radical arise directly from the H_2SO_4 (D_2SO_4) solvent. However, in view of the known ease of rearrangement of methyl benzenes in H_2SO_4 ,⁽²³⁾ another possibility is that these

two protons result from intermolecular methyl addition reactions. This second alternative would then require that, of the 20 protons in the HMB radical, only the two with the 5.4 gauss splitting readily exchange with D_2SO_4 . In order to distinguish between these alternatives, we have also prepared the HMB radical species in media which do not contain exchangeable protons.

Two aprotic reagents which have been employed as electron acceptors for the preparation of aromatic radical cations are $I_2^{(68)}$ and $SbCl_5$ (Section 3.4.2.). Figure 65 shows the ESR spectrum obtained for a 3×10^{-3} M solution of HMB in molten I_2 at $125^\circ C$. The spectrum consists



N-7001

Figure 65. ESR of a 3×10^{-3} M Solution of HMB in Molten I_2 at $125^\circ C$

of at least 23 equally-spaced lines about 1 gauss wide with a separation of 1.7 gauss. The spectrum is incompletely resolved; but the 1.7 gauss spacing is, within experimental error, identical to the 1.68 gauss splitting observed for HMB in H_2SO_4 .

Because of the poor resolution, the individual satellite lines arising from the 5.40 gauss splitting cannot be discerned. In order to ascertain whether this 2-proton splitting is present in the HMB- I_2 spectrum, an SESRS comparison which takes into account the incomplete resolution was performed. It was found that the line intensities for the spectrum in which the 2-proton splitting is omitted fall off much more rapidly than in the experimental curve. On the other hand, the SESRS spectrum for the 12-6-2 assignment appeared to be in much better agreement with experiment. Figure 66 shows a quantitative comparison of the line intensities for these two computed spectra with those obtained from the experimental curve. This comparison confirms the 12-6-2 assignment for the HMB- I_2 spectrum.

When a dilute solution of HMB in CH_2Cl_2 is treated with $SbCl_5$, a red color develops and the sample exhibits an ESR signal identical to that for HMB in H_2SO_4 (Figure 58). The ESR observations with both I_2 and $SbCl_5$ prove that all 20 protons in the HMB radical arise from HMB molecules. Since only two of the protons exchange with deuterium in D_2SO_4 , their bonding must be quite different from that of the other 18 protons.

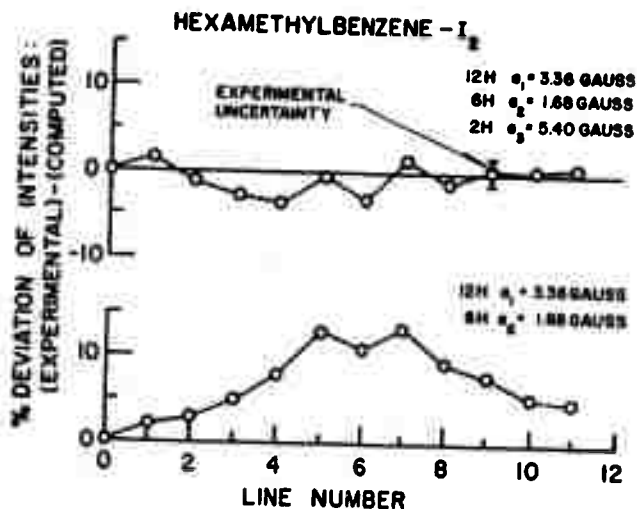


Figure 66. Correlation Diagrams for the ESR Spectrum of HMB in Molten I_2 ; Experimental Intensities Taken from the Curve in Figure 65; Line Number Zero is the Central Line of the Spectrum

N-7098

3.4.4.3.4. g-Factors

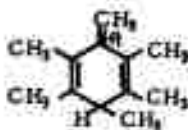
The g-factor of the radical formed from HMB in H_2SO_4 (Figure 58) was determined to be 2.0024 ± 0.0001 . Within experimental error, this value is identical to that found for hydrocarbon positive ions.⁽⁶⁷⁾ This g-factor seems to eliminate the possibility that the HMB radical is a quinone cation similar to that formed by the oxidation of p-xylene in H_2SO_4 - $K_2S_2O_8$ solution.^(78, 79) Oxygen-containing free radicals generally have considerably higher g-values, viz., between 2.0037 and 2.0047.⁽⁶⁷⁾ Since g-factors for semiquinone cations have not been reported, we have measured the g-factor of the duroquinone cation in H_2SO_4 - $Na_2S_2O_8$ ⁽⁷⁸⁾ and have indeed found the high value 2.0035 ± 0.0001 . These g-factor results show that the radical from HMB does not contain oxygen.

The g-factor for the HMB radical in molten I_2 had the unusually high value of 2.0057. However, we have found anomalously high g-factors for other radical cations in molten iodine. For example, the perylene radical cation in molten I_2 had the remarkably high g-value of 2.0090 ± 0.0003 . The large spin-orbit coupling constant of iodine⁽⁶⁷⁾ may be responsible for the large positive g-shifts when molten I_2 is used as a solvent.

3.4.4.4. NMR Studies of the Reactions of Hexamethylbenzene with Strong Acids

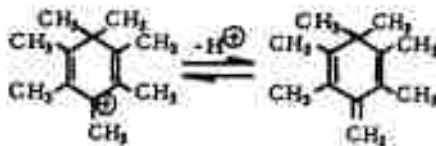
The ESR coupling constant assignment for the radical ion from HMB shows that HMB must undergo molecular rearrangement in strongly acidic media. Rearrangement reactions of methyl benzenes in strong acids (the Jacobsen Reaction) are well known.^(82,83) Furthermore, the mechanism of these rearrangements has been postulated to involve free-radical intermediates.⁽⁸⁸⁾

Several recent NMR studies have demonstrated chemical exchange and rearrangement reactions of HMB in the presence of strong acids. Maclean and Mackor⁽⁸⁹⁾ studied the NMR of HMB in HF-BF_3 at -85°C and obtained a resolved spectrum of the protonated hexamethylbenzonium ion (LII).



(LII)

At room temperature, the NMR spectrum collapsed to a single peak due to rapid proton exchange reactions. These exchanges were postulated to occur intramolecularly within the ion (LII). Birchall and Gillespie⁽⁹⁰⁾ have observed similar effects for solutions of HMB in HSO_3F . However, they postulated a mechanism of exchange in which the proton of the ion (LII) exchanged with the solvent. Doering, et al.,⁽⁹¹⁾ have reported NMR data for the very stable heptamethylbenzonium ion (LIII) which results from the rearrangements of methyl benzenes in the presence of Friedel-Craft catalysts. This ion can alternately be produced from HMB and CH_3OH in H_2SO_4 . The ion (LIII) can readily be converted to its conjugate base (LIV).



(LIII)

(LIV)

We have made NMR measurements of HMB in H_2SO_4 , D_2SO_4 , and $\text{SbCl}_5\text{-CH}_2\text{Cl}_2$. In 98 per cent H_2SO_4 at 25°C , only a single broad absorption at 2.35 ppm was observed. This peak can be attributed to the ion

associated with the two equivalent protons ($a_H = 5.40$ gauss) were larger than those for the $M = 0$ transitions and were strongly temperature and viscosity dependent. In the case of the highly-hindered dinitrodurene, Freed and Fraenkel⁽⁸⁸⁾ attributed the alternation in widths to an out-of-phase correlation of a modulation of the isotropic hyperfine splittings by the two equivalent nitrogen nuclei. If the 6-membered ring of radical (LV) were nonplanar, a hindered rotation of the CH_2 group would result in out-of-phase correlated motions of the two protons.

There was also a very slight asymmetry between the +1 and -1 transitions. This effect was most noticeable for the spectrum at $-2^\circ C$ (Figure 62), in which the low-field satellite of the central line is slightly less intense, and thus wider, than the high-field satellite. If it can be assumed⁽⁸⁸⁻⁹⁰⁾ that the component of the g tensor perpendicular to the aromatic ring is less than the average of the in-plane components, we are led to the result that the CH_2 proton coupling constants are negative. This result is in agreement with theory⁽⁹⁷⁾ and with experimental results on irradiated malonic acid^(98, 99) and diphenylpicrylhydrazyl.^(100, 101)

3.4.4.6. Conclusions

The stable radical from the oxidation of HMB is presumed to be the hexamethylbenzyl radical ion (LV) which is formed by the rearrangement of HMB in strong Lewis acids. The stability of (LV) is consistent with similar observations by von E. Doeing, et al., for the related diamagnetic ion (LIII) and its conjugate base (LIV). The observation of this stable radical in the acid catalyzed rearrangement of HMB suggests that free radical intermediates may be involved in Jacobsen rearrangements of other methylated benzenes. This proposal has recently been made by Bohlmann and Riemann.⁽⁸⁸⁾

We have indeed observed an ESR spectrum for durene in $SbCl_5 - CH_2Cl_2$ and in H_2SO_4 which is different from the spectrum for (LV). This spectrum transforms rapidly into that for the HMB radical (LV) as a result of methyl rearrangements. Pentamethylbenzene and pentamethylbenzyl chloride were also found to undergo immediate rearrangement in H_2SO_4 to the Radical (LV).

3.4.5. SESRS (Simulation of Electron Spin Resonance Spectra) Computer Program

3.4.5.1. Introduction

The identification by ESR of free radical intermediates in thermal decomposition and carbonization reactions requires that the hyperfine spectrum be analyzed in terms of nuclear coupling constants and the number of equivalent nuclei having a given coupling constant. The main difficulty of reducing a complex ESR hyperfine spectrum to coupling constants is the complicating effect of overlapping lines. The ultimate proof that a correct assignment of coupling constants has been made can be obtained only by reconstructing a spectrum from the coupling constants, which takes into

account actual line widths and shapes. Since computing and plotting such reconstructed spectra by hand is a practical impossibility, Stone and Maki⁽⁵⁶⁾ developed a "Simulation of Electron Spin Resonance Spectra" (SESRS) Fortran program which could be used with a large computer such as the IBM 7090. A brief description of the program (Appendix I of their paper) is included below.

3.4.5.2. Program Description

Appendix I: SESRS Computer Program (Stone and Maki)

"Complex ESR spectra with many overlapped line shapes can often be analyzed and measured by judicious use of the relatively few completely resolved lines. However, it is desirable to reconstruct the spectrum in order to verify both the analysis and the accuracy of the coupling constants. A Fortran program SESRS (Simulation of ESR Spectra) has been devised for this purpose. The principal features of SESRS are a short running time and the ability to superimpose any number of spectra with predetermined relative intensities. Input data consist of the coupling constants, linewidth, and relative intensity of each spectrum. Nuclei with $I=\frac{1}{2}$ and $I=1$ are considered, and up to 50 coupling constants can be accommodated for each type. The linewidth must be constant throughout each spectrum, and the line shape is Lorentzian, but any other desired line shape can easily be substituted. Output is returned in two forms: graphical and tabular. The graphical output is a spectrum plotted by the computer; it is useful for preliminary comparison with the experimental spectrum. The tabular output includes a list of X and Y coordinates adjusted so that the resulting graph will have the same proportions as the observed spectrum.

"The computational scheme used in SESRS is designed to minimize running time. For this reason, all coupling constants are rounded off to the nearest 0.005G, which is sufficiently accurate for most ESR results. The spectrum is generated in two memory blocks, A and B, each of which contains 6000 consecutively numbered locations. During computation, each location n accumulates numbers whose final sum represents the intensity of the derivative resonance signal at a magnetic field of 0.005 mG. The evaluation of intensities from a line-shape formula is relatively time consuming, so only one 'parent' line is computed in this fashion. The rest of the spectrum is generated simply by accumulating multiples of the parent line at appropriate intervals of magnetic field (locations). Accumulating is a very rapid computer operation.

"A simplified example will illustrate the method. Consider a radical containing one proton with $\alpha_1^H = 2$ G and two equivalent protons with $\alpha_1^H = 3$ G. The linewidth is 0.1 G. Initially, the value in every location in both memory blocks is cleared. Next, the parent line is generated in Block A by computing the intensity with the derivative Lorentzian formula in each of the first 320 locations, with the center of the line in Location 160. Thus a total of 16 linewidths are used to produce a lineshape in the SESRS program. The next step is the inclusion of the 2-G coupling constant for a single proton. The number in each location n of block A is added into both location n and location $(n+400)$ of Block B. This operation produces two line shapes in B, separated by 400 locations, or 2G. Block A is then cleared. To include the 3-G coupling constant for two equivalent protons, the value in each location n of Block B is added into both locations n and $(n+1200)$ of Block A, and twice the value is added into location $(n+600)$ of Block A. Now Block A contains the complete spectrum. The extension to more complex radicals is straightforward. In actual practice, only half of the spectrum is generated.

"The remainder of the program arranges such details as locating the center of the spectrum, adjusting the intensities of the various superimposed spectra, and organizing the output. The running time is roughly proportional to the number of different coupling constants rather than to the number of lines, and this relationship provides great efficiency for complex spectra. To synthesize the spectrum of terephthalaldehyde-2,5- d_2 anion, for example, which contains 198 lines from three species, an IBM 7090 computer required about 45 sec."

In cooperation with Union Carbide's central computing department, we have somewhat altered Stone and Maki's program and made arrangements to have the computed results transferred directly from magnetic tape to graphical form using a CALCOMP plotter.

Figure 67 shows an example of how useful and necessary such a detailed comparison is. The central curve (3055) is the experimental ESR spectrum for diazobenzil decomposed thermally in biphenyl at 180°C.⁽⁴⁾ Educated guesses of the coupling constants were made by constructing line spectra. The following were chosen:

$$\begin{aligned} 2H, a_1 &= 2.88 \text{ gauss;} \\ 4H, a_2 &= 2.67 \text{ gauss;} \\ \text{and } 4H, a_3 &= 1.17 \text{ gauss.} \end{aligned}$$

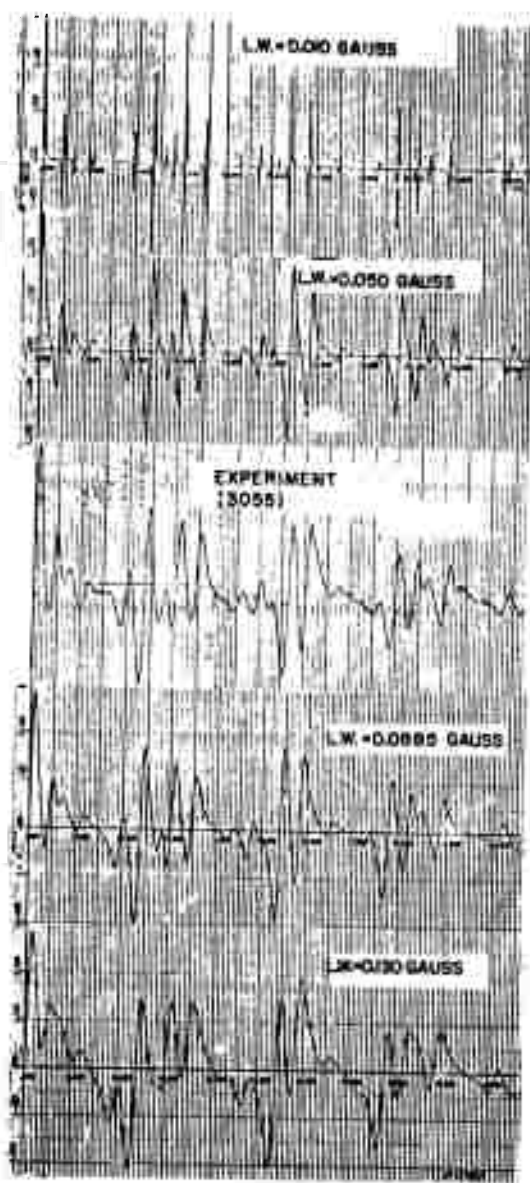


Figure 67. Comparison of Experimental and Computed ESR Spectra for Thermally Decomposed Diazobenzil

N-5408

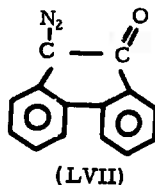
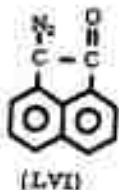
The four computed curves were obtained using these coupling constants, assuming Lorentz-shaped lines and the linewidths indicated. The experimental curve and the curve computed using a linewidth of 0.0885 gauss are essentially identical.

With the aid of this program, we are now able to make our coupling constant assignments much less ambiguously. Isotopic substitution becomes a further practical proof of assignment no matter how complicated the resultant spectra. The SESRS program can also be used when there is more than one species present. This experimental situation has arisen several times, but, until now, interpretation was not attempted because of the complexity of the curves.

3.5. ESR Studies of the Thermal Decomposition of Diazo Compounds

3.5.1 Introduction

In contrast to most pyrolysis reactions, the thermal decomposition of diazo compounds leads to easily identifiable products. The thermal reaction mechanisms and the role of free radical intermediates are, therefore, more easily determined. Previous reports have described ESR studies for the pyrolyses of diphenyldiazomethane and some of its derivatives and for the pyrolyses of diazofluorene and diazobenzil. The present report describes ESR results for two diazoketones, 2-diazoacenaphthenone (LVI) and diazophenanthrone (LVII), as well as the results of further analysis of the spectrum from 9-diazofluorene. (4,5) Diazaoacenaphthenone is of particular interest because of its close structural similarity to acenaphthylene.



3.5.2. 2-Diazo-1-acenaphthenone (LVI)

A 1:100 solution of (LVI) in biphenyl begins to decompose between 150°C and 200°C. A weak, but complex ESR hyperfine structure is observed. At 240°C, a second, much more intense signal begins to appear and grows quite rapidly. The initial weak signal disappears leaving the simple, symmetrical signal shown in Figure 68. Even though there is considerable line overlap, the approximate experimental line spectrum in Figure 69 was constructed. A computed line spectrum for two equivalent nitrogens and two pairs of equivalent protons is shown in the lower half of the figure. The agreement, in spite of line overlap, seems definite. An SESRS computer comparison will, of course, clinch the assign-

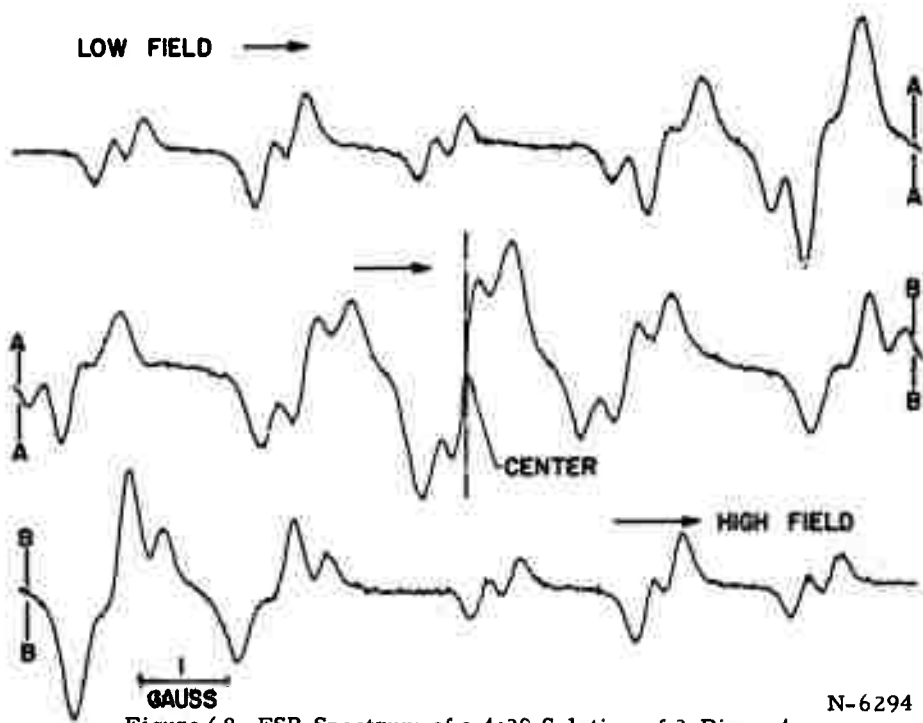


Figure 68. ESR Spectrum of a 1:20 Solution of 2-Diazo-1-acenaphthenone (LVI) in Biphenyl at 196°C

N-6294

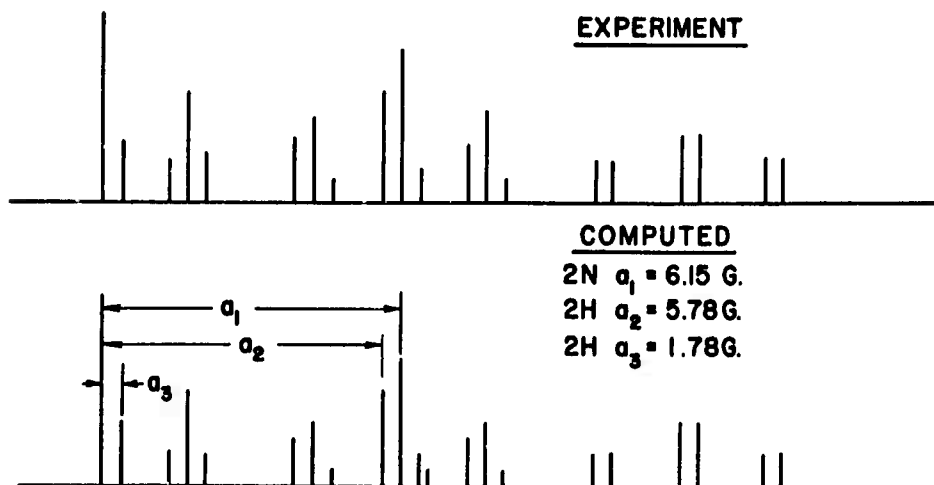


Figure 69. Comparison of Experimental and Computed Line Spectra for (LVI)

N-6295

ment. Furthermore, there are three more weak lines which the assignment predicts in the wings beyond the end of the page. The required field region was not covered in the experimental curve and will be examined in detail.

There is one other possible assignment of coupling constants. Six equivalent protons would yield seven lines with a 1:6:15:20:15:6:1 ratio of intensities, whereas two equivalent nitrogens yield five lines with 6.7:13.3:20:13.3:6.7 intensity ratios. If the weakest proton lines were not observed, it would be extremely difficult to tell the difference. However, a 10-proton radical seems very unlikely in view of the fact that the starting molecule contains only six protons. An SESRS comparison would again be useful and could eliminate one or the other of the possible assignments.

As mentioned previously, a weak but complex spectrum initially was observed at lower temperatures. The disappearance of the first spectrum at 190°C, the temperature at which the curve in Figure 68 was run, was at first thought to be irreversible. However, upon cooling the same sample to 90°C, the complex spectrum reappeared and a superposition of the two spectra was observed (Figure 70).

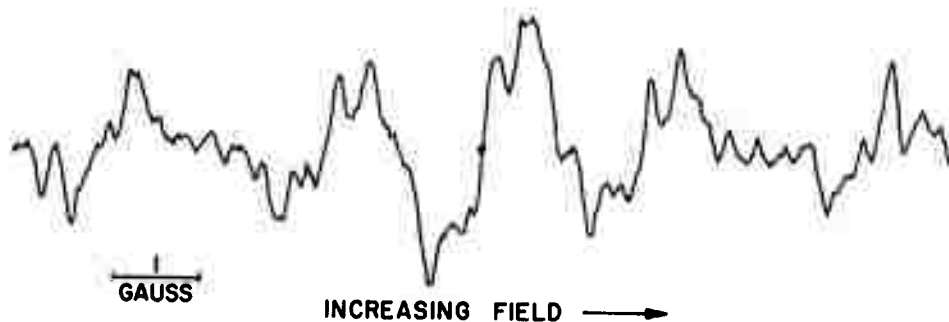


Figure 70. Superposition of Spectra for the Two Radicals Formed During the Thermal Decomposition of (LVI); Measurement Made at 90°C

The first point of interest is that the two spectra do not appear to have the same center. This fact is easily seen by noting the presence of a center of symmetry in Figure 68 but the absence of such a symmetry element in Figure 70. There is the possibility of a quadratic field dependence for extremely large splittings, but those observed in Figure 68 are not that large; furthermore, there is no detectable deviation from centrosymmetry in Figure 68. Thus, the g -values for the two radicals must be different. It is difficult to tell which is larger, but this fact could be determined experimentally for the signals for separate radicals. The g -values will provide evidence concerning which radicals contain oxygen or nitrogen.

Since the products of the decomposition of (LVI) are still not known, a discussion of the mechanism and radical intermediates is somewhat premature. It will be of interest to see if the radical intermediates from (LVI) are at all similar to those obtained in the thermal decomposition of acenaphthylene itself.

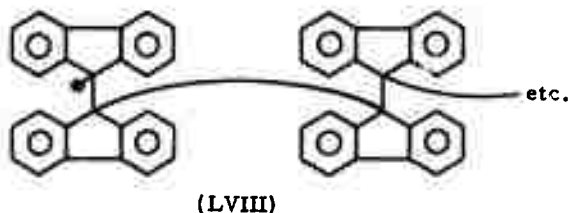
3.5.3. Diazophenanthrone (LVII)

Diazophenanthrone (LVII) begins to decompose near 180°C and a 1:20 solution of (LVII) in biphenyl exhibits resolved hyperfine structure at this temperature. However, a polymeric product forms which is apparently insoluble in biphenyl. Quenching a sample from 200°C to 90°C destroys the hyperfine structure, but the signal reappears upon reheating to 200°C. A better knowledge of the reaction products will be required before an analysis of the spectrum is attempted.

3.5.4. Thermally Decomposed Diazofluorene

A comparison of SESRS curves and experiment for the radical from the pyrolysis of 9-diazofluorene is shown in Figure 71. The sets of coupling constants were not chosen arbitrarily but were based on reasonable free radical structures which might be expected to be formed in diazo decomposition reactions. The two top curves (18 and 19) and the bottom curve (21) were so obviously different from the experimental curves that they were eliminated immediately. Curves 20 and 17 are close, but a careful inspection shows that only curve 20 is in quantitative agreement with experiment. The coupling constant assignment made previously⁽⁶⁾ (Curve 17) on the basis of an inaccurate line spectrum must be discarded.

The only reasonable free radical containing 16 protons in four groups of 4 equivalent protons is either a radical ion of the dimer $\Delta^{9,9'}$ -bifluorene or a neutral radical (LVIII) which forms one end of a polymer chain.



3.6. Synthesis of Organic Compounds for Pyrolysis Studies

Several compounds were synthesized for thermal reaction studies.

3.6.1. 2-Diazo-2-(4-methoxyphenyl) acetophenone

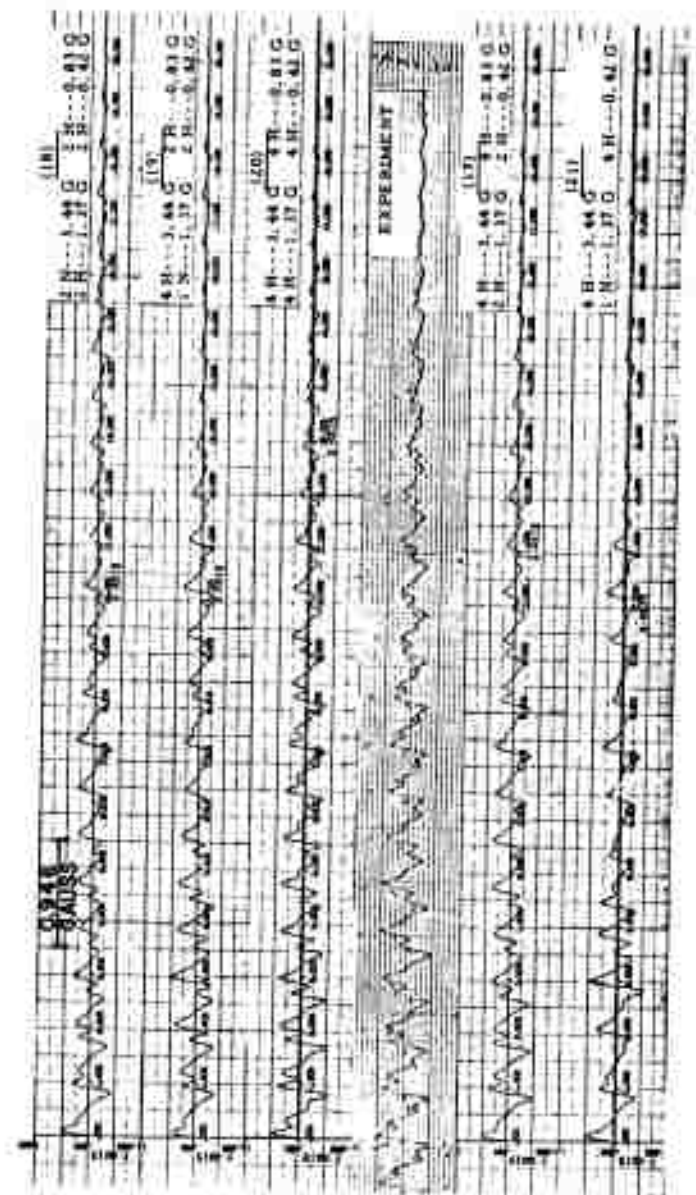
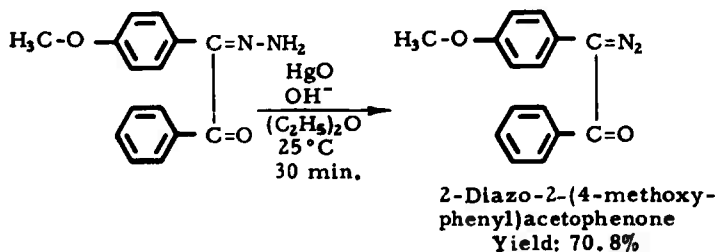
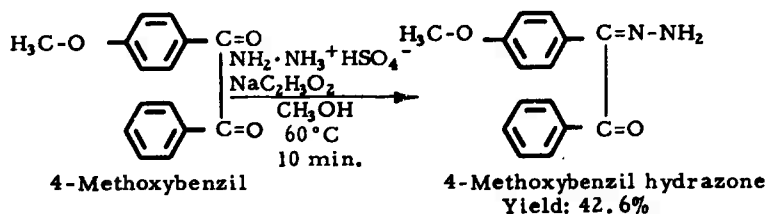


Figure 71. SESRS Comparisons of ESR Spectrum of Radical From Thermally Decomposed Diazofluorene
N-5855

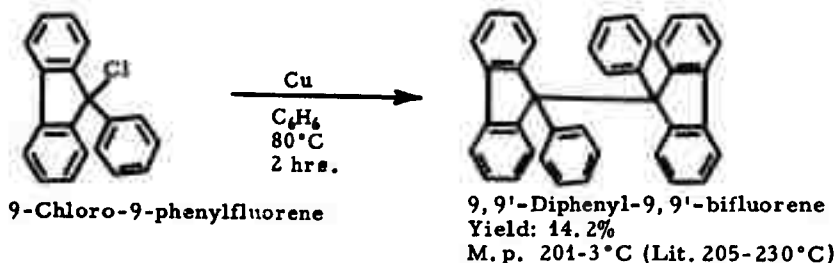
This compound was prepared for further ESR studies of the diazobenzil system. The substitution of a methoxy group in one ring would destroy the symmetry of the diazobenzil molecule and could be used for identification of the diazobenzil radical species.⁽⁴⁾

Methoxybenzil was converted to a hydrazone by treatment with hydrazine sulfate. The hydrazone was then converted to the diazo compound using the method of Nenitzescu and Solomonica.^(10a) The carbonyl group para to the methoxy group should be more reactive than the adjacent carbonyl group. The hydrazone formation should occur as shown below.



3.6.2. 9,9'-Diphenyl-9,9'-Bifluorene

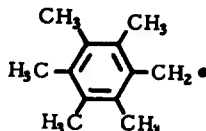
The method of Schlenk, Herzenstein, and Weickel^(10a) was used to synthesize this compound. The precursor, 9-chloro-9-phenylfluorene, was prepared as described previously.⁽⁴⁾



It is thought that this compound should thermally dissociate into 9-phenylfluorene radicals. ESR studies of this dissociation process would be of considerable assistance in those studies being performed on the related compounds 9,9'-bifluorene and $\Delta^{9,9'}$ -bifluorene.

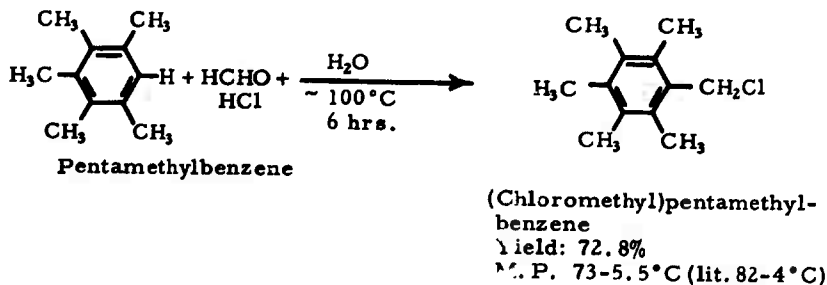
3.6.3. (Chloromethyl)pentamethylbenzene

One of the possible free radical products from the oxidation of hexamethylbenzene is the pentamethylbenzyl radical (LIX).



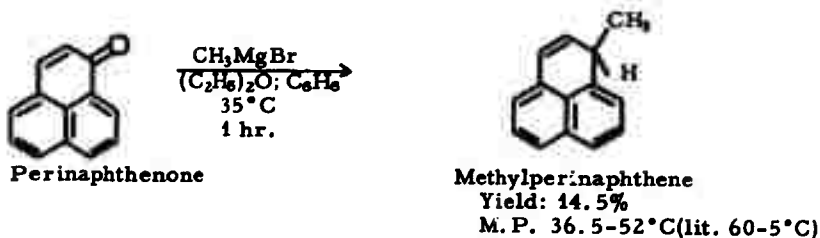
(LIX)

A possible direct route to (LIX) could be the thermal dissociation of the corresponding pentamethyl benzyl halide. (Chloromethyl)pentamethylbenzene was therefore prepared by the method of Aitken, Badger, and Cook⁽¹⁰⁴⁾ and was then employed for ESR thermal decomposition studies. ESR studies subsequently showed that (LIX) was not formed by the oxidation of hexamethylbenzene.



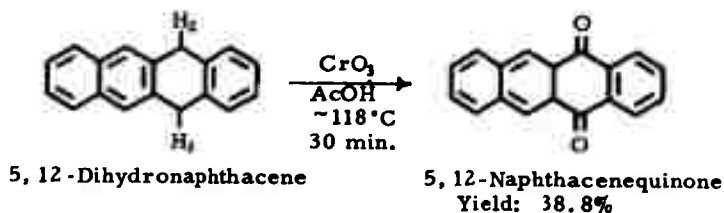
3.6.4. Methylperinaphthene

Methylperinaphthene should thermally decompose into a methylated perinaphthenyl radical, a possible intermediate in the pyrolysis of acenaphthylene.⁽⁶⁾ This compound was synthesized by the addition of methyl magnesium bromide to perinaphthenone. This method was previously employed by Craig, Jacobs, and Lavin.⁽¹⁰⁵⁾

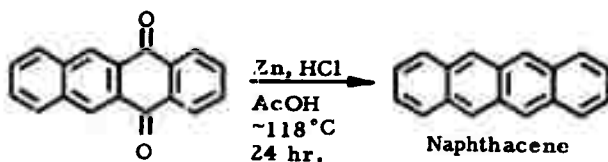


3.6.5. Naphthacene Dimer

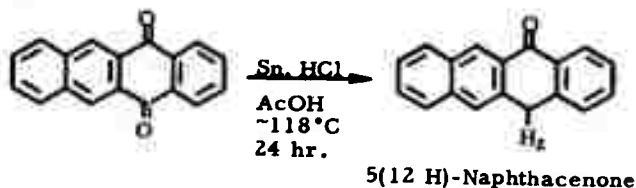
Two attempts have been made to prepare a dimer of naphthacene. One employed a method analogous to that used for the synthesis of dianthranyl.⁽⁴⁾ This method consists of reducing naphthacenequinone with zinc or tin and hydrochloric acid. The naphthacenequinone was prepared using the method of Gabriel and Leupold.⁽¹⁰⁸⁾



The first attempt to prepare the dimer using zinc, resulted in the formation of the unsubstituted hydrocarbon, naphthacene.



Zinc is apparently too strong a reducing agent for this reaction.⁽¹⁰⁷⁾ A second attempt to produce the dimer using tin, which is less reactive, was made. This reagent was employed by Bell and Waring in the preparation of dianthranyl.⁽¹⁰⁹⁾ The product of this reduction is believed to be 5(12 H)-naphthacenone and the reaction is



Apparently, it is not possible to proceed from the quinone to the dimer. An alternate route which could lead to the dimer involves a coupling reaction of 5-bromonaphthacene.

3.7. Polymerization of Aromatic Hydrocarbons and Heterocyclic Compounds Under Pressure

Most of the unsubstituted or substituted aromatic hydrocarbons or heterocyclic compounds which have been discussed above relative to thermal behavior comprise compounds which yield significant quantities of "carbon" on heating at atmospheric pressure. This result implies that their molecular size or structure is such that reaction occurs with condensation to larger molecular size before the atmospheric boiling or sublimation temperature is attained. Investigation of the thermal behavior of such compounds is obviously readily accomplished without the necessity of the more elaborate equipment required for super-atmospheric pressures.

The use of super-atmospheric pressure, however, permits the study of the thermal behavior of compounds of quite simple structure. Aromatic hydrocarbons with only two rings (such as naphthalene and biphenyl), methyl-substituted two-ring compounds (such as 1-methyl or 2-methylnaphthalene), and three-ring compounds (such as anthracene, phenanthrene, and the three isomeric terphenyls) all yield significant amounts of condensed polymeric material at super-atmospheric pressures. The critical temperatures of the three-ring or four-ring aromatics are sufficiently high (618° to 653°C for the three terphenyls) for a two-phase (liquid-gas) system to be maintained throughout thermal treatment, (until the solid polymer phase appears) with the liquid phase of substantially higher density than the gas (vapor) phase. For a two-ring compound such as naphthalene, with a critical temperature of 475°C, a single-phase system generally develops during the initial stages of thermal treatment. With a sufficiently high ratio of mass of initial charge to the volume of the vessel, a single-phase (dense fluid) system is attained at temperatures well below the critical temperature. With continued thermal treatment, a larger fraction of the initial material is converted to higher molecular weight compounds, and a two-phase system reappears prior to the formation of solid polymer.

3.7.1. Previous Investigations

The thermal and catalytic reactions of hydrocarbons in general and of the aromatic hydrocarbons in particular have been extensively investigated during the past one hundred years, the scientific studies probably having been initiated by Bertholet.⁽¹⁰⁸⁾ The earlier as well as the more recent studies have been reviewed by many authors.⁽¹¹⁰⁻¹¹⁴⁾

Much of the earlier work was done in the vapor phase, with and without catalysts such as iron, nickel, or aluminum chloride. There are few references to the reactions of hydrocarbons under substantial pressure prior to the pioneer work on the use of such conditions by Ipatieff.⁽¹¹⁵⁾

It is of interest to note that in discussing the destructive hydrogenation of aromatic hydrocarbons with an initial hydrogen pressure of 70 atmospheres in the presence of mixed catalysts of Al_2O_3 with iron, copper, or copper oxide, Ipatieff reports:⁽¹¹⁶⁾

"Anthracene, when heated with hydrogen under pressure, proved to be a most unstable compound. The chief product resulting from this reaction was coke. After heating 100 g of anthracene for 8 hours at $480^\circ C$, about 30 g of thick, brown liquid was obtained, which was not investigated. The remainder of the anthracene was converted into a mass of porous coke."

Later workers have confirmed the relatively facile polymerization of anthracene in contrast to other three-ring compounds such as phenanthrene and the terphenyls.

Detailed studies of the thermal behavior of aromatic compounds under pressure have been reported by Sachanen and Tilicheev⁽¹¹⁷⁾ and by Tilicheev and Shchitikov.⁽¹¹⁸⁾ Madison and Roberts⁽¹¹⁹⁾ studied the rate of condensation, generally in the liquid phase, of 43 aromatics and related heterocyclic compounds. Lang, Buffleb, Kalowy, and Zander⁽¹²⁰⁾ have reported extensive work on the pyrolysis of naphthalene, pyrene, 1-methyl- and 2-methyl-naphthalene, phenanthrene, fluorene, anthracene, acenaphthene, and mixtures of some of these two- to four-ring aromatic hydrocarbons with benzene. Although carried out in the vapor phase at a temperature of 700° to $800^\circ C$, and with only casual mention of "coke" formation, this work has led to the isolation and definitive identification of products which in all probability are also intermediates in the thermal polymerization of these aromatic hydrocarbons to solid polymeric products.

The use of aromatic hydrocarbons as the coolant or combined coolant and moderator for nuclear reactors has led to investigations of their thermal behavior, both in the absence and in the presence of a radiation field.⁽¹²¹⁻²⁵⁾

Studies of the polymerization of aromatic hydrocarbons on cracking catalysts have been reported.⁽¹²⁶⁾

Few of these studies were directed primarily toward determining the effect of structure of starting material and of conditions of thermal treatment on the properties of the solid polymer or "raw coke". Investigations along these lines, with evaluation of polymers in the form of small graphite rods made with the calcined polymers as the filler component, have been carried out in previous work of the Carbon Products Division of Union Carbide Corporation.⁽¹²⁷⁻¹²⁸⁾ Studies have been made at Pennsylvania State University on the characteristics of the polymeric materials produced by thermal treatment of various hydrocarbons of known structure, either in the liquid phase under pressure or in the vapor phase.⁽¹²⁹⁻¹³²⁾ Characterization of the type of material produced, both at the temperature of preparation and after heat-treatment to various temperatures in the range to $3000^\circ C$, was generally accomplished by X-ray powder diffraction examina-

tion. R. C. Nunn⁽¹²¹⁾ studied the intermediate stages of polymerization in anthracene "tar", defined as the benzene-soluble portion of the thermally treated anthracene.

3.7.2. Objectives of the Present Work

The objectives of the present work on thermal polymerization under pressure have included:

- a) Subjecting compounds of known structure to thermal treatment under pressure at temperatures and times which lead to the formation of a solid polymer, on a scale sufficient to evaluate the calcined polymer as the filler component in small graphite rods.
- b) Extending the scale of operations to the preparation of enough polymer (two to three kilograms) from certain selected initial materials to permit the fabrication of graphite specimens of a size ($2\frac{1}{2}$ inches in diameter by $2\frac{1}{2}$ inches in length) sufficient to allow measurement of graphite properties both with and across grain.
- c) Acquiring a more detailed understanding of the mechanisms and kinetics of the polymerization of aromatic hydrocarbons and related compounds which require the use of super-atmospheric pressure.

3.7.3. Equipment and Procedures

Most of the work was carried out in a $3\frac{1}{2}$ -inch ID, 7-inch OD, 30-inch inside length 347 stainless steel pressure vessel with a working pressure of 6000 lbs./in.² at 600°C. The vessel is equipped with heads (covers) at both top and bottom, with self-sealing modified Bridgeman closures.⁽¹²³⁾ Thermowells extended through both covers; the upper thermowell being immersed in the material being processed. Heat was supplied by chrome-steel-sheathed strip heaters strapped on the outside surface of the pressure vessel; the top and bottom heads were provided with quartz fabric heating mantles to avoid serious temperature gradients at the two ends.

Temperature control was provided by a program controller and time-proportioning circuit. The control couple was located between the outside of the vessel and one of the strip heaters. A multipoint instrument recorded temperatures at the top, middle, and bottom of the outside wall of the vessel, in the top and bottom thermowells, and at various points on the electrically-traced external piping. Pressure was controlled at any desired value up to rated pressure by a pneumatic controller with interchangeable Bourdon tubes and orifices.

In contrast to commercial materials such as petroleum residues and thermal tars (for which the off-products of thermal treatment are generally liquid or gaseous) many of the aromatic hydrocarbons are solid or yield products in thermal treatment which are solid at room temperature.

To avoid plugging by such material, the external lines were electrically traced (with heating tapes) and the pressure control and recording elements provided with diaphragm seals (also heated).

A "hot" receiver was provided in the external circuit, with heated lines to the receiver, for products solid at room temperature. The gas and vapors were led past the hot receiver to a water-cooled condenser, a "cold" receiver, a wet-test meter, and bulbs to collect samples for gas-chromatographic analysis. During the course of the work, an "event marker" pen was provided for one of the recorders; this pen was actuated each time the wet-test gas meter made one revolution (three liters), providing a record of the rate of gas evolution after the control pressure had been attained.

The desired objective was to obtain a material balance between initial material and polymer, distillates, and gas. Although generally the "unaccounted for" mass was 5 weight per cent or less, losses reached 10 per cent on occasion, requiring redesign of various points of the system. There was generally some holdup in the external lines, particularly for the lower molecular weight compounds such as naphthalene. Complete recovery of the solids and liquids produced in the form of "mist" at the pressure control or depressurizing valves was seldom attained, particularly at high rates of gas evolution.

The material to be thermally processed was generally placed in a stainless steel inner container ($3\frac{1}{8}$ -inch OD) inserted into the pressure vessel. Experiments comparing the stainless steel "liner" with a borosilicate glass liner (and a borosilicate glass sheath on the thermocouple well) did not reveal any significant catalytic effect of the stainless steel in contact with the material.

Materials solid at room temperature were melted in the liner, the liner with contents was inserted in the pressure vessel, and the top head was closed. After the contents were cooled to a temperature at which the vapor pressure of the starting material was reasonably low, the air in the vessel was displaced by repetitive (at least three times) pressurizing to 500 to 1000 lb./in.² with helium and exhausting to atmospheric pressure. Helium was employed, in part because of its high purity, but largely because its use simplified the chromatography of the gas samples. Initial pressure of helium was generally atmospheric, again to simplify the calculations of mass balance.

During the latter part of the program, a top cover for the pressure vessel was obtained (interchangeable with the original top cover) which was equipped with a motor-driven packless stirring device⁽¹³⁴⁾ with a shaft and impellers extending to within 1 inch of the bottom of the stainless steel liner. A tachometer indicated the revolutions per minute of the inner (driven) shaft, and the output of the tachometer was suitably converted to provide a signal which was recorded on the multi-point instrument. The decrease in RPM of the stirrer, eventually to zero, served as a relative indication of the increasing viscosity of the material

being thermally processed, the stalling providing an indication of the production of an essentially solid polymer at the temperature and pressure of the experiment.

The procedures for calcining the raw polymer (to 1000°C), forming $\frac{3}{4}$ -inch diameter by 6-inch length rods by extrusion, baking, graphitizing, and measuring coefficients of thermal expansion and specific electrical resistance have been described in a previous report.⁽¹³⁵⁾

3.7.4. Effect of Hydrocarbon Structure on Polymer Properties

The dominant effect of initial hydrocarbon structure on the properties of the resultant "graphite" has been extensively discussed in previous sections of this report. The effect of structure has also been found for the lower molecular weight compounds which require the use of super-atmospheric pressure.

3.7.4.1. Compounds Which Lead to Nongraphitizing Carbons

Tables 45 and 46 give data on the material balances, the temperature and pressure conditions of thermal polymerization, the properties of the 3000°C heat-treated polymers, and on graphite rods prepared using the 1000°C heat-treated polymers as the filler component for a series of compounds which lead to nongraphitizing carbons.






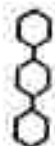
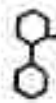

In Tables 45 and 46 (and in the succeeding tables), the temperatures given are the maximum temperatures during the period of solid polymer formation, that is, temperatures representing the peak of the exotherms discussed in a later section. The data for "moles gas per mole of charge" represent the amount of gas produced during the entire period of heating, including that produced (often at higher temperatures) after the exotherm.

The thermal expansion data were measured with-grain, and are mean values over the temperature range 30° to 100°C. The interplanar spacings were measured on the 3000°C heat-treated polymers by the procedure discussed in an earlier section of this report. The helium densities were measured using a purge-type Beckman pycnometer; the size of the 3000°C heat-treated powder was in the range of 45 to 60 per cent through 200 mesh (Tyler sieve series).

The characterization of the 3000°C heat-treated materials as non-graphitic or turbostratic carbons is based on the large interplanar c-axis spacing, the failure to observe a 101 line in the X-ray diffraction film, the low helium density of the 3000°C heat-treated polymers, and the high electrical resistance of the 3000°C heat-treated rods employing the 1000°C calcined polymers as filler components.

The first four materials in Tables 45 and 46 represent the series of 6-5-6 three-ring compounds, that is, two end rings with 6 carbon atoms and a middle ring of 5 carbon atoms, or of 4 carbon atoms and one nitrogen, oxygen, or sulfur atom. The other five materials are biphenyl, the

Table 45. Data on Thermal Polymerization of Compounds Leading to Nongraphitizing Carbons

Experiment No.	Initial Material		Material Balance, Weight Per Cent			Moles Gas Per Mole Charge	Temperature °C	Maximum Pressure lb/in ²	Grams Charge
			Polymer	Distillate	Gas				
255-124-1	Fluorene		78.9	7.3	10.8	3.0	0.999	1025	1007
255-160-9	Carbazole		91.7	0.4	5.4	4.0	0.387	483	2178
255-159-37	Dibenzofuran		78.8	12.9	5.3	3.0	0.491	537	2297
255-129-93	Dibenzothiophene		83.3	4.5	7.1	5.2	0.775	512	1011
255-159-19	Biphenyl		51.7	37.7	5.5	5.1	0.567	535	2167
255-129-39	p-Terphenyl		65.8	19.6	7.6	7.0*	0.726	521	1361
255-159-29	o-Terphenyl		73.5	16.9	6.3	3.3	0.898	506	2191
255-161-171	m-Terphenyl		73.3	17.7	5.8	3.3	0.830	530	2443
255-129-87	Hydrogenated Terphenyls		31.0	45.8	19.0	4.2	1.891	489	2011

* Known loss of gas.

Table 46. Characteristics of 3000°C Heat-Treated Polymers-Nongraphitizing Carbons

3000°C HT Rod Properties with grain								
Expt. No.	Initial Material	CTE 10 ⁻⁶ °C ⁻¹	Spec. Resistance 10 ⁻⁴ ohm cm	Interplanar Spacing, Å				Helium Density 3000°C HT Polymer g cm ⁻³
				3000°C HT Polymer				
				002	004	006	008	
124-1	Fluorene	+ 3.48	26.40	3.383	3.378	3.376	-	2.10
160-9	Carbazole	+ 2.91	45.55	3.409	3.415	-	-	1.66
159-37	Dibenzofuran	+ 3.04	35.40	3.409	3.412	-	-	1.75
129-93	Dibenzothiophene			3.45	3.41	-	-	1.60
159-19	Biphenyl	+ 3.07	31.85	3.43	3.41	-	-	1.78
129-39	p-Terphenyl	+ 3.15	30.70	Too diffuse	3.42	-	-	1.57
159-29	o-Terphenyl	+ 3.13	36.80	3.42	3.40			1.82
161-71	m-Terphenyl	+ 3.06	35.00					
129-87	Hydrogenated Terphenyls	+ 3.77	21.20	3.386	3.364	3.362	-	2.01

three isomeric terphenyls, and a mixture of partially hydrogenated terphenyls. * All nine compounds yield polymers which, on further heat treatment, lead to nongraphitizing carbons. Some quantitative variations appear: the polymers from the partially hydrogenated terphenyl mixture and from fluorene are somewhat less turbostratic than the others on the basis of 1) lower interplanar spacings and resolution of the third order reflection (006 line), 2) somewhat higher helium densities for the 3000°C heat-treated polymers, and 3) lower specific resistances in the 3000°C heat-treated formed rods.

As noted in Section 3.8., the polymer from p-terphenyl shows a low initial helium density after 1000°C heat treatment, with a drift with time to higher values. This behavior is characteristic of all of the compounds in Tables 45 and 46 for which such data were obtained. These 1000°C heat-treated materials thus parallel the behavior found by Franklin for certain carbonized coals.⁽¹³⁶⁾ The properties are quite similar to those found for the turbostratic carbons formed by heat treatment of cellulose⁽¹³⁷⁾ or of certain cross-linked polymers such as phenolformaldehyde resins or furfuryl alcohol resins.⁽¹³⁸⁾

Although it is not clear to what extent the term "glassy carbon" has been preempted for one particular type of turbostratic carbon,⁽¹³⁹⁾ the materials of Tables 45 and 46 can be quite literally described as glassy carbons in that they look like black glass (obsidian); this appearance remains unchanged after heating to 3000°C. The very diffuse X-ray diffraction lines are similar to those observed for materials in the glassy state.

The polymer from fluorene can be characterized as "glassy needles" in appearance. There is no evidence, however, that use of the calcined polymer as a filler component would lead to anisotropy in 3000°C heat-treated formed shapes.

* HB-40, Monsanto Chemical Company

3.7.4.2. Compounds Which Lead to Isotropic Graphite

Tables 47 and 48 give data (corresponding to that given in Tables 45 and 46) for fluoranthene and 9,9'-bifluorene. These two compounds yield polymers which are dull and quite dense. The 3000°C heat-treated polymers have an inter-planar spacing definitely greater than that observed for the materials described in the next section. The 4th order reflection (008 line) is resolved in some instances, however, and the helium densities appear only slightly lower than the well-ordered graphites. The 101 line is resolved in the X-ray diffraction spectrum, and the 3000°C heat-treated materials will leave a mark when rubbed on paper; the highly turbostratic carbons of the preceding section do not mark paper at all.

Graphite prepared from the 1000°C heat-treated polymers shows a high coefficient of thermal expansion, a specific resistance somewhat higher than those measured for materials of the next section, but far less than those obtained for the glassy carbons of Section 3.7.4.1. The graphite is quite isotropic, as shown in Section 3.8. for the material prepared from fluoranthene.

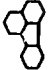

The properties of the graphite derived from these two materials is very similar to those of graphite derived from the coking of air-blown vacuum residues (described in Section 4.2.).

3.7.4.3. Compounds Which Lead to Anisotropic Graphite

Tables 49 and 50 give corresponding data for a series of compounds which lead to highly-ordered graphite, as evidenced by interplanar spacings in the range of 3.356 to 3.358 Å, resolved 4th order reflections, sharply resolved 101 lines, and helium densities close to the theoretical value for single crystal graphite.

For many of the compounds, the thermal polymers are quite highly oriented when judged by the with-grain thermal expansion of the extruded rods employing the 1000°C heat-treated polymers as filler component. The with-grain thermal expansion is often slightly negative over the temperature range of 30-100°C. Such low thermal expansions in the with-grain direction are interpreted to signify a considerable extent of orientation of the individual crystallites within the particles of the filler component; that is, the a-b axes of the crystallites composing the macroscopic particles are roughly parallel to each other and constitute a macroscopic type of order which extends over distances of 40 microns (40,000 Å) or more, which is much beyond the instrumental broadening limit (~2000 Å) for X-ray determination of crystallite size. There is no implication that the particles are by any means single crystals. Their porosity alone, as well as many other considerations, would militate against any such conclusion. This relative orientation is established in the thermal polymerization process, that is, at 400° to 525°C, and appears quite analogous to the crystalline type of condensation polymer.

Table 47. Data on Thermal Polymerization of Compounds Leading to Isotropic Graphites



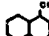
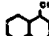
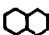
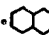


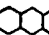
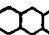

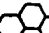
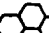
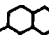
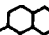

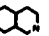

Experiment No.	Initial Material	Material Balance, Weight Per Cent				Moles Gas per Mole of Charge	Temperature °C	Maximum Pressure lb/in. ²	Grams Charge
		Polymer	Pitch or Tar	Distillate	Gas				
255-124-41	Fluoranthene 	88.2	-	2.5	7.4	0.834	487	1080	1613
255-160-23	Fluoranthene	89.4	4.8	0.4	5.6	-0.2	497	1700	2338
255-129-31	9,9'-Bifluorene 	84.9	-	3.6	8.9	1.226	-	1490	1455

* Known loss of gas.

Table 48. Characteristics of 3000°C Heat-Treated Polymers - Isotropic Graphites

Exper. No.	Initial Material	3000°C HT			Interplanar Spacing, Å			Helium Density 3500°C HT Polymer g./cm. ³
		CTE / 10 ⁻⁶ °C ⁻¹	Spec. Resistance / 10 ⁻⁴ ohm/cm.	with graph	3000°C HT Polymer	3000°C HT Polymer	3000°C HT Polymer	
124-41	Fluoranthene	+5.48	12.46		0.02	3.54	3.54	2.21
160-23	Fluoranthene	+5.45	12.10		0.02	3.54	3.54	2.21
124-31	9,9'-Bifluorene	+4.17	10.70		0.02	3.54	3.54	2.21

Table 49. Data on Thermal Polymerization of Compounds Leading to Anisotropic Graphite

Sample No.	Starting Material	Monomer	Yield, %	Gas, %	Distillate, %	Residue, %	Monomer, %	Melting Point, °C	Temperature, °C	Weight Percent, %	Viscosity, %
255-144-37	Naphthalene		38.4	4.5	19.3	4.4	8.8 *	8.516	400	1710	1012
255-128-17	Naphthalene		45.5	20.2	1.7	9.8	10.8	0.436	400	1000	1000
255-120-63	1-Methylnaphthalene		33.2	-	-	-	-	-	427	1700	2184
255-160-31	1-Methylnaphthalene		49.2	8.8	28.2	10.8	5.0	0.954	455	1900	2272
255-159-87	2-Methylnaphthalene		63.5	-	18.2	12.7	5.6	1.09	460	1910	2166
255-160-1	2,3-Dimethylnaphthalene		49.7	-	29.1	10.4	10.8 *	> 1.03	455	1920	1872
255-123-1	Acenaphthene		63.5	-	21.8	14.3	0.5	1.10	-	1040	1094
255-120-89	Acenaphthylene		80.7	-	5.8	10.3	3.2 *	0.786	-	1020	1141
255-144-29	Anthracene		83.3	-	5.0	5.5	6.2 *	0.578	430	1530	1403
255-145-61	Anthracene		84.6	4.0	1.8	7.0	2.5	0.368	415	1900	2190
255-144-1	9,10-Dihydroanthracene		75.5	-	6.1	11.1	7.3 *	1.140	-	1480	1604
255-144-55	Phenanthrene		82.2	-	6.1	9.1	2.6	1.042	473	1500	1201
255-160-51	Phenanthrene		84.1	-	5.2	4.6	6.1 *	0.538	525	1900	2301
255-144-21	Pyrene		88.6	-	1.1	7.7	2.6 *	1.135	-	1520	1592
255-144-71	Pyrene		88.4	-	0.9	5.2	5.5	0.810	480	1510	1495
255-159-45	Quinoline		74.9	-	12.7	9.5	3.1	0.638	450	1560	2403
255-161-21	Isoquinoline		75.3	-	9.0	5.8	10.0 *	> 0.45	462	1920	2358
255-159-9	Acridine		86.2	-	1.5	5.3	7.1 *	0.560	443	1560	2136

* Known loss of gas.

Table 50. Characteristics of 3000°C Heat-Treated Polymers - Anisotropic Graphites

Exper. No.	Initial Material	3000°C HT Rod Properties		3000°C HT Polymer Interplanar Spacing, Å	Helium Density 3000°C HT Polymer g cm ³
		CTE with-grain 10 ⁻⁶ /°C ⁻¹	Spec. Resistance 10 ⁻⁶ ohm cm		
144-37	Naphthalene	- 0.04	7.55		
128-17	Naphthalene	+ 2.02	10.00	3.358	2.261
120-63	1-Methyl naphthalene	+ 0.25	7.60	3.358	
160-31	1-Methyl naphthalene	+ 0.17	8.30		
159-87	2-Methylnaphthalene	0.00	7.40		
160-1	2,3-Dimethylnaphthalene	+ 0.07	8.45		
123-1	Acenaphthene	- 0.02	8.10		
120-89	Acenaphthylene	- 0.10	8.05		
144-29	Anthracene	- 0.02	8.45	3.357	2.261
144-1	9,10-Dihydroanthracene	- 0.05	7.60	3.356	2.260
144-55	Phenanthrene	+ 0.01	7.60	3.357	
160-51	Phenanthrene	+ 1.04	9.50	3.358	2.27
144-21	Pyrene	+ 1.34	8.00	3.358	
144-71	Pyrene	+ 2.93	6.10	3.358	2.22
159-45	Quinoline	+ 0.78	10.30	3.358	
161-21	Isoquinoline	+ 0.30	7.30		
159-9	Acridine	+ 0.40	9.30	3.356	2.23

As shown in Table 50 for naphthalene and phenanthrene, the degree of orientation in the polymer from a given compound does depend upon the conditions of polymerization: there is less orientation (as judged by the with-grain thermal expansion of the derived graphite rods) when the conversion from a viscous liquid to an essentially solid polymer occurs at the higher temperature, and, hence, more rapidly. The polymers are distinctively different in appearance; the polymer formed more slowly is more "crystalline". The interplanar spacings are identical within the accuracy of measurement, and the variation in the thermal expansion of the derived graphite is considered to result from a varying degree of macroscopic orientation in the polymer.

Graphite with very low with-grain thermal expansion has not yet been derived from pyrene, and it is possible that a highly crystalline polymer cannot be prepared from pyrene. The polymers prepared so far from quinoline do not lead to graphite with very low thermal expansion, although the graphite derived from the isomeric isoquinoline indicates a substantial degree of orientation in the polymer.

3.7.5. Kinetics of Thermal Polymerization

For all compounds which have been studied in detail so far, the transition from a liquid mixture to a polymer which is a solid at the temperature and pressure of the experiment has been found to occur at a definite stage of the thermal reaction. This transition step in the overall sequence of reactions is substantially exothermic, and the time of initiation of the exotherm has been utilized to relate the rate of reaction to the temperature.

An exotherm which is typical for the higher range of temperatures for naphthalene is illustrated in Figure 72.

In Figure 72, ΔT (the left ordinate) is the difference between the temperature indicated by a thermocouple in the material (initially naphthalene) and the temperature of the external wall of the pressure vessel at approximately mid-height. The right-hand ordinate is this latter external wall temperature. The abscissas are the times in hours from the start of heating. A moderate increase in ΔT occurred at 25.5 hours, with the main exotherm initiating at 26.0 hours. The exotherm peaked after the heat to the external wall was shut off by a protective circuit operated by a second thermocouple in the internal thermowell.

A rough approximation of the heat evolved was made by assuming that 1.5 kg of the original charge of 1.875 kg of naphthalene was in the liner at the time the main exotherm occurred, using a value for the specific heat of 0.55 gram calorie $g^{-1} C^{-1}$ * and ignoring any heat transfer from the liner to its environment. This estimate was 60 kilocalories. With the further assumption that the average species at the time of the initiation of the exotherm could be represented as binaphthyls (molecular weight of 254 g), a

* Based on the value given in Reference 122 for 2,2'-binaphthyl at 427°C.

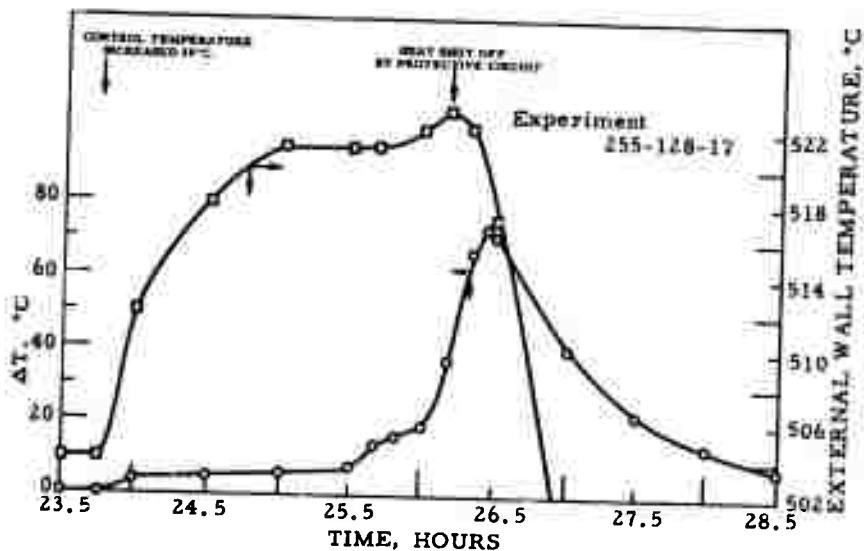


Figure 72. Exotherm in the Thermal Polymerization of Naphthalene (Experiment 128-17)

N-3887

heat of polymerization of ~10 kilocalories per mole was found. This value is comparable to values for heats of polymerization for styrene, vinyl acetate, isoprene, etc.⁽¹⁴⁰⁾ If we can accept the indicated 2°C rise in the external wall temperature as representing reaction heat transferred, we can add ~30 more kilocalories of energy release and arrive at ~15 kilocalories per mole for the heat of polymerization. It is obvious that the data obtained in this manner cannot be very precise, but they are believed to be in the correct range.

The correlation of the initiation of this exotherm with the transition from a liquid phase to a solid phase is based on the following observations:

1. If the time of thermal treatment is limited to a point "just short" of the initiation of the exotherm, the product is a pitch which is definitely fusible.
2. If the supply of heat is terminated just after the exotherm, the product is an infusible solid with a characteristic frozen-in bubble structure.

Experiments of this nature have been made for naphthalene, fluoranthene, p-terphenyl, anthracene, and quinoline. With naphthalene, anthracene, and quinoline, the product obtained by interruption of the heat

supply shortly after the exotherm peaked was composed of an infusible solid and some unconverted tar. The latter would have been converted by a longer time of heating.

Stopping "just short" of the initiation of the exotherm requires a fairly precise calculation of time at temperature. In an experiment with naphthalene, one in which calculation did not take adequate account of somewhat higher temperatures and a larger initial charge, the exotherm had initiated and progressed to the extent of 7°C. Although the heat was turned off immediately and a cold air blast applied to the external wall of the pressure vessel, it was quite impossible to quench the polymerization reaction. One of the thermocouples in the internal thermowell* showed an increase in temperature of 42.5°C in a 20-minute period after the heat was turned off and cooling air applied. At this time, the temperature indicated by the internal thermocouple was 100°C above the temperature in the lower internal thermowell (which would normally cool at the same rate as the upper internal thermowell). An exothermic reaction is, of course, normally difficult to quench once it has reached a certain stage. This experiment served to remove any remaining doubt as to the reality of the phenomenon.

More direct evidence of the close correlation of the occurrence of the exotherm with the transition from a liquid to an essentially solid polymer was obtained in experiments in which the charge was stirred from the beginning of thermal treatment (after melting for materials solid at room temperature), using a packless agitator (described in Section 3.7.3) with the rate of rotation (RPM) of the inner stirrer shaft recorded. Results of typical experiments are shown in Figures 73 and 74 for p-terphenyl and fluoranthene, respectively. In these two figures, the abscissae are the times in hours, and the various ordinates are:

- a) ΔT in °C, the temperature difference between the material in the liner (measured by a thermocouple in the internal thermowell) and the temperature of the external wall of the pressure vessel (at mid-height).
- b) RPM, the revolutions per minute of the inner (driven) shaft with attached impellers.
- c) $\Delta P/\Delta \theta$, rate of pressure rise in lbs./in.² per hour for the period prior to reaching the control pressure.
- d) $\Delta G/\Delta \theta$, rate of gas evolution in liters per hour for the period after reaching the control pressure.
- e) In Figure 74, T, in °C, the temperature of the material in the liner.

* A total of five thermocouples were in the internal thermowell in this experiment.

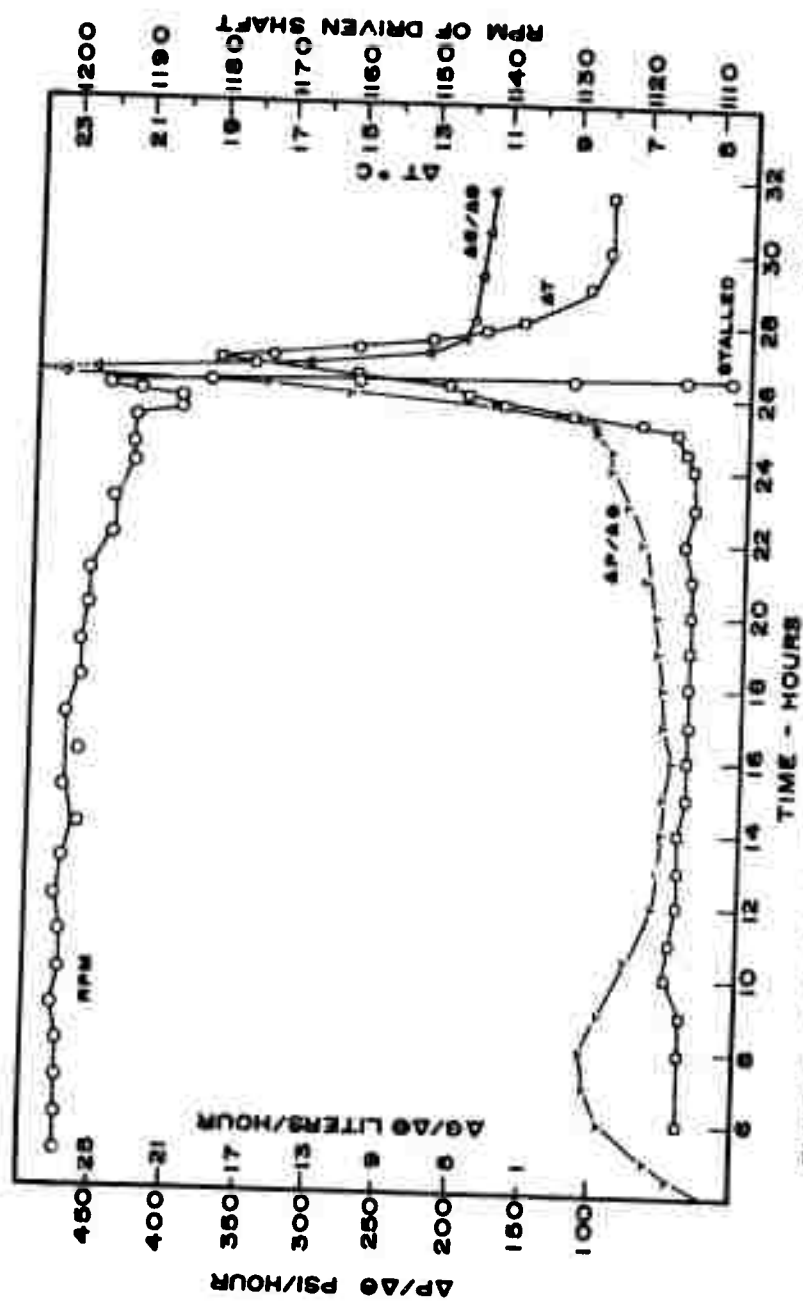


Figure 73. Transition to Solid Polymer in the Thermal Polymerization of p-Terphenyl (Experiment 160-24) N-7144

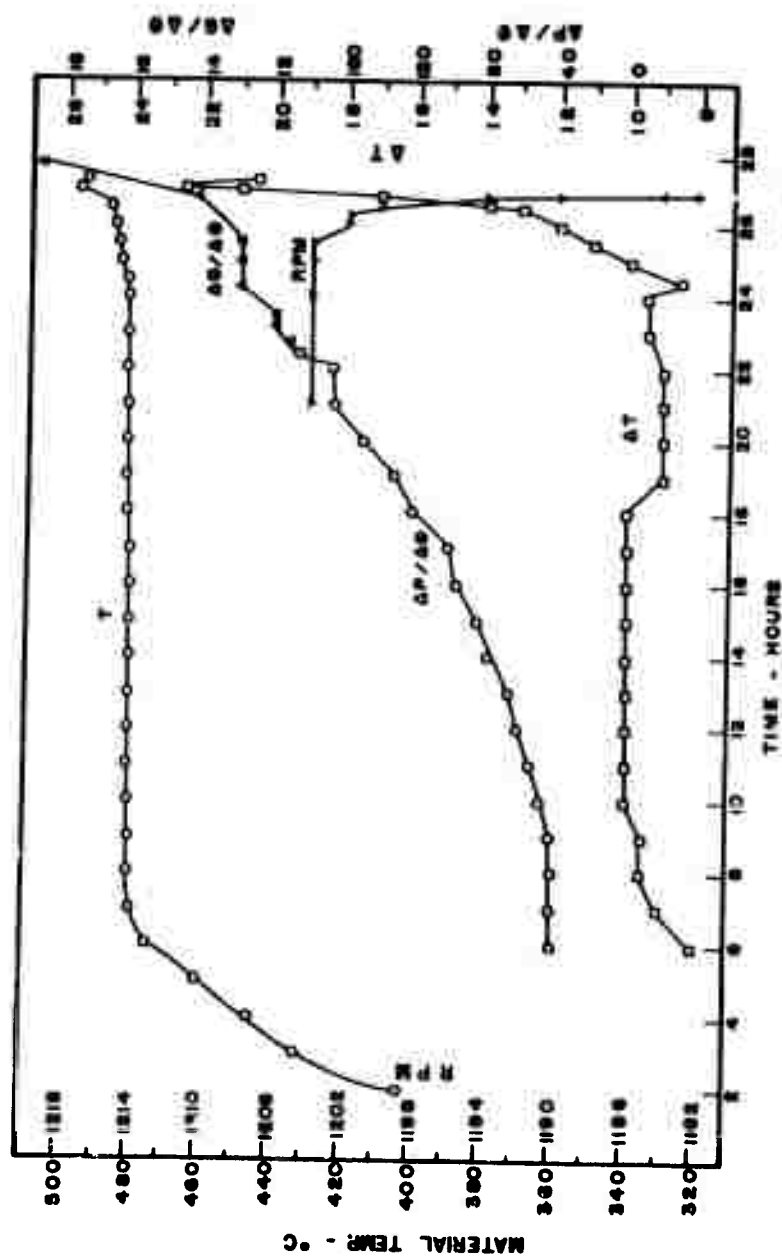


Figure 74. Transition to Solid Polymer in the Thermal Polymerization of Fluoranthene (Experiment 60.72)

The close correspondence in time between the occurrence of the exotherm and the sharply decreasing RPM of the agitator to complete stalling is evident in these figures.

The experiments using naphthalene, anthracene, and quinoline gave similar results.

3.7.5.1. Dependence of Rate of Polymerization on Temperature

The time of initiation of the exotherm accompanying the transition to a solid polymer appears to follow the Arrhenius relation between specific rate constant (k) and Kelvin temperature (T):

$$k = A \exp(-B/T) = A \exp(-E/RT)$$

$$\text{or } \ln k = \ln A - (B/T),$$

where $\ln A$ is the intercept and $-B$ the slope of the assumed linear relation between $\ln k$ and $1/T$. A is interpreted as a frequency factor (dimensionally correct only for first order kinetics) and E as an energy of activation. R is the gas constant.

The time to initiation of the exotherm can be interpreted as the time necessary to reduce the concentration of charge material to $\frac{1}{N}$ of its initial value. This time can be related to the specific rate constant for first order kinetics by

$$k = \theta_{1/N}^{-1} \ln N,$$

where k is the reaction rate constant

$\theta_{1/N}$ is the time to reduce the concentration of a reactant to $\frac{1}{N}$ of its initial value.

For a reaction of kinetic order m , the equation becomes

$$k = (N^{m-1} - 1) (m - 1)^{-1} C_0^{1-m} \theta_{1/N}^{-1}$$

where C_0 is the initial concentration.

For first order kinetics, $-\ln(\theta_{1/N})$ is plotted against $\frac{1}{T}$; the slope (but not the intercept) is independent of N . For higher order kinetics, $-\ln(C_0^{m-1} \theta_{1/N})$ should be plotted against $\frac{1}{T}$ if C_0 varies among the experiments.

Figures 75, 76, and 77 are Arrhenius plots of the data for naphthalene, fluoranthene and p-terphenyl, respectively. θ is the adjusted time, in hours, to the initiation of the reaction isotherm. Because of the high thermal resistances in the equipment, considerable time is required to bring the charge material to temperature. The temperature readings as a function of time were divided into groups covering up to 20°C (5°C for the higher temperature groups). An adjusted time θ_s at T_s (the selected temperature), was obtained from the actual time (θ_g) at the average temperature (T_g) for each group by the relations:

$$\log_{10} (\theta_g / \theta_s) = b \left[\left(\frac{1000}{T_g} \right) - \left(\frac{1000}{T_s} \right) \right]$$

and

$$\theta = \sum_g \left(\frac{\theta_g}{\theta_s} \right) \theta_s$$

where b is a constant in the assumed relation

$$\log_{10} (1000/\theta) = a + b (1000/T)$$

A first rough value of b could be obtained from the data and the procedure was iterated to an essentially constant value of b . Two iterations were usually sufficient.

In Figures 75 to 77, the number adjoining each point identifies the individual experiment. In Figure 76, Experiment 124-41 involved comparably long time periods at three different temperatures. The lower point is plotted for a temperature which is the weighed average of these three time periods. The upper point (marked +) is the temperature at which the exotherm initiated.

In Figure 77, only the data for p-terphenyl were used for the least-squares line. The points for single experiments on biphenyl, m-terphenyl, and o-terphenyl are shown on the same plot. The velocity of the overall reaction to a solid polymer for biphenyl and m-terphenyl appears quite comparable to that for p-terphenyl; the velocity for o-terphenyl is substantially higher. Data at a single temperature obviously gives no clue as to whether this difference represents a change in frequency factor or in energy of activation.

The information obtained for various compounds from the variation of the time to this stage of the reaction (initiation of the transition exotherm) with temperature is summarized in Table 51. The second column, n , is the number of experiments and the third column, E , the activation energy in kilocalories calculated from the least-squares slope. The

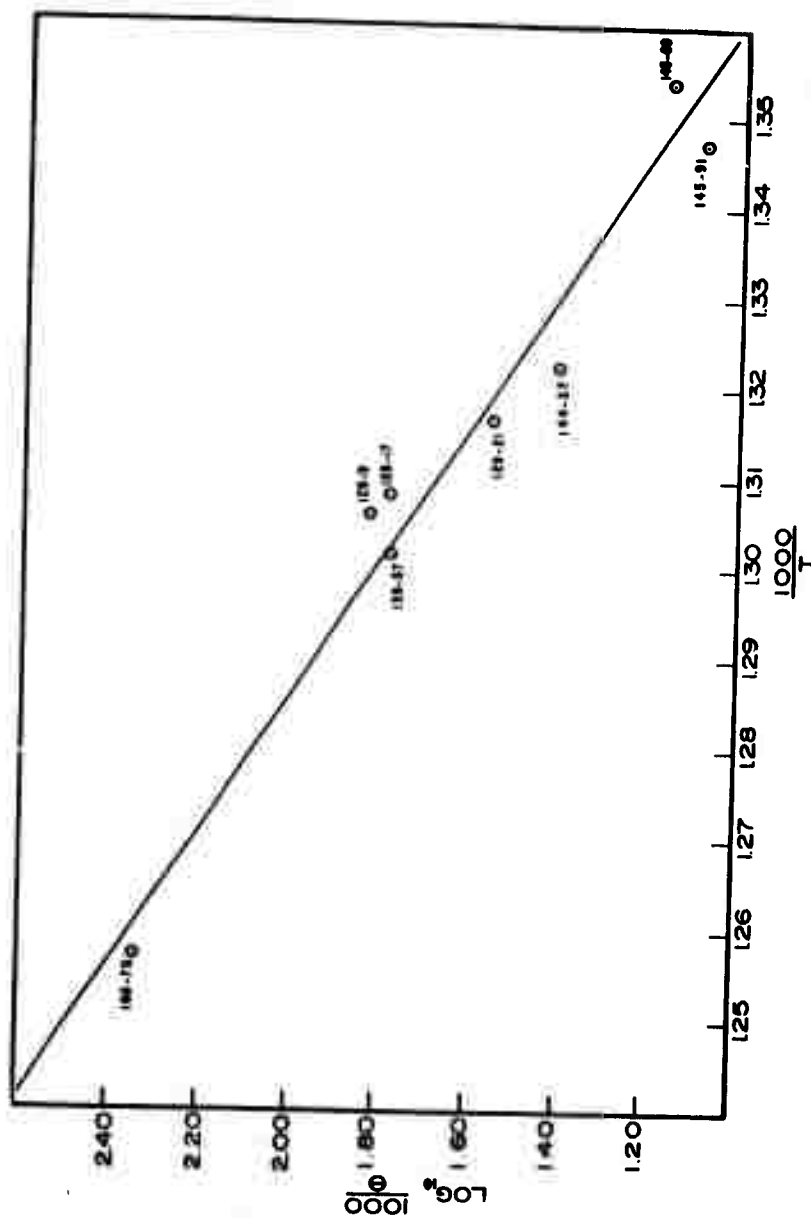


Figure 75. Arrhenius Plot for Transition to Solid Polymer - Naphthalene
(θ in Hours) N-7145

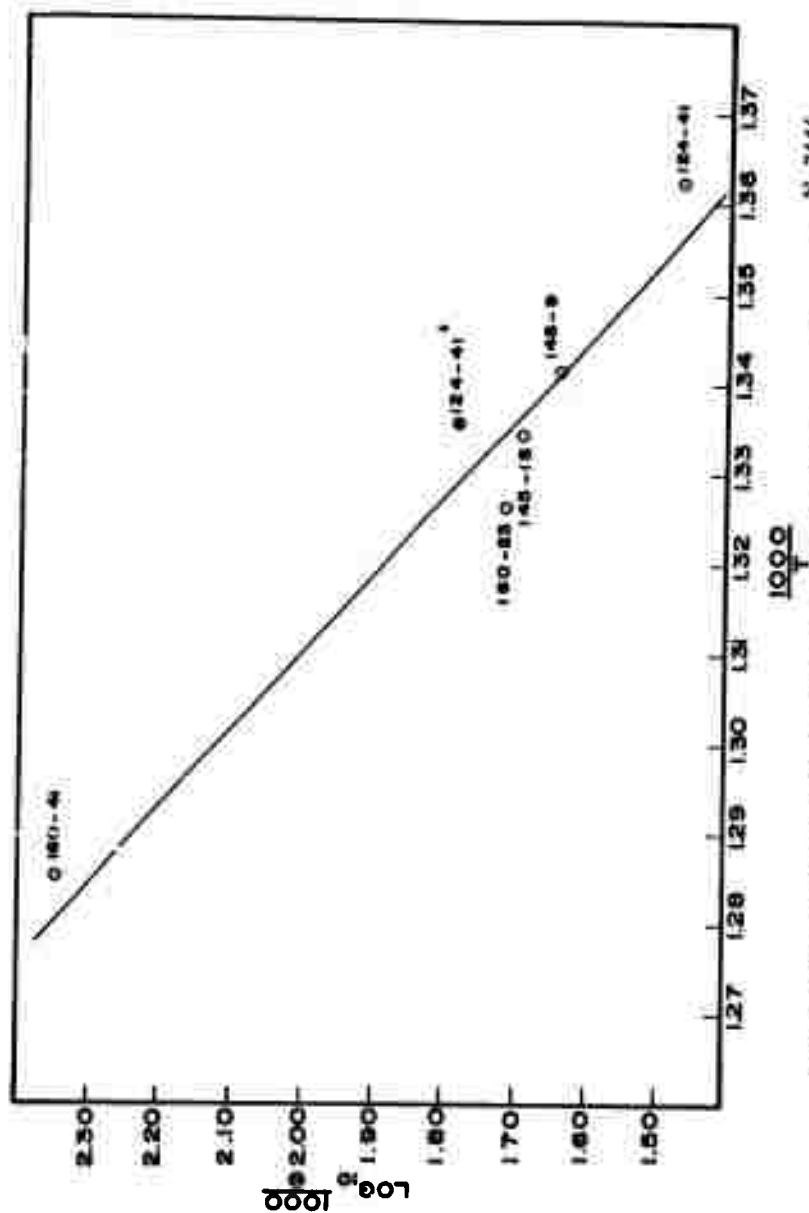


Figure 76. Arrhenius Plot for Transition to Solid Polymer - Fluoranthene
N-7146
(6 in Hours)

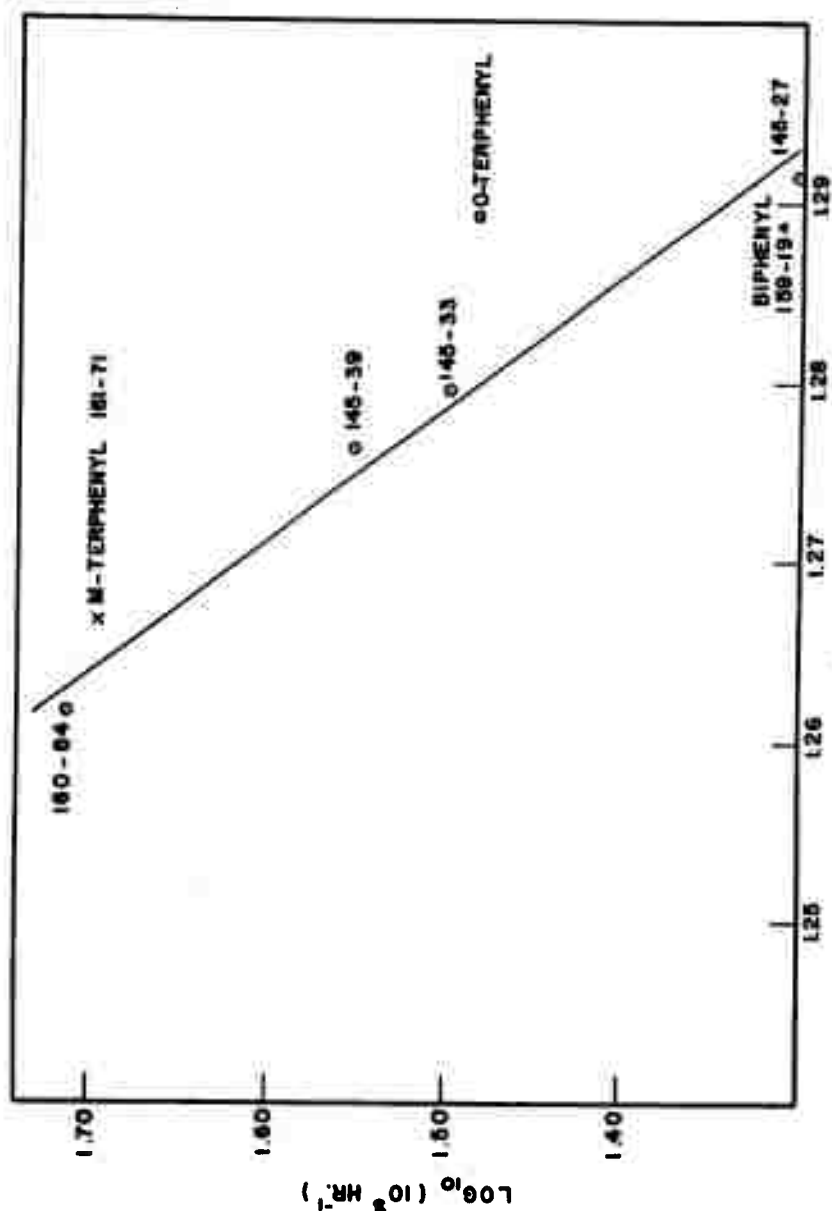


Figure 27. Arrhenius Plot for Transition to Solid Polymer - p-Terphenyl
(τ in Hours)

N-7147

Table 51. Summary of Data on Temperature Dependence of Rate of Polymerization

Initial Material	n	E kilocalories	E ^o kcal.	E [*] kcal.	A ₁ Sec. ⁻¹	A ₂ Liter mole ⁻¹ sec. ⁻¹	Range in Temperature °C
p-Terphenyl	4	62.3	6.0	-	5.1 · 10 ¹²	5.0 · 10 ¹²	501-519
Naphthalene	8	60.7	4.8	93.0	7.4 · 10 ¹²	7.3 · 10 ¹²	466-522
Phenanthrene	3	54.8	9.2	98.5	2.6 · 10 ¹¹	2.6 · 10 ¹¹	467-506
Fluoranthene	5	52.7	6.5	-	8.1 · 10 ¹⁰	7.9 · 10 ¹⁰	461-505
Quinoline	3	45.4	7.4	-	3.7 · 10 ⁹	3.6 · 10 ⁹	432-471
Anthracene	3	54.4	4.1	-	1.0 · 10 ¹³	1.0 · 10 ¹³	402-444

* Reported by Tilicheev. (118)

fourth column is the standard deviation of the slope of the assumed linear relation, expressed in kilocalories. The fifth column gives values of the activation energy, reported by Tilicheev. (118) Tilicheev's values were derived from data on the fraction of starting material converted when the aromatic hydrocarbons were heated (in a pressure vessel) for various periods of time and at different temperatures with fractional conversions ranging up to 0.40 for naphthalene and to 0.76 for phenanthrene.

The sixth and seventh columns are values for A₁, the Arrhenius frequency factor on the assumption of first-order kinetics, and for A₂, the coefficient of the exponential factor on the assumption of second-order kinetics. In the calculation of A₁ and A₂, the values N = 10 and C₀ = 4.0 moles/liter were taken for all compounds. Quantitative data have been obtained on the fractional conversion at a stage of reaction near the initiation of the transition exotherm only for naphthalene; the high partial pressure of the remaining naphthalene is a complication. Elution chromatography has indicated that the fractional conversion of fluoranthene at a stage shortly before the transition exotherm is of the order of 0.9, but this value has not yet been quantitatively established by fractional distillation. The initial concentration expressed as moles per liter will necessarily vary from one compound to another and with temperature. It is strongly dependent on the ratio of mass of initial material to total available volume for reduced temperatures (T/T_c where T_c is the critical temperature in °K) of ~0.9 or higher.

The values given in Table 51 represent an interpretation of the data, with assumed values for N and C₀, in terms of a conventional specific rate constant and concentration of the initial reactant. Table 52 presents values obtained from the same data for the coefficients a and b in the equation

$$\log_{10} \left(\frac{1000}{\theta} \right) = a + b \left(\frac{1000}{T} \right),$$

which can be rearranged to give

Table 52. Temperature Dependence of Time of Solid Polymer Formation

Initial Material				Time in Hours to Solid Polymer Formation			Initial Charge *	
	a	b	a'	450°C	500°C	550°C	Moles/liter	g/cm ³
p-Terphenyl	18.90	-13.61	15.90	830	51	4.3	1.52-2.80	0.349-0.644
Naphthalene	19.07	-13.27	16.07	190	12.4	1.12	2.54-4.92	0.325-0.630
Phenanthrene	17.61	-11.97	14.61	87.5	7.4	0.85	1.73-3.31	0.308-0.591
Fluoranthene	17.10	-11.53	14.10	70	6.5	0.81	2.82-3.03	0.570-0.612
Quinoline	15.76	-9.93	12.76	9.4	1.21	0.201	4.75-4.78	0.613-0.617
Anthracene	19.21	-11.88	16.21	1.65	0.143	0.0167	2.02-3.25	0.360-0.580

* Ratio of mass of initial charge to total volume.

$$\log_{10} \theta = b' (1000/T) - a',$$

where $b' = -b$, $a' = a - 3$, and θ is the time (in hours) to the initiation of the transition exotherm. Calculated times to this transition stage at 450°C, 500°C, and 550°C are given in Table 52 using the experimentally determined coefficients a and b .

Anthracene is the most reactive (to thermal polymerization) of the compounds in Table 52. Acridine is more reactive than anthracene, but data are available at only one temperature.

The range in charge density is given in the last two columns as grams per cc and as moles per liter. These data represent the initial concentration of reactant only when the temperature and pressure correspond to single-phase conditions.

The rate of the exothermic reaction of transition from liquid to solid polymer accelerates with temperature as does the overall reaction. Consequently, the exotherms are much more pronounced and peak much more rapidly at the higher temperatures. In the lower range of temperatures and with a reduction in the amount of initial charge, the time of initiation of the exotherm cannot always be identified with precision. In the single experiment with 9,9'-bifluorene, the time of transition could not be located from the record. A close control of the exterior vessel wall temperature is necessary to ensure positive identification of small changes in the differential temperature (ΔT).

3.7.5.2. Kinetic Order of the Reaction

The thermal cracking of petroleum refinery streams is generally described in terms of first-order kinetics.⁽¹⁴¹⁻¹⁴³⁾ Tilicheev⁽¹¹⁸⁾ offered evidence that the thermal reactions of aromatic hydrocarbons such as naphthalene and phenanthrene followed first-order kinetics, and the initial stages (below 20 per cent conversion) of the thermal reaction of biphenyl and the terphenyls have been reported to show first-order kinetics.⁽¹³⁸⁾

Madison and Roberts⁽¹¹⁹⁾ have, however, presented convincing evidence that the thermal reaction ("pyrolysis") of an aromatic hydrocarbon such as anthracene, where condensation to higher molecular weight products is a dominant aspect of the overall reaction, follows kinetics of order higher than first.

The present work (described below) indicates that the order of the reaction is higher than one and is probably two; however, the parameter of initial concentration of reactant has not yet been varied over a sufficient range to obtain conclusive evidence.

When the compounds are subjected to thermal treatment alone, (i. e., not in admixture with a supposedly inert solvent), the initial concentration of reactant is dependent on the initial charge density (mass per total volume of reactor) and the reduced temperature, T_r . With anthracene, phenanthrene, and fluoranthene, the temperatures of the experiments (last column of Table 51) and the initial charge densities (last column of Table 52) are such that two fluid phases (vapor and liquid) are present, with the density of the liquid phase considerably greater than that of the vapor phase and with a high value for the ratio

$$m_l / m_v,$$

where m_l is the mass in the liquid phase and m_v is the mass in the vapor phase.

For these compounds and temperatures, the initial charge density can be varied considerably between a lower limit (at which the liquid phase disappears) and an upper limit (at which the vapor phase is squeezed out of existence) without appreciable effect on the concentrations in the liquid or vapor phases, although the mass ratio obviously will vary. The experiments of Madison and Roberts⁽¹¹⁹⁾ with anthracene in the vapor phase were well below the lower limit (initial charge densities of 0.0034 and 0.072 moles/liter), and the "liquid phase" (two-phase) experiment was between these limits (initial charge density of 1.7 moles/liter).

At temperatures at which anthracene is converted to a solid polymer at a rate which is not so slow as to require exorbitant times nor so fast that equilibrium temperatures cannot be established, the initial concentration can be varied by use of a solvent which is assumed to be inert at these temperatures. The data of Table 52 favor the use of p-terphenyl from the standpoint of reaction velocity at a temperature of $\sim 435^\circ\text{C}$. These are indications, however, that biphenyl and the terphenyls might act as hydrogen acceptors in this lower temperature range; thus, naphthalene was chosen as inert solvent for an initial trial of this procedure. Data on this trial are given in Table 53. The time to initiation of the transition exotherm could not be used because the internal thermowell was poorly chosen and did not extend close enough to the bottom of the liner. Furthermore, the presence of the nonreacting naphthalene decreases the

Table 53. Kinetic Order in Thermal Polymerization of Anthracene

Expt. No.	Grams Anthracene	Grams Naphthalene	Estimated Initial Concentration at 430°C Moles/liter	Time * Hours	At t, °C	Adjusted Time at 430°C Hours	θ_1	$\frac{(C_0)_1}{(C_0)_2}$
144-29	1403	-	4.45	13.34	425.0	9.87	2.24	2.58
161-31	1110	1272	1.72	17.60	434.4	22.15		

* Time in hours to a maximum in $\Delta P/\Delta \theta$

magnitude of the exotherm (higher ratio of heat-absorbing-species to heat-releasing-species). The time to a maximum in $\Delta P/\Delta \theta$, the rate of increase of pressure with time, was used. As indicated in Figures 73 and 74, this maximum (or a maximum in $\Delta G/\Delta \theta$, rate of gas released, after the control pressure is attained) is closely associated with the transition exotherm for many of the compounds studied, including anthracene. This maximum, however, cannot be located as precisely as the time of initiation of the exotherm.

The times in the two experiments were adjusted to the same temperature (430°C), using the activation energy previously found (Table 52). Concentrations were estimated by using the value for anthracene of T_B/T_0 (ratio of Kelvin temperature of the boiling point at 1 atmosphere to the Kelvin critical temperature) of 0.685 suggested by Ambrose.⁽¹⁴³⁾ This ratio leads to an estimate of 897°K (624°C) for the critical temperature of anthracene, with T_B taken as 614.6°K (341.4°C).⁽¹⁴⁴⁾ Densities of liquid anthracene for the saturated liquid state were then calculated from generalized tables,^(145,146) employing the experimental density⁽¹⁴⁴⁾ of 0.9457 g/cc at 254.5°C.

The volume of naphthalene "solvent" was calculated from Zhuravlev's experimental values for liquid density.⁽¹⁴⁷⁾ It was assumed that no volume change occurred on mixing, an assumption that is probably justified in a lower temperature range but not necessarily at the temperatures of this experiment.

From the relation given previously for second-order kinetics

$$\theta_{1/N} = \frac{N-1}{K} \left(\frac{1}{C_0} \right),$$

it follows that, for the same N,

$$\frac{\theta_2}{\theta_1} = \frac{(C_0)_1}{(C_0)_2}.$$

The last two columns in Table 53 compare these two ratios. Second-order kinetics are indicated, although the experiments should be extended over a wider range in concentration and with modifications of procedure to delineate the initiation of the exotherm.

A substantial portion of the naphthalene in the initial mixture was recovered. Carbon-14 tracer experiments would be required, however, to establish that the naphthalene was truly inert, i.e., to determine that none of the naphthalene was incorporated into the structure of the solid polymer.

The indications of second-order kinetics from the data of Table 53 are, of course, for a late stage of the thermal reaction, with an estimated N of 10 (0.9 fractional conversion of the initial reactant). The indication from the experiments of Madison and Roberts⁽¹¹⁹⁾ of kinetics of order higher than first, however, apply to the early stages of the reaction.

The kinetic order in the thermal "cracking" of aromatic hydrocarbons has been investigated^(118, 120) by distillation after varying periods of time at temperature to determine the amount of initial reactant converted to products of higher or lower boiling range. For low conversion, a high accuracy in determining the fraction converted may be required to distinguish between first-order and second-order kinetics. It is convenient to consider the fraction of initial reactant, F , which remains unconverted at time θ as

$$F = C/C_0,$$

where C is the concentration of reactant at time θ and C_0 the initial concentration (F is often measured as a mass or volume fraction). For first-order kinetics,

$$\ln F = -k\theta;$$

and, for second-order kinetics,

$$\frac{F-1}{F} = -C_0 k\theta.$$

Unless cognizance is taken of a possible change in C_0 from one experiment to another, the $C_0 k$ becomes a constant k . Since a series expansion of $\ln F$, valid for $F > 0.5$, is

$$\ln F = \frac{F-1}{F} + \frac{1}{2} \left(\frac{F-1}{F} \right)^2 + \frac{1}{3} \left(\frac{F-1}{F} \right)^3 + \dots,$$

the above two expressions differ only by the higher order terms, and this difference is small for $F > 0.5$.

3.7.5.3. Behavior of Naphthalene

The critical temperature of naphthalene (475°C) falls within the "useful" range of temperatures for investigation of the thermal polymerization reaction. The term "useful range" implies that the rate of reaction will be neither so slow as to require an experiment of several weeks duration nor so rapid that an initial temperature equilibrium cannot be established. The initial phase conditions and reactant concentrations varied considerably with charge density in the experimental work on naphthalene.

The critical constants employed for naphthalene together with the sources of the data referenced are given in Table 54.

Table 54. Critical Constants of Naphthalene

Critical Temperature		Critical Pressure		Critical Density	Critical Volume	Critical Compressibility Factor
^{°K}	^{°C}	Atm.	lbs./in. ²	g/cc	cm ³ /g mole	z _c (dimensionless)
748.3	475.2 ⁽¹⁴⁸⁾	40.6 ⁽¹⁴⁹⁾	597	0.3148 ⁽¹⁴⁷⁾	407.2	0.269

The term z_c in Table 54 is the critical compressibility factor

$$z = \frac{PV}{RT} ; \quad z_c = \frac{P_c V_c}{RT_c} ,$$

where the subscript c refers to the pressure, temperature, molar volume and compressibility factor at the critical point.

Depending upon the initial charge density, the phase conditions at temperatures below the critical temperature may be single-phase gas (vapor), two-phases (liquid and vapor) in equilibrium (saturated or orthobaric conditions), or a single-phase dense fluid.

Table 55 shows the amounts of naphthalene used, the initial helium pressure (at room temperature), and the "initial" pressure at the approximate time thermal equilibrium was established at the temperature indicated. The total available volume in the pressure vessel and in the external lines and gauges varied slightly among the experiments, depending on the liner and the thermowells used; this volume averaged 3895 cm³. The single-phase density value is the ratio of mass of charge to total available volume.

The temperature, pressure, and density are expressed in Table 55 in the form of the reduced parameters

$$T_r = T/T_0; P_r = P/P_0; d_r = d/d_0 = V_0/V,$$

with the subscript *c* signifying critical conditions, *T* the Kelvin temperature, *P* the absolute pressure, *d* the density, and *V* the molar volume.

Table 55. Reduced Parameters for the Initial Conditions of Naphthalene Polymerization

Exper. No.	Naphthalene Charge Grams	Initial He Pressure lb/in ²	"Initial" Pressure lb/in ² at t °C	Single Phase Density, g cm ⁻³	Reduced Parameters			
					Temperature T _r	Pressure P _r	Density d _r	(Corr.) ⁴⁴ Density d' _r
145-53	2360	115	1405	0.5779	0.990	2.353	1.836	1.944
145-69	2357	15	1135	0.6026	0.986	1.901	1.914	1.931
144-37	2074	15	935	0.5360	1.006	1.566	1.703	1.718
144-13	2100	15	985	0.5427	1.008	1.650	1.724	1.739
159-67	1252	15	755	0.3177	1.025	1.265	1.009	1.031
159-57	2471*	15	1935	0.6269	1.025	3.241	1.991	2.001
160-75	1440	15	1000	0.3644	1.069	1.675	1.158	1.174
162-11	2202	15	1600	0.5399	1.067	2.680	1.715	1.726

* Actual initial charge 2540 grams; 69 grams of naphthalene evolved on reaching temperature (see text).
 ** Approximately corrected for the effect of helium gas present.

The values in the last column of Table 55 for d'_r represent an attempt to correct for the helium initially present in the vessel. The values given are based on the assumption of Amagat's law of additive volumes, although neither Amagat's law nor Dalton's law can be expected to hold for the conditions of these experiments. No data could be located on which to base a more elaborate treatment of the mixture of helium and naphthalene. Unless dissolved in the liquid phase at lower temperature stages of the run, much of the helium is located in the lines and gauges external to the vessel (and at a lower temperature) and is probably not in equilibrium with the material in the vessel.

In the experiments using the larger initial amounts of naphthalene, the density exceeds that of the saturated liquid at temperatures considerably below the critical temperature. Zhuravlev's⁽²⁴⁷⁾ experimental data for the densities of the liquid and gas phases of the orthobaric (saturated) liquid in the temperature range 400° to 470°C are given in Table 56.

Thus, in Experiment 159-57, the single-phase density exceeds that of the orthobaric liquid at ~410°C. The vapor phase is, so to speak, squeezed out of existence at this relatively low temperature, an additional degree of freedom develops with the disappearance of the vapor phase, and the pressure increases with increase in temperature at a much more rapid rate than the orthobaric rate: $\left(\frac{dP}{dT}\right)_\sigma$, where the subscript σ refers

Table 56. Orthobaric Liquid and Vapor Densities of Naphthalene⁽¹⁴⁷⁾

Temperature °C	Density of Liquid g cm ⁻³	Density of Gas g cm ⁻³
400	0.6410	0.0617
420	0.5989	0.0850
440	0.5510	0.1139
460	0.4935	0.1522
470	0.4590	0.1770

to the saturated liquid-vapor system. The values of pressure observed, expressed as P_r in Table 55, are reasonably concordant with the values calculated from tables of the generalized properties of fluids.⁽¹⁴⁶⁾

The effect of initial charge density on the variation of pressure with time at temperature is illustrated in Figures 78 and 79. In Figure 78, the initial charge density was not much greater than the critical density. The pressure rose to a near-constant level then rose at an accelerating rate as the rate of fixed gas (H_2 , CH_4 , C_2H_6 , etc.) formation increased.

In Figure 79 (for Experiment 159-57) with an initial charge density of about twice the critical density, the pressure rose rapidly to the control pressure. During a period of about 1 hour, with the control valve open, 69 grams of naphthalene were evolved from the vessel. Only a small amount of gas (less than 1 liter) was evolved during this period, some of which undoubtedly was helium. The pressure then decreased to a minimum value before again rising at an accelerated rate to the control pressure.

During the period of decreasing pressure, it appears that the naphthalene is being converted into higher molecular weight compounds (higher boiling materials with higher critical temperatures). These compounds must be, in part, partially hydrogenated species. With continued time at temperature, the rate of fixed gas formation (H_2 , CH_4 , etc.) increases and the pressure again rises from a minimum value. Although it is probable that (at a given temperature and constant total volume) naphthalene in solution with these higher molecular weight compounds would exert a lower specific pressure (i.e., per gram or per mole) than in the pure state, it appears that the major reason for the decreasing pressure is the reduction in amount of naphthalene present by virtue of its conversion to these higher molecular weight compounds.

It was originally considered that the time of minimum pressure for the experiments with a high initial charge density could be considered

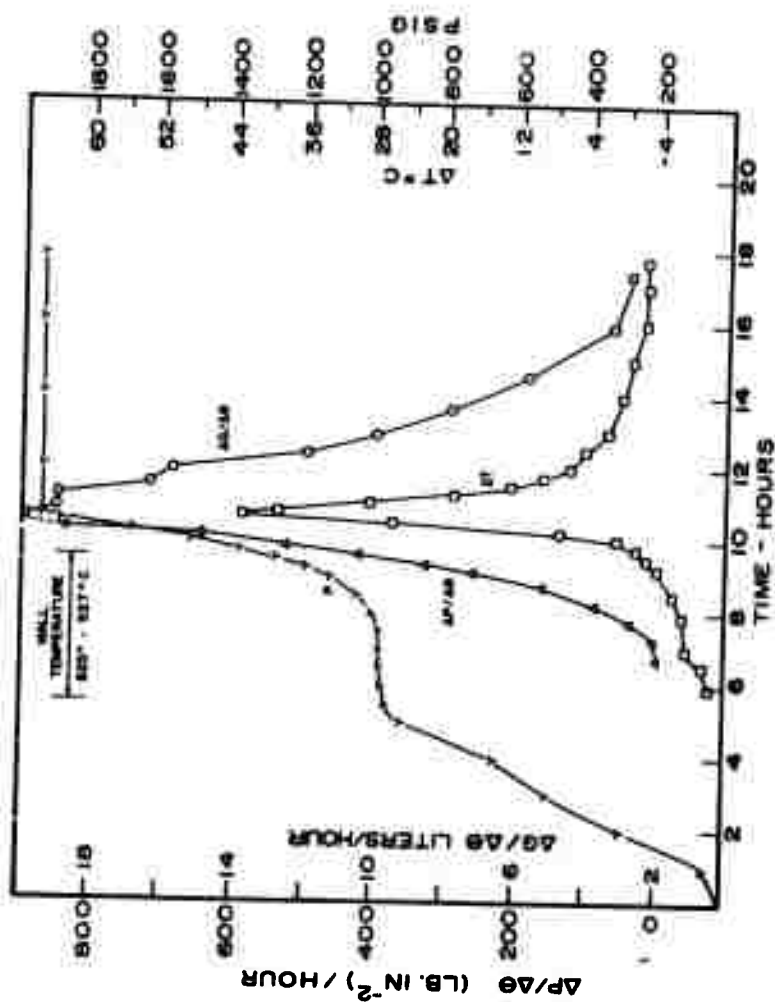


Figure 7A. Thermal Polymerization of Naphthalene - Reduced Density of 1.17 (Experiment 160-75) N-7148

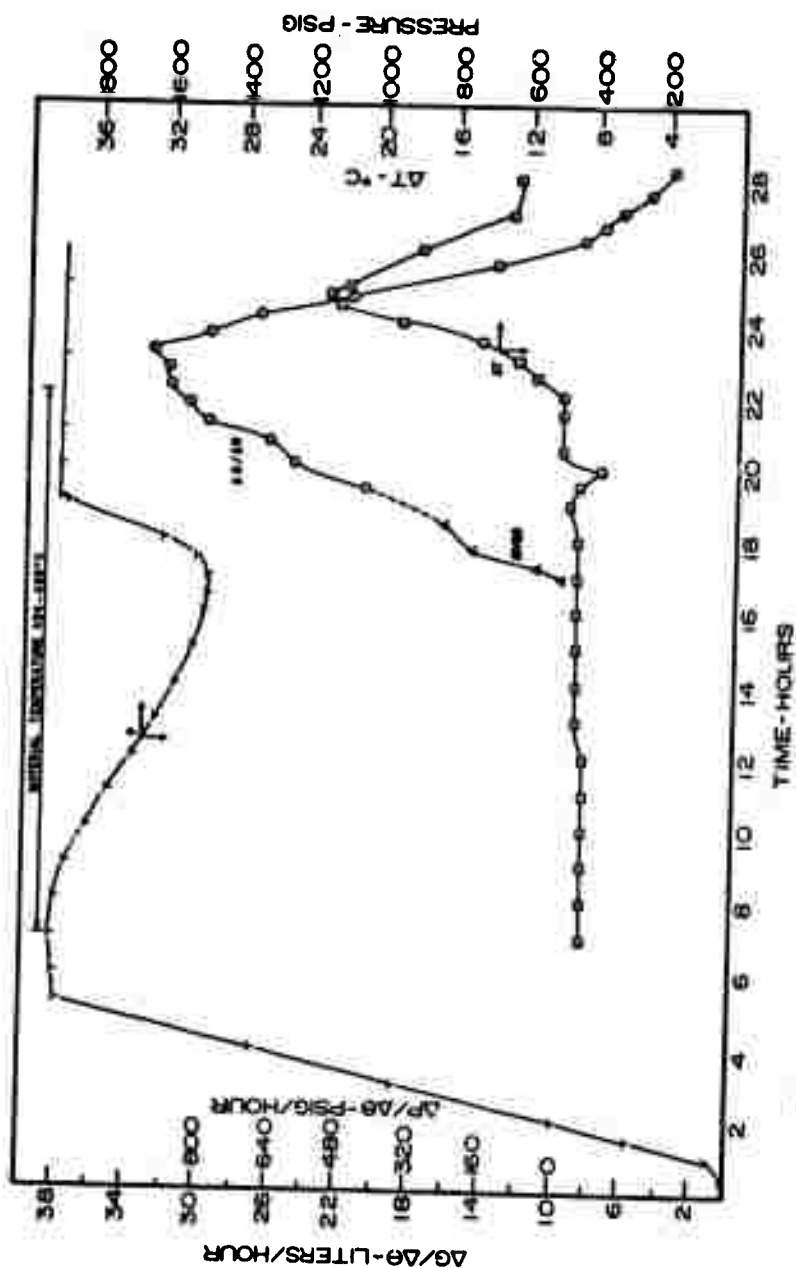


Figure 79. Thermal Polymerization of Naphthalene - Reduced Density of N-7149
2.00 (Experiment 159-57)

as a definite stage in the reaction, corresponding to a definite value of N , where $N = C_0/C_\theta$, C_0 being the initial concentration of reactant and C_θ the concentration of reactant at time θ .

Figure 80 is a plot for such times to a minimum pressure as a function of temperature, on the basis of first-order kinetics

$$\log_{10} \left(\frac{1000}{\theta} \right) = a + b \left(\frac{1000}{T} \right)$$

and Figure 81 is a similar plot on the assumption of second-order kinetics

$$\text{and } \log_{10} \left(\frac{1000}{C_0 \theta} \right) = c + d \left(\frac{1000}{T} \right).$$

The least-squares coefficients, the derived activation energies, and the standard deviations of the slope (expressed in kilocalories) are given in Table 57.

As evident from the figures and from the standard deviations in Table 57, the deviations from the assumed linear plot are considerably greater than those found for times required to carry the experiment to the point of initiation of the exotherm (Figure 75 and Table 51).

Additional analysis has indicated that:

- 1) The "time to minimum pressure" is directly applicable only to the experiments with high initial charge density. Where the initial charge density was appreciably lower (Experiments 159-67 and 160-75), this corresponding time was taken as the start of the rise in pressure from the initial flat portion. These times do not appear to represent the same stage of reaction, i. e., the same value of N . A time that does appear to represent the same stage is a maximum in $\Delta^2 P / \Delta \theta^2$. Location of this maximum, however, requires more exact control of the vessel temperature and greater detail in the pressure record than was obtained in the earlier experiments.
- 2) The initial charge density should be varied over a greater range (at constant temperature) to obtain significant information on the order of the reaction.
- 3) After partial conversion of the naphthalene and reappearance of a two-phase system, the concentration of naphthalene in this liquid phase becomes more or less independent of the original charge density. The latter is a valid indication of initial concentration only for the early stages of the reaction.

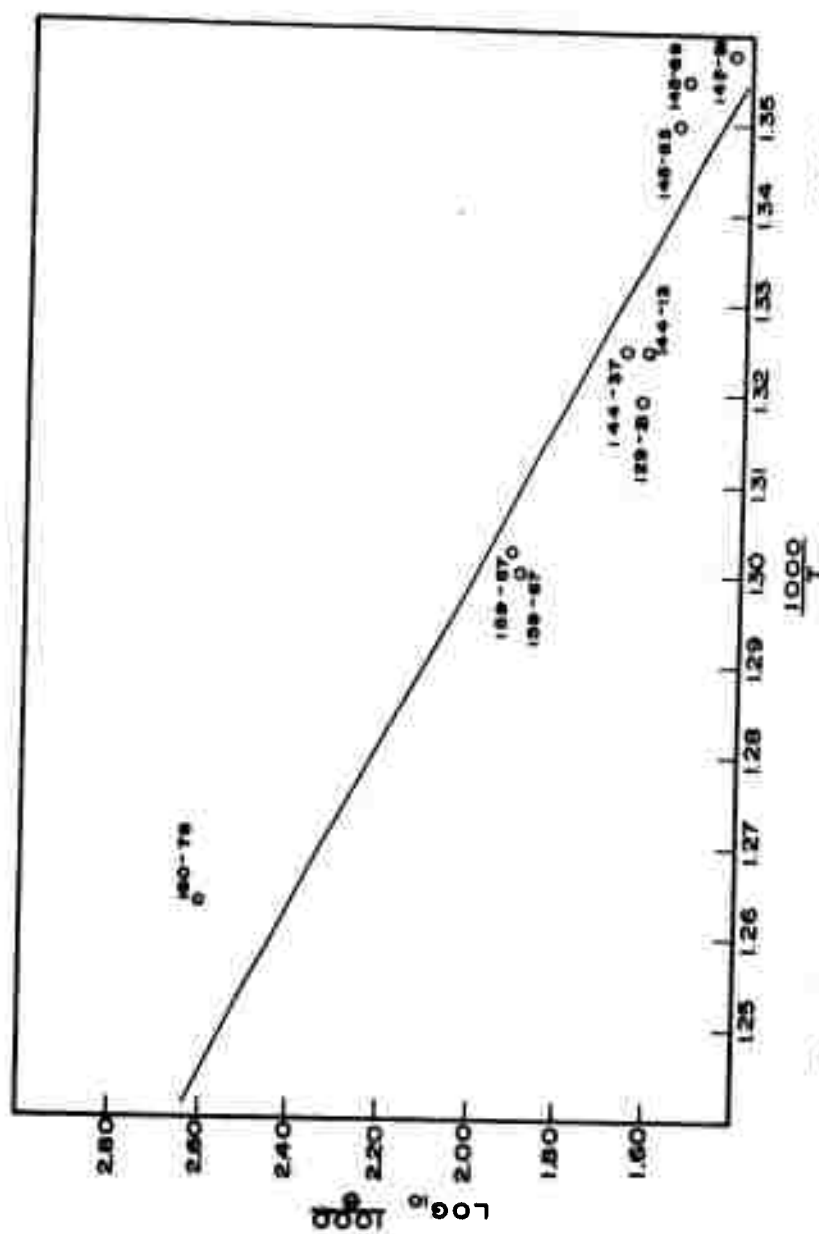


Figure 80, Arrhenius Plot - Time to Minimum Pressure for First-Order Kinetics (Naphthalene) N-7:50

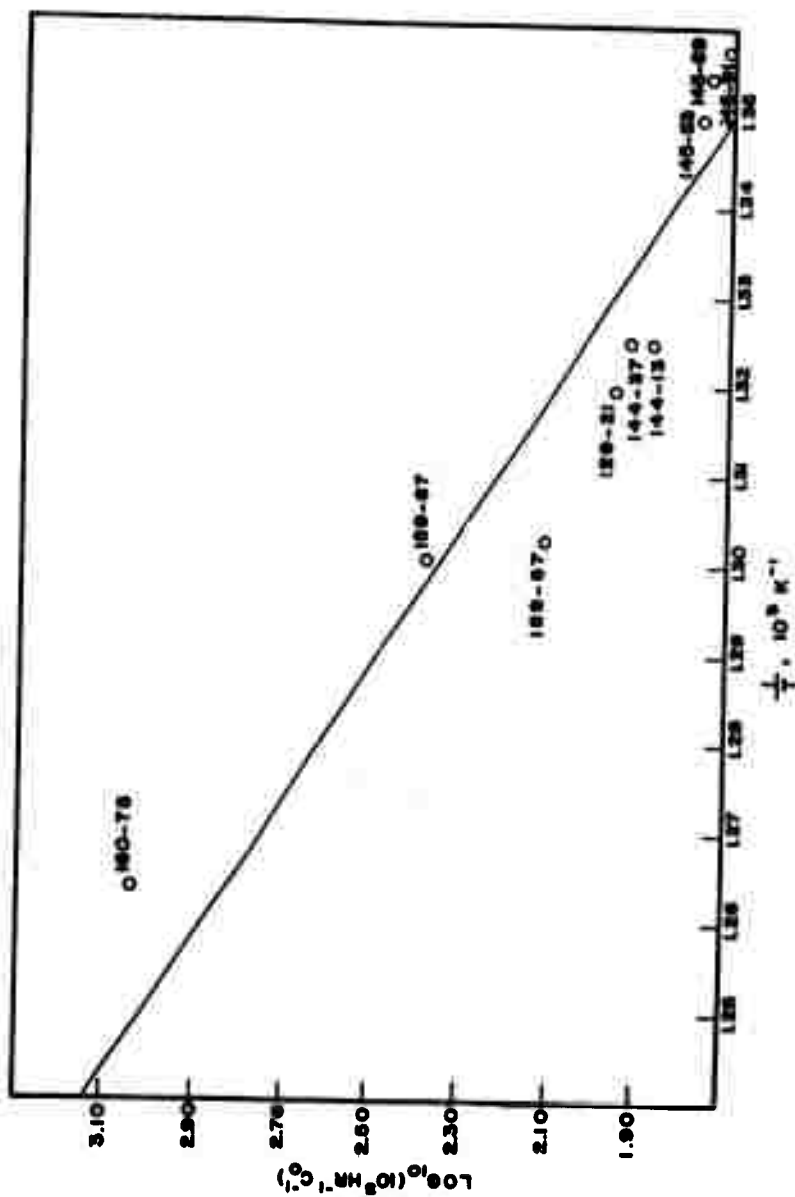


Figure 81. Arrhenius Plot - Time to Minimum Pressure for Second-Order Kinetics (Naphthalene) N-7172

Table 57. Coefficients and Statistics for Figures 80 and 81

Figure No.	a or c	b or d	E Kilocalories	σ_E kcal.
80	16.13	-10.87	49.7	7.4
81	19.32	-13.05	59.7	8.4

5.7.5.4. Additional Observations

As discussed previously, the major exotherm is closely correlated with the transition to a solid polymer. Other exothermic and endothermic phenomena have been noted, as illustrated in Figure 82 for fluoranthene. There appears to be a small exotherm followed by a slight endotherm, with the latter followed almost immediately by the major exotherm of transition. The smaller exotherm has been quite definitely observed with naphthalene, also, and appears to be correlated with a maximum in $\Delta^2 P / \Delta \theta^2$ for both compounds.

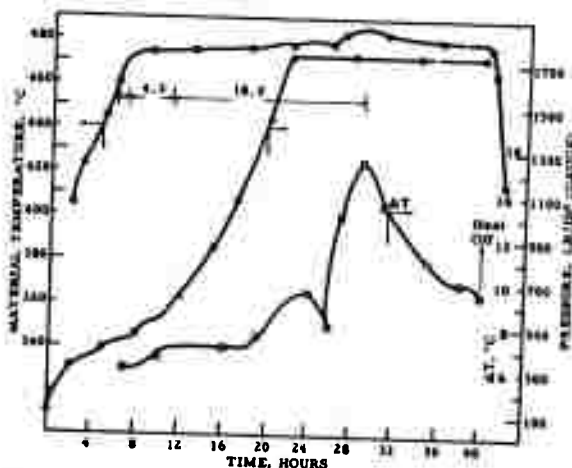


Figure 82. Time-Temperature-Pressure- ΔT Record for Polymerization of Fluoranthene (Experiment 255-145-15)

N-6726

It was considered possible that the endotherm shown in Figure 82 was an artefact resulting from reaching the control pressure and consequent loss of heat energy from the system in the form of the sensible heat of the gases discharged through the pressure control valve. That

this case does not apply for fluoranthene was shown by another experiment (145-9), which showed the same sequence of a small exotherm, a slight endotherm, and, finally, the major exotherm. As a result of a plug in the line to the pressure controller, the control valve did not open during the run and no gas was discharged.

With naphthalene, a slight decrease in material temperature has been observed as the control valve opens on reaching the control pressure. Considerable vapor (which condenses to a solid in the receiver) is evolved along with fixed gases, and the heat loss from the system is much greater than with fluoranthene; this loss more directly affects the material temperature.

3.7.6. Stoichiometry of the Reaction

Gas samples were taken at intervals during many of the experiments. Generally, samples were obtained only after the control pressure had been reached and gas was being released through the pressure control valve, or when depressurizing the vessel after the end of an experiment. During the last part of the program, partial success was obtained in taking gas samples from the system prior to reaching the control pressure.

Data are given in Table 58 on the amount and composition of gases evolved during the thermal polymerization of naphthalene. The first four rows represent experiments in which the time of reaction was in all cases short of the time of transition to a solid polymer. Control pressure was not reached and the gas samples were taken while depressurizing the vessel after cooling. The last five rows represent experiments which were carried to the stage of solid polymer formation and (except for 145-91) generally with heating continued after the exotherm, often to higher temperatures than the temperature at which solid polymer formation occurred.

In the first group (short of solid polymer formation), the percent naphthalene converted to other products was calculated from the amount of naphthalene recovered by a fractional distillation.

For the second group, the distillate (sublimate) evolved during the run (or during depressurization) was fractionally distilled to determine naphthalene content. The data in the table do not take into account naphthalene remaining in admixture with the solid polymer. This condition is appreciable only when the volatile content of the polymer is high, as for Experiments 145-69 and 159-57, as shown in the next to the last column as the weight loss on heating to 1000°C.

The data indicate that a relatively small amount of the hydrogen abstracted from the naphthalene molecules in the formation of compounds of higher molecular weight species of higher atomic C/H ratio was in the form of molecular hydrogen. The formation of CH_4 , C_2H_6 , and C_3H_8 , on the other hand, accounts for the abstraction of 1.5 to 1.9 moles of total hydrogen per mole of naphthalene converted.

Table 58. Stoichiometry in Thermal Polymerization of Naphthalene

Expt. No.	Naphthalene Converted, %	Moles Gas Per mole Naphthalene Converted	Average Analysis of Gas			Moles Molecular N ₂ per Mole Naphthalene Converted	Total Moles H ₂ in Gas per Mole Naphthalene Converted	Gram Atoms C in Gas per Mole Naphthalene Converted	Weight Loss 1000°C HT %	Pressure lb./sq. in.	Unaccounted for in Material Balance, %
			H ₂	CH ₄	C ₂ H ₆						
124-93	14.3	0.189	21.8	61.4	15.1	1.7	0.050	-	-	Plugged line ^a	0.8
161-61	34.9	0.259	21.7	52.4	18.6	2.3	0.066	0.221	-	1450 ^a	0.4
144-13	44.0	0.248	17.6	60.5	18.4	3.3	0.040	0.393	-	1155 ^a	2.5
144-53	51.6	0.283	17.6	60.5	18.4	3.3	0.040	0.393	-	1200 ^a	9.1
Solid Polymers											
145-91	87.8	0.722	12.7	71.7	13.5	2.2	0.092	1.483	8.54	1680	8.6
145-69	82	0.807	13.4	72.5	12.3	1.8	0.108	0.827	14.90	1700	7.9
159-57	76.5	0.848	14.3	64.5	18.6	2.6	0.117	0.896	16.2	1900	4.4
129-21	73.3	0.942	14.3	73.3	6.7	4.6	0.144	1.888	4.26	1600	4.7
129-9	59.8	0.951	14.4	73.3	7.4	4.8	0.137	1.925	3.76	1200	0

^a Control pressure not reached - no gas or sublimate evolution during run.

No definite evidence has yet been obtained to assess the possibility that molecular hydrogen may first be formed and at a later time, as the partial pressure of H_2 increases, react with various species present (hydrogenolysis or hydrocracking). The end result is the same as a hydrogen transfer reaction followed by thermal cracking of the hydrogenated species. The hydrogenolysis reaction should be dependent upon hydrogen partial pressure and possibly be catalytically accelerated by the metal of the pressure vessel or liner (see, however, Section 3.7.7.).

Fractional distillation of the materials formed in the first group and of the vapors evolved in the experiments of the second group indicated the formation of small amounts of compounds of lower molecular weight than naphthalene. Benzene, toluene, and xylene were definitely identified by analytical fractional redistillation and nuclear magnetic resonance spectroscopy. The amounts found were so small that it was suspected that they may have been present in the original naphthalene. Fractional distillation of 3 kg of the original naphthalene and examination of the fractions by NMR spectroscopy, however, revealed no trace of these compounds.

After removal of the unconverted naphthalene, the products from some of the experiments of the first group of Table 58 (and some of the pressure distillates of the second group) were fractionally distilled in vacuo. The compounds 2,2'-binaphthyl and perylene have been definitely identified and it is presumed that the other compounds isolated and identified by Lang, Buffleb and Kalow^(12a) are also present. In addition to such aromatic hydrocarbons, NMR spectroscopy showed that a partially hydrogenated species was present in a fraction which distilled immediately prior to the distillation of the 2,2'-binaphthyl. This compound (or mixture of compounds) has not yet been identified. It is quite sensitive to oxidation.

The gases evolved in the thermal polymerization of fluoranthene were similar both in amount and composition to those from naphthalene. The total gas evolved ranged from 0.73 to 0.88 moles per mole of initial charge for total times corresponding to a solid polymer of 4.7 to 6.7 per cent volatile content. Very little distillate is evolved when fluoranthene is polymerized at pressures in the range of 1000 to 2000 lbs./in.², and it is presumed that there is no great quantity of fluoranthene in admixture with these solid polymers. These values should thus correspond closely to moles of gas per mole of fluoranthene converted.

The composition of the gas evolved during the thermal treatment of p-terphenyl was not greatly different from that evolved from naphthalene and fluoranthene for a sample taken from the vessel after the formation of a solid polymer. We did obtain samples in one experiment at much earlier time periods as shown in Table 59. The first three samples of gas were taken from the external (pressurized) lines into a small 10 cm³ capacity pressure vessel. The last sample was of gas evolved after the control pressure had been reached. The first three samples probably represent

Table 59. Composition of Gas in Vessel at Various Times,
Experiment 160-84 (p-Terphenyl)

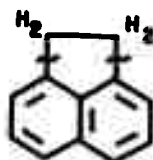
Sample	Mole Per Cent				Time in Hours after Material Temperature Reached 500°C	Remarks
	H ₂	CH ₄	C ₂ H ₆	C ₃ H ₈		
84-a	91.4	7.2	1.4	0	4	
84-b	82.7	13.3	4.0	0	6.8	
84-c	42.0	46.3	11.7	0	17.5	Before Exotherm
84-d	12.3	67.1	19.0	0	24.9	After Exotherm

the gas composition at times earlier than shown, since the total volume of the external pressurized system of lines, valves, gauges, etc. is ~105 cm³, and diffusion does not occur very rapidly in the small-diameter tubing used. The data do show that the H₂ content is higher and the CH₄ and C₂H₆ content lower in the earliest stages of thermal treatment. The compound C₃H₈ appears to form not at all or at least to a very limited extent with p-terphenyl, and little or no C₃H₈ was found in gas samples taken during thermal treatment of biphenyl and o-terphenyl.

The methylnaphthalenes showed a decidedly different gas composition. Samples taken during the earliest stages of thermal treatment show a high preponderance of CH₄. A sample taken during the thermal treatment of 1-methylnaphthalene 4 hours after reaching temperature (425°C) contained 1.9 mole per cent H₂, 94.7 mole per cent CH₄, and 3.4 mole per cent C₂H₆. The H₂ content actually increased with continued time of thermal treatment, and a sample from the vessel at the end of this experiment (solid polymer formation) contained 7.7 mole per cent H₂, 86.6 mole per cent CH₄, and 5.6 mole per cent C₂H₆.

The samples of gas taken during the thermal treatment of pyrene showed unusually high values for H₂ content. At the end of one experiment (solid polymer formation), the gas analyzed 31.8 mole per cent H₂, 55.4 mole per cent CH₄, 11.8 mole per cent C₂H₆, and 1.0 mole per cent C₃H₈. Samples taken earlier showed values as high as 50.6 per cent H₂.

A sample of gas taken at an intermediate period of the thermal treatment of acenaphthene contained 9.8 per cent H₂, 49.6 per cent CH₄, 34.5 per cent C₂H₆, and 5.5 per cent C₃H₈. The high value for C₂H₆ suggests that both of the bonds indicated in the diagram are often severed (not simultaneously) during thermal treatment (thermal dealkylation).



A considerable quantity of lower boiling compounds is formed in the thermal treatment of biphenyl. Fractional distillation of the "pressure distillate" from Experiment 159-19 using biphenyl as the initial charge showed a considerable amount of benzene and much smaller amounts of toluene and ethylbenzene. The material balance on the fractional distillation is shown in Table 60. The first three fractions were redistilled in an analytical distillation column; benzene, toluene and ethylbenzene were identified by NMR spectroscopy. The amount of benzene found (calculated from the amount of pressure distillate and the data of Table 60) indicates that 20 per cent of the molecules of biphenyl converted can be accounted for by the net reaction



The hydrogen is probably abstracted by phenyl radicals from molecules of biphenyl which then condense to higher molecular weight species.

Table 60. Composition of Pressure Distillate from Biphenyl Polymerization

	Weight Per Cent
Benzene	47.6
Toluene	1.5
Ethylbenzene	0.7
Biphenyl	30.6
Residue	17.5
Loss	2.1

3.7.6.1. Ultimate Analysis of the Solid Polymers

Analytical data on the solid polymers produced by thermal treatment of aromatic hydrocarbons or heterocyclic compounds are given in Table 61. The atomic C/H ratios for the polymers produced from a given compound will depend on the time and temperature of heat treatment after the occurrence of solid polymer formation. The last column gives the weight loss on heating the polymers to 1000°C; these data serve as a measure of the extent of after-treatment. The sulfur contents of the polymers, except for the polymer from dibenzothiophene, are quite low. The sulfur found in the polymers from the hydrogenated terphenyl mixture (Experiment 129-87) and from 9, 10-dihydroanthracene (Experiment 144-1) are believed to be a result of carry-over from preceding experiments with compounds which contained high sulfur. One of the experiments with pyrene showed 0.34 per cent sulfur in the polymer, but the other experi-

Table 64. Ultimate Analysis of Polymers

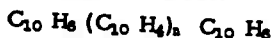
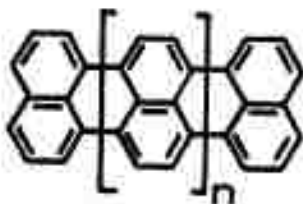
Expt. No.	Initial Material	Weight Per Cent				C/H Atomic Ratio	Highest Temp. of Thermal Treatment, °C	Weight Loss or Heating to 1000°C %
		C	H	N	O			
124-1	Fluorene	95.73	3.90	< 0.01	< 0.03	2.06	520	4.97
159-37	Dibenzofuran	93.56	3.70	< 0.01	< 0.01	2.12	530	8.84
129-93	Dibenzanthracene	72.89	2.89	15.84	< 0.03	2.12	535	6.11
159-19	Biphenyl	95.12	4.08	< 0.01	< 0.03	1.96	535	7.92
129-39	p-Terphenyl	95.65	4.10	< 0.01	< 0.01	1.96	516	8.64
129-87	Hydrogenated Terphenyls	94.68	4.18	< 0.01	< 0.01	1.90	515	8.60
129-31	9, 9'-Bifluorene	95.49	4.23	< 0.01	< 0.02	1.89	485	4.97
129-9	Naphthalene	96.13	3.21	< 0.01	< 0.02	2.51	533	3.76
129-21	Naphthalene	96.00	3.23	< 0.01	< 0.01	2.49	527	4.26
144-37	Naphthalene	96.08	3.71	< 0.01	< 0.01	2.59	480	6.27
145-69	Naphthalene	95.96	3.95	< 0.01	< 0.02	2.04	470	14.90
145-61	Anthracene	96.2	3.6	< 0.01	< 0.05	2.24	600	4.04
144-1	9, 10-Dihydroanthracene	95.73	3.45	< 0.01	< 0.63	2.33	520	4.89
144-55	Phenanthrene	95.40	4.10	< 0.01	< 0.16	2.33	525	4.68
144-21	Pyrene	95.98	3.23	< 0.34	< 0.03	2.49	520	3.55
144-71	Pyrene	96.62	2.99	< 0.01	< 0.02	2.71	520	3.66

ments showed 0.01 per cent sulfur with the same lot of pyrene; again, carry-over is believed responsible for the first result.

Appreciable O_2 contents were found for all the polymers. Except for dibenzofuran (which contains oxygen), this result may be due to slight oxidation of the polymer after removal from the pressure vessel rather than necessarily reflecting oxygen-containing impurities in the initial materials.

It will be noted that the atomic C/H ratio is greater than 2.6 only for Experiment 144-71 with pyrene. The molecular size of the polymer thus would not need to be very large for the assumption of a fully aromatic structure. Coronene (see Table 14) and periflanthene (see XXX in Section 3.3.3.5.) have an atomic C/H ratio of 2.00, and the dicoronylene prepared by Zander and Franke⁽¹⁶⁰⁾ has an atomic C/H ratio of 2.40.

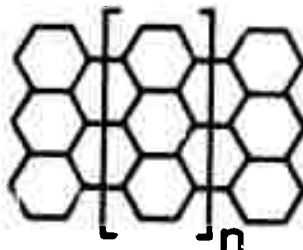
The assumption of a poly-rylene structure (the "dimer" is perylene) derived from naphthalene



would entail a limiting C/H ratio of 2.5 (n very large) and, in general, the C/H ratio would be

$$C/H = \frac{5(n+2)}{2(n+3)} = \frac{2.5 + (5/n)}{1 + (3/n)}, \quad n > 0.$$

A similar assumption of a "poly-anthene" structure (the "dimer" is bisanthene) derived from anthracene,



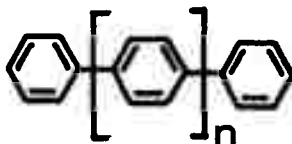
would entail a limiting C/H ratio of 3.5 and, in general,

$$\frac{C}{H} = \frac{7(n+2)}{2n+7} = \frac{3.5 + (7/n)}{1 + \frac{3.5}{n}} \quad (n > 0)$$

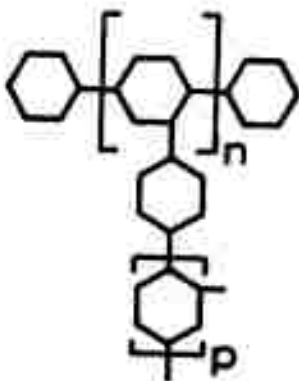
The C/H ratio for such an assumed polyanthene structure would be 2.33 for $n = 1$ (teranthene), or higher than found for the 600°C anthracene polymer.

It is quite possible that the solid polymers are not fully aromatic; that is, they may be partially hydrogenated. The gas evolved on further heating to 750°C is high in hydrogen (although still with a considerable CH₄ content) and it is possible that this result represents dehydrogenation. In any event, it appears that either the average molecular weight of the polymer is of moderate magnitude if fully aromatic, or the polymer is partially hydrogenated.

The C/H atomic ratios of 1.9 to 2.0 for the polymers from biphenyl and p-terphenyl eliminate the simple polyphenylene structure



since this compound would have a C/H ratio of 1.5 for n very large. A structure such as



would approximate the stoichiometry (C/H approaching 2.0) and would not be expected to be a "crystalline" polymer.

3.7.7. Possible Catalytic Effects

Experiments were conducted with phenanthrene to determine the magnitude of possible catalytic effects of the material used for the liner (stainless steel). Data are given in Table 62. In the second experiment, the liner was borosilicate glass, and the stainless steel thermowell was sheathed with a borosilicate glass tube so that the liquid phase was in contact only with glass.

Table 62. Comparison of Stainless Steel and Glass Liners

Expt. No.	Liner Material	Material Balance, Weight Per Cent				Time to Exotherm at		Calculated time at 500°C Hours	Spec. Resist. 10^{-6} ohm cm	CTE $\frac{1}{10^6} \text{ } ^\circ\text{C}^{-1}$
		Polymer	Distillate	Gas	Unaccounted For	Hours	°C			
161-51	Stainless Steel	84.1	5.2	7.3	3.4	6.59	505.5	8.47	9.50	1.03
161-65	Glass	85.7	5.0	7.5	1.8	7.96	495.1	6.35	8.60	0.95

No differences in yields of products or in the rate of overall reaction are evident. The adjusted times to the initiation of the transition exotherm are based on the energy of activation previously reported (Table 51) and cannot be very precise, since this energy of activation was calculated only from these two runs plus one additional run (Experiment 144-55). Samples of gas taken at corresponding times (when depressurizing after completion of thermal treatment and cooling) were very similar in composition, the H_2 content actually being somewhat higher for the experiment using the stainless steel liner. The properties of the graphite rods prepared using the polymers from the two experiments (after heat treatment at 1000°C) are quite comparable, with the higher temperature in Experiment 161-51 expected to give a higher with-grain thermal expansion for the derived graphite (see Section 3.7.4.3.).

No catalytic effects of the stainless steel liner can be discerned.

3.7.8. Mechanisms of Thermal Polymerization Under Pressure

A first attempt can be made to suggest a series of reaction steps for the thermal polymerization of naphthalene. Much more information than is presently available would be required to distinguish among the various possible mechanisms. The suggested series of steps is based on the following experimental observations:

- The overall reaction appears to be higher than first-order, and probably is second-order.
- Relatively little molecular hydrogen is formed per mole of naphthalene converted.

- c. Partially hydrogenated aromatic compounds are formed. The formation of such species has been definitely established for some aromatic hydrocarbons (Section 3.3.) and strongly indicated for naphthalene. So far, however, no particular species has been identified for naphthalene.
- d. With many compounds (including naphthalene), the transition to a solid polymer is accompanied by a high rate of formation of CH_4 , C_2H_6 , and C_3H_8 , indicating a correlation between the velocity of thermal cracking and that of the formation of solid polymer.

Additional premises stem from generally accepted principles:

- e. The CH_4 , C_2H_6 and C_3H_8 are more probably generated by the thermal cracking of partially hydrogenated species than by rupture of the carbon-carbon bonds in fully aromatic (unsubstituted) molecules.
- f. The free radicals formed from the larger fused-ring aromatic hydrocarbons are strongly stabilized by resonance. It appears useful to suggest more reactive free radical species as the "key intermediates".

An intermediate comprising a partially hydrogenated p-quinoid (or o-quinoid) free radical species has been proposed by deTar and Long for the reaction of aroyl peroxides in benzene at relatively high dilution. ^(151, 152) A similar species can be suggested for the thermal reaction of naphthalene, as shown in Figure 83.

The "steps" are numbered 1 through 6. Following in part the terminology generally applied to chain reactions, ⁽¹⁵³⁾ these steps are called:

1. Initiation
2. Rearrangement (ring fusion accompanied by hydrogen shift)
3. Propagation
4. Termination by coupling of two free radicals
5. Termination by disproportionation of two free radicals
6. Thermal cracking (carbon-carbon bond scission).

The initiation step 1 (a) is represented as bimolecular, in accord with the indications of second-order kinetics for the overall reaction. The following steps, 1 (b) and 1 (c), suggest possibilities for further reaction of the hydrogen atom generated in 1 (a). These hydrogen atoms, however, can be supposed to take part in step 6. The species labeled IV has the

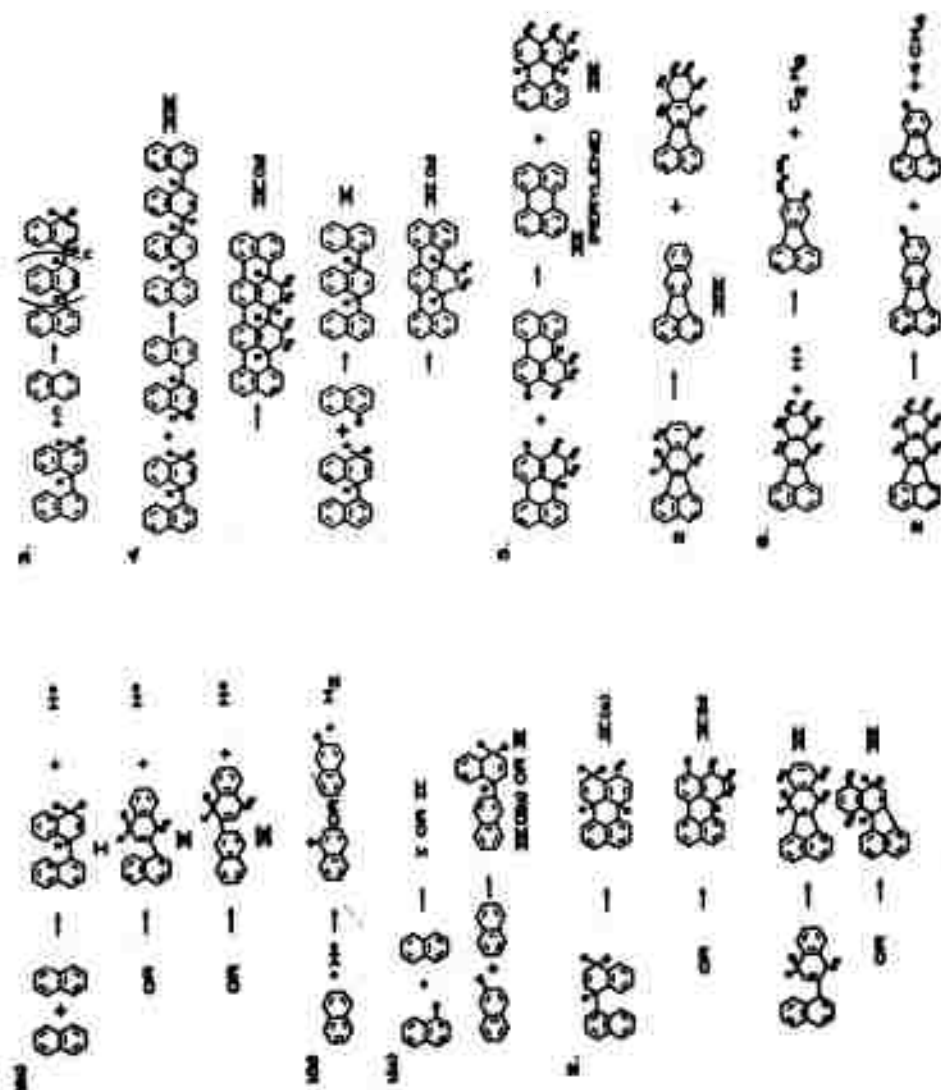


Figure 8C. Possible Mechanisms in the Thermal Polymerisation of Naphthalene
N-7185

same skeletal structure as II: both are dihydro-1, 2'-binaphthyl free radical species. The partially-hydrogenated free radical species of Step 1 have been shown as 1', 4'-dihydro structures (p-quinoid type), but 1', 2'-dihydro or 2', 3'-dihydro (o-quinoid) structures could be written. Presumably, even a 2', 6'-dihydro structure (amphi-quinoid) is a possibility.

Step 2 (a) represents further ring fusion accompanied by hydrogen shift and rearrangement of an isotetralin structure to a tetralin structure. Examples are given for the 1, 1'-binaphthyl and the 1, 2'-binaphthyl types.

Step 3 represents a propagation step. No evidence has been obtained that n is very large in the early stages of the reaction. A large n would imply the formation of a high molecular weight species (in the early stages), as in a typical free radical initiated vinyl polymerization. It is possible, however, that a variant of Step 6 could be decreasing polymer size whereas Step 3 was tending to increase the polymer size.

Again, following de Tar and Long, Step 4 represents coupling of free radicals. The compound 1', 4', 1'', 4''-tetrahydro-p-quaterphenyl (corresponding to VIII) was isolated by de Tar and Long.

Presumably, further ring fusion, accompanied by hydrogen shift, might occur in Step 4 as well as in Step 2 as indicated for IX (b) and XI (b). *

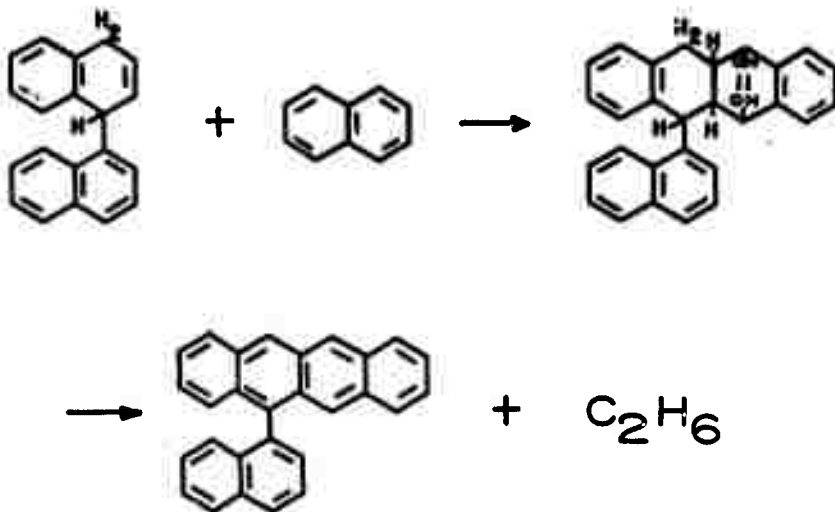
The coupling of two different radical species would form X, a 1', 4'-dihydro-1, 1', 4', 1''-ternaphthyl.

Step 5 represents a termination step by disproportionation of two radical species. The compounds XII (perylene), XIV [benzo(k)fluoranthene], and the isomeric benzo(j)fluoranthene (from the disproportionation of two radicals VII) were isolated and identified in the studies of Lang, et al.,^(120a) on the pyrolysis of naphthalene.

Step 6 represents the "thermal cracking" reaction (carbon-carbon bond scission); here, one is immediately faced with a large number of possible mechanisms, of which two are indicated in Figure 83. The first implies competition with 1 (b) for hydrogen atoms and is invoked to reduce further the necessity of molecular hydrogen formation as the concentration of hydrogenated species increases. The second represents a stoichiometric series of steps rather than a single mechanistic step, since it is highly improbable that four CH_4 molecules would be eliminated simultaneously. The thermal cracking step is assumed to represent a prolific source of additional radical species. This reasoning is in accord with the observed accelerated rate of CH_4 , C_2H_6 , and C_3H_8 (and H_2) evolution synchronous with the transition to a solid polymer.

* The designation (b) is for a tetralin structure; the isotetralin structure would be designated (a).

A possibility that could lead to the generation of a sub-structure with 4 ortho-fused rings is a Diels-Alder reaction:

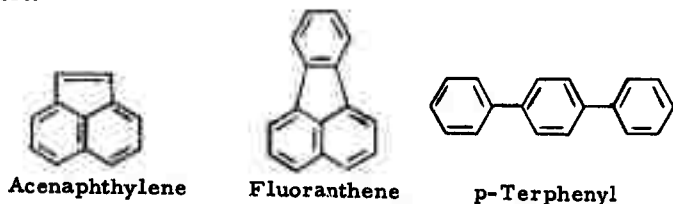


The increase in stability by elimination of the etheno bridgehead and aromatization might favor such a process. The reaction has been written for a 1,4-dihydro species resulting from the disproportionation of two free radicals. It is possible that it might occur with a radical species, the product then necessarily being a free radical. Such a reaction would serve to aromatize by the elimination of considerable hydrogen (as ethane) without reducing the total number of rings.

Each of the aromatic species created becomes a candidate for participation in the initiation steps 1 (a), 1 (b), and 1 (c). In a sense, the initial charge material (e.g., naphthalene) serves as a combination of reactant and solvent or diluent for these larger molecular weight species, which are probably more "reactive" than the initial material. Since they are generated from the initial material, the general course of the reaction is consecutive, rather than competitive, as indicated by the observations that the Arrhenius rate law is followed to a moderate degree of precision.

3.8. Preparation and Properties of Bulk Graphites from Model Aromatic Compounds

Bulk graphites (0.75-inch diameter extruded rods and 2.5-inch diameter molded plugs) were fabricated from cokes prepared from three model aromatic compounds (acenaphthylene, fluoranthene, and p-terphenyl), the pyrolyses of which were the subject of intensive physico-chemical investigations as described in Sections 3.1., 3.2., 3.3., and 3.7., of this report.



Acenaphthylene coke was prepared at atmospheric pressure by the beaker coking method.⁽¹³⁶⁾ Fluoranthene and p-terphenyl cokes were prepared at superatmospheric pressure, as described in Section 3.7. of this report. Analytical data on the 500°C raw and 1000°C calcined cokes are given in Table 63. The 1000°C calcined fluoranthene and p-terphenyl cokes were extremely hard, dense, and abrasive; as a consequence, there was a large increase in the ash contents of these cokes when they were milled to flours.

Table 63. Analytical Data on Raw and Calcined Cokes from Acenaphthylene, Fluoranthene and p-Terphenyl

Coke Derived From	Condition of Coke	% Ash	% S	Helium Density, g/cc
Acenaphthylene	500°C Raw	0.32	None	-
Acenaphthylene	1000°C Crushed	0.30	None	1.970
Acenaphthylene	1000°C Crushed	0.41	None	1.971
Fluoranthene	500°C Raw	-	-	-
Fluoranthene	1000°C Crushed	0.008	None	-
Fluoranthene	1000°C Milled	2.31	None	1.936
p-Terphenyl	500°C Raw	-	-	-
p-Terphenyl	1000°C Crushed	0.082	-	-
p-Terphenyl	1000°C Milled	1.49	None	1.83 - 2.13*

* Sample shows drift with time from lower to higher value.

Extruded rods and molded plugs were prepared from the 1000°C milled coke flours in accordance with previously established procedures.⁽¹³⁶⁾ Extrusion conditions and extruded rod properties in the green, 1000°C baked, and 3000°C graphitized states are summarized in Table 64. Both 30 medium coal tar pitch and a synthetic acenaphthylene pitch (106°C m. p.) were used as binders for the acenaphthylene coke. The use of synthetic pitch resulted in a graphite exhibiting a lower thermal expansion, higher sonic modulus of elasticity, higher strength, and higher helium density than that which was obtained by using the coal tar pitch. The presence of 2 pph iron oxide in the mix increased bulk density and strength and lowered the resistance of graphites prepared with 30 medium pitch binder. On the other hand, iron oxide had relatively little effect on graphites prepared with acenaphthylene pitch binder. Fluoranthene coke produced a strong, hard, high bulk density, high thermal expansion graphite, the helium density of which was slightly less than that of acenaphthylene graphite. The p-terphenyl coke also produced a strong, hard graphite; however, it possessed low bulk and helium densities, a high resistance, and an intermediate thermal expansion.

Molding conditions and molded plug properties in the green, 1000°C baked, and 3000°C graphitized state are summarized in Table 65. Two plugs were molded from each coke and the structure was examined in the green, baked, and graphitized states by xeroradiography. All plugs exhibited good structure. No iron oxide was used in these mixes.

The data in Table 65 indicate that acenaphthylene coke produces a soft, highly anisotropic graphite, whereas fluoranthene and p-terphenyl cokes produce hard, highly isotropic graphites which are considerably stronger than the acenaphthylene graphite. The properties of the fluoranthene graphite stem, in part, from the large amount of shrinkage between the baked and graphitized stages (~ 15 volume per cent as compared to 3 to 4 volume per cent for the acenaphthylene-coke-based plugs). The p-terphenyl-coke-based-plugs showed an 8 volume per cent shrinkage between the baked and graphitized stages, but the final density of the graphitized plug was low because of low green and baked densities. The high resistance of this material is accounted for, in part, by the low bulk density and, in part, by the high degree of disorder in the coke.

These results demonstrate that the initial molecular structure of aromatic compounds has a profound effect on the properties of cokes and bulk graphites prepared therefrom. Although the number of compounds investigated in this phase of the program was not large, the results of experimental work in Sections 3.1., 3.2., and 3.3. of this report make it clear that there is a systematic relationship between initial molecular structure and final graphite properties. This relationship becomes less certain, however, when the pyrolyses are carried out under pressure, since it has been found that the properties of cokes and graphites produced from certain polynuclear aromatic hydrocarbons can be significantly altered by manipulation of the coking conditions (see Section 3.7. of this report).

Table 64. Summary of Data on 0.75-Inch Diameter Extruded Rods Fabricated from Acenaphthylene, Fluoranthene, and p-Terphenyl Cokes

Coke	Pitch Used	Pitch Level	2 phr Fe ₂ O ₃ Added, %	Extrusion Temp., °C	Condition Pressure, lb/in ²	Rod Density, g/cc	3000 °C Graphite Properties (mp) ^a								
							CTE, 10 ⁻⁶ /°C	Sp. Resist. (30-100 °C), 10 ⁻⁴ ohm-cm	Modulus, 10 ¹⁰ lb/in ²	Tensile Strength, 10 ³ lb/in ²					
						Green	1000 °C	Density g/cc	10 ⁻⁶ /°C	10 ⁻⁴ ohm-cm	10 ¹⁰ lb/in ²	10 ³ lb/in ²	Value	Density g/cc	
Acenaphthylene	30 Mod.	33	No	110	6970-7190	1.59	1.46	1.53	8.52	0.69	1.209	1718	40 kg	24	2.186
Acenaphthylene	30 Mod.	35	Yes	110	6940-6970	1.62	1.52	1.57	8.05	0.62	1.364	2073	40 kg	38	
Acenaphthylene	30 Mod.	36	No	115	6970-7190	1.59	1.49	1.54	5.87	0.56	1.562	2382	40 kg	25	2.297
Acenaphthylene	30 Mod.	39	Yes	115	7410-7850	1.60	1.51	1.54	6.03	0.53	1.555	2356	40 kg	38	
Fluoranthene	30 Mod.	31	No	110	2830-3485	1.72	1.64	1.67	10.00	5.19	1.419	5889	5	95	2.172
p-Terphenyl ^b	30 Mod.	31	No	110	15,245-20,040	1.45	1.33	1.41	30.25	3.15	1.393	3596	5	83	1.780

^a Represents average of two determinations (both-grain direction). All measurements at room temperature.

^b 40 kg scale = 40 lb load and 1/2-inch ball. 5 kg scale = 100 lb load and 1/2-inch ball

^a Represents average of two determinations (half-grain direction). All measurements at room temperature.
 40 kg scale = 40 kg load and 1/2-inch ball. 10³ scale = 100 kg load and 1/2-inch ball.

Table 65. Summary of Data on 2.5-Inch Diameter Molded Plugs Fabricated from Acenaphthylene, Fluoranthene, and p-Terphenyl Cokes

Coke	Pitch Used	Pitch Level	Condition Pressure, lb/in ²	Temp., °C	Plug Density, g/cc	Bulk Density, g/cc	Orientation, 3000°C	CTE, 10 ⁻⁶ /°C	Sp. Resist. (30-100°C), 10 ⁻⁴ ohm-cm	Modulus, 10 ¹⁰ lb/in ²	Tensile Strength, 10 ³ lb/in ²	Bulk Density, g/cc	CTE, 10 ⁻⁶ /°C	Sp. Resist. (30-100°C), 10 ⁻⁴ ohm-cm	Modulus, 10 ¹⁰ lb/in ²	Tensile Strength, 10 ³ lb/in ²	Bulk Density, g/cc
Acenaphthylene	31	147	5	2.3	2.9	1.603	1.493	1.529	WG	1.528	8.97	1.56	476	1228	40 kg	21	2.208
Acenaphthylene	31	149	5	2.3	2.9	1.616	1.482	1.519	WG	1.531	12.87	3.03	415	1062	40 kg	24	
Fluoranthene	36	119	5	2.3	2.8	1.606	1.603	1.622	WG	1.515	8.65	1.64	445	1186	40 kg	11	2.264
Fluoranthene	36	119	5	2.3	2.8	1.606	1.603	1.622	WG	1.530	11.92	2.54	405	893	40 kg	13	
p-Terphenyl	36	119	5	2.3	2.9	1.585	1.634	1.665	WG	1.704	11.65	5.83	1.050	2561	5	84	2.160
p-Terphenyl	36	119	5	2.3	2.9	1.601	1.344	1.443	WG	1.800	11.90	6.35	1.075	2746	5	80	
p-Terphenyl	36	120	5	2.3	2.9	1.601	1.344	1.443	WG	1.827	11.01	5.93	1.155	2732	5	90	2.164
p-Terphenyl	36	120	5	2.3	2.9	1.601	1.344	1.443	WG	1.443	25.87	3.46	1.171	3321	5	80	1.777
p-Terphenyl	36	120	5	2.3	2.9	1.601	1.344	1.443	WG	1.548	27.60	3.57	1.175	2967	5	81	
p-Terphenyl	36	120	5	2.3	2.9	1.601	1.344	1.443	WG	1.435	26.04	3.41	1.101	3062	5	74	1.773
p-Terphenyl	36	120	5	2.3	2.9	1.601	1.344	1.443	WG	1.426	29.22	3.58	1.123	2670	5	67	

^a Represents average of three determinations. All measurements at room temperature.
 40 kg scale = 40 kg load and 1/2-inch ball. 10³ scale = 100 kg load and 1/2-inch ball.

4. BENCH-SCALE INVESTIGATIONS

Bench-scale effort has centered around basic investigations into the preparation of isotropic high thermal expansion graphites.

The investigations have included 1) the seeding of coker charge stocks and an asphaltic hydrocarbon with finely divided carbonaceous materials, 2) the air blowing of various charge stocks prior to coking, 3) the coking of a naturally occurring asphalt, and 4) the effects of certain processing variations during graphite manufacture.

The applications for isotropic high thermal expansion graphite are nuclear moderator graphites and substrate materials for coating with various carbides and metals for oxidation protection.

We have also attempted to produce isotropic cokes of intermediate thermal expansion levels by 1) causing coking to occur in a liquid phase thus producing regular shaped coke particles and 2) by coking selected mixtures of an asphaltic hydrocarbon and other coker charge stocks.

Chemical and physical characterization of various coker charge stocks was completed by the Carbon Products Division Research Laboratory. We did not attempt to statistically correlate this data with graphite properties since the sample population was too small.

Studies to improve binder qualities have included a) removing by extraction portions of coal tar pitches which do not contribute to binder strength and b) thermal and catalytic cracking of heavy petroleum stocks before distilling to a pitch. Statistical analyses have been performed in an attempt to correlate binder properties with flexural strength of 3-inch molded graphite plugs.

4.1. Seeding Experiments

Raw cokes are formed through a polymerization reaction in which relatively small molecules combine to form larger molecules under given conditions of time, temperature, and pressure. If the arrangement of the carbon atoms (crystallites) approaches that of a graphite lattice, the coke is said to be well ordered and exhibits a high degree of anisotropy in thermal expansion. In the seeding process, a finely divided carbonaceous material which interferes with the growth of the well-ordered crystallites, is added to the coker charge stock. The fabricated graphite billets then exhibit relatively high* and isotropic** thermal expansions.

The seeded cokes were processed either by coking in a pressure autoclave at a pressure of 50 lbs./in.² gauge, or by coking in beakers at atmospheric pressure; and then the cokes were calcined to 1000°C and

* 3 to 6 x 10⁻⁶/°C near room temperature.

** Approximately equal with- and across-grain values.

mixed with coal tar pitch. Extruded rods, $\frac{5}{8}$ inch in diameter by 6 inches in length, and molded billets, 3 inches in diameter by 3 inches in length, were formed, baked, and graphitized. Physical property measurements were made on samples obtained from the graphitized material.

4.1.1. Conducting Blacks as Seed Materials

Two carbon blacks, Cabot Vulcan XC-72R and Columbian Conductex SC have been evaluated as seed materials for atmospheric and for vacuum residuums. The blacks have a chain-like structure, similar to acetylene black, and are claimed to be higher in electrical conductivity than acetylene black.

Physical characteristics of the XC-72R black, Conducted SC black, and acetylene black are presented in Table 66.

Table 66. Physical Characteristics of Cabot Vulcan XC-72R, Columbian Conductex SC and Shawinigan Acetylene Black

Name of Black	Particle Diameter	Surface Area
	Millimicrons, Arithmetic Mean from Electron Microscope Measurements	Square Meters/Gram from Nitrogen Adsorption Measurements
Cabot Vulcan XC-72R	29	190
Columbian Conducted SC	17	200
Shawinigan Acetylene Black	50	64

Physical property data for graphitized extruded and molded billets produced from atmospheric and vacuum residuum cokes seeded with Conductex SC and Vulcan XC-72R blacks are presented in Table 67. For comparison, data for graphitized extruded and molded billets produced from cokes seeded with acetylene black are also presented.

The Conductex SC as a seed material produced a graphite with a considerably lower thermal expansion value than the graphite made with acetylene black.

The atmospheric residuum and vacuum residuum seeded with Vulcan XC-72R black produced extruded and molded graphitized billets with inconsistent electrical resistance and thermal expansion values. Upper limits for thermal expansion of the Vulcan XC-72R-seeded materials appear to be lower than those for acetylene black-seeded materials.

High strengths were measured on graphite billets produced from Vulcan XC-72R and acetylene black-seeded atmospheric residuum and vacuum residuum cokes.

Table 67. Physical Property Data for Graphitized Extruded and Molded Billets Produced from Atmospheric and Vacuum Residuum Cokes Seeded with Con-
ductex SC and Vulcan XC-72R

Code No.	Calculated Composition of Calcined Coke	Extruded 8-inch Diameter Graphitized Billet Data			Molded 3-inch Diameter Graphitized Billet Data					
		Specific Resistance		Thermal Expansion (10 ⁻⁶ /°C) W. G.	Specific Resistance		Thermal Expansion (10 ⁻⁶ /°C) W. G.			
		0-cm x 10 ⁴ W. G.	10-cm x 10 ⁴ W. G.		0-cm x 10 ⁴ W. G.	10-cm x 10 ⁴ W. G.				
A. Seeding of Atmospheric Residuum by Conductex SC Black										
T-44	86.1 wt. % Atmospheric Residuum 11.9 wt. % Conductex SC Black	11.27		3.23	12.49	12.43	3.86	2490	2170	
T-17	79.0 wt. % Atmospheric Residuum 21.0 wt. % Conductex SC Black	15.40		4.83	-	-	-	-	-	
T-16	77.0 wt. % Atmospheric Residuum 23.0 wt. % Conductex SC Black	12.97		4.08	-	-	-	-	-	
B. Seeding of Atmospheric Residuum by Vulcan XC-72R Black										
T-45	92.5 wt. % Atmospheric Residuum 7.5 wt. % Vulcan XC-72R Black	21.14		5.34	No Molded Billets Processed					
T-46	86.1 wt. % Atmospheric Residuum 10.9 wt. % Vulcan XC-72R Black	11.87		4.23	13.07	13.84	4.42	4.39	2540	1940
T-45	82.0 wt. % Atmospheric Residuum 12.9 wt. % Vulcan XC-72R Black	12.55		4.43	12.79	13.61	4.76	4.86	2990	2280
T-46	87.5 wt. % Atmospheric Residuum 12.5 wt. % Vulcan XC-72R Black	19.04		4.54	20.06	22.26	4.93	5.00	3300	2540
T-48	84.7 wt. % Atmospheric Residuum 15.3 wt. % Vulcan XC-72R Black	12.17		5.30	13.31	16.46	4.89	5.02	4020	2540
T-47	84.3 wt. % Atmospheric Residuum 15.7 wt. % Vulcan XC-72R Black	12.86		4.47	14.24	10.63	4.72	4.93	3410	2370
CR-121	84.0 wt. % Atmospheric Residuum 16.0 wt. % Vulcan XC-72R Black	21.67		5.19			5.42	5.56		
T-48	84.0 wt. % Atmospheric Residuum 16.0 wt. % Vulcan XC-72R Black	17.32		4.74	13.31	16.46	4.89	5.02	4020	2540
CR-119	77.0 wt. % Atmospheric Residuum 23.0 wt. % Vulcan XC-72R Black	20.39		5.05	20.98	29.49	5.25	5.62	3860	1690
C. Seeding of Vacuum Residuum by Vulcan XC-72R Black										
T-49	94.8 wt. % Vacuum Residuum 5.2 wt. % Vulcan XC-72R Black	9.59		3.89	12.62	13.01	4.39	4.76	2880	2400
T-50	91.3 wt. % Vacuum Residuum 6.7 wt. % Vulcan XC-72R Black	14.16		4.44	13.47	14.69	4.67	4.91	3100	2810
T-43	87.2 wt. % Vacuum Residuum 12.8 wt. % Vulcan XC-72R Black	17.36		4.80	18.06	19.86	5.22	5.33	2980	2580
T-44	83.3 wt. % Vacuum Residuum 16.7 wt. % Vulcan XC-72R Black	15.16		4.69	15.86	17.50	4.78	5.33	3250	3010
CR-117	80.1 wt. % Vacuum Residuum 19.9 wt. % Vulcan XC-72R Black	21.66		5.37	23.99	26.01	5.12	5.17	4050	2805
D. Control Data - Seeding of Vacuum Residuum and Atmospheric Residuum by Acetylene Black										
R-11	93.2 wt. % Vacuum Residuum 6.8 wt. % Acetylene Black	-		4.33	10.69	11.22	4.55	4.82	2710	2100
CR-86	95.0 wt. % Vacuum Residuum 5.0 wt. % Acetylene Black	21.10		5.47	18.73	20.28	5.50	5.43	3490	2930
CR-89	81.7 wt. % Atmospheric Residuum 18.3 wt. % Acetylene Black	20.14		5.74	20.90	21.72	5.39	5.29	2450	2970
CR-93	76.9 wt. % Atmospheric Residuum 23.1 wt. % Acetylene Black	17.30		5.16	17.99	22.37	5.20	5.18	3770	2080

For any given thermal expansion level, electrical resistance values tend to be slightly lower for graphitized billets produced from Vulcan XC-72R-seeded cokes than those for acetylene black-seeded materials. Some data inconsistencies were noted.

Vulcan XC-73R black appears to be an acceptable substitute for acetylene black when seeded cokes suitable for producing graphites up to $5.0 \times 10^{-6}/^{\circ}\text{C}$ (30-100 $^{\circ}\text{C}$) thermal expansion level are required.

4.1.2. Seeding of Gilsonite by Acetylene Black

Seeding of Gilsonite Selects, an asphaltic hydrocarbon, with a channel black has been reported previously⁽⁴⁾ to give an isotropic, high thermal expansion coke. Gilsonite Selects was dry-blended with the carbon black for this experiment.

The coking of Gilsonite materials in a delayed coker would require dispersion and dilution of the solid material in a diluent. Gilsonite VB, another form of solid Gilsonite, has been diluted in a 1:1 ratio with light catalytic cycle oil and seeded with acetylene black. This mixture (49.25 weight per cent Gilsonite VB, 49.25 weight per cent light catalytic cycle oil, 1.5 weight per cent shawinigan acetylene black) has been coked by bench-scale methods.

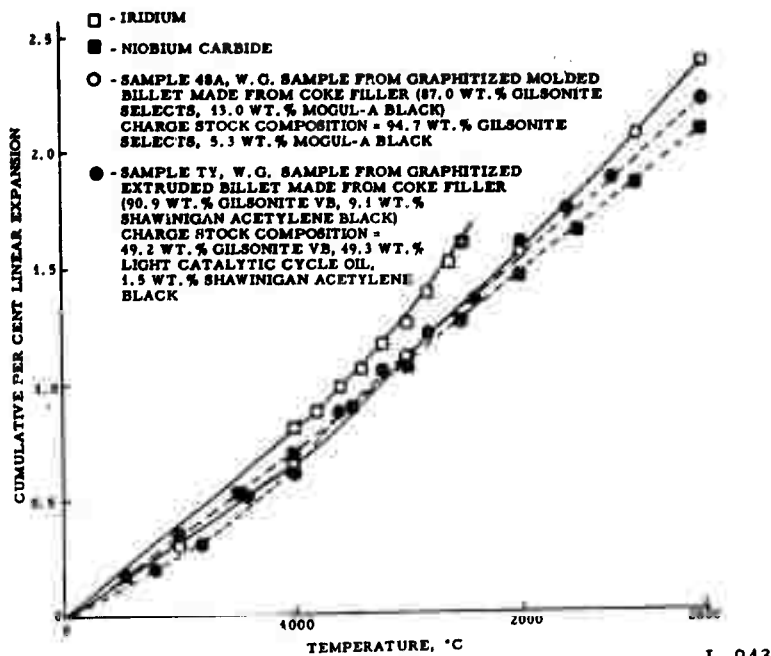
Figure 84 compares the high-temperature thermal expansion characteristics of graphitized billets produced from this material and from the undiluted seeded Gilsonite Selects with those of niobium carbide and iridium. The thermal expansion level of iridium was not attained; however, the thermal expansion of the two seeded cokes matches that of niobium carbide fairly well.

4.1.3. Lewis Acids

Ferric chloride is a Lewis acid (electron acceptor) which is known to act as a catalyst in the chlorination and subsequent polymerization of simple aromatic compounds. A mixture containing 3.1 weight per cent anhydrous ferric chloride in vacuum residuum, when coked at atmospheric pressure, yielded a coke which resulted in graphitized extruded billets having an average with-grain thermal expansion (30-100 $^{\circ}\text{C}$) of $3.97 \times 10^{-6}/^{\circ}\text{C}$.⁽⁵⁴⁾

To determine whether the thermal expansion elevation noted above is due to the catalytic action of ferric chloride or to the mechanical hindrance of orderly crystallite growth, further experiments using ferrous chloride (not a Lewis acid) and ferric chloride were made. As shown in Table 68, the effect of ferrous chloride on thermal expansion elevation is just as pronounced as the effect of anhydrous ferric chloride in the previous experiment. Raw coke yields in all cases were similar.

The results indicate that the effect on thermal expansion elevation realized by the use of small quantities of ferric chloride in vacuum



L-913

Figure 84. Cumulative Per Cent Linear Expansion Versus Temperature Relationships for Various High Thermal Expansion Materials

Table 68. Graphitized Extruded Billet Data for Vacuum Residue Coking Charge Material Containing Ferric Chloride (Lewis Acid) and Ferrous Chloride (Not a Lewis Acid)

Composition of Charge Material	Fe in Charge Material	Weight Per Cent		Average Thermal Expansion (30-100°C) 10 ⁻⁴ /°C
		Raw Coke Yield	Fe in Raw Coke	
96.9 wt. % Vac. Res. 3.1 wt. % Ferric Chloride (FeCl ₃)	1.07	24.51	4.37	3.97
95.2 wt. % Vac. Res. 4.8 wt. % Ferric Chloride (FeCl ₃)	1.64	25.10	6.53	2.57
95.2 wt. % Vac. Res. 4.8 wt. % Ferrous Chloride (FeCl ₂)	1.13 2.18	24.70	4.58 8.83	3.89

residuum is merely mechanical; possible catalytic effects of this Lewis acid are not primarily responsible for the thermal expansion elevation.

4.1.4. Investigation of Methods for Dispersing Acetylene Black in Coking Charge Stocks

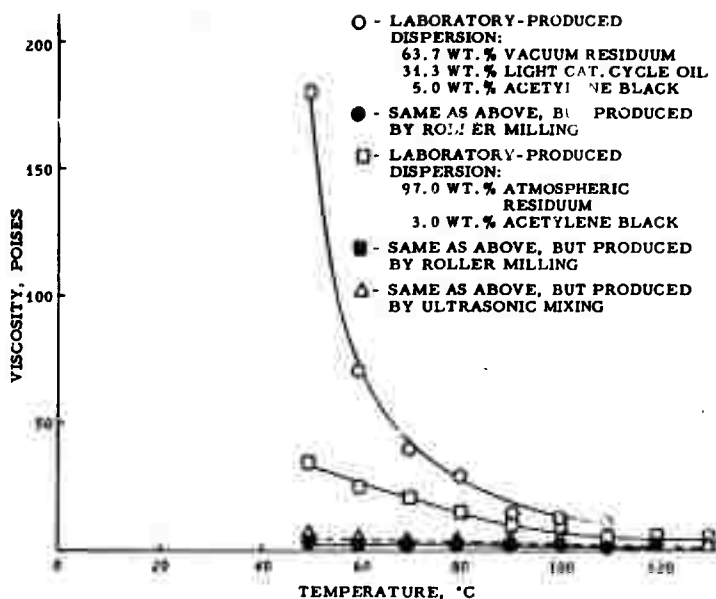
Prior work⁽⁴⁾ with high thermal expansion cokes has indicated that graphitized molded billets processed from an atmospheric residuum or vacuum residuum coke containing 12 to 23 weight per cent acetylene black in the calcined coke exhibited fairly isotropic with- and across-grain thermal expansion values as high as $5.8 \times 10^{-6}/^{\circ}\text{C}$ (30-100°C. These results prompted the consideration of acetylene black-seeded atmospheric residuum or diluted vacuum residuum as charge materials for initial pilot coker trials to produce a high thermal expansion coke.

For continuous operation in the experimental coker, a uniform agglomerate free dispersion is required. To minimize pumping difficulties and to prevent excessively high furnace pressures, a dispersion having viscosity characteristics similar to vacuum residuum is desired. Compared to channel or gas furnace blacks, acetylene black is very difficult to disperse in coking charge stocks. Lumpy, high-viscosity dispersions had resulted with vacuum residuum even at low black concentrations. Diluting agents, such as light catalytic cycle oil, were required to reduce dispersion viscosities.

Samples of atmospheric and vacuum residuum were submitted for dispersion trials to several commercial dispersion manufacturing companies, which use roller milling methods to disperse pigments in liquid carriers. Dispersions produced by roller milling techniques were of very high quality (free of agglomerates). Several additional types of intensive mixing equipment were also investigated. Dispersions produced using an ultrasonic mixer (Sonic Engineering Corporation, Norwalk, Connecticut) were of a similar quality. The ultrasonic system could be installed directly in the line at the refinery and was more convenient. As shown in Figure 85, the viscosities of dispersion samples made by ultrasonic mixing or roller milling are considerably lower than those processed in this laboratory by less intensive mixing methods (propeller-type mixer). An ultrasonic mixing unit was rented for use at Robinson, Illinois, to produce the required dispersion.

4.1.5. Effects of Diluents and High-Pressure Coking

Although dispersions of acetylene black in atmospheric residuum were chosen for initial pilot coker trials, vacuum residuum-acetylene black dispersions, cut with a diluting agent such as light catalytic cycle oil, would be a possible commercial adaptation. In commercial coking operations, the use of elevated coking pressure is desirable to increase the coke yield. Experiments were performed in the laboratory autoclave to determine the effects of diluting agents and high coking pressure on the characteristics of coke produced from vacuum residuum-acetylene black dispersions.



L-919

Figure 85. Viscosity Versus Temperature Relationships for Dispersions of Acetylene Black in Residual Feedstocks

Table 69 presents the physical property data for graphites produced from these cokes. No significant physical property differences are indicated. The 500 lbs./in.² run gave the expected increased yield but did not noticeably decrease the thermal expansion of the graphite.

4.2. Air Blowing of Coker Charge Stocks

The air-blowing process consists of controlling air flow into petroleum residues for determined periods of time and temperature until a desired gel, semisol or sol-asphalt is produced. The mechanism consists of dehydrogenation and condensation of unsaturated linkages. The rate of change is determined by the oil, resin, asphaltene and free carbon content. Highly-disordered cokes result from thermal decomposition of the asphalts.

4.2.1. Laboratory Air-Blowing Experiments

A modified laboratory pitch still was used for air-blowing experiments. A flowmeter in the air supply line provided metering of the air. The air was directed into the kettle and up through the mixer blades to provide good contact between the air and the charge stock. A paramagnetic-

Table 69. Physical Property Data for Graphitized Extruded and Molded Billets Processed From Seeded Cokes, Effect of Diluent and Coking Pressure

Composition of Charge Stock	Coking Pressure lbs./in. ² g	Raw Coke Yield w/o	Acetylene Black in Calcined Coke w/o	Extruded $\frac{1}{2}$ -Inch Diameter Graphitized			Molded 3-Inch Diameter Graphitized		
				Specific Resistance Ω -cm $\times 10^{-4}$ W. G.	Billet Data Specific Resistance Ω -cm $\times 10^{-4}$ W. G.	Thermal Expansion (30-100°C), $10^{-7}/^{\circ}\text{C}$ W. G.	Specific Resistance Ω -cm $\times 10^{-4}$ W. G.	Billet Data Specific Resistance Ω -cm $\times 10^{-4}$ W. G.	Thermal Expansion (30-100°C), $10^{-7}/^{\circ}\text{C}$ W. G.
94.70 wt. % Vacuum Residuum 5.30 wt. % Acetylene Black	50	30.2	18.6	18.21		5.38	17.52	18.00	5.02
63.27 wt. % Vacuum Residuum 3.56 wt. % Acetylene Black	50	21.3	17.1	18.43		5.48	15.22	20.57	5.10
33.17 wt. % Light Cat. Cycle Oil									
54.66 wt. % Vacuum Residuum 3.07 wt. % Acetylene Black	50	19.0	17.1	16.07		5.29	16.15	17.45	5.04
42.27 wt. % Light Cat. Cycle Oil									
63.27 wt. % Vacuum Residuum 3.56 wt. % Acetylene Black	500	25.8	12.7	19.30		5.48	17.40	18.00	5.22
33.17 wt. % Light Cat. Cycle Oil									

type oxygen analyzer continuously monitored the product gas and provided a guide to the degree of reaction. Whenever severe exothermic reactions occurred during the air-blowing process, cooling water was circulated around the kettle, and nitrogen replaced the air flow. At the end of the run, the system was flushed with nitrogen, cooled to about the lowest temperature at which the product would still flow and the material was drained into a receiving drum. The residuum that had been air blown previously was of an intermediate-type (a mid-continent crude source).⁽⁴⁾ A naphthenic-type residuum (Michigan crude source) and a paraffinic-type residuum (Pennsylvania crude source) were air blown and evaluated on bench-scale. The charge properties, the blowing conditions and the blown product properties for the naphthenic and paraffinic materials are listed in Tables 70 and 71.

Graphitized extruded billets ($\frac{5}{8}$ -inch in diameter by 6 inches in length) were produced from the different air-blowing experiments and tested for specific resistance and thermal expansion properties. These properties for graphites produced from naphthenic and paraffinic stocks are reported in Tables 72 and 73. The graphite thermal expansions obtained for paraffinic-, naphthenic- and intermediate-types of source stock were plotted against the asphaltene content of the source stock (n-pentane insoluble) in Figure 86. The room-temperature with-grain thermal expansion (extruded billets) upper limits were about 5.5 , 4.8 , and $5.5 \times 10^{-6}/^{\circ}\text{C}$ (30 - 100°C), respectively, for the paraffinic-, naphthenic-, and intermediate-type stocks. A with-grain thermal expansion of about $5.0 \times 10^{-6}/^{\circ}\text{C}$ (30 - 100°C) was obtained at a relatively low asphaltene content in the paraffinic stock. The intermediate and naphthenic stocks did not crest until a 50 per cent asphaltene content was achieved.

Data for graphitized molded billets (3 inches in diameter), produced from naphthenic and paraffinic stocks, are summarized in Tables 74 and 75. An approach to isotropic graphite thermal expansion values can be seen for the different air-blown charge stocks. Specific resistance remains low while flexural strengths increase as air-blowing severity increases. Bench-scale air blowing of the intermediate-type residuum was carried out by the Witco Chemical Company, the Trumbull Asphalt Company and the Advanced Materials Laboratory. A production-scale run was made by the Trumbull Asphalt Company. The asphalts were coked at atmospheric pressure, calcined and processed into extruded billets. Properties of these asphalts and thermal expansion values for the graphitized extruded billets appear in Table 76. The thermal expansion variation is considered small.

4.2.2. Diluent Effects

When charged to the experimental delayed coker, a high-melting point ($>150^{\circ}\text{C}$) asphalt must be preheated or diluted to reach sufficient fluidity for processing. Since the present experimental coker design would not permit the preheating of asphalts to 300°C (a viscosity of 100 poises), various diluents were investigated. The diluents with distillation results are listed in Table 77.

Table 70. Operating Conditions and Properties for the Paraffinic-Type Residuum Charge and Various Air-Blown Paraffinic-Type Residuum Samples

Run No.	Charge	PS-125	PS-126	PS-127	PS-129
Operating Conditions					
Air-Blowing Temperature, °C		252	300	340	380
Air-Blowing Hold Time, Hrs.		4.5	4.5	4.5	4.5
Asphalt Yield, Wt. %		93.2	76.2	42.4	14.0
Asphalt Properties					
Asphaltene, Wt. %	0.5	1.0	4.8	6.3	42.5
Quinoline Insoluble, Wt. %	Trace	Trace	Trace	Trace	2.9
Benzene Insoluble, Wt. %	Trace	Trace	Trace	Trace	6.3
Conradson Carbon, Wt. %	1.56	5.95	11.98	14.59	28.6
Carbon, Wt. %	85.80	84.55	84.30	85.10	87.00
Hydrogen, Wt. %	13.22	12.77	11.14	11.23	9.89
Ash, Wt. %	0.04	0.04	0.06	0.08	0.16
Melting Point, °C	-	-	66	-	158
Density, g/cc	0.89	0.91	.90	.96	1.00

Table 71. Operating Conditions and Properties for the Naphthenic Residuum Charge and Air-Blown Naphthenic-Type Residuum Samples

Run No.	Charge	PS-112	PS-113	PS-114	PS-123	PS-124
Operating Conditions						
Air-Blowing Temperature, °C		280	295	300	335	360
Air-Blowing Hold Time, Hrs.		4	3.5	5	4.5	4
Asphalt Yield, Wt. %		87.2	94.4	*	80.3	56.0
Asphalt Properties						
Asphaltene, Wt. %	4.9	32.6	28.1	38.0	42.3	44.3
Quinoline Insoluble, Wt. %	Trace	0.4	0.5	0.5	0.2	2.7
Benzene Insoluble, Wt. %	Trace	2.2	0.9	1.4	1.7	2.9
Conradson Carbon, Wt. %	7.7	20.6	18.4	20.1	23.6	28.9
Carbon, Wt. %	84.10	83.36	82.25	85.5	85.64	87.00
Hydrogen, Wt. %	10.28	10.47	10.51	10.17	10.31	8.94
Ash, Wt. %	0	0.01	0.08	0	0.03	0.05
Sulfur, Wt. %	0.19	0.36	0.39	0.33	-	-
Melting Point, °C	15	97	103	130	172	202
Density, g/cc	0.94	1.00	0.99	1.00	1.02	0.99
*Spillage of product occurred.						

Table 72. Graphite Properties for Extruded Billets Produced from Non Air-Blown and Air-Blown Paraffinic-Type Residuum

<u>Sample No.</u>	<u>Charge</u>	<u>PS-125</u>	<u>PS-126</u>	<u>PS-127</u>	<u>PS-129</u>
Billet Bulk Density, g/cc					
Green	1.70	1.71	1.66	1.70	1.70
Bake	1.53	1.55	1.46	1.60	1.58
Graphite	1.61	1.72	1.65	1.77	1.79
N	5	5	6	6	6
Specific Resistance, $10^{-4}\Omega\text{-cm}$					
Maximum	13.00	9.39	17.96	13.14	13.19
Minimum	10.43	8.16	15.81	9.81	11.36
Average	11.85	8.82	16.78	12.09	12.47
N	5	5	6	6	6
Thermal Expansion, $10^{-6}/^{\circ}\text{C}$ (30-100°C)					
Maximum	2.89	3.74		5.18	5.71
Minimum	2.60	3.38	4.85	4.82	5.35
Average	2.74	3.51	5.05	5.0	4.47
N	5	5	6	6	6

Table 73. Graphite Properties for Extruded Billets Produced from Non Air-Blown and Air-Blown Naphthenic-Type Residuum

<u>Sample No.</u>	<u>Charge</u>	<u>PS-112</u>	<u>PS-113</u>	<u>PS-114</u>	<u>PS-123</u>	<u>PS-124</u>
Billet Bulk Density, g/cc						
Green	1.64	1.69	1.70	1.67	1.67	1.69
Bake	1.53	1.52	1.52	1.48	1.46	1.59
Graphite	1.61	1.68	1.68	1.62	1.57	1.75
N	6	6	6	6	5	6
Specific Resistance, $10^{-4}\Omega\text{-cm}$						
Maximum	7.76	9.33	9.76	10.97	12.81	8.80
Minimum	6.10	8.25	8.80	10.07	11.37	7.77
Average	7.18	8.77	9.45	10.71	12.06	8.49
N	6	6	6	6	5	6
Thermal Expansion, $10^{-6}/^{\circ}\text{C}$ (30-100°C)						
Maximum	0.97	3.87	4.26	4.46	4.76	4.58
Minimum	0.60	3.55	4.02	4.17	4.64	4.14
Average	0.73	3.68	4.09	4.25	4.72	4.44
N	6	6	6	6	5	6

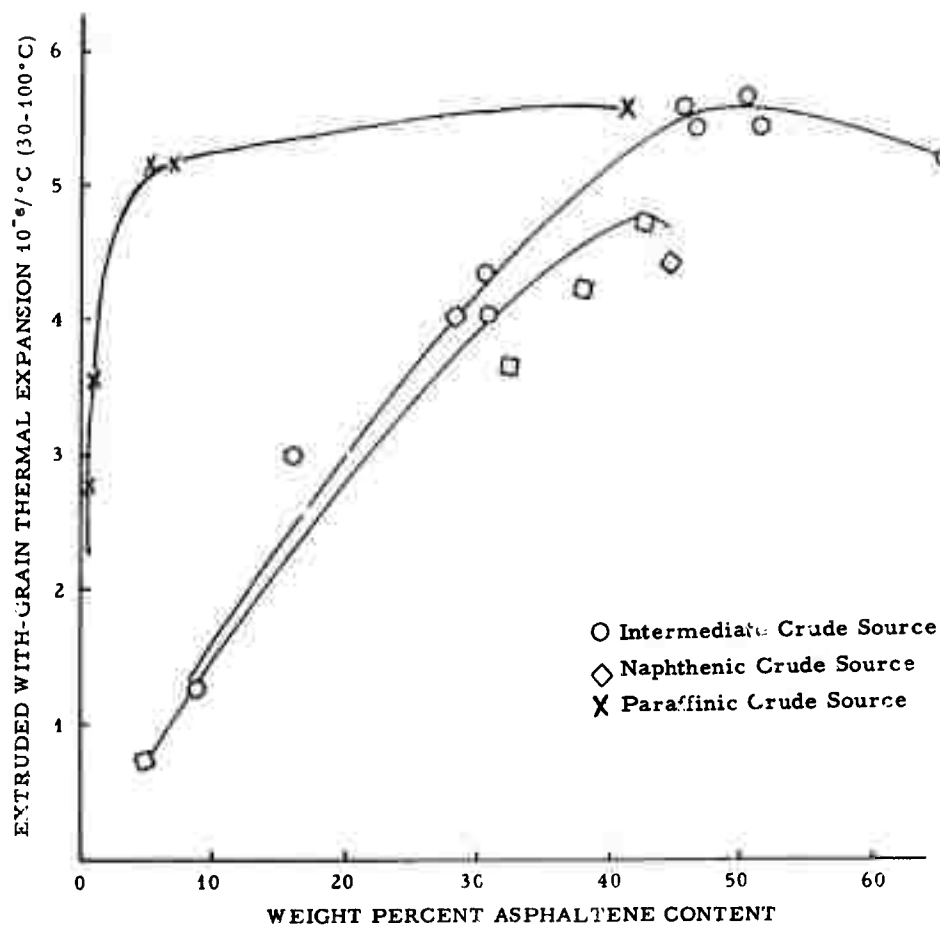


Figure 86. Thermal Expansion (30-100°C) of Extruded Graphite Articles as a Function of Asphaltene Content of the Charge Stocks

Table 74. Graphite Properties for Molded Billets Produced from Non Air-Blown and Air-Blown Naphthenic-Type Residuum

Sample No.	Charge	PS-112		PS-113		PS-114		PS-123		PS-124	
Billet Bulk Density, g/cc											
Green	1.63	1.66	1.66	1.66	1.63	1.61	1.61	1.61	1.62	1.62	1.62
Bake	1.54	1.55	1.53	1.53	1.52	1.49	1.49	1.53	1.53	1.53	1.53
Graphite	1.55	1.72	1.65	1.65	1.66	1.60	1.60	1.60	1.71	1.71	1.71
N	1	2	2	2	2	2	2	2	2	2	2
Specific Resistance, 10 ⁻⁴ Ω-cm											
Maximum	9.60	14.39	10.52	13.57	12.89	11.25	13.32	11.38	13.08	13.74	13.41
Minimum	8.33	10.79	8.16	10.66	10.19	11.89	8.91	7.26	7.55	9.39	11.33
Average	8.90	12.29	9.62	11.54	12.41	10.19	11.25	10.11	11.81	12.24	12.05
N	5	7	6	5	6	6	8	6	7	3	3
Thermal Expansion, 10 ⁻³ /°C (30-100°C)											
Maximum	1.66	2.67	5.29	4.89	4.69	4.69	5.16	5.16	5.29	-	-
Minimum	1.53	2.40	3.95	4.36	4.56	4.69	5.16	5.02	5.09	-	-
Average	1.56	2.55	4.51	4.67	4.63	4.79	5.16	5.09	5.21	5.89	5.96
N	4	4	4	2	2	2	2	4	4	1	1
Young's Modulus, 10 ⁸ lbs./in. ²											
Maximum	0.76	0.43	1.02	0.91	0.91	1.07	0.96	1.01	0.91	1.17	1.11
Minimum	0.52	0.32	0.95	0.75	0.77	0.93	0.78	0.86	0.84	0.91	1.00
Average	0.64	0.41	0.99	0.84	0.97	0.99	0.86	0.91	0.87	1.08	1.04
N	5	6	6	5	6	6	7	6	7	3	3
Flexural Strength, lbs./in. ²											
Maximum	1330	1010	2850	2100	2570	2790	2390	2970	2440	3285	2520
Minimum	1420	620	2260	1570	2330	2410	1810	2100	1770	2795	2060
Average	1220	820	2580	1910	2410	2400	2020	2410	2160	3000	2310
N	4	7	6	7	5	6	8	6	7	3	3

Table 75. Graphite Properties for Molded Billets Produced from Non Air-Blown and Air-Blown Paraffinic-Type Residuum

Sample No.	Charge*	PS-125		PS-126		PS-127		PS-129	
Billet Bulk Density, g/cc									
Green	1.54								
Bake	1.54								
Graphite	1.56								
N	2	1.62	1.56	1.56	1.67	1.66			
		1.52	1.39	1.55	1.55	1.53			
		1.68	1.56	1.70	1.70	1.73			
	1								
Specific Resistance, 10 ⁻⁴ Ω-cm									
Maximum	15.73	18.17	9.19	10.78	13.94	17.24	18.69	17.37	
Minimum	12.47	15.51	9.11	10.66	17.67	16.38	12.37	11.16	12.21
Average	13.99	16.91	9.15	10.72	18.89	13.16	14.82	14.67	14.40
N	3	4	2	2	3	2	4	4	7
Thermal Expansion, 10 ⁻⁶ /°C (10 ⁻⁶ /100° F)									
Maximum	2.96	3.69	4.33	4.73	5.22	5.56	5.76	6.16	6.29
Minimum	2.56	3.09	4.06	4.53	4.69	5.29	5.56	5.49	5.89
Average	2.76	3.41	4.20	4.63	4.96	5.12	5.43	5.83	6.01
N	4	4	2	2	2	2	2	4	4
Young's Modulus, 10 ⁴ lbs./in. ²									
Maximum	0.69	0.44	0.92	0.90	1.11	1.04	1.23	1.10	1.30
Minimum	0.63	0.39	0.91	0.81	1.00	0.86	1.21	0.94	1.24
Average	0.65	0.42	0.91	0.86	1.06	0.95	1.22	1.04	1.24
N	3	3	2	2	3	4	2	4	7
Flexural Strength, lbs./in. ²									
Maximum	4400	800	2430	1890	3270	2990	3590	2920	4050
Minimum	4020	760	2230	1830	3050	2430	3310	2410	3660
Average	1060	770	2330	1860	3130	2730	3450	2700	3860
N	3	3	2	2	3	4	2	3	4

* Coked at 50 psig while all other materials were coked at atmospheric pressure

Table 76. Evaluation of Air-Blown Vacuum Residuum

Air Blowing Operators	Penetration 100 g, 5 Sec. (ASTM D-5)		Melting Point, °C (Cube in Air)	Asphaltenes % (n-Pentane Insoluble)	Average Graphite With Grain Thermal Expansion (30-100°C) 10 ⁻⁶ °C
	77°F	150°F			
Advanced Materials Laboratory	9.0	28.7	168	46.1	5.45
Witco Chemical Company	7.3	35.7	157	48.8	5.77
Trumbull Asphalt Company	7.8	28.7	173	46.2	5.75
Trumbull Asphalt Company (Production Run)	9.0	39.0	164	42.6	5.57

Table 77. Atmospheric Distillation Results (ASTM D-158) for Asphalt Diluents

	Kerosene	Diesel Oil	Light Catalytic Cycle Oil
Initial Boiling Point, °F	372	390	422
10 wt. Per Cent Distilled, °F	396	470	480
50 wt. Per Cent Distilled, °F	432	530	522
90 wt. Per Cent Distilled, °F	480	586	578
End Point, °F	538	628	614

Each of the diluents was combined with an air-blown vacuum residuum asphalt for viscosity evaluation. Figures 87, 88, and 89 present the viscosity as a function of temperature at different concentrations of the asphalt A-117 (air-blown intermediate-type residuum).

Each diluent was combined with A-117 asphalt in a 50:50 weight ratio and batch coked. The coke was used to form $\frac{5}{8}$ -inch diameter extruded rods which were baked and graphitized. Thermal expansion values for the graphitized billets are presented in Table 78. The addition of diluent results in a slight decrease in thermal expansion with little differences seen among the diluents.

4.2.3. Commercial Air-Blown Asphalts

Several commercial air-blown asphalts were evaluated as sources for high thermal expansion graphite. The code number and

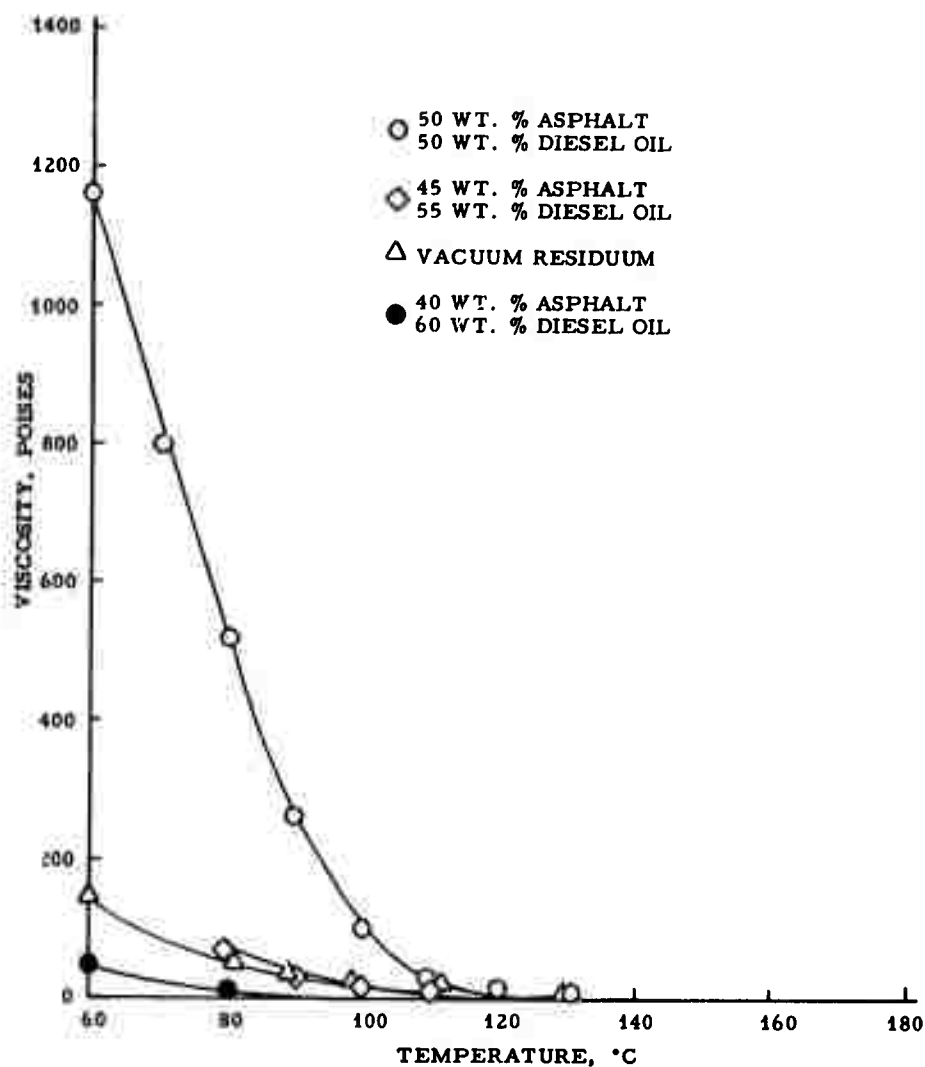


Figure 87. Viscosities of Diesel Oil Diluted Asphalt as Compared to Vacuum Residuum L-914

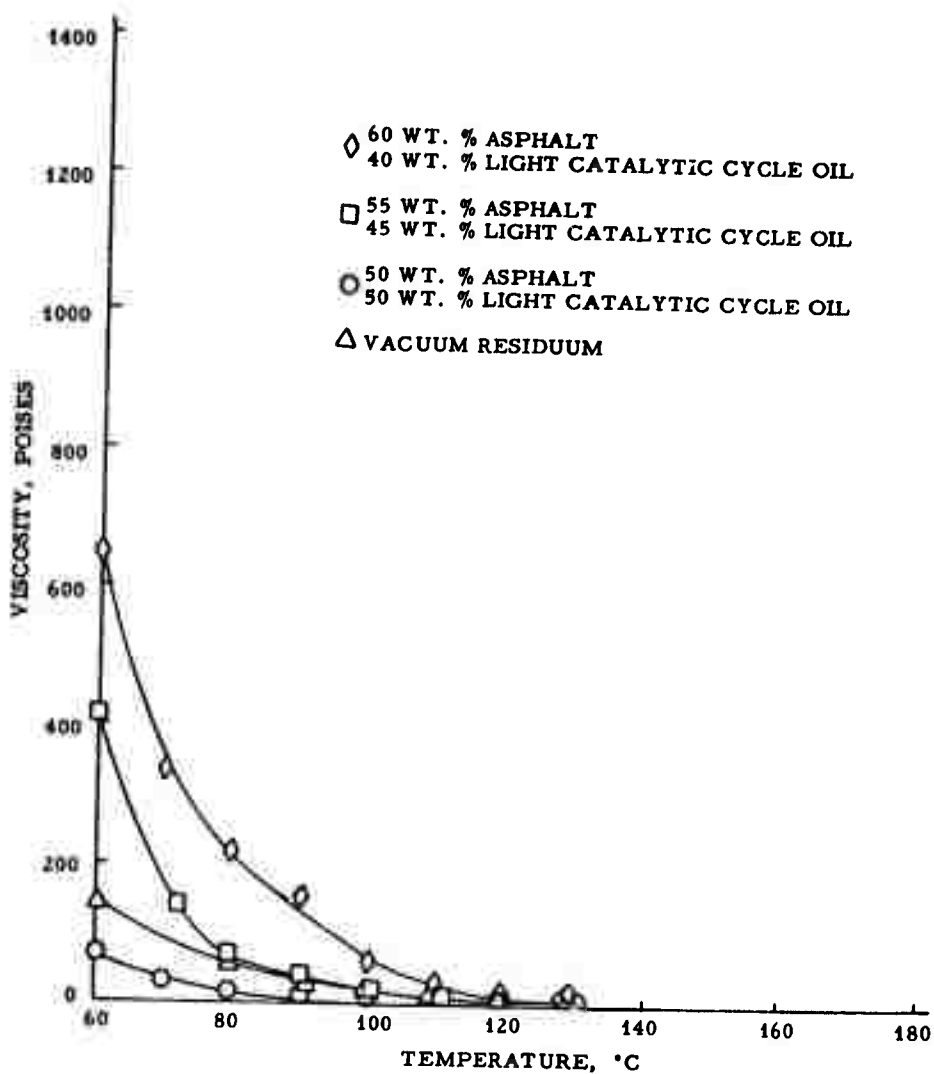


Figure 88. Viscosities of Light Catalytic Cycle Oil Diluted L-915 Asphalt as Compared to Vacuum Residuum

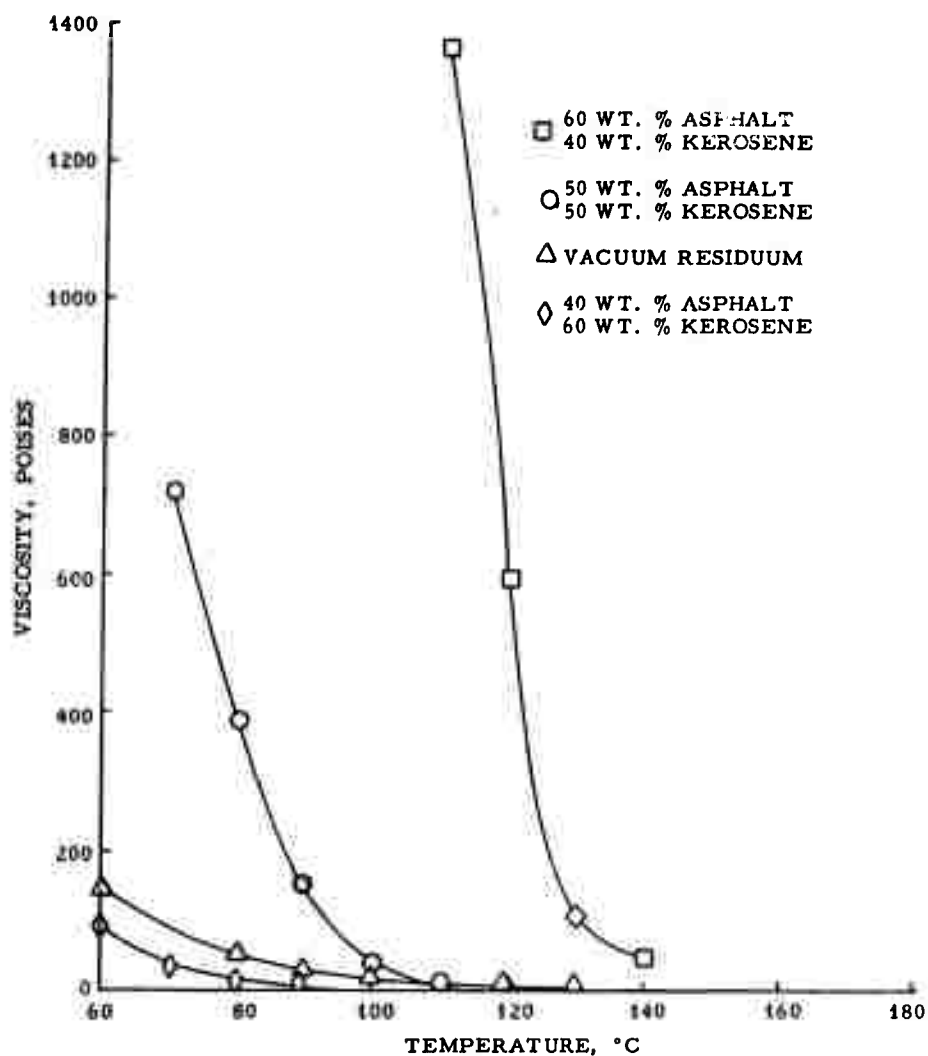


Figure 89. Viscosities of Kerosene Diluted Asphalt as L-916 Compared to Vacuum Residuum

Table 78. Graphite Thermal Expansion Evaluation
for Diluted Asphalt Coking Charges

	With-Grain Graphitized Extruded Billet Thermal Expansion, $10^{-6}/^{\circ}\text{C}$ (30-100 $^{\circ}\text{C}$)			
	N	Max.	Min.	Avg.
Undiluted Asphalt	6	5.79	5.73	5.75
50 wt. Per Cent Asphalt:				
50 wt. Per Cent Kerosene	6	5.58	5.48	5.51
50 wt. Per Cent Asphalt:				
50 wt. Per Cent Diesel Oil	6	5.65	5.41	5.55
50 wt. Per Cent Light Catalytic:				
50 wt. Per Cent Cycle Oil	6	5.67	5.49	5.60

sources of the different asphalts are listed in Table 79. Physical and analytical properties for the asphalts are listed in Table 80.

Table 79. Titles and Sources of Evaluated Commercial
Air-Blown Materials

Sample Code No.	Source	Venders' Title of Material
A-115	Trumbull Asphalt Co., Chicago, Illinois	No. 60 Stock
A-116	" " "	No. 63 Stock
A-118	Witco Chemical Co., Lawrenceville, Ill.	Witresin
A-119	" " "	No. 38 M. R.
A-120	" " "	No. 200 M. R.
A-121	Witco Chemical Co., Perth Amboy, N. J.	Witresin
A-122	" " "	No. 38 M. R.
A-123	" " "	B-2
A-125	Witco Chemical Co., Lawrenceville, Ill.	No. 38 M. R. Simulated Hammond, Ind., Formula
A-126	" " "	Special Experimental Resin

Table 80. Properties of Commercial Air-Blown Material

Sample Code No.	Penetration 100 g. 5 Sec. (ASTM D-5) 77°F 150°F	Melting Point, °C (Cube in Air)	Weight Per Cent						
			Asphaltene % (n-Pentane Insoluble)	Conradson Carbon	Benzene Insoluble	Quinoline Insoluble	Ash %	Sulfur %	
A-115	4.2	21.0	162	52.6	26.9	0.37	0.06	0.05	1.71
A-116	0.5	6.0	165	64.5	31.6	1.03	0.08	0.07	3.01
A-118	1.0	11.0	132	54.5	30.6	2.28	0.18	0.04	0.47
A-119	1.7	12.7	168	57.3	24.7	0.98	0.16	0.04	0.77
A-120	2.0	14.3	167	54.9	28.7	0.84	0.14	0.05	0.74
A-121	0.0	12.7	136	57.9	30.3	0.15	0.11	0.08	1.37
A-122	2.0	23.0	156	54.1	27.6	0.10	0.08	0.07	1.67
A-123	1.0	16.0	175	58.1	29.2	0.36	0.32	0.06	3.37
A-125	6.0	22.0	163	50.8	25.7	1.12	0.11	0.04	1.25
A-126	0.2	7.0	123	90.1	33.4	-	0.40	0.23	1.19

Extruded billets, 5/8-inch in diameter by 6 inches in length, were formed, baked and graphitized using coke made from the different commercial asphalts. Physical properties of the graphitized billets are presented in Table 81. Samples A-119, A-122 and A-125 are the most promising high thermal expansion graphite sources. The prime material for further investigation is A-119 because of its low sulfur level. (This is the material selected for Pilot-Scale Coker Cycles 78S and 78N.)

4.2.4. Asphalt Characterization

Previous work showed that asphaltene content (n-pentane insoluble) of the same type source stocks could be related to final graphite thermal expansion.⁽¹⁵⁶⁾ A densimetric method of characterization similar to that described by Corbett⁽¹⁵⁶⁾ was used to examine several coking feed stocks. A diagram of the densimetric analysis procedure is shown in Figure 90. By determining the weight per cent carbon, weight per cent hydrogen, and molecular weight of the malthene (petrolene) portion or n-pentane soluble, different characteristic calculations can be performed.

In Table 82 the properties of the coking charges and extruded billet graphite thermal expansion values are tabulated. The densimetric calculations for the coking charges are listed in Table 83. A relationship between both malthene molecular weights and number of carbon atoms per molecule, by the densimetric method, to graphite thermal expansions (30-100°C) is shown in Figure 91.

4.2.5. Natural Asphalt

A Wyoming "Fourbear" asphaltic crude oil was vacuum-topped to yield 57 weight per cent residuum. Residuum properties are presented in Table 84. The high sulfur content can be objectional for material used in making graphite. The residuum was coked, calcined and molded into 3-inch diameter billets. Thermal expansion values for the graphite billets are listed in Table 85.

4.2.6. Experiments to Develop Isotropic Cokes of Intermediate Thermal Expansion Levels

Graphite materials having intermediate isotropic thermal expansion characteristics [$2.0 - 4.0 \times 10^{-6}/^{\circ}\text{C}$ (30-100°C)] might have superior thermal shock resistance characteristics when compared to commercially available anisotropic graphites. Various experiments were devised and performed in an attempt to produce materials of this type.

4.2.6.1. Coking of Gilsonite VB and Slurry Oil or Vacuum Residuum Mixtures

One proposed method was to coke mixtures of Gilsonite materials, which result in fairly isotropic high thermal expansion cokes, and vacuum residuum or slurry oil, which result in comparatively low and anisotropic thermal expansion cokes.

Table 84. Physical Properties for Extruded Graphite Billets Produced from Commercial Air-Blown Materials

Sample Code No.	Average Bulk Density g/cc	With Grain Specific Resistance, Ω -cm $\times 10^{-4}$		With Grain Thermal Expansion (30-100°C), $10^{-6}/^{\circ}\text{C}$		
		Max.	Min.	Avg.	Max.	Min.
A-115	1.55	12.90	11.01	11.95	5.38	5.35
A-116	1.69	11.65	10.24	10.75	4.61	4.52
A-118	1.58	9.19	7.61	8.21	2.04	1.86
A-119	1.47	15.98	15.68	15.83	5.90	5.87
A-120	1.56	11.48	5.58	10.94	5.41	5.18
A-121	1.67	12.13	11.37	11.66	5.47	5.23
A-122	1.54	15.59	13.67	14.76	5.85	5.55
A-123	1.46	15.56	14.45	15.09	5.22	5.07
A-125	1.56	-	-	-	6.13	6.05
A-126	1.57	6.74	6.34	6.51	1.41	1.17

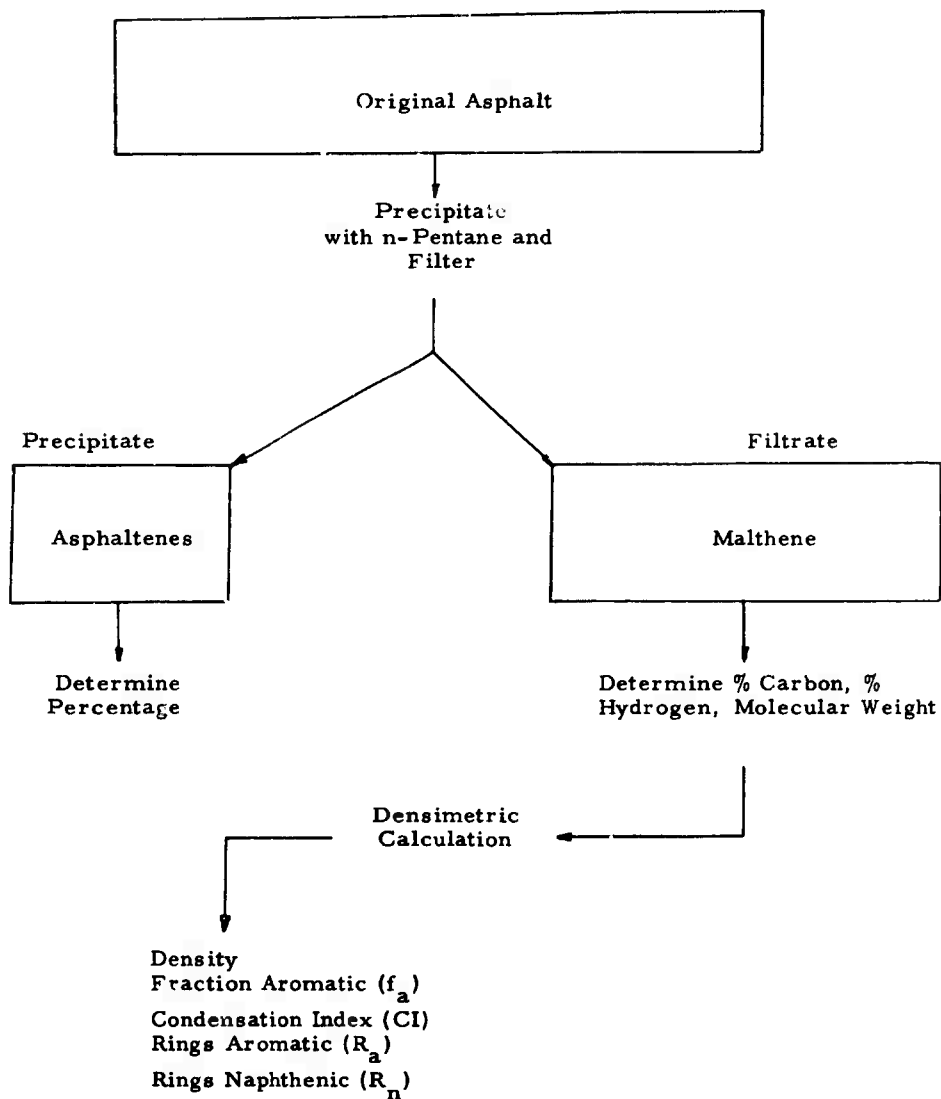


Figure 90. Method of Separation and Densimetric Analysis

Table 82. Coking Charge Characterization of Materials Used in the Densimetric Calculations

Code No.	P-4	P8-17	P8-76	P8-45	P-9	P8-119	P-11	P8-117	P8-57	A-119	A-126
Material	Vac. Resid.	Vac. Resid.	Vac. Resid.	Vac. Resid.	Slurry Oil	Slurry Oil	Thermal Tar	Thermal Tar	Thermal Tar	Air Blown Material	Commercial
Air Blowing Temperature, °C	Not	270	300	280	Not	250	Not	270	275	Air Blown Material	Commercial
Air Blowing Time, Hrs.	Air	5	5	6.5	Air	5	Not	68.4	67.5	Air Blown Material	Commercial
Air Blown Against Liquid, Wt. Per Cent	Blown	Spillage	87.7	91.0	Blown	82.9	Blown	68.4	67.5	Air Blown Material	Commercial
Coking Charge Characteristics											
Asphaltenes, Wt. per cent	11.3	30.5	44.6	46.1	15.8	84.3	2.3	72.0	79.1	42.2	90.1
Resins, Wt. per cent	0.0	Trace	Trace	0.3	Trace	0.7	0.1	0.4	0.3	6.1	0.4
Condensates, Wt. per cent	0.0	Trace	Trace	0.3	Trace	0.7	0.1	0.4	0.3	6.1	0.4
Benzenes, Wt. per cent	13.8	18.4	20.9	15.9	2.2	25.3	3.4	2.9	17.8	1.0	10.7
Conradson Carbon, Wt. per cent	0.4	0.4	0.4	0.4	5.3	34.82	9.4	33.0	32.7	24.7	33.4
Sulfur, Wt. per cent	0.01	0.01	0.03	0.04	0.01	0.0	0.1	0.1	0.2	0.9	1.2
Ash, Wt. per cent	87.19	85.9	86.6	87.2	89.3	88.8	91.79	90.0	90.0	84.0	84.2
Hydrogen, Wt. per cent	11.16	10.5	10.1	10.3	9.4	7.5	8.11	7.1	6.8	9.3	6.7
Density, g./cc.	1.09	1.02	1.00	1.03	1.01	0.95	1.05	1.12	1.17	1.05	1.16
Melting Point, °C	15	102	155	167	12	11	-----	92	140	168	123
Penetration, mm. 100°	-----	24.0	10.0	9.0	-----	24.0	-----	0	0.5	1.7	0.0
Graphitized Surface Area, sq. ft./g. (10-100°C)	1.47	4.36	5.14	5.45	0.45	0.93	0.28	0.67	2.29	5.84	1.27

Table 83. Malthene Properties and Densimetric Calculations for Various Coker Charge Stocks and Asphalts

Code No.	P-4	PS-77	PS-76	PS-45	P-9	PS-419	P-11	PS-417	PS-32	A-119	A-126
Malthene Material Properties:											
Carbon, wt. per cent	85.64	83.78	85.58	85.42	88.93	87.67	91.19	89.81	90.14	85.36	85.97
Hydrogen, wt. per cent	11.51	11.34	11.93	12.46	10.23	11.08	8.53	8.85	9.03	11.99	9.24
Density, g/cc	0.96	0.94	0.91	0.90	0.96	0.96	1.04	1.02	1.03	0.96	1.03
Molecular Weight	868	839	957	1015	305	358	179	328	361	970	474
Densimetric Calculations:											
$d_{20/4} = \text{density} = 1.4673 - 0.0431 (\%H) =$	0.97	0.98	0.95	0.93	1.03	0.99	1.10	1.09	1.08	0.95	1.07
$H/C = \text{hydrogen/carbon ratio} = 11.92 (\%H/\%C) =$	1.60	1.61	1.66	1.74	1.37	1.51	1.12	1.18	1.19	1.67	1.28
$Mc/d = \text{atomic molar volume} = 1201/(d_{20/4} \times \%C) =$	14.44	14.65	15.42	15.12	13.16	13.84	11.97	12.27	12.34	14.81	13.06
$(Mc/d)_{\text{c}} = \text{molar volume corrected for hetero atoms}$ $= Mc/d - 6.0 \frac{100 - \%C - \%H}{\%C} =$	14.24	14.30	15.25	14.97	13.10	13.75	11.95	12.18	12.28	14.62	9.62
$fa = \text{fraction aromatic} = 0.09 (Mc/d)_{\text{c}} = 1.45 (H/C) + 0.77 =$	0.16	0.21	0.23	0.12	0.37	0.27	0.56	0.52	0.51	0.17	0.17
$C, L = \text{Condensation Index} = 2 - H/C - fa =$	0.24	0.18	0.11	0.14	0.26	0.22	0.32	0.31	0.30	0.16	0.55
$No, C = \text{Average number of carbon atoms}$ $= (\%C \times M. W.)/1201 =$	61.89	58.58	68.25	72.25	22.58	26.13	13.59	24.53	27.12	68.94	33.93
$R = \text{total number of rings per mole}$ $= No, C (C, L)/2 + 1 =$	8.43	6.27	4.75	6.06	3.94	3.87	3.17	4.80	5.10	6.62	7.92
$No, CA = \text{number of carbon in aromatic rings} = fa \times (No, C) =$	9.90	12.30	15.70	8.67	8.35	7.06	7.61	13.00	13.80	11.72	5.77
$RA = \text{number of aromatic rings per mole} = (No, CA - 2)/4 =$	1.98	2.58	3.43	1.67	1.59	1.27	1.40	2.75	2.95	2.34	0.94
$PN = \text{number of naphthenic rings per mole} = R - RA =$	6.45	3.69	1.32	4.39	2.35	2.60	1.77	2.05	2.15	4.19	6.98

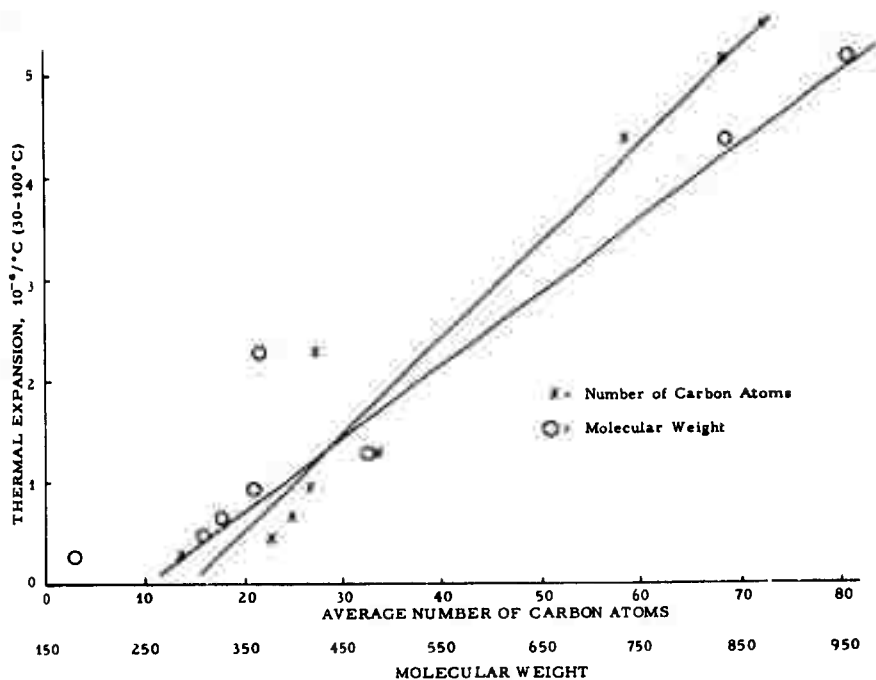


Figure 91. Graphite Thermal Expansion as a Function of Malthene Molecular Weight and Number of Carbon Atoms per Molecule

Table 84. Properties of Vacuum Residuum from Fourbear Crude Oil

Melting Point, °C	60
Penetration, 77°F	
100 g, 5 Sec. (ASTM D-5)	82
Weight Per Cent Content	
Asphaltene (n-Pentane Insoluble)	27.8
Quinoline Insoluble	0.25
Benzene Insoluble	0.35
Conradson Carbon	21.3
Ash	0.07
Sulfur	3.88

Table 85. Thermal Expansion Values for Graphite
Using a Topped Fourbear Crude Source

	With Grain	Across Grain
Average Thermal Expansion $10^{-6}/^{\circ}\text{C}$ (30-100°C)	2.75	3.22

4.2.6.1.1. Coking of Gilsonite VB and Slurry Oil Mixtures

Slurry Oil produces coke having a low anisotropic thermal expansion as shown in Tables 86 and 87. Slurry oil and Gilsonite VB mixtures, with light catalytic cycle oil as a diluting agent of negligible coking value, was coked at atmospheric pressure. Increasing slurry oil content resulted in lowered thermal expansion values, but the mixtures did not produce cokes having low anisotropy.

4.2.6.1.2. Coking of Gilsonite VB and Vacuum Residuum Mixtures

As shown in Tables 86 and 87, vacuum residuum yields a coke having a moderate thermal expansion level of somewhat less anisotropy than slurry oil coke. Mixtures of vacuum residuum, Gilsonite VB and light catalytic cycle oil diluent were coked at atmospheric pressure. Higher vacuum residuum contents resulted in lower thermal expansion values, but no cokes were produced having thermal expansion values below $3.5 \times 10^{-6}/^{\circ}\text{C}$ (30-100°C). Fair isotropy of thermal expansion was maintained. Although additional mixtures with increased vacuum residuum contents were not coked, it is likely that increased anisotropy and lower thermal expansion values would have resulted.

4.2.6.2. Coking of Charge Stocks in High-Boiling Organic Compounds

A proposed method for producing isotropic cokes of various thermal expansion levels is to coke in a liquid medium which does not volatilize appreciably until the coking cycle has been completed. Presumably the formation of coke in a refractory liquid medium should result in regularly-shaped coke particles.

Table 88 presents physical property data for graphitized molded billets processed from vacuum residuum and slurry oil cokes produced in high-boiling organic liquids. The results may be summarized as follows:

4.2.6.2.1. Coking of Vacuum Residuum in a Polyphenyl Mixture

The carrier medium for the coking is a mixture of polyphenyls which undergoes a weight loss of approximately 12 per cent during coking to 470°C, with a 1000°C calcined coke yield of approximately 16 weight

Table 86. Physical Property Data for Graphitized $\frac{5}{8}$ -Inch Diameter Extruded Billets Processed from Cokes Produced from Gilsonite and Vacuum Residue or Slurry Oil Mixtures

Code No.	Composition of Charging Charge Stock	Composition of Calcined Coke	Average Bulk Density, g/cc			Specific Resistance, $\Omega\text{-cm} \times 10^{-6}$			Thermal Expansion, (30-100°C), $10^{-4}/^{\circ}\text{C}$		
			Feen	Bike	Graph	N	Max.	Avg.	N	Min.	Avg.
T-53	18.2 wt. % Slurry Oil 54.5 wt. % Gilsonite VB 27.3 wt. % Light Catalytic Cycle Oil Diluent	14.4 wt. % Slurry Oil 85.6 wt. % Gilsonite VB	1.74	1.60	1.66	6	7.17	5.73	6	2.77	2.71
T-55	27.3 wt. % Slurry Oil 45.4 wt. % Gilsonite VB 27.3 wt. % Light Catalytic Cycle Oil Diluent	22.2 wt. % Slurry Oil 76.8 wt. % Gilsonite VB	1.73	1.57	1.66	5	7.12	5.79	6	1.71	1.59
T-54	18.2 wt. % Vacuum Resid. 54.5 wt. % Gilsonite VB 27.3 wt. % Light Catalytic Cycle Oil Diluent	17.9 wt. % Vacuum Residue 82.1 wt. % Gilsonite VB	1.72	1.62	1.78	6	8.19	5.18	6	4.10	3.75
T-56	27.3 wt. % Vacuum Resid. 45.4 wt. % Gilsonite VB 27.3 wt. % Light Catalytic	28.2 wt. % Vacuum Residue 71.8 wt. % Gilsonite VB	1.71	1.63	1.74	6	9.20	7.76	6	3.72	3.54
T-57	100 wt. % Slurry Oil (Control Run)	100 wt. % Slurry Oil	1.62	1.55	1.57	6	10.12	9.49	6	0.91	0.58
T-59	100 wt. % Vacuum Resid. (Control Run)	100 wt. % Vacuum Residue	1.64	1.57	1.62	6	9.24	8.91	6	1.50	1.44
0-3	100 wt. % Gilsonite VB (Control Run)	100 wt. % Gilsonite VB	1.68	1.70	1.70	6	10.54	9.58	6	4.05	3.90

Table 87. Physical Property Data for 3-Inch Diameter Graphitized Molded Billets Processed from Gilsonite and Vacuum Residuum or Slurry Oil Mixtures

Code No.	Composition of Coking Charge Stock	Composition of Calcined Coke	Average Bulk Density, g/cc		Specific Resistance, 5-cm x 10 ³			Thermal Expansion, (10-100°C), 10 ⁻⁶ /in.			Young's Modulus, 10 ³ lbs./in. ²			Flexural Strength, 10 ³ lbs./in. ²		
			Green	Red	Max.	Min.	Ave.	Max.	Min.	Ave.	Max.	Min.	Ave.	Max.	Min.	Ave.
T-53	16.2 wt. % Slurry Oil 83.8 wt. % Vacuum Residuum 27.3 wt. % Light Catalytic Cycle Oil Diluent	14.4 wt. % Slurry Oil 85.6 wt. % Gilsonite VB	1.71	1.65	1.70	2		W. G. 8.36 A. G. 9.47	6.78 8.85	7.58 9.20	8		1.11 0.79	0.77 0.71	0.97 0.76	6 8
T-55	27.3 wt. % Slurry Oil 45.4 wt. % Gilsonite VB 27.3 wt. % Light Catalytic Cycle Oil Diluent	23.2 wt. % Slurry Oil 76.8 wt. % Gilsonite VB	1.66	1.63	1.65	2		W. G. 9.02 A. G. 11.29	8.31 9.24	8.63 10.42	4		0.86 0.82	0.73 0.50	0.79 0.36	4 8
T-54	16.2 wt. % Vacuum Residuum 83.8 wt. % Gilsonite VB 27.3 wt. % Light Catalytic Cycle Oil Diluent	17.9 wt. % Vacuum Residuum 82.1 wt. % Gilsonite VB	1.65	1.65	1.76	2		W. G. 10.43 A. G. 12.86	6.72 8.30	8.73 9.93	7 6		1.14 0.94	0.74 0.70	0.99 0.92	4 4
T-56	27.3 wt. % Vacuum Residuum 45.4 wt. % Gilsonite VB 27.3 wt. % Light Catalytic	28.2 wt. % Vacuum Residuum 71.8 wt. % Gilsonite VB	1.65	1.64	1.75	2		W. G. 9.33 A. G. 10.98	7.94 9.72	8.86 10.19	6		1.03 0.83	0.90 0.76	0.96 0.79	6 6
T-57	100 wt. % Slurry Oil (Control Run)	100 wt. % Slurry Oil	1.56	1.49	1.52	2		W. G. 16.93 A. G. 27.74	12.16 22.02	15.05 24.54	5 4		0.62 0.29	0.41 0.23	0.53 0.26	5 8
T-59	100 wt. % Vacuum Residuum (Control Run)	100 wt. % Vacuum Residuum	1.34	1.48	1.52	1		W. G. 15.94 A. G. 18.55	12.47 16.84	14.19 17.66	9 9		0.76 0.54	0.44 0.31	0.63 0.46	9 9
0 - 3	100 wt. % Gilsonite VB (Control Run)	100 wt. % Gilsonite VB	No data available.													

Table 88. Physical Property Data for Graphitized Extruded and Molded Billets Produced from Vacuum Residuum and Slurry Oil Cokes Produced in the Presence of High-Boiling Organic Compounds

Code No.	Calculated Composition of Charge Material	Extruded 1-inch Diameter Graphitized Billet Data				Molded 3-inch Diameter Graphitized Billet Data				Remarks		
		Specific Resistance, $0\text{-cm} \times 10^{-8}$		Thermal Expansion, $(10\text{-}100^{\circ}\text{C}), 10^{-6}/^{\circ}\text{C}$		Specific Resistance, $0\text{-cm} \times 10^{-8}$		Thermal Expansion, $(10\text{-}100^{\circ}\text{C}), 10^{-6}/^{\circ}\text{C}$				
		W. G.	A. G.	W. G.	A. G.	W. G.	A. G.	W. G.	A. G.			
S-15	50 wt. % Vacuum Residuum 50 wt. % Polyphenyl	16.42		3.39		17.99	19.11	3.28	3.96	2161	2216	Residual polyphenyl not extracted after coking.
S-16	67 wt. % Vacuum Residuum 33 wt. % Polyphenyl	12.11		3.81		No molded billets processed.						Residual polyphenyl not extracted after coking.
P-4	100 wt. % Vacuum Residuum (Control Run)	7.88		1.31		9.82	13.24	2.02	3.00	1860	1860	
S-18	80 wt. % Slurry Oil 20 wt. % Polyphenyl	14.37		1.98		No molded billets processed.						Residual polyphenyl not extracted after coking.
T-35	82.5 wt. % Slurry Oil 17.5 wt. % Polyphenyl	7.90		1.45		11.04	11.74	3.19	2.89	2280	2404	Residual polyphenyl extracted by hot C_6H_6 after coking.
T-32	82.5 wt. % Slurry Oil 17.5 wt. % p-Terphenyl	6.63		0.39		No molded billets processed.						p-Terphenyl completely vaporized during coking.
C.R. 116	75 wt. % Slurry Oil 25 wt. % Phenyl Silane	10.14		1.37		12.56	14.77	1.83	2.66	1549	911	Residual phenyl silane not extracted after coking.
C.R. 123	73.8 wt. % Slurry Oil 26.2 wt. % Phenyl Silane	16.06		2.20		16.03	17.68	2.47	3.08	1629	1186	No residual liquid phenyl silane noted after coking.
P-9	100 wt. % Slurry Oil (Control Run)	8.61		0.42		10.58	15.23	0.79	2.40	1109	789	

per cent. The coking of vacuum residuum in polyphenyl, followed by calcination without extracting the carrier, resulted in a fairly isotropic graphite. The isotropy may have been due in part to the polyphenyl coke which was present after calcination.

4.2.6.2.2. Coking of Slurry Oil in a Polyphenyl Mixture

The coking of slurry oil normally yields a low thermal expansion coke. The coking of slurry oil in polyphenyl with the carrier extracted prior to calcination, resulted in a graphite of moderately low thermal expansion characteristics. The wide difference between the with-grain thermal expansion values of the extruded and molded billets indicates a high degree of anisotropy.

4.2.6.2.3. Coking of Slurry Oil in p-Terphenyl

The coking of slurry in p-terphenyl, which sublimates during the latter stages of the coking cycle, resulted in graphitized extruded billets which do not vary significantly in thermal expansion level from those produced from slurry oil which has been coked without using a high-boiling carrier.

4.2.6.2.4. Coking of Slurry Oil in a Phenyl Silane

The coking of slurry oil at 50 lbs./in.² gauge in a phenyl silane, which has a distillation range of approximately 430 to 510°C at atmospheric pressure, resulted in a more isotropic graphite material than is obtained with control slurry oil coke.

In order to maintain the high-boiling carrier in a liquid state throughout the coking range, a similar mixture of slurry oil in a phenyl silane was coked at 500 lbs./in.² gauge. The pressure was released at the completion of the heating cycle. The coke yield indicated that part of the phenyl silane had been coked. This material was more isotropic and had a higher thermal expansion than that produced in the lower pressure run. The extent to which the phenyl silane coke influenced the overall coke properties is unknown. To determine the practicality of these methods for producing relatively isotropic cokes of intermediate thermal expansion levels, we would have to perform additional experiments varying mixtures and coking pressures.

4.2.7. Preservation of High Thermal Expansion Properties Through Graphite Processing

The low-scrap manufacture of graphite articles of moderately large cross-sectional area requires the use of a filler which has been calcined to a high temperature. This is true particularly with the isotropic high thermal expansion seeded and air-blown cokes. The extremely high shrinkages during the graphitization cycle would make the use of a 1000°C or a 1350°C calcined material very difficult.

The use of graphitized or high-temperature calcined fillers lowers the potential thermal expansion level of the final graphitized product. The influence of this factor on the properties, particularly thermal expansion, of graphitized molded billets processed using the isotropic high thermal expansion air-blown materials, has been studied.

Figure 92 shows the processing variations which have been studied. Graphite properties of billets produced by these methods are listed in Table 89.

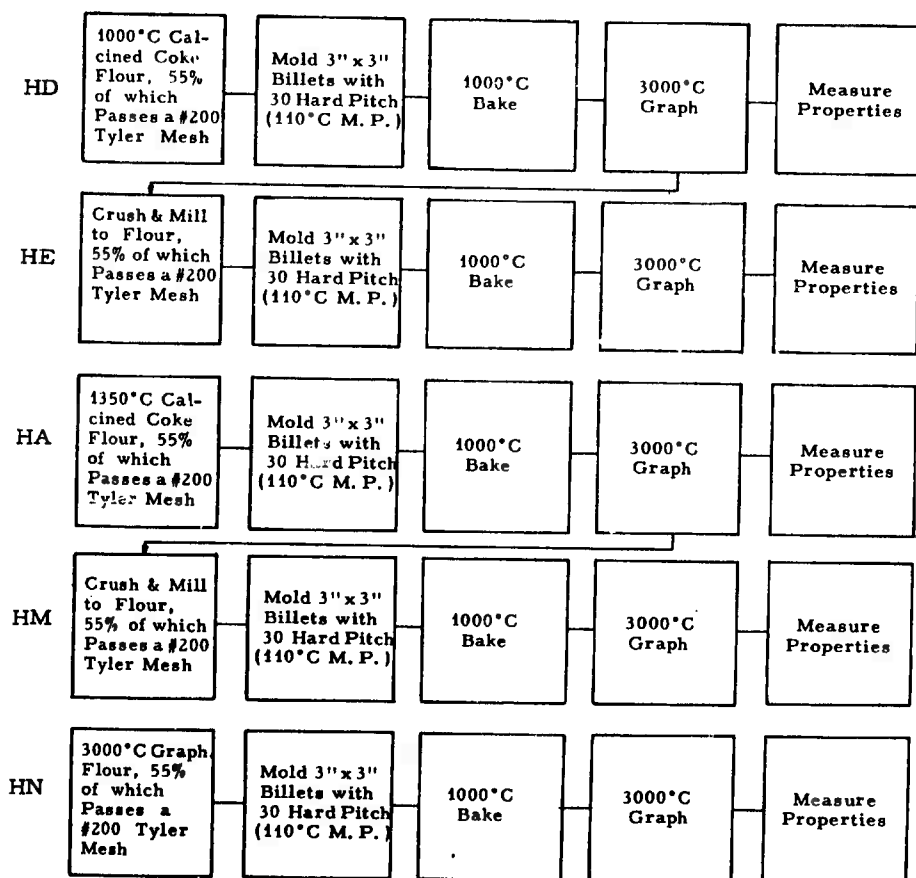


Figure 92. Billet Processing Variations Using Coke Produced in Pilot Coker (Cycles 68S and 69N) from Kerosene-Diluted Air-Blown Vacuum Residuum Produced by Trumbull Asphalt Company

Table 89. Graphitized 3-Inch Diameter by 3-Inch Length Molded Billet
Properties for Billets Produced Using Fillers of Various
Heat-Treatment Temperatures

Group No.	HD**		HE		HA		HM		HN	
Billet Bulk Density, g/cc										
Green	1.59		1.84		1.71		1.71		1.68	
Bake	1.47		1.76		1.54		1.68		1.62	
Graph	1.62		1.74		1.66		1.63		1.56	
	W. G.	A. G.	W. G.	A. G.	W. G.	A. G.	W. G.	A. G.	W. G.	A. G.
Specific Resistance, 10^{-10} Ω -cm										
Max.	14.24	14.56	18.08	18.99	14.47	14.68	16.19	16.67	17.45	24.35
Min.	12.07	8.89	15.80	15.98	12.92	12.63	13.33	14.51	15.84	18.24
Ave.	13.12	12.58	16.77	17.37	13.36	13.73	14.55	15.91	16.81	20.06
Thermal Expansion 30-100°C. x $10^{-6}/^{\circ}\text{C}$										
Max.	5.96	5.96	5.62	5.56	5.44	5.43	4.36	4.76	4.23	4.29
Min.	5.63	5.64	5.46	5.49	5.29	5.02	4.22	4.56	3.90	4.16
Ave.	5.73	5.77	5.36	5.52	5.40	5.25	4.29	4.64	4.03	4.22
Young's Modulus, 10^6 lbs./in. ²										
Max.	1.26	1.21	1.10	1.19	1.29	1.24	0.88	0.77	0.76	0.56
Min.	0.99	1.00	1.15	1.03	1.04	0.99	0.75	0.73	0.55	0.48
Ave.	1.17	1.13	1.22	1.12	1.17	1.11	0.79	0.74	0.69	0.52
Flexural Strength, lbs./in. ²										
Max.	4876	3853	3141	2707	4596	3572	2537	2045	1495	1065
Min.	3171	2306	2796	2162	3244	2257	1857	1605	974	746
Ave.	4010	3110	2590	2420	3900	2690	2000	1810	1310	1310

*Denotes volume expansion rather than shrinkage.

**See Figure 92 for group designation.

In groups HD, HA, and HM, 1000°C, 1350°C, and 3000°C heat-treated materials, respectively, were used and processed direct to the final graphite product. A decrease in thermal expansion and strength values and an increase in electrical resistance were noted with increasing filler heat-treatment temperatures. The use of 1000°C or 1350°C calcined material may be impractical for commercial processing of large cross section graphite articles.

Samples of the coke calcined at 1000°C and at 1350°C were made into molded billets and graphitized. After the billets had been graphitized, they were crushed and used as filler for additional processing. Fairly high thermal expansion values were preserved where the graphitized filler prepared from 1000°C calcined material was used (group HE). As shown in Table 89, the group HE billets were significantly higher in thermal expansion than the group HM billets, which were processed similarly to the HE billets using the 1350°C calcined starting material.

4.2.8. Solvent Extraction Experiments

Coke structure is dependent on the concentrations of different molecular species in the coker charge stock. Changing these concentrations or removing certain species may produce new types of coke from conventional charge stocks. This section deals with changing a particular stock; i.e., vacuum residuum (VR), by solvent extraction.

4.2.8.1. Paraffinic Solvents

The following procedure was used with each solvent. One part of VR was mixed with weight ratios of 1, 2, 5, and 10 parts of the solvent to be tested. After thorough mixing, the samples were centrifuged at room temperature in graduated tubes, and the level of the resinous or sludgy residue determined with an ultraviolet light. Table 90 shows the volume of sludge in the charge stock (for given volumes of solvent and charge stock). Pentane was the lowest molecular weight solvent used and dodecane the highest.

A poor solvent was needed for the resinous material so that as much sludge as possible could be separated from the VR. As expected, the lower the molecular weight of the solvent the more sludge phase was found, and the branched chain form produced even more. The double-bonded solvents showed little sludge phase.

Normal pentane and normal heptane at a 10 to 1 solvent to VR ratio were selected to produce a coker charge stock for the bench scale work. Pentane solubles, heptane solubles and a combination of 13.4 per cent heptane insolubles in 86.6 per cent VR were coked, calcined and processed through to finished 3-inch diameter molded graphite billets of $\frac{5}{8}$ -inch diameter extruded billets. Table 91 gives the properties of the finished graphite articles as compared with a VR graphite billet.

Table 90. Volume Per Cent Sludge Removed from Vacuum Residuum with Various Solvents

Wt. Ratio Solvent/ Vac. Resid.	n-Pentane	Ligroin*	n-Heptane	n-Decane	n-Dodecane	Solvent				Pentene	Octene
						Iso-pentane (2-methyl butane)	Iso-Heptane (2,4-dimethyl- pentane)	Iso-Octane (2,2,4-trimethyl pentane)			
1	0.8	T**	0.6	T	T	0.6	-	0.3	0.6	T	
2	16.6	T	8.2	0.5	0.5	40.6	-	22.5	2.0	0.9	
5	47.4	23.7	47.8	7.5	12.6	60.5	56.7	39.3	46.6	T	
10	44.4	45.8	24.6	14.1	15.1	81.4	76.0	58.9	27.3	T	
20			17.3								
40	59.4										

* A saturated fraction of petroleum boiling in the range 20-135°C

** Trace

* A saturated fraction of petroleum boiling in the range 20-135°C

** Trace

Table 91. Properties of Graphite Billets Made from Vacuum Residuum and its Heptane and Pentane Solubles and Insolubles

Property*	3-Inch Diameter Molded Billets						½-Inch Diameter Extruded Rods					
	Vacuum Residuum		Heptane Solubles		Insolubles**		Vacuum Residuum		Pentane Solubles		Heptane Solubles	
Binder Level, pph	30		36		34		32		34		36	
Green Density, g/cc	1.61		1.603		1.617		1.66		1.648		1.675	
Baked Density, g/cc	1.56		1.542		1.583		1.54		1.542		1.550	
Graphitized Density, g/cc	1.56		1.564		1.589		1.66		1.620		1.597	
Volume Shrinkage (bake to graph) %	4.61		5.67		6.67		12.26		6.50		7.84	
Weight Loss (bake to graph) per cent	4.84		4.28		6.26		5.16		-		4.92	
Specific Resistance, 10 ⁻⁴ ohm-cm	11.34		8.28		8.19		~ 10		6.96		6.34	
W. G.	15.02		11.35		10.19		----		----		----	
A. G.												
Young's Modulus, 10 ⁶ lbs/in. ²												
W. G.	0.69		0.70		0.79		----		----		----	
A. G.	0.48		0.45		0.57		----		----		----	
Flexural Strength, lbs/in. ²												
W. G.	1386		1476		1919		----		----		----	
A. G.	1051		1021		1385		----		----		----	
Thermal Expansion (30-100°C), 10 ⁻⁶ /°C												
W. G.	2.07		2.04		2.40		1.28		2.33		1.5-	
A. G.	3.45		3.15		3.27		----		----		----	

* Average of from 1 to 6 samples.

** Because of low yield, heptane insoluble was combined with vacuum residuum to give a charge stock containing 13.4 per cent heptane insoluble.

Yield data and differences in the chemical properties of the soluble and insoluble portions of the VR are compared to the original VR in Table 92. The pentane solubles of VR produced an extruded graphite with 82 per cent higher thermal expansion and a 30 per cent lower specific resistance than the untreated VR.

Table 92. Properties of Vacuum Residuum and Its Heptane and Pentane Solubles and Insolubles

Property	Vacuum Residuum	Pentane		Heptane	
		Solubles	Insolubles	Solubles	Insolubles
Specific Gravity, g/cc	0.956	0.938	1.050	0.947	1.15
Benzene Insolubles, wt. %	0.0	0.0	0.7	0.2	0.8
Quinoline Insolubles, wt. %	0.0	0.0	0.5	0.0	0.4
Conradson Carbon, wt. %	13.8	10.2	32.7	12.2	46.6
Ash, wt. %	0.02	0.01	0.17	0.02	0.32
Carbon/Hydrogen, wt. ratio	87.39/11.16	-	87.46/9.21		88.18/6.91
Sulfur, wt. %	0.38	0.34	0.50	-	0.63
Molecular wt.	991	952	1288	1001	1772
Yield, wt. % (10:1 solvent:VR ratio)		91.7	6.3	93.1	4.6

The heptane solubles and insolubles-plus-VR produced a graphite having a more isotropic thermal expansion than VR graphite. The insoluble plus VR portion had greater strength than the VR graphite.

The limited number of experiments has indicated an approach to isotropic thermal expansion through 1) a reduction of across-grain thermal expansion using the heptane soluble portion as a coker charge stock, and 2) an increase in with-grain thermal expansion using the heptane insoluble and VR as a coker charge stock.

4.2.8.2. Aromatic and Other Solvents

The procedure used for paraffin solvents was also tried with other solvents; however the solvent was either almost completely miscible or almost completely immiscible with the VR. No further work was done with the solvent. Table 93 shows the solvents tested.

4.2.9. Characterization of Complex Raw Materials

4.2.9.1. Coker Feed Stocks

Previous work⁽¹³⁵⁾ has shown that a general characterization of hydrocarbon feed stocks via its prior history, e. g., virgin residues or thermal and/or catalytic stocks, has yielded a rough correlation to the quality of the coke obtained when processed through to graphite.

Table 93. Aromatic and Other Solvents Used with Vacuum Residuum

Solvent	Miscible (M) or Immiscible (I) At Room Temperature
Acetone	I
Acetone - 5 % H ₂ O	I
Aniline - 5 % H ₂ O	I
Ethylene Glycol	I
Furfural	I
Furfuryl Alcohol	I
Methanol	I
Methanol - 10 % H ₂ O	I
Phenol	I
Phenol - 5 % H ₂ O	I
Benzene	M
Cyclohexane	M
Gasoline	M
Kerosene	M
Pyridine	M
Toluene	M
Xylene	M

Prior history is not always known, however, so a more quantitative picture of the chemical species is desired. The variables, e.g., coke yield, ash, per cent carbon, per cent hydrogen, etc.; while not related to molecular structure, could influence the quality of the coke and indicate species that are undesirable.

The charge stocks investigated were of two basic types, e.g., virgin residues and cracked stocks. Of the five virgin materials, two were atmospheric residues from a paraffinic (P-28) and an intermediate (P-16) base crude oil. The other three were vacuum residua from an intermediate (P-11), an intermediate-naphthenic (P-13), and a naphthenic (P-26) base crude oil. Of the three cracked stocks, two were residua from a catalytic cracking operation of gas oils with one (P-10) being followed by a thermal cracking operation. P-11 was the residue from a thermal cracking of gas oils.

The materials were processed by laboratory coking of the charge stocks at equivalent conditions of time, temperature and pressures. The cokes were then calcined to 1000°C, crushed, milled to a 55 flour (55 per cent through 200 mesh), and hot-mixed with a 140°C melting point coal tar pitch. The mix was made into $\frac{5}{8}$ -inch OD extruded rods and 3- by 3-inch molded plugs. Each piece was baked to 1000°C and graphitized to 2800°C. Graphite property data is shown in Table 94.

Table 94. Graphite Property Data (Beaker Coked-Extruded Rods)

Code No.	P-28	P-4	P-16	P-13	P-26	P-9	P-10	P-11
Raw Coke Yield, %	6.5	23.3	10.0	13.4	21.4	21.0	28.6	20.8
Specific Resistance, μ ohm-cm								
Maximum	13.00	9.24	8.19	-----	7.76	7.67	7.96	-----
Minimum	10.43	8.91	7.20	-----	6.10	6.75	7.35	-----
Average	11.85	9.04	8.05	7.56	7.18	7.21	7.54	8.16
Thermal Expansion, $10^{-6}, ^\circ\text{C}$ (30-100°C)								
Maximum	2.89	1.50	1.32	1.38	0.97	0.46	0.52	0.52
Minimum	2.60	1.44	1.26	1.35	0.60	0.43	0.40	0.43
Average	2.74	1.47	1.29	1.36	0.73	0.45	0.49	0.47

A correlation of the data obtained from the raw material and the final material characterization was attempted. The small number of samples available makes the statistical basis for conclusions weak; however, certain trends can be illustrated.

The techniques used were:

1. Structural Analysis

- a. Nuclear magnetic resonance
- b. Silica gel chromatography

2. Ultimate Analysis

- a. Carbon, per cent
- b. Hydrogen, per cent
- c. Sulfur, per cent
- d. Nitrogen, per cent
- e. Oxygen, per cent
- f. Ash, per cent

3. Molecular Weight (average)

4. Coke Yield (Conradson carbon)

5. Specific Gravity

4.2.9.1.1. Discussion of Analytical Procedures

Most procedures listed above are standard within the industry and will not be discussed in this report.

The most recent and promising analytical method is Nuclear Magnetic Resonance (NMR). In this procedure, a characterization based on hydrogen distribution including fused aromatic rings, substituted aromatic, olefinic, and alkyl groups is made.

The NMR spectra were recorded from a 10 per cent solution of the material in carbon disulfide. The spectra were obtained with a Varian A-60 spectrometer.

Proton (hydrogen) resonance absorptions were chemically classified according to Table 95. The raw materials have been assumed to possess predominantly hydrocarbon distributions.

Table 95. Chemical Shifts, δ , of Protons in Graphite Raw Materials

Proton Type	δ , p.p.m.
Heterocyclic (fused aromatic)	8.0-8.6
Aromatic ArH	7.0-8.0
Olefinic H-C=C-	5.0-6.0
Aromatic Methylene ArCH ₂ -	3.0-4.0
Aromatic Methyl ArCH ₃	2.2-3.0
Olefinic Methyl CH ₃ -C=C-	1.7-2.2
Nonaromatic Methylene -CH ₂ -CH ₂ -	1.2-1.4
Nonaromatic Methyl CH ₃ -C \leq	0.7-1.1

The NMR spectra were integrated in order to determine quantitatively the various proton types. The quantitative classification of the aliphatic hydrogen resonances cannot be considered precise due to overlapping of the various integral peaks. Aromatic/aliphatic ratios were also determined. Since the aromatic and aliphatic proton peaks are well separated, these ratios are believed to be accurate to within 2 per cent.

4.2.9.1.2. Discussion of NMR Results on Coker Feed Stocks (See Table 96)

a. Vacuum Residua

The three different vacuum residua are roughly comparable in composition. The aromatic contents are quite low and there is a preponderance of alkylated aliphatic species. The P-26 appears to have a slightly higher aromatic hydrogen content than the P-4 and P-13.

b. Atmospheric Residuum (Marathon Oil)

The hydrogen distribution of the atmospheric residuum P-16 is quite similar to that of the vacuum residua. The P-16 however, has a

Table 96. Properties of Commercial Coker Charge Stocks

Code No.	Type	Company	Location	Base of Crude Oil ⁽¹⁾	Virgin Stocks				Cracked Stocks			
					P-28	P-4	P-16	P-13	P-26	P-9	P-10	P-11
					Atm. Resid.	Vacuum Residuum	Atmos. Residuum	Vacuum Residuum	Vacuum Residuum	Decant. Oil	Thermal Cracking Tar	Thermal Cracking Tar
					Elk Refining	Marathon Oil	Marathon Oil	Marathon Oil	Marathon Oil	Marathon Oil	Marathon Oil	Pure Oil
					Falling Rock, West Va.	Robinson, Illinois	Robinson, Illinois	Texas City, Texas	Deerfoot, Michigan	Robinson, Illinois	Robinson, Illinois	Heath, Ohio
					P	I	I	I	N	-	-	-
					0.04	0.02	0.02	0.02	0	0.05	0.01	0.01
					0.10	0.10	0.10	0.10	0.19	0.06	0.06	0.07
					0.195	0.195	0.195	0.195	0.195	0.195	0.195	0.195
					84.03	86.21	85.94	86.08	86.77	85.08	85.08	85.08
					Carbon, %	Carbon, %	Carbon, %	Carbon, %	Carbon, %	Carbon, %	Carbon, %	Carbon, %
					12.63	10.84	11.63	11.15	11.46	9.70	9.70	9.70
					Hydrogen, %	Hydrogen, %	Hydrogen, %	Hydrogen, %	Hydrogen, %	Hydrogen, %	Hydrogen, %	Hydrogen, %
					1.57	1.67	1.62	1.64	1.64	1.77	1.77	1.77
					Conradson Carbon, %	Conradson Carbon, %	Conradson Carbon, %	Conradson Carbon, %	Conradson Carbon, %	Conradson Carbon, %	Conradson Carbon, %	Conradson Carbon, %
					0.2-0.1	0.1-0.7	0.4-0.3	0.7-0.5	0.7-0.5	7.6-12.7	4.5-10.0	4.5-10.0
					Oxygen, %	Oxygen, %	Oxygen, %	Oxygen, %	Oxygen, %	Oxygen, %	Oxygen, %	Oxygen, %
					0.1-0.2	0.6	0.5-0.6	0.6-0.8	0.5-0.5	0.3	0.3	0.3-0.6
					Nitrogen, % ⁽²⁾	Nitrogen, % ⁽²⁾	Nitrogen, % ⁽²⁾	Nitrogen, % ⁽²⁾	Nitrogen, % ⁽²⁾	Nitrogen, % ⁽²⁾	Nitrogen, % ⁽²⁾	Nitrogen, % ⁽²⁾
					1.0-0.2	0.6	0.5-0.6	0.6-0.8	0.5-0.5	0.3	0.3	0.3-0.6
					Vanadium, ppm ⁽³⁾	Vanadium, ppm ⁽³⁾	Vanadium, ppm ⁽³⁾	Vanadium, ppm ⁽³⁾	Vanadium, ppm ⁽³⁾	Vanadium, ppm ⁽³⁾	Vanadium, ppm ⁽³⁾	Vanadium, ppm ⁽³⁾
					1.0	0.6	0.5-0.6	0.6-0.8	0.5-0.5	0.3	0.3	0.3-0.6
					Molecular Weight	Molecular Weight	Molecular Weight	Molecular Weight	Molecular Weight	Molecular Weight	Molecular Weight	Molecular Weight
					1028	960-990	500	586	1100	130	370	270
					Mechnolab ⁽⁴⁾	Mechnolab ⁽⁴⁾	Mechnolab ⁽⁴⁾	Mechnolab ⁽⁴⁾	Mechnolab ⁽⁴⁾	Mechnolab ⁽⁴⁾	Mechnolab ⁽⁴⁾	Mechnolab ⁽⁴⁾
					786-797	754-901	374-495	607-628	785-800	286-296	321	272
					Distillation	Distillation	Distillation	Distillation	Distillation	Distillation	Distillation	Distillation
					270-274	270-274	270-274	270-274	270-274	270-274	270-274	270-274
					Characterization Analysis by Silica Gel Liquid Chromatography, (4) (weight per cent)	Characterization Analysis by Silica Gel Liquid Chromatography, (4) (weight per cent)	Characterization Analysis by Silica Gel Liquid Chromatography, (4) (weight per cent)	Characterization Analysis by Silica Gel Liquid Chromatography, (4) (weight per cent)	Characterization Analysis by Silica Gel Liquid Chromatography, (4) (weight per cent)	Characterization Analysis by Silica Gel Liquid Chromatography, (4) (weight per cent)	Characterization Analysis by Silica Gel Liquid Chromatography, (4) (weight per cent)	Characterization Analysis by Silica Gel Liquid Chromatography, (4) (weight per cent)
					Aromatic, %	Aromatic, %	Aromatic, %	Aromatic, %	Aromatic, %	Aromatic, %	Aromatic, %	Aromatic, %
					Non-aromatic, %	Non-aromatic, %	Non-aromatic, %	Non-aromatic, %	Non-aromatic, %	Non-aromatic, %	Non-aromatic, %	Non-aromatic, %
					Oxygen, %	Oxygen, %	Oxygen, %	Oxygen, %	Oxygen, %	Oxygen, %	Oxygen, %	Oxygen, %
					Loss, %	Loss, %	Loss, %	Loss, %	Loss, %	Loss, %	Loss, %	Loss, %
					Characterization Analysis by Nuclear Magnetic Resonance Spectroscopy (Atom per cent)	Characterization Analysis by Nuclear Magnetic Resonance Spectroscopy (Atom per cent)	Characterization Analysis by Nuclear Magnetic Resonance Spectroscopy (Atom per cent)	Characterization Analysis by Nuclear Magnetic Resonance Spectroscopy (Atom per cent)	Characterization Analysis by Nuclear Magnetic Resonance Spectroscopy (Atom per cent)	Characterization Analysis by Nuclear Magnetic Resonance Spectroscopy (Atom per cent)	Characterization Analysis by Nuclear Magnetic Resonance Spectroscopy (Atom per cent)	Characterization Analysis by Nuclear Magnetic Resonance Spectroscopy (Atom per cent)
					Hydrogen, %	Hydrogen, %	Hydrogen, %	Hydrogen, %	Hydrogen, %	Hydrogen, %	Hydrogen, %	Hydrogen, %
					Aromatic Hydrogen	Aromatic Hydrogen	Aromatic Hydrogen	Aromatic Hydrogen	Aromatic Hydrogen	Aromatic Hydrogen	Aromatic Hydrogen	Aromatic Hydrogen
					Aliphatic, %	Aliphatic, %	Aliphatic, %	Aliphatic, %	Aliphatic, %	Aliphatic, %	Aliphatic, %	Aliphatic, %
					Non-aromatic Hydrogen	Non-aromatic Hydrogen	Non-aromatic Hydrogen	Non-aromatic Hydrogen	Non-aromatic Hydrogen	Non-aromatic Hydrogen	Non-aromatic Hydrogen	Non-aromatic Hydrogen
					(ArCH ₃), %	(ArCH ₃), %	(ArCH ₃), %	(ArCH ₃), %	(ArCH ₃), %	(ArCH ₃), %	(ArCH ₃), %	(ArCH ₃), %
					Aromatic Methyl Hydrogen	Aromatic Methyl Hydrogen	Aromatic Methyl Hydrogen	Aromatic Methyl Hydrogen	Aromatic Methyl Hydrogen	Aromatic Methyl Hydrogen	Aromatic Methyl Hydrogen	Aromatic Methyl Hydrogen
					(CH ₃ -C-CH ₃), %	(CH ₃ -C-CH ₃), %	(CH ₃ -C-CH ₃), %	(CH ₃ -C-CH ₃), %	(CH ₃ -C-CH ₃), %	(CH ₃ -C-CH ₃), %	(CH ₃ -C-CH ₃), %	(CH ₃ -C-CH ₃), %
					Olefinic Methyl Hydrogen	Olefinic Methyl Hydrogen	Olefinic Methyl Hydrogen	Olefinic Methyl Hydrogen	Olefinic Methyl Hydrogen	Olefinic Methyl Hydrogen	Olefinic Methyl Hydrogen	Olefinic Methyl Hydrogen
					Non-aromatic Methylene Hydrogen	Non-aromatic Methylene Hydrogen	Non-aromatic Methylene Hydrogen	Non-aromatic Methylene Hydrogen	Non-aromatic Methylene Hydrogen	Non-aromatic Methylene Hydrogen	Non-aromatic Methylene Hydrogen	Non-aromatic Methylene Hydrogen
					Aliphatic	Aliphatic	Aliphatic	Aliphatic	Aliphatic	Aliphatic	Aliphatic	Aliphatic
					Peaks	Peaks	Peaks	Peaks	Peaks	Peaks	Peaks	Peaks
					(CH ₃ -C-), %	(CH ₃ -C-), %	(CH ₃ -C-), %	(CH ₃ -C-), %	(CH ₃ -C-), %	(CH ₃ -C-), %	(CH ₃ -C-), %	(CH ₃ -C-), %
					Aromatic Carbon, %	Aromatic Carbon, %	Aromatic Carbon, %	Aromatic Carbon, %	Aromatic Carbon, %	Aromatic Carbon, %	Aromatic Carbon, %	Aromatic Carbon, %
					Aliphatic Carbon, %	Aliphatic Carbon, %	Aliphatic Carbon, %	Aliphatic Carbon, %	Aliphatic Carbon, %	Aliphatic Carbon, %	Aliphatic Carbon, %	Aliphatic Carbon, %
					No. of Carbon atoms (whole sample) ⁽⁵⁾	No. of Carbon atoms (whole sample) ⁽⁵⁾	No. of Carbon atoms (whole sample) ⁽⁵⁾	No. of Carbon atoms (whole sample) ⁽⁵⁾	No. of Carbon atoms (whole sample) ⁽⁵⁾	No. of Carbon atoms (whole sample) ⁽⁵⁾	No. of Carbon atoms (whole sample) ⁽⁵⁾	No. of Carbon atoms (whole sample) ⁽⁵⁾
					56-74	56-74	56-74	56-74	56-74	56-74	56-74	56-74
					(1) P. B. Baffin, I. J. L. Baffin, U.S. Bureau of Mines Report Invest 3279, September, 1915	(1) P. B. Baffin, I. J. L. Baffin, U.S. Bureau of Mines Report Invest 3279, September, 1915	(1) P. B. Baffin, I. J. L. Baffin, U.S. Bureau of Mines Report Invest 3279, September, 1915	(1) P. B. Baffin, I. J. L. Baffin, U.S. Bureau of Mines Report Invest 3279, September, 1915	(1) P. B. Baffin, I. J. L. Baffin, U.S. Bureau of Mines Report Invest 3279, September, 1915	(1) P. B. Baffin, I. J. L. Baffin, U.S. Bureau of Mines Report Invest 3279, September, 1915	(1) P. B. Baffin, I. J. L. Baffin, U.S. Bureau of Mines Report Invest 3279, September, 1915	(1) P. B. Baffin, I. J. L. Baffin, U.S. Bureau of Mines Report Invest 3279, September, 1915
					(2) Underwood Method	(2) Underwood Method	(2) Underwood Method	(2) Underwood Method	(2) Underwood Method	(2) Underwood Method	(2) Underwood Method	(2) Underwood Method
					(3) Dumas Method	(3) Dumas Method	(3) Dumas Method	(3) Dumas Method	(3) Dumas Method	(3) Dumas Method	(3) Dumas Method	(3) Dumas Method
					(4) Spectrophotometric	(4) Spectrophotometric	(4) Spectrophotometric	(4) Spectrophotometric	(4) Spectrophotometric	(4) Spectrophotometric	(4) Spectrophotometric	(4) Spectrophotometric
					(5) Estimated from molecular weight	(5) Estimated from molecular weight	(5) Estimated from molecular weight	(5) Estimated from molecular weight	(5) Estimated from molecular weight	(5) Estimated from molecular weight	(5) Estimated from molecular weight	(5) Estimated from molecular weight
					(6) Estimated from boiling point and density, I.E.C., Vol. 27, No. 12, 1460-1464, December, 1915	(6) Estimated from boiling point and density, I.E.C., Vol. 27, No. 12, 1460-1464, December, 1915	(6) Estimated from boiling point and density, I.E.C., Vol. 27, No. 12, 1460-1464, December, 1915	(6) Estimated from boiling point and density, I.E.C., Vol. 27, No. 12, 1460-1464, December, 1915	(6) Estimated from boiling point and density, I.E.C., Vol. 27, No. 12, 1460-1464, December, 1915	(6) Estimated from boiling point and density, I.E.C., Vol. 27, No. 12, 1460-1464, December, 1915	(6) Estimated from boiling point and density, I.E.C., Vol. 27, No. 12, 1460-1464, December, 1915	(6) Estimated from boiling point and density, I.E.C., Vol. 27, No. 12, 1460-1464, December, 1915
					(7) Estimated from molecular weight	(7) Estimated from molecular weight	(7) Estimated from molecular weight	(7) Estimated from molecular weight	(7) Estimated from molecular weight	(7) Estimated from molecular weight	(7) Estimated from molecular weight	(7) Estimated from molecular weight
					(8) MW = % Carbon + 12	(8) MW = % Carbon + 12	(8) MW = % Carbon + 12	(8) MW = % Carbon + 12	(8) MW = % Carbon + 12	(8) MW = % Carbon + 12	(8) MW = % Carbon + 12	(8) MW = % Carbon + 12

higher concentration of alkanes than the latter. The aliphatic CH_3 and CH_2 peaks account for 90 per cent of the total hydrogen in the atmospheric residuum and for only about 80 per cent of the total in the vacuum residuum.

c. Atmospheric Residuum (Elk Refining)

The NMR behavior of P-28 was quite unusual. Only a highly broadened combined aliphatic CH_3 - and CH_2 - peak could be observed. The $(\text{CH}_3)_4\text{Si}$ reference peak was also considerably broadened. These results indicate the presence of many soluble free radicals in the F-28 resin. Such paramagnetic products would probably be aromatic and not observable by NMR. These results are consistent with the high thermal expansion of the resultant graphite.

d. Slurry Oil (Marathon Oil)

The slurry oil, P-9, is considerably more aromatic than the vacuum residua and contains some heterocyclic or large polycyclic systems. The lower aliphatic hydrogen content is reflected by the decreased aliphatic CH_2 and olefinic CH_3 NMR absorptions.

e. Thermal Residuum (Marathon Oil)

The P-10 material is even more aromatic than the slurry oil. A large number of aromatic alkyl groups are in evidence. The aliphatic CH_2 and CH_3 and the olefinic CH_3 contents are quite low. The composition of this material should lead to a very thermally reactive material.

f. Thermal Tar (Pure Oil)

The total aromatic content of the thermal tar is comparable to that of the thermal residuum sample. A significant difference, however, is observed between the NMR spectra of these two materials. The thermal tar shows sharp individual methyl absorptions at about 2.2, 2.4, and 2.6 ppm. These peaks are associated largely with methyl groups on small aromatic ring systems, e. g.: benzene and naphthalene. The aromatic methyl peak for the thermal residuum is typically broad and falls between 2.3 and 2.8 ppm. This broad peak can be attributed to a complex mixture of methylated aromatics which includes ring systems larger than naphthalene. The aromatic proton peak of the thermal tar is at higher fields than that of the thermal residuum which again indicates the presence of larger ring systems in the latter.

NMR offers a precise means of ascertaining the percentage of aromatic hydrogen. Listed in Table 97 are the aromatic and aliphatic hydrogen contents of the various raw materials. As long as the raw materials are soluble, the NMR integral curves accurately determine the relative numbers of hydrogens directly on aromatic rings and those on aliphatic side chains.

Table 97. Hydrogen Composition of Graphite Raw Materials

Material	%ArH	%AlH
P-4	1.3	98.7
P-13	1.8	98.2
P-26	3.7	96.3
P-9	19.4	80.6
P-10	30.4	69.6
P-11	34.1	65.9
P-16	3.4	96.6
P-28	----	----

In order to determine the extent of aromatic carbon, we must take into account not only the aromatic/aliphatic hydrogen ratio, but also the extent of substitution and average aromatic ring size. The hydrogen distribution data can be corrected to reflect aromatic/aliphatic carbon ratios if the following assumptions are made:

1. All aromatic carbon atoms are substituted by either hydrogen or alkyl groups.
2. All the aliphatic carbons contain at least one hydrogen substituent.

These assumptions become less valid when the average aromatic ring size becomes greater than one or when tertiary aliphatic groups are present.

Listed in Table 98 are the aromatic and aliphatic carbon percentages calculated with these assumptions. The aromatic contents are believed to be minimum values since the presence of any larger ring systems would raise these percentages. Included in Table 98 are the percentages of aromatics by weight which have been determined by elution chromatography. These values are not believed to be as reliable as the data obtained by NMR. The chromatographic method does not exclusively separate aliphatic and aromatic components. Furthermore, it is the actual aromatic carbon content rather than the amount of compounds containing aromatic rings which should be related to coking behavior.

NMR analyses of petroleum-derived raw materials indicate a wide distribution of proton types ranging from heterocyclic and large fused aromatic-ring protons to those associated with long-chain aliphatic groups. In order to determine how these proton types are distributed molecularly within the total material, a representative petroleum oil was chromatographically extracted and the chromatographic extracts were examined by NMR.

Table 98. Aromatic Carbon Content of Raw Materials

Material	NMR*		Chromatography**	
	% Aromatic C	% Aliphatic C	% Aromatic C	% Aliphatic C
P-4	10.5	89.5	32.2	60.5
P-13	13.6	86.4	41.9	53.8
P-26	15.5	84.5	--	--
P-9	43.2	56.8	61.4	33.0
P-10	59.2	40.8	63.6	32.1
P-11	63.0	37.0	89.8	5.0
P-16	11.6	88.4	35.2	58.4
P-20	79.5	20.5	95.5	0.1

*Atom per cent of carbon.

**Weight per cent of components.

The material chosen was the slurry oil P-9 which was chromatographically extracted with a variety of solvents over an alumina column. A total of 57 fractions were collected. These fractions were combined on the basis of similarity of IR spectra into groups and NMR spectra were then obtained for the combined fractions. The hydrogen distribution data for each group are given in Table 99.

Table 99. Hydrogen Composition of Slurry Oil P-9 and Chromatographed Fractions*

Fractions	Heter.***	ArH%	Olef. %	ArCH ₂ %	ArCH ₃ %	CH ₂ -C=C%	CH ₂ -CH ₂ %	CH ₂ -CH ₃ %
(1) P-9 (unchromatographed)	2.3	17.1	-	4.8	14.9	Slight	44.8	16.0
(2) Fract. 1-3	-	-	-	-	-	-	75.0	25.0
(3) Fract. 4-5	8.0	27.8	3.4	8.5	34.0	Slight	14.2	4.0
(4) Fract. 6-11	8.4	33.3	-	12.4	35.9	~ 2.6	5.2	2.0
(5) Fract. 12-20	6.9	40.1	-	8.9	34.3	-	-	9.8***
(6) Fract. 21-30	15.5	35.8	-	10.0	29.4	-	-	9.0***
(7) Fract. 31-49	13.6	32.0	-	6.1	37.4	-	-	10.1***
(8) Fract. 50-57	Highly aromatic, insoluble in CS ₂							

*Hydrogen composition is measured in atom per cent.

**Also includes polycyclic aromatics.

***The aliphatic CH₂ and CH₃ peaks could not be separated in these materials.

The first major products collected from P-9 were combined into fractions 1-3. This material was aliphatic and waxlike. NMR integration of the aliphatic CH₂ and CH₃ peaks indicated an average molecular size of 11 carbon atoms for this wax. At least 80 per cent of the aliphatic hydrogen found for P-9 could be attributed to this waxlike material.

The next extract, fractions 4-5, contained some of the aliphatic wax but was predominantly aromatic with a high degree of aromatic methyl substitution. Fractions 6-11 are almost entirely aromatic with extensive CH_3 and CH_2 substitution on the aromatic rings. Fractions 12-20 are similar to 6-11 except that the minor aliphatic CH_2 and CH_3 peaks are no longer separable.

In fractions 21-49, the aromatic proton peak at 8.0 to 8.6 ppm has noticeably increased. Although this peak is listed in the heterocyclic column, it is more likely the result of fused polycyclic ring systems such as phenanthrenes and anthracenes, which absorb in this region. The final fractions, 50-57, are highly aromatic and insoluble in CS_2 .

These results demonstrate that the high degree of aliphatic hydrogen in P-9, and presumably in other petroleum-derived raw materials, is associated with an aliphatic waxlike material which should not contribute to any extent to the coking value. The aromatics in P-9 are largely methylated, a factor which should increase their thermal reactivity.

4.2.9.1.3. Correlation Studies of Coker Feed Stocks

As previously indicated, no statistical correlation was attempted due to the small number of samples and the large number of variables. The following trends were noted:

Aromatic carbon content can be related to coke yields although this relationship is not quantitative as seen in Table 100.

Table 100. Relationship of Aromatic Carbon Content to Coke Yield

Number	Aromatic Carbon, % C _A , %	Conradson Carbon, %	Raw Coke Yield, % Atmos. Pressure Coking
<u>Vacuum Residuum</u>			
P-4	10.5	14.1-15.6	23.3
P-13	13.6	5.6-7.5	13.4
P-26	15.5	7.8	21.4
<u>Atmos. Residua</u>			
P-28	0	1.6-2.4	6.5
P-16	11.6	5.5-6.3	10.0
<u>Catalytic Residuum (Decant Oil)</u>			
P-9	43.2	7.6-12.7	21.0
<u>Thermally Cracked (Decant Oil)</u>			
P-10	59.2	15.2-18.6	28.6
<u>Thermal Residue from Virgin Gas Oil</u>			
P-11	63.0	10.0-11.8	20.8

An approximate relation between the thermal expansion and the aromatic carbon concentration in the coke can be shown from the data in Table 101. The aromatic carbon concentration is measured as

$$\frac{C_A}{\text{Coke Yield}} = \frac{(\text{gms aromatic carbons/gms feed stock})}{(\text{gms of coke/gms feed stock})} = \frac{\text{gms aromatic carbons}}{\text{gms of coke}}$$

and is a direct measure of the carbon atoms in the coke that contribute to the ultimate structure of the graphite.

Table 101. Relationship of Thermal Expansion to Aromatic Carbon Content of Feed Stocks

Charge Stock	C _A , %	Yield, % (Atm. Coked)	C _A , % Yield, %	Thermal Expansion 10 ⁶ /°C (30-100°C)		
				Atrm-Coked Avg.	Extruded Rod Max.	Min.
<u>Vacuum Residuum</u>						
P-4	10.5	23.3	0.45	1.47	1.50	1.44
P-13	13.6	13.4	1.01	1.15	1.16	1.13
P-26	15.5	21.4	0.72	0.73	0.97	0.60
<u>Atmos. Residua</u>						
P-28	0	6.5	0	2.74	2.89	2.60
P-16	11.6	10.0	1.16	1.29	1.32	1.26
<u>Catalytic Residuum (Decant Oil)</u>						
P-9	43.2	21.0	2.06	0.45	0.46	0.43
<u>Thermally Cracked (Decant Oil)</u>						
P-10	59.2	28.6	2.07	0.49	0.52	0.40
<u>Thermal Residue from Virgin Gas Oil</u>						
P-11	63.0	20.8	3.03	0.47	0.52	0.43

*C_A = gms aromatic carbon/gms feed stock

4.2.9.2. Asphalts

Air oxidation of petroleum hydrocarbon feed stocks has been employed in the production of high thermal expansion cokes and graphites.

A number of the air-blown products have been examined by standard analytical methods. In addition, a study of the chemical effects of the oxidation has been made using nuclear magnetic resonance, infrared analysis, and electron spin resonance techniques.

The materials which were examined, along with a description of their origin, are given in Table 102.

Table 102. Air-Blown Asphalts Examined

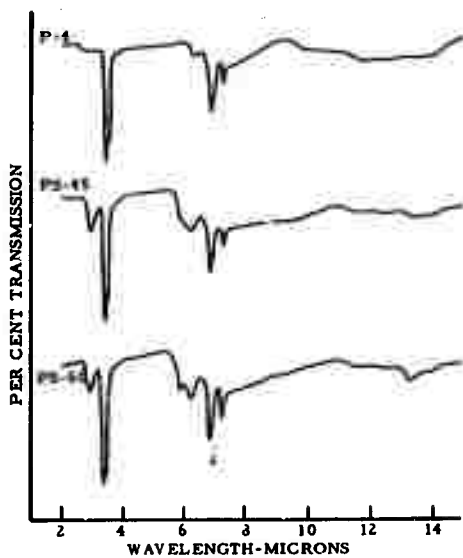
Initial Charge Stock	Asphalt	Origin
P-4	PS-44 PS-45 PS-60	Residue from the vacuum distillation of an intermediate crude
P-26	PS-114 PS-124	Residue from the vacuum distillation of a naphthenic crude
P-28	PS-127 PS-129	Residue from the atmospheric distillation of a paraffinic crude
P-9	PS-80 PS-51 PS-111	Residue from the distillation of catalytically cracked mixed gas oil

4.2.9.2.1. IR Analysis of Air-Blown Asphalts

Figures 93 and 94 display a series of infrared spectra for air-blown asphalts produced from the vacuum residuum P-4 and the slurry oil P-9.

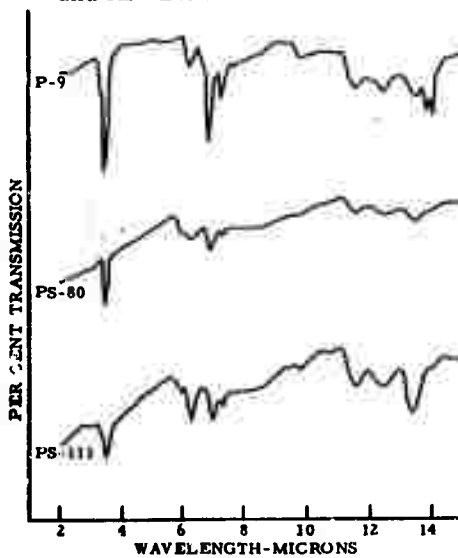
The IR spectra in Figure 93 indicates a small increase in the aromatic content during the air blowing of P-4. The IR spectrum of PS-60 in Figure 93 shows the definite growth of the aromatic substitution peak at 13 microns. The most significant change, however, is the appearance of the carbonyl group with an IR band at 5.9 microns. The appearance of this group provides evidence of direct oxidation.

The P-9 behaves similarly to the P-4 during air blowing. The IR spectrum of PS-80 in Figure 94 shows the increase in aromaticity and extensive C=O formation. The paraffinic component (absorptions at 13.75 and 13.95 microns) found in P-9 appears to be absent in the PS-80. This constituent has either been oxidized or been more likely volatilized in the process. The infrared spectrum of PS-111 shows a considerable increase in aromaticity plus an unexpected decrease in carbonyl content. This result is consistent since the carbonyl function which is introduced by oxidation serves as a site of bond cleavage in the aromatic ring systems. This



N-6367

Figure 93. Infrared Spectra of Vacuum Residuum P-4 and Air-Blown Products



N-6368

Figure 94. Infrared Spectra of Slurry Oil P-9, and Air-Blown Products

cleavage should produce nonplanar radical entities and thus induce the formation of disordered graphite.

4.2.9.2.2. NMR Analyses of Air-Blown Asphalts

NMR spectra were obtained for all of the air-blown asphalts listed in Table 103. Many of the asphalts possessed limited solubility in CS_2 and therefore only the CS_2 soluble portions could be examined. The NMR spectra for these products were uninformative. At best, only the single aliphatic CH_2 and aliphatic CH_3 peaks at 0 to 2 ppm could be resolved. The aromatic proton absorptions were highly broadened and unresolved. In many instances, the aliphatic bands as well as the reference $(\text{CH}_3)_4\text{Si}$ peak were extensively broadened. These results could be attributed to the presence of large concentrations of soluble free radicals in the air-blown asphalts.⁽¹⁸⁷⁾ Free radical formation through oxidative dehydrogenation is believed to be an important chemical effect of air blowing.

Figure 95 shows a series of NMR spectra for the air-blown asphalts derived from slurry oil P-9. The first air-blown product, PS-80, resembles the starting P-9 in its dominant composition, although the resolution of the spectrum has somewhat deteriorated. Continued oxidation results in the production of the asphalt PS-51, which shows an almost complete absence of the aliphatic CH_3 absorption at 0.9 ppm. The aliphatic CH_2 peak at 1.2 ppm is still prominent, but the aromatic proton peaks at 7.0 to 8.0 ppm and the aromatic CH_3 peaks at 2.0 to 3.0 have been appreciably broadened. With extended air blowing, the spectra obtained for PS-111 is observed. The aromatic proton and aromatic methyl peaks are extremely broad and almost lost in the noise. A broadened aliphatic CH_2 peak is still evident. The reference $(\text{CH}_3)_4\text{Si}$ proton peak at 0.0 ppm is also evidently highly broadened. These results suggest that continued air oxidation results in an increase concentration of soluble free radicals. The quantitative results of any NMR analysis of such materials are felt to be unreliable.

4.2.9.3. Electron Spin Resonance

4.2.9.3.1. Electron Spin Resonance (ESR) of Air-Blown Asphalts

The broad NMR lines observed for the air-blown asphalts strongly suggested the presence of high concentrations of free radicals. Since free radicals are known to be important in determining the paths of carbonization reactions, detailed ESR measurements were performed for two representative oils and their air-blown asphalt products. The two oils chosen for the study were P-9, a highly aromatic slurry oil, and P-4, a relatively nonaromatic vacuum residuum. The conduction ESR in graphites made from two air-blown materials produced from P-4 and P-9 was also investigated. Table 103 summarizes the ESR data for the oils and air-blown asphalts. The ESR results are discussed in the following sections.

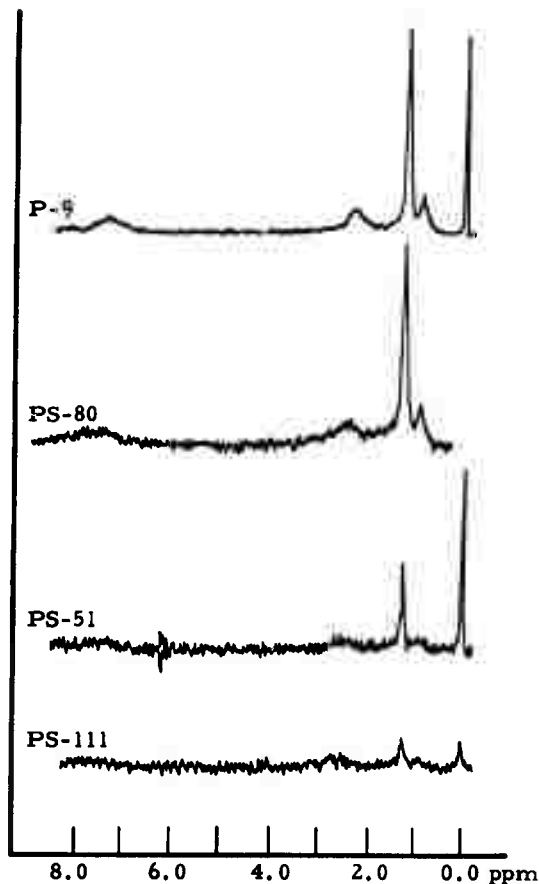


Figure 95. NMR Spectra of Air-Blown Asphalts from Slurry Oil P-9 N-6710

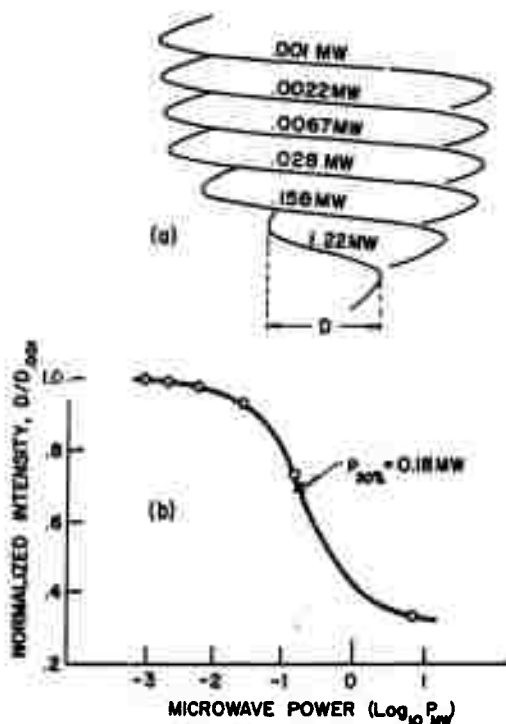
Table 103. ESR Results for Air-Blown Refinery Oils

	Saturation P _{30%} (mw.)	Linewidth (δ_F)		
		Gauss	Spins/gram	g-Factor
P-9 (Slurry Oil)	0.15	7.6	0.72×10^{18}	2.00260
PS-80 (Air-blown P-9)	0.037	5.1	5.0	2.00298
PS-51 (Air-blown P-9)	0.080	5.7	7.0	2.00285
PS-111 (Air-Blown P-9)	0.18	5.7	21.6	2.00259
P-4 (Vacuum Residuum)	0.45	4.8	1.2×10^{18}	2.00259
PS-44 (Air-Blown P-4)	0.23	4.4	2.8	2.00286
PS-45 (Air-Blown P-4)	0.33	4.5	4.4	2.00285
PS-60 (Air-Blown P-4)	0.33	4.7	3.7	2.00286

4.2.9.3.2. Saturation Measurements

The ESR signals in all the oils and air-blown asphalts were easily saturated. Saturation of the ESR is a result of a long spin-lattice relaxation time for the unpaired electrons in the organic free radicals in the materials. Long relaxation times are observed for all carbonized materials which have not been heated above $\sim 400^\circ\text{C}$.^(15a)

The results of saturation measurements on sample PS-111 are shown in Figure 96. The derivative curves in Figure 96 (a) were measured using superheterodyne detection. The saturation measurements were made by removing a known amount of attenuation between the Klystron and the sample and adding the same amount between the sample and the detector. By this method, all the curves would be the same height in the absence of saturation.



N-7115

Figure 96. Saturation Measurements on Sample PS-111: (a) ESR Curves for Different Microwave Powers; (b) Normalized Intensity as a Function of Microwave Power

The saturation curve in Figure 96 (b) was obtained by plotting the normalized heights, $D/D_{.001}$ vs. the log of the microwave power. The height $D_{.001}$ used for normalization corresponds to the unsaturated situation. The quantity $P_{30\%}$ is the microwave power required to produce 30 per cent saturation (decrease in height). For similar materials having saturation curves of the same shape, $P_{30\%}$ would be directly proportioned to T_1 , the spin-lattice relaxation time. Although a quantitative calibration to determine absolute T_1 's was not made, previous measurements showed that a value of $P_{30\%} = .18$ mw corresponded to a T_1 of between 10^{-4} and 10^{-6} seconds. For a relative comparison of samples, the $P_{30\%}$ values are listed in Table 103. Note that the oxidation of both P-4 and P-9 produces a sharp drop in $P_{30\%}$, followed by an increase with further oxidation.

Unlike many other low temperature cokes and chars, ⁽¹⁵⁹⁾ physically adsorbed atmospheric oxygen has no apparent effect on the spin-lattice relaxation time (or linewidth) of the ESR for all these materials. The reason is that the starting oils and air-blown products are tar-like and have a very low surface area.

4.2.9.3.3. Free Radical Concentration

The ESR results clearly show that air blowing increases significantly the free radical concentration in the oils P-4 and P-9. The free radical concentration (electron spins/gram) in Table 103 increases by a factor of 30 for the aromatic oil P-9 but only by a factor of 3 or 4 for the nonaromatic P-4.

The spin concentration determinations involve two important assumptions. First, all the ESR lines have a Lorentz shape; and second, the paramagnetism follows Curie's Law. Although we have not tested these assumptions quantitatively, the appearance of the curves and the known behavior of other low-temperature carbonaceous materials ⁽¹⁵⁸⁾ indicate that these assumptions are valid for all the oils measured. In order to avoid saturation, all spin concentration measurements were made at a microwave power of 30 microwatts. Figure 97 shows the ESR signal for an 87 milligram sample of P-9. The ruby signal is used as an internal calibration of instrument sensitivity. The spin concentration (taking amplifier gains into account) is directly proportional to the produce S^2D , which is also proportional to the static paramagnetic susceptibility of the material.

4.2.9.3.4. g-Factors

The g-factor for a material which exhibits ESR is defined by the basic resonance equation

$$h\nu = g\beta H,$$

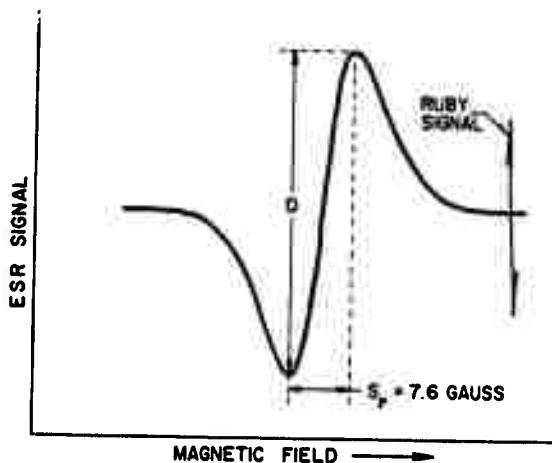


Figure 97. ESR Signal for P-9; (The Parameters D and S_p and the Height of the Ruby Signal are used to Calculate Free Radical Concentration) N-7116

where H = the magnetic field at maximum absorption (zero slope on the derivative curve),

β = the Bohr magneton,

h = Planck's constant,

and ν = the microwave frequency.

For a free electron, the g -factor is 2.0023. For unpaired electrons in free radical molecules, the g -factor differs from this value depending on the types of atoms in the molecule and the strength of interaction of the unpaired electrons with the atoms. For example, the g -factor for aromatic hydrocarbon radicals can exhibit g -factors as high as 2.005.⁽¹⁶⁰⁾ Since g -factors for the SR oils and asphalts could be measured with an accuracy of 1 or 2 parts in 200,000, it was possible to differentiate between hydrocarbon radicals and oxygen-containing radicals.

Table 103 lists the g -factors for the oils and their air-blown products. For the aromatic slurry oil, there is initially a large increase in g -factor with air blowing followed by a decrease to the original value after considerable air blowing. For the nonaromatic vacuum residuum, the initial increase is not as great. Furthermore, additional air blowing

does not change the g -value further. The significance of these changes in g -value with air blowing is discussed in Section 4.2.9.3.7.

4.2.9.3.5. Linewidths

The linewidths S_F , measured between peaks on the derivative curve (Figure 97) are shown in the third column of the table. The linewidths are typical of those observed for low-temperature cokes and chars.^(15a) Again, due to the small surface areas of the samples, no effects of atmospheric oxygen on the linewidth were observed.

4.2.9.3.6. ESR of Graphites Made from Air-Blown Asphalts

The conduction electrons in graphite also exhibit an ESR.^(16b, 16a) The line shape and g -factor of the signal are indicative of the crystalline size and impurity content of the graphite.

We examined small chips of two graphite samples made from PS-80-34-5 (an air-blown P-9) and PS-45-32-3 made from PS-45 (an air-blown P-4). The ESR curve for the former is shown in Figure 98(a), and for the latter in Figure 98(b). The curve (a) is typical of that obtained for highly graphitic materials prepared from petroleum cokes.^(16a) The broad asymmetric absorption extending to lower magnetic fields is due to incomplete averaging of the g -factor anisotropy by electron motion. The curve (b) is typical of that observed for graphites of small crystallite size, such as lampblack-base graphite.^(16a) The g -factor of 2.014 and the relatively sharp signal indicate fairly complete averaging of the anisotropy by rapid electron diffusion between crystallites.

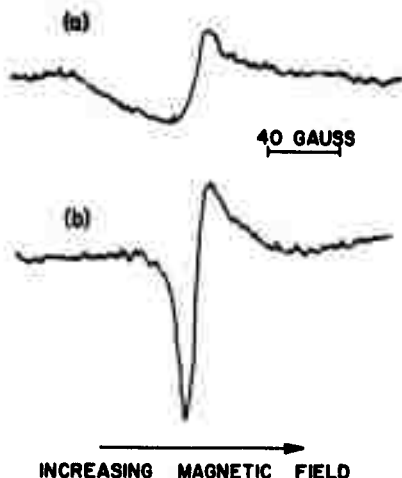


Figure 98. ESR of Graphites Made from Air-Blown Asphalts: (a) PS-80, (b) PS-45

N-7117

4.2.9.3.7. Discussion

The increase in free radical concentration by air blowing is consistent with the NMR observations of the increase in broadening with air blowing shown in Figure 95. In fact, as Gutowsky and Tai have found,⁽¹⁵⁷⁾ the linewidth of an NMR signal can be used to determine free radical concentrations in solution.

The identity of the free radicals formed by oxidation and the mechanism of their formation is not known. IR measurements show that oxidation increases the aromaticity of the starting oils and also introduces carbonyl groups. De Ruiter and Tschamler,⁽¹⁶⁸⁾ who observed an increase in the free radical content of coals with oxidation, suggested semiquinone formation. This same mechanism seems reasonable for the increase in free radicals in the asphalts resulting from air blowing.

Air blowing produces much larger changes in the aromatic oil P-9 than in the nonaromatic oil P-4. Although the extent of air blowing may not have been identical for the two materials, the melting point and oxygen analysis data in Table 104 do indicate that both the P-4 and P-9 series were altered by approximately the same amount. We concluded that the oxidation of aromatic oils produces more free radicals than the oxidation of nonaromatic oils.

The g-factor measurements indicate that the free radicals formed by oxidation contain oxygen. The fixation of oxygen was also observed in the infrared spectra and the chemical analyses of these materials. With further air blowing, the g-factor (at least in the case of materials derived from P-9) decreases. This result is consistent with the oxygen analyses in Table 104, which show a loss of oxygen with continued air blowing.

The saturation measurements indicate that the oxygenated radicals have a somewhat longer spin-lattice relaxation time than the radicals initially present. The changes in saturation properties correlate with the changes of the other ESR properties in Table 103.

The ESR measurements on the graphite samples show that the graphite made from an air-blown product of the aromatic P-9 oil has a much larger crystallite size than that made from the air-blown product of the much less aromatic P-4 oil. Apparently, even though air blowing can cause increased disorder in the final graphite, air-blown P-9 still produces a fairly well-ordered graphite.

4.2.9.4. Bench-Scale Graphite Evaluation of Air-Blown Asphalts

Property data of graphites made from various petroleum oils and their air-blown products are compared in Table 104 with the physical and chemical properties of the base material.

A qualitative relationship exists between thermal expansion of the graphite and C/H ratio - Conradson Carbon - asphaltenes - melting point of the charge stock.

Hydrogen and carbon distribution by NMR fails to yield any clues due to extreme peak broadening of the NMR spectrum.

Free radical analysis through ESR techniques holds the best hope for correlation although it was shown that the extent of free radical formation was a function of aromaticity of the base oil.

A statistical analysis was not performed due to the large number of variables and small number of samples.

It would be desirable in any future program to expand the analytical approach to encompass a chromatographic separation scheme followed by application of ESR, IR, etc., techniques to each fraction.

As with coker feed stocks, any measurements which are dependent on molecular structure would be helpful in determining the quality of the resultant coke and graphite.

4.3. Pitch Binder Studies

The following approach will be limited to a statistical study of 1) the variation of graphite properties (including strength) due to sample preparation, and 2) the variation of flexural strength with binder properties.

4.3.1. Binders and the Sample Making Process

4.3.1.1. Physical Property Variation of 3-Inch Diameter Molded Plugs

In order to find the expected variation of a standard billet for comparison with experimental materials, 31 3-inch diameter by $3\frac{1}{2}$ -inch length molded graphite billets were prepared and tested.

The binder used was a typical 110°C melting point coal tar pitch (30 hard) made by Barret Division of Allied Chemical Corporation. The filler was a calcined petroleum coke supplied by Continental Oil Company.

Normal preparation of these billets consisted of sizing the filler to a 55 flour, mixing with 32 parts per hundred of pitch and molding to a green density of about 1.63. The billets were then baked to 1000°C followed by graphitization to approximately 2800°C. Density, volume shrinkage and weight loss information was obtained on the billets. After processing, the billets were cut into $\frac{1}{2}$ - by $\frac{1}{2}$ - by $2\frac{1}{2}$ -inch samples. About three with-grain and four across-grain samples for bulk density, specific resistance, Young's modulus, and flexural strength measurements could be obtained from each billet. An additional two samples in each grain direction could be obtained for thermal expansion measurements (30-100°C).

Average property values were established for each billet and then these averages combined and manipulated to give the statistical information shown in Table 105. Variation was greatest for volume shrinkage and thermal expansion measurements (about 40 and 25 per cent of the

Table 105. Statistical Data for 3-Inch Diameter Molded Plugs

Property	Plugs Made With 30 Hard Coal Tar Pitch and Commercial Coke			Plugs Made With Petroleum Pitch and Commercial Coke		
	N	X	σ	N	X	σ
Green Density, g/cc (molded billets)	31	1.631	0.035	20	1.586	0.039
Baked Density, g/cc (1000°C baked billets)	31	1.536	0.035	20	1.501	0.017
Graphitized Density, g/cc	31	1.529	0.026	20	1.506	0.035
Volume Shrinkage, per cent (from bake to graphitization)	30	2.54	0.972	20	3.20	2.27
Weight Loss, per cent (from bake to graphitization)	29	3.16	0.419	20	2.946	0.381
Specific Resistance, 10 ⁻⁴ ohm cm, W/G Averages	26	12.96	1.999	18	13.13	1.828
	26	19.05	4.030	18	20.56	3.292
Maxima	26	13.71	1.529	18	13.71	1.930
Minima	26	20.87	4.644	18	21.89	3.869
Averages	26	12.21	1.625	18	12.47	1.835
Young's Modulus, 10 ⁶ lbs/in ²	26	17.31	3.980	18	19.16	2.940
	26	0.603	0.957	18	0.600	0.031
Maxima	26	0.363	0.050	18	0.321	0.030
Minima	26	0.635	0.060	18	0.636	0.046
Averages	26	0.385	0.061	18	0.341	0.029
Flexural Strength, lbs/in ²	26	0.577	0.059	18	0.561	0.036
	26	0.342	0.045	18	0.297	0.035
Maxima	26	1077	154	18	1007	160
Minima	26	771	160	18	681	121
Averages	26	1166	174	18	1095	176
Thermal Expansion, 10 ⁻⁶ /°C	26	834	171	18	761	135
	26	1001	141	18	899	182
Maxima	26	698	148	18	590	140
Minima	26	1.36	0.336	18	1.364	0.334
Averages	27	2.52	0.331	18	2.681	0.482
Flexural Strength, lbs/in ²	26	1.44	0.317	18	1.446	0.341
Thermal Expansion, 10 ⁻⁶ /°C	26	2.59	0.367	18	2.797	0.530
Maxima	26	1.27	0.370	18	1.279	0.351
Minima	26	2.44	0.315	18	2.561	0.482

respective averages) and least for bulk density (less than 3 per cent of the average). The flexural strength data was used for the regression analysis studies in Section 4.3.1.2.

In order to compare the standard billets with an experimental material, 20 billets were made using the calcined coke, and an experimental petroleum pitch similar to 30 hard pitch. Processing was carried out as before, and the results are reported in Table 105. The greatest variation was in volume shrinkage and thermal expansion, and there was less variation in Young's modulus.

Analytical properties of the two pitches are given in Table 106.

Table 106. Analytical Properties of 30 Hard Pitch and an Experimental Petroleum Pitch

Property	30 Hard Pitch	Petroleum Pitch
Melting Point, °C (CIA)	110	111
Specific Gravity, g/cc	1.338	1.26
Benzene Insolubles, weight per cent	30.0	27.1
Quinoline Insolubles, weight per cent	12.7	3.41
Conradson Carbon, weight per cent	54.9	55.3
Carbon/Hydrogen, weight ratio	92.98/4.22	93.71/5.14
Ash, weight per cent	0.11	0.011
Sulfur, weight per cent	0.50	0.50
Molecular weight	> 700	---

4.3.1.2. Graphite Flexural Strength Versus Binder Characteristics

4.3.1.2.1. Regression Analysis of Graphite Flexural Strength Versus Binder Properties

The relationship between flexural strength of graphite and its binder properties is not precisely known. There are, however, several properties that are believed to contribute to the strength. Among these are:

[Benzene Insoluble content, weight per cent
 Quinoline Insoluble content, weight per cent
 Conradson Carbon, weight per cent
 Melting Point, °C
 Specific Gravity, g/cc
 Carbon Content, weight per cent
 Hydrogen Content, weight per cent
 Carbon/Hydrogen, atomic ratio
 Ash, weight per cent]

Regression analyses were used to try to relate these properties to the flexural strength of 67 sets of 3-inch diameter molded graphite billets. A variety of experimental petroleum, coal tar and other pitches was used as binder with petroleum coke. Billets were made as described in Section 4.3.1.1., but with some variations in amount of binder and billet density. The binder properties and flexural strengths for each set of billets are shown in Table 107.

The stepwise multiple regression used with the data did not show high correlation for any combination of the variables used. This included:

1. Each property separately
2. The square of each property separately
3. The logarithm of each property separately
4. Combinations of the properties and/or squares
5. Combinations of the logarithms of the properties
6. Combinations of all possible cross products of the properties

The number of regression steps was limited to 50, hydrogen content was deleted because of high correlation with carbon content.

The best coefficient of variation obtained was ± 24 per cent. For 95 per cent confidence limits a predicted value could be in error by about 475 lbs./in.² (based on an average with-grain strength of 950 lbs./in.²).

The standard deviation of the 67 sets of billets was 355 lbs./in.². Use of the regression equation reduced this to 228 lbs./in.². In Section 4.3.1.1. it was shown that the billet-making process introduced an error (standard deviation) of about 154 lbs./in.². The remaining 74 lbs./in.² was unaccounted for and indicated that the binder properties measured did not include all the contributing properties, that the variables were used incorrectly, or that the reproducibility of experiments and tests was too poor for the relationship among the variables to be found from only 67 data sets. The most heavily weighted properties were carbon content, benzene insolubles, and specific gravity.

The regression equations are shown in Table 108. In addition to use of the regression equation, correlation coefficients were tested for the binder properties versus each other. There were no significant correlations ($R^2 > 0.75$).

4.3.1.2.2. Flexural Strength Versus a Characterization Factor

Charette and Bischofberger⁽¹⁸⁴⁾ found a correlation between compressive strength of carbon anodes and a characterization factor obtained

Table 107. Binder Characteristics and Graphite Flexural Strength

Code Number	Benzene Insolubles Per Cent	Quinoline Insolubles Per Cent	Conradson Carbon Per Cent	Melting Point °C	Specific Gravity g/cc	Carbon Per Cent	Hydrogen Per Cent	Atomic C/H	Flexural Strength	
									W/G	lbs./in. ² A/G
P-105	21.0	1.5	50.9	120	1.25	92.50	5.11	1.52	743	489
P-106	1.9	0.1	49.9	110	1.20	92.11	6.14	1.26	1031	695
P-109	1.9	0.3	29.2	71	1.06	87.96	9.08	0.81	379	275
P-110	27.1	3.4	54.4	111	1.26	93.66	5.27	1.49	1160	960
P-511	14.8	10.2	57.2	102	1.30	92.60	4.50	1.73	1618	1106
P-510	30.1	10.4	58.7	115	1.31	92.60	4.53	1.48	842	523
P-512	32.0	11.3	60.8	124	1.33	93.50	4.40	1.77	1568	1045
P-513	33.0	10.0	56.5	97	1.29	92.28	4.72	1.64	1299	871
P-514	38.0	9.4	53.9	85	1.27	93.22	4.88	1.60	1021	798
P-515	31.1	10.5	56.6	106	1.29	92.04	4.71	1.64	1184	677
P-521	34.2	10.9	54.5	110	1.27	92.25	4.96	1.55	729	643
P-521	38.2	10.9	54.5	110	1.27	92.25	4.96	1.55	1106	644
P-525	40.3	10.7	53.4	95	1.27	92.50	5.25	1.47	623	439
PE-55	32.0	2.6	42.6	102	1.32	92.70	6.40	1.22	631	415
PE-56	32.8	2.1	45.3	103	1.22	93.50	6.00	1.31	1385	899
PE-56	32.8	2.1	45.3	103	1.22	93.50	6.00	1.31	940	748
PE-56	32.8	2.1	45.3	103	1.22	93.50	6.00	1.31	1059	896
PE-57	15.1	2.1	41.4	98	1.23	93.06	5.84	1.34	1327	971
PE-65	3.1	0.2	25.8	61	1.11	91.49	7.28	1.05	726	551
PE-67	3.8	0.1	38.1	90	1.25	92.94	6.40	1.22	87	697
PE-68	15.4	2.1	59.4	146	1.25	93.46	5.34	1.47	1270	1033
PE-69	5.7	2.1	38.9	82	1.19	93.13	6.34	1.23	1059	802
PE-70	3.8	0.1	45.8	104	1.21	93.01	6.04	1.29	1052	837
PE-72	28.5	17.0	56.2	107	1.38	94.09	4.06	1.93	1291	706
PE-73	35.1	21.3	66.0	148	1.36	94.22	3.79	2.08	1683	1380
PE-74	31.4	17.5	55.4	106	1.34	93.81	4.03	1.95	1270	882
PE-91	13.8	2.1	49.0	114	1.22	93.12	5.58	1.40	812	775
PE-92	13.3	0.5	52.0	138	1.22	93.62	5.39	1.46	992	954
PE-93	37.7	3.7	54.6	123	1.39	92.77	5.39	1.44	1424	969
PE-94	2.6	0.7	42.1	104	1.21	92.72	5.59	1.39	886	713
PE-95	20.5	13.3	42.1	95	1.27	93.54	4.45	1.76	1192	824
AT-1	0.0	0.0	26.0	88	1.05	86.23	9.39	0.77	2715	1339
AT-2	0.2	0.0	27.2	185	1.06	85.09	8.94	0.80	752	369
AT-4	0.3	0.0	35.2	140	1.00	86.06	8.95	0.81	512	342
AT-5	0.4	0.0	39.3	172	1.01	86.50	8.47	0.85	490	382
TR-200	15.9	0.1	37.0	106	1.22	92.01	5.83	1.32	1075	364
TR-260	24.1	0.3	42.5	139	1.23	92.00	5.67	1.16	1245	779
TR-290	30.5	0.3	44.0	152	1.24	91.73	5.47	1.41	1890	1063
PE-101	1.7	0.3	38.3	84	1.20	90.70	6.14	1.23	1606	834
PE-41	14.8	27.4	44.2	105	1.27	92.20	5.30	1.30	406	352
Q-8	5.1	0.0	37.8	74	1.33	88.43	4.57	1.62	1139	0
HT-11	0.0	0.0	24.0	53	0.98	90.85	7.30	1.04	665	329
HT-17	10.0	0.8	37.6	111	0.74	84.63	7.93	0.90	657	437
HT-26	19.8	1.1	50.6	112	1.25	89.93	8.62	0.88	1162	697
HT-28	2.3	0.4	34.7	94	1.14	90.83	6.67	1.14	612	480
HT-30	1.9	0.1	36.8	94	1.16	91.64	6.56	1.17	1008	673
HT-32	0.0	0.0	34.8	95	1.16	91.27	6.77	1.13	856	558
HT-34	0.3	0.0	36.3	93	1.15	91.61	6.77	1.14	710	564
16160	19.2	1.1	54.1	119	1.25	92.14	4.99	1.54	1040	810
16167	1.4	0.2	51.0	113	1.21	91.15	5.49	1.39	1240	810
16261	0.5	0.1	45.8	117	1.15	89.25	6.60	1.13	770	490
16263	0.3	0.3	43.2	121	1.11	81.59	8.06	0.85	520	400
PR RES	4.7	4.2	43.1	94	1.18	93.75	5.75	1.47	1056	832
PE-29	37.0	24.5	44.2	99	1.25	82.00	5.70	1.21	398	272
P-105-GC	27.7	16.5	57.7	131	1.28	92.19	4.69	1.65	1141	631
P-105-TB	25.7	6.5	54.2	121	1.29	92.89	4.87	1.60	480	293
P-105-TC	29.5	1.3	54.0	120	1.28	94.10	4.81	1.64	720	410
P-105-TD	33.7	16.8	58.7	130	1.32	93.94	4.48	1.76	1088	695
P-105-TH	38.2	21.2	60.7	137	1.33	94.56	4.21	1.88	1222	825
PE-121	4.2	0.2	32.6	63	0.22	92.25	6.95	1.11	563	438
PE-130	24.8	2.4	48.5	109	1.23	92.21	5.67	1.36	420	325
PE-34	20.0	3.2	43.8	77	1.28	92.80	4.80	1.62	778	585
PE-504	26.3	7.6	44.7	94	1.26	89.58	5.05	1.49	541	598
PE-808	28.6	12.9	45.9	95	1.27	88.83	5.13	1.45	529	546
PE-806	31.9	18.2	41.2	97	1.26	84.19	5.38	1.31	442	390
LP	13.7	0.3	27.6	100	1.13	83.87	7.93	0.89	481	360
PE-63	17.7	2.4	41.8	98	1.30	91.80	4.70	1.64	1029	738
Acornap.	17.2	0.2	57.0	118	1.28	94.57	4.81	1.65	1275	919

Table 108. Regression Equations Formed for Binder Properties Versus Flexural Strength

Equation Number	Dependent Variable Manipulation	Number of Data Sets	Number of Variables in Regression Equation	Average of Flexural Strengths lbs./in. ²	Standard Deviation of Flexural Strengths lbs./in. ²	Standard Error of Regression Equation, lbs./in. ²	(1-R ²)*
W/G 1	linear, cross products and quadratics	67	9	950	±355	±228	0.355
2	logarithms (base e)	67	2	6.78 (log)	±0.402 (log)	±0.305 (log)	0.558
A/G 3	linear, cross products and quadratics	66	5	664	±243	±165	0.424
1	Flexural Strength = 1.09 (BI ²) + 3.64 (QI ²) + 415. (SpG ²) - 4.34 (BI x QI) + 0.38 (BI x MP) - 55.6 (BI x SpG) + 3.32 (QI x CC) - 1.17 (QI x MP) + 5.23 (% C x C/H) - 177						
2	Log "	" = 0.333 (log MP) + 7.11 (log % C) - 26.9					
3	Flexural Strength = 0.62 (BI ²) + 2.44 (QI ²) - 2.37 (BI x QI) - 12.8 (BI x SpG) + 10.9 (CC x C/H) + 129						
BI = Benzene Insolubles QI = Quinoline Insolubles SpG= Specific Gravity MP = Melting Point CC = Conradson Carbon %C = Per Cent Carbon C/H = Atomic Ratio of Carbon to Hydrogen							
$*R^2 = \left[\sum_i (\bar{y} - y_i)^2 - \sum_i (y_i - \hat{y}_i)^2 \right] / \sum_i (\bar{y} - y_i)^2$ <p>where \bar{y} = average of sample measurements y_i = observed sample measurements \hat{y}_i = calculated values (from the regression equation)</p>							

from the benzene insoluble content of the binder times the atomic C/H ratio of the benzene insoluble material times the atomic C/H ratio of the benzene soluble material.

The same type of correlation was found here for flexural strength of graphite billets versus the characterization factor, but with only seven data sets. Three commercial petroleum pitches, an experimental petroleum pitch, and three experimental coal tar pitches were used to find the results shown in Figure 99. Although there is a reasonable fit for the points given, there is not enough data to confidently determine the correct line for prediction of flexural strengths from the characterization factor.

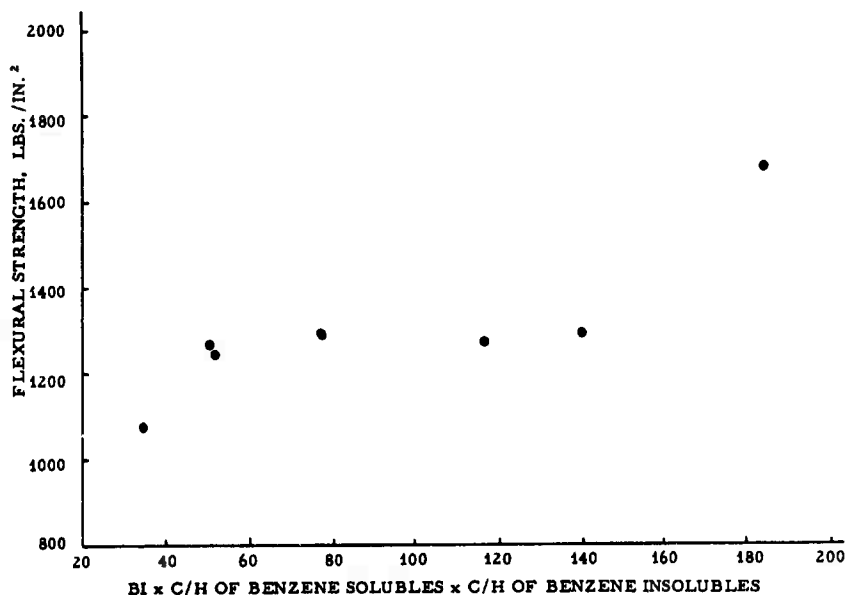
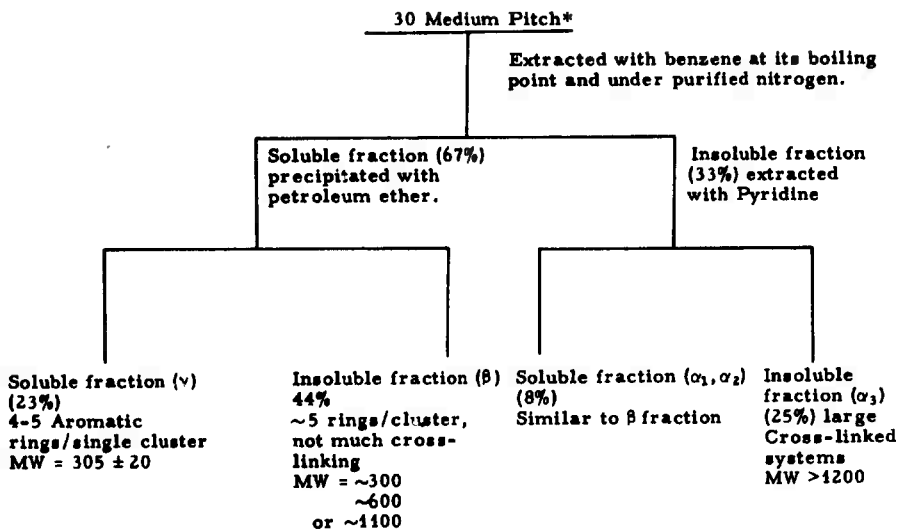


Figure 99. Relationship of Flexural Strength Versus Characterization Factor (BI x C/H of Benzene Solubles x C/H of Benzene Insolubles)

4.3.2. Solvent Extraction Experiments

de Ruiter, et.al,⁽¹⁰⁰⁾ suggested that the main contributors to the binding power of a typical coal tar pitch (30 medium) were those portions having molecular weights between 300 and 1200. Their pitch fractions were obtained by extracting the pitch with benzene, pyridine, and petroleum ether as shown in Figure 100.



* de Reuter, op. cit.

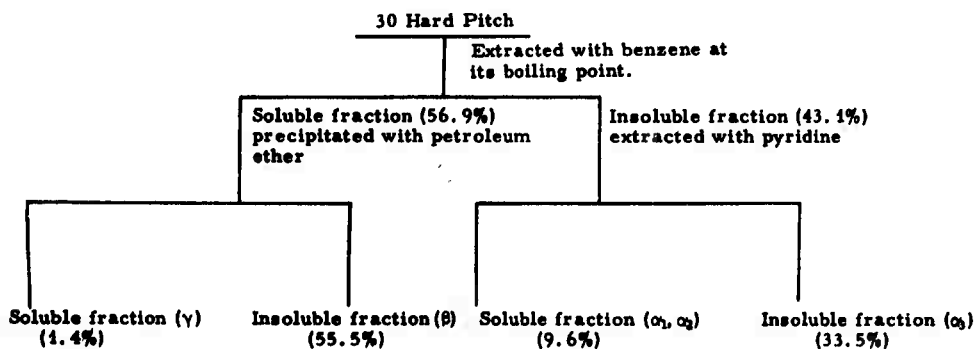


Figure 100. Extraction of 30 Medium and 30 Hard Pitch

An attempt was made here to extract 30 hard pitch in a similar manner and use the combined α_1 , α_2 , and β portions of Figure 100 as a higher strength binder. Graphite rods and billets so made are compared with a standard graphite billet in Table 109. Although the extract pitch had a lower softening point, the volume shrinkage (bake-to-graphitization) was reduced, and the with-grain flexural strength showed a 35 per cent increase.

Table 109. Properties of 30 Hard Pitch, 30 Hard Pitch Extract (α_1 , α_2 , and β Portions) and the Resultant Graphites

Pitch	30 Hard Pitch	30 Hard Pitch Extract
<u>Property</u>		
Melting Point, °C (CIA)	110	74
Specific Gravity, g/cc	1.34	1.33
Benzene Insolubles, weight per cent	30.0	5.08
Quinoline Insolubles, weight per cent	12.7	0.0
Conradson Carbon, weight per cent	54.9	37.8
Carbon/Hydrogen, weight ratio	92.98/4.22	88.43/4.57
Ash, weight per cent	0.11	-
Sulfur, weight per cent	0.50	0.48
Molecular Weight	>700	380
<u>Processing Data</u>		
	Molded Billets	Molded Billets
Binder Level, pph	32	32
Bulk Density, g/cc (Graphite)	1.529	1.455
Volume Shrinkage, per cent (bake to graph.)	2.54	0.56
Weight Loss, per cent (bake to graph.)	3.16	2.77
<u>Graphite Properties</u>		
Specific Resistance, 10^{-4} ohm-cm,	W/G 12.96 (26)*	13.58 (6)
	A/G 19.05 (26)	23.44 (7)
Young's Modulus, 10^6 lbs/in ² ,	W/G 0.60 (26)	0.62 (6)
	A/G 0.36 (26)	0.34 (8)
Flexural Strength, lbs/in ²	W/G 1080 (26)	1465 (4)
	A/G 770 (26)	610 (3)
Thermal Expansion (30-100°C) 10^6 /°C	W/G 1.36 (27)	1.69 (2)
	A/G 2.52 (26)	2.98 (3)
<u>*No. of samples in ()</u>		

4.3.3. Thermal and Catalytic Cracking Experiments

As shown in Section 4.2.9., most aromatic petroleum stocks contain a large amount of aromatic alkyl groups which tend to act as an internal diluent and thus lower specific gravity and coking value. Two methods have been tried to upgrade the quality of petroleum pitches,

namely, thermal and catalytic cracking of tars with subsequent distillation to a pitch.

The starting materials used were a thermal residuum (TR) from Marathon Oil Company and a thermal tar (TT) from Pure Oil Company. These stocks are refinery bottoms with the properties shown in Table 110.

Table 110. Properties of Marathon Oil Company Thermal Residuum and Pure Oil Company Thermal Tar

Property	Thermal Residuum	Thermal Tar
Ash, weight per cent	0.01	0.00
Sulfur, weight per cent	0.56	0.07
Conradson Carbon, weight per cent	12.30	11.30
Benzene Insoluble, weight per cent	6.24	1.02
Quinoline Insoluble, weight per cent	0.01	0.00
Carbon, weight per cent	90.10	91.79
Hydrogen, weight per cent	8.60	8.11
Atomic C/H	0.88	0.95
Molecular Weight	370.00	306.00
Density, g/cc	1.08	1.05
Flash Point, °C	323.00	235.00

4.3.3.1. Thermal Cracking

Table 111 shows time-temperature conditions for the three thermal cracking runs made.

Table 111. Thermal Cracking Conditions for Thermal Tar and Thermal Residuum (TT and TR)

Run No.	Charge	Temp. °C	Time hrs.
HT - 1	TT	250	41.6
2	TR	300	140.0
25	TR	416	11.0

At up to 300°C for 140 hours no useful alteration was made in the charge stock properties, but heating to the normal boiling point with reflux and 12.6 per cent distillation changed several properties of the TR as shown in Table 112.

Table 112. Properties of Marathon Thermal Residuam Before and After High-Temperature Thermal Cracking

Property	Thermal Residuam	Heat-Treated Thermal Residuam (HT-25)
Specific Gravity, g/cc	1.08	1.16
Benzene Insoluble, wt. %	6.24	12.00
Quinoline Insoluble, wt. %	0.01	1.90
Conradson Carbon, wt. %	12.30	33.80
Molecular Weight	323.00	385.00

This thermally cracked TR was stripped to a 102°C melting point pitch and used as binder to make graphite billets. Table 113 compares the properties of these billets with a typical coal tar pitch (30 hard pitch), and with pitch made from uncracked TR.

Table 113. Properties of Graphite Made from Thermally Cracked and Uncracked Thermal Residuam and from 30 Hard Pitch

	Uncracked Thermal Residuam			Thermally Cracked Thermal Residuam (HT-25)			30 Hard Pitch	
	Rods*	W/G**	A/G	Rods	W/G	A/G	W/G	A/G
Binder Level, pph	30		30	30		30		32
Green Density, g/cc	1.660	1.603		1.618	1.639		1.631	
Baked Density, g/cc	1.498	1.497		1.539	1.517		1.536	
Graphitized Density, g/cc	1.487	1.525		1.550	1.551		1.529	
Specific Resistance, 10^{-4} ohm-cm	7.95	10.50	16.76	7.82	11.54	19.80	12.96	19.05
Young's Modulus, 10^6 lbs./in. ²	----	0.58	0.32	----	0.60	0.31	0.60	0.36
Flexural Strength, lbs./in. ³	----	1042	660	----	1162	697	1077	771
Thermal Expansion, (30-100°C), $10^{-6}/^{\circ}\text{C}$	0.35	1.25	2.38	0.06	0.96	2.73	1.36	2.52

* $\frac{3}{8}$ -Inch Diameter Extruded Billets
 ** $\frac{1}{8}$ -Inch Diameter Molded Billets, $\frac{3}{8}$ - by $\frac{1}{8}$ - by $2\frac{1}{8}$ -Inch Samples, 3 to 8 Samples for Each Determination

On the basis of just a few samples, the thermally cracked TR produces a binder that showed no significant improvement over the non-treated petroleum pitch. In both cases, however, the graphite properties were equivalent to graphite properties of materials made with a coal tar pitch binder.

4.3.3.2. Catalytic Cracking

Table 114 shows time-temperature conditions for the eight catalytic cracking runs made.

Table 114. Catalytic Cracking Conditions for Thermal Tar and Thermal Residuum (TT and TR)

Run No.	Charge	Temp. °C	Time, hrs.	Catalyst
HT-3	TR	125	40.0	1% AlCl ₃ (Anhydrous)*
4	TR	125	40.0	2% FeCl ₃ (Anhydrous)
5	TR	225	40.0	2% FeCl ₃ (Anhydrous)
6	TR	225	40.0	2% FeCl ₃ (Anhydrous)
27	TT	260	7.0	5% Silica - Alumina
29	TT	250	7.3	5% Cobalt - Molybdate
31	TT	250	5.2	5% Cobalt Oxide
33	TT	250	5.8	5% Raney Nickel

*Some water pick-up suspected

The anhydrous aluminum and ferric chlorides and Raney nickel (which is pyrophoric) were added to the charge stocks prior to heating. The other catalysts were added in small amounts after the final temperature was reached. The catalysts were filtered out at the end of the run.

Although there was vigorous reaction during catalyst addition, no large changes were found in the charge stock properties (see Table 115). The cracked TT was stripped to a 90-100°C melting point pitch and used as binder for graphite billets. Table 116 gives comparative values of the graphite properties for the cracked and uncracked TT.

Table 115. Properties of Pure Oil Thermal Tar Before and After Catalytic Cracking Experiments

	Thermal Tar	Heat-Treated Thermal Tar and Catalyst			
		Cobalt Molybdate	Silica Alumina	Cobalt Oxide	Raney Nickel
Specific Gravity, g/cc	1.05	1.03	1.08	1.09	1.01
Benzene Insoluble, wt. %	1.02	0.06	0.08	0.00	0.07
Quinoline Insoluble, wt. %	0.00	0.00	0.34	0.00	0.00
Conradson Carbon, wt. %	11.26	12.23	12.52	13.34	11.31
Ash, wt. %	0.00	0.02	0.11	0.00	0.01
Molecular weight	306.00	424.00	221.00	308.00	245.00

Table 116. Properties of Graphite Made from Catalytically Cracked and Uncracked Thermal Tar and 30 Hard Pitch

	Catalytically Cracked Thermal Tar																	30 Hard Pitch
	Uncracked Thermal Tar			Silica-Alumina Catalyst		Cobalt-Molybdate Catalyst			Cobalt Oxide Catalyst			Raney Nickel Catalyst						
	KGs	W/G	A/G	KGs	W/G	A/G	KGs	W/G	A/G	KGs	W/G	A/G	KGs	W/G	A/G	W/G	A/G	
Binder Level, pph	30	28		28	28		30	30		30	30		30	30			32	
Green Density, g/cc	1.599	1.591		1.606	1.570		1.591	1.600		1.605	1.565		1.594	1.662			1.531	
Baked Density, g/cc	1.429	1.475		1.456	1.473		1.456	1.457		1.452	1.463		1.450	1.453			1.536	
Graphitized Density, g/cc	1.424	1.459		1.440	1.464		1.453	1.427		1.458	1.535		1.449	1.367			1.529	
Specific Resistance, 10^{-4} ohm-cm	10.05	16.56	17.36	9.52	12.98	19.07	10.10	14.20	21.26	10.02	16.04	23.26	10.22	15.33	23.63		12.96	19.05
Young's Modulus, 10^4 lbs./in. ²	-----	0.43	0.22	-----	0.46	0.26	-----	0.57	0.30	-----	0.47	0.26	-----	0.51	0.27		0.60	0.36
Flexural Strength, lbs./in. ²	-----	641	415	-----	662	481	-----	1008	573	-----	856	558	-----	710	564		1077	771
Thermal Expansion, (30-100°C), $10^{-6}/^{\circ}\text{C}$	0.49	1.51	2.24	0.11	1.35	2.52	0.28	1.55	2.81	0.70	1.43	2.60		0.35	1.37	2.90	1.36	2.52

* 9/8-Inch Diameter Extruded Billets

oo 3-Inch Diameter Molded Billets, 1/2- by 1/2- by 2-1/2-Inch Samples, 3 to 8 Samples for Each Determination

As with the thermally cracked TR, the catalytically cracked TT stock produced billets slightly inferior to 30 hard pitch, with lower strengths and higher specific resistance.

4.4. Pilot-Scale Coker Experiments

4.4.1. Isotropic High Thermal Expansion Coke

To produce ton quantities of high thermal expansion coke from air-blown or carbon-seeded charge stocks, a series of experiments were carried out in the 1/100 scale pilot coker located on the site of the Marathon Oil Company in Robinson, Illinois. Two experiments were performed in May and two in August, 1964. All experiments ran satisfactory under the conditions outlined in Table 117.

Table 117. High Thermal Expansion Isotropic Cokes, Operating Conditions and Yields

Cycle No.	Hrs.	Drum Pressure lbs./in. ²	Fresh Feed Rate bbls./day ⁽¹⁾	S.V. ⁽²⁾ hr. ⁻¹	Furnace Outlet Temperatures, °F		Inlet °F	Outlet °F	Raw Coke Bulk Density lbs./cu. ft. (g)	Yield, Weight Percent					
					2BA	2BB				Oil	Gas	Case-line	Raw Coke Gas (%)	Raw Coke (%)	
<u>Fresh Feed: Trumvac 1 (Air-Blown Vacuum Residuum - Kerosene, diluted 1/1 Volume Per Cent)</u>															
68S	23	35	172.8	36	666	934	875	725-790	62.9	77.6	6.1	5.2	11.1	15.4	
69N	24	33	171.5	34	665	934	842	765-784	62.1	65.0	19.9	4.7	10.4	15.8	
<u>Fresh Feed: Atmospheric Residuum, 3.0 Weight Per Cent Acetylene Black</u>															
708	31	30	174	39	650	932	874	780-795	67.4	56.1	12.7	6.1	24.9	15.6	
<u>Fresh Feed: Atmospheric Residuum, 2.0 Weight Per Cent Acetylene Black</u>															
76N	25.3	31	174	37	652	938	865	781	70.4	60.0	14.7	4.5	20.9	17.6	
<u>Fresh Feed: Witmar 1 (MR-38 - Light Catalytic Cycle Oil, Diluted 1/1 Weight Per Cent)</u>															
78S	24	30	167	36	652	938	875	774	61.8	70.9	3.9	4.7	20.53	20.1	
78N	24	30	183	39	651	938	875	864	61.8	65.1	6.9	4.8	23.30	19.7	

⁽¹⁾No recycle (once through coking)

⁽²⁾S.V. = Space Velocity (Fresh feed rate, gal./hr. ÷ furnace volume (gal.) above 750°F = 1/hr., indication at residence time)

⁽³⁾Measured at the Advanced Materials Laboratory

⁽⁴⁾Marathon data

⁽⁵⁾Calculated from measured bulk density

⁽¹⁾ No recycle (once through coking)

⁽²⁾ S.V. = Space Velocity (Fresh feed rate, gal./hr. ÷ furnace volume (gal.) above 750°F = 1/hr., indication at residence time)

⁽³⁾ Measured at the Advanced Materials Laboratory

⁽⁴⁾ Marathon data

⁽⁵⁾ Calculated from measured bulk density

The coking unit was operated on a once-through basis (no recycle) with the fractionator bypassed through the evaporator then through the last two furnace coils prior to entering the coke drum (Figure 101). It was necessary to operate a heat exchanger ahead of the evaporator to minimize the heating load on the furnace coils. Recycle coking through four furnace coils had been used on all previous experiments in this unit.

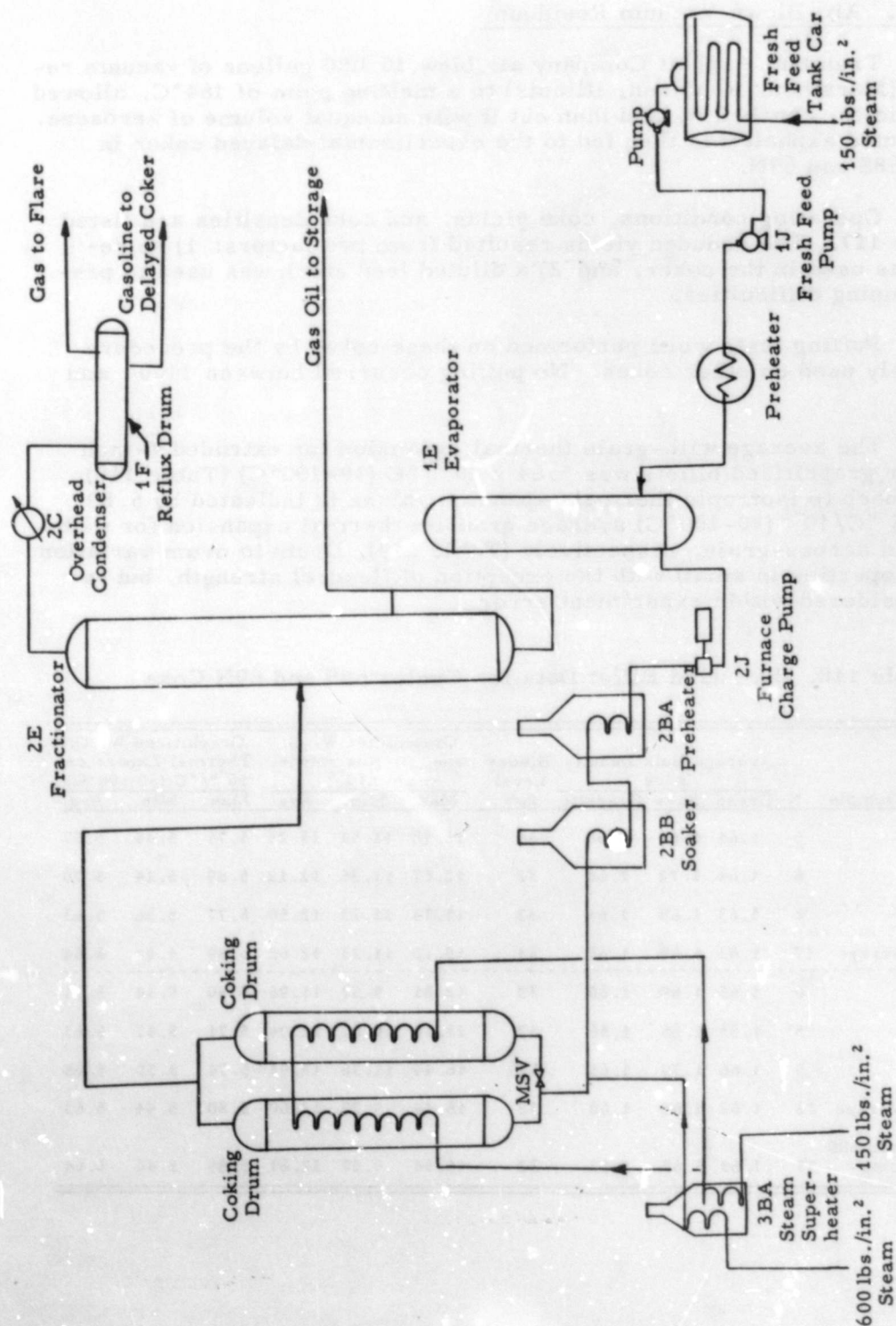


Figure 101. Schematic of Pilot-Scale Coker Operation for Producing a High Thermal Expansion Graphite-Source Material

L-917

4.4.1.1. Air-Blown Vacuum Residuuum

Trumbull Asphalt Company air blew 10,000 gallons of vacuum residuum (Marathon, Robinson, Illinois) to a melting point of 164°C, allowed it to solidify, crushed it, and then cut it with an equal volume of kerosene. This diluted asphalt was then fed to the experimental delayed coker in Cycles 68S and 69N.

Operating conditions, coke yields, and coke densities are listed in Table 117. The reduced yields resulted from two factors: 1) no re-cycle was used in the coker, and 2) a diluted feed stock was used to prevent pumping difficulties.

Puffing tests were performed on these cokes by the procedure previously used on other cokes. No puffing occurred between 1100° and 3000°C.

The average with-grain thermal expansion for extruded $\frac{5}{8}$ -inch diameter graphitized billets was $5.64 \times 10^{-6}/^{\circ}\text{C}$ (30-100°C) (Table 118). An approach to isotropic thermal expansion values is indicated by 5.89 and 5.95×10^{-6} (30-100°C) average graphite thermal expansion for with-grain and across-grain, respectively (Table 119). Drum to drum variation in all properties is small with the exception of flexural strength, but is still considered within experiment error.

Table 118. Extruded Billet Data for Cycles 68S and 69N Coke

Cycle Drum Sample	N	Average Bulk Density g/cc			Binder Level pph	Graphitized W. G. Specific Resistance, $\Omega\text{-cm} \times 10^{-4}$			Graphitized W. G. Thermal Expansion, $10^{-6}/^{\circ}\text{C}$ (30-100°C)		
		Green	Bake	Graphite		Max.	Min.	Avg.	Max.	Min.	Avg.
68S-Top	5	1.61	1.66	1.58	34	15.18	11.54	13.25	5.71	5.44	5.57
68S-Core	6	1.64	1.72	1.68	32	12.87	11.26	12.12	5.89	5.44	5.70
68S-Bottom	6	1.63	1.68	1.61	32	13.74	11.23	12.59	5.77	5.56	5.63
68S-Drum Average	17	1.63	1.69	1.63	33	15.18	11.23	12.62	5.89	5.44	5.64
69N-Top	6	1.65	1.69	1.60	32	12.81	9.57	11.96	5.80	5.44	5.61
69N-Core	5	1.55	1.65	1.56	32	13.36	10.61	12.06	5.71	5.47	5.63
69N-Bottom	5	1.66	1.70	1.65	32	16.44	11.38	13.91	5.74	5.50	5.65
69N-Drum Average	16	1.62	1.68	1.60	32	16.44	9.57	12.60	5.80	5.44	5.63
Average of Both 68S and 69N Drums	33	1.63	1.69	1.62	32	16.44	9.57	12.61	5.89	5.44	5.64

Table 149. Graphitized Molded Billet Data for Cycles 68S and 69N Coke

Cycle Drum Sample	Specific Resistance, 10 ⁻⁸ Ω-cm				Thermal Expansion, 10 ⁻⁶ /°C (30-100 °C)				Young's Modulus, lbs./in. ² x 10 ⁶				Flexural Strength, lbs./in. ²				
	N	Max.	Min.	Avg.	N	Max.	Min.	Avg.	N	Max.	Min.	Avg.	N	Max.	Min.	Avg.	
68S-Top	W. G.	3	13.74	11.31	12.41	4	5.82	5.62	5.70	3	0.97	0.87	0.91	3	1920	1460	1740
	A. G.	3	16.52	12.28	14.95	4	5.96	5.49	5.70	5	0.79	0.54	0.68	3	1660	1340	1450
68S-Core	W. G.	4	14.41	9.14	11.39	4	5.82	5.69	5.75	5	1.18	0.64	0.96	4	3140	1250	2260
	A. G.	4	16.52	9.18	13.84	3	6.29	5.96	5.11	5	1.07	0.73	0.94	2	2250	1470	1860
68S-Bottom	W. G.	5	14.23	9.48	12.14	4	6.22	5.89	6.10	5	1.29	1.03	1.19	4	3560	2380	3050
	A. G.	3	11.91	10.43	11.10	3	6.22	5.89	6.09	4	1.15	1.07	1.10	4	2990	2060	2420
68S-Drum Average	W. G.	12	14.23	9.14	11.96	12	6.22	5.62	5.85	13	1.29	0.64	1.04	11	3560	1250	2405
	A. G.	10	16.52	9.18	13.35	10	6.22	5.49	5.94	14	1.15	0.54	0.89	9	2990	1340	1970
69N-Top	W. G.	2	15.33	11.85	13.59	2	6.19	6.09	6.13	3	1.50	1.07	1.26	3	2350	1810	2000
	A. G.	7	17.94	10.63	14.07	2	6.29	6.29	6.29	7	1.04	0.68	0.81	7	2180	1230	1500
69N-Core	W. G.	4	13.07	11.05	11.97	2	6.09	5.76	5.92	5	1.25	0.83	1.10	4	4380	2610	3490
	A. G.	6	18.71	13.07	15.13	3	6.29	5.76	6.00	5	0.97	0.83	0.90	5	2810	2010	2440
69N-Bottom	W. G.	5	15.03	11.85	12.96	3	5.89	5.82	5.84	5	1.20	0.38	0.96	5	3410	2390	2960
	A. G.	4	18.75	13.87	15.66	4	5.96	5.69	5.78	5	1.11	0.46	0.82	4	3140	1960	2530
69N-Drum Average	W. G.	11	15.33	11.05	12.71	7	6.19	5.76	5.95	13	1.50	0.38	1.08	12	4380	1810	2900
	A. G.	17	18.75	10.63	14.92	9	6.29	5.69	5.97	17	1.11	0.46	0.84	16	3140	1230	2050
Average of Both 68S and 69N Drums																	
W. G.	23	15.33	9.14	12.32	19	6.22	5.62	5.89	26	1.50	0.38	1.06	23	4380	1250	2660	
A. G.	27	18.75	9.18	14.34	19	6.29	5.49	5.95	31	1.11	0.46	0.86	25	3140	1230	2030	

4.4.1.2. Commercial Air-Blown Asphalt

In experimental delayed coker Cycles 78S and 78N, 71,200 pounds of No. MR-38 asphalt (Witco Chemical Company, Lawrenceville, Illinois) cut with about an equal weight of light catalytic cycle oil (422° to 614°F boiling range) was coked. The asphalt was slowly added to a recirculating flow of catalytic cycle oil and pumped through an ultrasonic mixer to insure homogenous mixing and pumped to a heated railway tank car. The cut material was then pumped to the coking unit as illustrated in Figure 101, and coked under the conditions outlined in Table 117.

Graphite property data for billets produced from these cokes are summarized in Tables 120 and 121. An approach to isotropic graphite thermal expansion is indicated by 5.42 and $5.45 \times 10^{-6}/^{\circ}\text{C}$ (30-100°C) average values for with-grain and across-grain, respectively. These values are less than those recorded for coke produced from air-blown vacuum residuum in Cycles 68S and 68N which had average with-grain and across-grain graphite thermal expansion of 5.89 and $5.95 \times 10^{-6}/^{\circ}\text{C}$ (30-100°C), respectively. We suspect that the light catalytic cycle oil reduced the thermal expansions to some extent although the effect was not this great in batch coking experiments (Section 4.2.2.2.).

4.4.1.3. Acetylene Black-Seeded Atmospheric Residuum

In experimental delayed coker Cycle 70S, 10,000 gallons of atmospheric residuum containing approximately 3 weight per cent acetylene black were coked. The acetylene black was introduced slowly into a rapidly recirculating stream of atmospheric residuum, followed by passage through an ultrasonic mixer to insure deagglomeration prior to storage in a heated railway tank car.

Table 120. Extruded $\frac{5}{8}$ -Inch Diameter Billet Data for Cycles 78S and 79N

Sample No.	78S-Top	78S-Middle	78S-Bottom	79N-Top	79N-Middle	79N-Bottom
Billet Bulk Density, g/cc						
Green	1.64	1.68	1.71	1.70	1.70	1.68
Bake	1.43	1.43	1.54	1.47	1.52	1.42
Graphite	1.68	1.65	1.74	1.58	1.69	1.63
N	6	6	6	5	6	5
Graphite Specific Resistance, $10^{-6} \Omega\text{-cm}$						
Maximum	10.17	10.01	9.31	11.60	14.85	10.40
Minimum	7.28	9.30	7.65	9.89	9.43	8.32
Average	8.91	9.58	8.65	10.74	11.56	9.18
N	6	5	6	5	6	5
Drum Average		9.05			10.39	
Run Average			9.92			
Graphite Thermal Expansion, $10^{-6}/^{\circ}\text{C}$ (30-100°C)						
Maximum	5.11	5.29	5.23	5.44	5.29	5.44
Minimum	4.82	5.20	4.79	5.29	4.99	4.70
Average	4.95	5.25	4.99	5.37	5.16	5.01
N	6	5	6	5	6	5
Drum Average		5.06			5.18	
Run Average			5.13			

Table 121. Molded 3-Inch Diameter Billet Data for
Cycles 78S and 78N

Sample No.	78S		78N	
Billet Bulk Density, g/cc				
Green	1.62		1.71	
Bake	1.50		1.50	
Graphite	1.67		1.64	
N	4		4	
Graphite Specific Resistance, $10^{-4} \Omega\text{-cm}$				
	W. G.	A. G.	W. G.	A. G.
Max.	11.56	12.83	12.09	13.21
Min.	8.78	9.55	9.40	10.90
Avg.	10.05	11.25	11.33	12.52
N	10	14	9	9
Run Avg. (w. g. / a. g.)	10.69/11.89			
Graphite Thermal Expansion, $10^{-6}/^{\circ}\text{C}$ (30-100°C)				
Max.	5.62	5.56	5.42	5.62
Min.	5.29	5.29	5.29	5.29
Avg.	5.47	5.47	5.36	5.44
N	8	7	7	7
Run Avg. (w. g. / a. g.)	5.41/5.45			
Graphite Young's Modulus, $10^{-6} \text{ lbs./in.}^2$				
Max.	1.18	1.06	1.41	1.17
Min.	0.95	0.84	1.03	0.92
Avg.	1.08	0.96	1.13	1.03
N	10	14	9	9
Run Avg. (w. g. / a. g.)	1.10/1.00			
Graphite Flexural Strength, lbs./in.^2				
Max.	5050	3990	4560	3650
Min.	3470	2760	3650	2910
Avg.	4000	3190	4120	3120
N	10	14	9	9
Run Avg. (w. g. / a. g.)	4060/3155			

Operating conditions, yield, and density data are presented in Table 117. As a result of single pass (no recycle) coking, a raw coke yield of only 14.7 weight per cent was obtained, as compared to the 20 to

22 weight per cent yield which would have been expected from recycle coking. The unexpectedly low coke yield resulted in a raw coke containing 19 to 20 weight per cent black; 13 to 14 weight per cent had been desired.

Properties of the graphitized billets (extruded and molded) produced from Cycle 70S coke are listed in Table 122. The high black content is reflected in low thermal expansion values, and in high electrical resistance. Higher flexural strengths had been expected.

Table 122. Processing and Physical Property Summary, Extruded and Molded Billets Processed from Acetylene Black-Seeded Atmospheric Residuum Coke Produced in Pilot Coker, Cycle 70S

Code No:	70S - Composite		
Wt. % Acetylene Black In Charge Stock**	3.17		
In Calcined Coke**	25-27		
	$\frac{3}{8}$ -Inch Dia. Extruded Billet Data	3-Inch Dia. Molded Billet Data	
Binder Level, pph	34	30	
Green Bulk Density, g/cc			
Max.	1.63	1.58	
Min.	1.62	1.56	
Ave.	1.63	1.57	
N	6	3	
Baked Bulk Density, g/cc			
Max.	1.42	1.52	
Min.	1.39	1.42	
Ave.	1.40	1.45	
N	6	3	
Graphitized Bulk Density, g/cc			
Max.	1.56	1.68	
Min.	1.52	1.53	
Ave.	1.54	1.59	
N	6	3	
Specific Resistance, $10^{-4} \Omega\text{-cm}$		W. G.	A. G.
Max.	22.08	23.54	24.20
Min.	20.53	17.48	19.26
Ave.	21.38	21.29	21.84
N	6	8	5
Sonic Modulus, 10^6 lbs./in.^2			
Max.		1.40	1.33
Min.		1.05	0.63
Ave.		1.19	0.92
N		8	5
CTE, $30\text{-}100^\circ\text{C} \times 10^{-6}/^\circ\text{C}$			
Max.	5.47	5.62	5.49
Min.	4.88	5.16	5.29
Ave.	5.00	5.36	5.41
N	6	6	4
Flexural Strength, lbs./in.^2			
Max.		4898	3383
Min.		1357	1807
Ave.		2738	2347
N		8	3

*CCl₄ Insoluble, through 0.45 Micron Millipore Filter (Marathon's analysis)

**Calculation based on (1) Marathon analysis of per cent black in charge stock, (2) coke yield by drum outage figures and (3) AML calcination yields.

In experimental delayed coker Cycle 76N, 10,000 gallons of atmospheric residuum containing 2 weight per cent asphaltene were coked. The purpose of this experiment was to produce a coke which would contain 13 to 18 weight per cent black after calcination, as compared to the 25 to 27 weight per cent black in the calcined seeded atmospheric residuum coke from Cycle 70S. The coke containing the lesser amount of black was expected to result in higher thermal expansion and strength levels, with lower electrical resistance.

Graphite property data for billets produced from the Cycle 76N coke are summarized in Table 123. Extruded billet thermal expansion increased slightly (approximately 6 per cent) over the Cycle 70S values; electrical resistance decreased approximately 13 per cent. In the case of the molded billets, with-grain and across-grain thermal expansion values were not significantly changed (less than 1 per cent), electrical resistance decreased 21 per cent and 24 per cent, and flexural strength values increased 33 per cent and 34 per cent, respectively.

4.4.2. Pilot-Scale Coker Performance and Recommendations

4.4.2.1. Original Design and Modifications

4.4.2.1.1. Fresh Feed Flow and Temperature Control

The original design utilized an orifice flow control meter on the fresh feed line. After a short period of running it became obvious that this instrument could not handle the high viscosity liquids and so a positive displacement meter was installed. The original orifice meter was satisfactory as a control meter.

To control recycle ratio, it is necessary not only to measure accurately fresh feed and combined feed (fresh feed plus recycle gas oil) but also to control temperatures in the fractionating system so that the tower bottom will receive a continuous steady flow of heavy recycle oil. The only heat in the fractionator comes from the overheads of the coking cycle with control of the top section coming from recycle of the gasoline and product gas oil streams. Since there can be no control of the heavy gas oil in the bottom of the fractionator, the low and variable temperature of the fresh feed entering this section resulted in unsteady liquid level and therefore a variation in recycle ratio, although the difference in fresh feed and combined feed gave a reasonable average figure. The installation of a heat exchanger in the fresh feed line prior to the fractionator minimized these difficulties.

4.4.2.1.2. Furnaces

The design of this unit utilized two pair of helical coil furnaces which can be operated in pairs of two singly, pairs of two in parallel, or as a unit in series. Most experiments were run with the furnaces in series in order to gain maximum amount of residence time at temperature. No major troubles were encountered except in the transfer lines

Table 123. Processing and Physical Property Summary, Extruded and Molded Billets Processed from Acetylene Black-Seeded Atmospheric Residuum Coke Produced in Pilot Coker, Cycle 76N

Code No:	76N Composite		
Wt. % Acetylene Black In Charge Stock*	2. 1-2. 2		
In Calcined Coke**	15-17		
	$\frac{3}{8}$ -Inch Dia. Extruded Billet Data	3-Inch Dia. Molded Billet Data	
Binder Level, pph	32	32	
Green Bulk Density, g/cc			
Max.	1.67	1.67	
Min.	1.61	1.63	
Avg.	1.65	1.65	
N	6	4	
Baked Bulk Density, g/cc			
Max.	1.47	1.50	
Min.	1.32	1.41	
Avg.	1.39	1.45	
N	6	4	
Graphitized Bulk Density, g/cc			
Max.	1.55	1.61	
Min.	1.41	1.54	
Avg.	1.49	1.57	
N	6	4	
Specific Resistance, 10^{-8} Ω -cm		W. G.	A. G.
Max.	19.90	21.75	22.36
Min.	16.98	12.50	10.22
Avg.	18.63	16.84	16.65
N	6	9	10
Sonic Modulus, 10^8 lbs./in. ²			
Max.		1.43	1.27
Min.		1.11	0.96
Avg.		1.31	1.08
N		9	10
CTE, 30-100°C x 10^{-6} /°C			
Max.	5.47	5.56	5.56
Min.	5.23	5.29	5.29
Avg.	5.33	5.39	5.42
N	5	6	7
Flexural Strength, lbs./in. ²			
Max.		4490	3800
Min.		3075	2750
Avg.		3671	3120
N		9	10
* CCl ₄ Insoluble, through 0.45 Micron Millipore Filter (Marathon's analysis)			
** Calculation based on (1) Marathon analysis of per cent black in charge stock, (2) coke yield by drum outage figures and (3) AML calcination yields.			

where the larger diameter tubing decreased the linear flow velocity to a point that some coking took place that forced shutdown.

The use of four furnaces in series resulted in a high-pressure drop at high flow rates. This situation limited the range of the time-temperature variable for operating at high coke drum pressures.

4.4.2.1.3. Pumps

With the exception of the fresh feed pump, all pumps were of the reciprocating type. In some experiments the feed rate was so slow that the pumps were throttled to the point of stalling.

The installation of hand bypasses from the discharge side to the suction side, and a pressure controller instead of a flow controller minimized these difficulties and gave much steadier flow.

4.4.2.1.4 Fractionator

The original Kellogg design called for a fractionator of 2 $\frac{2}{3}$ -foot ID by 40-foot length. Instead, an existing refinery tower, 2 $\frac{2}{3}$ -foot ID by 50-foot length was used. This turned out to be too large for the volume of the overhead products in most of the experiments. The end point on the overhead products could not be controlled due to the small volume, and therefore the recycle oil could not be controlled.

4.4.2.1.5. Flow Rates of Overhead Liquid Products

Orifice meters (without bypasses) and positive displacement meters (with bypasses) were alternately used to measure product flows. Due to the wide range of product yields, neither performed 100 per cent satisfactorily.

4.4.2.1.6. Steam Superheater

This unit performed satisfactorily after check valves were installed in the steam inlet to the furnace coils to prevent backing up of the feed stock, and block valves were installed in the steam coil outlet around the coke drums to hold pressure.

4.4.2.2. Recommended Change in Design

4.4.2.2.1. Furnaces

A new unit should have only one heater. If a combination of heaters is necessary, they should be of a common ID with the transfer lines of the same size. The piping should be such that there would be no 90° connections but sweeping bends in order to minimize coke deposits at these points.

4.4.2.2.2. Pumps

The pumps should be of a centrifugal type to give smoother flow.

4.4.2.2.3. Fractionator

A smaller fractionating tower should be designed so that better control of the overhead products and the recycle oil can be accomplished.

4.4.2.2.4. Flow Rates of Overhead Liquid Products

All liquid product streams should have a high and low range positive displacement meter with a bypass around each so that good yield data can be obtained.

4.5. Graphite Fabrication

Graphite property variation and property adjustment through control of raw materials has been demonstrated by large-scale evaluation.

4.5.1. Low Thermal Expansion Cokes

4.5.1.1. Materials and Processes

Two different batches of pressure-cured (R process) graphite have been fabricated using cokes from controlled raw materials. One batch was low thermal expansion coke, and the other batch an intermediate thermal expansion coke. These cokes were produced from the pilot-scale experimental coker at Robinson, Illinois and, at the time, represented cokes at extremes of the thermal expansion scale. The low thermal expansion coke was made from slurry oil charge stock at high drum pressure (350 lbs./in.²), and the intermediate thermal expansion coke from vacuum residuum charge stock at low drum pressure (50 lbs./in.²), with high pressure steam injection into the hot-oil stream between furnace and coke drum. The cokes were then processed into "RVA-type" graphite as outlined by the "A" process flow sheet in Figure 102. The different lots of graphite were designated as RT-0033 from slurry oil stock, and RT-0034 from vacuum residuum stock. The coke used in grade RVA is made from charge stock combining a thermal tar with various other nonaromatic hydrocarbons in a routine commercial coker operation.

Samples of RT-0033 and RT-0034 were resin-impregnated and re-baked to give RT-0035 and RT-0036, respectively. This treatment produced a "CFZ-type" graphite.

4.5.1.2. Properties

After fabrication of 12 blocks of RT-0033 and 14 blocks of RT-0034, comparison was made on samples cut from the individual blocks, according to the sampling diagram in Figure 103. Five blocks each of

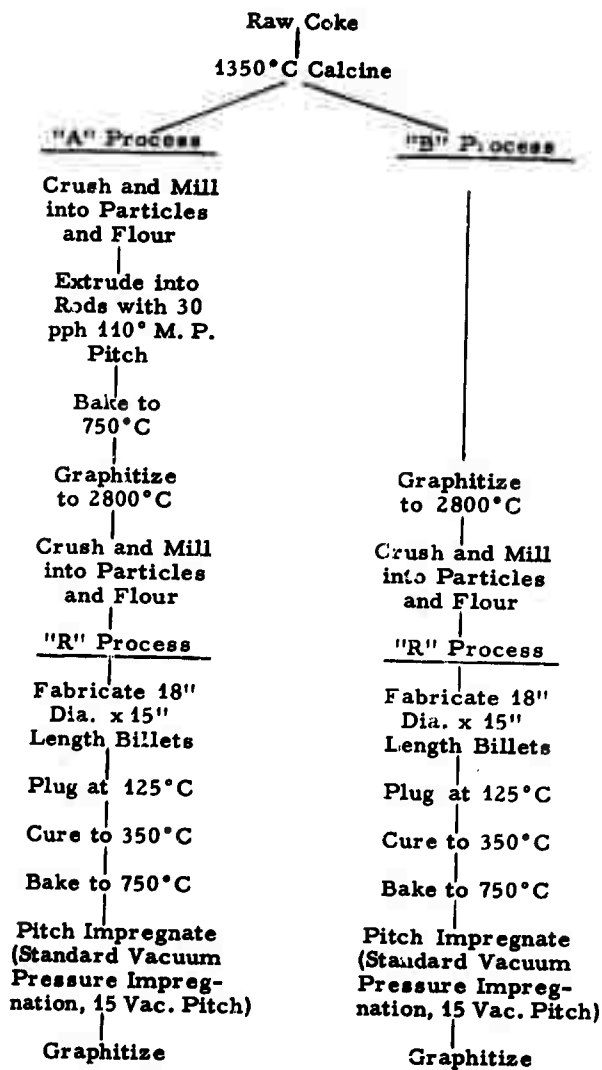


Figure 102. Processing Raw Cokes

SAMPLE DENOMINATION	PROPERTIES TO BE MEASURED
A. ACROSS GRAIN	SPECIFIC RESISTANCE YOUNG'S MODULUS FLEXURAL STRENGTH BULK DENSITY
B. WITH GRAIN	THERMAL EXPANSION
C. WITH GRAIN	COMPRESSIVE STRENGTH
D. WITH GRAIN	SPECIFIC RESISTANCE YOUNG'S MODULUS FLEXURAL STRENGTH BULK DENSITY
E. ACROSS GRAIN	THERMAL EXPANSION
F. ACROSS GRAIN	COMPRESSIVE STRENGTH

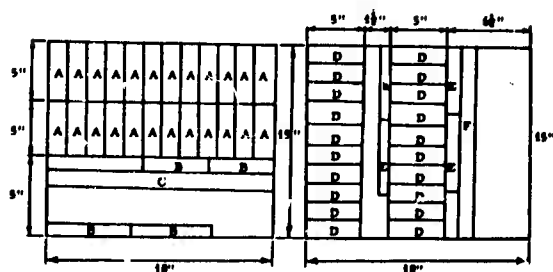
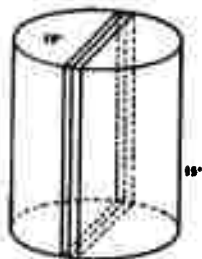


Figure 103. Sampling Diagram of Graphite Blocks

L-164

RT-0035 and RT-0036 were also sampled this way. Table 124 lists the room-temperature properties of these grades along with the properties of RVA and CFZ.

Two points were evident from the data of Table 124:

1. The character of the coke used in forming is carried through to the finished graphite article.
2. Variability in bulk density and compressive strength has been substantially reduced in cokes from a controlled source.

Comparison of properties on samples cut from the individual blocks of RT-0035 and RT-0036, can be made from Tables 125 through 135. Data on RT-0033 and RT-0034 was given in the first year's report.⁽⁴⁾ High-temperature thermal expansion and mercury porosimetry data for all four grades are shown in Figures 104 through 115.

Table 124. Room-Temperature Properties of RT-0033 Through RT-0036, RVA and CFZ

	RT-0033 ⁽²⁾		RT-0034 ⁽³⁾		CFZ ⁽⁴⁾		RT-0035 ⁽⁵⁾		RT-0036 ⁽⁶⁾	
	RVA ⁽¹⁾									
Bulk Density, g/cc										
\bar{X} (σ)	1.838		1.868		1.91		1.947		1.931	
σ	0.019		0.014		0.01		0.011		0.015	
N	312		545		40		202		204	
	W.G.	A.G.	W.G.	A.G.	W.G.	A.G.	W.G.	A.G.	W.G.	A.G.
Specific Resistance, 10 ¹⁰ Ω -cm										
\bar{X}	12.21	15.73	9.50	15.36	10.90	12.98	8.38	13.8	9.60	11.39
σ	0.37	0.96	0.44	0.95	0.61	0.75	0.84	0.74	0.51	0.64
N	149	162	258	287	284	330	104	98	104	100
Young's Modulus, 10 ⁶ lbs./in. ²										
\bar{X}	1.837	1.301	1.775	0.944	1.727	1.272	1.89	1.50	1.934	1.441
σ	0.073	0.094	0.086	0.048	0.053	0.050	0.07	0.04	0.093	0.048
N	128	162	258	287	284	330	14	16	104	98
Flexural Strength, lbs./in. ²										
\bar{X}	3800	2995	3314	2111	3809	3123	3980	3410	4100	3381
σ	321	203	260	280	236	240	340	260	272	224
N	135	121	258	287	284	330	14	16	101	98
Compressive Strength, ⁽⁸⁾ lbs./in. ²										
\bar{X}	9960	9000	6225	6377	11,995	11,999	9990	12,080	7944	8163
σ	1308	2000	385	254	153	556	1420	750	1280	1580
N	46	46	118	120	140	140	12	11	49	50
Thermal Expansion, 10 ⁻⁶ /°C										
Mean 30-100°C										
\bar{X}	4.65	2.77	1.12	2.52	2.25	2.94	1.94	2.64	1.17	2.46
σ	0.09	0.07	0.09	0.10	0.07	0.09	-	-	0.17	0.23
N	12	12	24	24	28	28	4	4	18	18

(1) Samples cut from 3 pieces, 33 inches in diameter by 42 inches in length.

(2) Samples cut from 12 pieces, 18 inches in diameter by 15 inches in length.

(3) Samples cut from 14 pieces, 18 inches in diameter by 15 inches in length.

(4) Samples cut from 1 piece 14 inches in diameter by 13 $\frac{1}{2}$ inches in length.

(5) Samples cut from 5 bisected pieces 18 inches in diameter by 15 inches in length.

(6) Samples cut from 5 bisected pieces 18 inches in diameter by 15 inches in length.

(7) \bar{X} = Average; σ = Standard Deviation; N = Number of Samples.

(8) One-inch cubes were used to test the RVA, RT-0033, CFZ, RT-0035, and RT-0036. One-inch diameter by one-inch long cylinders were used for the RT-0034 tests. The cylindrical specimen usually gives results ~10 per cent higher than the cube specimen and mere comparison of the data is not valid; however, the uniformity of the pieces is illustrated.

Table 125. Bulk Density, g/cc, Property Variation
for RT-0035

Block Number	N*	\bar{X} *	σ *
230	40	1.951	0.006
233	42	1.931	0.008
234	40	1.952	0.007
238	40	1.954	0.006
239	40	1.950	0.007
All Samples	202	1.947	0.011
Piece-to- Piece Variation	5	1.947	0.094

Table 126. Bulk Density, g/cc, Property Variation
for RT-0036

Block Number	N	\bar{X}	σ
270	40	1.926	0.005
271	40	1.949	0.005
274	40	1.919	0.014
275	42	1.922	0.011
276	42	1.939	0.013
All Samples	204	1.931	0.015
Piece-to- Piece Variation	5	1.931	0.013

* N = Number of Samples; \bar{X} = Average Value; σ = Standard Deviation.

Table 127. Specific Resistance, $10^{-4} \Omega\text{-cm}$, Property Variation for RT-0035

Block Number	With Grain			Across Grain		
	N	\bar{X}	σ	N	\bar{X}	σ
230	20	8.39	0.329	20	13.37	0.728
233	22	8.45	0.422	20	14.14	0.737
234	20	8.59	0.281	20	14.16	0.770
238	20	8.46	0.256	20	13.94	0.440
239	22	8.06	0.218	18	13.33	0.544
All Samples	104	8.38	0.355	98	13.80	0.742
Piece-to-Piece Variation	5	8.38	0.199	5	13.80	0.409

Table 128. Specific Resistance, $10^{-4} \Omega\text{-cm}$, Property Variation for RT-0036

Block Number	With Grain			Across Grain		
	N	\bar{X}	σ	N	\bar{X}	σ
270	20	0.976	0.030	20	1.155	0.034
271	20	0.879	0.033	20	1.037	0.030
274	20	0.987	0.021	20	1.198	0.025
275	22	1.001	0.017	20	1.153	0.036
276	22	0.952	0.033	20	1.152	0.046
All Samples	104	0.960	0.051	100	1.139	0.064
Piece-to-Piece Variation	5	0.960	0.048	5	1.139	0.032

Table 129. Young's Modulus, 10^6 lbs./in.², Property Variation for RT-0035

Block Number	With Grain			Across Grain		
	N	X	σ	N	X	σ
230	20	1.952	0.087	20	1.080	0.026
233	22	1.894	0.069	20	1.041	0.044
234	20	1.993	0.068	20	1.090	0.049
238	20	1.836	0.079	20	1.020	0.033
239	22	1.990	0.056	18	1.091	0.035
All Samples	104	1.934	0.093	98	1.064	0.048
Piece-to-Piece Variation	5	1.934	0.067	5	1.064	0.032

Table 130. Young's Modulus, 10^6 lbs./in.², Property Variation for RT-0036

Block Number	With Grain			Across Grain		
	N	X	σ	N	X	σ
270	20	1.796	0.042	20	1.436	0.027
271	20	1.839	0.026	20	1.481	0.017
274	20	1.812	0.029	20	1.448	0.043
275	22	1.767	0.037	20	1.388	0.030
276	22	1.805	0.028	20	1.453	0.029
All Samples	104	1.803	0.040	100	1.441	0.043
Piece-to-Piece Variation	5	1.803	0.026	5	1.441	0.034

Table 131. Flexural Strength, lbs./in.², Property Variation for RT-0035

Block Number	With Grain			Across Grain		
	N	X	σ	N	X	σ
230	20	3745	215	20	2455	154
233	21	3697	344	20	2505	139
234	20	3743	322	20	2327	280
238	19	3678	178	20	2464	166
239	21	3726	378	18	2516	149
All Samples	101	3718	295	98	2452	194
Piece-to-Piece Variation	5	3718	294	5	2452	72

Table 132. Flexural Strength, lbs./in.², Property Variation for RT-0036

Block Number	With Grain			Across Grain		
	N	X	σ	N	X	σ
270	19	3922	218	19	3379	108
271	20	4246	188	19	3453	162
274	18	4213	244	20	3468	226
275	22	4000	315	20	3397	170
276	22	4131	250	20	3379	160
All Samples	101	4100	272	98	3381	224
Piece-to-Piece Variation	5	4100	139	5	3381	56

Table 133. Compressive Strength, lbs./in.², Property Variation for RT-0035

Block Number	With Grain			Across Grain		
	N	X	σ	N	X	σ
230	9	8634	871	10	7303	1730
233	10	8049	658	10	8162	1580
234	10	7994	1090	10	7933	1480
238	10	7584	1340	10	9113	253
239	10	7529	1790	10	8305	1750
All Samples	49	7944	1280	50	8163	1580
Piece-to-Piece Variation	5	7944	445	5	8163	655

Table 134. Compressive Strength, lbs./in.², Property Variation for RT-0036

Block Number	With Grain			Across Grain		
	N	X	σ	N	X	σ
270	10	11,341	1530	10	11,982	190
271	10	11,738	1270	10	11,950	603
274	10	12,348	1510	10	11,010	2140
275	10	9,944	2000	10	12,543	2840
276	9	11,309	1410	10	12,319	819
All Samples	49	11,109	1770	50	11,961	1990
Piece-to-Piece Variation	5	11,109	920	5	11,961	586

Table 135. Room-Temperature Thermal Expansion of RT-0035, RT-0036, and CFZ

Block Number	With Grain			Across Grain		
	N*	\bar{X}	σ	N	\bar{X}	σ
<u>RT-0035</u>		$\times 10^{-6}$ (30-100°C)		$\times 10^{-6}$ (30-100°C)		
230	2	1.24		2	2.40	
233	2	0.94		2	2.64	
234	2	1.20		2	2.36	
238	10	1.31	0.10	10	2.36	0.18
339	2	1.17		2	2.54	
All Samples	18	1.17	0.17	18	2.46	0.23
Piece-to-Piece Variation	5	1.17	0.14	2	2.46	0.13
<u>RT-0036</u>						
270	10	2.47	0.12	8	2.90	0.08
271	2	2.38		2	3.06	
274	2	2.54		10	2.98	0.08
275	2	2.48		2	2.80	
276	2	2.33		2	2.96	
All Samples	18	2.94	0.11	24	2.91	0.11
Piece-to-Piece Variation	5	2.44	0.09	5	2.94	0.10
<u>CFZ</u>						
	4	1.94		4	2.64	

* N = No. of samples; \bar{X} = Average; σ = Standard Deviation

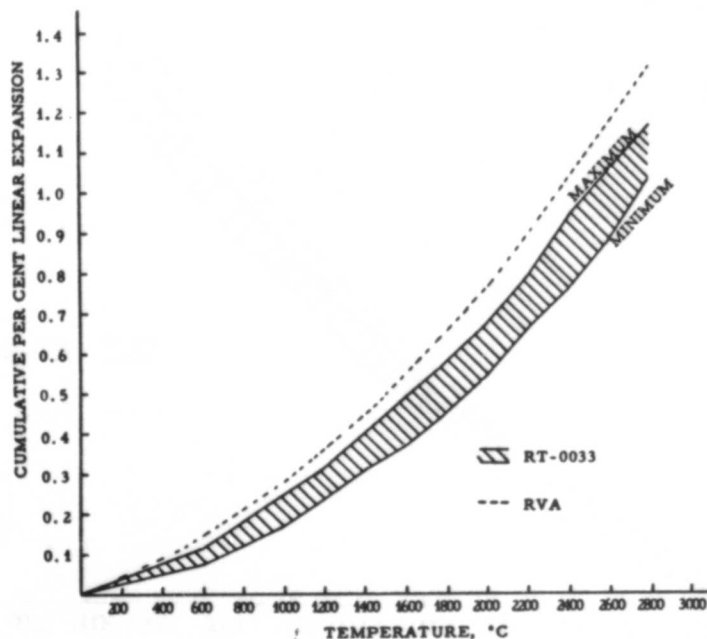


Figure 104. High-Temperature Thermal Expansion for L-920 With-Grain RT-0033 and RVA

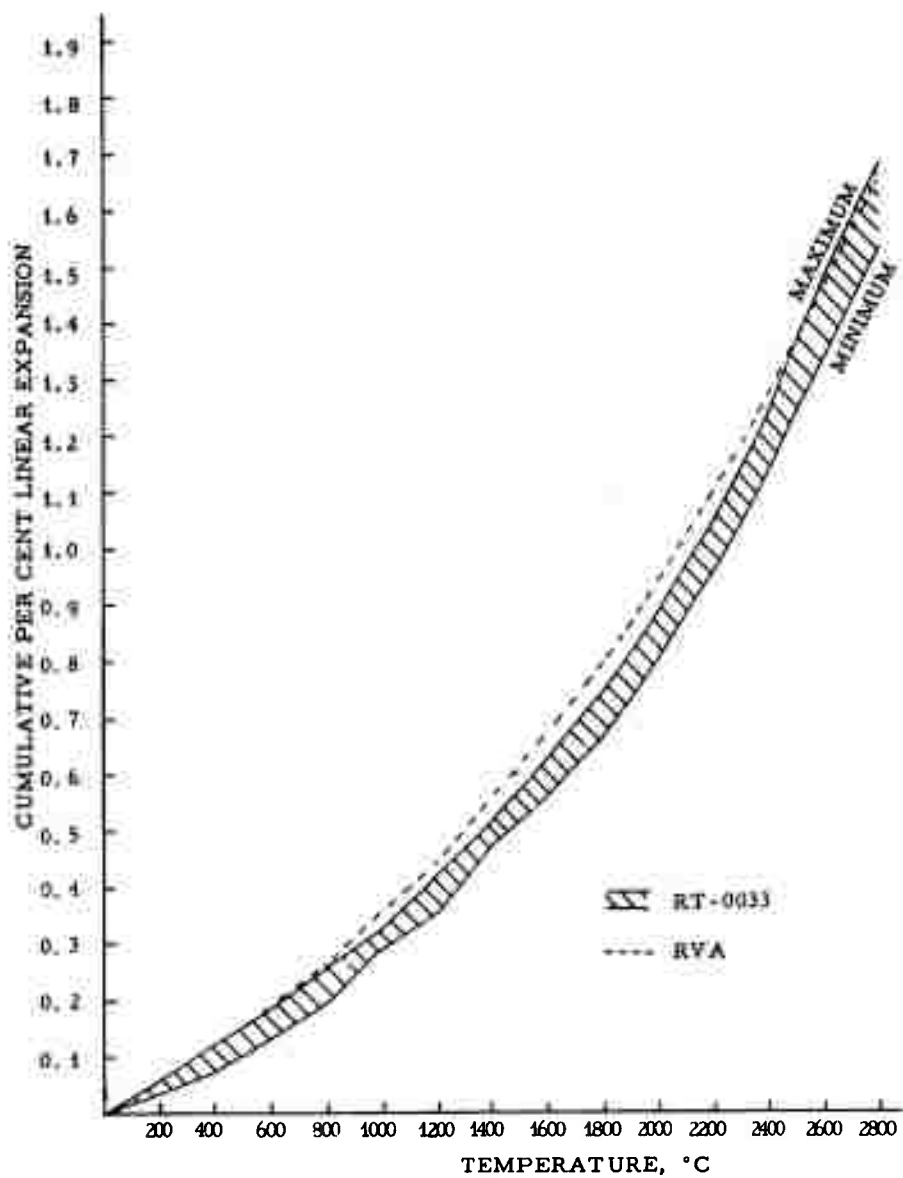


Figure 105. High-Temperature Thermal Expansion L-921
for Across-Grain RT-0033 and RVA

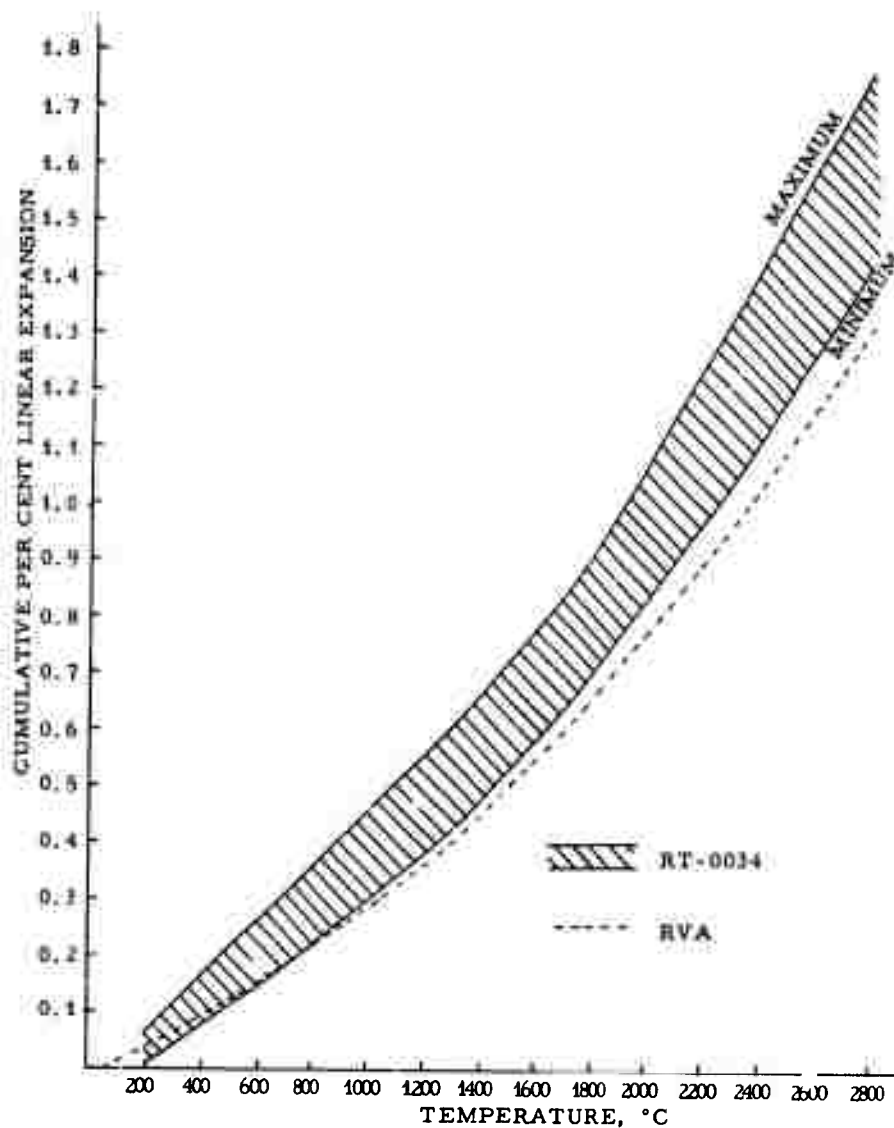


Figure 106. High-Temperature Thermal Expansion
for With-Grain RT-0034 and RVA

L-922

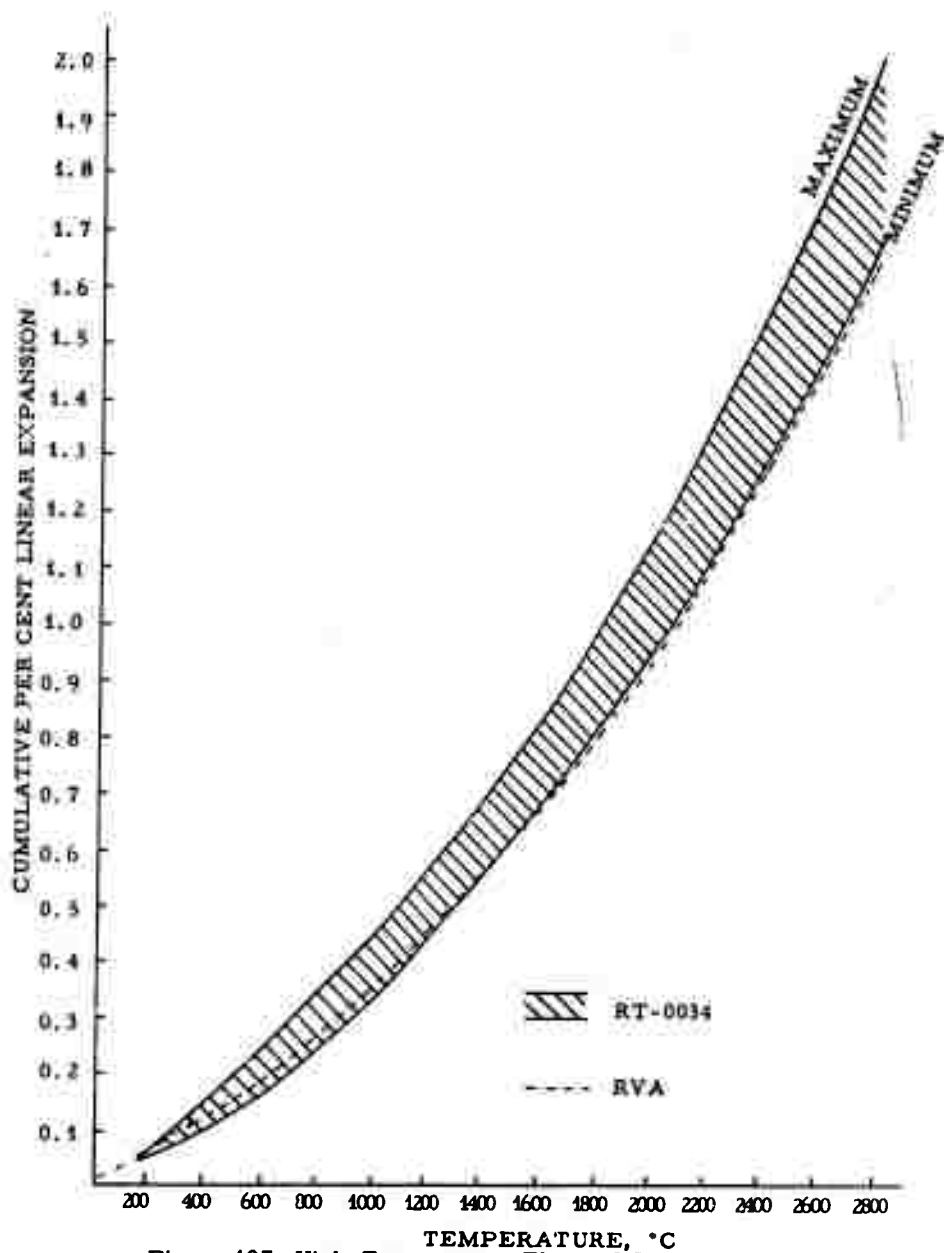


Figure 107. High-Temperature Thermal Expansion
for Across-Grain RT-0034 and RVA

L-923

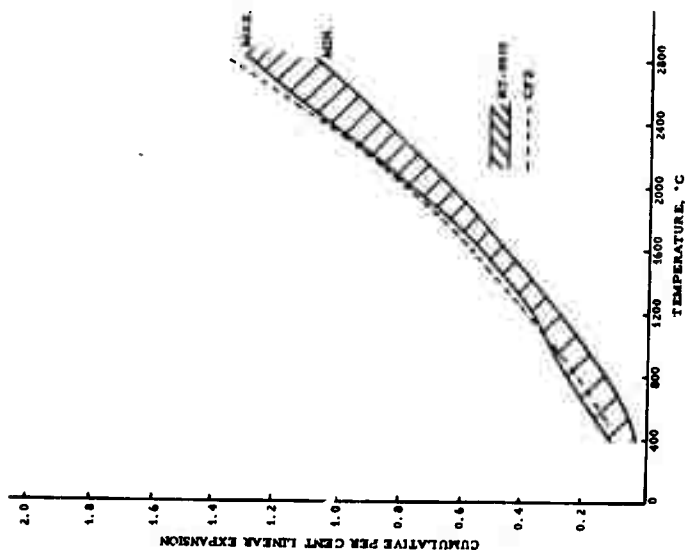


Figure 108. High-Temperature Thermal Expansion for With-Grain RT-0035 and CFZ

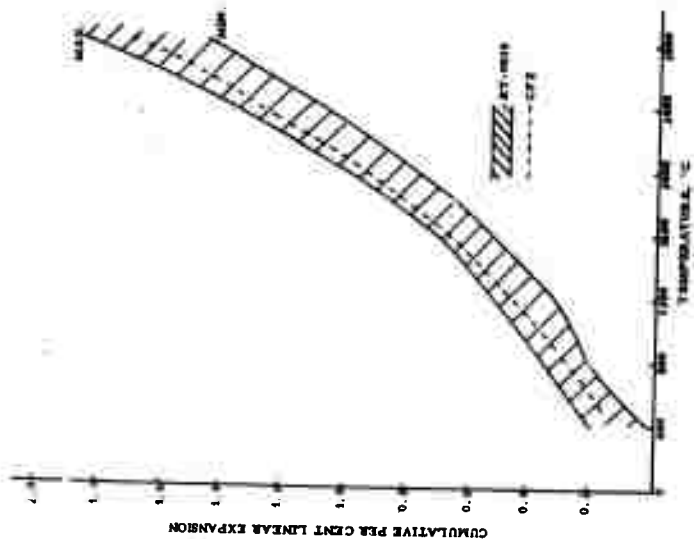


Figure 109. High-Temperature Thermal Expansion for Across-Grain RT-0035 and CFZ

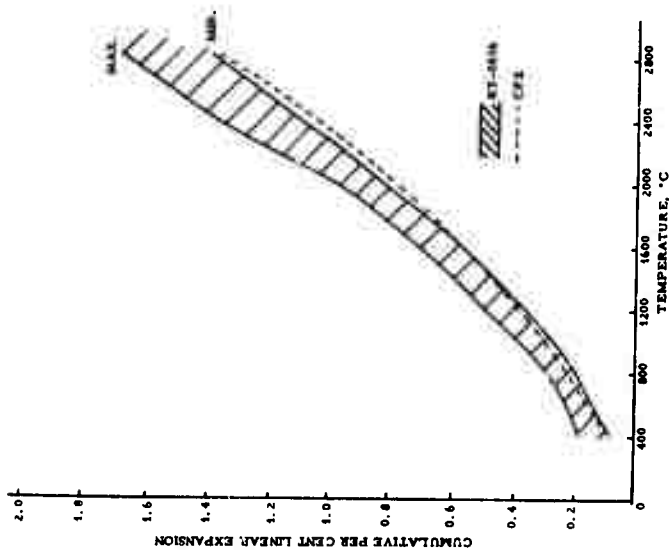


Figure 110. High-Temperature Thermal Expansion for With-Grain RT-0036 and CFZ

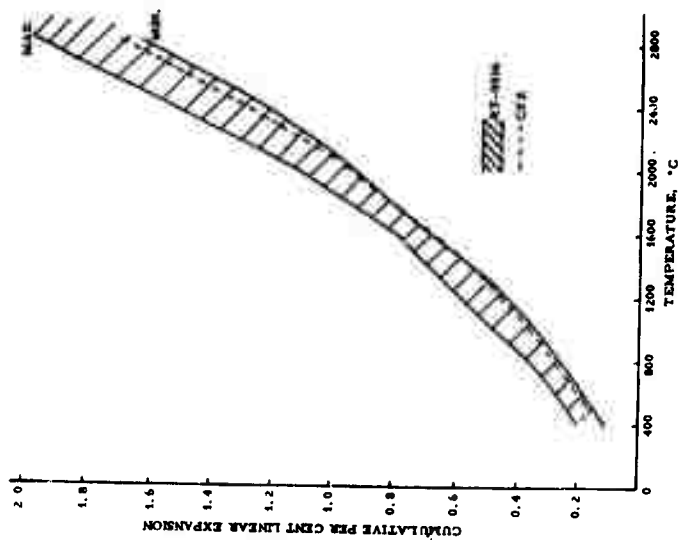
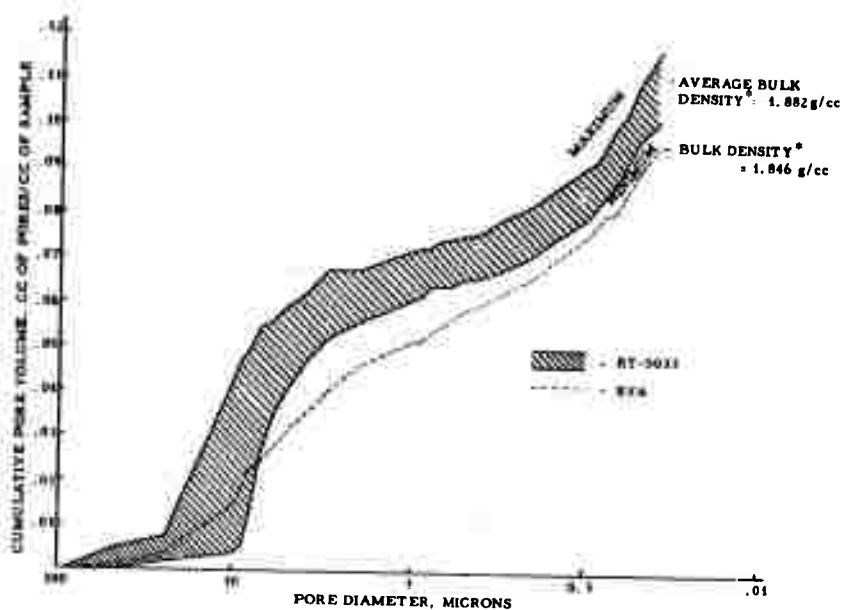


Figure 111. High-Temperature Thermal Expansion for Across-Grain RT-0036 and CFZ



* BULK DENSITY DETERMINED BY MERCURY DISPLACEMENT

Figure 112. Pore Size Distribution of Grades RT-0033 L-165 and RVA

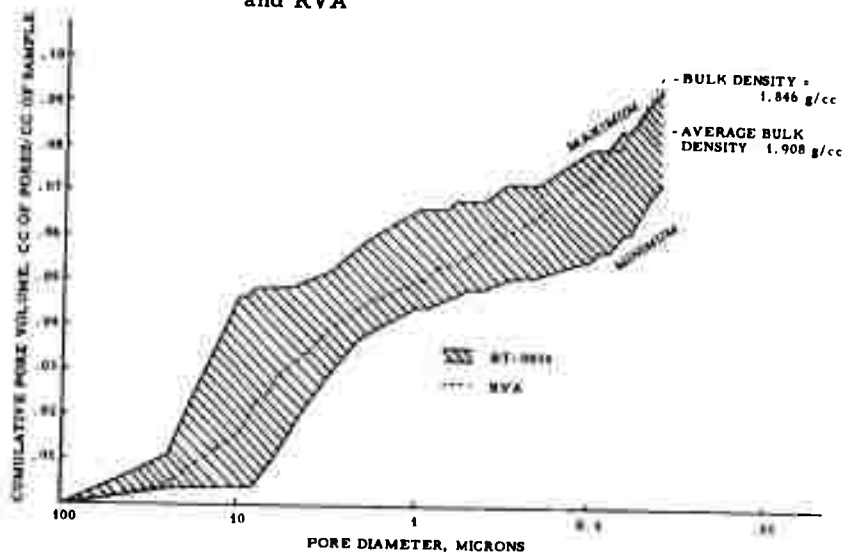


Figure 113. Pore Size Distribution of Grades RT-0034 L-924 and RVA

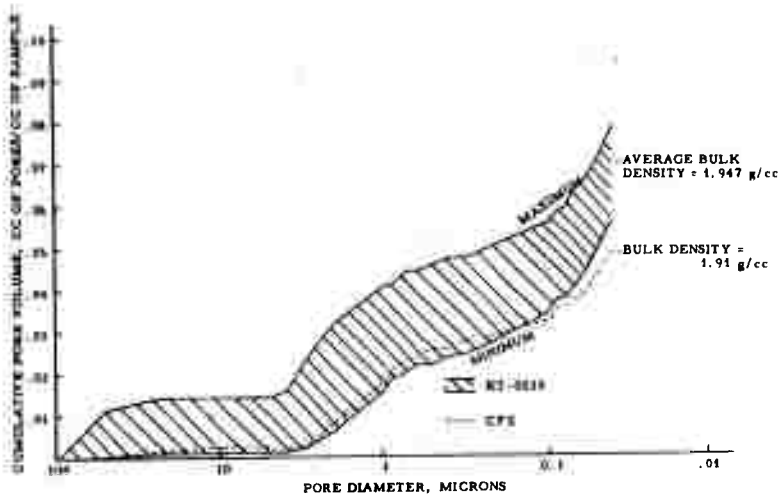


Figure 114. Pore Size Distribution of Grades RT-0035 and CFZ

L-925

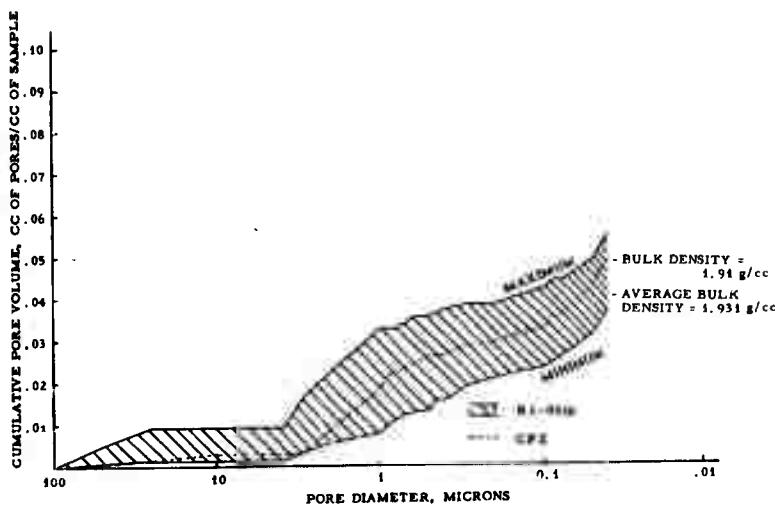


Figure 115. Pore Size Distribution of Grades RT-0036 and CFZ

L-926

4.5.2. High Thermal Expansion Coke

4.5.2.1. Materials and Processes

Pressure-cured graphite billets were prepared from the high thermal expansion cokes produced from air-blown vacuum residuum and carbon-seeded atmospheric residuum charge stocks. Two grades (RT-0037 and RT-0040) were made as shown in the "A" Process of Figure 102. Two additional grades (RT-0041 and RT-0044) were made as shown in the "B" Process of Figure 102. Table 136 identifies each of the RT grade numbers.

Table 136. Grade Designation for Graphites from Various Cokes

Raw Material for Coke	Process	Grade
Air-Blown Vacuum Residuum	A	RT-0037
	B	RT-0041
2.0% Acetylene Black-Seeded Atmospheric Residuum	A	RT-0040
	B	RT-0044

In the various "A" and "B" processing steps involving the crushing and grinding of coke and graphite materials, the seeded and air-blown cokes were considerably harder than the slurry oil or vacuum residuum materials. The carbon black-seeded cokes were harder than the air-blown cokes.

In the case of the carbon-seeded and air-blown materials, binder levels for billet fabrication by the "A" processing step were less than for the "B" processing steps. Slightly lower binder levels were required for the seeded materials than for the air-blown materials.

Billet curing times for the seeded and air-blown materials were considerably longer than for the slurry oil or vacuum residuum materials. Required curing time for billets formed from the carbon black-seeded materials were greater than for those formed using the air-blown materials. The poor electrical and thermal conductivity of the billets containing carbon black were responsible for the extended curing times in this case. "B" process billets required longer curing times than "A" process billets.

Baking and graphitizing schedules similar to those used for vacuum residuum (RT-0034) and slurry oil (RT-0033) pressure-cured billets were successfully used in processing the above materials.

4.5.2.2. Properties

Testing of three to five blocks each of RT-0037, -0040, -0041, and -0044 produced the data shown in Table 137. A comparison of properties on samples cut from the individual blocks can be made from Tables 138 to 143. High-temperature thermal expansion and mercury porosimetry data are shown in Figures 116 to 127.

Table 137. Physical Properties of Grades RT-0037, -0040, -0041, -0044

	RT-0037			RT-0040			RT-0041			RT-0044		
	N*	\bar{X}	σ	N	\bar{X}	σ	N	\bar{X}	σ	N	\bar{X}	σ
Bulk Density, g/cc	196	1.856	0.008	156	1.799	0.007	83	1.832	0.010	115	1.782	0.010
Specific Resistances, 10^{-4} ohm-cm												
W/G	83	14.930	0.182	72	17.080	0.365	15	14.230	0.408	46	14.880	0.240
A/G	113	17.150	0.423	84	19.800	0.670	15	16.570	0.932	69	19.850	0.649
Young's Modulus, 10^4 lbs./in. ²												
W/G	83	1.610	0.040	72	1.520	0.040	47	1.520	0.050	46	1.490	0.040
A/G	113	1.230	0.060	84	1.140	0.100	36	1.110	0.160	69	1.000	0.070
Flexural Strength, lbs./in. ²												
W/G	83	3,010	256	72	2,747	250	47	2,635	200	46	2,529	120
A/G	113	1,759	206	84	1,469	297	36	1,597	289	69	1,471	170
Compressive Strength, lbs./in. ²												
W/G	48	12,497	862	41	10,910	1,398	30	11,513	1,094	29	9,470	491
A/G	38	11,790	717	36	10,660	820	30	10,759	1,344	29	9,100	504
Thermal Expansion, (30-100°C), $10^{-6}/^{\circ}\text{C}$												
W/G	15	4.232	0.158	12	4.424	0.102	8	4.310	0.042	9	2.877	0.024
A/G	15	4.525	0.242	12	4.893	0.164	9	4.580	0.100	9	2.520	0.095

Table 138. Bulk Density, g/cc Property Variations for RT-0037, -0040, -0041 and -0044

Block Number		N*	\bar{X}	σ
RT-0037	1	37	1.860	0.004
	2	40	1.858	0.008
	3	40	1.852	0.009
	4	40	1.853	0.009
	5	39	1.859	0.006
All Samples		196	1.856	0.008
RT-0040	1	40	1.795	0.008
	2	34	1.804	0.006
	4	42	1.798	0.007
	5	40	1.802	0.004
All Samples		156	1.799	0.007
RT-0041	1	28	1.831	0.014
	2	25	1.835	0.008
	3	30	1.830	0.011
All Samples		83	1.832	0.010
RT-0044	1	37	1.789	0.014
	2	40	1.782	0.010
	3	38	1.776	0.005
All Samples		115	1.782	0.010

* N = Number of Samples; \bar{X} = Average Value; σ = Standard Deviation.

Table 139. Specific Resistance, $10^{-4} \Omega\text{-cm}$, Property Variation for RT-0037, -0040, -0041, and -0044

Block Number		With Grain			Across Grain		
		N	\bar{X}	σ	N	\bar{X}	σ
RT-0037	1	16	14.97	0.20	21	16.77	0.27
	2	18	14.83	0.15	22	17.09	0.38
	3	18	14.94	0.17	22	17.43	0.37
	4	16	15.01	0.20	24	17.38	0.41
	5	15	14.88	0.15	24	17.04	0.36
All Samples		83	14.93	0.182	113	17.15	0.428
RT-0040	1	18	17.55	0.39	22	20.04	0.48
	2	18	16.86	0.15	16	20.40	0.50
	4	18	17.02	0.18	24	19.18	0.50
	5	18	16.89	0.12	22	19.81	0.56
All Samples		72	17.08	0.37	84	19.80	0.67
RT-0041	1	5	14.08	----	5	16.10	----
	2	5	14.22	----	5	16.45	----
	3	5	14.39	----	5	17.16	----
All Samples		15	14.23	0.41	5	16.57	0.93
RT-0044	1	14	14.82	0.33	23	19.44	0.42
	2	16	14.94	0.22	24	20.09	0.80
	3	16	14.87	0.15	22	20.03	0.45
All Samples		46	14.88	0.24	69	19.85	0.65

Table 140. Young's Modulus, 10^6 lbs./in.^2 , Property Variation for RT-0037, -0040, -0041, and -0044

Block Number		With Grain			Across Grain		
		N	\bar{X}	σ	N	\bar{X}	σ
RT-0037	1	16	1.58	0.04	21	1.25	0.06
	2	19	1.61	0.04	22	1.27	0.06
	3	18	1.61	0.03	22	1.20	0.07
	4	16	1.62	0.03	24	1.22	0.05
	5	15	1.63	0.04	24	1.22	0.06
All Samples		83	1.61	0.04	113	1.23	0.06
RT-0040	1	18	1.55	0.02	22	1.20	0.04
	2	18	1.46	0.03	16	0.99	0.07
	4	18	1.53	0.02	24	1.21	0.06
	5	18	1.52	0.03	22	1.11	0.05
All Samples		72	1.52	0.04	84	1.14	0.10
RT-0041	1	16	1.51	0.06	12	1.22	0.09
	2	13	1.52	0.03	12	1.12	0.13
	3	18	1.53	0.05	12	0.98	1.15
All Samples		47	1.52	0.05	36	1.11	0.16
RT-0044	1	14	1.54	0.03	23	1.06	0.04
	2	16	1.46	0.02	24	0.99	0.08
	3	16	1.48	0.02	22	0.97	0.03
All Samples		46	1.49	0.04	69	1.00	0.07

Table 141. Flexural Strength, lbs./in.², Property Variation for RT-0037, -0040, -0041, and -0044

Block Number		With Grain			Across Grain		
		N	\bar{X}	σ	N	\bar{X}	σ
RT-0037	1	16	2721	187	21	1760	193
	2	18	3109	260	22	1723	226
	3	18	3129	181	22	1834	208
	4	16	3009	196	24	1787	188
	5	15	3055	237	24	1693	201
All Samples		83	3010	256	113	1759	206
RT-0040	1	18	2773	646	22	1512	226
	2	18	2510	226	16	1106	324
	3	18	2621	105	24	1648	201
	4	18	2945	131	22	1495	194
All Samples		72	2747	250	84	1469	297
RT-0041	1	16	2660	216	12	1779	143
	2	13	2567	206	12	1543	296
	3	18	2663	181	12	1468	317
All Samples		47	2635	200	36	1597	289
RT-0044	1	14	2567	132	23	1594	94
	2	16	2487	126	24	1407	204
	3	16	2539	94	22	1418	123
All Samples		46	2529	120	67	1473	170

Table 142. Compressive Strength, lbs./in.², Property Variation for RT-0037, -0040, -0041, and -0044

Block Number		With Grain			Across Grain		
		N	\bar{X}	σ	N	\bar{X}	σ
RT-0037	1	10	12,697	550	7	11,449	937
	2	10	13,125	960	9	12,393	567
	3	9	12,244	486	8	11,454	718
	4	9	12,728	698	7	11,886	397
	5	10	11,689	943	7	11,642	305
All Samples		48	12,497	862	38	11,790	717
RT-0040	1	9	12,247	864	8	11,584	725
	2	10	9,256	903	9	9,891	282
	4	11	11,480	1,087	9	11,038	654
	5	11	10,740	754	10	10,271	350
All Samples		41	10,910	1,398	36	10,660	820
RT-0041	1	10	11,451	994	10	10,939	1,580
	2	10	11,827	1,390	10	10,999	1,540
	3	10	11,260	864	10	10,340	321
All Samples		30	11,513	1,094	30	10,759	1,344
RT-0044	1	10	9,945	271	10	9,668	236
	2	9	9,353	463	10	8,642	233
	3	10	9,099	258	9	8,962	225
All Samples		29	9,470	491	29	9,100	504

Table 143. Thermal Expansion (30-100°C), 10⁶/°C, Property Variation for RT-0037, -0040, -0041, and -0044

Block Number		With-Grain			Across Grain		
		N	\bar{X}	σ	N	\bar{X}	σ
RT-0037	1	3	4.32	-	3	4.73	-
	2	3	4.15	-	3	4.67	-
	3	3	4.14	-	3	4.54	-
	4	3	4.26	-	3	4.37	-
	5	3	4.32	-	3	4.37	-
All Samples		15	4.23	0.158	15	4.53	0.242
RT-0040	1	3	4.46	-	3	4.97	-
	2	3	4.30	-	3	4.90	-
	4	3	4.51	-	3	4.89	-
	5	3	4.43	-	3	4.81	-
All Samples		12	4.42	0.102	12	4.89	0.164
RT-0041	1	3	4.32	-	3	4.61	-
	2	2	4.28	-	3	4.60	-
	3	3	4.32	-	3	4.53	-
All Samples		8	4.31	0.042	9	4.58	0.100
RT-0044	1	3	2.85	-	3	3.44	-
	2	3	2.89	-	3	3.55	-
	3	3	2.93	-	3	3.57	-
All Samples		9	2.87	0.024	9	3.52	0.095

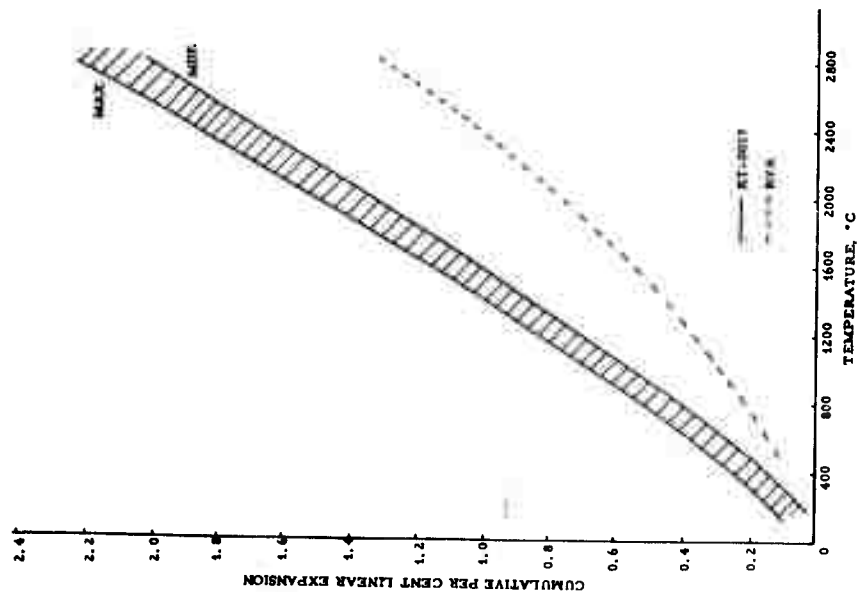


Figure 116. High-Temperature Thermal Expansion for With-Grain RT-0037 and RVA

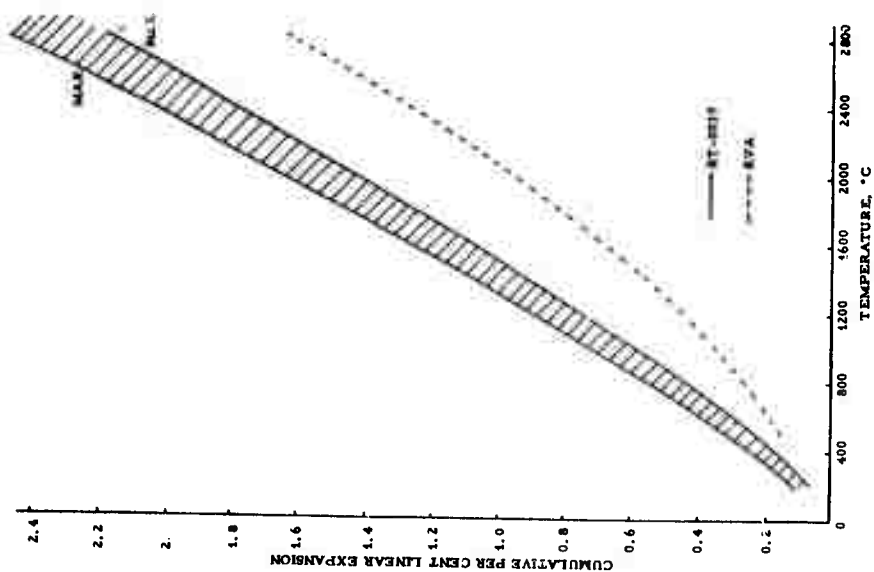


Figure 117. High-Temperature Thermal Expansion for Across-Grain RT-0037 and RVA

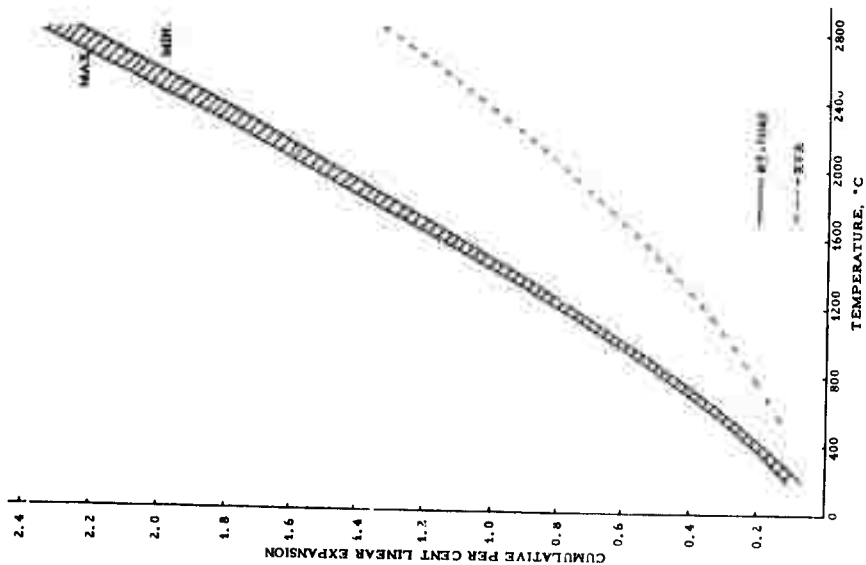


Figure 118. High-Temperature Thermal Expansion for With-Grain RT-0040 and RVA

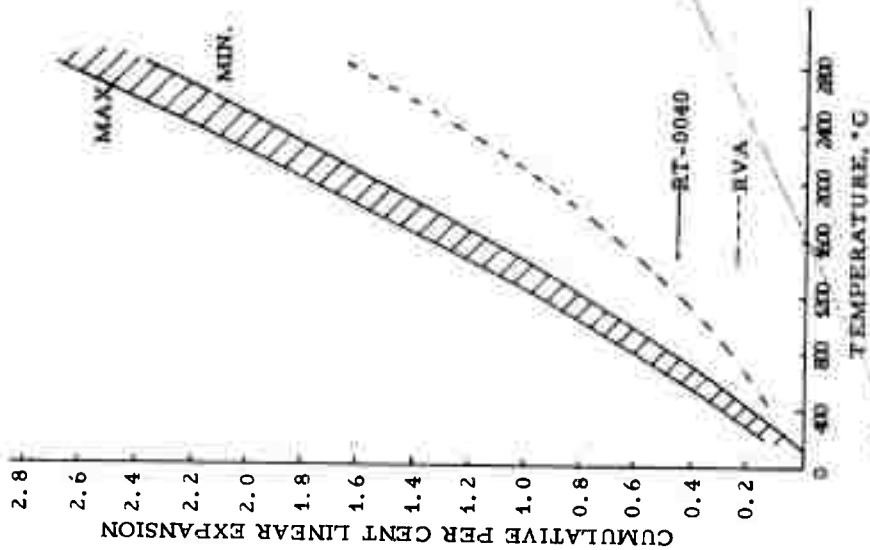


Figure 115. High-Temperature Thermal Expansion for Across-Grain RT-0040 and RVA

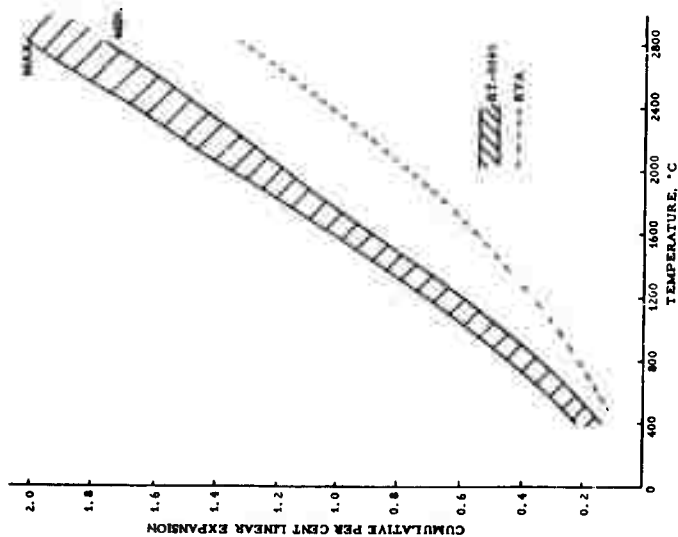


Figure 120. High-Temperature Thermal Expansion for With-Grain RT-0041 and RVA

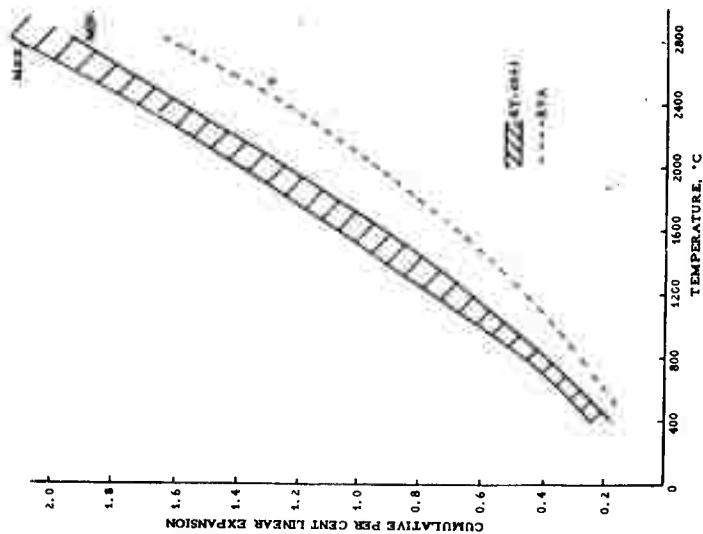


Figure 121. High-Temperature Thermal Expansion for Across-Grain RT-0041 and RVA

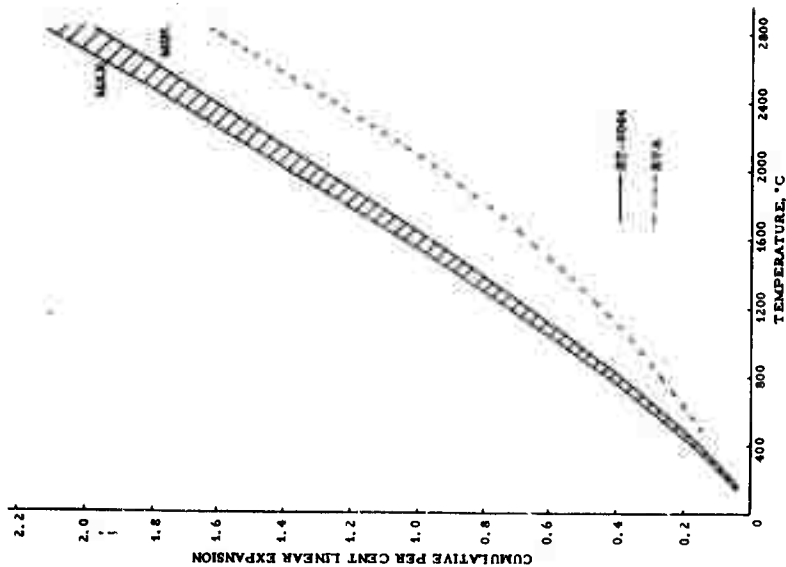


Figure 122. High-Temperature Thermal Expansion for With-Grain RT-0044 and RVA

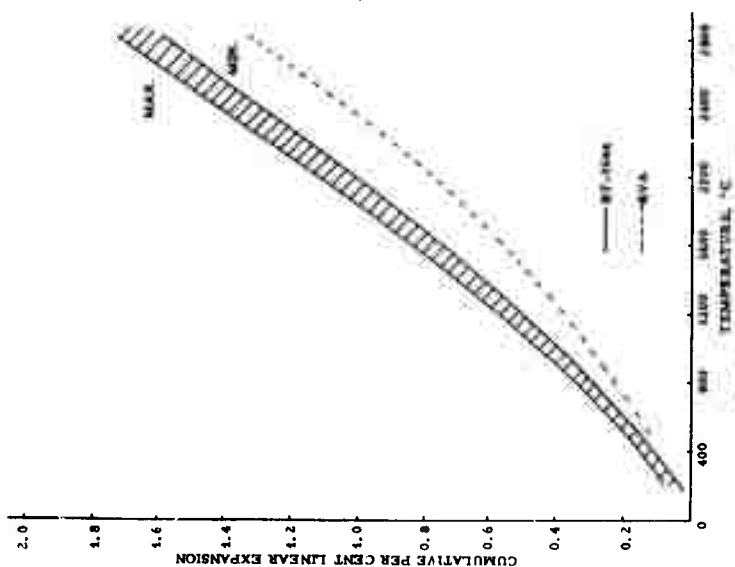


Figure 123. High-Temperature Thermal Expansion for Across-Grain RT-0044 and RVA

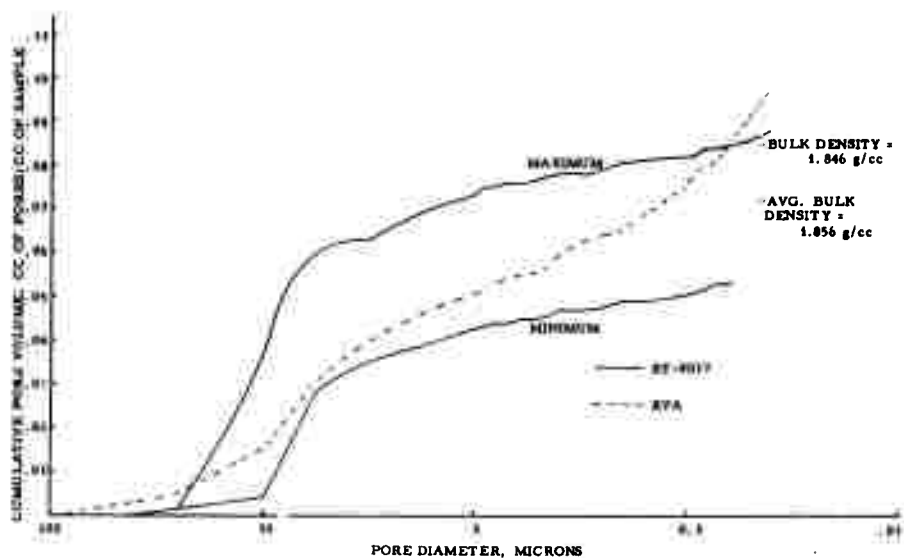


Figure 124. Pore Size Distribution of Grades RT-0037 and RVA

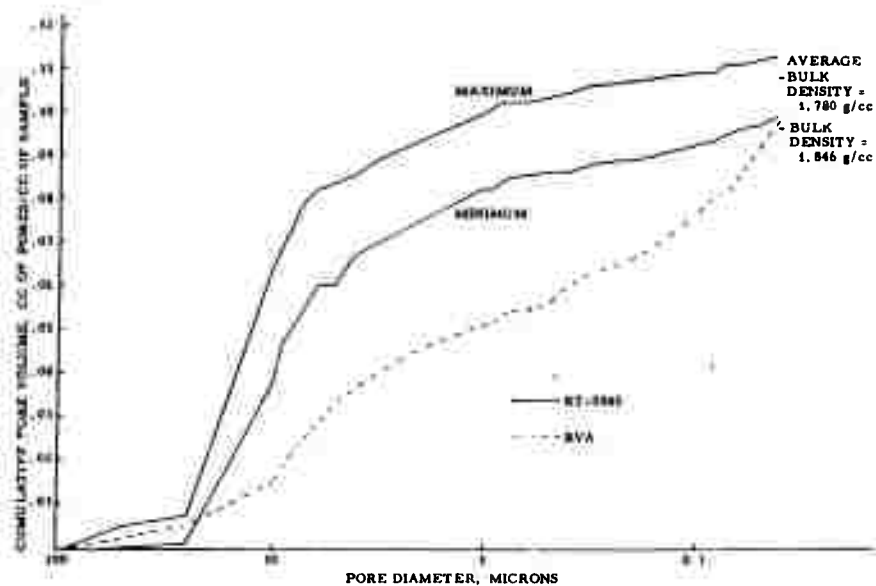


Figure 125. Pore Size Distribution of Grades RT-0040 and RVA

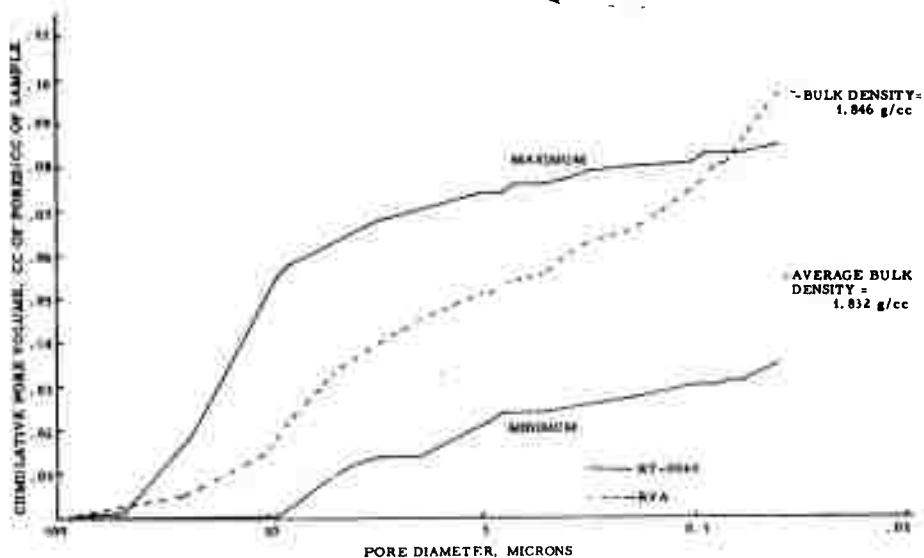


Figure 126. Pore Size Distribution of Grades RT-0041 and RVA

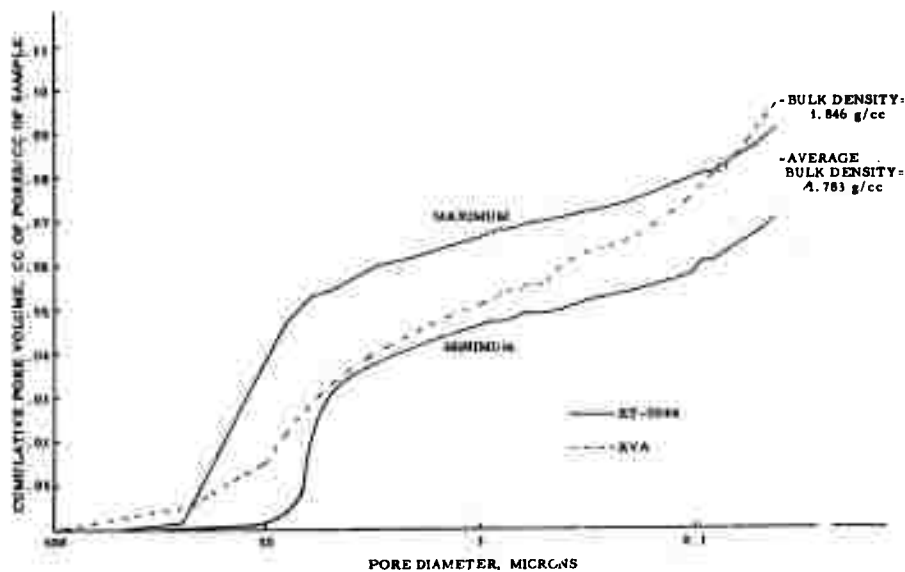


Figure 127. Pore Size Distribution of Grades RT-0044 and RVA

5. REFERENCES

1. Edstrom, T., and I. C. Lewis, "Thermal Reactivity of Aromatic Hydrocarbons," WADD Technical Report 61-72, Volume X and Supplement to Volume X.
2. Lewis, I. C., and T. Edstrom, "Carbonization Studies of Polynuclear Aromatic Hydrocarbons," WADD Technical Report 61-72, Volume XXVII.
3. Ruland, W., private communication.
4. Improved Graphite Materials for High-Temperature Aerospace Use, ML-TDR-64-125, Vol. I, "Research and Development for Improved Graphite Materials."
5. Singer, L. S., and I. C. Lewis, "An Electron Spin Resonance Study of Thermal Decomposition Reactions of Organic Compounds," WADD Technical Report 61-72, Volume XVI.
6. Singer, L. S., and I. C. Lewis, Carbon 2, 115 (1964).
7. Dziewonski, K., and Z. Leyko, Chem. Ber. 47, 1679 (1914).
8. Clar, E., K. F. Lang, and H. Scheulz-Kresow, Chem. Ber. 88, 1520 (1955).
9. Dziewonski, K., Chem. Ber. 53, 2173 (1920).
10. Clar, E., "Polycyclic Hydrocarbons," Academic Press, New York, N. Y., (1964).
11. Waldmann, H., and G. Pollak, J. Prakt. Chem. 150, 113 (1938).
12. McConnell, H. M., J. Chem. Phys. 24, 764 (1956).
13. Carrington, A., Quarterly Rev. 17, 67 (1963).
14. Tuttle, T. R., and S. I. Weissman, J. Am. Chem. Soc. 80, 5342 (1958).
15. Carrington, A., F. Dravineks, and M. C. R. Symons, J. Chem. Soc. 947, (1959).
16. deBoer, E., and S. I. Weissman, J. Am. Chem. Soc. 80, 4549 (1958).
17. Hoijsink, G. J., J. N. Townsend, and S. I. Weissman, J. Chem. Phys. 34, 507 (1961).

REFERENCES (CONT'D)

18. Weissman, S. I., E. de Boer, and J. J. Conradi, *J. Chem. Phys.* 26, 963 (1957).
19. Hoijtink, G. J., and W. P. Weijland, *Rec. Trav. Chem.* 76, 836 (1957).
20. Aalbersberg, W. I., G. J. Hoijtink, E. L. Mackor, and W. P. Weijland, *J. Chem. Soc.* 3049 (1959).
21. Baughan, E. C., T. P. Jones, and L. G. Stoodley, *Proc. Chem. Soc.* 274 (1963).
22. Weissman, S. I., E. de Boer, and J. J. Conradi, *J. Chem. Phys.* 26, 963 (1957).
23. Stenngren, G. E., and J. Kommandeur, *J. Chem. Phys.* 35, 1636 (1961).
24. Hsu, K., S. Chin, T. Chin, and Y. Tand, *Ko Hsuch Tung Pao* 12, 47 (1964); *C. A.* 61, 1412 (1964).
25. Rooney, J. J., and R. C. Pink, *Proc. Chem. Soc.* 142 (1961).
26. Singer, L. S., and J. Kommandeur, *J. Chem. Phys.* 34, 133 (1961).
27. Hirota, K., and K. Kuwata, *Bull. Chem. Soc. Japan* 36, 229 (1963).
28. Rooney, J. J., and R. C. Pink, *Trans. Far. Soc.* 58, 1632 (1962).
29. Krauss, H., and V. Defner, *Z. Naturfor.* 19b, 1 (1965).
30. Matsunaga, Y., *Bull. Chem. Soc. Japan* 34, 1293 (1961).
31. de Boer, E., and A. P. Proat, *Mol. Phys.* 8, 291 (1964).
32. Hilpert, S., and L. Wolf, *Ber. Deut. Chem. Ges.* 46, 2215 (1913).
33. Brass, K., and E. Tengler, *Chem. Ber.* 46, 2215 (1913); K. Brass and H. Eichler, *ibid.*, 67, 779 (1934).
34. Aalbersberg, W. I., G. J. Hoijtink, E. L. Mackor, and W. P. Weijland, *J. Chem. Soc.* 3055 (1959).
35. Das, M., and S. Basu, *Spect. Acta* 17, 897 (1961).
36. Matsunaga, Y., *Bull. Chem. Soc. Japan* 34, 893 (1961).
37. Kinoshita, M., *Bull. Chem. Soc. Japan* 35, 1137 (1962).

REFERENCES (CONT'D)

38. Leftin, H. P., and M. C. Hobson, Jr., *Advances in Catalysis* 14, 115 (1963).
39. *Gmelin's Handbuch der Anorganischen Chemie*, Vol. 18 B₂, p. 441.
40. Townsend, M. G., and S. I. Weissman, *J. Chem. Phys.* 32, 309 (1960).
41. Coulson, C. A., and A. Golebiewski, *Proc. Roy. Soc.* 71, 1961.
42. Fukui, K., T. Yonezawa, and H. Shingo, *J. Chem. Phys.* 20, 722 (1952).
43. Bolton, J. R., A. Carrington, and A. D. McLachlan, *Mol. Phys.* 5, 31 (1962).
44. Colpa, J. P., and J. R. Bolton, *Mol. Phys.* 6, 273 (1963).
45. Russell, G. A., E. G. Jansen, E. T. Strom, *J. Am. Chem. Soc.* 84, 4155 (1962).
46. Evans, A. G., B. J. Tabner, *J. Chem. Soc.* 5560 (1963).
47. Carrington, A., and J. dos Santos Veiga, *Mol. Phys.* 5, 285 (1962).
48. Bolton, J. R., and A. Carrington, *Mol. Phys.* 4, 270 (1961).
49. Katz, T. J., and H. L. Strauss, *J. Chem. Phys.* 32, 1873 (1960).
50. Carrington, A., and J. dos Santos Veiga, *Mol. Phys.* 5, 21 (1962).
51. Brown, T., *J. Chem. Phys.* 41, 2223 (1964).
52. Frankel, G. K., *J. Chem. Phys.* 37, 1489 (1962).
53. Hausser, K. H., L. Mongini, and R. van Stienwinkel, *Z. Naturfor*, 19a, 777 (1964).
54. Iwaizumi, M., and T. Isobe, *Bull. Chem. Soc. Japan* 37, 1651 (1964).
55. Stone, E. W., and A. H. Maki, *J. Chem. Phys.* 38, 1999 (1963).
56. Giacometti, G., P. L. Nordio, and M. V. Pavan, *Theor. Chim. Acta* 1, 404 (1963).
57. Sayetta, T. C., and J. D. Memory, *J. Chem. Phys.* 40, 2748 (1964).
58. Tuttle, T. R., Jr., R. L. Ward, and S. I. Weissman, *J. Chem. Phys.* 25, 189 (1956).

REFERENCES (CONT'D)

59. Murrell, J. N., and J. Tanaka, *Mol. Phys.* 7, 363 (1964).
60. Brass, K., and K. Fanta, *Ber. Deut. Chem. Ges.* 69B, 1 (1936).
61. Brass, K., and E. Tengler, *ibid.* 64, 1650 (1931).
62. Handa, T., *Bull. Chem. Soc. Japan* 35, 1361 (1962).
63. Herbststein, F. H., and G. M. J. Schmidt, *J. Chem. Soc.* 3314 (1954).
64. Nyburg, S. C., *Acta Cryst.* 7, 779 (1954).
65. Suzuki, H., *Bull. Chem. Soc. Japan* 33, 389 (1960).
66. Adam, F. C., and S. I. Weissman, *J. Am. Chem. Soc.* 80, 2057 (1958).
67. McLachlan, A. D., *Mol. Phys.* 3, 233 (1960).
68. We have omitted from these correlations the data for the azulene and pyrene radical ions for which large negative spin densities have been predicted by theory and confirmed by experiment. The coupling constants for the naphthalene dimer have been doubled and are shown as triangles in Figures 49, 50, and 51.
69. Symons, M. C. R., "The Identification of Organic Free Radicals by Electron Spin Resonance," in V. Gold, Ed., *Advances in Physical Organic Chemistry*, 1:289 (1963).
70. Reference 20, p. 3051.
71. Balk, P., S. de Bruijn, and G. J. Hoijsink, *Rec. trav. chim.* 76 907 (1957).
72. Reference 34, p. 3056.
73. de Boer, E., and S. I. Weissman, *Rec. trav. chim.* 76 824 (1957).
74. Reference 23, p. 1637.
75. Paul, D. E., D. Lipkin, and S. I. Weissman, *J. Am. Chem. Soc.* 78 116 (1956).
76. Bolton, J. R., and A. Carrington, *Mol. Phys.* 4, 497 (1961).
77. Bolton, J. R., *J. Chem. Phys.* 41, 2455 (1964).
78. Bolton, J. R., and A. Carrington, *Proc. Chem. Soc.* 174 (1961).
79. Hulme, R., and M. C. R. Symons, *J. Chem. Soc.* 1120 (1965).

REFERENCES (CONT'D)

80. Brivati, J. A., R. Hulme, and M. C. R. Symons, *Proc. Chem. Soc.* 384 (1961).
81. Carter, M. K., and G. Vincow, *Bull. Am. Phys. Soc., Series 2*, Vol. 10, 374 (1965).
82. Jacobsen, O., *Chem. Ber.* 19, 1209 (1886).
83. Smith, L. I., *Organic Reactions* 1, 370 (1942).
84. Kilpatrick, M., and H. H. Hyman, *J. Am. Chem. Soc.* 80, 77 (1958).
85. Freed, J. H., and G. K. Fraenkel, *J. Chem. Phys.* 41, 699 (1965).
86. Kommandeur, J., *Mol. Phys.* 4, 509 (1961).
87. Blois, M. S., H. W. Brown, and J. E. Maling, "Free Radicals in Biological Systems," Academic Press, New York (1961), p. 117.
88. Bohlmann, F., and J. Riemann, *Chem. Ber.* 97, 1515 (1964).
89. Maclean, C., and E. L. Mackor, *Mol. Phys.* 4, 241 (1961).
90. Birchall, T., and R. J. Gillespie, *Can. J. Chem.* 42, 502 (1964).
91. Doering, W. von E., M. Saunders, H. G. Boyton, H. W. Earhart, E. F. Wadley, W. R. Edwards, and G. Laber, *Tetrahedron* 4, 178 (1958).
92. Fessenden, R. W., and R. H. Schuler, *J. Chem. Phys.* 39, 2147 (1963).
93. Freed, J. H., and G. K. Fraenkel, *J. Chem. Phys.* 41, 699 (1965).
94. de Boer, E., and E. L. Mackor, *J. Chem. Phys.* 38, 1450 (1963).
95. McConnell, H. M., and R. E. Robertson, *J. Phys. Chem.* 61, 1018 (1957).
96. Stone, A. J., *Proc. Roy. Soc. A* 271, 424 (1963); *Mol. Phys.* 6, 509 (1963).
97. McConnell, H. M., and D. Chestnut, *J. Chem. Phys.* 28, 107 (1958).
98. McConnell, H. M., C. Heller, T. Cole, and R. W. Fessenden, *J. Am. Chem. Soc.* 82, 766 (1960).

REFERENCES (CONT'D)

99. Cole, T., and C. Heller, J. Chem. Phys. 34, 1085 (1961).
100. Anderson, M. E., G. E. Pake, and T. R. Tuttle, Jr., J. Chem. Phys. 33, 1581 (1960).
101. Gutowsky, H. S., H. Kusumoto, T. H. Brown, and D. H. Anderson, J. Chem. Phys. 30, 860 (1959).
102. Nenitzescu, C. D., and E. Solomonica, Organic Syntheses Coll. Vol. 2, A. H. Blatt, ed., 496 (1955).
103. Schlenk, W., A. Herzenstein, and T. Weickel, Chem. Ber. 43, 1754 (1910).
104. Aitken, R. R., G. M. Badger, and J. W. Cook, J. Chem. Soc. 331 (1950).
105. Craig, Lyman C., Walter A. Jacobs, and George L. Lavin, J. Biol. Chem. 139, 277 (1941).
106. Gabriel, S., and E. Leupold, Chem. Ber. 31, 1284 (1898).
107. Fieser, L. F., J. Am. Chem. Soc. 53, 2329 (1931).
108. Bell, F., and D. H. Waring, J. Chem. Soc. 267, (1949).
109. Bertholet, Marcellin Pierre Eugene (1827-1907), Les Carbures d'hydrogene, 1901 (Gauthier-Villars, Paris). Other specific references to Bertholet's pioneer work are noted in Reference 110.
110. Egloff, Gustav, Reactions of Pure Hydrocarbons, especially Chapter V (pp. 478-666), "Reactions of Aromatic Hydrocarbons," 1937 (Reinhold, New York).
111. Sachanen, A. N., Conversion of Petroleum; (a) 1st Edition, 1940 (Reinhold, New York); (b) 2nd Edition, 1948 (Reinhold, New York).
112. Kinney, C. R., "Pyrolytic Reactions of Aromatic Hydrocarbons," in The Chemistry of Petroleum Hydrocarbons, Volume II, pp. 113-136, B. T. Brooks, et al., Editors, 1955 (Reinhold, New York).
113. Steacie, E. W. R., Atomic and Free Radical Reactions, 2nd Ed., Vols. I and II, 1954 (Reinhold, New York).
114. Hurd, C. D., The Pyrolysis of Carbon Compounds, 1929 (The Chemical Catalog Co., New York).

REFERENCES (CONT'D)

115. Ipatieff, Vladimir N., Catalytic Reactions at High Pressures and Temperatures, 1936 (MacMillan, New York).
116. Reference 115, p. 398.
117. Sachanen, A. N., and M. D. Tilicheev, Chemistry and Technology of Cracking, 1932 (Chemical Catalog Company, New York).
118. Tilicheev, M. D., and V. K. Shchitkov, "Cracking of Aromatic Hydrocarbons under pressure," Foreign Pet. Tech. 5, 393-420, 481-540 (1937); 6, 43-74 (1938); 7, 343-375 (1939).
119. Madison, J. J., and R. M. Roberts, "Pyrolysis of Aromatics and Related Heterocyclics," Ind. Eng. Chem. 50, 237-250 (1958).
120. Lang, K. E., H. Buffleb, J. Kalowy, and M. Zander, Chem. Ber. (a) 90, 2888-2893 (1957); (b) 90, 2894-2898 (1957); (c) 91, 2866-2870 (1958); (d) 93, 303-309 (1960); (e) 94, 523-526 (1961); (f) 94, 1075-1082 (1961); (g) 94, 1871-1876 (1961); (h) 95, 1049-1051 (1962).
121. Bolt, R. O., and J. G. Carroll, Proc. 1st Inter. Conf. on the Peaceful Uses of Atomic Energy, 7, 546-555, 1956 (United Nations, New York).
122. Zartman, I. F., "Organic Materials," in Reactor Handbook, Vol. I, 943-954, C. A. Tipton, Editor, 1960 (Interscience, New York).
123. Halas, D. R. de, Proc. 2nd Inter. Conf. on the Peaceful Use of Atomic Energy 29, 287-291, 1958 (United Nations, Geneva).
124. Trilling, C. A., et al., ibid., 292-311.
125. G  umann, T., and J. M. Rayroux, Helv. Chim. Acta 45, 1563-71 (1962).
126. Appleby, W. G., J. W. Gibson, and G. M. Good, Ind. Eng. Chem. Prod. Res. Develop. 1, 102-110 (1962).
127. Winslow, N. M., unpublished report, National Carbon Company Research Laboratory, ERC-249, February 4, 1947.
128. Mitchell, C. V., unpublished report, National Carbon Company Research Laboratory, ERC-368, November 27, 1956.
129. Kinney, C. R., and E. del Bel, "Pyrolytic Behavior of Unsubstituted Aromatic Hydrocarbons," Ind. Eng. Chem. 46, 548-556 (1954).

REFERENCES (CONT'D)

130. Milliken, S. R., "The Nature and Formation of Carbon and Graphite," Doctorate Thesis, The Pennsylvania State University, January 1954; C. R. Kinney, "Studies on Producing Graphitizable Carbons," Proceedings of the Second Conference on Carbon, June 1955, pp. 83-92, 1956 (Waverly, Baltimore).
131. Nunn, R. C., "A Study of the Carbonization and Graphitization of Anthracene," Doctorate Thesis, The Pennsylvania State University, June 1955 (University Microfilms, Ann Arbor); C. R. Kinney, R. C. Nunn, and P. L. Walker, Jr., "Carbonization of Anthracene and Graphitization of Anthracene Carbons," Ind. Eng. Chem. 49, 880-884 (1957).
132. Conroy, J. S., R. S. Slysh, D. B. Murphy, and C. R. Kinney, "Studies on Producing Graphitizable Carbons," Proceedings of the Third Conference on Carbon, June 17-21, 1957, pp. 395-403, 1959 (Pergamon, New York).
133. United States Patent 2,424,449 (Autoclave Engineers, Inc.).
134. United States Patent 2,996,363 (Autoclave Engineers, Inc.).
135. Stout, C. F., M. Janes, and J. A. Biehl, "Studies of the Quality of Petroleum Coke from a Pilot-Scale Delayed Coker," WADD Technical Report 61-72, Volume XXXVI, October 1963.
136. Franklin, R. E., Trans. Faraday Soc. 45, 274-286, 668-682 (1949).
137. Davidson, H. W., and H. H. W. Losty, G. E. C. Journal 30, 22-30 (1963).
138. Kipling, J. J., et al., Carbon 1, 315-328 (1964).
139. Yamada, S., and H. Sato, Nature (London) 193, 261-62 (1962).
140. Billmeyer, F. W., Jr., Textbook of Polymer Science, pp. 289-90, 1962 (Interscience, New York).
141. Nelson, W. L., Petroleum Refinery Engineering, 4th Edition, 1958 (McGraw-Hill, New York).
142. Hirsch, J. H., and E. K. Fisher, "Conditions and Results of Thermal Cracking for Gasoline," in The Chemistry of Petroleum Hydrocarbons, Vol. II, 27-60, 1955 (Reinhold, New York).
143. Ambrose, D., Trans. Faraday Soc. 59, 1988-93 (1963).
144. Egloff, G., Physical Constants of Hydrocarbons, Vol. IV, pp. 180-181, 1947 (Reinhold, New York).

REFERENCES (CONT'D)

145. Hougen, O. A., K. M. Watson, and R. A. Ragatz, Chemical Process Principles, 2d Ed., Vol. II, 556-638, 1959 (Wiley, New York).
146. Reid, R. C., and T. K. Sherwood, The Properties of Gases and Liquids, 1958 (McGraw-Hill, New York).
147. Zhuravlev, D. I., J. Phys. Chem. (USSR) 9, 875-82 (1937); C. A. 31, 8287 (1937).
148. Ambrose, D., J. D. Cox, and R. Townsend, Trans. Faraday Soc. 56, 1452-59 (1960).
149. Schröer, E., Z. physik. Chem. B49, 271-8 (1941); C. A. 36, 6389 (1942).
150. Zander, M., and W. Franke, Chem. Ber. 91, 2794-97 (1958).
151. de Tar, D. F., and R. A. J. Long, J. Am. Chem. Soc. 80, 4742-43 (1958).
152. Fieser, L. F. and M. Fieser, Advanced Organic Chemistry, p. 671, 1961 (Reinhold, New York).
153. Laidler, K. S., Chemical Kinetics, 1950 (McGraw-Hill, New York).
154. Reference 4, p. 128.
155. Reference 4, p. 119.
156. Corbett, L. W., Division of Petroleum Chemistry Preprint, American Chemical Society, Volume 9, No. 2, pp B81-88, April 1964.
157. Gutowsky, H. S., and Julia Chow Tai, J. Chem. Phys. 39, 208 (1963).
158. Singer, L. S., Proceedings of the Fifth Carbon Conference, Vol. II, p. 37, Pergamon Press, Oxford (1963).
159. Singer, L. S., W. J. Spry, and W. H. Smith, Proceedings of the Third Carbon Conference, p. 121, Pergamon Press, Oxford (1959).
160. Blois, M. S., Jr., H. W. Brown, and J. E. Maling, Free Radicals in Biological Systems, p. 117, Academic Press, New York, (1961).
161. Wagoner, G., Phys. Rev. 118, 647 (1960).

REFERENCES (CONT'D)

162. Singer, L. S., and G. Wagoner, J. Chem. Phys. 37, 1812 (1962).
163. de Ruiter, E., and H. Tschamler, Brennstoff-Chem. 40, 41 (1959); 42, 311 (1961).
164. Charette, L. P., and G. T. Bischofberger, Binders for Carbon Electrodes in the Aluminum Industry, Ind. Eng. Chem. 47, 1412-1415, (July 1955).
165. de Ruiter, E., J. F. M. Oth, V. Sandor, and H. Tschamler, "Characterization of Binders in the Fabrication of Graphite Bodies," WADD Technical Report 61-72, Supplement to Volume XI.

DOCUMENT CONTROL DATA - R&D

(Security classification of title, body of abstract and indexing annotation must be entered when the overall report is classified)

1. ORIGINATOR'S NAME (Author) Union Carbide Corporation Carbon Products Division Advanced Materials Laboratory, Lawrenceburg, Tenn. and Research Laboratory, Parma, Ohio		2a. REPORT SECURITY CLASSIFICATION <u>Unclassified</u>	
3. REPORT TITLE Improved Graphite Materials for High-Temperature Aerospace Use Vol. III Further Research and Development for Improved Graphite Materials		2b. GROUP N. A.	
4. DESCRIPTIVE NOTES (Type of report and inclusive dates)			
5. AUTHOR(S) (Last name, first name, initial) Lafayette, P. G. (Program Director)			
6. REPORT DATE February 1966		7a. TOTAL NO. OF PAGES 381	7b. NO. OF REFS 165
8a. CONTRACT OR GRANT NO. AF 33(657)-11171 A. PROJECT NO. 7350 C. Task No. 735002		8b. ORIGINATOR'S REPORT NUMBER(S) ML-TDR-64-125 Volume III 8c. OTHER REPORT NUMBER(S) (Any other numbers that may be assigned this report) N. A.	
10. AVAILABILITY/LIMITATION NOTICES This document is subject to special export controls and each transmittal to foreign governments or foreign nationals may be made only with prior approval of the Metals and Ceramics Division (MAM), Air Force Materials Laboratory, Wright-Patterson AFB, Ohio			
11. SUPPLEMENTARY NOTES		12. SPONSORING MILITARY ACTIVITY Air Force Materials Laboratory MAMC Wright-Patterson AFB, Ohio	
13. ABSTRACT The pyrolysis mechanisms and thermal reactivity of aromatic and heterocyclic compounds are appreciably modified by substitution with nitrogen-, oxygen-, and halogen-containing groups. Aromatic nuclei with strongly activating side groups generally lead to a disordered graphitic structure. The hydrocarbons which yield well-ordered graphites consist largely of fused planar aromatic compounds. The complex mixtures of aromatic compounds that make up the normal raw materials for carbon and graphite form highly-ordered graphites. Pyrolysis studies have been performed for eleven model aromatic hydrocarbons and for two oxygenated aromatics. The planarity of the condensation products of the initial free radical intermediates determines the degree of ordering of the resulting graphite. Electron spin resonance (ESR) studies indicate that free radical intermediates may play an important role in the acid catalyzed rearrangements of methyl benzenes. Aromatic hydrocarbons and related heterocyclic compounds with two to four rings which produce no residue at atmospheric pressure have been thermally polymerized at super-atmospheric pressures. Graphite bodies have been fabricated using coke filler material prepared by pyrolysis of selected model aromatic compounds. The physical properties of the fabricated bodies are strongly influenced by the molecular structure of the starting compounds. Examination of controlled commercial charge stocks was continued and an effort to correlate the nuclear magnetic resonance and electron spin resonance of these			

Page 1 of 2 pages

DD FORM 1 JAN 64 1473

Unclassified
Security Classification

Unclassified
Security Classification

14. KEY WORDS	LINK A		LINK B		LINK C	
	ROLE	WT	ROLE	WT	ROLE	WT
Carbon Graphite Pyrolysis Aromatic Compounds Heterocyclic Compounds Electron Spin Resonance Cokes Pitch						

INSTRUCTIONS

1. **ORIGINATING ACTIVITY:** Enter the name and address of the contractor, subcontractor, grantee, Department of Defense activity or other organization (corporate author) issuing the report.

2a. **REPORT SECURITY CLASSIFICATION:** Enter the overall security classification of the report. Indicate whether "Restricted Data" is included. Marking is to be in accordance with appropriate security regulations.

2b. **GROUP:** Automatic downgrading is specified in DoD Directive 5200.10 and Armed Forces Industrial Manual. Enter the group number. Also, when applicable, show that optional markings have been used for Group 3 and Group 4 as authorized.

3. **REPORT TITLE:** Enter the complete report title in all capital letters. Titles in all cases should be unclassified. If a meaningful title cannot be selected without classification, show title classification in all capitals in parentheses immediately following the title.

4. **DESCRIPTIVE NOTES:** If appropriate, enter the type of report, e.g., interim, progress, summary, annual, or final. Give the inclusive dates when a specific reporting period is covered.

5. **AUTHOR(S):** Enter the name(s) of author(s) as shown on or in the report. Enter last name, first name, middle initial. If military, show rank and branch of service. The name of the principal author is an absolute minimum requirement.

6. **REPORT DATE:** Enter the date of the report as day, month, year, or month, year. If more than one date appears on the report, use date of publication.

7a. **TOTAL NUMBER OF PAGES:** The total page count should follow normal pagination procedures, i.e., enter the number of pages containing information.

7b. **NUMBER OF REFERENCES:** Enter the total number of references cited in the report.

8a. **CONTRACT OR GRANT NUMBER:** If appropriate, enter the applicable number of the contract or grant under which the report was written.

8b, 8c, & 8d. **PROJECT NUMBER:** Enter the appropriate military department identification, such as project number, subproject number, system numbers, task number, etc.

9a. **ORIGINATOR'S REPORT NUMBER(S):** Enter the official report number by which the document will be identified and controlled by the originating activity. This number must be unique to this report.

9b. **OTHER REPORT NUMBER(S):** If the report has been assigned any other report numbers (either by the originator or by the sponsor), also enter this number(s).

10. **AVAILABILITY/LIMITATION NOTICES:** Enter any limitations on further dissemination of the report, other than those

imposed by security classification, using standard statements such as:

- (1) "Qualified requesters may obtain copies of this report from DDC."
- (2) "Foreign announcement and dissemination of this report by DDC is not authorized."
- (3) "U. S. Government agencies may obtain copies of this report directly from DDC. Other qualified DDC users shall request through _____."
- (4) "U. S. military agencies may obtain copies of this report directly from DDC. Other qualified users shall request through _____."
- (5) "All distribution of this report is controlled. Qualified DDC users shall request through _____."

If the report has been furnished to the Office of Technical Services, Department of Commerce, for sale to the public, indicate this fact and enter the price, if known.

11. **SUPPLEMENTARY NOTES:** Use for additional explanatory notes.

12. **SPONSORING MILITARY ACTIVITY:** Enter the name of the departmental project office or laboratory sponsoring (paying for) the research and development. Include address.

13. **ABSTRACT:** Enter an abstract giving a brief and factual summary of the document indicative of the report, even though it may also appear elsewhere in the body of the technical report. If additional space is required, a continuation sheet shall be attached.

It is highly desirable that the abstract of classified reports be unclassified. Each paragraph of the abstract shall end with an indication of the military security classification of the information in the paragraph, represented as (TS), (S), (C), or (U).

There is no limitation on the length of the abstract. However, the suggested length is from 150 to 225 words.

14. **KEY WORDS:** Key words are technically meaningful terms or short phrases that characterize a report and may be used as index entries for cataloging the report. Key words must be selected so that no security classification is required. Identifiers, such as equipment model designation, trade name, military project code name, geographic location, may be used as key words but will be followed by an indication of technical content. The assignment of links, rules, and weights is optional.

DOCUMENT CONTROL DATA - R&D

(Security classification of title, body of abstract and indexing annotation must be entered when the overall report is classified)

1. ORIGINATING ACTIVITY (Corporate author)

2a. REPORT SECURITY CLASSIFICATION

2b. GROUP

3. REPORT TITLE

4. DESCRIPTIVE NOTES (Type of report and inclusive dates)

5. AUTHOR(S) (Last name, first name, initial)

6. REPORT DATE

7a. TOTAL NO. OF PAGES

7b. NO. OF REFS

8a. CONTRACT OR GRANT NO.

9a. ORIGINATOR'S REPORT NUMBER(S)

b. PROJECT NO.

9b. OTHER REPORT NO(S) (Any other numbers that may be assigned this report)

10. AVAILABILITY/LIMITATION NOTICES

11. SUPPLEMENTARY NOTES

12. SPONSORING MILITARY ACTIVITY

13. ABSTRACT CONTINUED

charge stocks with the final graphite properties was attempted. Bench-scale effort was centered around investigations into the preparation of isotropic high thermal expansion graphites and studies to improve binder qualities. Four pilot-scale coker runs to produce high thermal expansion isotropic cokes were made at the Marathon Oil Company in Robinson, Illinois. A commercial air-blown asphalt produced a lower thermal expansion and a higher strength material than that obtained from the air-blown vacuum residuum. A 2 per cent concentration of acetylene black in atmospheric residuum produced a coke with lower electrical resistance and higher strength than that of the 3 per cent concentration. Cokes from vacuum residuum and slurry oil charge stocks were formed into graphite. The test results show that original coke properties affect the final graphite properties. The high thermal expansion cokes were more difficult to process and resulted in graphite having a high compressive strength.

Page 2 of 2 pages

DD FORM 1 JAN 64 1473

Security Classification

Security Classification

14.	KEY WORDS	LINK A		LINK B		LINK C	
		ROLE	WT	ROLE	WT	ROLE	WT

INSTRUCTIONS

1. **ORIGINATING ACTIVITY:** Enter the name and address of the contractor, subcontractor, grantee, Department of Defense activity or other organization (*corporate author*) issuing the report.

2a. **REPORT SECURITY CLASSIFICATION:** Enter the overall security classification of the report. Indicate whether "Restricted Data" is included. Marking is to be in accordance with appropriate security regulations.

2b. **GROUP:** Automatic downgrading is specified in DoD Directive 5200.10 and Armed Forces Industrial Manual. Enter the group number. Also, when applicable, show that optional markings have been used for Group 3 and Group 4 as authorized.

3. **REPORT TITLE:** Enter the complete report title in all capital letters. Titles in all cases should be unclassified. If a meaningful title cannot be selected without classification, show title classification in all capitals in parenthesis immediately following the title.

4. **DESCRIPTIVE NOTES:** If appropriate, enter the type of report, e.g., interim, progress, summary, annual, or final. Give the inclusive dates when a specific reporting period is covered.

5. **AUTHOR(S):** Enter the name(s) of author(s) as shown on or in the report. Enter last name, first name, middle initial. If military, show rank and branch of service. The name of the principal author is an absolute minimum requirement.

6. **REPORT DATE:** Enter the date of the report as day, month, year, or month, year. If more than one date appears on the report, use date of publication.

7a. **TOTAL NUMBER OF PAGES:** The total page count should follow normal pagination procedures, i.e., enter the number of pages containing information.

7b. **NUMBER OF REFERENCES:** Enter the total number of references cited in the report.

8a. **CONTRACT OR GRANT NUMBER:** If appropriate, enter the applicable number of the contract or grant under which the report was written.

8b, 8c, & 8d. **PROJECT NUMBER:** Enter the appropriate military department identification, such as project number, subproject number, system numbers, task number, etc.

9a. **ORIGINATOR'S REPORT NUMBER(S):** Enter the official report number by which the document will be identified and controlled by the originating activity. This number must be unique to this report.

9b. **OTHER REPORT NUMBER(S):** If the report has been assigned any other report numbers (either by the originator or by the sponsor), also enter this number(s).

10. **AVAILABILITY/LIMITATION NOTICES:** Enter any limitations on further dissemination of the report, other than those

imposed by security classification, using standard statements such as:

- (1) "Qualified requesters may obtain copies of this report from DDC."
- (2) "Foreign announcement and dissemination of this report by DDC is not authorized."
- (3) "U. S. Government agencies may obtain copies of this report directly from DDC. Other qualified DDC users shall request through _____."
- (4) "U. S. military agencies may obtain copies of this report directly from DDC. Other qualified users shall request through _____."
- (5) "All distribution of this report is controlled. Qualified DDC users shall request through _____."

If the report has been furnished to the Office of Technical Services, Department of Commerce, for sale to the public, indicate this fact and enter the price, if known.

11. **SUPPLEMENTARY NOTES:** Use for additional explanatory notes.

12. **SPONSORING MILITARY ACTIVITY:** Enter the name of the departmental project office or laboratory sponsoring (paying for) the research and development. Include address.

13. **ABSTRACT:** Enter an abstract giving a brief and factual summary of the document indicative of the report, even though it may also appear elsewhere in the body of the technical report. If additional space is required, a continuation sheet shall be attached.

It is highly desirable that the abstract of classified reports be unclassified. Each paragraph of the abstract shall end with an indication of the military security classification of the information in the paragraph, represented as (TS), (S), (C), or (U).

There is no limitation on the length of the abstract. However, the suggested length is from 150 to 225 words.

14. **KEY WORDS:** Key words are technically meaningful terms or short phrases that characterize a report and may be used as index entries for cataloging the report. Key words must be selected so that no security classification is required. Identifiers, such as equipment model designation, trade name, military project code name, geographic location, may be used as key words but will be followed by an indication of technical content. The assignment of links, rules, and weights is optional.